

NASA CONTRACTOR  
REPORT

NASA CR-2523



N75-24677

NASA CR-2523

LIGHT AIRCRAFT LIFT, DRAG,  
AND MOMENT PREDICTION -  
A REVIEW AND ANALYSIS

*Frederick O. Smetana, Delbert C. Summey,  
Neill S. Smith, and Ronald K. Carden*

*Prepared by*  
NORTH CAROLINA STATE UNIVERSITY  
Raleigh, N.C. 27607  
*for Langley Research Center*



NATIONAL AERONAUTICS AND SPACE ADMINISTRATION • WASHINGTON, D. C. • MAY 1975



1. Report No. NASA CR-2523	2. Government Accession No.	3. Recipient's Catalog No.	
4. Title and Subtitle LIGHT AIRCRAFT LIFT, DRAG, AND MOMENT PREDICTION - A REVIEW AND ANALYSIS		5. Report Date May 1975	6. Performing Organization Code
		8. Performing Organization Report No.	
7. Author(s) Frederick O. Smetana, Delbert C. Summey, Neill S. Smith, and Ronald K. Carden		10. Work Unit No. 760-60-01-0900	11. Contract or Grant No. NGR 34-002-179
9. Performing Organization Name and Address North Carolina State University Raleigh, North Carolina 27607		13. Type of Report and Period Covered Contractor Report	
		14. Sponsoring Agency Code	
12. Sponsoring Agency Name and Address National Aeronautics and Space Administration Washington, DC 20546			
15. Supplementary Notes  Topical report.			
16. Abstract The historical development of analytical methods for predicting the lift, drag, and pitching moment of complete light aircraft configurations in cruising flight is reviewed. Theoretical methods, based in part on techniques described in the literature and in part on original work, are then developed in detail. These methods form the basis for understanding the computer programs presented in the remainder of the work. Programs are given to: (1) compute the lift, drag, and moment of conventional airfoils, (2) extend these two-dimensional characteristics to three dimensions for moderate-to-high aspect ratio unswept wings, (3) plot complete configurations, (4) convert the fuselage geometric data to the correct input format, (5) compute the fuselage lift and drag, (6) compute the lift and moment of symmetrical airfoils to $M = 1.0$ by a simplified semi-empirical procedure, and (7) compute, in closed form, the pressure distribution over a prolate spheroid at $\alpha = 0$ . Comparisons of the predictions with experiment indicate excellent lift and drag agreement for conventional airfoils and wings for $C_L < 0.8$ . Limited comparisons of body-alone drag characteristics yield reasonable agreement. Also included are discussions for interference effects and techniques for summing the results of 1-5 above to obtain predictions for complete configurations.			
17. Key Words (Suggested by Author(s)) Aerodynamic characteristics, prediction techniques, lift estimation, drag estimation, computer programs, numerical methods		18. Distribution Statement  Unclassified - Unrestricted  New Subject Category 02	
19. Security Classif. (of this report) Unclassified	20. Security Classif. (of this page) Unclassified	21. No. of Pages 492	22. Price* \$12.00



# TABLE OF CONTENTS

	Page
LIST OF FIGURES . . . . .	viii
LIST OF TABLES. . . . .	xiv
GENERAL INTRODUCTION. . . . .	1
LITERATURE REVIEW AND THEORETICAL BASIS OF COMPUTER PROGRAMS. . . . .	5
Literature Review. . . . .	6
Introduction. . . . .	6
The Airfoil in Inviscid Flow. . . . .	7
The Airfoil in Viscous Flow . . . . .	21
Compressibility . . . . .	23
Extension to Three Dimensions . . . . .	25
Treatment of Viscous Effects: Drag . . . . .	31
Fuselage Contributions To Lift, Drag, and Moment. . . . .	36
Interference Effects. . . . .	47
Unified Analytical Treatments of Wing-Body Characteristics. . . . .	49
A Theory for the Prediction of Lift, Drag, and Pitching Moment of Light Aircraft Wings. . . . .	50
Introduction. . . . .	50
Representation of an Airfoil in Two-Dimensional Flow. . . . .	54
Treatment of Viscous Effects. . . . .	71
Extension To Three Dimensions: The Finite Wing . . . . .	87
Concluding Remarks. . . . .	104
A Theory for the Prediction of Lift, Drag, and Pitching Moment of Light Aircraft Fuselages. . . . .	105
Inviscid Flow Over Fuselages. . . . .	105

TABLE OF CONTENTS (Continued)

	Page
Viscous Flow Over Fuselages . . . . .	113
Concluding Remarks. . . . .	133
Interference Effects. . . . .	135
Wing-Tail Interference . . . . .	135.
Lift of an Isolated Fuselage . . . . .	139
Interaction Between Wing Lift and Fuselage Lift. . . . .	144
Drag Interaction Effects . . . . .	145
Lift and Drag of Complete Configurations. . . . .	147
 PROGRAM FOR THE CALCULATION OF TWO-DIMENSIONAL WING AERODYNAMIC COEFFICIENTS. . . . .	 153
Introduction. . . . .	154
General Program Theory. . . . .	156
General Program Modifications . . . . .	162
Changes Concerning the Airfoil Geometry Specification . . . . .	168
Thickness and Camber Solution Modifications . . . . .	171
Boundary Layer Modifications. . . . .	173
Coefficient Modification. . . . .	175
Discussion of Program Results . . . . .	178
 EXTENSION TO THREE DIMENSIONS. . . . .	 211
Introduction. . . . .	212
General Program Theory and Operation. . . . .	219
Modifications Required to Adapt the CDC "STALL" Program to IBM Equipment. . . . .	223
General Program Modifications . . . . .	224
Changes Concerning Reynolds Number. . . . .	226

TABLE OF CONTENTS (Continued)	Page
Changes Concerning Airfoil Data Storage. . . . .	227
Discussion of Program Results. . . . .	229
	231
PROGRAMS FOR THE CALCULATION OF BODY AERODYNAMIC COEFFICIENTS . . . .	
Introduction . . . . .	232
Specifications of Input Data with Verification by Plotting . . . .	234
General Program Theory for Inviscid Body Program . . . . .	238
General Program Modifications . . . . .	243
Streamline Modification and Boundary Layer Calculation . . . . .	247
Addition of Wake Body. . . . .	251
Discussion of Program Results. . . . .	256
REFERENCES. . . . .	259
APPENDICES. . . . .	269
A - Two-Dimensional Wing Aerodynamic Characteristics Program . . . .	270
User Instructions . . . . .	270
Program Listing . . . . .	275
Sample Output . . . . .	291
B - Polynomial Fit of Two-Dimensional Data . . . . .	300
User Instructions . . . . .	300
Program Listing . . . . .	303
Sample Output . . . . .	306
C - Airfoil-to-Complete-Wing Program . . . . .	310
User Instructions . . . . .	310
Program Listing . . . . .	314
Sample Output . . . . .	322

TABLE OF CONTENTS (Continued)

	Page
D - PLOT Program. . . . .	323
User Instructions. . . . .	323
Plotting Software Modifications. . . . .	333
Program Listing. . . . .	341
Sample Output. . . . .	356
E - CONVERT Program . . . . .	369
Program Listing. . . . .	370
Sample Output. . . . .	372
F - NCSU BODY Program . . . . .	376
User Instructions. . . . .	376
Program Listing. . . . .	382
Sample Output. . . . .	400
G - Theoretical Basis of Oeller's Method. . . . .	405
H - Rapid, Inviscid Computation of the Pressure Distribution of Airfoils for Mach Numbers Less Than or Equal To 1.0 . . . . .	411
User Instructions - TRINSON. . . . .	426
Program Listing - TRINSON. . . . .	429
Sample Output - TRINSON. . . . .	430
User Instructions - COMPR. . . . .	431
Program Listing - COMPR. . . . .	435
Sample Output - COMPR. . . . .	440
User Instructions - TRANSON. . . . .	442
Program Listing - TRANSON. . . . .	445
Sample Output - TRANSON. . . . .	446



TABLE OF CONTENTS (Continued)

	Page
I - A Computer Program Providing Rapid Evaluation of Closed-Form Solution for the Flow About a Prolate Spheroid Moving Along Its X-Axis. . . . .	447
User Instructions . . . . .	449
Program Listing . . . . .	451
Sample Output . . . . .	452
J - Supplementary Bibliography . . . . .	453

## LIST OF FIGURES

	Page
1. Modification of camber line due to boundary layer displacement thickness. . . . .	157
2. Thickness effects due to boundary layer displacement thickness. . . .	158
3. Schematic of control point averaging. . . . .	159
4. NCSU computer program flow chart. . . . .	161
5. Sample airfoil with longest chord line. . . . .	164
6. Location of chord line for $\alpha=0$ . . . . .	165
7. Example airfoil in reference system for $\alpha=1$ option . . . . .	166
8. Rotated airfoil after longest chord line has been calculated. . . . .	166
9. Reference line for the angle of attack for both $\alpha$ options. . . . .	169
10. Effect of each of the drag modifications on the drag coefficients of the 23012 airfoil at a Reynolds number of 3.0 million . . . . .	177
11. General shape of the 15 airfoils investigated for lift and drag characteristics. . . . .	182
12. Comparison of 2-D lift and drag coefficients of the 0009 airfoil at a Reynolds number of 3,000,000 . . . . .	185
13. Comparison of 2-D lift and drag coefficients of the 2424 airfoil at a Reynolds number of 2,900,000 . . . . .	186
14. Comparison of 2-D lift and drag coefficients of the 2424 airfoil at a Reynolds number of 9,000,000 . . . . .	187
15. Comparison of 2-D lift and drag coefficients of the 4412 airfoil at a Reynolds number of 3,000,000 . . . . .	188
16. Comparison of 2-D lift and drag coefficients of the 4412 airfoil at a Reynolds number of 9,000,000 . . . . .	189
17. Comparison of 2-D lift and drag coefficients of the 4412 airfoil at a Reynolds number of 6,000,000 with fixed upper and lower surface leading edge transition to approximate standard roughness. . . . .	190

LIST OF FIGURES (Continued)

	Page
18. Comparison of 2-D lift and drag coefficients of the 4421 airfoil at a Reynolds number of 3,000,000 . . . . .	191
19. Comparison of 2-D lift and drag coefficients of the 23012 airfoil at a Reynolds number of 3,000,000 . . . . .	192
20. Comparison of 2-D lift and drag coefficients of the 23012 airfoil at a Reynolds number of 8,800,000 . . . . .	193
21. Comparison of 2-D lift and drag coefficients of the 23021 airfoil at a Reynolds number of 3,000,000 . . . . .	194
22. Comparison of 2-D lift and drag coefficients of the 63-006 airfoil at a Reynolds number of 3,000,000 . . . . .	195
23. Comparison of 2-D lift and drag coefficients of the 63 <sub>2</sub> -615 airfoil at a Reynolds number of 3,000,000. . . . .	196
24. Comparison of 2-D lift and drag coefficients of the 63 <sub>3</sub> -618 airfoil at a Reynolds number of 3,000,000. . . . .	197
25. Comparison of 2-D lift and drag coefficients of the 63 <sub>4</sub> -421 airfoil at a Reynolds number of 3,000,000. . . . .	198
26. Comparison of 2-D lift and drag coefficients of the 64 <sub>1</sub> -412 airfoil at a Reynolds number of 3,000,000. . . . .	199
27. Comparison of 2-D lift and drag coefficients of the 64 <sub>4</sub> -421 airfoil at a Reynolds number of 3,000,000. . . . .	200
28. Comparison of 2-D lift and drag coefficients of the Whitcomb airfoil at a Reynolds number of 1,900,000. . . . .	201
29. Comparison of 2-D lift and drag coefficients of the Whitcomb airfoil at a Reynolds number of 9,200,000. . . . .	202
30. Comparison of 2-D lift and drag coefficients of the TN D-7071 airfoil at a Reynolds number of 9,000,000 (note experimental drag coefficients are not available). . . . .	203
31. Comparison of pressure coefficients of the TN D-7071 airfoil at a Reynolds number of 9,000,000 and angle of attack of 3.4 degrees. . . . .	204
32. Comparison of pressure coefficients of the TN D-7071 airfoil at a Reynolds number of 9,000,000 and angle of attack of 12.4 degrees. . . . .	205

LIST OF FIGURES (Continued)

	Page
33. Comparison of pressure coefficients of the TN D-7071 airfoil at a Reynolds number of 9,000,000 and angle of attack of 18.7 degrees. . . . .	206
34. Comparison of 2-D lift and drag coefficients of the S-14.1 airfoil (Ref. 108) at a Reynolds number of 600,000. . . . .	207
35. Predictions of $C_L$ variation with Mach Number at $\alpha = 0^\circ$ and a Reynolds number of 3,000,000 for the 23012 airfoil . . . . .	208
36. Predictions of $C_D$ variation with Mach Number at $\alpha = 0^\circ$ and a Reynolds number of 3,000,000 for the 23012 airfoil . . . . .	209
37. Comparison of original and modified program three-dimensional coefficient values for the 64218 root-64412 tip case . . . . .	214
38. Comparison of experimental and calculated three-dimensional coefficient values for the 64420 root-64412 tip case . . . . .	215
39. Comparison of experimental and calculated three-dimensional coefficient values for the 4420 root-4412 tip case . . . . .	216
40. Comparison of experimental and calculated three-dimensional coefficient values for the 23020 root-23012 tip case . . . . .	217
41. Planform of the three-dimensional test cases from Reference 78 . . . . .	218
42. Flow chart of major logic in FITIT . . . . .	221
43. Flow chart of major logic in FUNC. . . . .	222
44. Schematic representation of the modified data look up procedure. . . . .	228
45. Example of a correct and an incorrect data set for the Cessna 182 fuselage . . . . .	235
46. The approximate representation of the body surface . . . . .	240
47. Orientation of body with respect to reference line . . . . .	245
48. New panel identification procedure for tracing streamlines . . . . .	250
49. Definition of wake body. . . . .	251
50. Panel boundaries on the original body and the wake body. . . . .	252
51. 3-1 ellipsoid with and without a wake body . . . . .	254
52. Cessna 182 Fuselage with and without a wake body . . . . .	255

LIST OF FIGURES (Continued) - Appendices

	Page
A-1. Format specification of input data for the 2-D characteristics program. . . . .	273
A-2. Example data set for the 2-D characteristics program. . . . .	274
A-3. Sample output of the 2-D characteristics program with IWRITE=0 (note that only upper surface inviscid and boundary layer solution information is shown here). . . . .	291
A-4. Sample output of the 2-D characteristics program with IWRITE=1. . .	295
A-5. Sample output of the 2-D characteristics program with IWRITE=2. . .	298
A-6. Sample output of the 2-D characteristics program with IWRITE=3. . .	299
B-1. Format specification of input data for the polynomial fit of 2-D data program . . . . .	301
B-2. Example data set for the polynomial fit of 2-D data program . . . .	302
B-3. Sample output of the polynomial fit of 2-D data program . . . . .	306
C-1. Format specification of input data for the airfoil-to-complete-wing program . . . . .	312
C-2. Example data set for the airfoil-to-complete-wing program . . . . .	313
C-3. Sample output of the airfoil-to-complete-wing program . . . . .	322
D-1. Orientation of body with respect to body reference axes for the PLOT programs. . . . .	338
D-2. Sample Cessna 182 data set for the PLOT program . . . . .	339
D-3. Example of the unplotted portion of the sample output for the PLOT program . . . . .	356
D-4. Plotted 3-view of the Cessna 182. . . . .	358
D-5. Orthographic projection of a Cessna 182 rolled $-45^\circ$ , pitched $10^\circ$ and yawed $-30^\circ$ with respect to the X-Z plane of symmetry . . . . .	359
D-6. Orthographic projection with hidden lines removed of a Cessna 182 rolled $45^\circ$ , pitched $10^\circ$ , and yawed $30^\circ$ with respect to the X-Z plane of symmetry. . . . .	360

LIST OF FIGURES (Continued) - Appendices

	Page
D-7. Orthographic projection of a Cessna 182 rolled $45^\circ$ , pitched $10^\circ$ , and yawed $160^\circ$ with respect to the X-Z plane of symmetry . . . . .	361
D-8. Orthographic projection of a Cessna 182 rolled $-45^\circ$ and yawed $-70^\circ$ with respect to the X-Z plane of symmetry . . . . .	362
D-9. Orthographic projection of a Cessna 182 rolled $-45^\circ$ , pitched $10^\circ$ , and yawed $-30^\circ$ with respect to the Y-Z plane. . . . .	363
D-10. Perspective view number 1 of the Cessna 182 . . . . .	364
D-11. Perspective view number 2 of the Cessna 182 (The reader should note that the viewer is under the aircraft looking up) . . . .	365
D-12. Plotted 3-view of the Cessna 182 fuselage . . . . .	366
D-13. Two orthographic projections of a Cessna 182 fuselage rolled $-45^\circ$ , pitched $10^\circ$ , and yawed $-30^\circ$ with respect to the X-Z plane of symmetry. The top view has hidden lines removed. . .	367
D-14. Orthographic projection with hidden lines removed of a Cessna 182 fuselage rolled $-45^\circ$ , pitched $10^\circ$ , and yawed $-30^\circ$ with respect to the Y-Z plane . . . . .	368
E-1. CONVERT program sample output of the Cessna 182 with 560 panels describing the half-body . . . . .	372
F-1. Orientation of body with respect to body reference axes for the NCSU BODY program. . . . .	378
F-2. Schematic of indexing scheme used for a 3-1 ellipsoid with 60 panels describing the half-body. . . . .	379
F-3. Format specification for the NCSU BODY program. . . . .	380
F-4. NCSU BODY program sample data set for a 3-1 ellipsoid with 100 panels describing the half-body. . . . .	381
F-5. NCSU BODY program sample output for the Cessna 182 with 560 panels describing the half-body using the IWRITE=0 option. . .	400
G-1. Geometry for potential flow calculation . . . . .	405
G-2. Airfoil approximation by polygon. . . . .	406

LIST OF FIGURES (Continued) - Appendices

	Page
G-3. Geometry for calculation of $K_{ij}, i \neq j$ . . . . .	407
G-4. Geometry for calculation of $K_{jj}$ . . . . .	409
H-1. Comparison of 16 point Weber, 32 point Weber, and 65 point Lockheed methods for predicting airfoil pressure distributions on the NCSU 0010 at $\alpha = 2.5^\circ$ . . . . .	414
H-2. Comparison of theory and experiment for one airfoil . . . . .	425
H-3. Format specification of input data for TRINSON. . . . .	427
H-4. Example data set for TRINSON . . . . .	428
H-5. Sample output for TRINSON . . . . .	430
H-6. Format specification of input data for COMPR. . . . .	433
H-7. Example data set for COMPR. . . . .	434
H-8. Sample output for COMPR . . . . .	440
H-9. Format specification of input data for TRANSON. . . . .	443
H-10. Example data set for TRANSON. . . . .	444
H-11. Sample output for TRANSON . . . . .	446
I-1. Format specification for SPHEROID . . . . .	449
I-2. Sample data set for SPHEROID. . . . .	450
I-3. Sample output for SPHEROID. . . . .	452

## LIST OF TABLES

	Page
1. Comparison of subroutines contained in the NASA program and the NCSU program. . . . .	164
2. Comparison of routines contained in the original and modified program . . . . .	224
3. Data file comparison for the XYZ and the NCSU BODY programs . . .	244
H-1. Position of pivotal points. . . . .	415
H-2. Weber coefficients $S^{(1)}$ for the 16 point method . . . . .	416
H-3. Weber coefficients $S^{(2)}$ for the 16 point method . . . . .	417
H-4. Weber coefficients $S^{(3)}$ for the 16 point method . . . . .	418
H-5. Weber coefficients $S^{(1)}$ for the 32 point method . . . . .	419
H-6. Weber coefficients $S^{(2)}$ for the 32 point method . . . . .	421
H-7. Weber coefficients $S^{(3)}$ for the 32 point method . . . . .	423



## GENERAL INTRODUCTION

The successful prediction of the performance of a new or modified aircraft depends as much on the availability of an accurate estimate of the configuration's lift and drag characteristics as on any one thing. Despite the importance of this task, the procedure used in the light aircraft industry and that taught in most universities has remained essentially a semi-empirical correlation of wind tunnel and flight test data plus a collection of useful rules of thumb. The major airframe manufacturers and their cognizant governmental laboratories have for some time sought both to reduce the time needed to develop these predictions and to increase their accuracy and reliability through the use of large-scale digital computers. Employing long-known, highly rigorous analytical computation methods which become too involved when applied to complete aircraft for one to perform manually, these groups have, within the last three-to-six years, achieved some remarkable successes in predicting the aerodynamic characteristics of complex geometric shapes.

It is the intention of the present work

- to review analytical and experimental developments in aerodynamics of the past 32 years, in particular those of the National Aeronautics and Space Administration,
- to identify those of special pertinence to the design of light aircraft and
- to develop from these easy-to-use design procedures.

Of necessity these procedures will involve digital computer programs. This approach follows that employed in earlier works in this series. Reference 1, for example, provides detailed computer programs for the prediction of point and path performance assuming that the lift, drag, and thrust characteristics are known. References 2 and 3 give programs for the calculation of stability derivatives and aircraft motions given the vehicle's geometric and inertial characteristics. Thus with these and the present work the reader can specify the aircraft geometry, mass distribution, and thrust applied to the air and expect to obtain the vehicle's performance and its handling qualities. He can then vary the geometry, etc. in a systematic fashion and find the shape giving the most satisfactory combination of performance and handling qualities.

While the availability of these programs will certainly be of great assistance in the overall design task, it should be noted that many areas of aircraft configuration design have not been treated in detail or have not been programmed for computer solution in the work to date. These include large excursions in the motions about an equilibrium position, performance in the horizontal plane, takeoff and landing, aerodynamic characteristics at high angles of attack and/or with deflected flaps, flight in turbulent air, calculation of stick and rudder forces and deflections, propeller slipstream effects, adequate representations of thrust horsepower and fuel

flow, and the effects of specific stability augmentation systems. It is the authors' ultimate intention to treat all of these problems in the manner of the programs included in the present work. They would, however, be pleased to receive suggestions from readers and users of the work as to the priority with which the problems should be attacked.

The present work departs from the practice of previous works in this series in that the computer programs presented are usually modifications (generally simplifications) of elaborate programs in use at government facilities rather than original efforts. This was done to take advantage of the rather substantial effort which went into the preparation of these programs. Each program which was used has shown good agreement with experiment in at least a limited number of cases. Such a practice also has a number of disadvantages:

1. The available documentation is usually very sketchy and frequently inconsistent with the program statements and/or logic. As a result it is very difficult to determine in detail the method on which the program is based and the validity and/or applicability of the methods.
2. The programs usually contain many more options than are needed for the present purposes. It is often difficult to unravel the program to the point that these unneeded options can be removed successfully.
3. The programs are usually written to take advantage of the characteristics of a particular machine which limits their transferability to other machines.
4. In every case the programs are written for very large machines. Smaller machines generally have insufficient storage capacity even to compile the programs. In order to use them on smaller machines one must devise a means of splitting a program into several parts or employing a form of virtual storage.

The present work represents an effort at overcoming these disadvantages. It begins with a review of the literature on the estimation of lift and drag characteristics of wings, wing-bodies, and complete aircraft configurations. Among those treated in this discussion are a group of government reports which describe computer programs for performing various portions of this estimation task in a rapid but accurate manner. Several of these programs appeared to offer a sufficient reduction in the cost of estimating the aerodynamic characteristics of new or modified designs that it seemed desirable to adapt them for use with light aircraft, the computer capabilities of this industry, and as an instructional device for fledgling designers. For these reasons, those portions of the programs dealing with the effects of flap deflections have been removed. The modified programs are therefore more applicable to the higher speed portions of the flight profile. Studies are currently underway of means for including the computation of these effects with reasonable additional computer requirements.

In the next section of the work the theoretical bases of the recommended programs are discussed starting from first principles. It should be emphasized that the methods described are not always exactly those used by the computer programs. The approach to the problem is usually the same but the details are frequently quite different. This has been done because, as noted above, the details of the methods actually used are obscure, at least to the present authors, and because a different treatment was regarded as being easier for those approaching the area for the first time to understand.

Following this discussion is a review of the changes in the programs, instructions for their use, and some sample results. Included also are appendices providing locally-written computer programs found useful for producing analytical check cases, simple approximate solutions to more general computations, or extensions of the range of the major programs to other speed regimes.

The present work is intended to serve several needs. Its primary function is to provide the practicing light aircraft designer with a powerful tool for reducing the engineering labor needed to develop a new airplane or revise an existing one. Hopefully, it is written at such a level and in sufficient depth that the user will be able to gain an understanding of the limitations imposed on the attainable accuracy by the choice of physical and mathematical models as well as an appreciation for the new capabilities provided by the programs and instructions for their use. By keeping the mathematical sophistication required for comprehension to a minimum and by emphasizing physical descriptions of the means by which flows over aircraft are represented, it is hoped that undergraduate aeronautical engineering students will also find the work both helpful and illuminating. It seems unfortunate that because of time limitations, a lack of technical maturity on the student's part, and a reluctance on many educators' part to depart from traditional practice, flight vehicle design is still taught largely as a semi-empirical art rather than as the near-science which it has lately become. Perhaps with the aid of these more powerful less time-consuming tools the student can now successfully complete more realistic design problems during his undergraduate education.



LITERATURE REVIEW AND THEORETICAL

BASIS OF COMPUTER PROGRAMS

# LITERATURE REVIEW

## INTRODUCTION

Given the task of creating an entirely new airplane, the designer will usually seek to devise first a wing geometry and, ultimately, a whole airplane geometry that

1. provides the required lift
2. has suitable stall characteristics
3. has minimum drag for good performance
4. has good stability and control characteristics
5. meets structural requirements
6. is easy to build.

He will usually select a configuration that satisfies the last two objectives reasonably well and then attempt to determine how well the configuration meets the other objectives. He recognizes that he need not calculate the aerodynamic forces acting on the vehicle with great accuracy in order to determine the flying qualities. On the other hand, if he is to predict the craft's performance with reasonable accuracy, he must know the lift and drag as precisely as possible.

From the viewpoint of designers active during the early years of this century the analysis process was very ill-defined. One did not then even know how much wing he should provide or what shape to make it in order to insure that his aircraft would fly. Being able to estimate how fast or how far his craft might go seemed a matter of secondary concern to the more urgent problem of how much lift is associated with a particular geometry. A systematic study of this problem would seem to begin with consideration of the lift developed by a slice or section out of the wing. Modeling the problem in this fashion has the advantage that one need consider only flow in two dimensions rather than in three, a great mathematical simplification. Further it would seem reasonable to assume that the fluid is inviscid if for no other reason than to take advantage of the extensive analytical studies (particularly those of Helmholtz (Ref. 4) and Kirchhoff (Ref. 5)) that had been carried out for this case during the nineteenth century. These studies had been successful at explaining several experimental facts and present far less mathematical difficulty than one would encounter working the more general equations for the flow of a viscous fluid formulated by Navier and by Stokes about 1840. A good account of much of this work may be found in Lamb (Ref. 6).

The immensity of the problem facing engineers in 1900 trying to devise a rational means of calculating wing lift can be better appreciated when

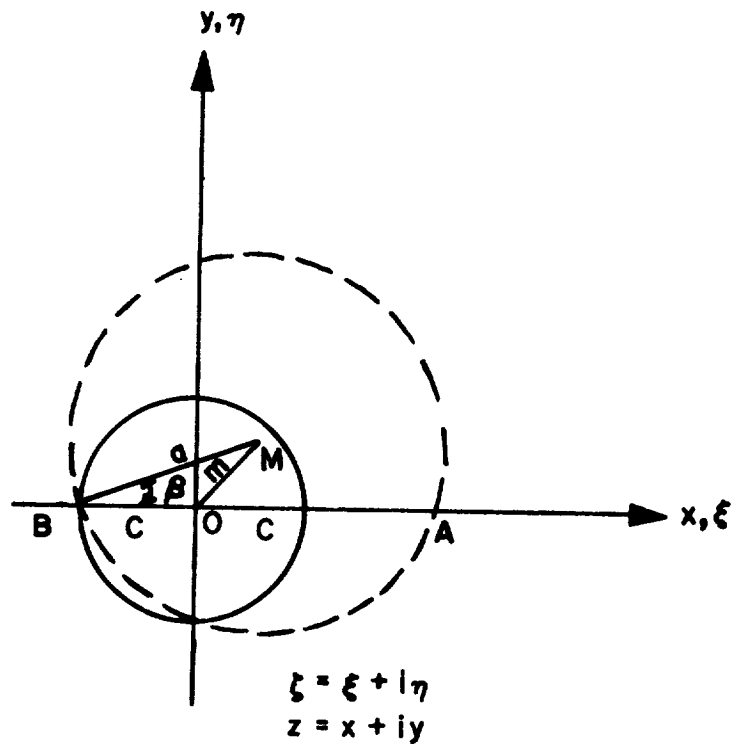
one realizes that in the contemporary view lift was the force reacting to the change in the momentum of the airstream striking the inclined lower surface of wing. Such a force would be proportional to  $\sin^2 \alpha$  where  $\alpha$  is the angle by which the lower surface is inclined to the wind. If one were to assume that a wing is flying at fifty miles an hour with  $\alpha = 6^\circ$ , then it could develop about 0.0635 pounds of lift per square foot of surface, according to this theory. Since it was then impossible to build a wing lighter than this weight, many scientists confidently predicted that man would never fly. More preceptive individuals noted however that the flight of gliders could not be explained by such small values of lift and therefore something must be wrong with the theory.

### THE AIRFOIL IN INVISCID FLOW

Lord Rayleigh had shown in 1878 that the swerving flight of a "cut" tennis ball could be explained at least in general terms by comparing it to the case of a cylinder placed in an inviscid uniform stream. By superposing a circulatory flow upon the cylinder, the cylinder developed a force normal to the direction of the uniform stream, directly proportional to the strength of the circulatory flow. This result along with the earlier work of Helmholtz and Kirchhoff was known to the German mathematician M. W. Kutta who was interested in why cambered airfoils produce lift at  $\alpha = 0$ . In a 1902 paper (Ref. 7) he studied a thin airfoil formed by a circular arc. He concluded that the only reasonable assumption one could make in view of what was known physically was that the flow velocity over the upper surface was equal to that over the lower surface at the trailing edge. The flow would therefore leave the surface smoothly at finite velocity. He was willing to accept the idea of an infinite velocity at the sharp leading edge, a situation studied by Helmholtz, in order to obtain an approximate solution for the lift. Von Kármán (Ref. 8) gives a highly readable account of this early work.

Joukowski (Ref. 9), working independently along somewhat parallel lines, was able to obtain exact solutions for a certain class of airfoils in inviscid flow. He first showed that when a cylindrical body of arbitrary cross-section moves with velocity,  $V$ , in a fluid whose density is  $\rho$  and there is a circulation of the magnitude,  $\Gamma$ , around the body, a force is produced equal to the product  $\rho V \Gamma$  per unit length of the cylinder. The direction of the force is normal both to the velocity,  $V$ , and the axis of the cylinder. Joukowski also assumed the flow to leave the airfoil smoothly at the trailing edge. By means of this hypothesis the whole problem of lift becomes purely mathematical: one has only to determine the amount of circulation so that for zero vertex angle at the trailing edge the velocity of the flow leaving the upper surface is equal to the flow leaving the lower surface. If the tangents to the upper and lower surfaces form a finite angle, the trailing edge is a stagnation point.

Joukowski then found a transformation,  $\zeta = z + C^2/z$ , by which a circle in the  $z$ -plane becomes an airfoil in the  $\zeta$ -plane. See the following sketch.



According to the transformation, a point represented by  $z = x + iy$  in the  $x, y$  plane is moved to a different location in the  $\xi, \eta$  plane. In the process, all the other points in the plane are moved in such a way that the figure of a circle in the  $x, y$  plane becomes an airfoil in the  $\xi, \eta$  plane. Under Joukowski's transform the shape of the airfoil may be changed to a considerable extent by moving the center of the circle (originally at 0) to some other location  $M$  while keeping the point at which the circle crosses the  $x$ -axis in the left half-plane at  $B$ . To see how this happens it is instructive to carry out a sample calculation.

The general equation of a circle is of course

$$(x - x_1)^2 + (y - y_1)^2 = a^2$$

where

$$x_1 = a \cos \beta - C = \frac{a^2 - C^2 - m^2}{2C}$$

$$y_1 = a \sin \beta$$

in the notation of the sketch. For simplicity one may assume that in this calculation  $\beta = 0$ . Then

$$[x - (a - C)]^2 + y^2 = a^2$$

or

$$y = \sqrt{2(a - C)x + 2aC - C^2 - x^2}$$



Now

$$\zeta = x + iy + \frac{C^2}{x + iy}$$

$$= x + iy + C^2 \left( \frac{x - iy}{x^2 + y^2} \right)$$

$$= x \left( 1 + \frac{C^2}{x^2 + y^2} \right) + iy \left( 1 - \frac{C^2}{x^2 + y^2} \right).$$

Substituting values for  $x^2 + y^2$  and  $y$  into this expression yields

$$\zeta = x \left( 1 + \frac{C^2}{2aC - C^2 + 2x(a - C)} \right) + i \left( 1 - \frac{C^2}{2aC - C^2 + 2x(a - C)} \right) \sqrt{2(a - C)x + 2aC - C^2 - x^2}.$$

Since  $a$  and  $C$  are arbitrary numbers, choosing  $x$  completely specifies the value of  $\zeta$ . For example, let  $C = 1$  and  $a = 1.1$ . For this special case the previous equation becomes

$$\zeta = x \left( 1 + \frac{1}{1.2 + 0.2x} \right) + i \left( 1 - \frac{1}{1.2 + 0.2x} \right) \sqrt{1.2 + 0.2x - x^2}.$$

The equation is easily evaluated and the results presented in tabular form. The table below may be extended to determine the shape of the resulting figure more accurately, if desired.

x	$\xi$	$\eta$
1.2	2.035	0.
1.	1.707	+.1855
1.	1.707	-.1855
0.5	0.885	+.236
0.5	0.885	-.236
0.	0.	+.182
0.	0.	-.182
-1.	-2.	0.

Even from this limited set of numbers, however, it is apparent that for these values of  $a$  and  $C$  the circle maps into a symmetrical airfoil-like figure of high thickness-to-chord ratio. Moving  $M$  to the right increases airfoil thickness while moving  $M$  in the  $y$ -direction adds camber to the airfoil. Note that the airfoil chord is approximately  $4C$ . Note also that point  $A$  becomes the leading edge of the mean camber line and point  $B$  the trailing edge of the airfoil under the transformation. When the angle of attack is changed, the flow strikes the airfoil from a different direction. To represent this situation, the strength of the circulation must be changed so that as far as the flow over the cylinder in the  $x$ - $y$  plane is concerned the forward stagnation point has moved to some new location obtained by rotating the line  $MA$  through an angle  $\alpha$ ,  $\alpha$  being positive when  $A$  moves down ( $y$  becomes negative). The location of the rear stagnation point must, for reasons pointed out in the next chapter, remain fixed during this operation.

Since the transformation is conformal, the fluid velocity and pressure which exist at any point on the surface of the cylinder can be related quantitatively, as indicated below, to those which exist at the corresponding point on the airfoil. Integration of these pressures in the direction normal to the free stream velocity then gives the airfoil lift (which is also the same as the lift produced by the generating cylinder).

For the cylinder, the surface velocity components are given by

$$u = V[\cos \alpha(1 - \cos 2\theta) + \sin \alpha \sin 2\theta] + \frac{\Gamma y}{2\pi a^2}$$

$$v = V[\cos \alpha \sin 2\theta - \sin \alpha(1 - \cos 2\theta)] - \frac{\Gamma x}{2\pi a^2}$$

while the surface pressures are given by

$$P_{\text{CIRCLE}} = P_{\text{STAGNATION}} - \frac{\rho}{2} (u^2 + v^2) .$$

Here  $\theta$  is the angular location of the point of interest on the surface measured from the negative x-axis. Hence  $x = a \cos \theta$  and  $y = a \sin \theta$ . One may use these values in the procedure outlined above to find that location on the airfoil corresponding to  $\theta$ . The velocity on the airfoil surface is simply the velocity at the equivalent point on the circle times  $|dz/d\zeta|$ . From the transform

$$\left| \frac{dz}{d\zeta} \right| = \left| \frac{1}{d\zeta/dz} \right| = \left| \frac{1}{1 - C^2/z^2} \right| = \left| \frac{z}{z - C^2/z} \right|$$

thus the airfoil surface pressure is given by

$$P_{\text{AIRFOIL}} = P_{\text{STAGNATION}} - \frac{\rho}{2} (u^2 + v^2) \left| \frac{z}{z - C^2/z} \right|^2 .$$

It is interesting to note that while the theory places no limit on the magnitude of  $\Gamma$ , a value greater than  $\Gamma = 2\pi Va$  means that the front and rear stagnation points have come together and are moving away from the circle along the ray  $\theta = -\pi/2$ , clearly a physically impossible situation since it would mean a strong cyclonic flow was present about the airfoil. In actual cases  $\Gamma$  seldom exceeds  $\pi Va/4$ .

The Joukowski transform technique was a great step forward in analyzing the lift of airfoils. It gives the correct variation of lift with angle of attack and predicts lift values which are very close to measured values at the same angles of attack. Unfortunately the Joukowski transform techniques also had a number of disadvantages:

1. It is an inverse technique, that is, one does not know beforehand precisely what the airfoil will look like. As a result it is difficult to use the technique to estimate the characteristics of a given airfoil.

2. It leads always to an airfoil with a cusp at the trailing edge. This is impractical structurally.
3. It leads to airfoils which have their minimum pressure point very far forward. Consequently, they have thick boundary layers, and therefore higher drag and lower maximum lift values than airfoils with the minimum pressure point further aft.
4. Being an inviscid theory, it cannot be used to estimate either lift characteristics near stall or drag values.
5. It is tedious to determine the ordinates of the airfoil accurately.

These deficiencies were soon recognized and many investigators set about devising more general transforms which could be used to represent a greater variety of airfoils, in particular those with finite trailing edge angles. Kármán and Trefftz (Ref. 10), von Mises (Ref. 11), Müller (Ref. 12), and Theodorsen (Ref. 13) were among the leaders in this effort, which by 1932 had reached the point where one could determine the lift characteristics of a great variety of airfoils. The great effort required to complete a calculation, however, discouraged thoughts of a further generalization in the transform technique. The following outline of Theodorsen's method will indicate the labor required.

The transform or mapping function is built up in two stages; in the first the airfoil profile in the  $z$ -plane is mapped into a contour in the  $\zeta'$ -plane through the use of the Joukowski transformation

$$z = \zeta' + \frac{c^2}{\zeta'}$$

It is desirable that the contour in the  $\zeta'$ -plane be as close to a circle as possible; for this reason the axes in the  $z$ -plane should be chosen with a view toward producing that result. This means that the airfoil should be distributed as near like an ellipse as possible with respect to the axes in the  $z$ -plane.

The second stage consists of finding a mapping function which will transform the near-circle in the  $\zeta'$ -plane to an exact circle in the  $\zeta$ -plane. Theodorsen used the transform

$$\zeta' = \zeta \exp \left( \sum_{n=1}^{\infty} \frac{C_n}{\zeta^n} \right),$$

where the coefficients  $C_n$ , complex in general, have to be determined.

A point on the near or pseudo circle in the  $\zeta'$ -plane is given by

$$\zeta' = C e^{i\psi(\theta)} e^{i\theta}$$

The factor  $e^{i\psi(\theta)}$  determines how much the contour in the  $\zeta'$ -plane departs from that of a circle. The relationship between points on the airfoil and points

on the pseudo-circle is given by the equations

$$x = 2C \cosh \psi \cos \theta$$

$$y = 2C \sinh \psi \sin \theta .$$

These two equations can be put into the form

$$2 \sin^2 \theta = P + \left[ P^2 + \left( \frac{y}{C} \right)^2 \right]^{1/2}$$

$$2 \sin^2 \psi(\theta) = -P + \left[ P^2 + \left( \frac{y}{C} \right)^2 \right]^{1/2} ,$$

where

$$P = 1 - \left( \frac{x}{2C} \right)^2 - \left( \frac{y}{2C} \right)^2 ,$$

which establishes the function  $\psi(\theta)$ .

Theodorsen describes a point on the exact circle in the  $\zeta$ -plane by the equation

$$\zeta = C e^{\psi_0} e^{i\phi} = R e^{i\phi}$$

where  $\psi_0$  is a constant not yet determined.  $R$  is, of course, also a constant. The relationship between points on the pseudo-circle and those on the exact circle is given by

$$\frac{C e^{\psi(\theta)} e^{i\theta}}{C e^{\psi_0} e^{i\theta}} = \frac{\zeta'}{\zeta} = \exp \left( \sum_{n=1}^{\infty} \frac{C_n}{\zeta^n} \right) .$$

Setting

$$\frac{C_n}{\zeta^n} = \frac{A_n + iB_n}{\zeta^n} = \frac{A_n + iB_n}{R^n} e^{-in\phi}$$

and equating real and imaginary parts one obtains

$$\psi - \psi_0 = \sum_{n=1}^{\infty} \frac{1}{R^n} (A_n \cos n\phi + B_n \sin n\phi)$$

$$\theta - \phi = \sum_{n=1}^{\infty} \frac{1}{R^n} (B_n \cos n\phi - A_n \sin n\phi) .$$

From these it follows that

$$\psi_0 = \frac{1}{2\pi} \int_0^{2\pi} \psi(\phi) d\phi$$

$$\frac{A_n}{R^n} = \frac{1}{\pi} \int_0^{2\pi} \psi(\phi) \cos n\phi d\phi$$

$$\frac{B_n}{R^n} = \frac{1}{\pi} \int_0^{2\pi} \psi(\phi) \sin n\phi d\phi .$$

The foregoing equations define  $\psi_0$ ,  $A_n$ , and  $B_n$  in terms of  $\psi(\phi)$  or, equivalently,  $\theta(\phi)$ . Since  $\psi(\theta)$  is usually not easily extracted and when it has been it is not a simple form, the evaluation of the various coefficients is best handled numerically or by a combination of graphical constructions, approximations, and iterations. Theodorsen's original method followed the second course. The original paper may be consulted for details. To use the method today one would employ numerical techniques.

Once the process has been completed by whichever means are employed, one then has the pressures and velocities at each point on the airfoil surface in terms of those at the equivalent point on the exact circle.

Analyses of the lift characteristics of various Joukowski airfoils in the meantime revealed that the thickness contributed little to the lift. It therefore seemed to some that if airfoils for which one had difficulty finding appropriate conformal transforms could be characterized by their mean camber lines only, then perhaps one would have a relatively simple, yet direct method of evaluating the lift and pressure distribution of arbitrary airfoils. Such an approach is obviously most appropriate when the actual airfoils are thin. These ideas were developed in the early 1920's by Munk (Ref. 14), Birnbaum (Ref. 15), and Glauert (Ref. 16).

In Glauert's conception the airfoil is replaced by its mean camber line which he assumed, never lies very far from the chord line. For this reason he felt justified in making the approximation that the velocities over the airfoil could be represented by a continuous distribution of vortices (or a sheet of vorticity)\* lying along the chord line. The variation in vorticity with chord location is not known initially. The velocity induced at point  $x'$  on the chord of the airfoil due to the vortex sheet is given by

$$v(x') = \int_0^c \frac{\gamma dx}{2\pi(x - x')} ,$$

---

\* The reader unfamiliar with the theoretical basis of the concept is referred to the next section of the present work or to Reference 17 for complete mathematical details.

where  $\gamma$  is the vortex strength per unit length. This induced velocity is actually calculated for a point on the chord but, according to Glauert's approximation, may be taken to be the same as the induced velocity at the corresponding point of the airfoil itself.\* Since the resultant of the free stream velocity and the induced velocity adjacent to the airfoil must be parallel to the surface at each point of the airfoil and since the flow angularities are small, one may write this statement as

$$\alpha + \frac{v}{V} = \frac{dy}{dx} ,$$

where  $dy/dx$  is the slope of the mean camber line at  $x'$ . It will be seen that these two equations are sufficient to provide a complete solution of the problem in terms of the shape of the curved line which represents the airfoil. The solution is obtained as  $\gamma(x)$ . Then according to Joukowski's theorem

$$L = \int_0^c \rho V \gamma dx$$

$$M = \int_0^c \rho V \gamma x dx \quad .$$

The method Glauert employed to find  $\gamma(x)$  is instructive because most subsequent calculative procedures use refinements of the same idea. Glauert first changed the independent variable  $x$  to  $\theta$  according to the transformation

$$x = \frac{c}{2} (1 - \cos \theta) .$$

He assumed that he could represent  $\gamma$  by a sine series in  $\theta$ :

$$\gamma = 2V \{A_0 \cot \theta/2 + \sum_{n=1}^{\infty} A_n \sin n\theta\} .$$

Hence

$$\gamma dx = cV \{A_0(1 + \cos \theta) + \sum_{n=1}^{\infty} A_n \sin n\theta \sin \theta\} d\theta ,$$

then

$$v(x') = \frac{V}{\pi} \int_0^{\pi} \frac{A_0(1 + \cos \theta) + \frac{1}{2} \sum_{n=1}^{\infty} A_n \{\cos (n-1)\theta - \cos (n+1)\theta\}}{\cos \theta' - \cos \theta} d\theta$$

---

\* Karamcheti (Ref. 17) presents a very detailed discussion of the relation of this approximation to the exact formulation.

$$= V \left\{ -A_0 + \frac{1}{2} \sum_{n=1}^{\infty} A_n \frac{\sin(n+1)\theta' - \sin(n-1)\theta'}{\sin \theta'} \right\}$$

$$= V \left\{ -A_0 + \sum_{n=1}^{\infty} A_n \cos n\theta' \right\} .$$

Substituting of this result in the second of the two original equations gives

$$\frac{dy}{dx} = \alpha - A_0 + \sum_{n=1}^{\infty} A_n \cos n\theta' .$$

According to the theory of Fourier series the coefficients  $A_n$  are determined from the shape of the airfoil by evaluating the integrals

$$\alpha - A_0 = \frac{1}{\pi} \int_0^{\pi} \frac{dy}{dx} d\theta$$

$$A_n = \frac{2}{\pi} \int_0^{\pi} \frac{dy}{dx} \cos n\theta d\theta$$

where  $dy/dx$  now is the slope of the surface at any  $x$  between 0 and  $c$  as a function of  $\theta$ . The integral can, of course, be evaluated piecewise if the functional form changes as  $\theta$  goes from 0 to  $\pi$ .

Glauert showed that one need find only  $A_0$ ,  $A_1$ , and  $A_2$  in order to determine  $C_L$  and  $C_{M_0}$ . Note that

$$\frac{L}{\frac{1}{2}\rho V^2 c} = C_L = \frac{2}{\rho c V^2} \int_0^{\pi} \rho c V^2 \{A_0 (1 + \cos \theta) + \sum_{n=1}^{\infty} A_n \sin n\theta \sin \theta\} d\theta$$

$$= 2\pi (A_0 + \frac{1}{2}A_1)$$

and similarly that

$$C_{M_0} = \frac{\pi}{2} (A_0 + A_1 - \frac{1}{2}A_2) = \frac{\pi}{4} (A_2 - A_1) - \frac{1}{4}C_L .$$

He also showed that

$$A_0 + \frac{1}{2}A_1 - \alpha = -\frac{1}{\pi} \int_0^{\pi} \frac{dy}{dx} (1 - \cos \theta) d\theta = \frac{2}{\pi} \int_0^{\pi} \frac{y}{c} \frac{d\theta}{1 + \cos \theta} ,$$

thus

$$C_L = 2\pi \left( \alpha + \frac{2}{\pi} \int_0^{\pi} \frac{y}{c} \frac{d\theta}{1 + \cos \theta} \right) .$$

Since Glauert also showed that

$$\int_0^\pi \frac{y}{c} \cos \theta \, d\theta = \frac{\pi}{4} (\alpha - A_0 - \frac{1}{2}A_2) ,$$

$$C_{M_0} = 2 \left( \int_0^\pi \frac{y}{c} \cos \theta \, d\theta - \frac{1}{2} \int_0^\pi \frac{y}{c} \frac{d\theta}{1 + \cos \theta} \right) - \frac{1}{4}C_L .$$

Values of  $C_L$  and  $C_{M_0}$  computed by this method Glauert found to be "in close agreement with experimental determinations of these quantities." The method can be seen to be considerably simpler to use than the transform technique. During the 1930's when designers sought to reduce wing drag by eliminating external bracing, they were forced by structural considerations to abandon the very thin airfoils they had been using until that time. They found that in order to predict the lift and moment characteristics of the newer and thicker airfoil sections that were then becoming the vogue, more elaborate analytical methods or extensive wind tunnel testing were necessary. One of these analytical methods took the following tack. Since the sum of solutions to the Laplace equation (the equation describing inviscid, incompressible flow) is also a solution, one can describe a thick, cambered airfoil at angle of attack by superimposing solutions for a curved line (Glauert's method), a flat plate at angle of attack (also represented by a vortex sheet), and a thick symmetrical airfoil at  $\alpha = 0$  (using a distribution of sources along the chord line). An example of such a built-up solution is given by Karamcheti (Ref. 17). Reference 18 provides an exposition of both the thin airfoil and Theodorsen approaches and indicates how these techniques were used to guide the very significant series of experimental investigations carried out during the 1930's by the NACA.

These investigations sought to measure in considerable detail aerodynamic characteristics of several general families of airfoils. Since these data were obtained in well-calibrated wind tunnels at flight Reynolds numbers and presented valid drag data as well, designers came to regard NACA TR-824, "A Summary of Airfoil Data," (Ref. 19) and its forerunners as their primary data source. It has only been within the last 20 years or so that interest in improved analytical methods has been rekindled. This revival perhaps can be attributed to the simultaneous occurrence of

1. recent, sharp escalation in the cost of making models and conducting tests,
2. the desire to optimize certain aspects of airfoil behavior and to investigate the characteristics of unconventional airfoils,
3. the appearance of the large digital computer which made it possible to consider the use of what had previously been rather laborious methods on a routine basis.



One of the first and most widely used methods of the current revival is that described by J. Weber (Refs. 20, 21). In the earlier of the two papers she treated the case of a symmetrical two-dimensional airfoil at angle of attack. By transforming an airfoil into a slit, she was able to show that the source distribution which she used to represent the thickness at zero lift can be placed along the chord line rather than on the surface with little error, provided the airfoil is no thicker than about 10% of the chord. With that assumption and the superposition of a vortex distribution on a flat plate at angle of attack, Weber obtained the equation

$$V(x,z) = \frac{V_o}{\sqrt{1 + \left(\frac{dz}{dx}\right)^2}} \left\{ \cos \alpha \left[ 1 + \frac{1}{\pi} \int_0^1 \frac{dz}{dx} \frac{dx'}{x - x'} \right] \right. \\ \left. \pm \sin \alpha \sqrt{\frac{1-x}{x}} \left[ 1 + \frac{1}{\pi} \int_0^1 \left( \frac{dz}{dx} - \frac{2z(x')}{1 - (1 - 2x')^2} \right) \frac{dx'}{x - x'} \right] \right\} .$$

The positive sign holds for the upper surface, the negative sign for the lower surface.  $V(x,z)$  is the velocity along the airfoil surface. The pressure coefficients along the surface are given by

$$C_p = 1 - \left( \frac{V(x,z)}{V_o} \right)^2 .$$

The most attractive feature of the method is Weber's technique for finding a numerical value of  $V(x,z)$ . She begins by making the following definitions

$$S^{(1)}(x) = \frac{1}{\pi} \int_0^1 \frac{dz}{dx'} \frac{dx'}{x - x'}$$

$$S^{(2)}(x) = \frac{dz}{dx}$$

$$S^{(3)}(x) = \frac{1}{\pi} \int_0^1 \left[ \frac{dz}{dx} - \frac{2z(x')}{1 - (1 - 2x')^2} \right] \frac{dx'}{x - x'} .$$

She then evaluates these quantities at specific points,  $x_v$ , along the chord using the representation

$$S^{(1)}(x_v) = \sum_{\mu=1}^{N-1} S_{\mu v}^{(1)} z_{\mu}$$

$$S^{(2)}(x_v) = \sum_{\mu=1}^{N-1} S_{\mu v}^{(2)} z_{\mu}$$

$$S^{(3)}(x_v) = \sum_{\mu=1}^{N-1} S_{\mu v}^{(3)} z_{\mu} + S_{Nv}^{(3)} \sqrt{\frac{\rho}{2c}} .$$

The coefficients  $S_{\mu v}^{(1)}$ ,  $S_{\mu v}^{(2)}$ ,  $S_{\mu v}^{(3)}$  are independent of airfoil shape and Weber gives tables of their values.  $N$  is the number of points used to approximate the airfoil (she gives tables for 8, 16, and 32 points). Point #1 is always at the trailing edge.  $\rho$  is the leading edge radius and  $c$  is the chord length. Weber also gives a table for finding  $x_v$  corresponding to a given value of  $v$ . These are the chordwise stations at which the pressure is calculated.  $z_{\mu}$  is the airfoil ordinate corresponding to the chord location given by

$$x_{\mu} = \frac{1}{2} \left( 1 + \cos \frac{\mu\pi}{N} \right)$$

where  $1 < \mu < N-1$ . It will be seen that with the aid of the tables of universal coefficients  $S_{\mu v}^{(1)}$ ,  $S_{\mu v}^{(2)}$ ,  $S_{\mu v}^{(3)}$  the pressure computation is carried out very easily using a desk calculator.

A significant feature of Weber's method is her retention of the factor  $1/\sqrt{1 + (dz/dx)^2}$  which materially improves the accuracy of the pressure computation near the leading edge. (See Appendix F.)

Weber extended her approach to treat cambered airfoils in a second paper (Ref. 21). She showed that two additional terms are required in the expression for pressure to account for camber:

$$c_p = 1 - \frac{\{\cos \alpha [1 + S^{(1)}(x) \pm S^{(4)}(x)] \pm \sin \alpha \sqrt{(1-x)/x} [1 + S^{(3)}(x)]\}^2}{1 + [S^{(2)}(x) \pm S^{(5)}(x)]^2}$$

where

$$S^{(5)}(x) = \sum_{\mu=1}^{N-1} S_{\mu v}^{(5)} z_{c\mu} = \left( \frac{dz_c}{dx} \right) x_v$$

$$S^{(4)}(x) = \sum_{\mu=1}^{N-1} S_{\mu v}^{(4)} z_{c\mu} = \frac{\Gamma(x_v)}{2V_o} .$$

The subscript "c" refers to the camber line. Weber gives tables for  $S_{\mu v}^{(4)}$  and  $S_{\mu v}^{(5)}$  and also provides some second order corrections to aid in predicting the pressure in the nose regions more accurately.

Comparisons between Weber's results and exact theory for Joukowski airfoils indicate that her method predicts pressures which are low by about 1%. Maximum camber must be less than about 4% of chord and thickness less than 10% of chord to obtain results of this accuracy, however.

The success of Weber's approach and its obvious adaptability to computer solution (see for example Reference 22) seems to have served as a spur to the development of more exact airfoil representation schemes which are practical only if carried out by digital computer. The method of Hess and Smith (Ref. 23) is among the best known of these developments. In this method the non-lifting airfoil surface is replaced by a source sheet with strength  $\sigma(s)$  where  $s$  is the distance measured along the airfoil surface. The sum of the velocity induced by the source sheet and the free stream velocity is forced to satisfy the condition that its component normal to the airfoil surface at each value of  $s$  is zero. This statement is written mathematically as a Fredholm integral equation of the second kind:

$$2\pi \sigma(s) + \oint \sigma(s') \ln r(s,s') ds' = F(s)$$

where  $r(s,s')$  is the distance between the point of interest,  $s$ , and any other point on the surface,  $s'$ ;  $\sigma(s')$  represent the source strength at points other than  $s$ ;  $\sigma(s)$  is the source strength at  $s$ ; and  $F(s)$  represents the component of the free stream velocity normal to the surface at  $s$ . The left side of the equation then represents the component of the velocity induced by the source sheet which is normal to the surface. Note that for a given airfoil in a stream of known speed the unknown quantity is  $\sigma(s')$  which occurs under the integral sign.

To solve this equation Hess and Smith make several approximations:

1. the contour of the airfoil can be represented by  $N$  straight line segments,
2.  $\sigma(s')$  is constant over each segment,
3. the integral is evaluated at only one point—generally the mid-point—of each segment.

This leads to a system of  $N$  simultaneous linear equations which can be solved to find  $\sigma$  on each segment. For good accuracy,  $N$  must be large, particularly in regions of high curvature. Knowing  $\sigma$  one can then find the tangential component of velocity from which one can compute the surface pressure.

To treat the lifting airfoil, Hess and Smith in effect superpose a vortex sheet of suitable strength so that the total flow satisfies the local tangency condition as well as the Kutta condition at the trailing edge.

Martensen (Ref. 24) chose a different approach. He represented the airfoil by a vortex sheet on its surface. By requiring that the strength

of the vortex sheet be identical to the velocity distribution on the surface of the airfoil, Martensen was able to show that in the interior of a closed vortex sheet the velocity is everywhere zero. Thus on the inner side of the vortex sheet the net tangential velocity which is a sum of that due to free stream and that due to the vortex sheet is zero, or

$$\frac{\Gamma(s)}{2} - \frac{1}{2\pi} \frac{\partial}{\partial n} \oint \Gamma(s') \ln r(s,s') ds' = V_{\infty} \left( \frac{dx}{ds} \cos \alpha + \frac{dy}{ds} \sin \alpha \right).$$

This equation has almost exactly the same form as that formulated by Hess and Smith.

To solve the equation Martensen chose, as did Hess and Smith, to replace the integral by a summation. As a result he also ended up solving a system of simultaneous equations. An equation expressing the Kutta condition is required to complete the formulation. Martensen's method while giving the velocity distribution on the surface as the solution to the system of equations does not give good results for very thin airfoils. The reason is that when the upper and lower surface control points are very close together, the vortices located there induce strong tangential velocities on each other. While this induced velocity actually decays very rapidly for points in the neighborhood of the control point, the method of approximating the integral which Martensen used assumes it to be a constant. Jacob (Ref. 25) used a different limiting approximation which improves the results but at the cost of restricting one's freedom in distributing the control points on the airfoil surface.

If an inviscid fluid flow is everywhere parallel to the surface of a closed body then the surface of the body can be represented by a streamline on which the stream function,  $\psi$ , is constant. Oellers (Ref. 26) used this idea to write

$$\psi = V_{\infty} y(s) \cos \alpha - V_{\infty} x(s) \sin \alpha - \frac{1}{2\pi} \oint \Gamma(s') \ln r(s,s') ds'.$$

To solve this equation for  $\psi$  and  $\Gamma(s')$ , the integral is approximated by a summation of the type used by Hess and Smith.

Chen (Ref. 27) made a very detailed comparison of the three foregoing methods. He found that when applied to airfoils for which analytical expressions for the pressure distribution are known, the Hess-Smith method always gives the correct value of circulation generated by the airfoil. On the other hand the computed surface velocity was found to be very sensitive to the coordinates of the control points. A tiny error in the input coordinates can produce a wavy behavior of large amplitude in the computed surface velocity, more so than is reasonable physically. Chen also tried approximating Martensen's integral in the same way Hess and Smith approximated theirs. He found that the resulting circulation was smaller than that found by Hess and Smith because the integration is carried out along straight line segments rather than curves. This also leads to some difficulties in the numerical computation because the

matrix of coefficients is ill-conditioned. Even after curvature effects are taken into account, the circulation computed by the Martensen-Jacob method, although larger, is still slightly smaller than that obtained by the Hess-Smith method. On the other hand, because it is a vortex sheet and tangential velocities which are considered by Martensen and Jacob, the computed results are not very sensitive to inaccuracies in the values of the input coordinates.

Chen prefers Oellers' method, primarily because it leads to fewer computational difficulties. Since it is an integral representation, no surface slopes must be computed, a process which always causes some loss in accuracy. Secondly, because the kernel of the integral equation is simpler in this formulation, the computing time required is generally less.

Several improvements in the transform approach to predicting airfoil characteristics have also appeared in recent years. Lighthill (Ref. 28) chose to specify the desired velocity distribution about the airfoil in closed form. Sato (Ref. 29) extended this approach to permit a velocity distribution of any kind to be specified. As worked out by Sato, the velocity distribution is assumed in such a way that front and rear stagnation points can be treated separately. A well-behaved function  $g(\theta)$  takes up the velocity distribution everywhere with the exception of the stagnation points and three constants which are imbedded. The constants are determined by  $g(\theta)$ , the fact that the airfoil is a closed curve, and the fact that the flow field at infinity is uniform. A set of initial values must be given to the three constants in order to obtain  $g(\theta)$  from the specified velocity distribution. This  $g(\theta)$  is then used to obtain a new set of values for the constants which will give a closed curve as the airfoil geometry. The process is repeated iteratively until the before and after constant values match. In this way Sato's method always guarantees an airfoil geometry giving the desired velocity distribution. Because of the repetitive nature of many of its steps and the need for piecewise integration, it is best done on a digital computer.

#### THE AIRFOIL IN VISCOUS FLOW

It was of course recognized that all of these approaches would give somewhat optimistic predictions of airfoil lift and no prediction at all of airfoil drag. It was therefore just a matter of time until efforts would be made to attempt to account for the effects of viscosity at least so far as the lift produced by an airfoil is concerned. Powell (Ref. 30) was one of the first to attack the problem in a fairly rigorous fashion. He modified the airfoil geometry in two ways to account for the effects of boundary layer displacement of the inviscid flow. To the airfoil thickness distribution (symmetrical about the mean camber line) he added the total displacement thickness evenly distributed between upper and lower surfaces. He recognized, however, that the displacement thickness is not the same in the two surfaces, being thicker

on the upper surface. He chose to account for this fact by reflexing the trailing edge, adding  $\frac{1}{2}(\delta^*_{upper} - \delta^*_{lower})$  to the ordinates of the mean camber line. Because the airfoil did not then physically close at  $x = c$ , he chose to set the upper and lower pseudo-surface velocities equal at  $x = c$  as a replacement for the Kutta condition. He then employed Weber's method to predict the surface pressures. Powell assumed in his computation that  $\delta^*(x)$  was available a priori. He also discussed the problem of "closing" the pseudo-airfoil in the wake as a means of finding reasonable surface slopes at  $x = c$ .

Apparently Powell's paper served as a source of inspiration for the work reported in Reference 31. Although the sketchy nature of the discussion in the report makes it difficult to ascertain precisely the heritage of the approach used or even its particulars, detailed examination of the computer program indicates that the authors (of the Lockheed Georgia Company) actually employed a combination of methods (vortex distribution on surface of a cambered airfoil plus a vortex distribution on a symmetrical airfoil) along with the idea discussed by Powell of modifying camber and thickness separately to account for boundary layer thickness. This represents somewhat of a departure from an earlier version of the computer program (Ref. 32) which is said to be based on Van Dyke's inviscid method (Ref. 33) and earlier British work on viscous corrections which was also considered by Powell. Van Dyke offered a way of treating thicker airfoils by transferring the surface tangency condition to the chord line with a Taylor series expansion. In other respects his approach is equivalent to Weber's.

The significant feature of the Lockheed program is its provision for arriving at the pseudo-airfoil shape in an iterative fashion. The program uses the inviscid pressure distribution and a fairly crude boundary layer computation to obtain the initial estimate of the displacement thickness. The displacement thickness is then used to get a new inviscid pressure distribution. The process is continued for five iterations until the pressure distribution used to compute the displacement thickness is virtually the same as that which one gets after adding the displacement thickness to the airfoil geometry. Computations of skin friction, transition of the boundary layer from laminar to turbulent flow, and location of the separation point are made at the same time. Program output is therefore airfoil lift, drag, and pitching moment as a function of angle of attack. It can also account for variations in free stream Mach number.

The program, which forms the basis of the modified version given herewith, was found, when compared with experimental results, (see for example Reference 52) to:

1. over-estimate the lift curve slope by 5% to 8%,
2. give very accurate estimates for the surface pressures except in the neighborhood of large suction peaks or incipient separation,

3. give rather poor estimates of section drag, errors of 30% to 50% being common at low-to-moderate angles of attack; in particular the integration of the inviscid pressures in the drag direction is frequently not zero.

Despite these difficulties, the success of the program and its inherent rigor makes it apparent that with improvements in the boundary layer computation method and in the numerical procedures used an accurate and reliable means of estimating all the aerodynamics characteristics of airfoils at subsonic speeds is at hand. Reference 31 is the basis for the presentation in the next chapter of a theory for the prediction of lift, drag, and moment characteristics of two-dimensional airfoils.

### COMPRESSIBILITY

To complete the discussion of developments in theoretical means for predicting the inviscid characteristics of light plane airfoils it is necessary to mention the effect of changes in Mach number. Although non-jet powered aircraft are not likely to reach speeds such that a local sonic point will exist on the airfoil, many do experience sufficiently high speeds to distort the  $M = 0$  pressure distribution significantly. Thus it is desirable to chronicle the efforts which have been made in describing these effects.

Despite the folklore that the speed of sound presented an impregnable barrier to the velocity of flight vehicles, it was recognized quite early by many aeronautical scientists that artillery shells, for example, frequently exceed this speed. One should therefore be able to develop an expression for the pressure forces on a body for situations where the compressibility of the air is not negligible. Studies later showed that by allowing the density to vary in the equations describing the motion of an inviscid fluid but retaining the idea that the airfoil was thin and therefore did not disturb the flow greatly, it was possible to describe the flow over airfoils by the equation

$$\left(1 - M_{\infty}^2\right) \frac{\partial^2 \phi}{\partial x^2} + \frac{\partial^2 \phi}{\partial y^2} = 0$$

along with suitable boundary conditions. This equation, however, can be written as

$$\frac{\partial^2 (\beta \phi)}{\partial x^2} + \frac{\partial^2 (\beta \phi)}{\partial (\beta y)^2} = 0$$

where  $\beta^2 = 1 - M_{\infty}^2$ , a constant. The form then is that of the Laplace equation with which hydrodynamicists and early aerodynamicists were already familiar. Consistent with the small disturbance idea is the representation of the pressure coefficient at an arbitrary point on the airfoil surface by

$$\begin{aligned}
C_P &= \frac{P_L - P_\infty}{\frac{\rho_\infty}{2} U_\infty^2} = \frac{1}{\frac{\rho_\infty}{2} U_\infty^2} \left[ P_{\text{STAG}} - \frac{\rho_\infty}{2} (U_\infty + u')^2 - P_{\text{STAG}} + \frac{\rho_\infty}{2} U_\infty^2 \right] \\
&= \frac{2}{\rho_\infty U_\infty^2} \left[ -\frac{\rho_\infty}{2} (U_\infty^2 + 2u'U_\infty + u'^2) + \frac{\rho_\infty}{2} U_\infty^2 \right] \\
&= \frac{2}{\rho_\infty U_\infty^2} \left[ -\rho_\infty U_\infty u' - \frac{\rho_\infty}{2} u'^2 \right] \\
&\approx -\frac{2u'}{U_\infty} .
\end{aligned}$$

But  $u' = \beta \frac{\partial \phi}{\partial x}$  and thus

$$C_P = -\frac{2\beta}{U_\infty} \frac{\partial \phi}{\partial x} .$$

For the case where  $\beta = 1$  (incompressible flow),

$$C_P = -\frac{2}{U_\infty} \frac{\partial \phi}{\partial x} .$$

Thus,

$$(C_P)_{\text{COMPRESSIBLE}} = \frac{C_{P \text{ INCOMP}}}{\sqrt{1 - M_\infty^2}} .$$

This simple relation was advanced about 1928 by Glauert and by Prandtl independently. It provides a good prediction of experimental results for local Mach numbers over the airfoil less than critical. It fails at higher Mach numbers because for rigor, the equation describing the flow must then contain an additional, non-linear term. This also makes it impossible to compare exactly the same airfoil at two different Mach numbers. Nevertheless, the fact that the Prandtl-Glauert formula permits one to find the pressure distribution over airfoils with reasonable accuracy for all Mach numbers less than that where the flow first becomes sonic merely by knowing the  $M = 0$  distribution led to a very serious search for parameters which can be used to determine when the flow over an airfoil at one Mach number is similar to that over a second airfoil at another Mach number and hence will have the same pressure distribution.

One of the most successful efforts in this direction was the formula

$$C_P = \frac{C_{P \text{ INC}}}{\sqrt{1 - M_\infty^2} + \frac{M_\infty^2}{\sqrt{1 - M_\infty^2} + 1} \left( \frac{C_{P \text{ INC}}}{2} \right)}$$



proposed by Kármán and Tsien in 1939. (Quoted in Reference 56.) Although not strictly applicable to the flow over the same airfoil at different Mach numbers, it has been used in this way with good results. A good discussion of the theoretical basis for comparing flows over bodies at one Mach number with flows over the same or related bodies at different Mach numbers is given in Chapter 10 of the text by Liepmann and Roshko (Ref. 57).

### EXTENSION TO THREE DIMENSIONS

The conceptual basis for expanding an airfoil section laterally into a finite wing can be traced to an 1894 paper by F. W. Lancaster. He elaborated these views in a book (Ref. 34) published in 1907. The mathematical expression of these ideas in a convenient form, however, seems to have originated with Prandtl (Ref. 35). He took a very simplified view of the wing, arguing that because the lift curve slope of all airfoils is nearly the same and because one cannot in any event determine viscous effects from an inviscid theory why not, then, for purposes of determining the effect of planform geometry or twist, represent the wing by just a line located at about the airfoil aerodynamic center. By placing a circulation about this line whose strength varies with the angle of attack of the wing, one can obtain a linear lift curve ( $C_L$  versus  $\alpha$ ) of the correct magnitude. Since such a vortex must either close or extend to infinity, Prandtl assumed that the vortex leaves each wing tip and extends, parallel to the fuselage, to some point very far downstream at which it closes; this can be considered to be at infinity for all practical purposes. Such a flow pattern is then consistent with the vortices observed leaving the tips of lifting wings. By superposing a series of vortices of different strengths and spans but assuming that they all "roll up" into one on leaving the tips, one can represent a rather arbitrary spanwise lift distribution.

Glauert (Ref. 16b) points out that the flow induced by this vortex system is normal to the span and to the direction of the aircraft's motion and is directed downwards in general. This downward flow velocity,  $w$ , is small compared with the flight velocity,  $U$ , but has the effect of reducing the angle with which the wing meets the oncoming flow,  $\alpha$ . The reduction in angle of attack is given by  $w/U$ . Since  $w$  varies over the span, the induced angle of attack also varies over the span. Further, since the lift is defined as the force normal to the flow direction, the presence of an induced flow angle  $w/U$  causes the lift force to tilt backwards, giving a component in the direction of the drag force. This induced drag,

$$D_i = \frac{w}{U} L$$

is an inviscid effect resulting from the finite extent of the wing span. It may be noted that the work done on the fluid by the induced drag appears as the kinetic energy of the trailing vortices.

In the lifting line theory, the characteristics of a monoplane airfoil are determined by first finding  $w$  and hence the effective angle of attack at each point along the span, then finding the corresponding two-dimensional lift and drag, and finally, integrating across the span. The first step in this process is determining  $w$  in terms of the strength of the trailing vortices. Between the points  $y$  and  $y + dy$  on the span, the circulation  $\Gamma$  can be assumed to fall by an amount  $-(d\Gamma/dy)dy$  and hence a trailing vortex of this strength springs from the element of span  $dy$ . There is therefore a sheet of trailing vortices extending across the span and the normal induced velocity,  $w$ , at any point  $y_1$  on the span contains contributions from all the trailing vortices in this sheet. At  $y_1$ , therefore,

$$w(y_1) = \int_{-b/2}^{b/2} \frac{-\frac{d\Gamma}{dy} dy}{4\pi(y - y_1)} .$$

It can also be shown that the circulation around a section of any wing (airfoil) is

$$\Gamma = \frac{1}{2} C_L c U = \frac{1}{2} C_{L\alpha} (\alpha - w/U) U .$$

Although  $C_{L\alpha}$  actually varies slightly with airfoil geometry it is usually taken to be a constant. This equation, in conjunction with the preceding one, makes it possible to determine the circulation and  $w$  for any wing in terms of the local values of  $c$  and  $\alpha$ . Note, however, that the first of these two equations is an integral equation because one of the unknowns,  $\Gamma$ , appears under the integral sign. This fact is responsible for much of the difficulty incurred in solving the wing lift problem because, in contrast to differential equations, few techniques exist for solving integral equations.

The technique which Glauert (Ref. 16b) suggested for solving the two equations proceeds as follows:

Call 
$$y = -\frac{b}{2} \cos \theta$$

and 
$$\Gamma = 2bU \sum_{n=1}^{\infty} A_n \sin n\theta .$$

Then 
$$w(\theta_1) = \frac{U}{\pi} \int_0^\pi \frac{\sum n A_n \cos n\theta}{\cos \theta - \cos \theta_1} d\theta = U \sum n A_n \frac{\sin n\theta_1}{\sin \theta_1}$$

from which it may be seen that at any point along the span

$$w \sin \theta = U \sum n A_n \sin n\theta .$$

The second equation connecting  $\Gamma$  and  $w$  becomes in this notation

$$2bU \sum A_n \sin n\theta = \frac{1}{2} C_{L\alpha} cU \left\{ \alpha - \frac{\sum n A_n \sin n\theta}{\sin \theta} \right\} .$$

Letting  $\mu = (C_{L\alpha} c)/(4b)$  one can write this as

$$\begin{aligned} \sum A_n \sin n\theta \sin \theta &= \mu \alpha \sin \theta - \mu \sum n A_n \sin n\theta \\ \text{or} \quad \sum A_n \sin n\theta (\mu n + \sin \theta) &= \mu \alpha \sin \theta . \end{aligned}$$

In general it is to be expected that  $\mu$  and  $\alpha$  are functions of  $\theta$ . The problem now is determining the values of the coefficients  $A_n$  which will satisfy the foregoing equation at every value of  $\theta$  along the span of the particular wing in question.

In passing one may note that since

$$\begin{aligned} L &= C_L \frac{\rho}{2} S U^2 = \int_{-b/2}^{b/2} b^2 \rho U^2 (\sum A_n \sin n\theta) \sin \theta d\theta \\ &= \pi b^2 \frac{\rho}{2} U^2 A_1 , \end{aligned}$$

then

$$A_1 = \frac{C_L S}{\pi b^2} = \frac{C_L}{\pi AR} .$$

From this result it appears that the wing lift is determined by the value of  $A_1$  and that the other coefficients in the series for the circulation,  $\Gamma$ , modify the shape of the spanwise lift distribution without altering the total lift.

The general procedure for obtaining the coefficients is to write as many equations as coefficients one desires to evaluate, each equation for a different value of  $\theta$ , and solve the resulting system for the coefficient values. For example, the system

$$\begin{aligned} A_1 \sin \theta_1 (\mu_1 + \sin \theta_1) + A_3 \sin 3\theta_1 (3\mu_1 + \sin \theta_1) + A_5 \sin 5\theta_1 (5\mu_1 + \sin \theta_1) \\ + A_7 \sin 7\theta_1 (7\mu_1 + \sin \theta_1) = \mu_1 \alpha_1 \sin \theta_1 \end{aligned}$$

$$\begin{aligned} A_1 \sin \theta_2 (\mu_2 + \sin \theta_2) + A_3 \sin 3\theta_2 (3\mu_2 + \sin \theta_2) + A_5 \sin 5\theta_2 (5\mu_2 + \sin \theta_2) \\ + A_7 \sin 7\theta_2 (7\mu_2 + \sin \theta_2) = \mu_2 \alpha_2 \sin \theta_2 \end{aligned}$$

$$A_1 \sin \theta_3 (\mu_3 + \sin \theta_3) + A_3 \sin 3\theta_3 (3\mu_3 + \sin \theta_3) + A_5 \sin 5\theta_3 (5\mu_3 + \sin \theta_3) \\ + A_7 \sin 7\theta_3 (7\mu_3 + \sin \theta_3) = \mu_3 \alpha_3 \sin \theta_3$$

$$A_1 \sin \theta_4 (\mu_4 + \sin \theta_4) + A_3 \sin 3\theta_4 (3\mu_4 + \sin \theta_4) + A_5 \sin 5\theta_4 (5\mu_4 + \sin \theta_4) \\ + A_7 \sin 7\theta_4 (7\mu_4 + \sin \theta_4) = \mu_4 \alpha_4 \sin \theta_4$$

can easily be solved for  $A_1, A_3, A_5,$  and  $A_7$  by algebraic techniques since the values of  $\theta_1, \theta_2, \theta_3, \theta_4, \mu_1, \mu_2, \mu_3, \mu_4,$  etc. are known from the wing geometry. The value of  $A_1$  becomes independent of  $n$  only when  $n$  is large.

Only odd coefficients occur in the series because the wing is assumed to be symmetric about its mid-span point.

The induced drag is found easily once the  $A_n$ 's are known. Since

$$D_i = \int_{-b/2}^{b/2} \frac{w}{U} L dy = \int_{-b/2}^{b/2} \rho w \Gamma dy = \int_{-b/2}^{b/2} \rho U^2 b^2 (\sum_n A_n \sin n\theta) (\sum_n A_n \sin n\theta) d\theta,$$

$$D_i = \pi b^2 \frac{\rho}{2} U^2 \sum_n A_n^2 .$$

Since  $A_1$  is independent of the planform shape, it follows that the induced drag will be a minimum when the other coefficients in the series are zero. The circulation for such a condition is then represented by

$$\Gamma = 2bU \frac{C_L}{\pi AR} \sin \theta = 2bU \frac{C_L}{\pi AR} \sqrt{1 - \cos^2 \theta} = 2bU \frac{C_L}{\pi AR} \sqrt{1 - 4y^2/b^2}$$

or the equation of an ellipse. An elliptical span-wise distribution of circulation (lift) can be obtained in practice by an elliptical variation of chord in the spanwise direction or by combinations of taper and twist.

During preliminary design one of the things one seeks to establish, at least approximately, is the relationship between aircraft attitude and lift developed. This entails finding the effect of the finite wing span on the slope of the lift curve. For infinite aspect ratio of course it is about  $2\pi$  per radian for all airfoils. The lifting-line theory, however, indicates that for an elliptical lift distribution—the most efficient type—there is a reduction in the effective angle of attack of  $C_L/\pi AR$ . To develop the same lift, the geometric angle of attack must then be  $\alpha_{2D} + C_L/\pi AR$ . The geometric angle of attack for finite-span wings can also be written

$$\alpha_{2D} \left( 1 + \frac{C_L \alpha_{2D}}{\pi AR} \right) = \alpha_{2D} \left( 1 + \frac{2}{AR} \right) = \alpha_{3D} .$$

Since  $C_{L\alpha_{2D}} \alpha_{2D} = C_{L\alpha_{3D}} \alpha_{3D}$  when the finite span wing develops the same lift as the infinite span wing, the three-dimensional lift-curve slope is

$$C_{L\alpha_{3D}} = \frac{2\pi}{1 + \frac{2}{AR}} \text{ per radian.}$$

The conclusion drawn from lifting line theory that an elliptical spanwise aerodynamic loading leads to minimum induced drag has been of particular interest to the designers of large aircraft. Since the performance gains resulting from minimum induced drag can be significant for such aircraft, designers have sought to devise methods capable of treating complex planforms more accurately and accounting for inviscid, non-planar effects (wing fences, end plates, engine pylons, etc.) in determining the lift distribution. The latter area has been of more than academic interest since the appearance of jet transports with pylon-mounted engines and boundary layer control fences. The computer program described by Lundry (Ref. 55) uses a transform technique to map the non-planar configuration into a type of lifting line and then computes the distribution of twist and camber necessary to minimize the induced drag.

Many other significant features of the aerodynamic characteristics of wings have been deduced using the lifting-line approach. This theory has its limits, however. Obviously it does not treat well the case where, because of sweep, there is a substantial spanwise flow component, nor is a single lifting line an adequate representation of a wing when the ratio of span to chord is not large. These deficiencies were recognized quite early, but because of the complexity of the generalization from lifting line to lifting surface and the use of high aspect ratio unswept wings until after World War II, solution techniques were long in developing. In 1950 Multhopp (Ref. 60) employed a generalization of the scheme above to make one of the first successful attacks on the problem.

The complexity one must contend with is easily seen in the expression for the local angle of attack (Ref. 43) at a point on the wing

$$\alpha(x_1, y_1) = -\frac{1}{8\pi} \int_{-b/2}^{b/2} \frac{dy}{(y_1 - y)^2} \int_{x=x_{l.e.}}^{x=x_{t.e.}} \Delta C_p(x, y) \left[ 1 + \frac{x_1 - x}{\sqrt{(x_1 - x)^2 + (y_1 - y)^2}} \right] dx$$

where  $\Delta C_p$  is the unknown load distribution and the bar through the integral sign denotes the principal value.

As in the lifting line theory, the unknown loading function is usually approximated by a series:

$$C_p(\xi, \eta) = \frac{2b}{c(\eta)} \sum_{r=0}^{N-1} a_r(\eta) h_r(X)$$

$$\text{with } h_r(X) = \frac{2}{\pi} \frac{\cos[\frac{\psi}{2} (2r + 1)]}{\sin(\psi/2)} ; \quad \xi = \frac{2x}{b} ; \quad \eta = \frac{2y}{b} ; \quad X = \frac{x - x_{l.e.}}{c} = \frac{1}{2}(1 - \cos \psi) ;$$

$$\psi = \cos^{-1} (1 - 2X) \quad \theta = \cos^{-1}(\eta)$$

$$a_r(\eta) = \frac{2}{m+1} \sum_{n=1}^m a_{rn} \sum_{\mu=1}^m \sin \mu\theta \sin \frac{\mu n \pi}{m+1}$$

This approach in effect replaces the unknown  $\Delta C_p(x, y)$  by  $mN$  unknown coefficients  $A_{rn}$ . The problem is then to calculate  $A_{rn}$  by satisfying the boundary condition  $\alpha(x_1, y_1)$  at suitable points distributed over the planform. The main numerical difficulty lies in determining the double integral due to each term in the respective loading.

Reference 43 discusses three methods of carrying out the integration which are of comparable accuracy and difficulty. The details of one of these, including the computer program (in Algol 60), is given in Reference 61. In the later work, the theory has been extended to treat slowly oscillating wings. Reference 41 makes some detailed appraisals of the accuracy of this and other methods developed in Europe. A similar approach for the non-oscillating case with the computer program given in FORTRAN is presented in Reference 39. Further details are discussed in Reference 44. A FORTRAN program of slightly different approach is given by Lamar in Reference 59. The effects on accuracy of certain assumptions for the form of the pressure distribution, the number of points at which the boundary conditions are satisfied, and the location of these points is discussed in Reference 38. Wagner, in Reference 47, gives a good summary of the present state of development of true lifting surface theory. He is particularly careful to distinguish this approach from the vortex lattice or other "finite element" approaches.

Because one seems compelled to employ a large system of simultaneous equations to approximate the lifting surface integral equation satisfactorily and because the choice of points at which the boundary condition is satisfied, the method of integration, and the complexity of the planform all effect to the accuracy of the results, investigators quickly began to search for alternate lifting surface methods. Although called by a variety of names, the most popular alternate is an extension of the idealized single horseshoe vortex representation of a wing given by Glauert (Ref. 16b). By dividing the wing surface into a finite number of flat rectangular panels, placing such a horseshoe vortex on each, and summing the contribution of all the vortices to the flow over a control point in each panel, one obtains a system of relatively simple equations which, when solved for the individual

vortex strengths, has been found to give remarkably good estimates of the pressure distribution over the wing. Reference 37 describes such an approach—called here a vortex lattice—and supplies a FORTRAN program for computing the lift and moment distribution and overall lift and moment characteristics of rather complex wings. This particular program can accept a maximum number of horseshoe vortices on the left side of the plane of symmetry of 120. Within this limit, the number of horseshoe vortices in any chordwise row may vary from 1 to 20 and the number of chordwise rows may vary from 1 to 50. It can treat wings with dihedral and/or sweep.

Reference 40 describes another perhaps more restricted computer-based approach while Reference 42 is a systematic mathematical study of the characteristics of the method and various solution techniques. Current work at the Boeing Company (Ref. 58) seems intended to reduce computation time and increase accuracy by using overlapping (both spanwise and chordwise) continuous distributions of vorticity over a set of panels on a paneled wing. The basic distributions are independent and each satisfies all the boundary conditions required of the final solution. Boundary conditions are satisfied in a least square error sense. Excellent results have been obtained thus far and consideration is now being given to including an automatic paneling routine in the program so that the user need only specify the wing geometry and the accuracy with which he wishes to calculate the downwash in order for the program to select, on an iterative basis, sufficient panels to satisfy this requirement.

All of these lifting surface and vortex-lattice theories suffer from twin faults: they are applicable only to planar wings, wings without thickness which lie entirely in the x-y plane, and they do not include the effects of viscosity. One interesting way of circumventing these problems for unswept, moderate-to-high aspect ratio wings is given in Reference 36. There, two dimensional data—obtained either from wind tunnel test or theoretical calculations which include the effects of thickness and viscosity—are extended to three-dimensions by using lifting-line theory to determine the effective local angle of attack at each point along the span, looking up the two-dimensional characteristics corresponding to that local angle of attack, and integrating the results in the spanwise direction. This method forms the basis of the discussion in the next chapter on extending the theory for predicting two-dimensional aerodynamic characteristics to treat complete wings.

#### TREATMENT OF VISCOUS EFFECTS: DRAG

Despite the fact that much of the aerodynamic behavior of an airplane can be deduced by considering air to be an inviscid fluid, one very important characteristic, its resistance to continued motion, arises directly from the viscosity of the air and necessitates the installation of a power plant and a store of fuel to operate that power plant. Unfortunately, adequate theoretical descriptions of this characteristic are very much more difficult to provide than are descriptions of the aircraft's lifting behavior. For this reason early designers relied almost exclusively on correlations of experimentally-determined drag with body shape and surface condition during the

preliminary design phase and on wind tunnel and flight tests of the actual configuration during the final stages of development. This procedure is still widely used. Reference 53 is an up-to-date compilation of the most widely accepted correlations along with procedures for using them to estimate the drag of complete subsonic aircraft. A similar approach is employed in Reference 62.

Analytical determination of the drag of bodies evolved from the work of Prandtl, who in 1904 proposed that the effects of viscosity could be considered to be confined to a thin layer of fluid immediately adjacent to the body surface (*i.e.*, a boundary layer). Such an assumption permits a considerable simplification to be made in the equations describing fluid motion in this region. Outside this region one can use the classical inviscid analysis. Other investigators then began to develop methods for solving the boundary layer equations, first for simple configurations such as flat plates and later for curved two-dimensional bodies. One of the more versatile techniques has been programmed for computer solution (Ref. 63). Although the technique treats compressible flows with heat transfer, the flow will be taken here to be incompressible and non-heat-conducting in order to describe the approach as simply as possible.

If one begins with the conventional momentum integral equation (equation 44 in the next chapter),

$$\frac{d\theta}{dx} + \frac{du_e}{dx} \left( \frac{2\theta + \delta^*}{u_e} \right) = \frac{v}{u_e^2} \left( \frac{\partial u}{\partial y} \right)_{\text{wall}} ,$$

and makes the following definitions

$$\ell \equiv \frac{\theta}{u_e} \left( \frac{\partial u}{\partial y} \right)_w ,$$

$$-n \equiv \frac{\theta^2}{v} \frac{du_e}{dx} ,$$

$$H \equiv \frac{\delta^*}{\theta} ,$$

then this equation can be written

$$-u_e \frac{d}{dx} \left( \frac{n}{\frac{du_e}{dx}} \right) = 2[n(H + 2) + \ell] = N$$

Correlation of N against n for a number of exact theoretical solutions of the boundary layer equations indicated to Cohen and Reshotko (Ref. 64) that one could take



$$N = A + Bn$$

where A and B are constants for flows with zero or favorable pressure gradients. Under these circumstances the equation can be integrated to yield

$$n = -Au_e^{-B} \frac{du_e}{dx} \int_0^x u_e^{B-1} dx$$

A = 0.44 and B = 5.5. Then,

$$\theta = \left( \frac{-nv}{\frac{du_e}{dx}} \right)^{1/2} .$$

Since exact theoretical solutions of the boundary layer equations give a unique correlation between n and  $\ell$ , this can be used to find  $(\partial u / \partial y)_w$ . Then one may use

$$A + Bn = 2 \left[ n \left( \frac{\delta^*}{\theta} + 2 \right) + \ell \right]$$

to find  $\delta^*$ .

The solution for the turbulent boundary layer case is obtained from a variant of the momentum integral analysis with experimental skin friction correlations. Transition is determined from a variant of the Schlichting Ulrich (sixth order polynomial representation of the velocity distribution) laminar boundary layer stability analysis.

Comparisons between predicted and measured values of  $\delta^*$  and  $\theta$  on an NACA 0012 airfoil were quite good, except in the immediate neighborhood of the transition point. It is to be expected, therefore, that predicted values of skin friction drag would also be quite good. To find the total drag on the airfoil, however, it would be necessary to find the change in the pressure distribution over the airfoil resulting from the presence of the boundary layer displacement thickness and add this to the skin friction drag or integrate completely across the wake to find the overall change in the momentum of the flow caused by the passage of the airfoil. Schlichting (Ref. 65) describes a method, based on the latter idea, which was developed by Squire and Young in 1938. The drag force per unit length of span represented by the momentum defect in the wake far downstream of the airfoil is

$$\frac{D}{b} = \int_{y=-\infty}^{y=+\infty} \rho u (u_\infty - u) dy$$

from which

$$C_D = \frac{D}{b} \frac{1}{\frac{\rho}{2} cu_\infty^2} = \frac{2}{c} \int_{y=-\infty}^{y=+\infty} \frac{u}{u_\infty} \left( 1 - \frac{u}{u_\infty} \right) dy = \frac{2\theta_\infty}{c} .$$

The problem, then, is to evaluate  $\theta_\infty$  in terms of the boundary layer characteristics over the airfoil.

The momentum integral equation of boundary layer theory is of course also valid in the wake behind a body. In the wake, however, the shearing stress at the wall is zero so that the equation for this circumstance becomes

$$\frac{d\theta}{dx} + \frac{du_e}{dx} \left( \frac{2\theta + \delta^*}{u_e} \right) = 0 .$$

$x$  now denotes the distance from the trailing edge of the body measured along the wake centerline. The foregoing equation can also be written as

$$\begin{aligned} \frac{1}{\theta} \frac{d\theta}{dx} &= - \left( \frac{2 + H}{u_e} \right) \frac{du_e}{dx} = - \left( 2 + H \right) \frac{u_\infty}{u_e} \frac{d(u_e/u_\infty)}{dx} \\ &= - \left( 2 + H \right) \frac{d}{dx} \left( \ln \frac{u_e}{u_\infty} \right) . \end{aligned}$$

Integration by parts of this equation along  $x$  from the trailing edge of the body (station 1) to a station very far downstream in the wake results in

$$\ln \theta \Big|_\infty^1 = - (H + 2) \ln \frac{u_e}{u_\infty} \Big|_\infty^1 + \int_\infty^1 \ln \frac{u_e}{u_\infty} \frac{dH}{dx} dx .$$

At the downstream station  $u_e = u_\infty$  and

$$\frac{\delta^*}{\theta} = \frac{\int \left( 1 - \frac{u_e}{u_\infty} \right) dy}{\int \frac{u_e}{u_\infty} \left( 1 - \frac{u_e}{u_\infty} \right) dy} = 1$$

thus,

$$\ln (\theta_1/\theta_\infty) + (H_1 + 2) \ln (u_{e1}/u_\infty) = \int_{H=1}^{H=H_1} \ln \frac{u_e}{u_\infty} dH$$

or

$$\theta_\infty = \theta_1 \ln \left( \frac{u_{e1}}{u_\infty} \right)^{H_1+2} \exp \left( \int_1^{H_1} \ln \frac{u_\infty}{u_e} dH \right) .$$

Now, if the integral on the right hand side and  $u_{e1}/u_\infty$  can be evaluated, one has the required explicit relationship between  $\theta_\infty$  and  $\theta_1$ . From an analysis of experimental data H. B. Squire proposed that one could assume

$$\frac{\ln (u_\infty/u_e)}{H - 1} = \frac{\ln (u_\infty/u_{e1})}{H_1 - 1} = \text{constant} .$$

Hence,

$$\ln (u_{\infty}/u_e) = \text{constant} (H - 1)$$

$$\int_1^{H_1} \ln \frac{u_{\infty}}{u_e} dH = \int_1^{H_1} (H - 1) \left[ \frac{\ln (u_{\infty}/u_e)}{H_1 - 1} \right] dH = \frac{\ln (u_{\infty}/u_{e1})}{H_1 - 1} \left( \frac{H^2}{2} - H \right) \Big|_1^{H_1}$$

$$= \left( \ln \frac{u_{\infty}}{u_{e1}} \right) \left( \frac{H_1 - 1}{2} \right) ;$$

with this result

$$\theta_{\infty} = \theta_1 \left( \frac{u_{e1}}{u_{\infty}} \right)^{H_1+2} \left( \frac{u_{\infty}}{u_{e1}} \right)^{\frac{H_1-1}{2}} = \theta_1 \left( \frac{u_{e1}}{u_{\infty}} \right)^{\frac{H_1+5}{2}} .$$

A typical value of  $H_1$  is 1.4. For this value

$$\theta_{\infty} = \theta_1 \left( \frac{u_{e1}}{u_{\infty}} \right)^{3.2}$$

and thus

$$C_D = \frac{2\theta_1}{c} \left( \frac{u_{e1}}{u_{\infty}} \right)^{3.2} .$$

To find  $C_D$ , then, one must know the value of the potential velocity (velocity outside the boundary layer) at the trailing edge and the value of the momentum thickness at the same place. One attempt to be more explicit is reported by Schlichting. Using relations for a flat plate H. B. Helmbold obtained

$$C_D = \frac{0.074}{R_e^{\frac{1}{2}}} \left\{ \int_{x_u/c}^1 \left( \frac{u_e}{u_{\infty}} \right)^{3.5} d\left(\frac{x}{c}\right) + 62.5 R_e^{\frac{1}{4}} \left( \frac{\theta_{\dagger}}{c} \right)^{5/4} \left( \frac{u_{e\dagger}}{u_{\infty}} \right)^{3.75} \right\}^{0.8}$$

for the drag due to the one surface of a wing. The subscript "+" refers to the point of transition from laminar to turbulent flow.

The method of Squire and Young can be extended fairly simply to axisymmetric bodies and was so done by Young in 1939. (ARC R&M 1947)

Cebeci, Mosinskis, and Smith (Ref. 54) studied the possibility of improving the estimation of the drag of two-dimensional and axisymmetric bodies by improving the laminar and turbulent boundary layer methods used as inputs to the Squire and Young method. They also sought the effect of better identification of the location of the transition region. They concluded that the total drag coefficients of two-dimensional bodies such as airfoils can with such improved techniques be calculated very accurately for  $\alpha \leq 6^\circ$ . For higher angles of attack "use of the Squire-Young formula introduces an error into the drag calculations. . .since the Squire-Young formula is applicable only to a symmetrical wake." It would seem, however, that this

restriction could be removed without excessive difficulty. They also found that by improving the theoretical turbulent boundary layer methods they could match 57 experimental values with an rms error of 2.9%

The total-drag coefficient of axisymmetric bodies, they found, can be calculated less accurately than the total drag coefficient of two-dimensional bodies. "The calculations show a great sensitivity to the choice of tail end location on the body and to the use of inviscid pressure distributions in the drag calculations." For more general three-dimensional bodies such as aircraft fuselages there are unfortunately no quasi-rigorous analytical methods now available and one must resort to techniques based on rather gross approximations or to correlations of experimental results.

The reader has no doubt observed by this time that a detailed discussion of ways to calculate the drag of bodies ultimately comes to a consideration of methods for solving the boundary layer equations. Even the simplest case of steady, two-dimensional, incompressible, laminar flow involves a non-linear partial differential equation for which a general closed-form solution is impossible. This is the reason for the proliferation of solution techniques one sees in the literature. Some of these involve a great deal of insight into the problem and others employ rather sophisticated mathematical techniques. For these reasons it seems appropriate not to discuss the various methods in detail here but rather to direct the reader to Reference 65 which is probably the best single source of information on the rationale behind the various solution techniques.

#### FUSELAGE CONTRIBUTIONS TO LIFT, DRAG, AND MOMENT

The isolated fuselage is generally a body with a plane of symmetry rather than an axis of symmetry. This situation effectively precludes accurate calculations of its lift and drag by relatively simple, closed-form methods. Thus, until recently, it was the practice to rely on the guidance provided by a few classical approximate theoretical treatments and determine the detailed lift and drag characteristics experimentally.

Sir Horace Lamb (Ref. 6) for example was able to find an exact expression for the potential about an ellipsoid with three unequal axes. The problem was treated somewhat more completely by Munk (Ref. 66) who was interested in its application to determining the aerodynamic characteristics of airship hulls. Timman (Ref. 49) extended the analysis to include flows with velocity components along two axes simultaneously. He then calculated the streamline patterns for such a case. From these one can get the inviscid pressure distribution over the surface. This could then serve as the basis of a boundary layer calculation. Timman in fact had previously developed a boundary layer computation method for such a body and Reference 49 was intended to supply the potential field needed to begin the calculation.

A 1941 paper by Hans Multhopp (Ref. 51) provided a quantum jump in theoretical understanding of the fuselage contribution to airframe lift and moment. The essence of his arguments are contained in the following excerpts taken from a translation of that paper.

*One notoriously neglected phase in the aerodynamics of aircraft is that of the fuselage. This is due, in the first instance, to the fact that the fuselage considered by itself is a comparatively simple structure the effects of which are apparently readily perceived. But its real effects come into evidence only in combination with other parts of the aircraft, especially with the wing; hence it becomes necessary to evolve a fuselage theory which includes this mutual interference.*

*The search for mathematically exact solutions for such interference problems is exceedingly bothersome throughout, as it would entail the development of a three-dimensional potential theory with very arbitrary boundary conditions; a problem to which hardly more than a few proofs of existence could be adduced.*

\*\*\*\*\*

*For the present task the performance mechanics are, in general, excluded, since drag problems usually must be left to experimental research.*

\*\*\*\*\*

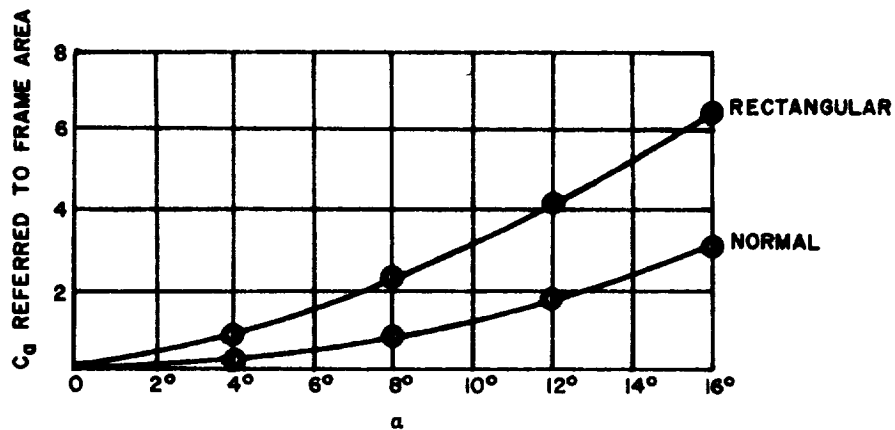
*Before proceeding to the analysis of the interference of the fuselage with the other parts of the airplane, a brief discussion of the phenomena observed on the fuselage, in the absence of all other airplane parts, is necessary.*

*On analyzing the conditions in frictionless parallel flow the first result is the total absence of resultant forces on the fuselage; the pressure distribution over the body merely affords free moments. These free moments are of some significance since they are proportional to the angle of attack of the fuselage and hence enter the stability quantities. The sign of these moments is such that the stability about the normal axis is lowered by the action of these free moments. On an axially symmetrical fuselage the free moment in flow along the fuselage axis is, of course, zero; on unsymmetrical fuselage forms or by appendages the axis for zero moment can be located at any other place. The free moment is produced by negative pressure on the upper side of the bow and on the lower side of the stern and positive pressure at the lower side of the bow and on the upper side of the stern. (See the figure at the top of the next page.)*

*The free moments can be computed in various ways. If time and patience are no object, a field of singularities substituting for the fuselage may be built up by means of potential theory methods.\* But for the task in hand Munk's method is much more suitable. He simply determined the asymptotic value for very slender fuselage forms and then added a correction factor dependent on the slenderness ratio, which he obtained by a comparison with the values of easily and accurately computable forms.*

---

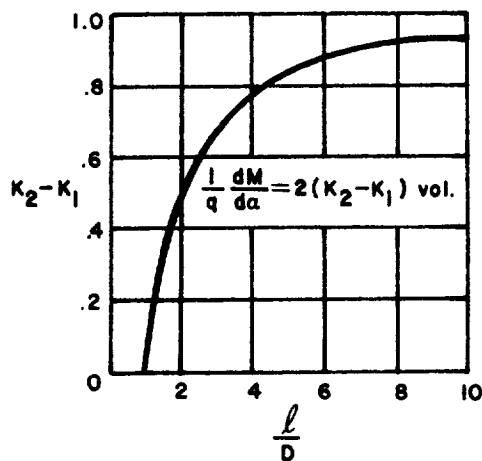
\* This is, in fact, just what is done in Reference 23; the computer makes it possible to be impatient and still accomplish the task quickly and accurately.



According to Munk, the unstable moment of a very slender body of revolution is

$$\frac{1}{q} \frac{dM}{d\alpha} = -2 \text{ vol. } ,$$

the effect of finite fuselage length being accounted for by the correction factor  $(K_2 - K_1)$  which depends on the slenderness ratio  $l/D$ . (See the accompanying sketch.) In this representation  $K_2$  is the air volume in ratio



to the fuselage volume by transverse motion of the fuselage\* and  $K_1$  that by longitudinal fuselage motion. For other than axially symmetrical surfaces it is

$$\frac{1}{q} \frac{dM_R}{d\alpha} = -\frac{\pi}{2} (K_2 - K_1) \int_0^l b_R^2 dx. \quad **$$

This is all that the consideration of the potential theory supplies concerning a single fuselage. But the actual behavior of the fuselage is not described by the potential flow alone. As soon as the flow past the fuselage ceases to be perfectly symmetrical, boundary-layer material accumulates more on one side than on the other and the flow conditions are altered. This results in additional forces at the fuselage and so becomes an appreciable factor in the moment balance of the fuselage. The point of application of the induced frictional lift or cross force is of course proportionally far aft at the fuselage.

As the dependence of frictional lift on angle of attack is strongly suggestive of a very similar course on wings of very small aspect ratio, its correlation suggests itself. For a wing of very small aspect ratio we get approximately for  $\alpha = 0$ :

$$\frac{1}{q} \frac{dA}{d\alpha} = \frac{\pi b^2}{2} \quad ***$$

\* The air volume depends upon the local air velocity\* which is found from an exact solution to the flow over an ellipsoid. (See Reference 66, Division C.) The formula for computing  $K_1$  is given (Ref. 66) as

$$K_1 = \frac{2 \left( \frac{1 - e^2}{e^3} \right) \left[ \frac{1}{2} \log \frac{1 + e}{1 - e} - e \right]}{2 - 2 \left( \frac{1 - e^2}{e^3} \right) \left[ \frac{1}{2} \log \frac{1 + e}{1 - e} - e \right]}$$

where  $e = \sqrt{1 - (a^2/b^2)}$  and  $a$  = the half axis and  $b$  = the largest radius of the ellipsoid.

\*\* The notation is that of the original paper. While somewhat different from present usage in the United States, its meaning, when taken in context, should be reasonably clear.

\*\*\* Assume a circular streamtube with diameter  $b$  equal to the wing span. The lifting force which the fluid applies to the wing results in a deflection of the streamtube according to Newton's Second Law of Motion:

$$L = \left[ \rho V \left( \frac{\pi b^2}{4} \right) \right] V \sin \epsilon$$

where  $\epsilon$  is the deflection angle of the streamtube. For small aspect ratios the wing chord is comparatively long. Thus the flow inclination seen by most of the wing is  $\epsilon$ . Hence for such situations one can take

a result readily derivable by means of certain momentum considerations which is in good agreement with the available test data for such wings. However, the conventional fuselage has no sharp sides; hence a temporarily unknown measure that denotes the width of the separating boundary layer substitutes for the width  $b$ . In place of it we correlate the lift to the maximum fuselage width  $b_R$  and introduce a form factor  $f$ , the exact determination of which might be a profitable field of experimental research; presumably it depends, above everything else, on the cross-sectional form of the fuselage, on its solidity, and on the location of appendages. Hence we put

$$\frac{1}{q} \frac{dA_R}{d\alpha} = \frac{\pi}{2} f b_R^2 .$$

The foregoing appraisal of the moments of the fuselage in free stream fails, because the flow pattern of the wings causes a very substantial variation of the flow at the fuselage. To begin with, the previously described frictional lift of the fuselage is not likely to exist, since the wing orientates the flow along the wing chord and even far aft of it with the result that no appreciable flow component transverse to the fuselage exists in the real zone of formation of the frictional lift. Hence there is some justification in assuming that the theoretically anticipated moments will afterward actually occur.

First of all the fuselage with wing differs from the fuselage alone in that the fuselage takes up a very substantial proportion of the lifting

\*\*\*continued

$$\alpha \approx \epsilon .$$

For small angles of attack the lift may then be written

$$L = \frac{\pi}{2} b^2 \frac{\rho V^2}{2} \alpha$$

from which

$$\frac{1}{q} \frac{dL}{d\alpha} = \frac{\pi}{2} b^2 .$$

Note that Multhopp uses the symbol  $A$  to designate lift. This result can also be obtained from the general expression for the dependence of lift-curve slope on aspect ratio (sweep angle and Mach number = zero):

$$C_{L\alpha} = \frac{2\pi AR}{2 + \sqrt{4 + AR^2}}$$

when  $AR \rightarrow 0$  this expression becomes

$$C_{L\alpha} = \frac{2\pi AR}{4} = \frac{2\pi b^2}{4S} = \frac{\pi}{2} \frac{b^2}{S} .$$

Then

$$L = C_{L\alpha} \alpha q S$$

and

$$\frac{1}{q} \frac{dL}{d\alpha} = \frac{\pi}{2} b^2 .$$



forces ordinarily carried by the wing section in its place. The point of application of the aerodynamic forces at the fuselage directly due to the circulation of the wing, is located at the same place as on the substitute wing section; separating this air force distribution for the moment leaves only a free moment which is solved from a simple momentum consideration.

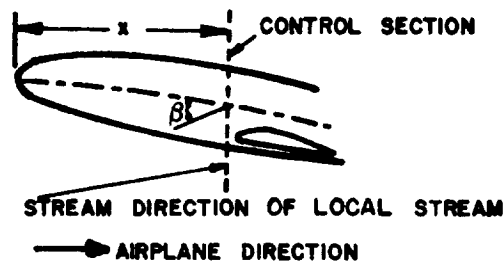
Next, the fuselage is assumed to be sufficiently long, so that, after fixing a reference plane at right angles to the flow direction that meets the fuselage at distance  $x$  from the nose, the integral over the pressure distribution of the fuselage portion ahead of the reference plane equals the vertical momentum passing through this area in unit time. Then, with  $\beta^*$  as the angle in yaw in the reference plane, that is, the angle which the flow would form with the fuselage axis if the fuselage were non-existent, and  $b_R$  as the fuselage width at this point, the lift of the thus segregated fuselage portion is:

$$\int_0^x \frac{dA_R}{dx} dx = \rho v^2 \beta \frac{\pi}{4} b_R^2 .$$

For, if the fuselage is long enough, the flow at right angles to the fuselage axis may be approximated to two-dimensional, and for the flow at right angles to an elliptic cylinder the comprised air volume, that is, the integral

$$\int \rho (v_n - v_{n_\infty}) df = \rho v_{n_\infty} \frac{\pi}{4} b_R^2 = \rho v \beta \frac{\pi}{4} b_R^2$$

is ( $v_n$  and  $v_{n_\infty}$  being the components at right angles to the cylinder axis) independent of the axes ratio of the ellipse. (Note the sketch below.)



Since this formula holds true even for a cylinder degenerated to a flat plate, its approximate use for all cross-section forms appears justified.

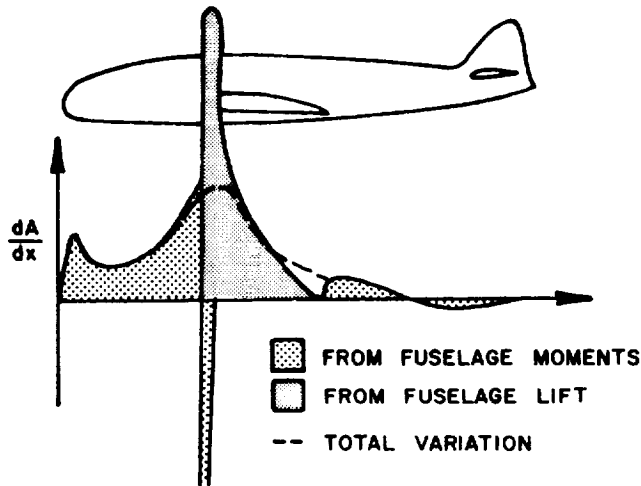
---

\*  $\beta$  is the angle the flow direction makes with the fuselage axis. If these vectors lie in the  $x$ - $z$  plane then  $\beta$  is the angle of attack.

Differentiation with respect to  $x$  then affords:

$$\frac{1}{q} \frac{dA}{dx} = \frac{\pi}{2} \frac{d}{dx} \left( \beta b_R^2 \right)$$

(The air load distribution along the typical fuselage is shown in the figure below)



By reason of the disappearance of  $b_R$  the so computed total fuselage lift is zero at both its ends, hence gives the desired free moments additionally supplied by the fuselage. This free moment is for any reference point

$$\frac{M_R}{q} = \frac{\pi}{2} \int_0^l \frac{d}{dx} \left( \beta b_R^2 \right) x dx$$

and, after partial integration:

$$\frac{M_R}{q} = - \frac{\pi}{2} \int_0^l \beta b_R^2 dx$$

For surfaces of revolution on which the flow is not disturbed by the presence of the wing, we get, because  $\beta = \text{constant}$

$$\frac{M_R}{q\beta} = - \frac{\pi}{2} \int_0^l D^2 dx = - 2 \text{ vol.}$$

or the same result as Munk's for the free moments of airship hulls. It then might be advisable to apply a correction factor to these free fuselage moments on Munk's pattern, containing the effect of the finite fuselage length, except for the difficulty of not quite knowing what slenderness ratio to apply. The reduction relative to the theoretical value is primarily due to the fact that the flow at the fuselage ends still varies somewhat from the assumed two-dimensional pattern; and while the rear end contributes almost nothing to the free fuselage moment, the portions of the fuselage directly before the wing, which certainly are not encompassed by this reduction through the effect of the finite length, contribute very large amounts. Hence the actual value for the correction factor is likely to be far closer to 1 than Munk's quantity ( $K_2 - K_1$ ).

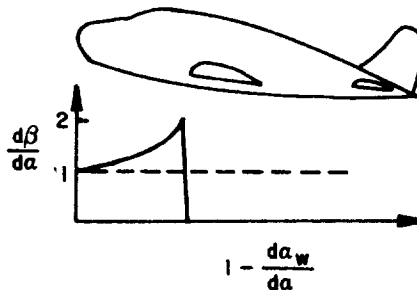
The presence of the wing is allowed for by relating  $\beta$  to the wing circulation. The change of the moment with the angle of attack is:

$$\frac{1}{q} \frac{dM_R}{d\alpha} = - \frac{\pi}{2} \int_0^l b_R^2 \frac{d\beta}{d\alpha} dx .$$

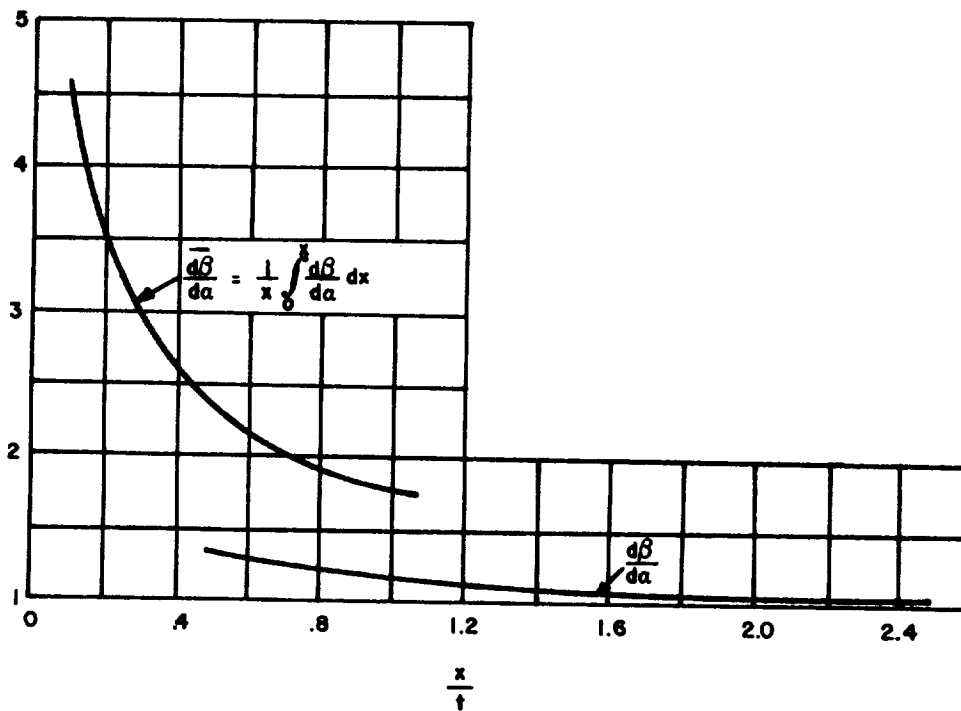
The change of the yawed flow with the angle of attack  $d\beta/d\alpha$  is expressed as follows: The flow in the region of the wing is practically parallel to the wing chord; hence  $d\beta/d\alpha = 0$ . Behind the wing the downwash reduces the yawed flow; at the fuselage stern in the vicinity of stabilizer and elevator there is obtained:

$$\frac{d\beta}{d\alpha} = 1 - \frac{d\alpha_w}{d\alpha} .$$

(This is depicted graphically in the accompanying sketch.)



It is sufficiently exact, when assuming that  $d\beta/d\alpha$  rises linearly from the wing trailing edge to this value. Before the wing  $d\beta/d\alpha$  is always greater than 1 because of the prevalent upwash. (This variation is shown in the graph below.)



For the determination of the fuselage effect on the lift distribution of the wing the flow transverse to the fuselage was assumed to be two-dimensional; then all the mathematical difficulties which the fuselage of itself would entail, can be removed by a conformal transformation of the fuselage cross section to a vertical slit. Then the calculation of the lift distribution for a wing-fuselage combination reduces to that of an equivalent wing, wherein the fuselage effect is represented by a change in chord distribution and also, to some extent, in the angle-of-attack distribution. Then the conventional methods of computing the lift distribution of a wing are fully applicable. Multhopp's transform forms the basis of the method discussed in detail in the next chapter for extending two-dimensional airfoil characteristics to three-dimensional wings. For that reason it will not be discussed further here.

As mentioned earlier, modern treatments of the fuselage contribution to airplane lift, drag, and moments usually represent the flow displacement caused by the presence of the fuselage through source distributions either on the fuselage surface (Ref. 23) or along the fuselage axis (Ref. 48). The three-dimensional source distribution (Ref. 23) can of course be extended to include the wing, etc. A means to account for lift, such as

a distribution of horseshoe vortices, must then be added and, finally, a consistent boundary layer computation must be included in order to complete the calculation. This is, all told, a very complex procedure. Some details of these treatments are given in the next chapter.

It should be noted that the treatment of the fuselage as a body surrounded by a boundary layer is tenable only so long as the angle of attack does not get very large. Reference 68 points out that when a thin cone exceeds an angle of attack of  $8^\circ$  or so vortices begin to be shed from the edges in the streamwise direction resulting in a larger-than-expected normal force coefficient.

Cebeci, Mosinskis, and Smith (Ref. 109) obtained some interesting results from their efforts to predict the drag coefficients of axisymmetric bodies. Their procedure took the following course:

1. Calculate the inviscid pressure distribution on the body using a distribution of sources technique (Ref. 23).

2. Consider the aft end of the body to occur at that longitudinal station where the pressure coefficient first returns to zero. Note that the inviscid source distribution method will always yield a stagnation point at the aft end. The point at which  $C_p = 0$  is therefore located somewhat upstream. For the fineness ratio 4-10 bodies which they studied, this point occurs at roughly 90% of the length. Bodies with blunt trailing edges such as ellipsoids and airship hulls were found experimentally to have separated boundary layers aft of the 85%-90% point so that the assumption of  $C_p = 0$  in this region is fairly reasonable. Some boundary layer separation also occurs on bodies which taper slowly to a point because the boundary layer cannot withstand a pressure rise to a stagnation value. Again, the assumption of separation at about the 90% or 95% point is probably reasonable although the ratio of boundary layer thickness to body radius at separation (used as indicated below) is different than for bodies with blunter trailing edges. Data presented in the paper indicates a pressure coefficient of about +0.1 in the separated flow region.

3. Calculate the boundary layer displacement thickness and momentum thickness at the point taken to be the trailing edge. When the body radius is expected to be large compared with the displacement thickness, a two-dimensional value for the momentum thickness is found to give better results.

4. Then use Granville's formula (Ref. 111)

$$C_D = \frac{4r_\theta}{R_0^2} \left( \frac{u_e}{u_\infty} \right)^{[7 \left( \frac{\delta^*}{\theta} + 2 \right) + 3]} / 8$$

to determine the total drag of the body. In this formula  $r_0$  is the radius of the body at the tail "end",  $R_0$  is the maximum radius,  $u_e$  is the flow velocity outside the boundary layer at the tail end of the body, and  $u_\infty$  is the free stream velocity. If the "end" is chosen to be that point at which  $C_p = 0$ , then  $u_e/u_\infty = 1.0$ .

For a fineness ratio 4.0 body (similar to an ellipsoid but having the tail end modified to come to a point) the method gave excellent agreement with experimental results up to a Reynolds Number of about 6 million. Above this value, the prediction was about 20% low. The skin friction drag constituted about 90% of the total drag in this case. For the fineness ratio 7.0 body (same contour) the agreement with experiment was excellent for all Reynolds Numbers and the skin friction constitutes virtually all the drag.

The airship hull (fineness ratio = 4.2) predictions agreed very well with experimental results for all Reynolds numbers. Skin friction was again about 90% of the total drag and flow separation occurred at about 90% of the length.

Cebeci, Mosinskis, and Smith comment that their studies showed a great sensitivity to the effective end location on the body to be used in the drag formulas and to the inviscid pressure distribution used in the drag calculations. They note also that the two-dimensional analog of Granville's formula really applies only to the case where the wake is symmetrical with respect to the body chord. This condition is not satisfied for  $\alpha > 6^\circ$ . Thus, a similar situation can be expected to prevail for axisymmetric bodies.

It would seem reasonable to expect that one might someday develop a version of Granville's formula for asymmetric bodies more representative of aircraft fuselages. To do this, however, it will be necessary to solve the three-dimensional boundary layer equations for the body in question and to develop a proper averaging method for final average values of  $\theta_{2-D}$ ,  $r_0$ ,  $R_0$ ,  $u_e/u_\infty$ , and  $\delta^*/\theta$ . Such bodies also require more careful scrutiny for the presence of and locations of flow separations. In a recent paper Cebeci, Mosinskis, and Smith (Ref. 109) address this problem for axisymmetric bodies. Using a finite difference method of numerically solving the axisymmetric boundary layer equations which included transverse curvature effects, they were able to predict the location of separation with less than 1% error. Their two-dimensional calculations also gave excellent results for separation on airfoils at high angles of attack. It should, perhaps, be pointed out at this point that finite difference techniques for solving the boundary layer equations take on the order of twenty times the computer time that are required for the less accurate momentum integral technique described in some detail in the next chapter.

A very recent analytical effort to describe the drag-producing separated flow behind bodies of revolution is described by Marshall and Deffenbaugh (Ref. 117). They first treat three-dimensional steady separation as equivalent to two-dimensional unsteady flow. This assumption, a heuristic one, is suggested primarily by experimental data. They then describe the two-dimensional unsteady wake by a distribution of inviscid point vortices superimposed on the un-

separated potential flow solution, suitably modified by diffusive effects. Their argument for following this tack is the way the wake is observed to develop with time. The object of this approach is to avoid solving the complete Navier-Stokes equations for the separated flow field by a laborious and lengthy finite-difference technique. Instead, one pieces together by computer an ensemble of relatively well-known solutions for sub-flow fields which together form the whole. This is essentially the approach followed by the present work although it differs in details. Marshall and Deffenbaugh include a computer program listing and user instructions in their report. They also compared results obtained by their method with experimental data. For a prolate spheroid  $C_n$  agreed with experiment for  $\alpha < 10^\circ$ .  $C_m$  agreed well for  $\alpha < 20^\circ$ . No drag computations were presented, however.

### INTERFERENCE EFFECTS

The flow at the junction of a wing and a fuselage is not that which one would obtain by combining the flows about isolated wings and fuselages. The flow about the wing modifies or influences the fuselage flow and vice versa. Hence the name interference effects. Küchemann and Weber (Ref. 64) provide two relatively simple means of determining the effect of the junction on the inviscid pressure distribution: (a) Ring vortices are placed on the surface of the body and their strengths are determined from the condition that their induced radial velocities are proportional to the slope of the wing-body junction in the streamwise direction; (b) A fictitious body, obtained by subtracting the wing thickness inside the body from the given body thickness, is considered and is replaced by a source distribution along the body centerline. Applied with care to situations which the models represent reasonably well, the methods give results for the interference velocities which agree well with experiment.

With the advent of the computer, computation of the three-dimensional potential field can be carried out on a fairly routine basis. Loeve (Ref. 50) describes a computer program for the calculation of subsonic flow about wing-body combinations. A three-dimensional distribution of sources on the surface of the wing and the body is used to represent the disturbance to the free stream caused by the presence of the non-lifting wing-body combination. The source strengths are so adjusted that the flow is always everywhere parallel to the surface of the wing-body. To treat the effects of lift, a system of horseshoe vortices is placed on the camber line of the wing.

The superposition of the flow due to sources located on the surface of a wing-body combination is also discussed by Hess and Faulkner (Ref. 46) who give some examples obtained through the aid of a computer program.

Success at treating the wing-body combination would naturally lead one to attempt a method for the determination of the inviscid pressure distribution on complete aircraft. The problem becomes tractable by considering the aircraft surface to consist of a finite number of panels (hence the name sometimes applied: finite element technique). As reported by Carmichel (Ref. 48), the computer program being used at the NASA/AMES Center represents

- (a) body thickness by line sources,
- (b) body lift by line doublets,
- (c) wing thickness by constant source panels,
- (d) wing lift by constant pressure panels, and
- (e) wing-body interference by constant pressure panels.

These finite element methods can be considered a "brute force" approach, in that if one is willing to expend the computer time, the accuracy of the computation can generally be improved by using more and smaller elements. Ultimately, limitations in machine accuracy and in the numerical methods used provide a bound for the accuracy which can be obtained.

A recent correlation of wing-body lift interference effects is provided by Reference 67. Five effects are noted: (1) body upwash on the local angle of the wing; (2) local body flow parameters such as dynamic pressure on the wing characteristics; (3) lift carry-over from the wing to the body; (4) wing upwash on the body ahead of the wing; (5) wing lifting vortices on the body behind the wing. The correlation provided in the paper suggests that one may find the lift on a wing-body combination as follows: (1) Find the lift-curve slope of the wing from

$$C_{L\alpha} = \frac{2\pi AR}{2 + \sqrt{4 + AR^2 \beta^2 (1 + \tan^2 \Delta / \beta^2)}}$$

where  $\beta^2 = 1 - M^2$  and  $\Delta$  is the sweep angle of the maximum thickness point on the wing. Aspect ratio here is based on exposed wing area, *i.e.* that part away from the fuselage.  $C_L$  is then based on the same area. (2) Multiply  $C_{L\alpha}$  thus found by an interference factor,  $F$ , given graphically in the paper. The present authors have determined that for  $M < 0.8$  this curve can be fit by the equation

$$F = 1 + 2\left(\frac{d}{b}\right) + 24\left(\frac{d}{b}\right)^4$$

where  $d$  = body diameter and  $b$  = wing span. Working through the numbers shows that most of the effect is lift carry over from the wing. Most of the remainder can be accounted for with Multhopp's transform. (See next section.)

The fact that viscous effects have been excluded from all of these computations tends to compromise their accuracy or applicability somewhat. To use them successfully, one must first be sure that no flow separations are present such as at wing-body junctions.

In addition to the effect on lift, wing-body interference also complicates the estimation of drag since the boundary layer flow around wing-body junctions, for example, is subject to an external pressure distribution which is the resultant of all the effects listed above. It is not surprising then



that interference drag at subsonic speeds is usually evaluated experimentally or from correlations of data on similar configurations. A "brute force" means of accounting for viscosity in evaluating interference effects, however, would seem to follow from the methods used to calculate the viscous pressure distributions on airfoils (Ref. 31).

#### UNIFIED ANALYTICAL TREATMENTS OF WING-BODY CHARACTERISTICS

By 1962 (Ref. 83) the potential flow about a three-dimensional, non-lifting body had been determined quite successfully through the expedient of representing the surface by an ensemble of connecting plane quadrilaterals, placing on each a source of undetermined strength, and then finding the source strengths by requiring that the total flow produced by the interaction of all the sources and the free stream be parallel to a point on each of the quadrilaterals. A rather large number of "panels" was found to be necessary to obtain results which agreed well with closed form analytical solutions for simple bodies. In addition one had to keep the areas of all panels nearly the same. Despite the very significant amount of computer time required for even the simplest of such computations, the prospect of being able to extend the scheme to include wings, other protuberances and/or lift and thereby treat entire practical configurations at one time was unusually attractive to industry researchers. As a result there are now a number of numerical methods and associated computer programs for treating all or part of the wing-body problem. Among these one may cite References 84, 85, 86, 87, 88, and 89. The differences among the various methods cited lie principally in the numerical procedures employed. Indeed, since these bear so heavily on the economic practicality of the methods, it is not surprising to find a paper (Ref. 93) dealing entirely with this facet of the prediction procedure. Finally, the review article by Widnall (Ref. 90) is quite helpful in distinguishing among the approaches to these and other aspects of the problem used by 19 other authors.

The use of such calculation procedures to examine other aerodynamic characteristics (stability derivatives for example) of complete configurations is discussed in References 91 and 92. Here also the procedures are useful for determining only those contributions to the parameter values which do not depend significantly upon viscous effects. The ability to integrate the determination of these effects into the procedures in a rational yet computationally-manageable way seems to be a skill yet to be learned.

# A THEORY FOR THE PREDICTION OF LIFT, DRAG, AND PITCHING

## MOMENT OF LIGHT AIRCRAFT WINGS

### INTRODUCTION

One of the fundamental tasks in aircraft design is the estimation of the forces which the air will exert on the vehicle during flight so that the structure may be made appropriately strong, the wings may be made sufficiently large to carry the desired load, and the engine may have sufficient power to propel the vehicle at the desired speed. Because no two masses may occupy the same space at the same time, the airplane must move air out of its way temporarily as it flies. To move air one must exert a force on it. Even the mere "sliding" of the air over the skin of the aircraft requires that one exert a force to overcome the friction.

To represent these phenomena quantitatively we consider a fictitious cube through which the air is moving. The cube is fixed to the airplane. Now in general, the velocity of the air moving across one face of the cube does not have to be the same as that moving across the opposite face. Thus we say that in any one of the three principal directions there is a net flux of mass across the cube boundaries given by

$$\rho \frac{\partial u_i}{\partial x_i}$$

where  $\rho$  represents the density of the fluid;  $u$ , the velocity;  $x$ , the length of the cube; and  $i$  indicates that it applies to any one of the three principal directions.

We assert that for the purpose of this analysis the volume occupied by a given mass of fluid always stays the same. As a result, if more net mass flows into the cube in one direction more must flow out in another direction. A mathematical statement of this concept is

$$\rho \frac{\partial u}{\partial x} + \rho \frac{\partial v}{\partial y} + \rho \frac{\partial w}{\partial z} = 0 \quad . \quad (1)$$

Newton's Second Law of Motion states in effect that the force required to change the direction of a mass, *i.e.* move it out of the way, is equal to the product of its mass and its acceleration. This force can be assumed to have three components, *i.e.* one along each principal axis, so that we should write three mathematical statements or equations to describe the complete picture:

$$\begin{aligned} F_1 &= ma_1 \\ F_2 &= ma_2 \\ F_3 &= ma_3 \end{aligned} \quad (2)$$

Now, acceleration is a time rate of change of velocity. But if the velocity crossing one face of the cube is different from that crossing an opposite face at the same time there has been a change in velocity with distance. The product of this change with distance and the velocity at any point in the cube is also an acceleration. For acceleration along x, one may write

$$a_1 = \frac{\partial u}{\partial t} + u \frac{\partial u}{\partial x} + v \frac{\partial u}{\partial y} + w \frac{\partial u}{\partial z} . \quad (3)$$

For the time being we will ignore the force applied to the airplane (and therefore also to the air, according to Newton's Third Law) by the air sliding over the skin. We note that air is caused to move by a pressure difference. In fact, the greater the pressure difference per unit distance the greater will be the force which causes the air to move. Thus, according to Equations (2) and (3) we write

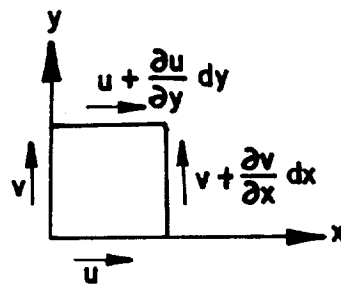
$$\begin{aligned} -\frac{\partial P}{\partial x} &= \rho \left[ \frac{\partial u}{\partial t} + u \frac{\partial u}{\partial x} + v \frac{\partial u}{\partial y} + w \frac{\partial u}{\partial z} \right] \\ -\frac{\partial P}{\partial y} &= \rho \left[ \frac{\partial v}{\partial t} + v \frac{\partial v}{\partial y} + u \frac{\partial v}{\partial x} + w \frac{\partial v}{\partial z} \right] \\ -\frac{\partial P}{\partial z} &= \rho \left[ \frac{\partial w}{\partial t} + w \frac{\partial w}{\partial z} + u \frac{\partial w}{\partial x} + v \frac{\partial w}{\partial y} \right] . \end{aligned} \quad (4)$$

At this point we will assume that the aircraft velocity is steady—unchanging in time—and that the speed of the air flowing over the airplane depends only upon its position with respect to the aircraft. This assumption permits us to ignore terms of the type  $\partial u/\partial t$  and to write Equation (4) as follows

$$\begin{aligned} -\frac{\partial P}{\partial x} &= \rho \left[ u \frac{\partial u}{\partial x} + v \frac{\partial u}{\partial y} + w \frac{\partial u}{\partial z} \right] \\ -\frac{\partial P}{\partial y} &= \rho \left[ v \frac{\partial v}{\partial y} + w \frac{\partial v}{\partial z} + u \frac{\partial v}{\partial x} \right] \\ -\frac{\partial P}{\partial z} &= \rho \left[ w \frac{\partial w}{\partial z} + u \frac{\partial w}{\partial x} + v \frac{\partial w}{\partial y} \right] . \end{aligned} \quad (5)$$

We will need these equations later to relate the pressure forces on wings and fuselages to the velocity of the air moving around them.

Let us now examine the imaginary cube through which we assume the air to be flowing. Consider one face as shown in the sketch below:



By assuming that the air slides over the surface of the airplane without applying any force to it we have in effect assumed that the air has no way of transmitting shearing forces to itself or to solid bodies with which it comes in contact. The measure of this shearing action is the viscosity of the fluid. We have assumed therefore that air is inviscid. Since we have no way of causing one fluid cube to shear against another it is reasonable to conclude that there is no way a fluid cube can be caused to rotate. From the sketch we see that a mathematical statement of this conclusion is

$$u \, dx + \left( v + \frac{\partial v}{\partial x} \, dx \right) dy - \left( u + \frac{\partial u}{\partial y} \, dy \right) dx - v \, dy = 0 \quad (6)$$

Simplifying the equation, one has

$$\frac{\partial v}{\partial x} \, dx \, dy - \frac{\partial u}{\partial y} \, dx \, dy = 0$$

or

$$\frac{\partial u}{\partial y} - \frac{\partial v}{\partial x} = 0 \quad (7)$$

Similar expressions can be obtained for the other five faces of the cube.

We move now to consider the consequences of the condition represented by Equation (7). A general differential  $d\phi$  can be written

$$d\phi = u \, dx + v \, dy + w \, dz \quad (8)$$

Since

$$d\phi = \frac{\partial \phi}{\partial x} \, dx + \frac{\partial \phi}{\partial y} \, dy + \frac{\partial \phi}{\partial z} \, dz \quad (9)$$

$$u = \frac{\partial \phi}{\partial x}, \quad v = \frac{\partial \phi}{\partial y}, \quad w = \frac{\partial \phi}{\partial z} \quad (10)$$

But

$$\frac{\partial^2 \phi}{\partial x \partial y} = \frac{\partial^2 \phi}{\partial y \partial x} \quad (11)$$

Therefore

$$\frac{\partial u}{\partial y} = \frac{\partial v}{\partial x}, \quad \frac{\partial v}{\partial w} = \frac{\partial w}{\partial y}, \quad \frac{\partial w}{\partial x} = \frac{\partial u}{\partial z} \quad (11)$$

Consequently, requiring that the fluid be irrotational means that  $d\phi$  is an exact differential. The integral of an exact differential is independent of the path of integration and depends only on the value of the function at the two end points. We say then that for an irrotational fluid a function  $\phi$ , called a velocity potential, exists such that its partial derivatives represent the components of the fluid velocity. See Equation (10).

Using this result in Equation (1) one may write

$$\frac{\partial^2 \phi}{\partial x^2} + \frac{\partial^2 \phi}{\partial y^2} + \frac{\partial^2 \phi}{\partial z^2} = 0 \quad (12)$$

This partial differential equation is called the Laplace Equation and is one of the most studied in the mathematical literature. Note that there is only one dependent variable. Thus if one can find a function  $\phi$  which satisfies the equation and the boundary conditions he should be able to find the velocity around a body represented by the boundary conditions. Note that since the Laplace Equation is linear, a sum of solutions is also a solution. We shall make use of this fact to represent complex bodies as a sum of simple solutions.

For the calculation of the lift and drag of aircraft wings we will restrict our attention for the time being to flow in a plane aligned with the airstream. Therefore we take  $w = 0$  and ignore derivatives with respect to  $z$ . We postulate that a function

$$\phi = \frac{\Gamma}{2\pi} \tan^{-1} \frac{y}{x} , \quad (13)$$

where  $\Gamma$  is a constant, is a solution of the equation

$$\frac{\partial^2 \phi}{\partial x^2} + \frac{\partial^2 \phi}{\partial y^2} = 0 . \quad (14)$$

Now

$$\frac{\partial \phi}{\partial x} = - \frac{\Gamma}{2\pi} \frac{y}{x^2 + y^2} \quad (15)$$

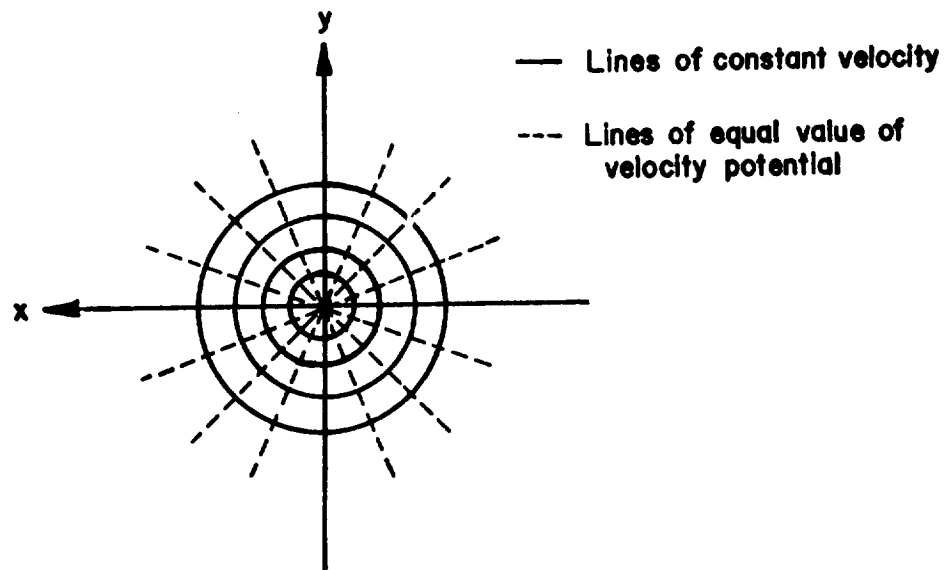
$$\frac{\partial \phi}{\partial y} = \frac{\Gamma}{2\pi} \frac{x}{x^2 + y^2} ,$$

hence

$$\frac{\partial^2 \phi}{\partial x^2} = - \frac{\Gamma}{2\pi} \frac{y(-2x)}{(x^2 + y^2)^2} \quad (16)$$

$$\frac{\partial^2 \phi}{\partial y^2} = \frac{\Gamma}{2\pi} \frac{x(-2y)}{(x^2 + y^2)^2} .$$

The sum of the two equations in (16) is seen to equal zero and thus Equation (13) is a solution of Equation (14). The figure below depicts this function.



For a given value of  $\Gamma$  the velocity decreases as  $1/(x^2 + y^2)^{\frac{1}{2}}$ . This type of flow is called a vortex. It is irrotational. The quantity  $\Gamma$  is called the vortex strength.

If the vortex is not located at the origin the expression for the potential becomes

$$\phi = \frac{\Gamma}{2\pi} \tan^{-1} \frac{y - y_0}{x - x_0} \quad (17)$$

where  $(x_0, y_0)$  is the location of the center of the vortex. Corresponding expressions for the velocity components are

$$u = -\frac{\Gamma}{2\pi} \frac{y - y_0}{(x - x_0)^2 + (y - y_0)^2} \quad (18)$$

$$v = \frac{\Gamma}{2\pi} \frac{x - x_0}{(x - x_0)^2 + (y - y_0)^2}$$

Now suppose we place a number of vortices in a plane and ask what is the velocity induced at a point  $(x, y)$ . We should be able to assume that the vortices may all be treated separately and that their contributions at a point may be summed to find the net velocity. We write therefore

$$\bar{u} = -\frac{1}{2\pi} \sum_{N=1}^k \frac{(y - y_{0N}) \Gamma_N}{(x - x_{0N})^2 + (y - y_{0N})^2} \quad (19)$$

$$\bar{v} = \frac{1}{2\pi} \sum_{N=1}^k \frac{(x - x_{0N}) \Gamma_N}{(x - x_{0N})^2 + (y - y_{0N})^2}$$

where  $k$  is the total number of vortices.

#### REPRESENTATION OF AN AIRFOIL IN TWO-DIMENSIONAL FLOW

Consider then the possibility of placing the vortices on the perimeter of an airfoil. If we can choose the strength of each vortex properly we should be able to make the net flow velocity along the airfoil surface satisfy, at least approximately, the boundary condition that the flow be parallel to the airfoil surface. To do this it is necessary to consider in addition the contribution of the free stream to the total flow picture. The velocity potential for a uniform stream is readily shown to be

$$\phi = -Vx \quad (20)$$

Hence, the effect of the free stream is to add a velocity  $V$  to  $\bar{u}$ . The boundary condition may then be stated as

$$\tan^{-1} \left( \frac{\bar{v}}{V + \bar{u}} \right) = \tan^{-1} \left( \frac{dy}{dx} \right)_{\text{wing}} - \alpha$$

or

$$\frac{\bar{v}}{V + \bar{u}} = \left( \frac{dy}{dx} \right)_{\text{wing}} - \tan \alpha \quad (21)$$

where  $\alpha$  is the angle of attack of the wing chord line.

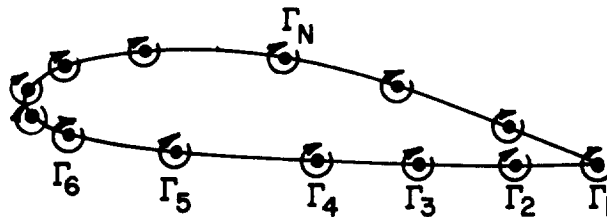
$\left( \frac{dy}{dx} \right)_{\text{wing}}$  is the slope of the wing surface (measured relative to the axis system) at the point where the boundary condition is to be satisfied. The use of this notation follows from the concept of describing the surface by the equation  $y = f(x)$ . The local value of the tangent to this curve is of course given by  $dy/dx|_x$ .

In Equations (19)  $\Gamma_N$ , the vortex strength at each of the  $k$  points, is unknown and must be found by applying the boundary condition  $k$  times, that is, by writing  $k$  equations. Since we can accommodate no more than  $k$  values of the surface slope, one usually depicts the airfoil as consisting of straight line segments connecting the vortex centers. For this reason one usually desires  $k$  to be large in order to describe thick or cambered airfoils accurately.

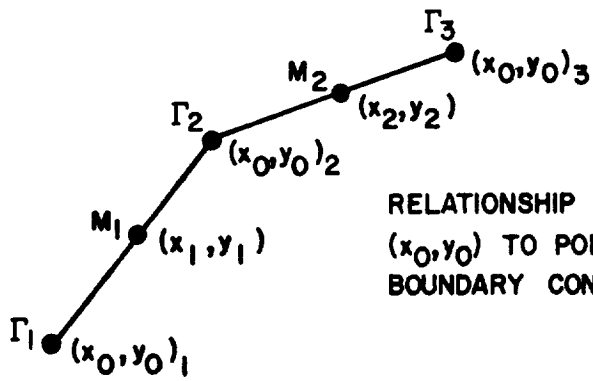
The concept for representing airfoils and the significance of the various symbols used in the text is illustrated in the sketches below.



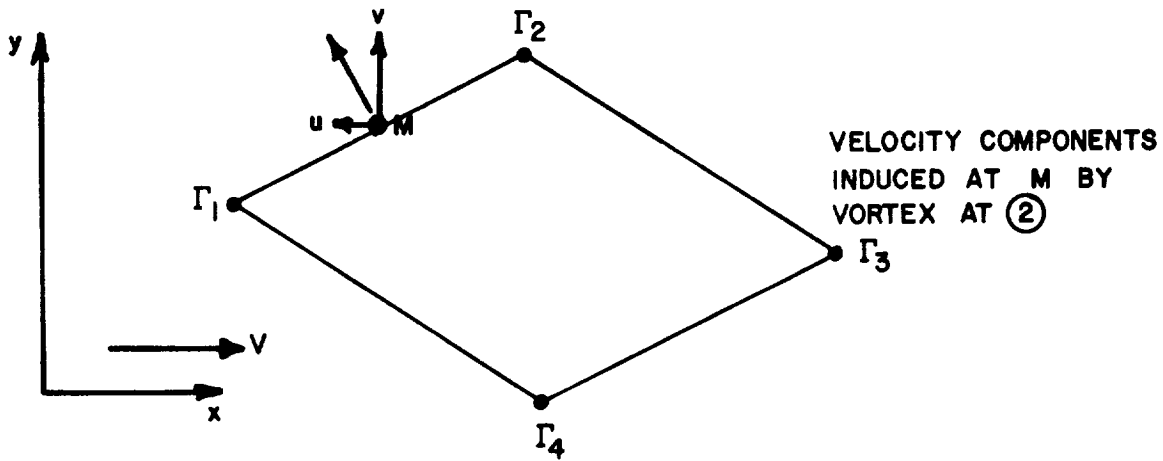
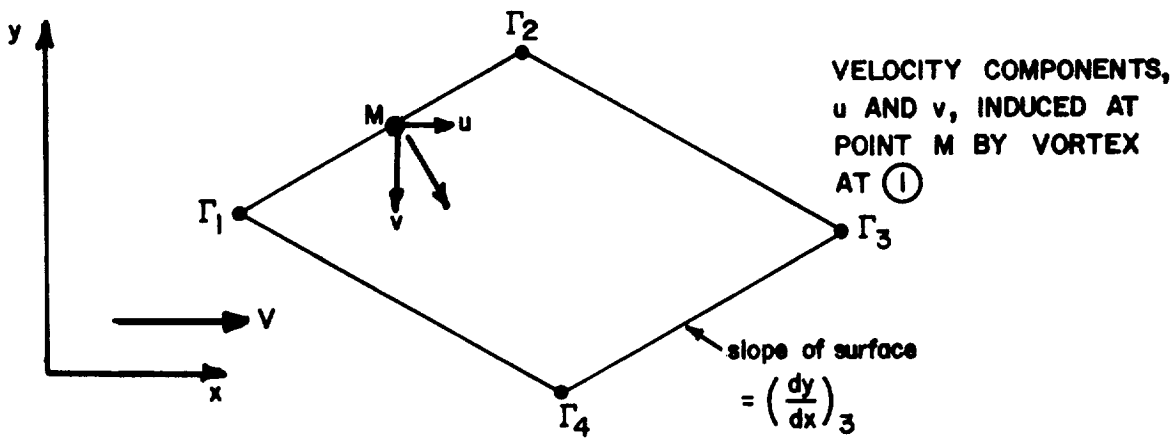
PHYSICAL AIRFOIL SHAPE



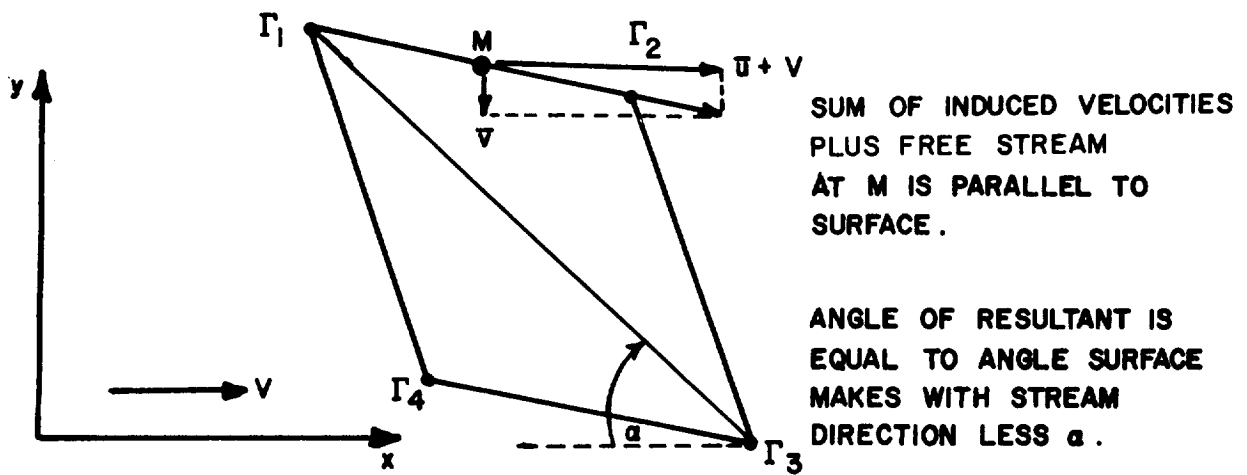
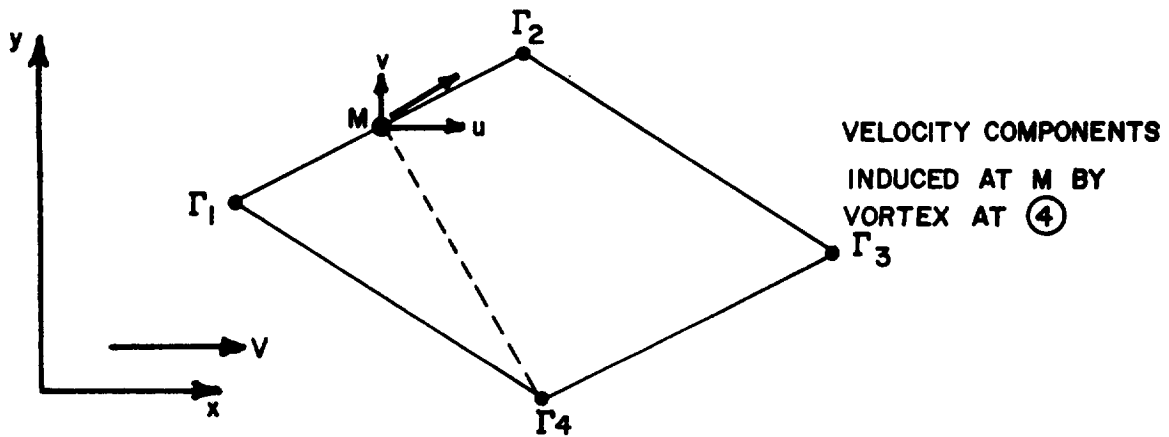
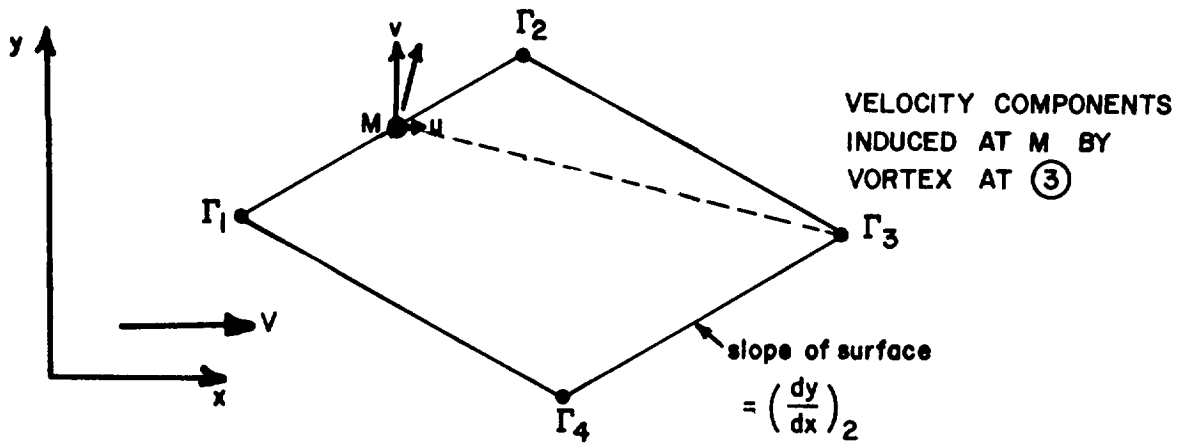
REPRESENTATION OF THE DISTURBANCE CAUSED IN A UNIFORM STREAM BY THE PRESENCE OF AN AIRFOIL THROUGH THE USE OF A DISTRIBUTION OF VORTICES OF DIFFERENT STRENGTHS PHYSICALLY SITUATED AS IF THEY WERE LOCATED ON THE AIRFOIL SURFACE. ARROWS INDICATE DIRECTION OF VORTEX FLOW AND DOTS SHOW LOCATION OF LINE VORTICES EXTENDING TO INFINITY INTO AND OUT OF PAPER.



RELATIONSHIP OF VORTEX CENTERS  
 $(x_0, y_0)$  TO POINTS (M) AT WHICH  
 BOUNDARY CONDITIONS ARE SATISFIED







Note that each vortex on the entire airfoil contributes its share to the net velocity which is produced at each M. Note also that we have chosen to bound each line segment by a vortex. This choice facilitates the description of point M in terms of the vortex locations as may be seen in the analysis below. We could have chosen instead to represent the airfoil by a group of line segments, locate a vortex at the 1/4 point, say, and satisfy the boundary condition at the 3/4 point on each line segment. Such a procedure requires that one first find the equation of each line segment and then locate the vortex and the control point (point where boundary condition is satisfied) on it.

Let us call the right-hand side of Equation (21)  $B_M$ , the tangent of the required flow angle at point M. M has coordinates (x, y). Let us also call

$$\frac{(y_M - y_{O_N})}{(x_M - x_{O_N})^2 + (y_M - y_{O_N})^2} = a_{MN} \quad (22)$$

$$\frac{(x_M - x_{O_N})}{(x_M - x_{O_N})^2 + (y_M - y_{O_N})^2} = b_{MN} \quad , \quad (23)$$

then

$$\begin{aligned} B_1 &= \frac{b_{11}\Gamma_1 + b_{12}\Gamma_2 + \dots + b_{1N}\Gamma_N + \dots + b_{1k}\Gamma_k}{V + a_{11}\Gamma_1 + a_{12}\Gamma_2 + \dots + a_{1N}\Gamma_N + \dots + a_{1k}\Gamma_k} \\ &\cdot \\ &\cdot \\ &\cdot \\ B_k &= \frac{b_{k1}\Gamma_1 + b_{k2}\Gamma_2 + \dots + b_{kN}\Gamma_N + \dots + b_{kk}\Gamma_k}{V + a_{k1}\Gamma_1 + a_{k2}\Gamma_2 + \dots + a_{kN}\Gamma_N + \dots + a_{kk}\Gamma_k} \end{aligned} \quad (24)$$

represents the system of equations which must be solved to find all the  $\Gamma$ 's.

To evaluate  $a_{MN}$  and  $b_{MN}$  in Equation (24) we need to locate points M in relation to  $(x_O, y_O)_N$ . For convenience we will choose M halfway between successive values of  $(x_O, y_O)_N$ . Now the line which extends from  $x_{O1}, y_{O1}$  to  $x_{O2}, y_{O2}$  is described by

$$y = y_{O1} + \left[ \frac{y_{O2} - y_{O1}}{x_{O2} - x_{O1}} \right] (x - x_{O1}) \quad . \quad (25)$$

If we let

$$x = x_{O1} + \frac{x_{O2} - x_{O1}}{2} \quad ,$$

then

$$y = y_{O1} + \frac{y_{O2} - y_{O1}}{2} \quad . \quad (26)$$

By generalizing Equation (26) to

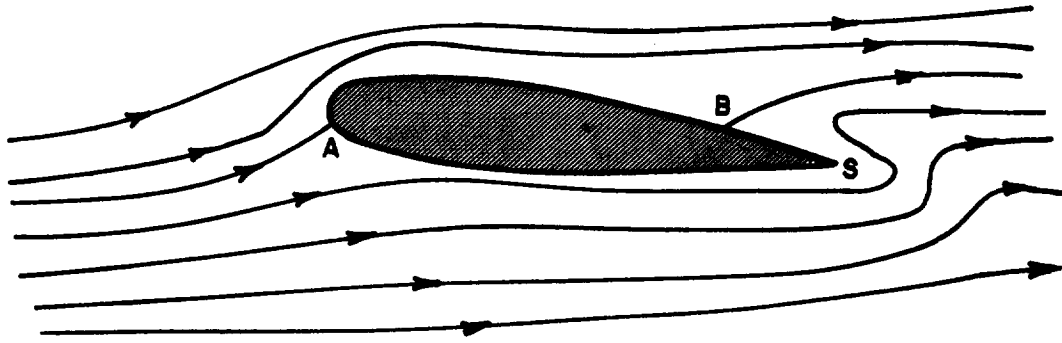
$$\begin{aligned}x_M &= x_{0N} + \frac{1}{2} (x_{0N+1} - x_{0N}) \\y_M &= y_{0N} + \frac{1}{2} (y_{0N+1} - y_{0N}) \quad ,\end{aligned}\tag{27}$$

we can find the coordinates of all except one of the points where the boundary conditions must be matched.

The reason one boundary value cannot be found by this procedure is that by tracing line segments between successive points we draw what can be termed an open polygon. Such a polygon has one less line segment than points. For example, if one numbers four arbitrary points and draws line segments from pt. one to pt. two, from pt. two to pt. three, and then from pt. three to pt. four, he will have only three line segments connecting the four points. As a result, the maximum value of M is therefore  $k - 1$ . Note that if  $N = k$  there is no  $k + 1$  point. We can resolve this difficulty by closing the polygon and giving one point two names, *i.e.*  $N = 1$  and  $N = k$ . While this step does not provide us with an extra line segment at which to match the boundary condition, it does permit one to invoke the physics of the problem to reduce the number of unknown  $T_N$ 's by one and thereby obtain a determinant system.

At this point the question is sure to arise in the mind of the uninitiated reader, why could not one simply locate one vortex and one control point on each line segment? The system is then completely determinant and there is no need to worry about finding another constraint. Unfortunately, such an approach encounters difficulties satisfying our present view of the physical situation. Consider for example the fact that with such a mathematical model we know the flow to be parallel to the line segments only at the control points. We do not know what the direction or magnitude of the resultant flow is anywhere else. The flow could very well cross the airfoil "surface". In particular we must be concerned about the situation at the trailing edge. Now we call one boundary for a quantity of flow a streamline. Far from the airfoil, or course, the streamlines are parallel. As the flow approaches the airfoil one streamline marks the exact line above which all the flow moves over the upper surface of the airfoil and below which all the flow moves over the lower surface of the airfoil. This line is called the stagnation streamline because at the point where it intersects the airfoil surface the flow velocity is exactly zero or stagnant.

The flow in the immediate neighborhood of this line obviously cannot move into the surface and it splits, half of it moves up and half down along the surface at this point with a net velocity of zero. Now, there must be another point of this type on the lee side of the airfoil where the flow around the airfoil comes together and leaves the surface. Where is this point located? Note the accompanying sketch.



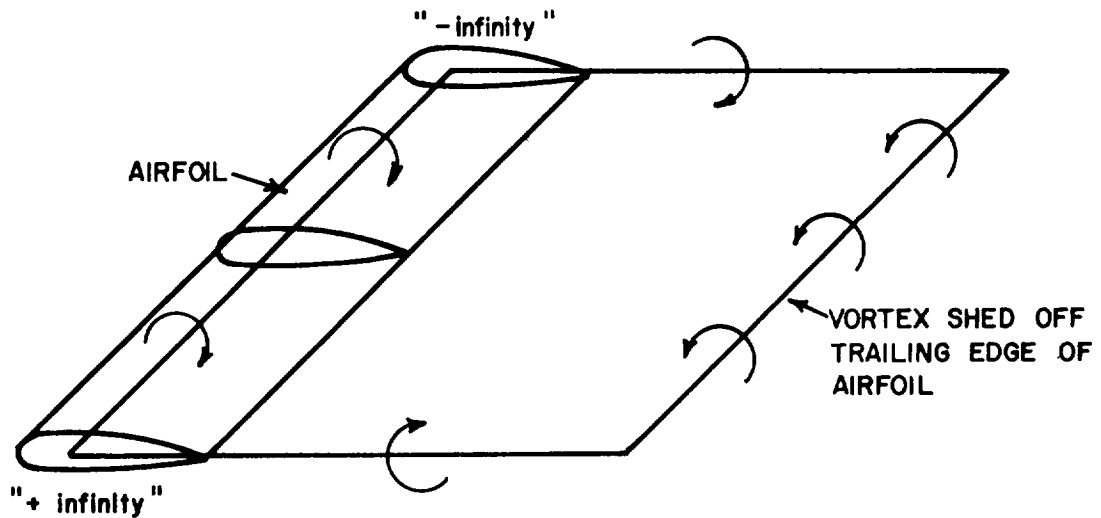
Point A here is the forward stagnation point. It would seem reasonable to locate B such that the distance the flow would have to travel between A and B over upper surface would be equal to the distance from A to B using a lower surface route. For low drag, airfoils usually have trailing edges, S, with very small radii of curvature. If the stream is to remain attached to the surface and flow smoothly around this sharp corner, then it must change direction very rapidly. This means there must then be portions of this region where the velocity is very high and, according to Equation 31, where the pressure is very low.

If the fluid experiences no frictional forces, the kinetic energy of its motion at S is just sufficient to drive it to the stagnation point B. Viscous forces, which are present in the actual case, retard this motion so that the fluid does not quite reach B but stops somewhere on the way. In fact, anytime the fluid does not quite reach B whether because of viscosity or not a counter flow is set up (see sketch below) as some



fluid seeks to move from the high pressure area at B to the low pressure area at S. This tends to separate the flow coming around S from the upper surface. The action of these two flows creates a vortex. This vortex, which is formed along the whole trailing edge of the airfoil, is unstable and separates from the trailing edge. It is carried along by the general motion.

According to Helmholtz's theorem, vortex cores are closed figures. Thus there must be a net circulatory flow around the entire airfoil in the clockwise direction which is attached (at infinity) to the vortex shed off the trailing edge (see following sketch). Incidentally, this



flow pattern can be seen in photographs taken of an airfoil just as it is set into motion. The flow is made visible by inserting the airfoil vertically into stagnant water on which finely ground aluminum powder is floating. Such a vortex is shed everytime there is a change in lift.

Simultaneously with the vortex shedding process and the creation of a net clockwise circulation around the airfoil itself, the stagnation point B is displaced until it resides approximately at S. The fluid then no longer moves around the trailing edge but flows off tangentially with equal velocity at both sides. The assumption that the flow will leave the trailing edge smoothly was put forward independently by Kutta and Joukowski. It is the salient point in the theory of lift because it determines the magnitude of the circulation. By means of this hypothesis the whole problem of lift becomes purely mathematical: one has only to determine the amount of circulation so that the velocity of the flow leaving the upper surface at the trailing edge is equal to that of the flow leaving the lower surface. The rule stated in this way applies to wings with zero vertex angle. If tangents to the upper and lower surfaces form a finite angle, the trailing edge is a stagnation point. Most airfoils with which we will be concerned have finite trailing edge angles; according to the Kutta-Joukowski hypothesis the flow velocity and hence the circulation at the trailing edge of these airfoils is zero. If we locate the first of the vortex filaments describing the airfoil at the trailing edge and require that the net velocity at this point be zero, we must also choose the strength of the vortex filament at that point to be zero since the velocity at the core of a vortex is infinite. At first thought one would simply take  $\Gamma_1 = \Gamma_k = 0$  but this would mean that there is one more equation in (24) than is necessary, something we know is not true. To skirt this mathematical problem we take

$$\Gamma_1 = - \Gamma_k \quad . \quad (28)$$

Obviously, if we have two vortices located at the same point with equal and opposite strengths the sum of those strengths (which is what we would see physically) is zero. Through this device we satisfy the requirement that a stagnation point will always exist at point 1. Simply saying that  $\Gamma_1 = \Gamma_k$  does not insure that  $\Gamma_1$  will come out to be zero even if point 1 is at the trailing edge. Finally, with these constraints Equations (24) now read

$$\begin{aligned}
 B_1 &= \frac{1}{V} \left[ (b_{11} - B_1 A_{11}) \Gamma_1 + (b_{12} - B_1 A_{12}) \Gamma_2 + \dots (b_{1N} - A_{1N} B_1) \Gamma_N + \right. \\
 &\quad \left. \dots (B_1 a_{1k} - b_{1k}) \Gamma_1 \right] \\
 B_{k-1} &= \frac{1}{V} \left[ (b_{(k-1)1} - B_{k-1} a_{(k-1)1}) \Gamma_1 + (b_{(k-1)2} - B_{k-1} a_{(k-1)2}) \Gamma_2 + \right. \\
 &\quad \left. \dots (b_{(k-1)N} - B_{k-1} a_{(k-1)N}) \Gamma_N + \dots (B_{k-1} a_{(k-1)k} - b_{(k-1)k}) \Gamma_1 \right]
 \end{aligned} \tag{29}$$

Equations (29) contain  $k - 1$  distinct values of  $\Gamma_N$  and  $k - 1$  values of  $B_M$  so that the system is solvable for all  $k - 1$  values of  $\Gamma_N$ . Admittedly, when  $k$  is a large number this is a task which is practical only when one is able to use a digital computer with sufficient storage (memory) to carry out the solution process. Generally, the process should be one able to accommodate a system of 65 or more simultaneous algebraic equations. The most favored method for solution of such large systems is a generalization of Cramer's Rule, familiar to college algebra students as a technique for solving systems of 3 or 4 simultaneous algebraic equations. Fortunately, the nature of the matrix form of this large system is such that the solution is less difficult than one might expect to encounter for systems of this size. Those readers interested in the mathematical details of the numerical methods one might employ for this purpose are referred to texts and papers on matrix algebra and in particular to papers on matrix inversion techniques. Since these techniques are not elementary (they are, fortunately, usually available as standard computer library programs) and since their details are not crucial to an understanding of the physical reasoning used to formulate Equations (29), they will not be discussed here.

A cautionary note regarding Equations (29) should, perhaps, be injected at this point. In their formulation, it was assumed that the coordinates of the vortex centers were measured from a fixed reference. Therefore, when the angle of attack changes, the locations of the vortex centers as well as the coordinates of the center of the connecting line segments change. In other words,  $a_{MN}$  and  $b_{MN}$  depend for their values upon the airfoil angle of attack. On the other hand, the local airfoil slope,  $((dy)/(dx))_{wing}$  can be taken as constant for all  $\alpha$  since the term  $\tan \alpha$  is subtracted from the slope to calculate the boundary condition, Equation (21). An alternate formulation considers the airfoil to be fixed and the flow to rotate as  $\alpha$  changes. The left hand side of Equation (21) will then read

$$\frac{\bar{v} + V \sin \alpha}{\bar{u} + V \cos \alpha}$$

while the right hand side will no longer have the term  $\tan \alpha$ .

In addition to the necessity of locating two vortex filaments at the trailing edge as discussed above, there is a second geometrical aspect which should be considered in choosing the locations of the other vortex filaments by which one represents the airfoil. This aspect is the surface curvature. Obviously, the line segments between filaments must be more numerous in regions of high curvature if one is to describe the surface accurately. Thus, for most airfoils the preponderance of points should be located near the leading edge. One can quantify this procedure by specifying that the distance from the line segment to the surface should never exceed a fixed, small percentage of the airfoil chord (distance from leading to trailing edge). The orientation of the local surface to the stream also has an effect on the vortex filament spacing. Surfaces nearly parallel to the free stream can be represented more accurately with a few filaments than surfaces with large inclinations.\*

The solution of Equation (29) is  $k$  values of  $\Gamma_N$  with  $\Gamma_1 = -\Gamma_k$ . Now that we have these values we ask how we may use them to find what is really of interest to us: the local pressures on the surface of the airfoil. We begin by considering how one might write a two-dimensional version of Equations (5) in a coordinate system with one axis tangent to stream line and the other normal to it. In such a coordinate system (5) reduces to

$$-\frac{\partial P}{\partial s} = \rho \tilde{u} \frac{\partial \tilde{u}}{\partial s} \quad (30)$$

where  $\tilde{u}$  is the total fluid velocity and  $s$  is the distance along the streamline. Equation (30) is easily integrated to yield

$$P_s = P + \frac{1}{2} \rho \tilde{u}^2 \quad (31)$$

$P_s$  is the stagnation pressure along a streamline, that is, the pressure which would exist if the fluid were brought to rest. It is usually assumed that the disturbances produced by the airfoil decay to zero at great distances upstream and downstream of the airfoil, *i.e.* at these stations. If the flow is uniform then the stagnation pressure must be the same along all streamlines. Since there is no mechanism in an irrotational, incompressible, inviscid flow by which the stagnation pressure can change,  $P_s$  is then the same on all streamlines throughout the flow field. It is easily evaluated since  $P_\infty$ ,  $\rho$ , and  $V$  are known in a given flow.

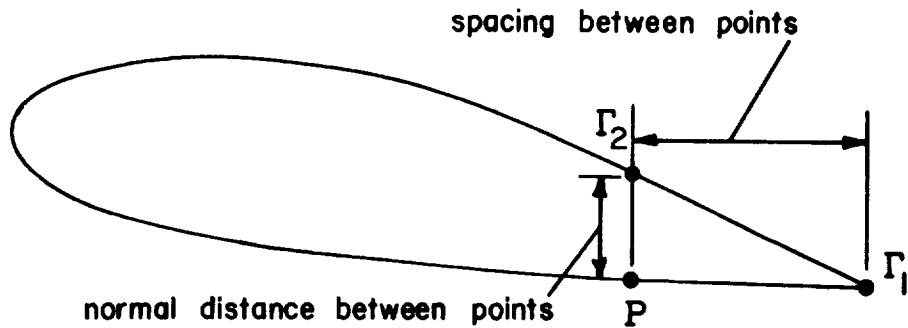
---

\* One might postulate that by representing both the boundary on which parallel flow is to be required and the vortex strength explicitly by continuous functions of the surface coordinates with continuous derivatives everywhere, the intervals over which these functions are fitted can be significantly larger, for equal accuracy, than the straight line segments (with their delta-function-like circulation strengths) used in the present approach. Larger segments, of course, means fewer (although perhaps more complex) equations to solve. Hess (Refs. 81, 82) studied this question at some length. He begins with the implicit assumption that one would always wish to represent the distribution of vorticity over the airfoil surface as a continuous distribution. The strength of the vorticity

---

\* CONTINUED

over any segment of the airfoil surface is then an integral of the vortex strength per unit length over that segment. Since this integral equation usually cannot be solved in general, one usually seeks to find approximate means of solution. Hess states that "the most straightforward means of evaluating the integral is by means of a quadrature formula that replaces the integral by a weighted sum of values of the integrand evaluated at certain points. That is, the effect of a continuous singularity distribution is approximated by a sum of concentrated point singularities...This is not a satisfactory procedure. The basic difficulty is that the velocity approaches infinity more rapidly in the neighborhood of a point singularity than it does near a finite-strength singularity distribution on an arc of a curve. Thus the spacing of the quadrature points must be small compared to all physical dimensions of the boundary. This is not practical for airfoils which are often quite thin." Near the trailing edge, particularly, the problem is quite difficult. "Adjacent to the corner the ratio of the normal distance between two points to the spacing between them is approximately the sine of the trailing edge angle, no matter how many points are used."

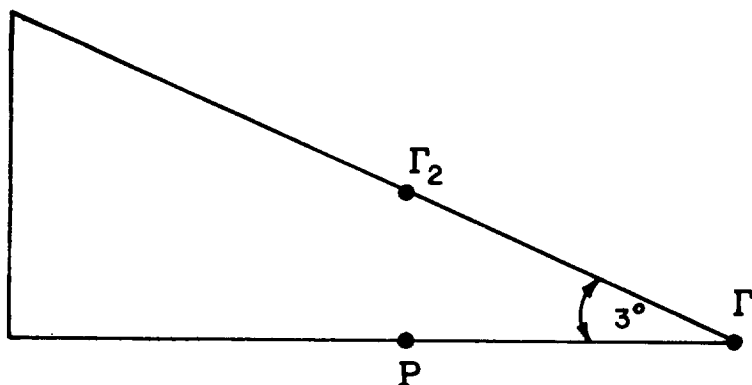


As a result, the velocity at  $P$  on the lower surface of the airfoil in the sketch above is dominated by the contribution from  $\Gamma_2$ , whereas in the integral representation the contribution from vorticity at some distance from  $\Gamma_2$  will still be significant.



\* CONTINUED

To illustrate these concepts consider the following example. Take two flat plates which join at an angle of  $3^\circ$ .



Place vortices  $\Gamma_1$  and  $\Gamma_2$  10 units apart as shown and assume  $\Gamma_1 = \Gamma_2$ . Now  $\Gamma_2$  induces a velocity which is parallel to the lower plate at P which has a magnitude equal to  $(\Gamma/2\pi)(1.91)$  while  $\Gamma_1$  induces a velocity at P which is normal to the plate and has a magnitude equal to  $(\Gamma/2\pi)(0.1)$ .

The integral representation for constant vortex strength per unit length is given by

$$v \approx \frac{1}{2\pi} \int_0^{10} \frac{\Gamma}{10} \left[ \ln \sqrt{1.002742 x^2 - .05483 x + .2742} \right] dx$$

$$\approx \frac{\Gamma}{2\pi} (1.37) .$$

Note that in this example the magnitude of the induced velocity at P is, as stated by Hess, less for a continuous distribution of vorticity than for a distribution of concentrated point singularities. It would appear, therefore, that the use of continuous distributions of vorticity would lead to less "wavy" flows in the neighborhood of airfoil surfaces and is therefore desirable.

---

\* CONTINUED

Hess systematically investigated the effectiveness of higher order approximations of the integral equation, including the use of curved surface elements and parabolically-varying vorticity. He found that the approach using flat elements with constant singularity is mathematically consistent as is the next higher-order approach with parabolic elements and linearly-varying singularity strength. The popular approach based on flat elements with linearly-varying singularity strength he shows to be mathematically inconsistent. Hess concludes that "(1) the higher order solutions give very little increase in accuracy for the important case of exterior flow about a convex body; (2) for bodies with substantial concave regions and for interior flows in ducts, the use of parabolic elements and linear varying singularity can give a dramatic increase in accuracy; and (3) the use of still higher order solutions leads to a rather small additional gain in accuracy."

The results which Hess obtained for the surface velocity on a semi-infinite body whose forward portion is a semi-circle concave to the flow has a particular bearing on the question of whether the use of higher order solutions can lead to shorter computational times for equal accuracy. Using 36 curved elements with linearly-varying source strengths he was able to recover the values given by the analytical solution. Even with five times that number of straight elements with constant source strengths—and, more importantly, one hundred times the computing time—he was not able to recover the correct values. The results were qualitatively correct but were quantitatively in error, particularly on the centerline.

Hess also studied the use of the various solutions on a highly cambered Kármán-Trefftz airfoil for which an analytical solution is known. Since the lower surface of this airfoil is concave, use of the higher order method was found to be necessary in order to obtain good agreement with the analytical result.

The implications of Hess's work, so far as the prediction of airfoil characteristics is concerned, are (1) for conventional airfoils little reduction in computational time—for the same accuracy—can be achieved by using fewer curved elements and linearly-varying singularity strengths, (2) for unconventional airfoils—airfoils with concave areas on their lower surfaces—use of the higher order solution will yield substantial improvements in accuracy for a given computational time.

Now the velocity along a streamline is given by

$$\sqrt{(V + \bar{u})^2 + \bar{v}^2} = \bar{u} \quad (32)$$

so that the fluid pressure which acts normal to the airfoil surface at point (x, y) is simply

$$P = P_{\infty} + \frac{1}{2} \rho V^2 - \frac{1}{2} [(\bar{u} + V)^2 + \bar{v}^2] \quad (33)$$

or

$$P = P_{\infty} - \frac{1}{2} \rho [\bar{u}^2 + \bar{v}^2 + 2\bar{u}V] .$$

Note that we have used all of the  $\Gamma_N$  found from a solution of (29) to determine  $\bar{u}$  and  $\bar{v}$  at a set of points (x, y) according to Equations (10). It may be well to note here that requiring the flow generated by the system of vortices to be parallel to the surface at the mid-segment points does not guarantee that it is also parallel to the surface everywhere. Thus it is prudent to select x, y for the pressure computation to be those same mid-segment points. Pressures at points inbetween are probably best found from a third order polynomial fit to four successive calculated values.

The net lift on the airfoil is obtained by integrating the components of the pressure which are normal to the free stream direction over the entire surface of the airfoil. Mathematically, this process can be expressed by

$$L = \cos \alpha \oint P(x) \cos \left[ \tan^{-1} \left( \frac{dy}{dx} \Big|_x \right) \right] dx - \sin \alpha \oint P(x) \sin \left[ \tan^{-1} \left( \frac{dy}{dx} \Big|_x \right) \right] dx . \quad (34)$$

The lift coefficient is then  $L/\frac{1}{2}\rho V^2 c$ .

To perhaps aid the reader in grasping some of the foregoing concepts, we will digress momentarily from the main thrust of our argument, retrace some of our steps and approach the calculation of airfoil lift from a slightly different direction. We will employ for this purpose the analysis given by von Kármán and Burgers in Volume II of the six volume set, Aerodynamic Theory, edited by W. F. Durand, (Julius Springer, 1935). Equations (19) when expressed in polar coordinates become

$$v_r = \sum_{N=1}^k \frac{\Gamma_N}{2\pi} \frac{r_{0N} \sin(\theta - \theta_{0N})}{r^2 + r_{0N}^2 - 2r r_{0N} \cos(\theta - \theta_{0N})}$$

$$v_{\theta} = - \sum_{N=1}^k \frac{\Gamma_N}{2\pi} \frac{r - r_{0N} \cos(\theta - \theta_{0N})}{r^2 + r_{0N}^2 - 2r r_{0N} \cos(\theta - \theta_{0N})} .$$

In these expressions it is assumed that the positive sign of the circulation corresponds to a clockwise rotation of the fluid and that the nose of the airfoil points to the left into the oncoming stream.  $v_{\theta}$  is positive in the counterclockwise direction. We now expand the velocities in a series containing decreasing powers of r. These series are convergent so long

as  $r$  is greater than any of the values  $r_1, r_2, \dots, r_n$ , that is, so long as the point where we wish to compute the velocity components is further from the origin than any point on the airfoil surface. Under these conditions, the first term in the denominator of each series above is dominant and one may write

$$v_r = \frac{1}{r^2} \sum_{N=1}^k \frac{\Gamma_N}{2\pi} r_{0N} \sin(\theta - \theta_{0N}) + \text{higher terms}$$

$$v_\theta = -\frac{1}{r} \sum_{N=1}^k \frac{\Gamma_N}{2\pi} - \frac{1}{r^2} \sum_{N=1}^k \frac{\Gamma_N}{2\pi} r_{0N} \cos(\theta - \theta_{0N}) + \text{higher terms} .$$

We now assume a uniform and parallel fluid motion with velocity component  $V_x$  and  $V_y$  to be superimposed on the flow produced by the vortex filaments. We apply to the fluid within a circle of radius  $r = K$  the theorem that the difference between the fluid momentum entering the circle and that leaving it is equal to the resultant of the forces acting on the fluid. The forces involved are (a) the pressure distributed along the circle and (b) the forces acting between the vortices and the fluid. The theorem may therefore be stated thus:

Resultant of forces = Resultant of pressures - Change in momentum

or 
$$F_x = - \oint P \cos \theta \, ds - \rho \oint W_n W_x \, ds$$

$$F_y = - \oint P \sin \theta \, ds - \rho \oint W_n W_y \, ds$$

where  $F_x, F_y$  are the resultant forces in the  $x$  and  $y$  directions,  $\theta$  locates the element  $ds$  and

$$W_n = V_x \cos \theta + V_y \sin \theta + v_r$$

$$W_x = V_x + v_r \cos \theta - v_\theta \sin \theta$$

$$W_y = V_y + v_r \sin \theta + v_\theta \cos \theta .$$

Then

$$F_x = -K \int_0^{2\pi} P \cos \theta \, d\theta - \rho K \int_0^{2\pi} (V_x \cos \theta + V_y \sin \theta + v_r) \cdot (V_x + v_r \cos \theta + v_\theta \sin \theta) d\theta$$

$$F_y = -K \int_0^{2\pi} P \sin \theta \, d\theta - \rho K \int_0^{2\pi} (V_x \cos \theta + V_y \sin \theta + v_r) \cdot (V_y + v_r \sin \theta + v_\theta \cos \theta) d\theta$$

$$\begin{aligned}
P &= P_{\infty} + \frac{1}{2}\rho(V_x^2 + V_y^2) - \frac{1}{2}\rho(V_x + v_r \cos \theta - v_{\theta} \sin \theta)^2 \\
&\quad - \frac{1}{2}\rho(V_y + v_r \sin \theta + v_{\theta} \cos \theta)^2 \\
&= P_{\infty} - \frac{1}{2}\rho(v_r^2 + v_{\theta}^2 + 2v_r[V_x \cos \theta + V_y \sin \theta] \\
&\quad + 2v_{\theta}[V_y \cos \theta - V_x \sin \theta]) \quad .
\end{aligned}$$

If  $K$  is large, then  $v_r \rightarrow 0$  and  $v_{\theta} \rightarrow -\frac{1}{K} \sum_{N=1}^k \frac{\Gamma_N}{2\pi}$  .

Further, the integral from 0 to  $2\pi$  of  $\sin \theta$ ,  $\cos \theta$ , and  $\sin \theta \cos \theta$  are all zero so that in computing  $F_x$  and  $F_y$  one need do only

$$\begin{aligned}
F_x &= K \int_0^{2\pi} \frac{\rho}{2} 2 v_{\theta} V_y \cos^2 \theta d\theta + K\rho \int_0^{2\pi} v_{\theta} V_y \sin^2 \theta d\theta \\
F_y &= -K \int_0^{2\pi} \frac{\rho}{2} 2 v_{\theta} V_x \sin^2 \theta d\theta - \rho K \int_0^{2\pi} v_{\theta} V_x \cos^2 \theta d\theta
\end{aligned}$$

which become

$$\begin{aligned}
F_x &= K\rho 2\pi v_{\theta} V_y \\
F_y &= -K\rho 2\pi v_{\theta} V_x \quad .
\end{aligned}$$

Then with  $v_{\theta} = -\frac{1}{K} \sum_{N=1}^k \frac{\Gamma_N}{2\pi}$  we have

$$\begin{aligned}
F_x &= -\rho V_y \sum_{N=1}^k \Gamma_N \\
F_y &= \rho V_x \sum_{N=1}^k \Gamma_N \quad .
\end{aligned}$$

In the case where the fluid motion is parallel to the x-axis we see that  $V_x = V$  and  $V_y = 0$  so that the resultant force or lift,

$\rho V \sum_{N=1}^k \Gamma_N$ , is normal to the direction of the stream. Since Joukowski

found that the lift of an airfoil is  $\rho V \Gamma$ , it is evident that the net circulation about the airfoil is the sum of the individual vortex filament strengths.

A simplified form of Equation (34) can also be used to show an interesting relationship between the vortex filament strengths and the surface velocities. Since

$$P(x) = P_{\infty} - \frac{\rho}{2} [\bar{u}^2 + \bar{v}^2 + 2\bar{u}\bar{v}]$$

we could take for  $\alpha = 0$  and an airfoil surface made up of straight line segments

$$L = \int P(x) \left( \frac{\Delta x}{\Delta s} \right)_x dx ,$$

where  $\left( \frac{\Delta x}{\Delta s} \right)_x$  represents the cosine of the angle formed by a particular line segment and the chord line. If we are willing to say that this cosine is always near unity then we may ignore the v-component in the velocity and also  $\bar{u}^2$  in comparison with  $2\bar{u}V$ . With these approximations we have for the lift

$$L = \oint [P_\infty - \frac{\rho}{2} (2\bar{u}V)]_x (\Delta x)_x dx .$$

Since we are discussing a surface made up of line segments  $(\Delta x)_x$  and we assume that the pressure is constant over each line segment, the integral is readily approximated by a series:

$$L = \sum_x \rho V \bar{u}_x (\Delta x)_{x_{upper}} + \sum_x \rho V \bar{u}_x (\Delta x)_{x_{lower}} .$$

Note that  $\oint P_\infty dx = 0$ . From a comparison between this expression for the lift and that in terms of the vortex filament strengths where

$$L = \rho V \sum_N \Gamma_N$$

we see that

$$\bar{u}_x = \frac{\Gamma_x}{(\Delta x)_x} .$$

In other words, the velocity induced along a segment of the airfoil surface is equal to the vorticity per unit length existing over that segment.

Some comments concerning the results of the procedure leading to (34) are appropriate at this point. First, it must be recalled that the procedure considers air to be an inviscid, incompressible fluid. Thus, there is no dissipative mechanism available to produce a drag. Hence, the integral of the streamwise components of the pressure force on the airfoil must, if the calculation has been carried out accurately and correctly, be zero, or in mathematical terms,

$$\begin{aligned} \sin \alpha \oint P(x) \cos \left[ \tan^{-1} \left( \frac{dy}{dx} \Big|_x \right) \right] dx \\ + \cos \alpha \oint P(x) \sin \left[ \tan^{-1} \left( \frac{dy}{dx} \Big|_x \right) \right] dx \leq 0.00005 . \end{aligned} \quad (35)$$

Carrying out the procedure indicated by Equation (35) is an excellent way to check the accuracy and validity of the method used to obtain a numerical result for Equation (34).

A second anomaly resulting from the use of an inviscid theory is that one cannot predict the approach of the phenomenon pilots call "stall." Physically, stall is characterized by a loss of lift and a sharp increase

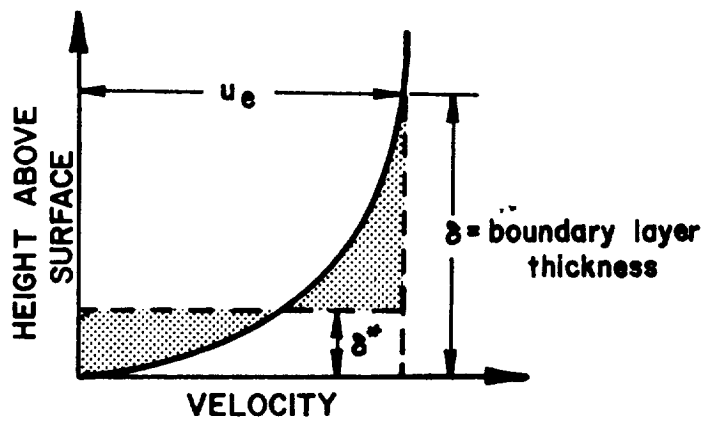
In drag as the wing's angle of incidence to the stream is increased. Thus an airfoil exhibits a maximum lift coefficient just prior to stall. It usually occurs at angles of incidence to the airstream ( $\alpha$ ) in the neighborhood of  $16^\circ$  to  $20^\circ$ . The inviscid theory, on the other hand, will predict maximum lift at  $\alpha \rightarrow 45^\circ$ . Despite this deficiency, the inviscid theory will generally give quite satisfactory predictions of lift for  $\alpha < 6^\circ$  or  $8^\circ$ .

### TREATMENT OF VISCOUS EFFECTS

It should be evident from the previous comments that to be able to make a realistic estimation of aircraft performance one must find some means to consider in the calculations the property by which air is able to resist the motion of aircraft and propellers: viscosity. It has been known for a long time that inclusion of this property in the equations describing fluid motion makes them (a) non-linear, (b) higher order, (c) consider energy transport, and, consequently, a pressure-density-temperature relation—factors which make them virtually insolvable in general. In one of the greatest contributions to the analytical description of physical reality, Ludwig Prandtl argued in 1904 that for most practical applications one could consider the effects of viscosity to be confined to a thin layer of the fluid immediately adjacent to the airfoil surface which he called the boundary layer. Prandtl argued that the remainder of the flow field can be treated quite adequately by retaining the fiction that the fluid is inviscid. If we assume that we have an acceptable method to calculate the lift on an airfoil-like body we must ask ourselves how can we include this viscous boundary layer in the treatment and what are its effects.

The concept of viscosity means that there is a transport or communication of the momentum of the fluid in one layer to the fluid in the adjacent layer. Whereas in inviscid theory we assumed that the fluid layer immediately adjacent to the surface of a flat plate has the same velocity as that far from the surface, we recognize that the stationary character of the surface must be known to the fluid immediately adjacent to it. This fluid cannot be moving very rapidly with respect to the surface because the molecules lose a significant portion of their tangential momentum in striking the stationary surface. This change in momentum appears as a frictional force on the surface. The layers outside the one closest to the surface, however, continually feed in additional momentum so that the net result is the development of a gradation in fluid velocity from the surface to the edge of the boundary layer. At the surface the velocity relative to the surface is zero. At the outer edge of the boundary layer the velocity is equal to that in the inviscid flow. See the following sketch.

Shown on the sketch is a graph of the variation of fluid velocity with height above a solid surface.  $u_\infty$  is the inviscid free stream velocity. A similar graph can be constructed at each streamwise location along the surface. Generally, the height over which the fluid velocity moves from zero to the inviscid free stream value, the distance labeled  $\delta$  on the graph, increases as one goes downstream.

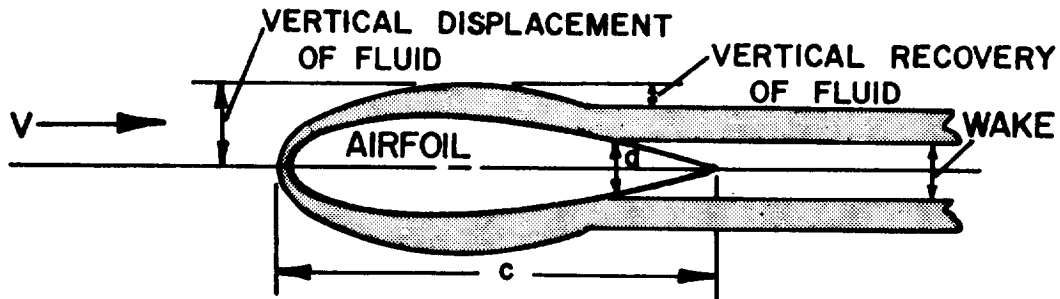


Looking at the sketch one notes that the two cross-hatched areas are approximately equal. This suggests that one could say, for purposes of modeling, that all of the fluid mass in the boundary layer is really concentrated in a region of uniform velocity  $u_e$  extending from  $\delta^*$  outward to  $\delta$  and that the region from the surface to  $\delta^*$  could be considered part of the body since in this model there is no fluid in it. It would seem then that a way of accounting for some of the effects of viscosity is to determine  $\delta^*$ , add this value to the airfoil ordinates, and recompute the lift values by inviscid theory based on this modified shape. As we shall see, this is an iterative process since the value of  $\delta^*$  depends upon the value of the surface pressures.

Because of the existence of the boundary layer and its accompanying viscous dissipation, the flow in the immediate area of the trailing edge has a lower stagnation pressure than that at the leading edge. Since the pressure just aft of the airfoil must be about the same throughout a plane normal to the stream, there will be a region formed by the confluence of the two surface boundary layers where the fluid velocity will be less than free stream. This is called a wake, that is, a region where the fluid is relatively static with respect to the airfoil. Wakes tend ultimately to diffuse and disappear downstream. A wake exists whether or not the boundary layer(s) separate from the airfoil. The wake is of course much thicker if there is separation.

Another way of looking at the effect of a wake is to note that in moving over an obstruction the fluid velocity increases in proportion to the vertical displacement of the obstruction at the particular streamwise location. As the velocity goes up, the pressure must come down, according to Equation (31). Then, having passed the peak of the obstruction, the fluid begins to decelerate and the pressure begins to rise. Now, the effect of the wake coming off the trailing edge of the airfoil is to prevent the inviscid flow from returning all the way to its original free stream value. See the sketch below. Consequently, the pressure at the beginning of this wake region, point "a" on the sketch, is substantially lower than stagnation pressure. Since the streamlines are essentially straight downstream of point "a" it means the flow is more or less uniform and the pressure over





the entire airfoil aft of point "a" is approximately constant at the low value that exists at point "a". An integral of the surface pressures in the streamwise direction is now not zero. There is a finite drag, called in this case the form drag since it is dependent for its value on the form or shape of the body.

To accommodate this situation within the bounds of our inviscid theory we can proceed as follows: take as our body shape the airfoil plus  $\delta^*$  up to  $x = c$ . At  $x = c$ , assume the body continues to extend downstream by an amount equal to

$$\left( \delta^* \frac{dy}{dx} \right)_{x=c},$$

the projections from the two surfaces coming together in a point at this location. By this device we artificially create the sharp trailing edge we must have to satisfy the condition  $\Gamma_1 = -\Gamma_k$ .  $\Gamma_1$  and  $\Gamma_k$  of course are then placed at this fictitious trailing edge point. Next we compute the pressures as a function of  $x$  (to  $x = c$  only) in the conventional manner and then employ (34) to obtain the lift and (35) to obtain the form drag. In essence then, we apply the pressures computed with the perturbed shape (geometric plus displacement thickness,  $\delta^*$ ) to the actual physical airfoil shape at the same chordwise station. There is of course some error involved in this procedure because the shape of the pseudo-body aft of  $x = c$  may cause the inviscid flow to decelerate somewhat more quickly than is actually the case and some of this effect will be apparent in the pressures calculated for points just upstream of the corners. In other words, it will tend to make the computed drag somewhat lower than it actually is. This effect is not serious as long as the wake is small compared with the airfoil thickness. Unfortunately, the model is not readily amenable to more sophisticated treatments of the wake effect\* and the problem of accuracy is probably best

---

\* Other schemes for treating the trailing edge condition which come to mind include (1) replacing the Kutta condition by the requirement that the vorticity shed into the wake from upper and lower surfaces be the same (2) extending the airfoil as a thin sheet along the wake centerline with the local curvature determined from considerations of the velocity distribution in the

---

\* CONTINUED

wake according to viscous theory and the fact that the change in the fluid momentum in the y-direction in the upwash and downwash (aft of the airfoil) fields must equal the airfoil lift. One may also consider the superposition of a vortex distribution related in some predetermined way to that found above which will make the integral of the pressures over the pseudo-airfoil in the drag direction equal to zero.

Callaghan and Beatty (Ref. 69) in their treatment represent the displacement thickness with a source near the trailing edge. The pseudo-body then never closes and the source strength must be chosen to yield the proper wake thickness.

The very interesting approach used by Bhateley and McWhirter (Ref. 80) to treat this problem is in some respects quite similar. They do not employ the Kutta condition and, in addition, locate a source of undetermined strength within the airfoil. They must therefore supply two additional boundary conditions to obtain a solvable system. These are obtained by specifying two pseudo airfoil surface points just behind the trailing edge on both the upper and lower surfaces. The condition of continued tangential flow to the last surface element is satisfied at these pseudo boundary points. This type of analysis permits them to treat with good accuracy airfoils with slightly blunted trailing edges. These configurations are currently of increasing popularity because they can yield higher lift coefficients for the same angle of attack than the same airfoils with sharp trailing edges.

Bhateley and McWhirter further apply this concept to airfoils with partially separated boundary layers. Thus they are able to predict the variations in  $C_L$ ,  $C_D$ , and  $C_m$  with  $\alpha$  up to  $\alpha_{STALL}$  quite accurately. In their method the conditions of tangential flow are satisfied only on that part of the body having attached flow. If the boundary layer calculations indicate that the lower surface flow will separate, this fact is ignored and the displacement thickness is computed in the usual fashion. The two additional corner points are generated: one very close to the separation point on the upper surface and the other at the trailing edge on the lower surface of the pseudo body. The condition of continued tangency of the lower surface flow at the additional boundary point is satisfied. In specifying the additional boundary point aft of the separation point on the upper surface the user must select, based on experience, other analysis, etc., the direction of the flow leaving the upper surface. No pressures are calculated in the separated flow region. The pressure distribution downstream of the separation point is assumed constant and equal to that value of the pressure obtained by linear interpolation of the last two boundary point pressures prior to the separation point.

---

\* CONTINUED

In this treatment, the separation point on the upper surface is considered to be the upper trailing edge point of a blunt trailing edge airfoil. It is easily seen, then, that the trailing edge thickness (and the source strength responsible for it) of the pseudo airfoil grows rapidly as  $\alpha_{\text{STALL}}$  is approached. The pseudo airfoil begins to take on the appearance of a blunt body. Blunt bodies, of course, are known to have relatively high drag and relatively low lift so that it is easily seen how this approach can be used to account for the change in airfoil behavior from a low drag, high lift, relatively wake-free body at moderate angles of attack to a high drag, low lift, large wake body at high angles of attack.

The success of such a technique is, of course, highly dependent upon the accuracy with which one can predict the location of the boundary layer separation point on the airfoil. For this purpose Bhateley and McWhirter use a finite difference method in place of the momentum integral method discussed here. Studies conducted by colleagues of the present authors indicate that the momentum integral technique predicts increasingly more rearward separation locations (compared with predictions of the finite difference technique) as the angle of attack increases. Thus the lift predictions will be too large and the drag predictions too small at higher angles of attack compared with those obtained using a finite difference approach. On the other hand, the finite difference technique was found to require 20 times the computing time needed by the momentum integral technique.

The considerable success enjoyed by Bhateley and McWhirter in predicting the pressure distributions on airfoils at high angles of attack however seems to be more a function of the boundary layer routine they use than because they use an embedded source and two off-body tangency conditions. One can obtain similar results, for example, by replacing the Kutta condition by a requirement that the pressures at the upper surface and lower surface separation points and all points inbetween over the aft portion of the airfoil be the same, provided one does not then wish to construct a new pseudo body and compute from this a new potential solution. The source and two off-body tangency conditions are needed to determine the shape of the pseudo body aft of the separation point and thus to determine the potential flow about the pseudo body.

For airfoils with sharp trailing edges (and no boundary layer) Bhateley and McWhirter chose the Kutta condition in one of two forms: the flow  $10^{-5}$  chord lengths behind the trailing edge is constrained to move in a direction which is an average of the airfoil surface slopes at the trailing edge or the net vorticity at the trailing edge is required to be zero.

handled for the present in a semi-empirical fashion, with the correction expected to be a function of angle of attack.

There is in addition to the form drag what is termed skin friction or shear drag, drag that is due directly to the sliding of the air over the airfoil surface. For well-streamlined shapes this accounts for perhaps 80% of the total drag. Reverting to our concept of momentum transport across layers of fluid as the drag mechanism, it is reasonable to postulate that the skin friction drag is proportional to the change in fluid velocity with distance from the surface. This may be expressed mathematically as

$$D_f = \mu A \left. \frac{du}{dy} \right|_{y=0} \quad (36)$$

where  $A$  is the surface area and  $\mu$  is the coefficient of viscosity, a property of the particular fluid which usually varies with temperature. A very accurate relation for air is that due to Sutherland:

$$\mu = \mu_{ref} \left( \frac{T}{T_{ref}} \right)^{3/2} \frac{T_{ref} + 198}{T + 198} \quad (37)$$

The values for temperature,  $T$ , should be given in  $^{\circ}R$ . For  $T_{ref} = 519^{\circ}R$ ,  $\mu_{ref} = 373 \times 10^{-9}$  slugs/ft-secs.

---

\* CONTINUED

The potential solution employed by Bateley and McWhirter represents the airfoil surface by straight line segments and the vorticity distribution by linear variations between values at the corner points. This seems a bit strange in view of Hess's comment in Reference 82.

The troublesome trailing edge condition has also been the subject of several recent, extended, theoretical investigations. Spence (Ref. 70) presents a very graphic explanation of the problems and argues that because of the presence of a viscous wake the circulation around the airfoil should be multiplied by the factor

$$1 - \left( \frac{C_D}{4\pi} \right) \left( \ln \frac{4}{C_D} \right) \quad .$$

For a typical two-dimensional value of  $C_D \approx 0.01$  this factor is about .995. Riley and Stewartson (Ref. 71) in examining the flow in the neighborhood of airfoil trailing edges conclude that if the angle of attack is small and the trailing edge angle is less than  $1/Re^{1/4}$  then the flow will be maintained, without separation, up to the trailing edge. This is obviously a necessary condition for treating the effects of the viscous wake in a more general way since it establishes the point at which the flow leaves the surface although not necessarily the angle at which it leaves or its radius of curvature.

It is apparent from an examination of (36) that the problem in evaluating  $D_f$  (and  $\delta^*$  for that matter) comes in finding

$$\left. \frac{du}{dy} \right|_{y=0}$$

as a function of position on the airfoil surface. One would like to integrate the local value of  $D_f$  over the total wetted surface to find the total skin friction drag. Several things complicate the problem:

1. The thickness of the boundary layer can be shown to depend upon the local Reynolds number,  $\rho V_x / \mu$ .
2. The character of the boundary layer—whether it flows in well-defined layers or lamina, or whether it flows in a more disorderly or turbulent fashion which one can only represent rather approximately—is also dependent upon the local Reynolds number and the condition of the surface. Further, the boundary layer may change from laminar to turbulent during the course of its travel over the airfoil.
3. The thickness of either a laminar or turbulent boundary layer depends upon the nature of the pressures outside the boundary layer. If the pressures are such that the flow tends to accelerate (high pressure upstream and lower pressure downstream) then the boundary layer grows very slowly. If the reverse is true (decelerating flow) the boundary layer grows rapidly. It may even separate from the surface entirely.

The analysis of two-dimensional boundary layer flows to find  $\delta^*(x)$  and  $C_f(x)$  where  $C_f = D_f / \frac{1}{2} \rho V^2 (\text{unit area})$  is considerably simplified if we are willing to assume (1) the flow is incompressible, (2) there is no heat transfer from the surface to the flow, (3) the boundary layer is laminar, and (4) the pressure across the boundary layer is constant. With these assumptions the mass conservation Equation (1) has the same form as in the inviscid analysis. The x-momentum Equation (5) has a viscous stress term

$$\mu \frac{\partial^2 u}{\partial y^2}$$

added to it while the y-momentum equation reduces to  $\partial P / \partial y = 0$ . Thus the equations for this analysis are written

$$\frac{\partial u}{\partial x} + \frac{\partial v}{\partial y} = 0 \tag{38}$$

$$u \frac{\partial u}{\partial x} + v \frac{\partial u}{\partial y} = - \frac{1}{\rho} \frac{\partial P}{\partial x} + \nu \frac{\partial^2 u}{\partial y^2} .$$

Since  $\partial P / \partial y = 0$ , we can use the relationship between pressure and velocity in the free stream just outside the boundary layer to express

$$- \frac{1}{\rho} \frac{\partial P}{\partial x} \text{ as } u_e \frac{\partial u_e}{\partial x} .$$

See for example Equation (30). With this, (38) becomes

$$\frac{\partial u}{\partial x} + \frac{\partial v}{\partial y} = 0 \quad (39)$$

$$u \frac{\partial u}{\partial x} + v \frac{\partial u}{\partial y} = u_e \frac{\partial u_e}{\partial x} + v \frac{\partial^2 u}{\partial y^2} .$$

Now if we multiply the first equation of (39) by  $(u_e - u)$  and subtract from this the second equation we obtain

$$\frac{\partial}{\partial x} [u(u_e - u)] + \frac{\partial}{\partial y} [v(u_e - u)] + (u_e - u) \frac{\partial u_e}{\partial x} + v \frac{\partial u_e}{\partial y} = -v \frac{\partial^2 u}{\partial y^2} . \quad (40)$$

The term  $\partial u_e / \partial y = 0$  because  $u_e$  does not change in the  $y$ -direction in the boundary layer. If we now define

$$\begin{aligned} \delta^* &= \int_0^\delta \left(1 - \frac{u}{u_e}\right) dy , \\ \theta &= \int_0^\delta \frac{u}{u_e} \left(1 - \frac{u}{u_e}\right) dy \end{aligned} \quad (41)$$

and rewrite (40) as

$$\begin{aligned} &\frac{\partial}{\partial x} \left[ u_e^2 \left( \frac{u}{u_e} \left[ 1 - \frac{u}{u_e} \right] \right) \right] + \frac{\partial}{\partial y} [v (u_e - u)] + u_e \left( 1 - \frac{u}{u_e} \right) \frac{\partial u_e}{\partial x} = -v \frac{\partial^2 u}{\partial y^2} \\ \text{or} \quad &\frac{\partial}{\partial x} \left[ u_e^2 \frac{\partial \theta}{\partial y} \right] + \frac{\partial}{\partial y} [v (u_e - u)] + u_e \frac{\partial \delta^*}{\partial y} \frac{\partial u_e}{\partial x} = -v \frac{\partial^2 u}{\partial y^2} , \end{aligned} \quad (42)$$

we can integrate with respect to  $y$  to obtain

$$\frac{\partial}{\partial x} \left[ u_e^2 \theta \right] + \int_0^\delta \left\{ \frac{\partial}{\partial y} [v (u_e - u)] \right\} dy + u_e \delta^* \frac{\partial u_e}{\partial x} = v \frac{\partial u}{\partial y} \Big|_{y=0} . \quad (43)$$

Note that

$$\int_0^\delta v \frac{\partial^2 u}{\partial y^2} dy = v \left[ \frac{\partial u}{\partial y} \Big|_{y=\delta} - \frac{\partial u}{\partial y} \Big|_{y=0} \right]$$

and by the first equation of (39)

$$\begin{aligned}
\int_0^\delta \left\{ \frac{\partial}{\partial y} \left[ v (u_e - u) \right] \right\} dy &= \int_0^\delta \left\{ - (u_e - u) \frac{\partial u}{\partial x} + v \frac{\partial u}{\partial y} - v \frac{\partial u}{\partial y} \right\} dy \\
&= \int_0^\delta \left\{ - (u_e - u) \frac{\partial u}{\partial x} + \frac{\partial u}{\partial y} \int_0^\delta \frac{\partial u}{\partial x} dy \right\} dy \\
&= \int_0^\delta \left\{ - (u_e - u) \frac{\partial u}{\partial x} \right\} dy + \int_0^\delta (u_e - u) \frac{\partial u}{\partial x} dy = 0.
\end{aligned}$$

Thus (43) is

$$\frac{d\theta}{dx} + \frac{2\theta + \delta^*}{u_e} \frac{du_e}{dx} = \frac{v}{u_e^2} \frac{\partial u}{\partial y} \Big|_{y=0} \quad (44)$$

We should note that (44) is only an approximate description of boundary layer flow because the process of integration used to obtain (43) in effect smooths out local departures from mean values. Further, although we intuitively understand what we mean by the outer edge of the boundary layer, the fact is we have never defined this value of  $y$  precisely. The approximate method, however, gives results which are within a few percent of those obtained with exact solutions in the few cases where the latter are known. For this reason and the ease with which it is applied to airfoil-like bodies, we shall find this approximate technique extremely useful. Empirical corrections to improve the agreement with experiment can be applied at the conclusion of the calculation if desired.

To complete the solution of (44), that is to find  $\delta^*(x)$  and  $\mu \frac{\partial u}{\partial y} \Big|_{y=0} (x)$  which we need to calculate the form drag and the skin friction drag respectively, we need an expression for  $u(y)$ . We shall assume, following Pohlhausen, that we can represent this function by the polynomial

$$\frac{u}{u_e} = A\eta + B\eta^2 + C\eta^3 + D\eta^4 \quad (45)$$

where  $\eta = y/\delta$ . We choose this polynomial because it is the lowest order polynomial which can represent the essential character of what we know of boundary layer flow and is the highest order polynomial for which we can easily evaluate the constants. The constants are found from the boundary conditions:

$$\begin{aligned}
\text{at } y = 0, \quad u = 0; \quad \frac{dp}{dx} = -\rho u_e \frac{du_e}{dx} \\
y = \delta, \quad u = u_e; \quad \frac{\partial u}{\partial y} = 0; \quad \frac{\partial^2 u}{\partial y^2} = 0 \quad .
\end{aligned} \quad (46)$$

The result is that

$$\begin{aligned}
A = 2 + \frac{1}{6} \frac{\delta^2}{v} \frac{du_e}{dx}; \quad B = -\frac{1}{2} \frac{\delta^2}{v} \frac{du_e}{dx} \\
C = -2 + \frac{1}{2} \frac{\delta^2}{v} \frac{du_e}{dx}; \quad D = 1 - \frac{1}{6} \frac{\delta^2}{v} \frac{du_e}{dx} \quad .
\end{aligned} \quad (47)$$

Substitution of (47) into (45) yields

$$\frac{u}{u_e} = 2\eta - 2\eta^3 + \eta^4 + \frac{1}{6} \frac{\delta^2}{\nu} \frac{du_e}{dx} \left( \eta - 3\eta^2 + 3\eta^3 - \eta^4 \right)$$

or

$$\frac{u}{u_e} = \left[ 2 + \frac{1}{6} \frac{\delta^2}{\nu} \frac{du_e}{dx} \right] \eta - \frac{1}{2} \frac{\delta^2}{\nu} \frac{du_e}{dx} \eta^2 - \left[ 2 - \frac{1}{2} \frac{\delta^2}{\nu} \frac{du_e}{dx} \right] \eta^3 + \left[ 1 - \frac{1}{6} \frac{\delta^2}{\nu} \frac{du_e}{dx} \right] \eta^4. \quad (48)$$

$du_e/dx$  of course is found from the potential, or inviscid, solution. Equation (48) may be substituted into (41) to obtain

$$\delta^* = \delta \left[ \frac{3}{10} - \frac{1}{120} \frac{\delta^2}{\nu} \frac{du_e}{dx} \right] \quad (49)$$

$$\theta = \delta \left[ \frac{37}{315} - \frac{1}{945} \frac{\delta^2}{\nu} \frac{du_e}{dx} - \frac{1}{9072} \left( \frac{\delta^2}{\nu} \frac{du_e}{dx} \right)^2 \right].$$

The local shearing stress on the surface,  $\mu \frac{\partial u}{\partial y}|_{y=0}$ , is simply

$$\frac{\mu u_e}{\delta} \left[ 2 + \frac{1}{6} \frac{\delta^2}{\nu} \frac{du_e}{dx} \right]. \quad (50)$$

To complete the numerical evaluation of  $\delta^*$  and the shearing stress,  $\tau_{y=0}$ , we substitute (49) and (50) into (44) to obtain

$$\begin{aligned} & \frac{37}{315} \frac{d\delta}{dx} - \frac{3\delta^2}{945 \nu} \frac{du_e}{dx} \frac{d\delta}{dx} - \frac{5\delta^4}{9072 \nu^2} \left( \frac{du_e}{dx} \right)^2 \frac{d\delta}{dx} - \frac{1}{945} \frac{\delta^2}{\nu} \frac{d^2 u_e}{dx^2} - \frac{2\delta^4}{9072 \nu^2} \frac{du_e}{dx} \frac{d^2 u_e}{dx^2} \\ & + \frac{2\delta}{u_e} \left[ \frac{37}{315} - \frac{1}{945} \frac{\delta^2}{\nu} \frac{du_e}{dx} - \frac{1}{9072} \left( \frac{\delta^2}{\nu} \frac{du_e}{dx} \right)^2 \right] \frac{du_e}{dx} + \frac{\delta}{u_e} \left[ \frac{3}{10} - \frac{1}{120} \frac{\delta^2}{\nu} \frac{du_e}{dx} \right] \frac{du_e}{dx} \\ & = \frac{\mu}{\rho u_e \delta} \left[ 2 + \frac{1}{6} \frac{\delta^2}{\nu} \frac{du_e}{dx} \right] \end{aligned}$$

or

$$\begin{aligned} & \left[ \frac{37}{315} - \frac{3\delta^2}{945 \nu} \frac{du_e}{dx} - \frac{5\delta^4}{9072 \nu^2} \left( \frac{du_e}{dx} \right)^2 \right] \frac{d\delta}{dx} - \frac{1}{945} \frac{\delta^2}{\nu} \frac{d^2 u_e}{dx^2} - \frac{2\delta^4}{9072 \nu^2} \frac{du_e}{dx} \frac{d^2 u_e}{dx^2} \\ & + \frac{2\delta}{u_e} \left[ \frac{37}{315} - \frac{1}{945} \frac{\delta^2}{\nu} \frac{du_e}{dx} - \frac{1}{9072} \left( \frac{\delta^2}{\nu} \frac{du_e}{dx} \right)^2 \right] \frac{du_e}{dx} + \frac{\delta}{u_e} \left[ \frac{3}{10} - \frac{1}{120} \frac{\delta^2}{\nu} \frac{du_e}{dx} \right] \frac{du_e}{dx} \\ & = \frac{\mu}{\rho u_e \delta} \left[ 2 + \frac{1}{6} \frac{\delta^2}{\nu} \frac{du_e}{dx} \right]. \quad (51) \end{aligned}$$



Equation (51) is a highly non-linear first-order ordinary differential equation with  $\delta$  the dependent variable and  $x$  the independent variable. Note that  $u_e$ ,  $du_e/dx$ ,  $d^2u_e/dx^2$  must all be supplied as data from the external, or potential, solution and the value of each of these quantities depends upon the particular value of  $x$ . The equation may be solved by predicting  $d\delta/dx$ , solving the resultant polynomial for  $\delta$  and then checking to be sure that the predicted value of  $d\delta/dx$  is sufficiently close to that found. If not, the process is repeated until sufficient accuracy is achieved. In the interests of speed and accuracy the solution is best obtained on a digital computer. The solution will be in the form of  $\delta$  for each value of  $x$  along the chord for each surface. By the use of the first equation of (49) and by (50) one can find then  $\delta^*(x)$  and  $\tau_{y=0}(x)$ . Schlichting (Ref. 65) gives the more common evaluation of (51).

As a check on the solution technique one can look at (51) as applied to a flat plate at zero angle of attack. Under these circumstances (51) reduces to

$$\frac{37}{315} \frac{d\delta}{dx} = \frac{2\mu}{\rho u_e \delta} \quad (52)$$

This has the solution

$$\frac{\delta^2}{2} = \frac{630}{37} \frac{x\mu}{\rho u_e}$$

or

$$\delta = \frac{5.84 x}{\sqrt{\frac{\rho u_e x}{\mu}}} = \frac{5.84 x}{\sqrt{Re_x}} \quad (53)$$

This overestimates the value of  $\delta$  by about 1.8% compared with more exact solutions.  $\delta^*$  is therefore also high by about 1.2%.

The effect of  $du_e/dx$  is to reduce  $\delta$  for a given  $x$  when  $du_e/dx$  is positive and increase it when  $du_e/dx$  is negative. Both types of behavior will be present on airfoils. From the leading edge to the crest on the upper surface of the airfoil  $du_e/dx$  will be positive. From the crest aft,  $du_e/dx$  will be negative. The boundary layer will therefore be very thin up to the crest and will begin to grow rapidly downstream of that point.

If the  $du_e/dx$  is sufficiently negative and persists for a sufficient extent of  $x$  it will cause the boundary layer to leave the surface. This condition is manifest to the pilot as a stall or loss of lift accompanied by a sharp increase in drag. Usually, the flight Reynolds number, airfoil geometry, and surface condition are such that the boundary layer becomes turbulent before separation occurs so that we will postpone our discussion of how to calculate the aerodynamic characteristics near maximum lift.

Assuming we now have the value of  $\delta^*(x)$  as calculated above, how do we use it to correct the surface pressure values obtained from the inviscid computation? By adding  $\delta^*$  upper surface to the actual upper surface ordinates and  $\delta^*$  lower surface to the actual lower surface ordinates we obtain a new fatter airfoil. We submit these new ordinates to the inviscid computation procedure and obtain a new pressure distribution. If  $du_e/dx$

is substantially different from what we used to compute  $\delta^*(x)$  we must use the new values of  $du_e/dx$  in a predictor-corrector scheme to compute a new  $\delta^*(x)$ . The process must be repeated until the values of  $du_e/dx$  obtained from the inviscid computation agree with what we used in computing  $\delta^*(x)$ . Generally, as speed and aircraft size increase, fewer iterations will be required to achieve satisfactory agreement because the boundary layer will be proportionately thinner.

As we have noted there are a number of things which can cause a laminar boundary layer to become turbulent: existence of a large Reynolds number, surface roughness, and to some degree the sign on  $du_e/dx$ . Because wings on light aircraft will usually experience a turbulent boundary layer on at least some portion of their surfaces it is necessary to examine how the procedure to calculate  $\delta^*$  and  $\tau_{y=0}$  are altered for this condition and how one determines when to change from laminar to a turbulent calculation. It should be recognized at the outset that turbulent motion is a very complex phenomenon, never successfully treated in a completely analytical fashion. It is necessary therefore to employ rather crude analytical models or semi-empirical correlations in order to retain the usual equations of motion (38) as the describing equations of the fluid behavior. Following this approach we observe that Equation (44) may also be used to represent turbulent boundary layer flow provided we use a suitable relation for skin friction in place of

$$\mu \left. \frac{\partial u}{\partial y} \right|_{y=0}$$

and a consistent expression for  $u(y)$ . One empirical formula for  $\tau_{y=0}$  which finds considerable use is that due to Ludwig and Tillmann (as quoted in Ref. 65):

$$\tau_{y=0} = \frac{\rho u_e^2 \left( 0.123 \times 10^{-0.678} \frac{\delta^*}{\theta} \right)}{\left( \frac{u_e \theta}{\nu} \right)^{0.268}} . \quad (54)$$

The relation for the velocity profile commonly used in related studies is

$$\frac{u}{u_e} = \left( \frac{y}{\delta} \right)^{\frac{1}{n}} , \quad (55)$$

where  $n$  is between 4 and 6, but is usually taken to be the latter value.

The use of (54) in (44) still leaves the equation non-integrable because an explicit relation between  $\delta^*$  and  $\theta$  has not been given. This could be developed from the definitions of  $\theta$  and  $\delta^*$ , (41) and (55), or the problem skirted by proceeding as follows: Multiply the second equation of (39) by  $u$  and then integrate with respect to  $y$ . We obtain what might be termed an energy integral equation

$$\frac{1}{u_e^3} \frac{d}{dx} \left[ u_e^3 \delta^{**} \right] = \int_0^{\delta} \frac{\tau_{y=0}}{\rho u_e^2} \frac{\partial}{\partial y} \left( \frac{u}{u_e} \right) dy , \quad (56)$$

analogous to the momentum integral Equation (44). The name of course refers to the fact that momentum times velocity has the units of energy. Note that

$$\delta^{**} = \int_0^{\delta} \frac{u}{u_e} \left( 1 - \frac{u^2}{u_e^2} \right) dy \quad . \quad (57)$$

It has been found experimentally that there exists a unique relationship between  $\delta^*/\theta$  and  $\delta^{**}/\theta$  which can be expressed as

$$\frac{\delta^{**}}{\theta} = \frac{1.269 \frac{\delta^*}{\theta}}{\frac{\delta^*}{\theta} - 0.379} \quad . \quad (58)$$

Experiments have also led to the conclusion that

$$\int_0^{\delta} \frac{\tau_{y=0}}{\rho u_e^2} \frac{\partial}{\partial y} \left( \frac{u}{u_e} \right) dy = \frac{0.56 \times 10^{-2}}{\left( \frac{u_e \theta}{\nu} \right)^{1/6}} \quad . \quad (59)$$

Substitution of these experimental results, (58) and (59), into (56) yields

$$\frac{1}{u_e^3} \frac{d}{dx} \left[ \frac{1.269 u_e^3 \frac{\delta^*}{\theta}}{\frac{\delta^*}{\theta} - 0.379} \right] = \frac{0.56 \times 10^{-2}}{\left( \frac{u_e \theta}{\nu} \right)^{1/6}} \quad (60)$$

while (54) substituted into (44) gives

$$\frac{d\theta}{dx} + \frac{2\theta + \delta^*}{u_e} \frac{du_e}{dx} = \frac{0.123 \times 10^{-0.678} \frac{\delta^*}{\theta}}{\left( \frac{u_e \theta}{\nu} \right)^{0.268}} \quad . \quad (61)$$

Simultaneous solutions of (60) and (61) will yield  $\delta^*(x)$  and  $\theta(x)$ . When these results are substituted into (54) one has  $\tau_{y=0}(x)$ . The skin friction drag is then computed by integrating  $\tau_{y=0}(x)$  over both surfaces:

$$D_f = \left[ \int_0^c \tau_{y=0}(x) dx \right]_{\text{upper surface}} + \left[ \int_0^c \tau_{y=0}(x) dx \right]_{\text{lower surface}} \quad . \quad (62)$$

The dimensions of  $D_f$  are force per unit span. As noted previously, at low angles of attack, the drag as computed by (62) should be about 4 times that found by (35). As  $\alpha$  increases, the form drag tends to predominate. The total drag of course is the sum of the drags calculated from (35) and (62).

The correct expression for  $\tau_{y=0}$  in (62) depends, as has been indicated, on whether the boundary layer is laminar or turbulent or some combination thereof. Generally one would expect that the boundary layer is laminar over the forward

portion of the wing and then changes—goes through what is called transition—to a turbulent boundary layer. Thus, Equation (50) would give the correct expression for  $\tau_{y=0}$  upstream of the transition point and (54) gives the correct expression for  $\tau_{y=0}$  downstream of this point. Since the boundary layer already has a finite thickness at the transition point, one chooses as a starting point for the turbulent calculation that point which will give the same  $\delta$  at the transition point as the laminar solution beginning at the leading edge. The laminar values of  $\tau_{y=0}$  and  $\delta^*$  are used up to transition and the turbulent values downstream. They are approximately the same at transition.

The beginning of transition has been found to occur at a Reynolds number between  $3 \times 10^5$  and  $4 \times 10^6$ . This is a very substantial range. As a point of reference consider that the Reynolds number per foot of chord for a airplane flying at 200 ft/sec at sea level is  $1.275 \times 10^6$ . Transition could, according to this criterion, occur anywhere from 4" from the nose to 3 ft from the nose. Since the chord for most light aircraft is at least 4 ft, the boundary layer on the aft portion of the wing will always be turbulent. Whether the transition begins 4" from the nose or 3 ft from the nose depends upon such things as surface roughness, free stream turbulence, and  $du_e/dx$ . The latter influence, however, is the only one which can be determined *a priori*, that is, before the wing is built and flown under particular conditions. It is, therefore, the only one we will attempt to evaluate.

A laminar boundary layer is said to be unstable—that is, it tends to become turbulent—when a velocity disturbance in this boundary layer can grow. Tollmein was able to show that a necessary and sufficient condition for neutral stability of disturbances in laminar boundary layers is the existence of a point of inflection in the boundary layer's velocity profile,  $u(y)$ .

Using a sixth order polynomial to represent the velocity profile, Schlichting and Ulrich were able to plot a relationship between the value of  $u_e \delta^*/\nu$  for which an inflection point exists and  $\delta^2 du_e/\nu dx$ . With this plot one can take the values of  $\delta$ ,  $\delta^*$ ,  $u_e$ ,  $du_e/dx$ , and  $\nu$  and determine whether or not the boundary layer is unstable. The precise distance between the onset of transition and the point of neutral stability as determined above depends upon the rate of amplification of disturbances in the boundary layer and consequently upon  $du_e/dx$  in that region. It has been found that plotting experimental data on a graph where

$$\left( \frac{u_e \theta}{\nu} \right)_{\text{transition}} - \left( \frac{u_e \theta}{\nu} \right)_{\text{neutral stability}}$$

is the ordinate and

$$\frac{\int_{x_{n.s.}}^{x_{tr}} \frac{\theta^2}{\nu} \frac{du_e}{dx} dx}{x_{tr} - x_{n.s.}}$$

is the abscissa leads to excellent correlation of the data. For a laminar boundary layer we know  $\theta$ ,  $u_e$ ,  $du_e/dx$ , and  $(\theta^2/\nu)(du_e/dx)$  as functions of  $x$ . We also know  $(u_e\theta/\nu)_{n.s.}$  because we know the relationship between  $\theta$  and  $\delta^*$ . Marching downstream of the neutral stability point we can easily find a  $u_e\theta/\nu$  and an  $x_{tr} = x_{n.s.}$  for each point. The other data then permits us to locate a point on the graph for each value of  $x$ . The first point which falls on or above the data correlation is taken as the  $x$ -location for which transition has taken place.

In addition to the change in  $\delta^*$  and  $\tau_{y=0}$  as one goes from laminar to turbulent boundary layer another type of behavior associated with boundary layer flows which significantly affects the lift, drag and moment characteristics of the airfoil in boundary layer separation is usually identified by the disappearance of the local skin friction, i.e. when

$$\left. \frac{du}{dy} \right|_{y=0} = 0 .$$

The geometry of very thin airfoils is such that regions of laminar separation or separation followed by reattachment confined to the front half of the airfoil are possible at moderate angles of attack. However, light aircraft operating at moderate Mach numbers can be expected to employ airfoils of 12% or greater thickness for which this type of phenomenon is not to be expected. The separation characteristic of thick airfoils is a turbulent separation from the region of the trailing edge. Thus, if one terminates the calculation of  $\delta^*$  and  $\tau_{y=0}$  at that angle of attack for which  $\tau_{y=0} = 0$  over a significant portion of the airfoil, he is reasonably assured of having closely approached  $C_{Lmax}$ . This is about the most one could expect of the procedure outlined above.

Perhaps it would now be appropriate to review briefly and comment upon the procedure for estimating the aerodynamic characteristics of airfoils as developed up to this point.

1. We first locate the vortex filaments, taking care that we space them sufficiently close together to represent the surface accurately. This is particularly important in regions of high curvature and/or regions where the surface slope is significantly different from the free stream flow direction.

2. Equations (29) are then solved for a particular angle of attack to obtain the values of all  $\Gamma_N$ . These values are then substituted into (19) to obtain the net induced velocities and the surface pressures computed from (33).

3. The lift and drag are evaluated by (34) and (35). The drag at this point should be zero.

4.  $u_e(x)$  is evaluated from (32) for both surfaces. Data smoothing procedures are employed to insure that the results represent physical reality as closely as possible with as few inflection points as possible.  $du_e/dx$  and  $d^2u_e/dx^2$  are then calculated numerically.

5.  $\delta^*(x)$  for both surfaces is then found from a solution to (57).  $\delta^*(x)$  is obtained from (49) and  $\tau_{y=0}$  from (50).

6. The location of transition is identified and the turbulent boundary layer computation begun using (60) and (61) and then (54). At the conclusion of this process one has complete values of  $\delta^*(x)$  and  $\tau_{y=0}(x)$  for both surfaces.

7.  $\delta^*(x)$  is then added to the physical ordinates of the airfoil along with artificial trailing edge found by extending the chord

$$\delta^*(c) \left/ \frac{dy}{dx} \right|_{x=c} .$$

8. The previous seven steps are then repeated for the new ordinates.

9. The new value of  $du_e/dx$  is compared with the value obtained from step 4. If they differ by more than a few percent, we modify our estimates of  $\delta^*(x)$  according whether  $du_e/dx$  seems to favor larger or smaller values of  $\delta^*$ .

10. The process is repeated until the final value of  $du_e/dx$  would give the same  $\delta^*(x)$  as used in the inviscid calculation. Obviously, care must be taken to insure that adequate precision is maintained during such an extensive series of computations, else the resulting numbers are meaningless.

11. The procedure is valid for a Mach number of zero. Since most light aircraft operate at Mach numbers not far above zero, the simple Prandtl-Glauert correction to the pressures for Mach number effects is usually quite adequate:

$$P_x = P_\infty + \frac{(P_x - P_\infty)M=0}{\sqrt{1 - M_\infty^2}} . \quad (63)$$

12. The corrected pressure is then applied to the physical boundaries of the airfoil to obtain the lift and form drag according to (34) and (35). The skin friction drag is computed with (62) using the most updated value of  $\tau_{y=0}(x)$ .

13. The pitching moment about the leading edge can be computed by integrating the product of the pressure forces and the distance from the nose

$$M = \oint P(x) x \cos \left[ \tan^{-1} \frac{dy}{dx} \Big|_x \right] dx + \oint P(x) y \sin \left[ \tan^{-1} \frac{dy}{dx} \Big|_x \right] dx. \quad (64)$$

There will also be a small contribution to the moment from the skin friction forces but these are (a) generally in the chordwise direction and (b) the moment generated by the friction on the upper surface opposes that generated by the friction on the lower surface. As a result the net contribution is generally small enough to neglect.

## EXTENSION TO THREE DIMENSIONS: THE FINITE WING

The theoretical procedure described above provides a means for estimating the aerodynamic characteristics of a section of an infinite wing. Real wings, of course, have to have ends and frequently, for reasons that will become apparent as the discussion proceeds, are tapered, twisted, and change airfoil sections with changes in span locations.

Some means must therefore be found to account for such influences in determining the aerodynamic characteristics of complete wings. The principal considerations in wing design are (1) low drag for good performance, (2) light weight with adequate strength for good payload capacity, and (3) fairly simple structure with few changes in shape for low cost in manufacturing. We shall be concerned here with means for calculating the lift, drag and moments of wings which we will assume satisfy the latter two criteria. We will also limit our consideration to unswept wings of moderate-to-high span-to-chord (aspect) ratio. Further, in order to keep the computation to a reasonable length we would like the technique we employ to use as much of the previous result as possible. In order to do so we ask the question, what are the effects of ends, twist, and taper? If an untapered wing has the same airfoil over its entire span then it would seem reasonable to conclude that, at least near the center, twisting the wing has the effect of changing the local angle of attack. It will be recalled that the two-dimensional calculation is carried out for specific angle of attack. Generally, both lift and drag increase with increasing angle of attack. Twist will therefore change the local lift and drag values.

The existence of a wing tip permits high pressure air from the lower surface of the wing to flow up around the tip to the low pressure regions on the upper surface. The result is that the lift in the tip regions is reduced and a vortex filament is created. This filament begins near the tip and extends downstream in a plane parallel to the fuselage. The fact that in theory vortices must be closed or infinite led to the thought that since a vortex is actually observed extending rearward from the tip regions of lifting wings, some sort of vortex system must also extend from tip to tip. If this is true, perhaps one could actually represent such a wing by a series of "horseshoe"-like vortices which "roll up" in the tip regions to form a single vortex extending to infinity. A series of horseshoe vortices with different strengths would enable one to represent a variety of lift distributions on a wing. If the wing has a moderate-to-high aspect ratio, little or no sweep, and moderate dihedral then it would seem that one could take the various vortex filaments as being co-linear with little error. Such an assumption, the so-called lifting-line theory of Prandtl, obviously leads to fewer mathematical difficulties than having to consider a chord-wise lattice of vortices or a lifting surface. Because most light aircraft wings meet the criteria for applicability of the lifting line theory and because we intend to use the theory only to modify our 2-dimensional results, we expect the procedure to give us accurate results.

It will be observed that a horseshoe system with the trailing vortex's velocity moving inboard over the upper surface and outboard under the lower surface induces an upwash component ahead of the wing and a downwash component behind the wing. This combination of upwash ahead and downwash

behind the wing is, in effect, a change in local angle of attack in so far as the flow facing a section of wing is concerned. The finite span of the wing can therefore be thought of as producing the same effect as does geometric twist. For consistency it would seem to be convenient to attempt to represent the effects of taper also as a change in local angle of attack. If we are successful in this endeavor, we have reduced the entire procedure for calculating the lift, drag, and moment characteristics of complete wings to one of (1) finding the effective local angle of attack by the lifting line theory, (2) determining the two-dimensional or section characteristics corresponding to these effective local values of  $\alpha$  by reference to equations or tables computed by the methods discussed above, and then (3) integrating these section characteristics over the entire wing area to average the values.

In current designs, wings are not free entities but are attached to large structures such as fuselages. It is important, therefore, to model the fuselage-wing junction region in such a manner that the effects of its presence can be handled within the framework of a method to calculate finite wing characteristics. We do this by mathematically transforming this region of the fuselage into a part of the wing. Other examples of the use of mathematical transformations to simplify the analysis of complex problems are well known. Problems involving flow through pipes, structural analysis of tubes, etc. become much simpler when transformed from Cartesian or rectangular coordinates to cylindrical coordinates. Differential equations become algebraic when transformed from the time domain to the frequency domain. Complex shapes, such as airfoils, can be transformed into circles about which the flow behavior is well known. The flow at any point about an airfoil can then be found by locating the equivalent point on the circle.

Generally, in selecting a transformation we seek one which either simplifies the mathematical representation of a physical situation or, as in the present case, distorts a complex shape into a simpler shape for which the physical phenomena are well understood and easily analyzed. We then go through an inverse transform to find how the well-understood behavior distorts in going back to the original physical situation. Devising a suitable transform is usually a trial and error process, guided by experience, skill, and to some extent, luck. Certain mathematical requirements must also be met, dependent upon the framework in which the transform is used. The transform used here was devised by H. Multhopp (Ref. 51).

The thought processes followed by Multhopp in devising the transform shown below for elliptical cross-section fuselages probably included these elements: Under the Joukowski transform,

$$\zeta = z + \frac{c^2}{z} ,$$

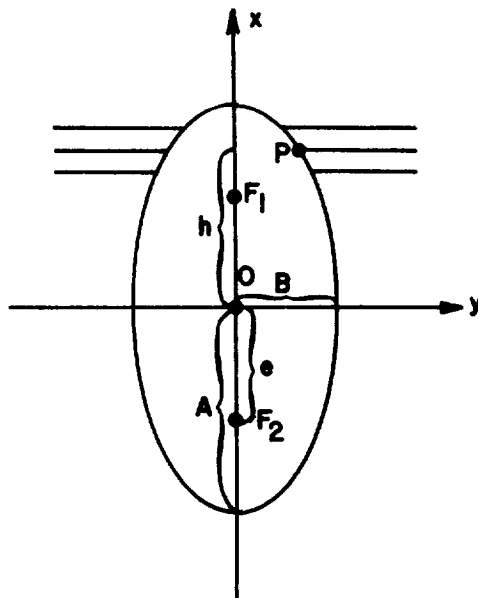
a circle in the  $z$ -plane with its center at the origin transforms to a flat plate along the  $\xi$ -axis in the  $\zeta$ -plane for positive values of  $c^2$ . If one takes  $c^2 = -1$ , then



$$\begin{aligned} \zeta &= \xi + i\eta = x + iy - \frac{1}{x + iy} \\ &= x + iy - \frac{x - iy}{x^2 + y^2} \\ &= x \left( 1 - \frac{1}{x^2 + y^2} \right) + iy \left( 1 + \frac{1}{x^2 + y^2} \right) \end{aligned}$$

and the circle (of radius 1.0) transforms into a flat plate along the  $\eta$ -axis in the  $\zeta$ -plane. From this result one concludes that a similar transform, suitably modified to account for elliptical fuselages and variable placement of the wing with respect to the origin, should produce the requisite figure.

Consider also the ellipse shown in the sketch below:



The properties of an ellipse are such that

$$A^2 - B^2 = e^2 ,$$

$$\frac{x^2}{A^2} + \frac{y^2}{B^2} = 1 ,$$

and

$$\overline{F_1P} + \overline{F_2P} = 2A .$$

From the last statement it follows that

$$2A = \sqrt{y^2 + (h - e)^2} + \sqrt{y^2 + (h + e)^2}$$

from which one can obtain

$$A^2 = y^2 + h^2 + e^2$$

or

$$B^2 = y^2 + h^2 \quad .$$

For points outside the ellipse we can generalize this by writing

$$a^2 = y^2 + h^2 + e^2$$

$$b^2 = y^2 + h^2$$

$$e^2 = a^2 - b^2 \quad .$$

It has been a feature of textbooks on hydrodynamics for some years to show that the equation for mapping an ellipse in the  $\omega$ -plane into a circle of radius  $\frac{1}{2}(A + B)$  in the  $z$ -plane is

$$z = \frac{1}{2} (\omega + \sqrt{\omega^2 - e^2}) \quad .$$

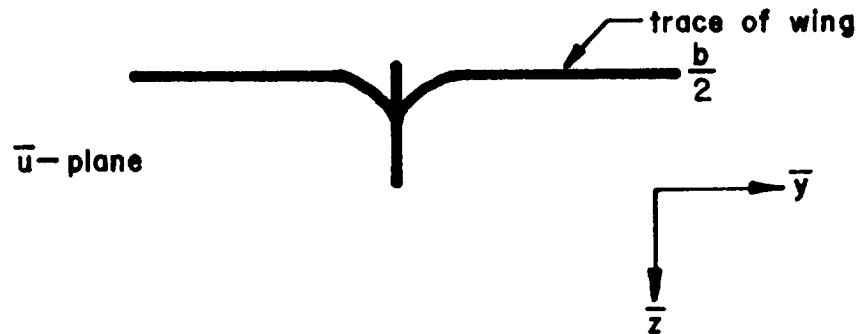
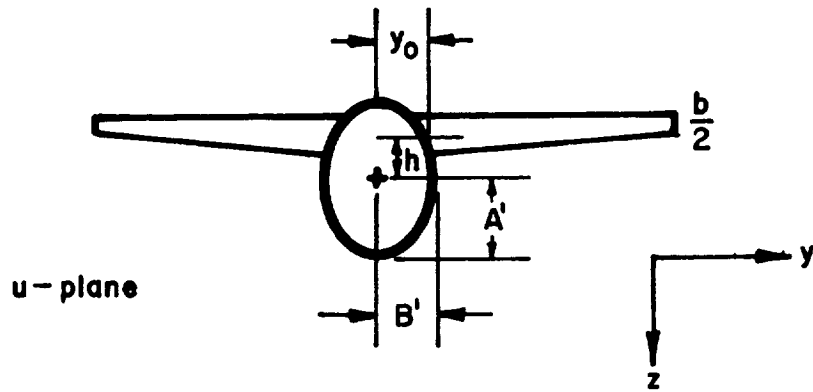
Thus to map the ellipse into a flat plate we write

$$\begin{aligned} \zeta &= z + \frac{\frac{1}{2}(A + B)^2}{z} = \frac{1}{2} (\omega + \sqrt{\omega^2 - e^2}) + \frac{\frac{1}{2}(A + B)^2 (\omega - \sqrt{\omega^2 - e^2})}{\omega^2 - \omega^2 + e^2} \\ &= \frac{(A^2 - B^2)}{2e^2} (\omega + \sqrt{\omega^2 - e^2}) + \frac{(A + B)^2}{2e^2} (\omega - \sqrt{\omega^2 - e^2}) \\ &= \left( \frac{A^2 - B^2}{2e^2} + \frac{A^2 + 2AB + B^2}{2e^2} \right) \omega + \left( \frac{A^2 - B^2}{2e^2} - \frac{A^2 + 2AB + B^2}{2e^2} \right) (\sqrt{\omega^2 - e^2}) \\ &= \left( \frac{2A^2 + 2AB}{2e^2} \right) \omega + \left( \frac{-2AB - B^2}{2e^2} \right) \sqrt{\omega^2 - e^2} \\ &= \frac{A}{A - B} \omega - \frac{B}{A - B} \sqrt{\omega^2 - e^2} \end{aligned}$$

which is the form employed by Multhopp.

The figure below shows how the trace of the wing-fuselage combination in the  $y$ - $z$  plane transforms from the physical  $u$ -plane to the  $\bar{u}$ -plane according to the relation

$$\bar{u} = \frac{1}{A' - B'} \left[ A' u - B' \sqrt{u^2 - A'^2 + B'^2} \right] \quad . \quad (65)$$



We use this transformation because it changes an elliptical fuselage into a thin vertical line which then provides no resistance to the vertical or induced component of flow over the wing. As we noted above, it is these vertical components which determine the magnitude of the local angle of attack. In essence, then, the transform distributes the flow components due to the fuselage over the span of the distorted wing. A similar transformation  $\bar{u} = u + R^2/u$  is used for circular fuselages. More complex shapes can be handled in the same fashion through the use of a suitable transform. By writing  $u$  and  $\bar{u}$  as complex variables

$$u = z + iy = a \cos \psi + ib \sin \psi \quad (66)$$

$$\bar{u}' = \bar{z} + i\bar{y}$$

and making the following definitions

$$a = \frac{1}{2} \left[ \sqrt{y^2 + (h - e')^2} + \sqrt{y^2 + (h + e')^2} \right]$$

$$b = \sqrt{a^2 - e'^2} \quad (67)$$

$$e = \sqrt{A'^2 - B'^2} = \sqrt{a^2 - b^2}$$

then

$$\begin{aligned}\bar{u} &= \frac{1}{A' - B'} \left[ A'u - B'\sqrt{u^2 - e'^2} \right] \\ &= \frac{1}{A' - B'} \left[ A'u - B'\sqrt{u^2 - a^2 + b^2} \right].\end{aligned}\quad (68)$$

But

$$\begin{aligned}u^2 - a^2 + b^2 &= a^2 \cos^2 \psi - b^2 \sin^2 \psi + 2abi \sin \psi \cos \psi - a^2 + b^2 \\ &= a^2(\cos^2 \psi - 1) - b^2(\sin^2 \psi - 1) + 2abi \sin \psi \cos \psi \\ &= a^2 \sin^2 \psi + b^2 \cos^2 \psi + 2abi \sin \psi \cos \psi \\ &= (b \cos \psi + ia \sin \psi)^2\end{aligned}\quad (69)$$

therefore,

$$\begin{aligned}\bar{u} &= \frac{1}{A' - B'} \left[ A'u - B'(b \cos \psi + ia \sin \psi) \right] \\ &= \frac{1}{A' - B'} \left[ A'z + iA'y - B'b \cos \psi - iB'a \sin \psi \right] \\ &= \frac{1}{A' - B'} \left[ (A'z - B'b \cos \psi) + i(A'y - B'a \sin \psi) \right] = \bar{z} + i\bar{y}.\end{aligned}\quad (70)$$

Comparing real and imaginary parts, one finds that

$$\bar{y} = \frac{1}{A' - B'} \left[ A'y - B'a \sin \psi \right].\quad (71)$$

Since

$$y = b \sin \psi = \sqrt{a^2 - e'^2} \sin \psi$$

then

$$\sin \psi = \frac{y}{\sqrt{a^2 - e'^2}}.$$

One may therefore write for  $\bar{y}$

$$\bar{y} = \frac{y}{A' - B'} \left[ A' - B' \frac{a}{\sqrt{a^2 - e'^2}} \right].\quad (72)$$

This relationship determines how points along the span in the physical or  $u$ -plane transform into the  $\bar{u}$ -plane.

We seek now to find how the flow in the neighborhood of the fuselage influences the flow direction and magnitude at each station along the wing's span. The real part of  $d\bar{u}/du$  in effect distributes the vertical components of the fuselage flow along the wing. If  $\alpha_B$  is the fuselage angle of attack in the  $\bar{u}$ -plane then the induced\* upwash along the span is given by

$$\Delta\alpha(y) = \left[ \frac{R}{du} \frac{d\bar{u}}{du} - 1 \right] \alpha_B \quad . \quad (73)$$

Because of the nature of the transformation  $\alpha_B$  will have the same value in either plane.

Now

$$\frac{d\bar{u}}{du} = \frac{1}{A' - B'} \left[ A' - \frac{B'u}{\sqrt{u^2 - e'^2}} \right] \quad . \quad (74)$$

The real part of  $d\bar{u}/du$  is, of course, its vertical component:

$$\begin{aligned} \frac{d\bar{u}}{du} &= \frac{1}{A' - B'} \left[ A' - B' \frac{a \cos \psi + ib \sin \psi}{b \cos \psi + ia \sin \psi} \right] \\ &= \frac{1}{A' - B'} \left[ A' - B' \frac{(a \cos \psi + ib \sin \psi)(b \cos \psi - ia \sin \psi)}{(b \cos \psi + ia \sin \psi)(b \cos \psi - ia \sin \psi)} \right] \\ \therefore \frac{R}{du} \frac{d\bar{u}}{du} &= \frac{1}{A' - B'} \left[ A' - B' \frac{ab(\cos^2 \psi + \sin^2 \psi)}{b^2 \cos^2 \psi + a^2 \sin^2 \psi} \right] \\ &= \frac{1}{A' - B'} \left[ A' - B' \frac{ab}{b^2 \left( 1 - \frac{y^2}{b^2} \right) + \frac{a^2 y^2}{b^2}} \right] \\ &= \frac{1}{A' - B'} \left[ A' - B' \frac{\frac{a}{\sqrt{a^2 - e'^2}}}{1 + \frac{e'^2 y^2}{(a^2 + e'^2)^2}} \right] \quad . \end{aligned} \quad (75)$$

If the wing is very thick at its junction with the fuselage then the actual  $\Delta\alpha$  obtained is less than that predicted by (73). It has been suggested that one should therefore reduce (73) by a factor  $T$ , taken as constant across the wing span, which is the ratio of the body cross-sectional area above and below the wing to the total frontal area of the body. The area of the

---

\* The amount by which the flow angularity exceeds that due to geometric inclination.

elliptical fuselage is of course  $\pi A'B'$ . The segment of the fuselage which represents a continuation of the wing has an area of approximately  $2y_0 t_{root}$ . Thus

$$T = 1 - \frac{2 y_0 t_{root}}{\pi A'B'} \quad (76)$$

and a more general expression for (73) is

$$\Delta\alpha(y) = T \alpha_B \left[ \frac{R}{du} \frac{d\bar{u}}{du} - 1 \right] \quad (77)$$

We could also have written (77) as

$$\Delta\alpha(y) = \alpha_B \left[ \left( \frac{R}{du} \frac{d\bar{u}}{du} \right)_T - 1 \right] \quad (78)$$

if we had known how to write

$$\left( \frac{R}{du} \frac{d\bar{u}}{du} \right)_T$$

explicitly. However, by comparing (77) and (78) we find that as a first approximation

$$\left( \frac{R}{du} \frac{d\bar{u}}{du} \right)_T = 1 + T \left[ \frac{R}{du} \frac{d\bar{u}}{du} - 1 \right] \quad (79)$$

In addition to the flow angularity induced along the wing by the presence of a fuselage there is also a flow angle (a downwash) induced by the lift associated with a finite wing. This angle in the  $\bar{u}$ -plane is written  $\bar{\alpha}_i(\bar{y})$ . We seek now to transform this angle into the  $u$ -plane so that we may see more easily its influence on the actual lift and drag of the local airfoil section. We note that the induced angle in the  $\bar{u}$ -plane multiplied by the real part of the change in  $\bar{u}$  for a given change in  $u$  is just the induced angle in the  $u$ -plane. Thus for thick airfoils

$$\alpha_i(y) = \bar{\alpha}_i(\bar{y}) \left[ \frac{R}{du} \frac{d\bar{u}}{du} \right]_T \quad (80)$$

This angle is negative in the usual sense. The geometric angle of attack of the wing can be given in terms of the angle of attack at the root and the twist relative to the root angle as a function of span:  $\alpha_e(y) = \alpha_R + \epsilon(y)$ . To the geometric angle we must add flow angularities due to body upwash,  $\alpha_B$ , and due to wing lift,  $\alpha_i$ . The result is that for thick wings the effective section angle of attack in the physical plane is given by

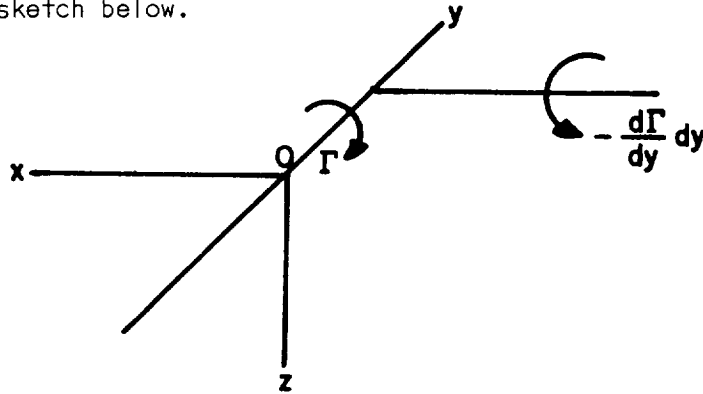
$$\alpha_e(y) = \alpha_R + \epsilon(y) + \left[ \alpha_B - \bar{\alpha}_i(\bar{y}) \right] \left[ 1 + \left( 1 - \frac{2 y_0 t_{root}}{\pi A'B'} \right) \cdot \left( \frac{1}{A' - B'} \left\{ A' - B' \frac{\frac{a}{\sqrt{a^2 - e'^2}}}{1 + \frac{e'^2 y^2}{(a^2 - e'^2)^2}} \right\} \right) - 1 \right] \quad (81)$$

with 
$$a = \frac{1}{2} \left[ \sqrt{y^2 + (h - A'^2 - B'^2)^2} + \sqrt{y^2 + (h + A'^2 - B'^2)^2} \right]$$

and 
$$e = \sqrt{A'^2 - e'^2} .$$

Note that with the exception of  $\bar{\alpha}_i(\bar{y})$  all the quantities in (81) can be determined from the geometry of the design.

For the evaluation of  $\bar{\alpha}_i(\bar{y})$  we employ a variant of the technique used to determine the inviscid velocity distribution about an airfoil section. Consider the sketch below.



Recall also that we had indicated previously that we would represent a wing by a group of horseshoe-like vortices which physically "roll-up" at the tips to form single trailing vortices. Thus the circulation  $\Gamma$  will vary along the span, being symmetrical about the point 0 and falling to zero at the tips. Between the point  $y$  and  $y + dy$  on the span the circulation decreases by an amount

$$- \frac{d\Gamma}{dy} dy .$$

Ideally, a trailing vortex of this strength springs from the element of span  $dy$ . There is therefore a sheet of trailing vortices extending across the span and the induced velocity normal to the free stream velocity must be obtained as the sum of the effects of all trailing vortices in this sheet.

To determine the form of the expression giving the sum of the effects of all trailing vortices consider first the case of a wing represented by a single horseshoe vortex. We see from Equation (15) that the velocity induced by a vortex at a point depends upon the distance from the point to the filament. In the following sketch the distance from P to the wing filament is PM. Now in Equations (15) the total velocity,  $\sqrt{u^2 + v^2}$ , is normal to the line,  $\sqrt{x^2 + y^2}$ , connecting the filament to the point at which one desires to know the velocity. One could therefore write

$$\sqrt{u^2 + v^2} = \frac{\Gamma}{2\pi\sqrt{x^2 + y^2}} . \tag{82}$$

It seems reasonable to conclude that at any point the velocity induced by a semi-infinite vortex filament is half that induced by an infinite vortex. Let us ask then what is the velocity induced at a point by a small segment of a vortex filament. We know that the velocity depends upon the distance from the segment to the point. If we call  $x^2 + y^2 = r^2$ , then this distance from the vortex segment at A' is  $r/\sin \theta_1$  where  $\theta_1$  is the angle PA'M in the sketch below.

Substitution of this expression for distance into an expression for the velocity induced at a point, say in the XOZ plane, by a segment of a semi-infinite vortex can be seen to yield

$$dV = \frac{\Gamma \sin \theta}{4\pi r} d\theta \quad . \quad (83)$$

Integration of (83) gives

$$V_1 = \frac{\Gamma}{4\pi} \left[ -\cos \theta \Big|_{\theta_1}^{\pi/2} \right] = \frac{\Gamma}{4\pi} \cos \theta_1 \quad . \quad (84)$$

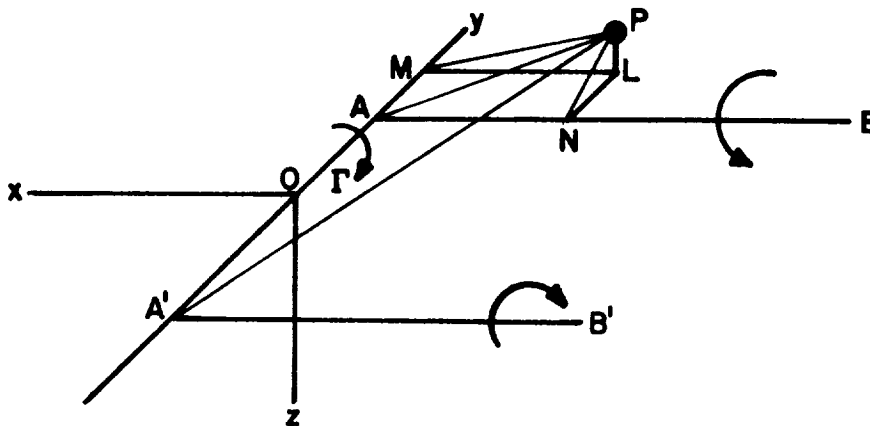
Calculation of the contribution to the velocity from the part of the filament beyond O yields

$$V_2 = \frac{\Gamma}{4\pi} \cos \theta_2 \quad (85)$$

so that the total induced velocity is given by

$$V = \frac{\Gamma}{4\pi} (\cos \theta_1 + \cos \theta_2) \quad . \quad (86)$$

In the notation of the sketch, the downwash velocity at point P (normal to PM) may be written





$$V = \frac{\Gamma}{4\pi PM} \left[ \cos PA'A + \cos PAA' \right]. \quad (87)$$

If we now assume that point P is located along the span at, say,  $y_1$ , then the distance from  $y_1$  to any other point is  $y_1 - y$ . Further, if  $\Gamma$  is variable along  $y$  then

$$\Gamma = \int_{-b/2}^{b/2} \frac{d\Gamma}{dy} dy.$$

One may therefore write the induced velocity at some point  $y_1$  along the span as

$$V \alpha_i(y_1) = \frac{1}{4\pi} \int_{-b/2}^{b/2} \frac{\frac{d\Gamma}{dy} dy}{y_1 - y}.$$

In the  $\bar{u}$ -plane this is simply

$$\bar{\alpha}_i(\bar{y}_1) = \frac{1}{4\pi V} \int_{-b/2}^{b/2} \frac{\frac{d\Gamma}{dy} d\bar{y}}{\bar{y}_1 - \bar{y}}. \quad (88)$$

If  $\bar{\alpha}_i(\bar{y}_1)$  is to be in degrees, we multiply the right hand side of (88) by  $180/\pi$ .

Unfortunately the circulation  $\Gamma$  about an airfoil is not readily measured nor is it a quantity which is easily thought of in physical terms. More commonly, the characteristic of an airfoil is stated in terms of its lift coefficient, a quantity easily measured and important in aerodynamic and structural design. It can be shown on analytical grounds (Ref. 9) that the lift per unit span of a wing is  $\rho V \Gamma$  where  $\rho$  is the air density. The lift coefficient is therefore

$$C_l = \frac{\rho V \Gamma}{\frac{1}{2} \rho V^2 c} = \frac{2\Gamma}{Vc};$$

hence

$$\Gamma = \frac{1}{2} C_l Vc. \quad (89)$$

Because both  $C_l$  and  $c$  can vary as functions of  $y$  we put

$$\frac{d\Gamma}{dy} = \frac{V}{2} \frac{d(C_l c)}{dy}$$

or in non-dimensional form

$$\frac{d\Gamma}{dy} = \frac{Vb}{2} \frac{d\left(\frac{C_{\ell}c}{b}\right)}{dy} \quad (90)$$

with (90), (88) becomes

$$\bar{\alpha}_i(\bar{y}_1) = \frac{180\bar{b}}{8\pi^2} \int_{-\bar{b}/2}^{\bar{b}/2} \frac{\left[ \frac{d\left(\frac{C_{\ell}\bar{c}}{\bar{b}}\right)}{d\bar{y}} \right]}{\bar{y}_1 - \bar{y}} d\bar{y} \quad (91)$$

where  $\bar{\alpha}_i(\bar{y}_1)$ , is now in degrees.

We note that the transformation (65) is an analytic function (and therefore conformal). It does not, however, affect geometric quantities in the chord-wise direction so that  $\bar{c} = c$ . Wing twist is also not affected, nor does the transformation affect quantities such as the local value of the circulation,  $\Gamma$ . In other words, the circulation or lift that exists at  $y$  in the  $u$ -plane is the same circulation or lift that exists at  $\bar{y}$  in the  $\bar{u}$ -plane:

$$C_{\ell}(y)c = \bar{C}_{\ell}(\bar{y})\bar{c} \quad (92)$$

The key to the evaluation of Equation (81) is therefore a suitable expression for  $C_{\ell}(y)c$ , the spanwise lift distribution. Unfortunately we do not know *a priori* what it is. We do know from the two-dimensional values calculated previously and the problem geometry what lift we would obtain if  $\bar{\alpha}_i(\bar{y})$  could be neglected. We have only to find  $\alpha_e(y)$  and the corresponding  $C_{\ell}$  comes from the two-dimensional data. We can assume some modification to the local angle of attack for 3-dimensional effects and see if our calculated value of  $\bar{\alpha}_i(\bar{y})$  is equal to the assumed value. If not, we can modify our assumption until it is. What we seem to require then is a systematic procedure for doing this.

Let us represent  $C_{\ell}(y)c/b$  by a series,

$$\frac{C_{\ell}(y)c}{b} = \sum_{n=1}^{\infty} A_n \sin \left[ n \cos^{-1} \left( \frac{-2\bar{y}}{\bar{b}} \right) \right] \quad (93)$$

and call  $\bar{\theta} = \cos^{-1} (2\bar{y}/\bar{b})$ . Then (91) could be written

$$\bar{\alpha}_i(\bar{y}_1) = \frac{180}{4\pi^2} \int_0^{\pi} \frac{\sum_{n=1}^{\infty} n A_n \cos n\bar{\theta}}{\cos \bar{\theta} - \cos \bar{\theta}_1} d\bar{\theta} \quad (94)$$

Since it can be shown that

$$\int_0^{\pi} \frac{\cos n\theta}{\cos \theta - \cos \phi} d\theta = \pi \frac{\sin n\phi}{\sin \phi} \quad (95)$$

$$\bar{\alpha}_i(\bar{y}_1) = \frac{180}{4\pi} \left[ \frac{\sum_{n=1}^{\infty} n A_n \sin n\bar{\theta}_1}{\sin \bar{\theta}_1} \right]. \quad (96)$$

To proceed with the evaluation of (96) one returns for the moment to (93). Let us assume that we can adequately represent the lift at each of  $m$  evenly spaced points along the span with a finite series of  $r - 1$  terms.  $m$  and  $r$  we assume are related by  $\bar{\theta} = m\pi/r$  and  $m = 1, 2, \dots, r - 1$ . In other words, we divide the range  $0 \leq \bar{\theta} \leq \pi$  into  $r$  intervals. Over each interval, the lift is a constant which we can represent by a finite series, the number of terms of which being also the number of points at which we calculate the lift. Thus, to use a large number of terms in the series to represent the lift in each interval, it is necessary to take a large number of intervals. The lift in each interval is written

$$\left( \frac{C_{\ell}(\gamma)c}{b} \right)_m = \sum_{n=1}^{r-1} A_n \sin n \frac{m\pi}{r} \quad (97)$$

for which

$$A_n = \frac{2}{r} \sum_{m=1}^{r-1} \left( \frac{C_{\ell}c}{b} \right)_m \sin n \frac{m\pi}{r}. \quad (98)$$

Substitution of this result into (96) yields

$$\bar{\alpha}_i(\bar{y}_1) = \frac{180}{4\pi \sin \bar{\theta}_1} \left\{ \sum_{n=1}^{\infty} n \left[ \frac{2}{r} \sum_{m=1}^{r-1} \left( \frac{C_{\ell}c}{b} \right)_m \sin n \frac{m\pi}{r} \right] \sin n\bar{\theta}_1 \right\}. \quad (99)$$

It will be readily recalled that

$$\sin \alpha \sin \beta = \frac{1}{2} [\cos (\alpha-\beta) - \cos (\alpha+\beta)] ;$$

with this identity (99) is

$$\bar{\alpha}_i(\bar{y}_1) = \frac{180}{4\pi r \sin \bar{\theta}_1} \left\{ \sum_{m=1}^{r-1} \left( \frac{C_{\ell}c}{b} \right)_m \sum_{n=1}^{r-1} n \left[ \cos n \left( \bar{\theta}_1 - \frac{m\pi}{r} \right) - \cos n \left( \bar{\theta}_1 + \frac{m\pi}{r} \right) \right] \right\} \quad (100)$$

where we have chosen to terminate the infinite series in (99) at  $r - 1$  terms for computational convenience.

We choose to evaluate the induced angle of attack at the same points along the span at which we are required to find  $C_{\ell}$ . To accomplish this we put  $\bar{\theta}_1 = k\pi/r$ . If we define

$$\beta_{mk} = \frac{180}{4\pi r \sin \frac{k\pi}{r}} \sum_{n=1}^{r-1} n \left[ \cos n \frac{(k-m)\pi}{r} - \cos n \frac{(k+m)\pi}{r} \right] \quad (101)$$

then

$$\bar{\alpha}_i(\bar{y}_i) = \bar{\alpha}_{ik} = \sum_{m=1}^{r-1} \left( \frac{C_{qc}}{b} \right)_m \beta_{mk} \quad (102)$$

Now if  $k = m$

$$\beta_{mk} = \frac{180}{4\pi r \sin \frac{k\pi}{r}} \sum_{n=1}^{r-1} n \left[ 1 - \cos \frac{2kn\pi}{r} \right] \quad (103)$$

The sum of the series is not easily found but can be shown by evaluating series of varying numbers of terms to be  $r^2/2$ ; hence

$$\beta_{mk} = \frac{180r}{8\pi \sin \frac{k\pi}{r}} \quad (104)$$

for

$$k = m \quad .$$

If  $k + m$  is even (and  $k \neq m$ ) then  $\beta_{mk}$  contains terms such as

$$\begin{aligned} & 1 \left[ \cos 1 \left( \frac{1-3}{4} \right) \pi - \cos 1 \left( \frac{1+3}{4} \right) \pi \right] \\ & + 2 \left[ \cos 2 \left( \frac{-2}{4} \right) \pi - \cos 2\pi \right] \\ & + 3 \left[ \cos 3 \left( \frac{-2}{4} \right) \pi - \cos 3\pi \right] = 0 \end{aligned}$$

which always sum to zero. In a similar fashion one can show that when  $k + m$  is odd

$$\beta_{mk} = \frac{180}{4\pi r \sin \frac{k\pi}{r}} \left[ \frac{1}{1 - \cos \frac{(k+m)\pi}{r}} - \frac{1}{1 - \cos \frac{(k-m)\pi}{r}} \right] \quad (105)$$

Note that the value of  $\beta_{mk}$  depends only on the number of spanwise stations used and is independent of wing aspect ratio or taper ratio.

The perceptive reader will note that (102) really does not supply us with more information regarding the spanwise variation of  $\bar{\alpha}_i(\bar{y}_i)$  than we had previously. It does, however, provide us with the physical and geometric

tools we need to work out a successful iterative procedure for finding the correct value of  $C_{\ell c}/\bar{b}$  as a function of span. That this is true will become apparent as we proceed. First, let us write (81) as

$$\alpha_e(y) = \alpha_k - \frac{R}{du} \sum_{m=1}^{r-1} \left( \frac{C_{\ell c}}{\bar{b}} \right)_m \beta_{mk} . \quad (106)$$

As a first approximation we will assume that the variation of lift coefficient with angle of attack,  $C_{\ell \alpha}$ , at any spanwise location,  $k$ , is constant. Then by writing

$$\alpha_e \left( C_{\ell \alpha} \frac{c}{\bar{b}} \right)_k = \left( \frac{C_{\ell c}}{\bar{b}} \right)_k + \Delta_k \quad (107)$$

we can define  $\Delta_k$  as the amount that must be added to the initial estimate for  $(C_{\ell c}/\bar{b})$  in order to obtain a new value which includes in it effects from other portions of the wing. A second iteration is formed as follows:

$$\left\{ \alpha_k - \frac{R}{du} \sum_{m=1}^{r-1} \left[ \left( \frac{C_{\ell c}}{\bar{b}} \right)_m + \Delta'_m \right] \beta_{mk} \right\} \left( C_{\ell \alpha} \frac{c}{\bar{b}} \right)_k = \left( \frac{C_{\ell c}}{\bar{b}} \right)_k + \Delta'_k . \quad (108)$$

Subtraction of (108) from (107) yields

$$\left( C_{\ell \alpha} \frac{c}{\bar{b}} \right)_k \left( \frac{R}{du} \right)_k \sum_{m=1}^{r-1} \Delta'_m \beta_{mk} = \Delta_k - \Delta'_k . \quad (109)$$

If we define

$$\left( \frac{C_{\ell \alpha} c}{\bar{b}} \right)_k \left( \frac{R}{du} \right)_k \frac{180r}{8\pi \sin \frac{k\pi}{r}} = G_{kk} , \quad (110)$$

then Equation (109) could be written as

$$\Delta'_k + G_{kk} \Delta'_k + \left[ \sum_{m=1}^{r-1} \Delta'_m \beta_{mk} \right]_{k \neq m} \left( \frac{C_{\ell \alpha} c}{\bar{b}} \right)_k \left( \frac{R}{du} \right)_k = \Delta_k . \quad (111)$$

Dividing by  $G_{kk}$  yields

$$\left( 1 + \frac{1}{G_{kk}} \right) \Delta'_k + \left[ \sum_{m=1}^{r-1} \frac{\beta_{mk}}{\beta_{kk}} \Delta'_m \right]_{k \neq m} = \frac{\Delta_k}{G_{kk}} . \quad (112)$$

Equation (112) represents  $r/2$  simultaneous equations which may be represented in matrix form as

$$[G_{ij}] \{\Delta_i'\} = \frac{1}{G_{kk}} \{\Delta_i\} \quad (113)$$

where  $[G_{ij}]$  is a matrix with all the principal diagonal elements equal to  $(1 + 1/G_{kk})$  and the other elements are  $\beta_{mk}/\beta_{kk}$ . The values to be added to one set of approximate values to obtain a better approximation are therefore given by

$$\{\Delta_i'\} = [G_{ij}]^{-1} \frac{1}{G_{kk}} \{\Delta_i\} \quad (114)$$

As a first approximation to the distribution of lift on the wing we use the expression (Ref. 36)

$$\frac{C_{lC}}{b} = C_{lC} \left( \frac{AR}{AR + 1.8} \right) \left( \frac{c}{c_R} \right) \left( \frac{c_R}{b} \right) \left( \frac{b}{b} \right) \left[ \frac{1}{2} + (1 + \lambda) \sqrt{1 - \left( \frac{2\bar{y}}{b} \right)^2} \right] \quad (115)$$

which, as can be seen, contains a simple aspect ratio correction and a simple taper ratio correction to a typical elliptical lift distribution. Here,  $AR$  is the aspect ratio,  $(b^2/\text{wing area})$ ,  $c_R$  is the root chord, and  $\lambda$  is the taper ratio or the ratio of the tip chord to the root chord. The value of  $C_{lC}$  on the right-hand side of this equation comes from the two-dimensional data corresponding to the local geometric angle of attack.

Now the flow in the tip regions and its effect on the overall wing characteristics is particularly difficult to determine quantitatively. The more inboard sections of a finite wing are influenced by the downwash generated by the horseshoe vortex system and the upwash due to the fuselage so that the primary effect there is a change in effective angle of attack. In the tip region, on the other hand, there is a substantial spanwise flow which detracts from the flow moving chordwise; consequently, the tip region is able to generate less lift than one would normally expect for a given free stream velocity. This of course reduces the total lift of the wing somewhat. To accommodate this loss in lift within the idea of using two-dimensional data at an appropriate angle of attack, we modify  $\alpha_e$  as given by (81) to read (Ref. 36)

$$\alpha_e' = \frac{[(\alpha_e - \alpha_{Z.L.})(1 - \sqrt{1 + 4/AR^2})]}{\sqrt{1 + \frac{4}{AR^2}}} \quad (116)$$

We then use  $\alpha_e'$  to look up the 3-dimensional value of the section lift coefficient from the 2-dimensional data.

If  $C_{lC}/b$  computed in this fashion is not sufficiently close to the initial estimate of  $C_{lC}/b$  than a correction given by (114) is added. The process is repeated until satisfactory agreement is obtained.

When a satisfactory lift distribution has finally been obtained, one can employ the same section data to find the profile drag and moment coefficient at each station along the wing. The local induced drag is simply a product of the lift and the induced angle of attack at that point. The overall force and moment coefficients are obtained by integrating the local values over the span. If one uses Simpson's rule for this integration, explicit relations for the lift, drag, and pitching moment can be obtained:

$$C_L = \left(\frac{\bar{b}}{b}\right)^2 AR \sum_{m=1}^{r-1} \left(\frac{C_{\ell}c}{b}\right)_m \left[ \frac{\pi}{6r} (3 - (-1)^m) \sin \frac{m\pi}{r} \right] \quad (117)$$

$$C_{D_i} = \frac{\pi}{180} \left(\frac{\bar{b}}{b}\right)^2 AR \sum_{m=1}^{r-1} \left[ \left(\frac{C_{\ell}c}{b}\right) \alpha_i \right]_m \left[ \frac{\pi}{6r} (3 - (-1)^m) \sin \frac{m\pi}{r} \right] \quad (118)$$

$$C_{D_o} = \left(\frac{\bar{b}}{b}\right)^2 AR \sum_{m=1}^{r-1} \left(\frac{C_{d_o}c}{b}\right)_m \left[ \frac{\pi}{6r} (3 - (-1)^m) \sin \frac{m\pi}{r} \right] \quad (119)$$

$$C_m = \frac{AR\bar{b}}{b^2c'} \sum_{m=1}^{r-1} (C_m c^2) \left[ \frac{\pi}{6r} (3 - (-1)^m) \sin \frac{m\pi}{r} \right] \quad (120)$$

where

$$C_m = C_{m_c/4} - \frac{x}{c} \left[ C_{\ell} \cos(\alpha_B - \alpha_i) + C_{d_o} \sin(\alpha_B - \alpha_i) \right] - \frac{z}{c} \left[ C_{\ell} \sin(\alpha_B - \alpha_i) - C_{d_o} \sin(\alpha_B - \alpha_i) \right] \quad (121)$$

and  $c'$  is the mean aerodynamic chord. Note that this integration is somewhat analogous to the process represented by

$$\frac{1}{bc'} \int_{-b/2}^{b/2} C_{\ell}c \, dy .$$

Since the computation of  $(C_{\ell}c/\bar{b})$  has really been carried out in the  $\bar{u}$ -plane so far as the wing span is concerned we must multiply our result by  $\bar{b}/b$  to transform it to the physical plane.  $AR$  is just  $b/c'$  and the average (aerodynamic not geometric) value of  $c$  over the span is  $c'$ . The term in brackets is the multiplier employed by Simpson's Rule. It is seen therefore that  $C_L$  is in fact an average over the span in the physical plane.

## CONCLUDING REMARKS

The totality of procedures described in this section for computing the aerodynamic characteristics of complete wings can be seen to be capable—at least in principle—of a very accurate representation of physical reality. The vortex filament distribution approach to determining the inviscid pressure distribution on airfoil sections leads in the limit of a multitude of filaments and high computational accuracy to very good results. The application of the lifting line concept to the correction of section characteristics for finite span effects also can yield very reliable results, provided the number of spanwise stations at which the characteristics are computed is large, computational accuracy is maintained, and the underlying assumptions of the lifting-line theory are not violated by the planform it is supposed to represent.

The approach used here has two principal advantages, insofar as the computation of light aircraft wing aerodynamic characteristics is concerned, when compared with the finite element or vortex lattice approach which has been discussed prominently in the literature of late:

- (1) three-dimensional drag data is obtained,
- (2) the computational time for an equally accurate potential solution is far less since, in effect, the spanwise integration of vorticity is replaced by a single integration along the lifting line. This, of course, is made possible by restricting the interest to unswept, moderate-to-high aspect ratio wings in subsonic flow.

The computation of the effects of fluid viscosity is the least rigorous and least accurate of the procedures. So long as the boundary layer is laminar and the wing surface smooth one could expect to obtain very acceptable drag and boundary layer displacement effects by successive refinement of the pseudo-airfoil shape using a more general polynomial for  $u/u_e$  if necessary. Laminar boundary layer methods inherently more accurate than the momentum integral technique are also available as computer programs and could be included if desired, at the cost, however, of greatly increased computer time. The local characteristics during boundary layer transition and for turbulent boundary layers are here computed by what may be termed state of the art techniques—not completely rigorous, but about as reliable as any available. The procedure is therefore expected to be less accurate as the need for a precise knowledge of boundary layer behavior increases—at high angles of attack or in the presence of surface irregularities.

Finally, we should mention that to translate these concepts into useful design tools we must also employ sound, efficient computational procedures. Although a treatment of the rationale behind the choice of one numerical method over another for a particular computation is beyond the scope of the present discussion, it must be emphasized that such decisions can be crucial both economically and technically. For this reason it is to be expected that the major improvements which occur in the procedure presented in this work, at least in the immediate future, will likely be in the area of computational effectiveness.



# A THEORY FOR THE PREDICTION OF LIFT, DRAG, AND PITCHING MOMENT OF LIGHT AIRCRAFT FUSELAGES

## INVISCID FLOW OVER FUSELAGES

In the preceding discussion we were concerned with a means of predicting the lift, drag, and moment characteristics of wings. An airplane, however, contains other parts which contribute to the overall aerodynamic force and moment experienced by the vehicle. Most notable of these is the fuselage. The fuselage contributes to the overall drag for two reasons: it has a large surface area against which the air can "rub" and in order to provide a finite volume in which to carry a useful payload it must move air "out of the way." It can also contribute some amount to the lift in addition to that provided by the bridging action between the two wings. This effect is usually significant only at high angles of attack. If the fuselage produces contributions to the lift and drag, then it is also likely to affect the pitching moment.

Because the fuselage is usually not a body of revolution but rather a three-dimensional body with a plane of symmetry its proper analytical representation is more difficult than that of an airfoil. In the case of an airfoil we were able to represent the surface by a series of line vortices. Because a vortex must either be closed or extend to infinity, the only vortex we can use to represent three-dimensional bodies is a ring. To be sure the ring can be contorted, but it must close. The geometric problems associated with describing such a ring leads us to ask whether there is another flow function for describing the inviscid flow about fuselages which may be easier to use. The point source is an elementary flow which can be described quite easily mathematically. The potential at the point  $(x, y, z)$  due to a source at  $(\xi, \eta, \zeta)$  is given by

$$\phi = \frac{-q}{4\pi} \frac{1}{[(x - \xi)^2 + (y - \eta)^2 + (z - \zeta)^2]^{1/2}} \quad (122)$$

where  $q$  is called the source strength. The components of the velocity associated with a source flow are then

$$u = \frac{q}{4\pi} \frac{(x - \xi)}{[(x - \xi)^2 + (y - \eta)^2 + (z - \zeta)^2]^{3/2}} \quad (123)$$

$$v = \frac{q}{4\pi} \frac{(y - \eta)}{[(x - \xi)^2 + (y - \eta)^2 + (z - \zeta)^2]^{3/2}} \quad (124)$$

$$w = \frac{q}{4\pi} \frac{(z - \zeta)}{[(x - \xi)^2 + (y - \eta)^2 + (z - \zeta)^2]^{3/2}} \quad (125)$$

That this flow is irrotational and satisfies the Laplace Equation is easily verified.

Physically, the three-dimensional source is a point from which fluid emanates in straight lines in all directions. The quantity of fluid emanating from the point depends upon the value of  $q$ . By placing a source in a uniform stream one in effect displaces the streamlines in the uniform stream because of local additions to the mass flow. By distributing sources in space and using a different strength for each source it is possible to cause the streamline pattern of the flow to simulate the shape of the windward side of complex bodies quite satisfactorily. To represent a closed body it is necessary to withdraw the mass added by the sources so that the streamlines can return to their original positions downstream of the body. We do this by means of a distribution of sources with negative values of the source strength, or sinks. Hence, the net source strength when integrated over a closed body is zero.

A source flow is also a flow which inherently cannot create a net circulation about a body. Consequently, it cannot be used to represent a situation where lift is present. Such situations can be simulated by a combination of sources, horseshoe vortices, and a uniform stream. Even though a distribution of sources in a uniform stream by itself cannot represent a lifting body, it is suitable for determining the inviscid pressure distribution on a non-lifting body. Then by adding a boundary layer one can determine both the form and friction drag of such bodies.

The technique by which such a calculation is carried out is very similar to that which we employed to determine the aerodynamic characteristics of airfoils. We begin by considering the body surface to be made up of a number of connected plane quadrilaterals. As the number of quadrilaterals approaches infinity, the polygon becomes the body identically. On each plane quadrilateral we place a source of undetermined strength. We require that the flow induced on any one quadrilateral through the interaction of all the sources with the uniform stream be parallel to the quadrilateral surface or that the flow velocity normal to the quadrilateral be zero. This gives us sufficient boundary conditions to write a determinant system of equations, one for each quadrilateral, which we can then solve to find the individual source strengths.

The total velocity induced at a point on the body surface by a series of sources distributed over the body can, following (19), be written

$$\begin{aligned}
 \bar{u} &= \frac{1}{4\pi} \sum_{N=1}^k \frac{q_N(x - \xi_N)}{[(x - \xi_N)^2 + (y - \eta_N)^2 + (z - \zeta_N)^2]^{3/2}} \\
 \bar{v} &= \frac{1}{4\pi} \sum_{N=1}^k \frac{q_N(y - \eta_N)}{[(x - \xi_N)^2 + (y - \eta_N)^2 + (z - \zeta_N)^2]^{3/2}} \\
 \bar{w} &= \frac{1}{4\pi} \sum_{N=1}^k \frac{q_N(z - \zeta_N)}{[(x - \xi_N)^2 + (y - \eta_N)^2 + (z - \zeta_N)^2]^{3/2}} .
 \end{aligned} \tag{126}$$

To complete the formulation of the equations, we must include the effects of the free stream velocity at  $(x, y, z)$  and define the normal to the surface at  $(x, y, z)$  so as to be able to state the requirement that the net flow be parallel to the surface. The free stream velocity just adds a term  $V_\infty$  to the  $u$ -component.

The surface in which the point  $(x, y, z)$  lies can, in general, be defined by the equation  $a'x + b'y + c'z + d' = 0$ . Each quadrilateral composing the fuselage will have a different range of values for  $x, y,$  and  $z$  as well as for  $a', b', c',$  and  $d'$ . The values of the coefficients  $a', b', c',$  and  $d'$  for a particular quadrilateral are found by solving for them from the system of equations

$$\begin{aligned} a'x_1 + b'y_1 + c'z_1 + d' &= 0 \\ a'x_2 + b'y_2 + c'z_2 + d' &= 0 \\ a'x_3 + b'y_3 + c'z_3 + d' &= 0 \\ a'x_4 + b'y_4 + c'z_4 + d' &= 0 \end{aligned} \tag{127}$$

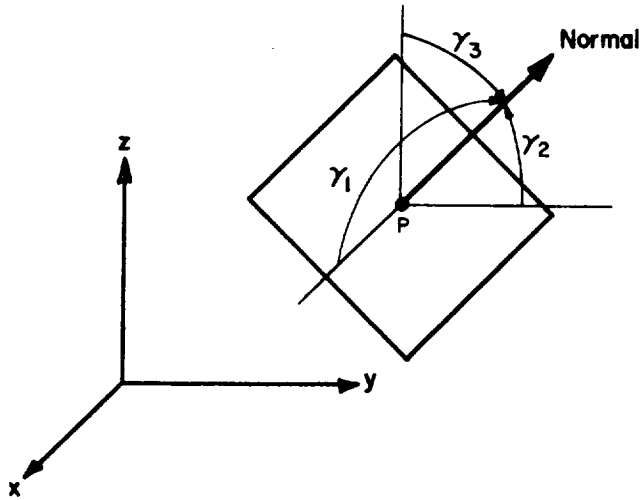
where  $(x_1, y_1, z_1), (x_2, y_2, z_2), (x_3, y_3, z_3)$  and  $(x_4, y_4, z_4)$  are four points all of which lie in the same plane. One can use for these points the four corners of the quadrilateral. One can also rewrite the equation for a plane surface in the form

$$\frac{a'}{\sqrt{a'^2 + b'^2 + c'^2}} x + \frac{b'}{\sqrt{a'^2 + b'^2 + c'^2}} y + \frac{c'}{\sqrt{a'^2 + b'^2 + c'^2}} z + \frac{d'}{\sqrt{a'^2 + b'^2 + c'^2}} = 0 .$$

Then the quantities

$$a = \frac{a'}{\sqrt{a'^2 + b'^2 + c'^2}}, \quad b = \frac{b'}{\sqrt{a'^2 + b'^2 + c'^2}}, \quad c = \frac{c'}{\sqrt{a'^2 + b'^2 + c'^2}}$$

are what are called the direction cosines of the normal to the plane  $ax + by + cz + d = 0$ . The reason for this may be seen from the sketch below. If we draw a line from point  $P$  normal to the plane in which it lies then  $a = \cos \gamma_1, b = \cos \gamma_2,$  and  $c = \cos \gamma_3$ .  $a', b',$  and  $c'$  are called direction numbers. The plane through point  $P(x_p, y_p, z_p)$  whose normal has direction numbers  $a', b',$  and  $c'$  is the graph of the equation  $a'(x - x_p) + b'(y - y_p) + c'(z - z_p) = 0$ . From this discussion we see that direction numbers and direction cosines are proportional.



The requirements that there be no flow normal to the surface is satisfied when

$$(\bar{u} + V_{\infty})\bar{a} + \bar{v}\bar{b} + \bar{w}\bar{c} = 0 \quad (128)$$

at one point on each quadrilateral. That this is true is easily seen if one writes the velocity as a vector,  $(\bar{u} + V_{\infty})\bar{i} + \bar{v}\bar{j} + \bar{w}\bar{k} = \bar{V}$ , and the normal as a vector,  $\bar{a}\bar{i} + \bar{b}\bar{j} + \bar{c}\bar{k} = \bar{N}$ . The scalar or dot product of two vectors is the product of their magnitudes times the cosine of the angle between them. Thus if  $\bar{V} \cdot \bar{N} = 0$  the two vectors are at right angles to one another. But  $\bar{V} \cdot \bar{N} = (\bar{u} + V_{\infty})\bar{a} + \bar{v}\bar{b} + \bar{w}\bar{c}$ . When this is zero the flow is parallel to the surface.

It will be recalled that in the two-dimensional case of the airfoil one could as easily chose the condition that the flow must be parallel to the surface as the condition that the flow velocity normal to that surface must be zero. They are equivalent statements and offer similar mathematical problems.\* In the three-dimensional case, however, one does not know *a priori* the direction of the flow parallel to the surface. For this reason, a single, fixed-value boundary condition becomes difficult to specify. Requiring that the velocity normal to the surface be zero on the other hand, removes this difficulty.

---

\* It has been pointed out by Chen (Ref. 27) that specifying that the tangent of the flow angle be the same as the local angle of the surface makes the solution less sensitive to errors in the coordinates of the surface than requiring that the flow velocity normal to the surface be zero.

While perhaps not evident in the discussion above there is a problem in relating points on the body surface to the coefficients of (127). Simply stated it is that the four points on the body surface closest to  $x, y, z$  do not necessarily lie in the same plane. In fact, it would be most remarkable if they did. Further, if the four corner points on any quadrilateral are "adjusted" so that they are in fact coplanar then the edges of that quadrilateral will not necessarily be colinear with the edges of adjacent quadrilaterals. The effect then is to represent the body by an ensemble of planar "scales," similar to those of a fish, rather than by something that resembles a wire gridwork. In the limit, however, as the number of quadrilaterals becomes very large, the two models become the same thing.

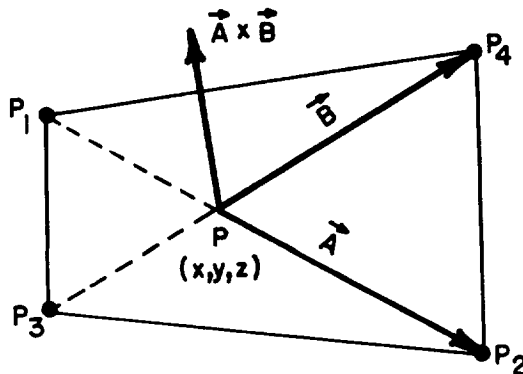
How then to resolve the dilemma? Forming triangular panels from three adjacent surface points insures that the three points are coplanar but, as one may readily observe, it also doubles the number of panels one needs to cover a given area. Since the computational time required to solve for the source strength on each panel varies approximately as the number of panels squared, one does not take such a step lightly. On the other hand if one is willing to "adjust" the corner points of a quadrilateral to make them coplanar, how should he proceed to insure that the calculated normal is nearly the same as the true normal to the body at  $x, y, z$ . One way which has been suggested (Ref. 23) approaches the problem by writing, first of all, equations for the two diagonals of the quadrilateral. This is straightforward since the two opposite corner points of a quadrilateral define a straight line uniquely. Now, if one is willing to say that these two lines are essentially coplanar, then the crossproduct of their vector representations is the normal to the quadrilateral. For example, the equation describing a line through points  $P_1(x_1, y_1, z_1)$  and  $P_2(x_2, y_2, z_2)$

$$\frac{x - x_1}{x_2 - x_1} = \frac{y - y_1}{y_2 - y_1} = \frac{z - z_1}{z_2 - z_1} \quad (129)$$

while the equations describing a line through points  $P_3(x_3, y_3, z_3)$  and  $P_4(x_4, y_4, z_4)$  are

$$\frac{x - x_3}{x_4 - x_3} = \frac{y - y_3}{y_4 - y_3} = \frac{z - z_3}{z_4 - z_3} \quad (130)$$

The various points and lines are depicted on the sketch below.



Now, the point at which the two lines have the same values of  $x$  and  $y$  (that is, the point at which they cross one another) is found by solving the two equations simultaneously to obtain

$$y = \frac{(x_1 - x_3) - y_1(x_2 - x_1)/(y_2 - y_1) + y_3(x_4 - x_3)/(y_4 - y_3)}{\frac{x_4 - x_3}{y_4 - y_3} - \frac{x_2 - x_1}{y_2 - y_1}}$$

$$x = x_1 - y_1 \left( \frac{x_2 - x_1}{y_2 - y_1} \right) + \left( \frac{x_2 - x_1}{y_2 - y_1} \right) \left[ \frac{(x_1 - x_3) - y_1(x_2 - x_1)/(y_2 - y_1) + y_3(x_4 - x_3)/(y_4 - y_3)}{\frac{x_4 - x_3}{y_4 - y_3} - \frac{x_2 - x_1}{y_2 - y_1}} \right] \quad (131)$$

$z$  is then found from

$$z = (y - y_3) \left( \frac{z_4 - z_3}{y_4 - y_3} \right)$$

or

$$z = (y - y_1) \left( \frac{z_2 - z_1}{y_2 - y_1} \right) \quad (132)$$

A vector beginning at  $P(x, y, z)$  and terminating at  $P_2(x_2, y_2, z_2)$  is represented by

$$\vec{A} = (x_2 - x)\vec{i} + (y_2 - y)\vec{j} + (z_2 - z)\vec{k} \quad (133)$$

while that beginning at  $P(x, y, z)$  and terminating at  $P_4(x_4, y_4, z_4)$  is represented by

$$\vec{B} = (x_4 - x)\vec{i} + (y_4 - y)\vec{j} + (z_4 - z)\vec{k} \quad (134)$$

The vector which is normal to the plane defined by  $\vec{A}$  and  $\vec{B}$  is then

$$\begin{aligned} \vec{A} \times \vec{B} &= (x_2 - x)(y_4 - y)\vec{k} - (x_2 - x)(z_4 - z)\vec{j} \\ &\quad + (y_2 - y)(z_4 - z)\vec{i} - (y_2 - y)(x_4 - x)\vec{k} \\ &\quad + (z_2 - z)(x_4 - x)\vec{j} - (z_2 - z)(y_4 - y)\vec{i} \end{aligned}$$

$$\begin{aligned} \vec{A} \times \vec{B} &= [(y_2 - y)(z_4 - z) - (z_2 - z)(y_4 - y)]\vec{i} \\ &\quad + [(z_2 - z)(x_4 - x) - (x_2 - x)(z_4 - z)]\vec{j} \\ &\quad + [(x_2 - x)(y_4 - y) - (y_2 - y)(x_4 - x)]\vec{k} \end{aligned} \quad (135)$$

The condition that the flow be parallel to the surface is then satisfied when

$$\vec{V} \cdot (\vec{A} \times \vec{B}) = 0$$

$$\begin{aligned} \text{or } (\bar{u} + v_\infty) [(y_2 - y)(z_4 - z) - (z_2 - z)(y_4 - y)] + \bar{v} [(z_2 - z)(x_4 - x) \\ - (x_2 - x)(z_4 - z)] + \bar{w} [(x_2 - x)(y_4 - y) - (y_2 - y)(x_4 - x)] = 0. \end{aligned} \quad (136)$$

For simplicity we will define the terms in brackets as  $\bar{a}$ ,  $\bar{b}$ , and  $\bar{c}$  respectively. Note that one must exercise care in choosing the labels for the points so that the normal  $(\vec{A} \times \vec{B})$  is always outward.

We have now found a means to represent the boundary condition of no flow across the surface of the body in terms of the coordinates of the corner points of the quadrilaterals making up the body. The system of equations one must then solve to find the individual source strengths is

$$\begin{aligned} & \left( v_\infty + \frac{1}{4\pi} \sum_{N=1}^k \frac{q_N(x_1 - \xi_N)}{[(x_1 - \xi_N)^2 + (y_1 - \eta_N)^2 + (z_1 - \zeta_N)^2]^{3/2}} \right) \bar{a}_1 \\ & + \frac{\bar{b}_1}{4\pi} \sum_{N=1}^k \frac{q_N(y_1 - \eta_N)}{[(x_1 - \xi_N)^2 + (y_1 - \eta_N)^2 + (z_1 - \zeta_N)^2]^{3/2}} \\ & + \frac{\bar{c}_1}{4\pi} \sum_{N=1}^k \frac{q_N(z_1 - \zeta_N)}{[(x_1 - \xi_N)^2 + (y_1 - \eta_N)^2 + (z_1 - \zeta_N)^2]^{3/2}} = 0 \\ & \quad \vdots \\ & \left( v_\infty + \frac{1}{4\pi} \sum_{N=1}^k \frac{q_N(x_k - \xi_N)}{[(x_k - \xi_N)^2 + (y_k - \eta_N)^2 + (z_k - \zeta_N)^2]^{3/2}} \right) \bar{a}_k \\ & + \frac{\bar{b}_k}{4\pi} \sum_{N=1}^k \frac{q_N(y_k - \eta_N)}{[(x_k - \xi_N)^2 + (y_k - \eta_N)^2 + (z_k - \zeta_N)^2]^{3/2}} \\ & + \frac{\bar{c}_k}{4\pi} \sum_{N=1}^k \frac{q_N(z_k - \zeta_N)}{[(x_k - \xi_N)^2 + (y_k - \eta_N)^2 + (z_k - \zeta_N)^2]^{3/2}} = 0 \quad . \end{aligned} \quad (137)$$

In these equations  $k$  = the number of quadrilaterals by which the surface is represented.  $x_k, y_k, z_k$  is the point on each quadrilateral at which the boundary condition is satisfied and  $\xi_k, \eta_k, \zeta_k$  is the point on each quadrilateral at which the source is located. Not making these points coincident will usually lead to less waviness in the surface pressures and velocities. If we choose to separate the source point from the point at which the boundary condition is satisfied, *i.e.*, the point at which the normal is computed, then we need to write an equation for a plane quadrilateral having its normal identical with that given by (135) and its corner points located at the same  $x$  and  $y$  locations but with slightly different  $z$  values. We need to do this in order to locate the source approximately on the surface in a known relationship to the corner points and to  $P(x,y,z)$ . From Equation (127) we see that since  $\bar{a}, \bar{b},$  and  $\bar{c}$  are now the direction numbers of the normal to the plane, picking one value of  $z$ , say  $z_1$  as lying on the physical surface permits one to solve for the other value of  $z$  and for  $d$ . If we choose to locate the source point at  $1/3$  the quadrilateral chord then the  $x$ -coordinate of the source point is given by

$$\frac{1}{2} \left[ x_1 + \frac{x_4 - x_1}{3} + x_3 + \frac{x_2 - x_3}{3} \right] = \xi_k . \quad (138)$$

The  $y$ -coordinate is given by

$$\frac{1}{2} \left[ y_3 + \frac{y_2 - y_3}{3} + y_1 + \frac{y_4 - y_1}{3} \right] = \eta_k . \quad (139)$$

The  $z$ -coordinate is then determined from the equation of that particular quadrilateral. If one wishes to move the point at which the boundary condition is satisfied to some other, fixed point along the quadrilateral chord, he could follow a similar procedure.

The source strengths,  $q_N$ , are then found by solving the rather large system of Equations (137) simultaneously. Given these values one can then find local velocity components from (126). The local pressure on the fuselage is then given by

$$P = P_\infty + \frac{1}{2}\rho[V_\infty^2 - (V_\infty + \bar{u})^2 - \bar{v}^2 - \bar{w}^2] . \quad (140)$$

Obviously, to obtain a reasonably accurate picture of the surface pressures, the number of quadrilaterals with which the surface is represented must be very large, particularly if the fuselage shape deviates significantly from that of a streamlined body. As was the case in the analysis of two-dimensional bodies (airfoils), conventional practice usually represents the potential by a constant source strength over the entire surface of a particular panel rather than by a point source as is done here. Use of the continuous distribution, it will be recalled, usually results in less waviness in the computed surface streamline. This streamline of course is required by our formulation to be parallel with the physical surface only at one point on each panel.



Because of the very large number of panels usually required to achieve reasonably accurate descriptions of the surface pressures on fuselage-like bodies, the opportunity to save substantial amounts of computer time or storage through the use of sophisticated numerical or mathematical procedures exists. Every program for performing such computations that the present authors have examined in detail (three at this writing) either carries out the calculation in pieces, takes advantage of the special character of the coefficient matrix in performing the inversion, recognizes that panels far away from the one on which the boundary condition is satisfied contribute little to the flow and therefore can be represented more approximately with no loss in accuracy, or uses line sources to represent all or part of the fuselage. Line sources, of course, can be used to greatly simplify the formulation of the problem, but unfortunately they can describe only slender fuselages adequately. A detailed discussion of the advantages and disadvantages of the various computation techniques is beyond the scope of the present work. This activity is mentioned merely to indicate to the reader that reducing the cost and complexity of the computations has already received considerable intelligent attention and is likely to be the subject of further intensive study in the near future.

By treating the fuselage as an isolated body, we have assumed implicitly that the fuselage is flying at such an inclination to the stream that it generates no lift other than by providing a bridge between the two halves of the wing. We shall also assume that the effect of the entire fuselage on the wing lift is adequately treated by the method of the previous section. Further, we shall assume that for purposes of finding the fuselage drag we can treat the fuselage as a free body, adding the wing-body interference effects later as an empirical or semi-empirical correction. These assumptions leave us with the necessity of determining only the boundary layer displacement and skin friction effects. In subsequent sections we shall examine some of the rationale for these assumptions and determine in a general way the conditions for which they are reasonable.

#### VISCOUS FLOW OVER FUSELAGES

The problem of determining the characteristics of a boundary layer flowing over a general, three-dimensional body is one of great fundamental interest. Unfortunately, the only known solutions are for axisymmetric bodies or other special cases. It is known, however, that if the body cross-sectional area and volume do not change rapidly in the streamwise direction and if there is no significant pressure gradient in the cross flow direction, then the boundary layer behaves in much the same way as it would on a two-dimensional body subject to the same history of pressure gradients in the streamwise direction. If we are willing to accept the restrictions and errors inherent in assuming that the three-dimensional boundary layer can be treated through such a concept, then we may use the techniques of the previous section to determine  $\delta^*$  and  $\tau_y=0$  along the

body streamlines<sup>†</sup>. One can obtain a reasonable estimate of the circumferential variation of  $\delta^*$  and  $\tau_{y=0}$  at any axial station by calculating  $\delta^*$  and  $\tau_{y=0}$  along a series of these lines approximately equally spaced in the circumferential direction.

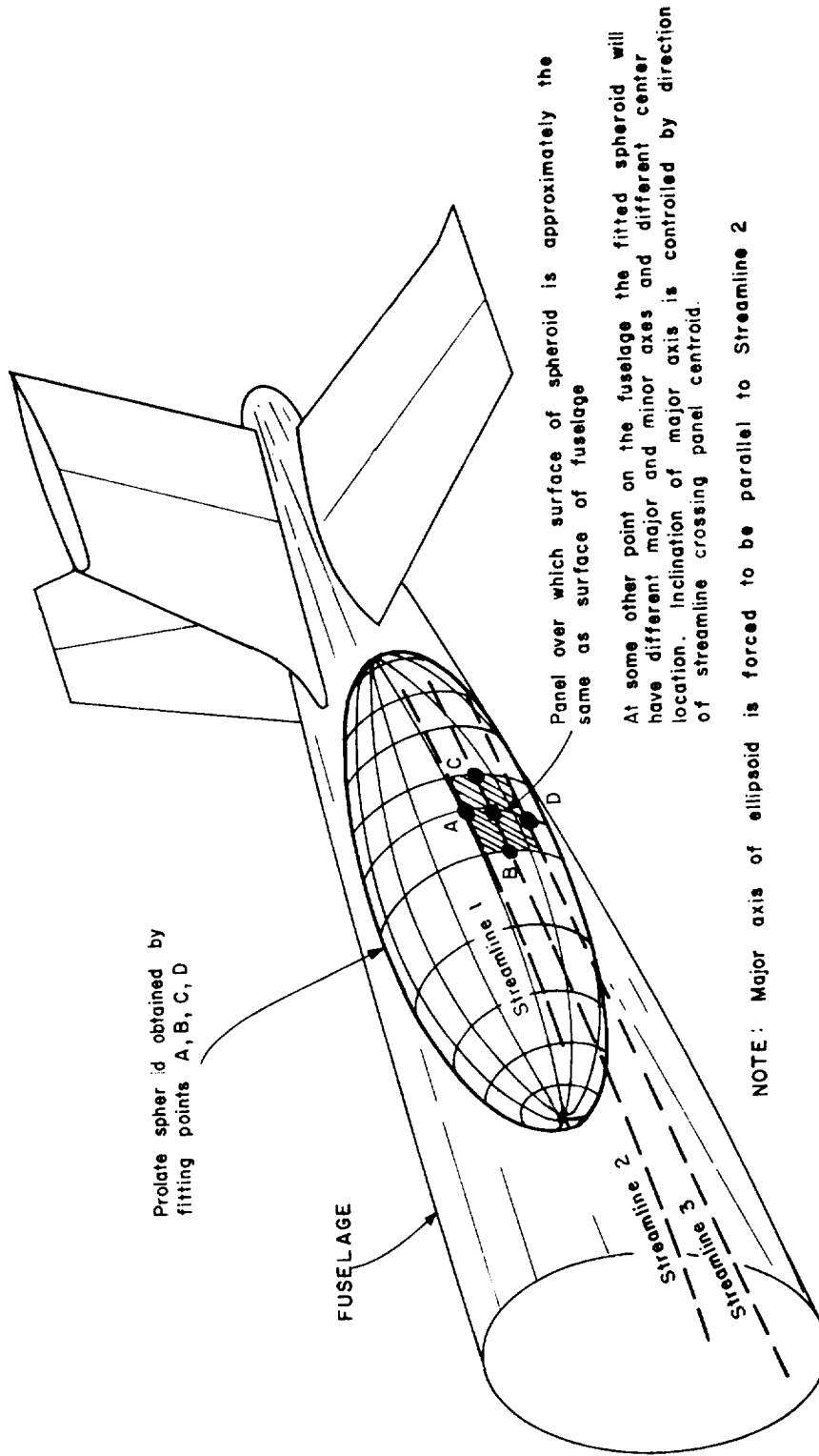
A new pseudo-surface can then be constructed by smoothing these displacements from the original surface and a new inviscid pressure distribution can then be calculated. This process for determining the fuselage drag follows essentially the same path as that employed earlier for determining airfoil drag except that the pressures and viscous shear must be integrated over appropriate areas rather than line segments. We will examine the process in somewhat more detail a little later.

One may argue with considerable justification that if the use of a two-dimensional-boundary-layer-along-streamlines procedure gives results which compare well with experimental values for a group of fuselages, then it should be regarded as satisfactory for engineering purposes on this basis alone. However, since it is not exceedingly difficult to determine—to a fair degree of approximation—the conditions under which the additional terms in the three-dimensional boundary layer equations are small compared with the two-dimensional-along-streamlines terms, we shall now make this determination in order to identify those cases where the results obtained by the procedure may be suspect.

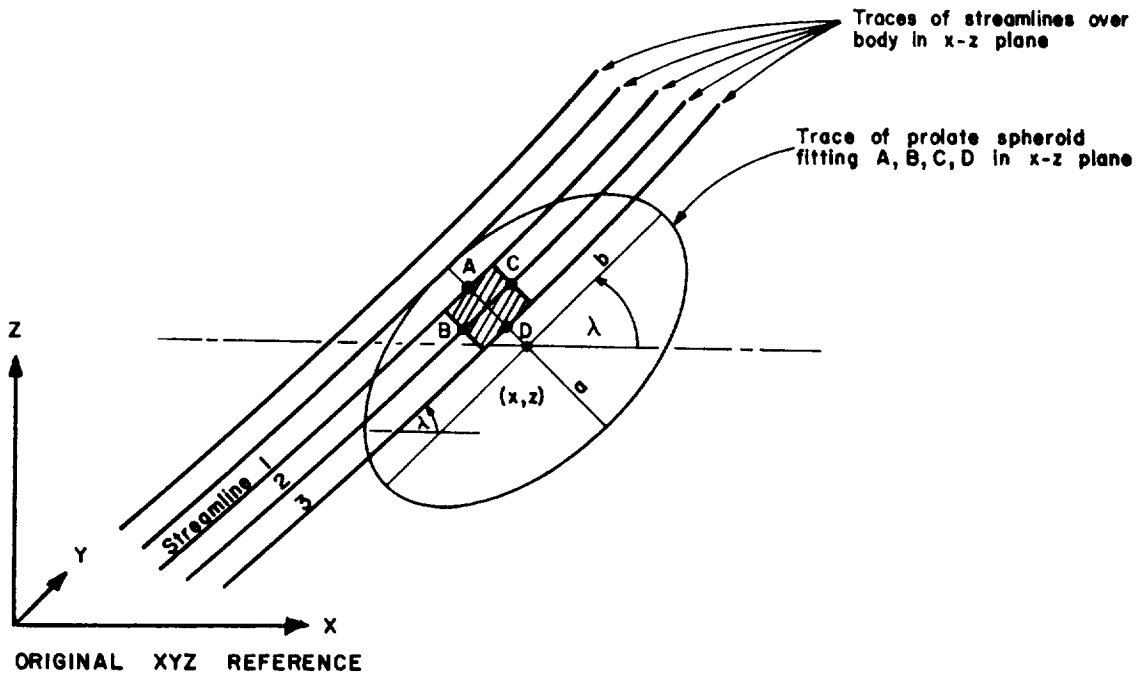
We begin by choosing to represent the fuselage locally by a section of a prolate spheroid with its major axis aligned with the local streamline and its center always in the x-z plane. The figures below depict this concept.

---

<sup>†</sup> Formally, two adjacent streamlines form the boundaries of the flow of a given quantity of fluid. The position of these lines on a body can be determined from the magnitude and direction of the flow over the surface.

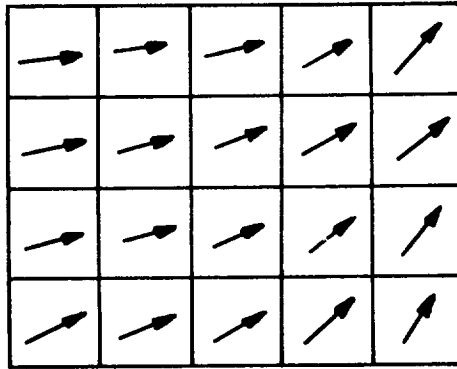


VIEW SHOWING HOW A SECTION OF A PROLATE SPHEROID WITH CENTER IN THE REFERENCE X-Z PLANE MAY BE USED TO REPRESENT THE SURFACE OF AN AIRCRAFT FUSELAGE LOCALLY

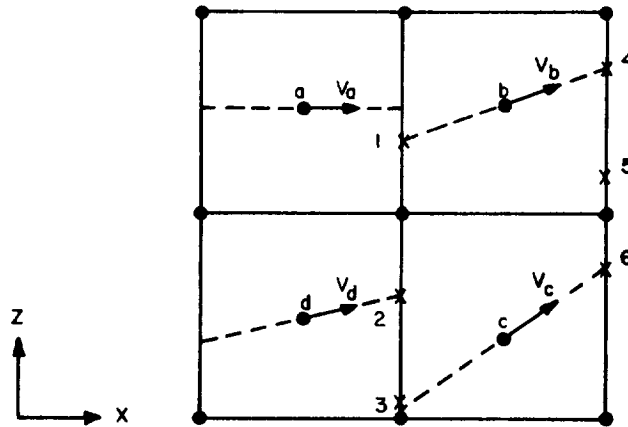


LOCATION OF SPHEROID WITH  
RESPECT TO REFERENCE AXES  
AND DEFINITION OF SYMBOLS

The solutions of equations (126) give us the magnitude and direction of the flow velocity at one point on each panel. If we observe a group of panels, as in the sketch below,



and place, at the point on each where the boundary condition is satisfied, a vector whose direction is the flow direction at that point and whose length is proportional to the flow magnitude, then we may employ the method of isoclines (Ref. 107, page 97) to sketch the streamlines. The streamlines, after all, represent the trajectories of given masses of fluid as they travel over the surface of the body. For computational purposes, however, it is preferable to describe these streamlines in a more analytical fashion. Consider the section of the surface shown in the sketch below:



From the magnitudes of the surface velocity components we know the direction of the flow at a, b, c, and d. Let us assume that this direction is constant across the panel (as shown by the dashed line). The quantity of flow that moves between b and c depends upon the distance between b and c and the average velocity between b and c. Since the quantity of fluid between two streamlines is always constant, the appearance of converging streamlines means that the flow velocity is increasing as the flow moves from left to right. If we assume that the fluid velocity at a given x-station between two streamlines can be considered to be constant, with a value between that along line 1-4 and that along line 3-6 at the same x-station, then the position of the streamline continuing to the right from point 2 will be related to points 4 and 6 as  $\left(\frac{\text{line } 2-3}{\text{line } 1-3}\right) = \left(\frac{\text{line } 5-6}{\text{line } 4-6}\right)$ . This insures that the quantity of fluid between 2 and 3 is the same as between 5 and 6. Further the magnitude of the velocity at 5 is that at 2 times  $\left(\frac{\text{line } 1-3}{\text{line } 4-6}\right)$ . Since we know the coordinates of the corner points on each planar panel as well as those of points a, b, c, and d in terms of the original reference axes, we may describe the line segment from 2-5 in this reference system without undue difficulty. We can do the same for other similar line segments and so relate the streamlines over the body to one another in an analytical fashion. The equation for any particular streamline will change of course as it crosses a panel boundary.

We recognize that the assumptions we made with regard to the velocity between streamlines and the straightness of streamlines across panels are true only in the limit of vanishing panel size. However, since we will generally employ more than 400 panels to represent a fuselage such assumptions should not introduce significant error in practice.

Having identified the location of the streamlines in this manner we proceed to orient the prolate spheroid by which we represent a section of the surface of the fuselage.

$$\text{Let } \lambda = \tan^{-1} \left[ \frac{z_{n+1} - z_{n-1}}{x_{n+1} - x_{n-1}} \right] \quad (141)$$

be the inclination of the streamline and  $z_{n+1}, x_{n+1}$  are the z and x coordinates of a point on the streamline just immediately downstream of the point of interest.  $z_{n-1}$  and  $x_{n-1}$  are then the coordinates of the point immediately upstream of the point of interest.  $\lambda$  defined in this fashion also represents the angle which the major axis of the spheroid makes with the original x-axis, as noted in one of the foregoing sketches.

This method of determining how the major axis should be oriented in order that it lie parallel to a streamline becomes indeterminate when the streamline is near the top or bottom of the fuselage. Indeterminacy occurs because

changes in flow direction are no longer confined principally to the x-z reference plane. For example, crossflow over the top of the fuselage may be evident only as a point in the x-z plane. The condition can be rectified by rotating ones viewpoint so that the changes in flow direction occur almost entirely in a plane normal to the direction of view. However, to illustrate the concept of fitting an arbitrary fuselage-like body locally by a prolate spheroid, we need work only with streamlines lying in a plane parallel to the x-z reference plane.

The equation for a prolate spheroid at the origin reads

$$\left(\frac{x}{b}\right)^2 + \left(\frac{y}{a}\right)^2 + \left(\frac{z}{a}\right)^2 = 1 \quad (142)$$

If, however, the origin is translated and the body rotated, both events taking place only in the x-z plane, the equation becomes

$$Ax^2 + By^2 + Cz^2 + Dxz + Ex + Fz + G = 0 \quad (143)$$

where

$$\begin{aligned} C &= (a^2 \sin^2 \lambda + b^2 \cos^2 \lambda) \\ B &= b^2 \\ A &= (a^2 \cos^2 \lambda + b^2 \sin^2 \lambda) \\ D &= 2(b^2 - a^2)\sin \lambda \cos \lambda \\ F &= 2x_1(b^2 - a^2)\sin \lambda \cos \lambda - 2z_1(b^2 \cos^2 \lambda + a^2 \sin^2 \lambda) \\ E &= 2z_1(b^2 - a^2)\sin \lambda \cos \lambda - 2x_1(b^2 \sin^2 \lambda + a^2 \cos^2 \lambda) \\ G &= 2x_1z_1(b^2 - a^2)\sin \lambda \cos \lambda + (b^2 x_1^2 + a^2 z_1^2)\sin^2 \lambda \\ &\quad + (a^2 x_1^2 + b^2 z_1^2)\cos^2 \lambda - a^2b^2 \end{aligned} \quad (144)$$

Since we have chosen to specify  $\lambda$  according to (141) and since the body cross-section in the original y-z plane is a circle, the number of unknown constant values is really only four:  $a$ ,  $b$ ,  $x_1$ , and  $z_1$ . We therefore rearrange the equation as follows:

$$a^2(h_1 + h_2 x_1 + h_3 z_1 + h_4 x_1 z_1 + h_5 x_1^2 + h_6 z_1^2) + b^2(h_7 + h_8 x_1 + h_9 z_1 + h_{10} x_1 z_1 + h_{11} x_1^2 + h_{12} z_1^2) = a^2 b^2 \quad (145)$$

In this form

$$\begin{aligned} h_1 &= z^2 \sin^2 \lambda + x^2 \cos^2 \lambda - 2xz \sin \lambda \cos \lambda \\ h_2 &= -2x \cos^2 \lambda + 2z \sin \lambda \cos \lambda \\ h_3 &= +2x \sin \lambda \cos \lambda - 2z \sin^2 \lambda \\ h_4 &= -2 \sin \lambda \cos \lambda \\ h_5 &= \cos^2 \lambda \\ h_6 &= \sin^2 \lambda \\ h_7 &= z^2 \cos^2 \lambda + y^2 + x^2 \sin^2 \lambda + 2xz \sin \lambda \cos \lambda \\ h_8 &= -2x \sin^2 \lambda - 2z \cos \lambda \sin \lambda \\ h_9 &= -2x \sin \lambda \cos \lambda - 2z \cos^2 \lambda \\ h_{10} &= 2 \sin \lambda \cos \lambda \\ h_{11} &= \sin^2 \lambda \\ h_{12} &= \cos^2 \lambda \end{aligned} \quad (146)$$

This equation we then fit to the fuselage surface at four points (A, B, C, D in sketch) to evaluate  $a$ ,  $b$ ,  $x_1$ , and  $z_1$ . We do this by choosing two points on the streamline of interest, one on either side of the point of interest, and one point on each of the adjacent streamlines as close to the point of interest as possible. We have then a system of four non-linear algebraic equations which we must solve to find  $a$ ,  $b$ ,  $x_1$ , and  $z_1$ . The equations are non-linear because they contain products of the unknowns, e.g.,  $x_1^2$ ,  $x_1 z_1$ .

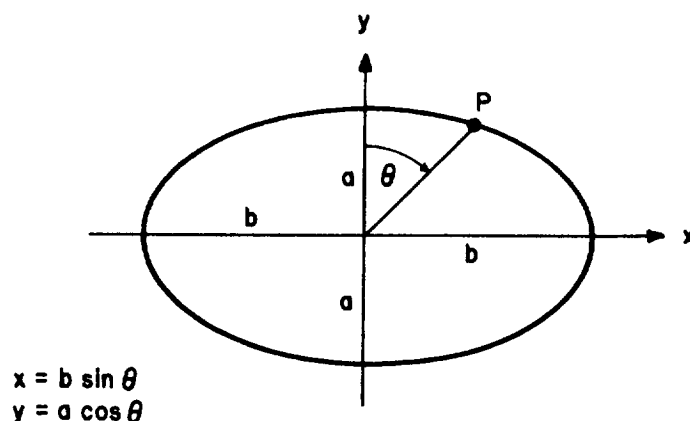
One method of solution for such a system of four equations is an adaptation of Newton's method for finding the roots of a single equation. In Newton's method one makes an initial estimate for the value of a root. If the estimate is reasonably close, the procedure yields a second approximation which is closer to the correct value. The procedure is repeated until the desired degree of accuracy is achieved. The generalization to a system of



four equations is outlined in Ref. 100, page 105. It is of course a numerical procedure of some length and is therefore best done on a computer.

Having found  $a$  and  $b$  for the particular prolate spheroid which represents the surface at the point of interest we ask how we might describe in orthogonal coordinates the length of a line along the surface of the spheroid. We wish to do this because the expression for the line element provides us with a means of characterizing the space (prolate spheroidal in this case). We may then use the boundary layer equations written in general curvilinear coordinates with the local values of the space inserted to evaluate the effects of body curvature on the values one might obtain for  $\tau_w$  and  $\delta^*$  using a momentum integral formulation.

Consider the figure below:



We recognize that the distance along the perimeter is given by

$$ds_1 = \sqrt{a^2 \cos^2 \theta + b^2 \sin^2 \theta} d\theta, \quad (147)$$

while if we rotate the figure about its x-axis the circumferential displacement of P is given by

$$ds_2 = a \cos \theta d\phi . \quad (148)$$

Thus, we can describe the distance traveled along the surface by the change in the values of two coordinates,  $\theta$  and  $\phi$ :

$$ds^2 = \{a^2 \cos^2 \theta + b^2 \sin^2 \theta\} d\theta^2 + a^2 \cos^2 \theta d\phi^2 \quad (149)$$

By specifying  $\lambda$  in the manner which we did we have virtually required that the major axis of the ellipsoid be parallel to the projection of the streamline in the x-z reference plane. In addition, by evaluating a and b in the manner described we have almost assured that the streamline is a section of the curve

$$\frac{\bar{x}^2}{b^2 \left[ 1 - \frac{\bar{z}^2}{a^2} \right]} + \frac{\bar{y}^2}{a^2 \left[ 1 - \frac{\bar{z}^2}{a^2} \right]} = 1 , \quad (150)$$

where  $\bar{z}$  may be treated as a constant. In other words, the streamline of interest is still an ellipse but may not be in the meridional plane. It will, however, lie parallel to this plane. The element of distance traveled along the surface in the streamwise direction now becomes

$$d\bar{s}_1 = \sqrt{a^2 \left( 1 - \frac{\bar{z}^2}{a^2} \right) \cos^2 \bar{\theta} + b^2 \left( 1 - \frac{\bar{z}^2}{a^2} \right) \sin^2 \bar{\theta}} d\bar{\theta} \quad (151)$$

while the distance in the crossflow direction is given by

$$d\bar{s}_2 = \sqrt{\bar{z}^2 + a^2 \left( 1 - \frac{\bar{z}^2}{a^2} \right) \cos^2 \bar{\theta}} d\bar{\phi} \quad (152)$$

$\bar{\theta}$  is a displacement about the z-axis in the plane  $z = \text{constant}$  while  $\bar{\phi}$  is a displacement about the x-axis in the plane  $x = \text{constant}$ . In terms of these

coordinates, the element of distance along the surface is given by

$$d\bar{s}^2 = \left[ a^2 \left( 1 - \frac{\bar{z}^2}{a^2} \right) \cos^2 \bar{\theta} + b^2 \left( 1 - \frac{\bar{z}^2}{a^2} \right) \sin^2 \bar{\theta} \right] d\bar{\theta}^2 + \left[ \bar{z}^2 + a^2 \left( 1 - \frac{\bar{z}^2}{a^2} \right) \cos^2 \bar{\theta} \right] d\bar{\phi}^2 \quad (153)$$

or 
$$d\bar{s}^2 = g_1^2 d\bar{\theta}^2 + g_2^2 d\bar{\phi}^2 . \quad (154)$$

For purposes of practical calculation we must still evaluate  $\bar{z}$ ,  $\bar{\theta}$ , and  $\bar{\phi}$ , in terms of the original body coordinates. The transformation equations for these quantities we can show to be

$$\bar{z} = (z - z_1) \cos \lambda + (x - x_1) \sin \lambda \quad (155)$$

$$\bar{\theta} = \tan^{-1} \left( \frac{(x - x_1) \cos \lambda - (z - z_1) \sin \lambda}{y} \right) \quad (156)$$

$$\bar{\phi} = \tan^{-1} \left( \frac{\bar{z}}{y} \right) \quad (157)$$

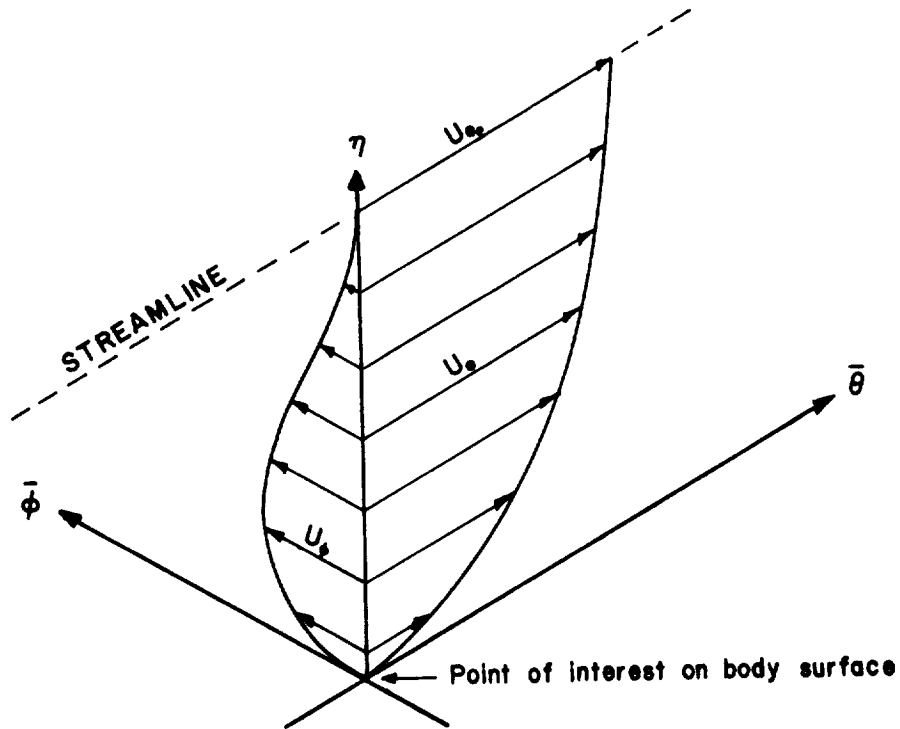
We now have the tools we need to describe streamwise and crossflow coordinates locally on the body in terms of the coordinates of points on the body surface as well as to write the boundary layer equations in this curvilinear coordinate system. We will not go through the derivation of the boundary layer equations in a general curvilinear coordinate system; rather we will employ those given for this case by Cebeci *et al.* (Ref. 99), rewritten in the present notation:

$$\frac{1}{g_1} \frac{\partial u_{\bar{\theta}}}{\partial \bar{\theta}} + \frac{\partial u_n}{\partial n} + \frac{\overset{\textcircled{1}}{1}}{g_2} \frac{\partial u_{\bar{\phi}}}{\partial \bar{\phi}} + \frac{\overset{\textcircled{2}}{u_{\bar{\theta}}}}{g_1 g_2} \frac{\partial g_2}{\partial \bar{\theta}} = 0$$

$$\frac{u_{\bar{\theta}}}{g_1} \frac{\partial u_{\bar{\theta}}}{\partial \bar{\theta}} + u_n \frac{\partial u_{\bar{\theta}}}{\partial n} + \frac{\overset{\textcircled{3}}{u_{\bar{\phi}}}}{g_2} \frac{\partial u_{\bar{\theta}}}{\partial \bar{\phi}} - \frac{\overset{\textcircled{4}}{u_{\bar{\phi}}^2}}{g_1 g_2} \frac{\partial g_2}{\partial \bar{\theta}} = - \frac{1}{\rho g_1} \frac{\partial P}{\partial \bar{\theta}} + \nu \frac{\partial^2 u_{\bar{\theta}}}{\partial n^2}$$

$$\frac{u_{\bar{\theta}}}{g_1} \frac{\partial u_{\bar{\phi}}}{\partial \bar{\theta}} + u_n \frac{\partial u_{\bar{\phi}}}{\partial n} + \frac{u_{\bar{\phi}}}{g_2} \frac{\partial u_{\bar{\phi}}}{\partial \bar{\phi}} + \frac{u_{\bar{\theta}} u_{\bar{\phi}}}{g_1 g_2} \frac{\partial g_2}{\partial \bar{\theta}} = - \frac{1}{\rho g_2} \frac{\partial P}{\partial \bar{\phi}} + \nu \frac{\partial^2 u_{\bar{\phi}}}{\partial n^2} \quad (158)$$

The velocities and directions are defined in the sketch below:



In these equations

$$\frac{\partial g_2}{\partial \bar{\theta}} = - \frac{\frac{1}{2} a^2 \left( 1 - \frac{\bar{z}^2}{a^2} \right) \sin^2 \bar{\theta}}{\sqrt{\bar{z}^2 + a^2 \left( 1 - \frac{\bar{z}^2}{a^2} \right) \cos^2 \bar{\theta}}} . \quad (159)$$

Despite the apparent generality of this form of the boundary layer equations we are still forced to assume when using them that the inviscid streamlines are displaced only in the  $n$ -direction by the presence of the boundary layer. We must do this in order that the metrics ( $g_1, g_2$ ) we compute at a point on the surface apply vertically through the boundary layer.

The differences between the two-dimensional boundary layer equations developed earlier and the present three-dimensional treatment lie in the four numbered terms and the third equation. We note that if the circumferential variation in pressures at a given  $x$ -station along the body is small compared with the change in pressures in the streamwise direction, then there is no significant force available to produce a crossflow. Since this term,  $\frac{\partial P}{\partial \bar{\phi}} \frac{1}{\rho g_2}$ , must, because of the basis on which the equation was written, be at least as large in magnitude as any term in the equation, we are justified in ignoring the third equation whenever  $\frac{\partial P}{\partial \bar{\phi}} \ll \frac{\partial P}{\partial \bar{\theta}}$ .

We now need to find the conditions under which the other four terms may be ignored. Unfortunately we cannot demonstrate these easily in a rigorous fashion. But we will observe that if  $\partial P / \partial \bar{\phi}$  is small then it is not likely that  $u_{\bar{\theta}}$  will be large; in fact, it will probably be no more than about 1/10 as large as  $u_{\bar{\theta}}$ . In that event, term number (4) is probably small compared with terms on the right hand side of the equation. Again, if  $\partial P / \partial \bar{\phi}$  is small we would not expect  $u_{\bar{\theta}}$  to change substantially from one  $\bar{\phi}$  value to another (for the same  $\bar{\theta}$ ). This, combined with the small value of  $u_{\bar{\theta}}$ , means that term (3) probably is also quite small. By the same argument we can ignore term (1). Term (2), however, is not small in regions of large changes in body curvature, i.e., near the nose or the tail of the spheroid. ( $\bar{\theta} \rightarrow \pm 90^\circ$ ). It is this term which accounts for the spreading of the flow as it moves straight downstream from the nose over the increasing surface area of the body.

It would appear, then, that as long as one observed the criteria

$$1. \quad \frac{\partial P}{\partial \bar{\phi}} \ll \frac{\partial P}{\partial \bar{\theta}}$$

and

$$2. \quad \bar{\theta} < \left| \frac{0.9\pi}{2} \right| \quad (160)$$

the use of a two-dimensional boundary layer calculation along streamlines would be a reasonable way of determining  $\delta^*$  and  $\tau_w$ .

By choosing a sufficient number of streamlines we can insure that at least one streamline will cross each panel somewhere near its center. The solution of the boundary layer equation along that streamline will then give us  $\tau_w$  and  $\delta^*$

near the centroid of each panel. Because of the very great amount of work involved in successively modifying the body shape to account for displacement thickness effects, we will for the present, adopt the policy of using the first calculation of  $\tau_w$  as the final value.

We could modify the body shape to account for displacement effects by adding

$$\delta^* = \frac{\bar{a}}{\sqrt{\bar{a}^2 + \bar{b}^2 + \bar{c}^2}} \quad (161)$$

to the x-dimension of all point on the panel

$$\delta^* = \frac{\bar{b}}{\sqrt{\bar{a}^2 + \bar{b}^2 + \bar{c}^2}} \quad (162)$$

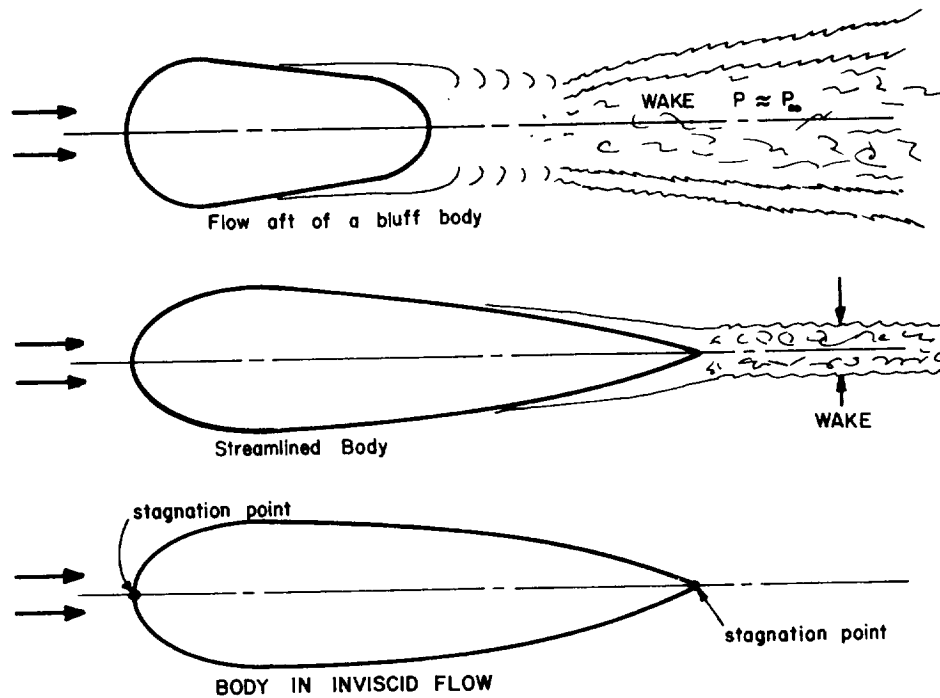
to the y-dimension and

$$\delta^* = \frac{\bar{c}}{\sqrt{\bar{a}^2 + \bar{b}^2 + \bar{c}^2}} \quad (163)$$

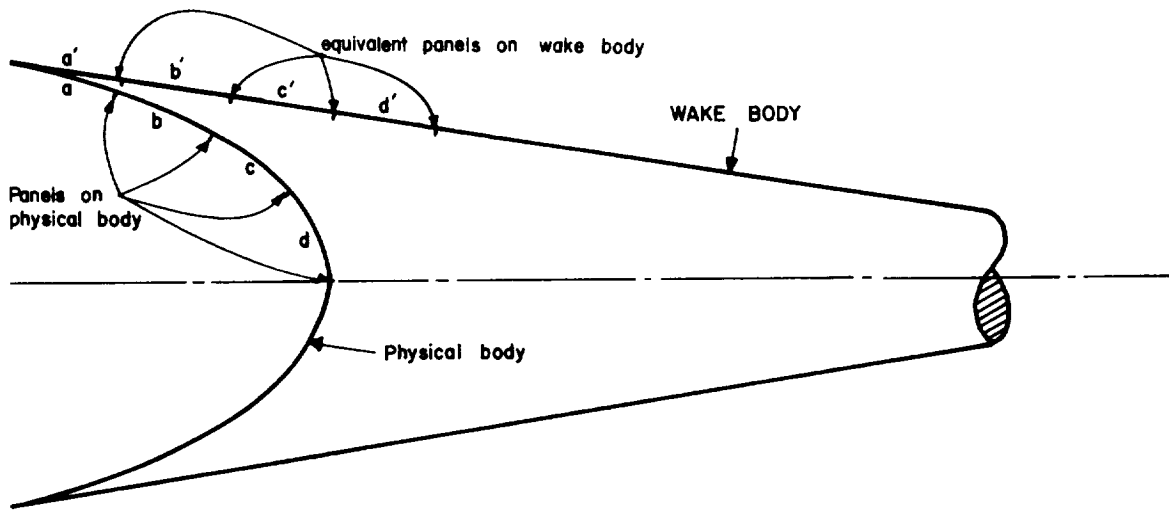
to the z-dimension,  $\bar{a}$ ,  $\bar{b}$ , and  $\bar{c}$  are given by equation (136).

However, the displacement thickness over the forward part of the body is usually small and the use made of this information on the rear part of the body in our drag calculations, as outlined below, is rather approximate. In these circumstances recomputation of the entire body contour does not appear to be warranted.

It must be constantly borne in mind that the approach used here for determining the pressures and velocities over the body surface is an inviscid one. As such, it always places a stagnation point at the downstream end of a closed body. As a result, the computation always leads to a prediction of rear stagnation pressures at the aft end of the body in what is physically a wake region. See the sketch below. The pressures in this wake are generally less than atmospheric immediately aft of the body and rise to the free stream value some distance downstream. The relatively low pressure exerted on that portion of the body's geometry opposite the high pressure stagnation region near the nose is the principal source of the force acting in the direction of the flow which we call form drag or pressure drag. Bodies producing extensive regions of flow separation will therefore have large pressure drags. It is apparent, therefore, that we must represent the wake effects with reasonable accuracy if we are to make meaningful drag computations.



How to include such a representation within the framework of our procedure for determining the inviscid flow field is the hurdle we must clear. Since the wake is a region of "dead" air relative to the body it seems reasonable to represent it by assuming it to be part of the physical body for purposes of calculating the inviscid flow field. Then, by assigning quadrilaterals to the surface of this wake-body which are of approximately the same area as those on the physical body, one can redo the inviscid computation to find the pressures on the wake-body. See the sketch below. The pressures on those panels of the wake-body which lie immediately above equivalent panels (quadrilaterals) on the physical body are then applied to the panels on the physical body along the normals to the physical body. The forces acting on the physical body are summed to find a lift and a drag. Since the pressures on the upstream portion of the wake-body will, if its contours are properly chosen, be less than those on the rear of the physical body according to the inviscid flow computation, the integration of forces will indicate a net drag on the body. Note that the total number of panels considered in the analysis is greater when the wake-body is present.



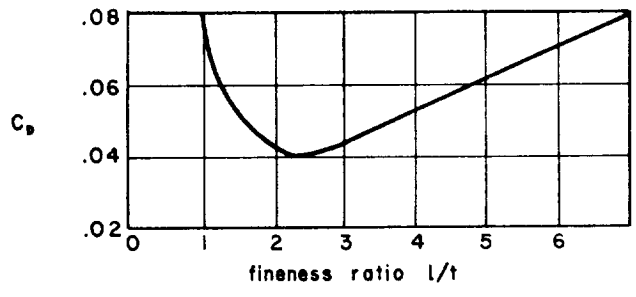
Pressures computed on panels a', b', c', and d' by the inviscid source distribution are applied to panels a, b, c, and d on the physical body before the integration of forces in the axial direction is carried out. Since these pressures are lower than those computed by source distribution on the physical body, a net drag is obtained on integration.

Some difficulty arises in attempting to specify the contours of the wake-body *a priori*. If the contours are significantly concave, the inviscid flow model will always produce a decelerating flow in these regions and, hence, rising pressures. The computed pressure drag will then be less than that actually present. Further, the boundary layer model used cannot predict the location of the actual flow separation point. Thus, there is some ambiguity in locating the upstream origin of the wake-body as well as how it should fair into the physical body.

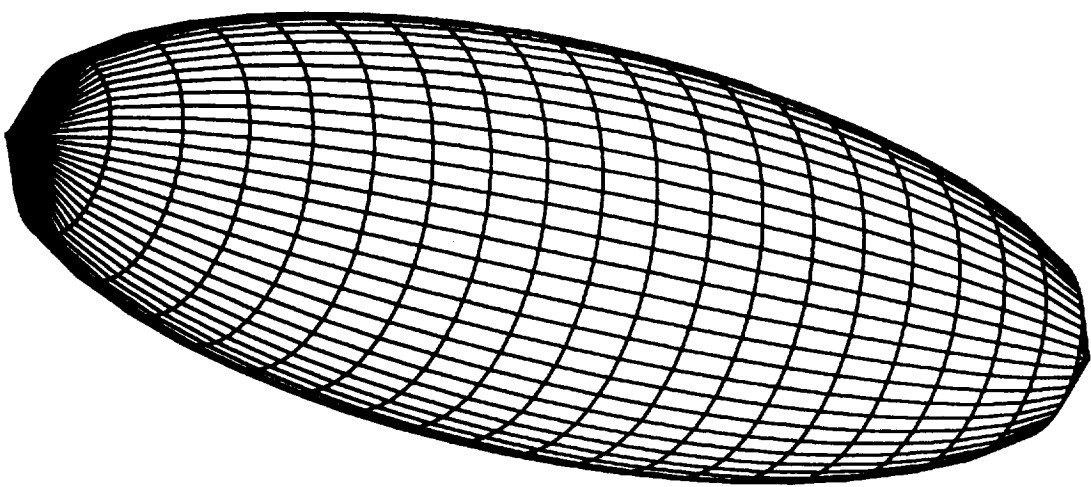
Consider, however, the drag data (Ref. 112) for airship hulls with geometries given in the following table.

$x/l$	$2y/t$	$x/l$	$2y/t$	$x/l$	$2y/t$
0	0	.150	.887	.600	.885
0.0125	.2	.200	.947	.700	.790
.0250	.335	.250	.982	.800	.665
.050	.526	.300	.998	.900	.493
.0750	.658	.350	.999	.950	.362
.100	.758	.400	.990	.980	.225
.125	.835	.500	.950	1.000	0

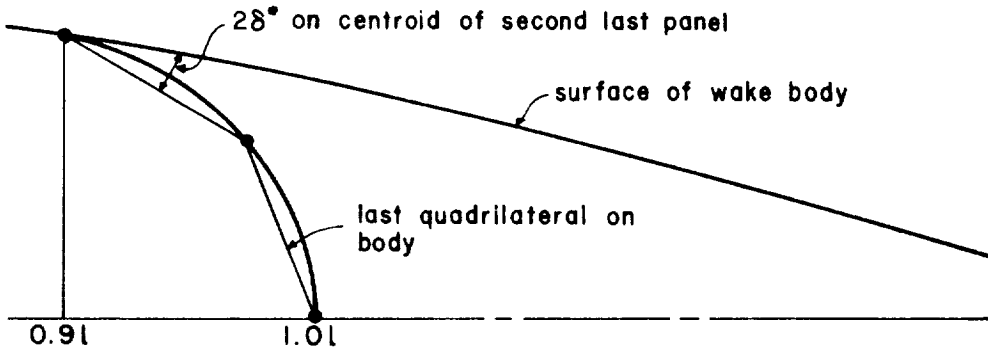




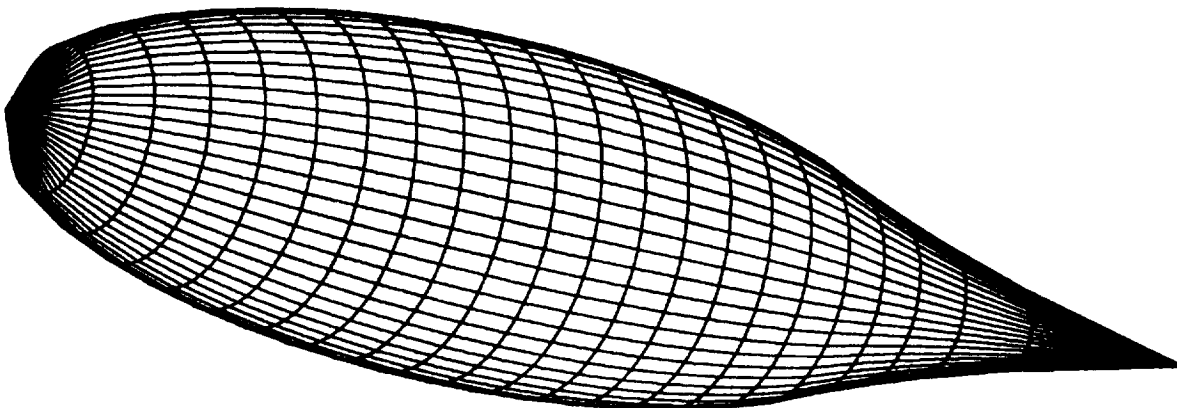
Note that the minimum combined skin friction and pressure drags occur at a fineness ratio of 2.1. The drag coefficient rises steeply for blunter bodies. It is thus, unlikely that fuselages will be blunter than a fineness ratio of 2 to 3. Calculations of the skin friction drag over a 3 to 1.0 ellipsoid (see sketch below) compared with the total measured drag indicate that the pressure



drag generated by such a body is about 25 percent of the total. As the fineness ratio increases this fraction of course decreases. The total drag is thus not particularly sensitive to small errors in determining the pressure drag on streamlined bodies. Let us, therefore, arbitrarily assume that the wake-body always begins at about the 0.9 $l$  point on the physical body. We will also assume that we can determine the initial surface slope of the wake-body from our calculation of the displacement thickness as indicated in the sketch below:



The wake-body surface we will gradually fair, via an exponential function, to a point sufficiently far downstream that the surface of the wake-body can be paneled with an even number of sets of panels in the streamwise direction. The panel areas are to be the same size as those on the physical body. It will be recognized that for thin wakes the termination point of the wake-body with this scheme is of necessity very far downstream. For thicker wakes, the termination point will be somewhat further upstream. The sketch below shows how the 3 to 1.0 ellipsoid appears with a wake-body appended.



The reader will recognize that an ellipsoid of revolution is one of the simplest bodies possible. Because the procedure outlined above gives reasonable results in such cases, does not mean that it will necessarily give reasonable results for more complex bodies, if applied in an arbitrary and capricious fashion. More complex bodies—of which light aircraft fuselages are excellent examples—can produce local separations as the flow rounds the cowling or encounters the windscreen and more general separations in the area aft of the cabin, for example. None of these situations can really be treated properly by the boundary layer theory employed. All one can do is insure that the fuselage geometry is adequately presented to the inviscid flow field computation and that when boundary layer computations indicate that separation is imminent, force the flow to continue attached (for computational purposes) until a more favorable pressure gradient is encountered. Sometimes these measures will yield acceptable results, sometimes not. The user must in most cases examine the results with caution and in detail, relying on past experience and experimental evidence to determine whether they are reliable. It is unfortunate that the requirement for the exercise of such substantial engineering judgement in this procedure has not yet been eased. However, in defense of this situation one may point out that in contrast to other aspects of the prediction of aerodynamic characteristics of complete configurations, the estimation of fuselage drag in a rigorous analytical fashion is now in its infancy and undergoing considerable flux. The method related herein was assembled by the present writers in the absence of suitable techniques in the literature. With the intense activity in the field, however, it would be surprising indeed if it were not soon superseded by methods more easily applied and using more accurate boundary layer models.

We have discussed above the methods by which we find the pressure and skin friction on individual panels or quadrilaterals. To determine the lift, drag, and pitching moment of the entire body we begin by finding first the component in either the z (lift) direction or the x (drag) direction, of the pressure on each panel. A product of this pressure component and the panel area (assuming of course that the pressure determined for a particular point on the panel exists everywhere on that panel) gives the force contributed by the panel to the total body force along either the z or x-axis. The pressure on a panel is exerted parallel to the normal to the panel. Thus, the component of the pressure in the z-direction is given by

$$P_{z_i} = P_i \left( \frac{\bar{c}}{\sqrt{\bar{a}^2 + \bar{b}^2 + \bar{c}^2}} \right)_i \quad (164)$$

while the component in the x-direction is

$$P_{x_1} = P_i \left( \frac{\bar{a}}{\sqrt{\bar{a}^2 + \bar{b}^2 + \bar{c}^2}} \right)_i \quad (165)$$

Formally, then, the lift is simply

$$L = \sum_{i=1}^k P_{z_1} A_i \quad (166)$$

where  $k$  is the number of panels on the body and  $A_i$  is the area of the  $i$ th panel. The pressure drag is

$$D_p = \sum_{i=1}^k P_{x_1} A_i . \quad (167)$$

The pitching moment is easily seen to be

$$M = \sum_{i=1}^k P_{z_1} (x_0 - x_i) A_i , \quad (168)$$

where  $x_0$  is the moment reference point and  $x_i$  is the  $x$ -coordinate of the  $i$ th panel.

If we call  $\gamma_x$ ,  $\gamma_y$ , and  $\gamma_z$  the direction cosines of the streamlines over the body, then the  $x$ -component of the skin friction on each panel, when summed over all panels on the body, becomes the skin friction drag:

$$D_f = \sum_{i=1}^k \tau_{w_i} \gamma_{x_i} A_i . \quad (169)$$

Skin friction contributions to the lift and pitching moment can be found in an analogous fashion. The total fuselage drag is the sum of the pressure drag and the skin friction drag, i.e.,

$$D = D_f + D_p . \quad (170)$$

## CONCLUDING REMARKS

In our determination of the lift, drag, and moment characteristics of light aircraft fuselages we have generally employed a procedure which is characterized by the following steps:

1. Represent the surface of the isolated fuselage by a number of quadrilaterals or four-sided panels.
2. In effect move all four corners of the panel into the same plane through the procedure which determines the direction of the normal.
3. Place a source of undetermined strength on each panel and require that the velocity induced by all sources plus that due to the free stream in the direction normal to the surface of each panel be zero.
4. Solve the resulting system of equations for the source strengths.
5. Compute the velocity over the body surface. From this, determine streamlines and surface pressures.
6. Perform two-dimensional, momentum-integral-type boundary layer computations along streamlines to find local values of  $\tau_w$  and  $\delta^*$ .
7. Integrate  $\tau_w$  over the surface to find the skin friction drag of the isolated fuselage.
8. Modify the body shape by attaching a wake-body toward the trailing edge and enlarging, if desired, the remainder of the body to account for displacement thickness effects.
9. Compute a new set of source strengths and surface pressures corresponding to the wake-body shape.
10. Integrate the surface pressures to find the lift, pressure drag, and pitching moment of the fuselage.

This procedure of course applies only to an isolated fuselage and does not account for flow interactions between the fuselage and the wing or tail plane. These are discussed in the following chapter. The procedure also does not account for the effects on drag of small protuberances such as extended landing gear. A suggested means of tying together the results of the various computations in this, the previous chapter, and the chapter on interactions, along with empirical results for small protuberances, is presented in the chapter on Lift and Drag Estimation of Complete Configurations.

We should mention also that the method developed here applies only to fuselages so inclined as to have minimum circumferential pressure gradients. This was done, it will be recalled, to permit the use of a simple boundary layer computation procedure along streamlines. With the need for many panels to adequately represent the body and the desire to have at least one streamline go through each panel near its centroid, the number of boundary layer calculations required to accomplish this is very substantial. In essence we are substituting a large number of two-dimensional computations which we know how to do for a smaller number, perhaps, of difficult and involved three-dimensional computations with which we have had little experience as yet. For this reason and the very large computer capacity required even for such an approach, we have not considered the case of flow approaching the fuselage with a vertical or sidewise component. The reader will recognize that because the formulation of our problem is linear, the effects of such components can be superimposed on the effects of the axial component. To include one of these components, however, is the equivalent, computationally, of repeating the problem. Considering only an axial onset flow limits the applicability of our treatment to cases where the fuselage angle of attack is always near zero, i.e., near cruise. We cannot, therefore, take adequate advantage of the ability of the wing program to yield reliable results up to  $C_L$ 's of about 0.8 except to account for variations in wing incidence angle. It is to be expected, however, that such restrictions will be relaxed through the use of improved methods which should be available from the major airframe manufacturers within the next few years.

## INTERFERENCE EFFECTS

In our previous discussion we mentioned that while we perform most of our aerodynamic calculations on isolated fuselages and wings we did realize that when these components are joined together to form practical configurations there are interactions between them not accounted for by the treatment of isolated components. We intimated that we would approach these interaction effects largely on an empirical basis. As may become evident from the discussion below, we are virtually forced to take this approach by the complexity of the problem.

### WING-TAIL INTERFERENCE

An aircraft's horizontal tail plane is flying in a very non-uniform flow field at least compared with the one seen by the main wing. In developing lift, the main wing imparts a downward component to the flow over it, a component which is not uniform across the span. Further, the wake produced by the main wing is a sheet-like region of low dynamic pressure which diffuses slowly as it moves downstream. These phenomena make it difficult to determine the orientation and magnitude of the flow striking the tailplane. Ferrari in Ref. 98 describes the situation aptly:

*"For wings of aspect ratio greater than 4.0 and sweep angles of less than 30°, the wings' system of bound vortices may be taken to be compressed into one single vortex, the axis of which is normal to the plane of symmetry and passes through the mean aerodynamic center of the lifting surface. The single vortex has a circulation that is variable in strength along the span; a trailing vortex sheet is shed across the whole breadth of this bound vortex core. The actual shape of the vortex sheet is rather difficult to specify inasmuch as it depends upon the particular velocities induced by the vortex system at the points occupied by the trailing vortex sheet.*

*The problem is complicated even more seriously because the trailing band of vortices is unstable. As a result of this instability the band tends to roll up at the edges in such a way that two distinct vortical corelike nuclei of appreciable size are formed, which are characterized by equal and opposite amounts of circulation...the complete rolling up of the vortices is accomplished only at a certain distance behind the rear edge of the wing, which may be calculated from the relationship  $0.56 \frac{b}{2} \frac{AR}{C_L}$ " where the symbol AR denotes aspect ratio and b is the wing span.*

*For most cases of interest however "the region of the vortex sheet which stands nearest to the stabilizer...is not yet involved in the roll-up phenomena."*

The usual way to treat the problem of determining the direction and magnitude of the flow approaching the stabilizer is to assume first of all that the wake is non-existent. This enables one to use an extension of the lifting line theory (as we shall do below) to find the flow angle anywhere in the downwash field. The effect of the wake is then added in a semi-empirical fashion.

Referring now to the figure following equation (82) we may, as we did in obtaining equation (87), write an expression for the downwash component of the flow velocity at any point aft of the wing, which includes contributions from the bound vortex (that running along the wing span) and the two trailing vortices:

$$\begin{aligned}
 w = \frac{\Gamma}{4\pi} & \left\{ \frac{-x}{x^2 + z^2} \left[ \frac{y + b/2}{\sqrt{x^2 + z^2 + (y + b/2)^2}} - \frac{y - b/2}{\sqrt{x^2 + z^2 + (y - b/2)^2}} \right] \right. \\
 & - \frac{y - b/2}{z^2 + (y - b/2)^2} \left[ 1 - \frac{x}{\sqrt{x^2 + z^2 + (y - b/2)^2}} \right] \\
 & \left. + \frac{y + b/2}{z^2 + (y + b/2)^2} \left[ 1 - \frac{x}{\sqrt{x^2 + z^2 + (y + b/2)^2}} \right] \right\} \quad (171)
 \end{aligned}$$

Positive z-direction is downward and positive x-direction is upstream. The other components of the induced velocity are

$$u = \frac{\Gamma}{4\pi} \frac{z}{x^2 + z^2} \left\{ \frac{y + b/2}{\sqrt{x^2 + z^2 + (y + b/2)^2}} - \frac{y - b/2}{\sqrt{x^2 + z^2 + (y - b/2)^2}} \right\} \quad (172)$$

$$\begin{aligned}
 v = \frac{\Gamma}{4\pi} \frac{z}{z^2 + (y - b/2)^2} & \left\{ 1 - \frac{x}{\sqrt{x^2 + z^2 + (y - b/2)^2}} \right\} \\
 - \frac{\Gamma}{4\pi} \frac{z}{z^2 + (y + b/2)^2} & \left\{ 1 - \frac{x}{\sqrt{x^2 + z^2 + (y + b/2)^2}} \right\}. \quad (173)
 \end{aligned}$$

The foregoing expressions give the velocity components induced by a single horseshoe vortex. In the usual case where it is necessary to represent



the actual distribution of circulation by superimposing a number of simple horseshoe vortices, the induced velocity components are calculated by replacing  $\Gamma$  by  $d\Gamma/d\eta$  and  $b/2$  by  $\eta$  in (171, 172, and 173) and the integrating the resulting expressions from  $\eta = 0$  to  $\eta = b/2$ .  $\Gamma(\eta)$  is known beforehand from the procedure which determines the three-dimensional lift distribution on the wing. Since this integration must be carried out for each point of interest, the mapping of the flow direction and magnitude in the region near the tail is a laborious process. The flow direction in the x-z plane is found from the expression

$$\epsilon = \sin^{-1} \left[ \frac{w}{V + u} \right], \quad (174)$$

while the magnitude is given by

$$\sqrt{w^2 + (V + u)^2}. \quad (175)$$

If the stabilizer is placed about three chord-lengths behind an aspect ratio 6.0 wing, it will be found that the downward angle will be about  $2SC_L/\pi b^2$  radians. For  $C_L = 0.6$  this is  $3.64^\circ$ .

The center of the vortex sheet describes a path in an x-z plane which can be found by integrating  $\epsilon$  with respect to x from the trailing edge of the wing rearward. Ferrari gives an expression, developed from experimental data, for the vertical displacement of this vortex sheet center which occurs because of the influence of the wake:

$$\Delta z = -\frac{1}{2} C_s \sin \alpha, \quad (176)$$

where  $C_s$  represents the length of separated flow over the airfoil (primarily the upper surface). The semi-thickness of the airfoil wake he states as

$$z_{\text{wake}} = 1.38 c C_{d_o}^{\frac{1}{2}} \left[ \frac{x}{c} + 0.15 \right]^{\frac{1}{2}}, \quad (177)$$

where  $C_{d_o}$  is the profile drag coefficient applying to the airfoil section located at the spanwise station at which the wake's behavior is being investigated. The magnitude of the velocity along the wake centerline Ferrari gives as

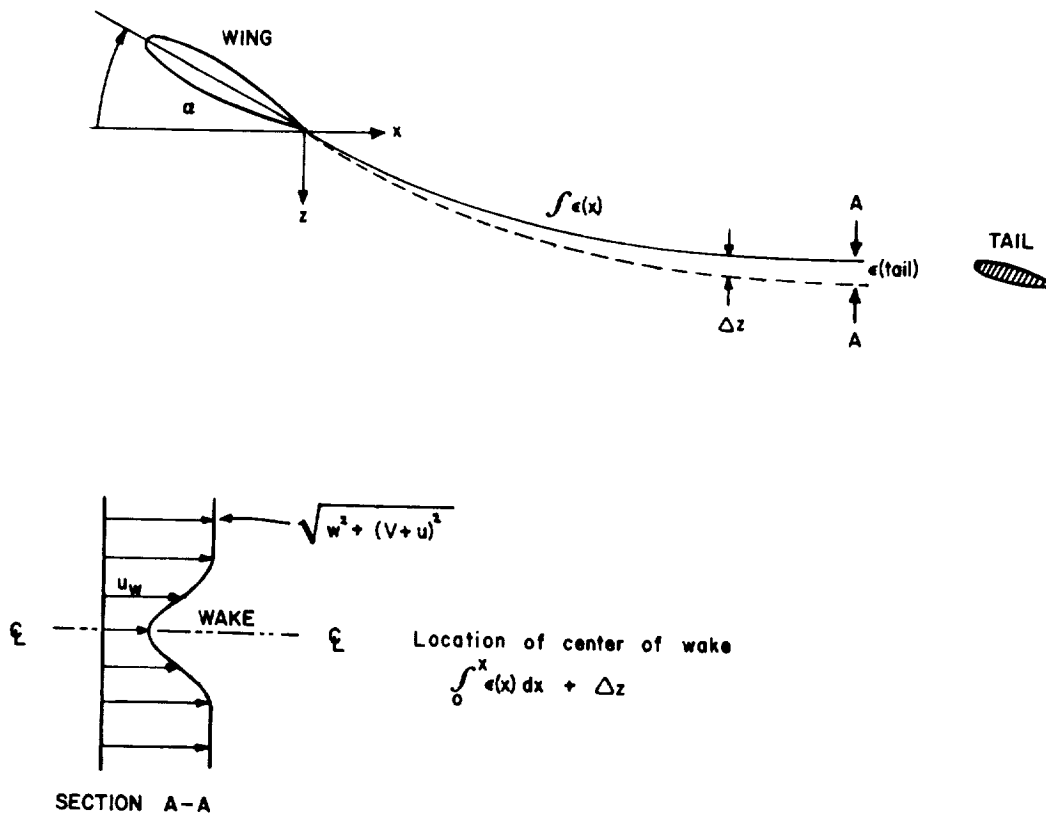
$$u_{w_c} = V \sqrt{1 - \frac{2.42 [C_{d_o}]^{\frac{1}{2}}}{\frac{x}{c} + 0.3}} \quad (178)$$

while the distribution of velocity vertically through the wake is

$$u_w = V \sqrt{1 - \frac{2.42 [C_{d0}]^{\frac{1}{2}}}{\frac{x}{c} + 0.3} \cos^2 \left( \frac{\pi \tilde{z}}{z_{wake}} \right)} \quad (179)$$

$\tilde{z}$  is to be measured from the wake centerline and  $\tilde{z}/z_{wake} \leq 1/2$ .

To summarize the procedure related above, we described the trace of the center of the vortex sheet shed by the wing in x-z plane at any value of y by an integration with respect to x of equation (174). Since this is an inviscid theory, we apply empirical corrections to account for viscosity effects. The actual wake centerline is displaced from the value given by the integration of (174) by an amount  $\Delta z$  from (176). The actual magnitude of the flow velocity across the wake is given by (179) rather than (175). Outside the wake region, the magnitude of the flow velocity is given by (175). The magnitude given by (175) should also be used in place of V in (179). These relationships are depicted in the figure below:



From the foregoing we have sufficient information to develop at least a semi-quantitative view of the disturbance which the wing produces in the flow field approaching the horizontal tail plane. With this view we can then proceed to calculate with reasonable accuracy the aerodynamic characteristics of this surface considering it to be a portion of a complete airframe. We do this by employing the theory for a complete wing in the presence of a fuselage developed in the previous chapter but substituting local values of  $(\alpha - \epsilon)$  for  $\alpha$  and  $u_w$  for  $V$  (if the tail plane is flying in the wing wake). Such a procedure ignores the presence of a thick boundary layer over the aft portion of the fuselage, the disturbance to the flow field caused by the vertical stabilizer, and the confluence of the body flow immediately downstream of the stabilizer. Since a thick boundary layer tends to smooth out disturbances and since it tends to make the fuselage appear to the flow to be longer and less rapidly varying in area than it actually is, it seems reasonable to conclude that for most configurations in cruise flight the effects ignored are small.

### LIFT OF AN ISOLATED FUSELAGE

It was pointed out in the discussion of the literature that a fuselage at angle of attack in inviscid flow should experience no net lift. Any lift generated is a result of viscous effects. In principle we could obtain the correct result by extending our treatment of forces on an isolated fuselage as presented in the previous chapter to include a vertical component in the onset flow and a boundary layer computation method which accepts circumferential pressure gradients and expanding flows. (It is of course possible that bodies of unusual shape will also generate lift in much the same way that wings do but we have not as yet added planar vortices to our treatment of the pressures on the fuselage to account for this.) Unfortunately, the procedure would assuredly be very lengthy. Since it is desirable in design work to have an indication of the relative importance of certain effects so that we know how precisely we will have to evaluate them, we would like to have a simpler means for establishing the magnitude of the fuselage lift and for identifying its source physically. One such means follows from the argument given below.

A very long circular cylinder whose axis is at angle  $\alpha$  with the oncoming flow has a flow about it which can be thought of as being made up of two non-interacting parts: first, an axial flow which cannot affect the lift although it does result in a skin friction drag; second, a crossflow which exhibits the same characteristics as the flow over a cylinder placed normal to a stream of velocity  $V \sin \alpha$ . For Reynolds numbers between  $4 \times 10^2$  and  $2 \times 10^5$  one finds from experiments (Ref. 65) that the drag coefficient of a cylinder normal to a stream is always about 1.1. This is, of course, a result of the separation of the flow from the cylinder near the  $90^\circ$  points and the creation of a large low pressure wake on the lee side. If the cross flow Reynolds number lies within this range, one would expect that a long, isolated cylinder will experience a force normal to its axis given by

$$N = 1.1 \frac{\rho}{2} (V^2 \sin^2 \alpha) l d . \quad (180)$$

$l$  is the length of the cylinder and  $d$  is its diameter. The force normal to the stream direction is then

$$L = N \cos \alpha . \quad (181)$$

Normalizing this force by the usual  $1/2 \rho V^2 d l$  gives

$$C_L = 1.1 \sin^2 \alpha \cos \alpha . \quad (182)$$

Most fuselages are not very long circular cylinders but have instead a nose which, even for the flow model assumed, i.e., noninteracting axial and crossflow components, experience an inviscid lift force. Usually, this force would be balanced by an equal and opposite force on the tail in inviscid flow, resulting in the development of a pitching moment but no net lift. If, however, the body is cut off so that the flow separates from the base and forms a viscous wake, the body appears to the inviscid flow to extend downstream for some distance at essentially constant diameter. The balancing force is then not developed and we are left with a net lift which is said to be potential or inviscid in origin. Following Ref. 101, we shall show how this arises.

We recall that the potential for the crossflow at station  $x$  on an infinite circular cylinder in cylindrical coordinates is written

$$\phi = -V \sin \alpha \left( r + \frac{a^2}{r} \right) \cos \theta \quad (183)$$

where  $a$  is the radius of the cylinder at station  $x$ ,  $r$  is the radial coordinate, and  $\theta$  is the angular coordinate measured from the forward stagnation point. The crossflow may also change in time as the flow moves along the axis of the cylinder so that the appropriate form of the Bernoulli equation giving the relation between pressure and velocity along a streamline is

$$\frac{P}{\rho} = -\frac{\partial \phi}{\partial t} - \frac{1}{2} \left[ \left[ \frac{\partial \phi}{\partial r} \right]^2 + \left[ \frac{\partial \phi}{r \partial \theta} \right]^2 \right] + c . \quad (184)$$

The three partial derivatives are given by

$$\frac{\partial \phi}{\partial t} = -V \sin \alpha \frac{\cos \theta}{r} 2a \frac{da}{dt} = -V \sin \alpha \cos \theta \frac{2a}{r} \frac{da}{dx} \frac{dx}{dt}$$

$$\frac{\partial \phi}{\partial r} = -V \sin \alpha \left(1 - \frac{a^2}{r^2}\right) \cos \theta . \quad (185)$$

$$\frac{\partial \phi}{r \partial \theta} = + \frac{V \sin \alpha}{r} \left(r + \frac{a^2}{r^2}\right) \sin \theta$$

Inserting these values into the Bernoulli Equation yields

$$\begin{aligned} \frac{P}{\rho} = & 2V^2 \sin \alpha \cos \alpha \frac{da}{dx} \frac{a}{r} \cos \theta - \frac{V^2 \sin^2 \alpha}{2} \left\{ \cos^2 \theta \left(1 - \frac{a^2}{r^2}\right)^2 \right. \\ & \left. + \left(1 + \frac{a^2}{r^2}\right) \sin^2 \theta \right\} + c \end{aligned} \quad (186)$$

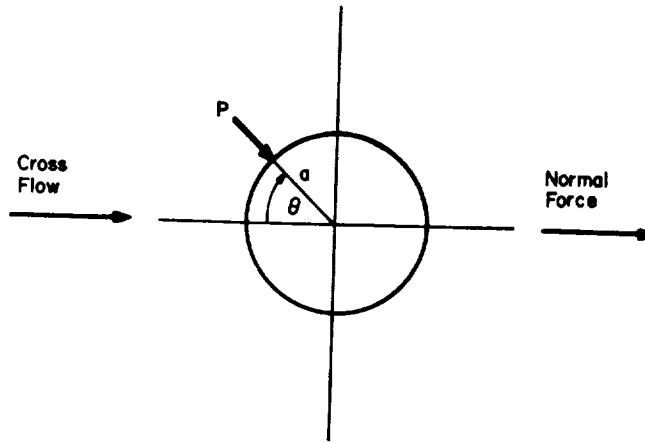
As  $r \rightarrow \infty$ , we must assume that  $P$  becomes  $P_\infty$ , the freestream value at infinity; hence

$$c = \frac{P_\infty}{\rho} + \frac{V^2 \sin^2 \alpha}{2} . \quad (187)$$

On the surface of the cylinder  $r = a$ . At this location the pressure is, accordingly,

$$\begin{aligned} \frac{P}{\rho} = & 2V^2 \sin \alpha \cos \alpha \frac{da}{dx} \cos \theta - \frac{V^2 \sin^2 \alpha}{2} \left[ 4 \sin^2 \theta \right] + \frac{P_\infty}{\rho} + \frac{V^2 \sin^2 \alpha}{2} \\ = & 2V^2 \sin \alpha \cos \alpha \frac{da}{dx} \cos \theta + \frac{V^2 \sin^2 \alpha}{2} \left[ 1 - 4 \sin^2 \theta \right] + \frac{P_\infty}{\rho} \end{aligned} \quad (188)$$

The force exerted by the crossflow, per unit length, on the cylinder is, as may be seen in the sketch below,



$$\begin{aligned} \frac{N}{l} &= \int_0^{2\pi} P a \cos \theta d\theta = \frac{\rho V^2}{2} \left[ \int_0^{2\pi} 2 a \sin 2 \alpha \frac{da}{dx} \cos^2 \theta d\theta \right. \\ &\quad \left. + \sin^2 \alpha \int_0^{2\pi} a(1 - 4 \sin^2 \theta) \cos \theta d\theta \right] + a \int_0^{2\pi} P_{\infty} \cos \theta d\theta . \end{aligned} \quad (189)$$

Since

$$\int_0^{2\pi} \cos \theta d\theta = 0 \quad \text{and} \quad \int_0^{\pi} \cos^3 \theta d\theta = 0 ,$$

$$\begin{aligned} \frac{N}{l} &= \frac{\rho V^2}{2} 4 a \sin 2 \alpha \frac{da}{dx} \int_0^{\pi} \cos^2 \theta d\theta \\ &= \frac{\rho V^2}{2} 2\pi a \frac{da}{dx} \sin 2 \alpha \end{aligned} \quad (190)$$

In producing a force on the cylinder the inviscid flow is deflected so that the lift is considered to act at an angle  $\alpha/2$  from the normal force:

$$\frac{L}{l} = \frac{\rho V^2}{2} 2\pi a \frac{da}{dx} \sin 2 \alpha \cos \frac{\alpha}{2} \quad (191)$$

This inviscid lift is developed by the body in addition to the viscous lift described earlier. The total lift is the sum of the two effects. We write therefore

$$\frac{L}{\rho V^2} = \int_0^l \left[ 2\pi a(x) \frac{da}{dx} \sin 2\alpha \cos \frac{\alpha}{2} + 2a(x) 1.1 \sin^2 \alpha \cos \alpha \right] dx \quad (192)$$

If we choose our reference area to be  $ld$  then

$$C_L = \frac{2}{ld} \int_0^l \left[ \pi a(x) \frac{da}{dx} \sin 2\alpha \cos \frac{\alpha}{2} + 1.1 a(x) \sin^2 \alpha \cos \alpha \right] dx \quad (193)$$

We note with interest that inviscid lift is present only when  $\frac{da}{dx} \neq 0$ , that is, primarily in the nose region of the body. We can easily make an approximate comparison between the predictions of this theory and experimental results taken on an ogive-cylinder-boattail ( $l/d = 12.7$ ,  $d = 5$ , nose length = 26.25) by assuming that the ogive can be satisfactorily represented by a cone and the boattailing can be ignored. Then  $da/dx = 0.125$ ,  $a(x) = 0.125x$  for  $x$  from 0 to 20;  $da/dx = 0$ ,  $a(x) = 2.5$  for  $x$  from 20 to 63.5. With these numbers

$$C_L = \frac{2}{317.5} \left[ \pi \sin 2\alpha \cos \frac{\alpha}{2} \frac{x^2}{128} \Big|_0^{20} + 1.1 \sin^2 \alpha \cos \alpha \left( \frac{x^2}{16} \Big|_0^{20} + 2.5x \Big|_{20}^{63.5} \right) \right] \quad (194)$$

$$C_L = 0.0619 \sin 2\alpha \cos \frac{\alpha}{2} + 0.573 \sin^2 \alpha \cos \alpha \quad (195)$$

The table below presents the results obtained with this formula and the comparable experimental data. Other experimental data on bodies of revolution may be found in Ref. 95.

$\alpha$	$C_L$ Theory	$C_L$ Experiment Ref. 96
4°	.0114	.0108
8°	.0280	.0233
12°	.0494	.0376
16°	.0744	.0536
20°	.1022	.0713

Qualitative agreement is seen to be quite good. The lack of quantitative agreement is no doubt a result of our failure to describe the shape of the experimental body with sufficient accuracy since the comparisons with experiment presented in Ref. 101 show good correlations.

To apply this theory properly to isolated fuselages, we can see from the foregoing development that we need to know

- (a) the fuselage geometry,
- (b) the crossflow drag coefficient at each axial station on the fuselage,
- (c) the crossflow potential function at each axial station, and
- (d) the extent of the fuselage over which the axial flow is essentially inviscid.

The latter we need in order to determine the axial extent over which we may need to consider potential forces. Frequently this point is taken to be the fuselage station at which the wing intersects the fuselage. The crossflow drag coefficient and crossflow potential function are often difficult to determine for non-circular bodies. We do know, however, that the crossflow drag coefficient for Reynolds numbers in the range  $10^2$ - $10^5$  is always less than about 1.4. (It has this value for a flat plate normal to the wind.) Since the inviscid lift term in (195) is linear and approximately equal to the viscous term for  $\alpha = 12^\circ$ , it seems reasonable to conclude that it would seldom be more than 30 percent greater than for the experimental configuration considered here. Thus, for all angles of attack of interest, the lift of an isolated fuselage can be expected to be less than 5 percent as great as the lift of a wing of the same planform area. Under conditions of cruising flight, the fuselage lift is probably around 1 percent of the wing lift. With the uncertainties involved in determining wing-body interference effects of this magnitude, fuselage lift alone can be justifiably ignored.

#### INTERACTION BETWEEN WING LIFT AND FUSELAGE LIFT

As long as the fuselage is long and thin and either circular or elliptical in cross section and the flow about the wing-body combination can be regarded as inviscid, Multhopp's transform technique discussed earlier adequately describes the effect of wing-body interference on overall lift. These conditions are seldom obtained in practice, however. It is of interest, therefore, to examine what method practicing designers use to describe this effect. Ref. 97 suggests that one assume a linear variation of lift with angle of attack and consider that the effect of the body on the wing lift, the wing on the body lift, and total wing-body lift are as given by the ratios in the following table:



body diameter / wing span	$L_{WB}/L_W$	$L_{BW}/L_W$	$L/L_W$
0	1.0	0	1.0
0.05	0.99	0.057	1.047
0.1	0.972	0.1215	1.094
0.15	0.956	0.170	1.127
0.2	0.936	0.224	1.16
0.25	0.907	0.270	1.18
0.30	0.882	0.308	1.19

$L_{WB}$  = wing lift in presence of body

$L_{BW}$  = body lift in presence of wing

$L_W$  = lift of wing without body

$L$  = Total lift

Examining the quantities in the table shows that as the body grows and begins to shield the wing, the wing lift falls off, but not as rapidly as the fuselage diameter increases. This indicates a substantial "bridging" effect and is about what one would predict from the Multhopp theory. The body's contribution to the total lift grows in direct proportion to its diameter. The total wing-body lift for fuselage width-to-span ratios typical of light airplanes is about 10 percent greater than for an isolated wing because of the flow wake existing over the fuselage. On the basis of our previous argument concerning the lift of isolated fuselages, it would appear that the interaction between the wing and the fuselage enhances the fuselage's contribution to the total lift. Experience with the flow over cylinders inclined to a stream (Ref. 102) would indicate that these effects actually are more non-linear with  $\alpha$  than would be suggested by the table above. In particular, if  $\alpha < 6^\circ$ , a common condition, certainly, for cruising flight, the crossflow wake is weaker than would be expected from linear considerations and the total lift under these conditions is probably about the same as for the wing alone or perhaps as small as that given by Multhopp's transform. Thus, it would seem reasonable to ignore lift interaction effects unless boundary layer calculations on the body alone indicate the likelihood of the formation of a wake on the upper side of the fuselage which would grow with small increases in angle of attack.

#### DRAG INTERACTION EFFECTS

During preliminary design it is usually assumed (Ref. 53) that the drag of wing-body combinations is the sum of the skin friction drag of the body and wing separately times a mutual interference factor plus the form drag of the combination. This mutual interference factor for the Mach numbers of interest in light aircraft is usually taken to be about 1.06 for Reynolds

numbers below  $2 \times 10^7$  and 0.93 for Reynolds number based on fuselage length above  $6 \times 10^7$ . A light aircraft with a 30' fuselage moving at 150 mph will have a Reynolds number of about  $4.5 \times 10^7$ . Thus for cruise conditions this interaction criterion would suggest that the drag interference effects are small.

Such interference criteria, however, cannot account for interactions which result in locally adverse pressure gradients on the wing or fuselage. These gradients often lead to flow separation (and accompanying high drag) at places like wing-fuselage junctions. Correction of these drag problems is usually relegated to the flight phase of the development program, the process being called "drag cleanup."

## LIFT AND DRAG OF COMPLETE CONFIGURATIONS

In the preceding chapters we have set forth theoretical methods by which one can determine the aerodynamic characteristics (lift, drag, and pitching moment) of airfoil sections and isolated fuselages at low and moderate angles of attack. We also presented an analytical method, valid for unswept wings at moderate-to-high aspect ratios, for correcting two-dimensional aerodynamic characteristics for the presence of the fuselage, taper, twist, changes in camber, and the finite extent of the wing. In addition, we discussed an analytical means by which one might determine the magnitude and direction of the flow approaching the horizontal tailplane. Further, we were able to show that for low-to-moderate angles of attack the fuselage contribution to the aircraft lift is usually negligible. We also noted the semi-empirical means by which drag interaction effects are frequently treated.

These various methods, interesting as they may be in themselves, remain largely academic exercises for the designer unless he can employ them effectively in the estimation of the lift and drag of complete configurations. It is really only in tasks of this kind that the advantages of more rigorous estimation procedures can be fully appreciated. For many reasons it is not yet practical to attempt to consolidate the various methods into a single computer program, the inner workings of which need not concern the user. It therefore requires some understanding of the basis for the various methods in order to apply them all to the same configuration and obtain useful results. We shall outline below a step-by-step procedure which should accomplish this objective.

1. Select the basis of the force coefficients. Normally we will take the wing planform area, including the portion covered by the fuselage, as the basic area.
2. From the geometry of the wing, including
  - (a) airfoil ordinates at several spanwise stations (at least root and tip)
  - (b) taper
  - (c) twist
  - (d) aspect ratio
  - (e) fuselage cross section at wing root and location of wing in relation to fuselage center,

determine the lift, drag, and pitching moment coefficients of the wing and the spanwise variation in circulation. These data come from the methods discussed in the chapter on wing characteristics. The spanwise circulation, it may be noted, is proportional to the final form of the spanwise variation in section

lift coefficient for a given  $\alpha$ . This information will be used later when we determine the flow conditions approaching the horizontal tailplane. Note also that for good results we should choose flight conditions for which  $C_L \leq 0.8$ .

3. Determine the drag force on the fuselage using the methods discussed in the chapter on fuselages. The methods will also give fuselage lift and pitching moment. The moment will be of interest if one seeks to perform stability computations at some later time. The lift given by these methods includes both the inviscid and viscous lifts discussed in the chapter on interference but of course does not include wing-body interference effects. This fuselage lift properly can be added to the wing lift; because it should be small compared with the wing lift, its computation can also serve as a check on the fuselage drag computation. If the fuselage lift is large, the fuselage drag values should be suspect.

4. Normalize the fuselage drag force by the wing area and the free-stream dynamic pressure.

5. Compute the magnitude and direction of the flow approaching the horizontal tailplane.

6. With these data, use the methods of (2) above to determine the lift, drag, and pitching moment of the horizontal tailplane.

7. Normalize by the wing area and freestream dynamic pressure.

8. Add the lift coefficients for the wing, fuselage, and horizontal tailplane together to obtain an overall lift coefficient. Do the same for drag and moment coefficients.

9. Multiply the total drag coefficient by a factor ranging from 1.06 at low Reynolds numbers ( $< 2 \times 10^7$ ) to 0.93 at high Reynolds numbers ( $< 6 \times 10^7$ ). Reynolds number is based on fuselage length.

10. Add in drag increments for protuberances as in Ref. 2 ( $C_{D_\pi}$  method) and for those interference effects which experience or test data indicates may be greater than normal. The  $C_{D_\pi}$  method is summarized below.

Protuberances such as handles, hinges, antennas, cover plates, etc., impose additional drag on the aircraft but their effects are not readily treated within the analytical framework discussed earlier. It has been common to account for such effects in the following manner:

The drag produced by some element of the aircraft can be written

$$D_e = C_{D_e} q S_w$$

where  $C_{D\pi}$  represents the drag coefficient of the element based on the wing area. It is, however, difficult to estimate the drag coefficient of many protuberances in terms of the wing area. These estimates are frequently made by comparing the protuberance with some simple shape which has been tested frequently. For example, the drag of a vertical antenna wire would be estimated by considering the wire to be a cylinder normal to a uniform stream. For most Reynolds numbers, the drag coefficient of such cylinders is given in classic texts as 1.2-1.3 based on a product of the wire diameter and its length. If one calls such a "natural" area  $A_\pi$  and the drag coefficient based upon it  $C_{D\pi}$ , then  $D_e$  is also given by

$$D_e = C_{D\pi} q A_\pi .$$

In terms of  $C_{D\pi}$  then,

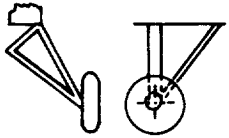
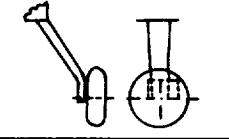
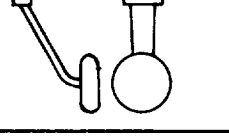
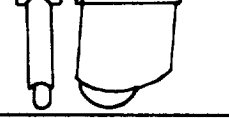
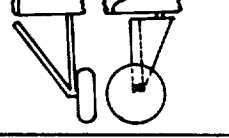
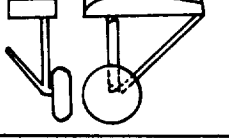
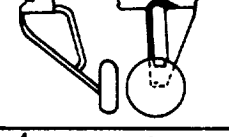
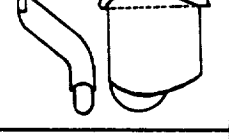

$$C_{D_e} = \frac{C_{D\pi} A_\pi}{S_w} .$$

The net contribution of all protuberances to the total airplane drag coefficient based on the wing area is thus simply

$$C_{D_{\text{Protuberances}}} = \frac{\sum_{\pi} C_{D\pi} A_\pi}{S_w} .$$

The same rationale applies to the contributions to the vehicle drag provided by the fuselage and tail surfaces. The reason for basing all contributions to the overall drag on the wing area is simply one of convenience. The wing area is the basic geometric parameter used in sizing the airplane during preliminary design and is therefore the parameter governing initial estimates of power required and performance.

Given below are  $C_{D\pi}$  values and the areas upon which they are based for some landing gear designs, nacelles, wing tanks, and wires and struts.

Configuration	Remarks	$f = C_{D_{\pi}} A_{\pi}$
	8.50-10 wheels, not faired . . . . . 8.50-10 wheels, faired . . . . . 8.50-10 wheels, no streamline members . .	1.67 1.50 3.83
	8.50-10 wheels, faired . . . . . 27-in. streamlined wheels, not faired . . . . .	0.74 0.98
	27-in. streamlined wheels, not faired . . 8.50-10 wheels, faired . . . . . 21-in. streamlined wheels, not faired . .	0.84 0.68 0.53
	8.50-10 wheels . . . . .	0.51
	8.50-10 wheels, not faired . . . . . 8.50-10 wheels, faired . . . . .	1.52 1.02
	8.50-10 wheels, not faired . . . . .	1.60
	24-in. streamlined wheels, & intersections filleted . . . . . 8.50-10 wheels, no fillets . . . . .	0.86 1.13
	8.50-10 wheels . . . . .	1.05
	Low pressure wheels, intersections filleted Low pressure wheels, no wheel fairing . . Streamlined wheels, round strut, half fork no fairing . . . . .	0.31 0.47
<b>Nose Gear</b>	For the nose gear $C_{D_{\pi}} = .5 \rightarrow .8$ based on $A_{\pi} = (\text{wheel diameter})(\text{wheel width})$	

COMPONENTS	AREA FOR DRAG CALCULATION	$C_{D\pi}$
<b>Nacelles</b>		
1. above wing, small airplane	Cross section area	.250
2. large leading edge nacelle, small airplane	Cross section area	.120
3. small leading edge nacelle, large airplane	Cross section area	.080
4. improved nacelle, no cooling flow	Cross section area	.050
5. improved nacelle, typical cooling air flow	Cross section area	.100
<b>Wing Tanks</b>		
1. centered on tip	Cross section area	.05-.07
2. below wing tip	Cross section area	.07-.10
3. inboard below wing	Cross section area	.15-.30
<b>Wires and Struts</b>		
1. smooth round wires and struts (per foot)	Frontal area	1.2-1.3
2. standard aircraft cable (per foot)	Frontal area	1.4-1.7
3. smooth elliptical wire (per foot)	Frontal area	0.6-0.4
fineness ratio 2:1		.35
fineness ratio 4:1		.3-.2
4. standard streamlined wire (per foot)	Frontal area	.45-.20
5. square wire (per foot)	Frontal area	.16-.20
6. streamlined struts (per foot)	Frontal area	.075-0.10

For smooth round wire of diameter less than  $\frac{1}{4}$  inch, assume two end fittings equivalent to three feet of wire.

For smooth round struts of diameter greater than  $\frac{5}{16}$  inch, assume two end fittings equivalent to one foot of strut.

For smooth elliptical wire, assume two end fittings equivalent to 10 to 15 feet of wire.

For square wire, assume two end fittings equivalent to two feet of wire.

For streamlined struts, assume two end fittings equivalent to five feet of strut if faired, ten feet if unfaired.

The contribution of the various protuberances to the total aircraft drag coefficient is commonly on the order of 3% to 5%.



**PROGRAM FOR THE CALCULATION OF TWO-DIMENSIONAL  
AERODYNAMIC COEFFICIENTS**

## INTRODUCTION

In order to predict the three-dimensional lift and drag characteristics of a general planform, one usually begins with the two-dimensional characteristics of the airfoils which constitute the wing. As noted in the literature review, a computer program which estimates the aerodynamic characteristics of multiple-component airfoils in subsonic, viscous flow already exists (Ref. 31). This program, originally written for NASA Langley under NASA Contract NAS1-9143, has undergone extensive in-house modification at NASA Langley; this modified version is available to the general public. To take advantage of the rather substantial effort which went into the preparation of this program, it was decided to use this NASA program as the basis for developing a suitable—in terms of accuracy and computational requirements—procedure for estimating the two-dimensional lift and drag characteristics of general airfoils.

Since the present report is concerned only with the prediction of characteristics of single-element airfoils and wings, a single element version of the program was obtained from NASA Langley. Although the NASA program was written for the CDC 6600 computer, only slight modification was required in order to use it on the IBM 370-165 computer at N. C. State University. Several airfoils were then investigated at NCSU to determine how well the program prediction of lift, drag, and pitching moment coefficients compared with the experimental data given in Reference 19. After several comparisons it was concluded that in general the predicted lift coefficient was high by 5 to 8 percent for moderately thick airfoils and 8 to 15 percent for very thick airfoils; the drag coefficient was usually high by at least 25% and sometimes as much as 75%. The program as obtained from Langley required 200K (K denotes 1,000 bytes) of core storage and a scratch disk (for matrix inversion use) for an IBM FORTRAN IV H-LEVEL run on the IBM 370-165 computer. The average execution time was 45 to 60 seconds for each airfoil angle of attack (a large portion of this time is input-output time for the scratch disk). Based on the above results the goals for the new program were set as follows:

- (1) modify the NASA program to improve the predicted lift and drag coefficients
- (2) reduce the size of the program to facilitate its use on smaller computers (~100K)
- (3) reduce the computational time required to evaluate the coefficients of a particular airfoil.

The extent to which the above goals were achieved is summarized below:

- (1) a marked improvement in the accuracy of the predicted lift and drag coefficients is evident by perusing Figure 12 through Figure 30
- (2) the modified program required only 106K of core storage with no scratch disk required

(3) the computational time required to evaluate the coefficients of a particular airfoil was reduced to 20 seconds or less.

In the following sections the reader will find a brief explanation of the theory upon which the program is based, a discussion of the various changes and modifications implemented in the NASA program, and a comparison of the predicted lift and drag coefficients (from both the original NASA program and the NCSU-modified program) with experimentally-determined coefficients.

## GENERAL PROGRAM THEORY

The only practical method currently available for predicting the viscous flow field about an airfoil involves an iterative procedure. The basic steps for this iterative procedure are:

- (1) obtain an inviscid flow solution for the basic airfoil
- (2) obtain a boundary layer solution based on the inviscid flow solution
- (3) construct a modified airfoil by adding the boundary layer displacement thickness to the original airfoil
- (4) obtain an inviscid flow solution for the modified airfoil
- (5) repeat steps (2) through (4) until some convergence criterion is satisfied, for example, the difference between two successive values of lift coefficient is less than some specified tolerance.

The above steps represent only an outline of the procedure to be used since there are many techniques available for obtaining inviscid and boundary layer flow solutions. For a discussion of many of the available techniques and how they are applied to particular problems, the reader should consult the literature review.

A detailed description of a logical solution procedure is given in the general theory of the previous section. However, for reasons noted in the general introduction, this procedure differs in some details from the method actually employed in the program. Thus, to insure clarity, a brief description of the actual solution procedures used in the modified NCSU program is given below.

It is of utmost importance to choose a solution procedure which can be relied on to converge in most cases. For the problem of the flow field about an airfoil, convergence depends primarily on the manner in which the displacement effects of the boundary layer are treated in the inviscid flow calculations. The program as supplied to NASA chose to model the influence of the boundary layer on the velocity distribution over the actual airfoil as two separate effects. The effect of the boundary layer on the lift is considered to be a modification of the camber line so as to effectively decrease the angle of attack of the airfoil. The change in camber is given by the difference in the magnitude of the upper and lower surface displacement thicknesses as shown in Figure 1.

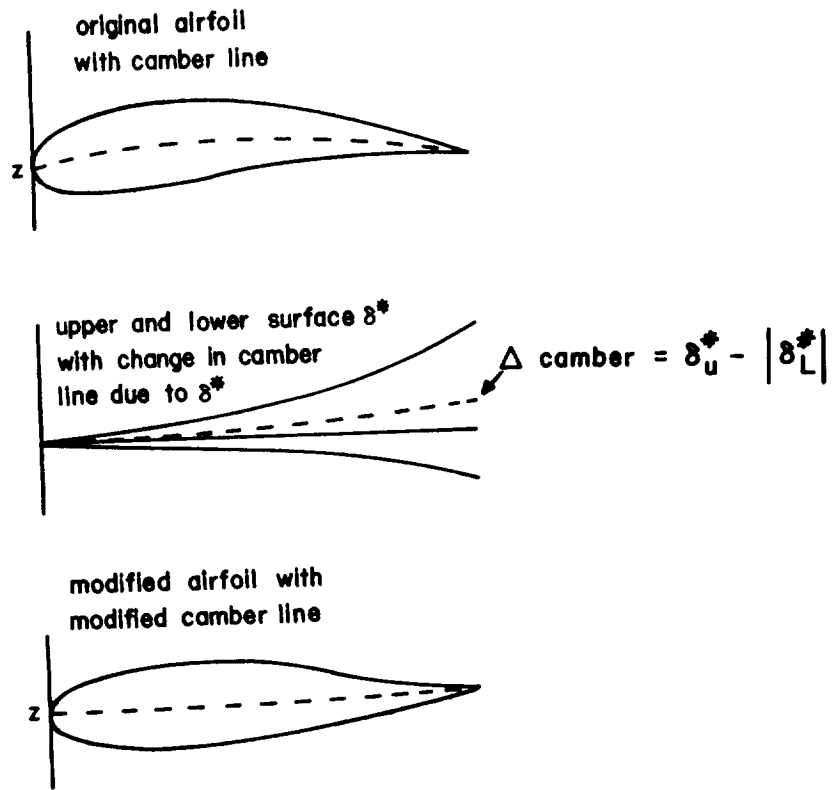


Figure 1. Modification of camber line due to boundary layer displacement thickness.

Thickness effects due to the existence of the boundary layer tend to relieve the stagnation condition in the trailing-edge region, giving rise to the pressure or form drag of the airfoil. This effect of the boundary layer on the drag was approximated by the difference of two "thickness" solutions (see Figure 2). The first thickness solution is for a symmetric airfoil at zero angle of attack with the same thickness distribution as the original airfoil plus boundary layer displacement thicknesses. The second thickness solution is also for a symmetric airfoil at zero angle of attack but with the same thickness distribution as the original airfoil. Since superposition is assumed to apply, the velocity distribution over the original airfoil is given by,

$$\left(\frac{v}{v_\infty}\right)_{\text{TOTAL}} = \left(\frac{v}{v_\infty}\right)_{\text{CAMBER}} + \left(\frac{v}{v_\infty}\right)_{\text{BT}+\delta^*} - \left(\frac{v}{v_\infty}\right)_{\text{BT}},$$

where BT stands for the basic thickness distribution of the original airfoil.

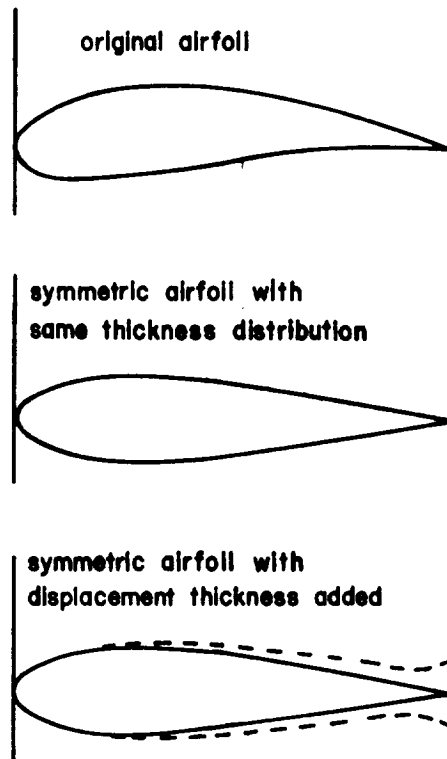


Figure 2. Thickness effects due to boundary layer displacement thickness.

During the initial phase of the investigation, the authors questioned the necessity of having to use superposition to model the various boundary layer displacement effects. It seemed that the boundary layer displacement effect could be modeled by simply adding the displacement thickness to the original airfoil. However, upon consultation with Mr. Harry L. Morgan, Jr., the authors were informed this approach had already been attempted at NASA Langley but was unsuccessful. Time simply did not permit the authors to investigate this possible solution procedure further.

The program as originally supplied to NASA Langley used a distributed vorticity method to calculate inviscid flow solutions. The airfoil was approximated by a closed polygon, and the distributed vorticity was assumed to vary linearly along each line segment of this polygon. The sum of the velocity induced by the distributed vorticity and the free stream velocity was forced to satisfy the condition that its component normal to the airfoil surface must be zero at the midpoint of each line segment. NASA replaced this inviscid solution procedure with a different distributed vorticity method based on Oeller's work (Ref. 26 and 27).<sup>\*</sup> Using the new

---

\* For the user's convenience, a derivation of the equations for Oeller's method is given in Appendix G.

procedure the airfoil is again approximated by a closed polygon, but the distributed vorticity is assumed to have a constant value per line segment. The solution is obtained by requiring that the stream function have the same constant value at each of the midpoints of the line segments (see page 405). Consider the two line segments shown in Figure 3. To obtain a

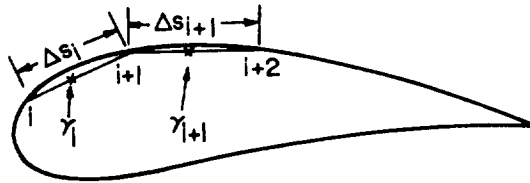


Figure 3. Schematic of control point averaging.

value for the local velocity at the point  $(i + 1)$  on the airfoil surface, it is necessary to use some type of averaging technique on the distributed vorticities  $\gamma_i$  and  $\gamma_{i+1}$ . The NASA program used an averaging procedure of the form,

$$\left(\frac{v}{V_\infty}\right)_{i+1} = \frac{1}{2} (\gamma_i + \gamma_{i+1}) \quad .$$

Strictly speaking this procedure is correct only if all the line segments have the same arc length. A somewhat better averaging procedure is obtained by using the following form,

$$\left(\frac{v}{V_\infty}\right)_{i+1} = (\gamma_i \Delta s_i + \gamma_{i+1} \Delta s_{i+1}) / (\Delta s_i + \Delta s_{i+1}) \quad .$$

This improved averaging technique was therefore incorporated into the NCSU-modified program.

To facilitate the understanding of the remainder of the programming theory, a program flow chart has been included and is presented in Figure 4. The remainder of this section will be concerned with the explanation of this flow chart.

As indicated in the flow chart, the program begins by calling subroutine READIT. As its name implies READIT is responsible for reading the input geometry and the ambient conditions. A call is then made to subroutine GEOM to obtain a set of 65 distributed solution points. A basic thickness velocity distribution  $\left(\frac{v}{V_\infty}\right)_{BT}$  is calculated next using subroutine VOVBT.

This velocity distribution is calculated only once for each airfoil because it is the basic thickness solution at zero angle of attack. Various arrays are then initialized and MAIN2 which controls the calculation of the inviscid flow solution is entered. The camber solution velocity distribution  $\left(\frac{v}{V_\infty}\right)_{CAMBER}$

is calculated in subroutine CAMBER. For all iterations after the first (zeroth in the program output), the "basic thickness plus displacement thickness" velocity distribution  $\left(\frac{V}{V_\infty}\right)_{BT+\delta^*}$  is calculated in subroutine VOVB. The three velocity distributions are combined to give the total velocity distribution for the airfoil,  $\left(\frac{V}{V_\infty}\right)_{TOTAL}$ . Using this velocity

distribution subroutine COMP is called to obtain the compressible pressure coefficients using the Karman-Tsien correction law. The location of the forward stagnation point is obtained from subroutine STAG and subroutine MAIN2 returns control to the mainline.

Subroutine MAIN3 is next entered to control the boundary layer calculations. A call is made to subroutine LAMNA2 to obtain the laminar boundary layer solution for the upper surface. At each point on the airfoil surface subroutine LAMNA2 makes a call to subroutine BLTRAN to see if boundary layer transition has occurred. Control remains in subroutine LAMNA2 until either laminar separation, boundary layer transition, or the end of the surface is encountered. If boundary layer transition has occurred, TURB2 is called to calculate the turbulent boundary layer solution. To insure stability in the computation the last seven boundary layer displacement thicknesses are replaced using a least squares fit obtained from subroutine LSQ\*. A calculation for the lower surface boundary layer is performed in a similar manner. The pressure coefficient and skin friction coefficients are integrated over the airfoil in subroutine LOAD, and the various aerodynamic and force coefficients are computed in MAIN3 before control is returned to the mainline. A check is then made to see if five iterations have been completed, a check is made to see if all the angles of attack have been used for the specified Mach number, and a check is made to see if the airfoil has been investigated at each of the specified Mach numbers. Once all the Mach numbers have been investigated, the program returns to subroutine READIT where it attempts to read another data set.

Although this description of the flow chart concludes the General Program Theory section, the reader is reminded that additional aspects of the theory must, of necessity, be discussed in explaining many of the modifications incorporated into the NCSU program. The next section will discuss program modifications of a general nature while later sections will be concerned with modifications of a more specific nature.

---

\* See page 79 of Reference 31 for the description of this displacement thickness smoothing procedure.



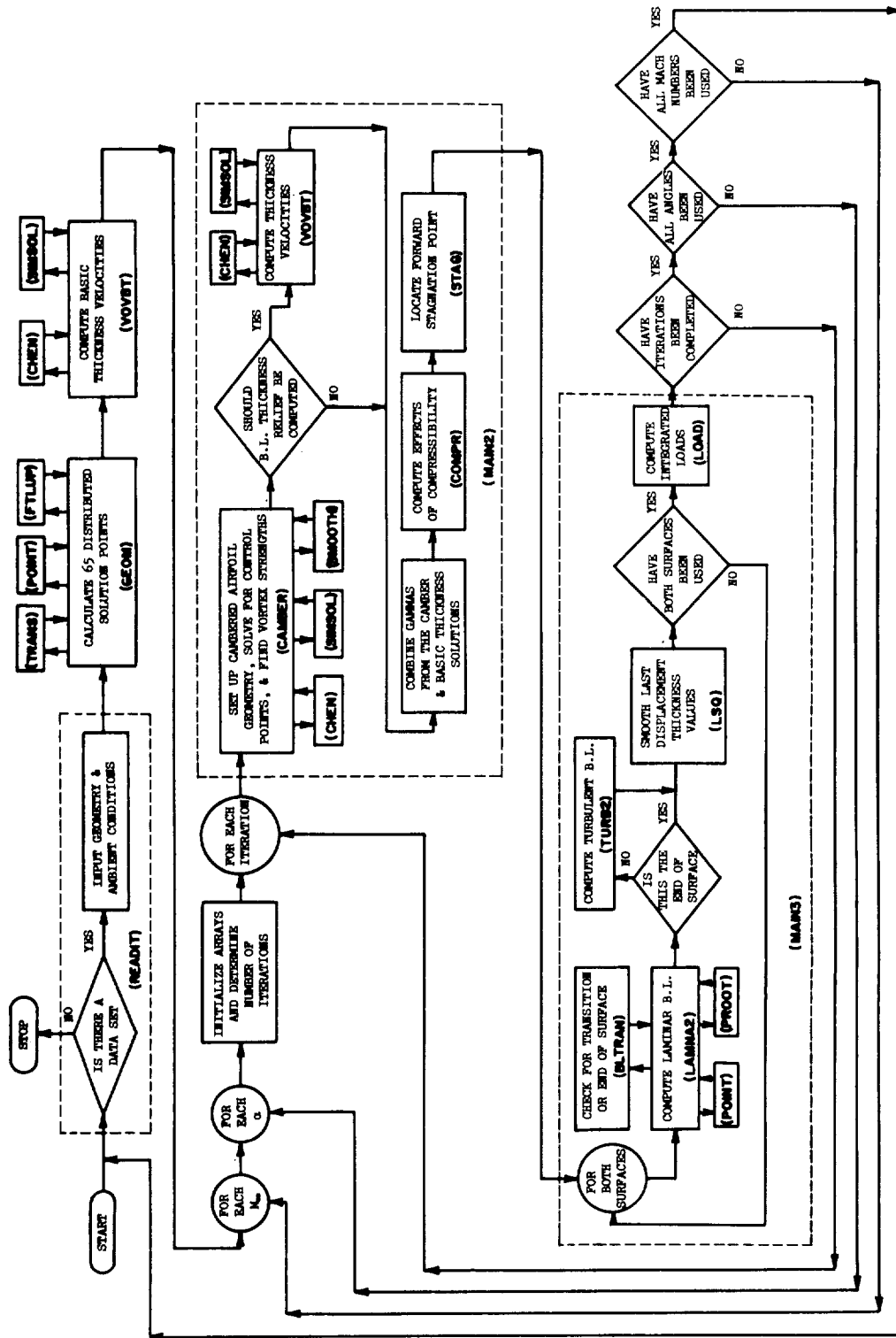


Figure 4. NCSU computer program flow chart.

## GENERAL PROGRAM MODIFICATIONS

Many of the changes made in the NASA program may be classified as general programming modifications applicable to the entire program rather than a particular subroutine; these general modifications are discussed below. Throughout the remainder of the text the program obtained from NASA Langley will be referred to as the NASA program while the modified program generated at N. C. State University will be referred to as the NCSU program.

The NASA program was run on the CDC 6600 computer using segmentation to reduce the core requirement. Since segmentation as such is not supported by IBM machines, the segmentation control cards were deleted. The NASA program also contained a PLOT subroutine which was used to plot the pressure coefficients. Inasmuch as plotting software may vary drastically from installation to installation, this subroutine was deleted from the program.

Although only a multi-component version of the program was originally supplied to NASA Langley (Ref. 31), a single element version was produced at NASA by deleting the confluent boundary layer and slot flow subroutines. This single element version was the program made available to N. C. State University. The program as supplied still contained variables in other subroutines which were used only for multi-component calculations and variables which were double subscripted to facilitate multi-component calculations (the second subscript was used to denote the particular component). These unnecessary variables and second subscripts are eliminated in the NCSU version of the program.

In the interest of clean coding, the COMMON statements were aligned and modified so that the Common variables have the same variable name in each of the subroutines in which they appear. Also, whenever possible the NCSU program makes use of Common transfer of information thus eliminating many of the subroutine arguments.

In the NASA program a Mach number extrapolation and smoothing process\* was applied to upper and lower surface trailing edge pressure coefficients in subroutine MAIN3 (statements 90 through 99 of NASA program). Since this pressure coefficient modification was found to produce a significant non-zero lift coefficient for a symmetrical airfoil at zero angle of attack, it was deleted in the NCSU program.

The NASA program also allowed the user to specify the total number of solution points desired for the airfoil investigated, up to 100 points. In order to minimize storage, several test cases were investigated to find a minimum value for the number of solution points which would still give valid aerodynamic coefficients. Calculations with 65 points produced

---

\* See pages 78 and 79 of Reference 31 for the description of this procedure.

coefficients which were within one or two percent of those predicted using 100 points; also, less than 65 points showed the trend of producing a larger percentage difference as the number of points were decreased. It was therefore decided that 65 solution points were the optimum number, and the NCSU program specifies the use of 65 solution points.

Several of the unnecessary WRITE and PRINT statements contained in the NASA program were deleted in the NCSU program to reduce total program size. To insure compatibility with other installations all input/output statements were changed to the forms READ(JREAD,C), WRITE(JWRITE,C), and WRITE(JPUNCH,C) where JREAD, JWRITE, and JPUNCH are the appropriate input/output numbers and C is some FORMAT statement number. The values of the input/output unit numbers are assigned by three specification statements at the beginning of the mainline of the NCSU program (JREAD=1, JWRITE=3, and JPUNCH=2). For installations having different input/output unit numbers these specifications may be changed. Only Hollerith field literal data specifications were permitted in the NCSU program to insure IBM-CDC machine compatibility.

The maximum number of angles of attack, specified as 5 in the NASA program, was increased to 10 in the NCSU program. Also, many of the subroutines contained in the NASA program were combined or deleted in the NCSU program to make it simpler and more efficient. A table comparing the subroutines contained in each of the programs is given below.

NASA PROGRAM	NCSU PROGRAM
MAIN	MAIN
READIT	READIT
GEOM	GEOM
DISTP }	
ROTRAN }	
MAIN2 }	
VOVBT }	VOVBT
THICK }	
COEFF }	CAMBER
VORTEX }	
CONTPT }	
EQUIV }	
CHEN	CHEN
COMPR	COMPR
STAG	STAG
MAIN3	MAIN3
LAMNA2	LAMNA2
BLTRAN	BLTRAN
TURB2	TURB2
TURB	
LOAD	LOAD
LSQ	LSQ
TRANS	TRANS
PROOT	PROOT
POINT	POINT

(continued on next page)

NASA PROGRAM	NCSU PROGRAM
SLOPE	
SMOOTH	SMOOTH
FTLUP	FTLUP
DIF	
SIMSOL	SIMSOL
FUNCTION LOCF(X)	

Table 1. Comparison of subroutines contained in the NASA program and the NCSU program.

In order to give the user the option of reducing the size of the NASA program output for a particular airfoil, an IWRITE control parameter was incorporated into the NCSU program. IWRITE is a program input variable which should have the value 0, 1, 2, or 3. IWRITE = 0 is the default write option which basically gives the complete output presented in the NASA program. An IWRITE of 1, 2, or 3 will yield reduced portions of the total output with IWRITE = 3 producing the minimum output for each airfoil tested. An example of the output generated for each of the IWRITE options is given in Figures A-3, A-4, A-5, and A-6 of Appendix A.

The angle of attack of an airfoil is generally defined as the angle between the free stream flow direction and the airfoil chord line. The program must therefore know the location of the chord line of the airfoil with respect to the x-axis of the reference system in order to calculate the correct aerodynamic coefficients as a function of angle of attack. In most cases the location of the chord line is known, and the airfoil coordinates are referenced with respect to this chord line. However, in some instances the chord line location may not be precisely defined, thus requiring the program to calculate a chord line to use as a reference line for the angle of attack. In general the most logical choice for the calculated chord line would be the longest line from the midpoint of the trailing edge to the nose of the airfoil. Thus, the program would choose line A as the chord line for the airfoil depicted in Figure 5.

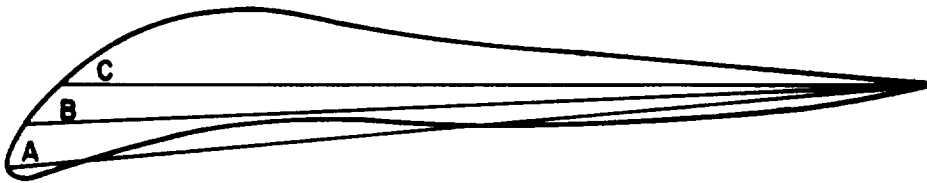


Figure 5. Sample airfoil with longest chord line.

Throughout this report a chord line calculated by the program in this manner will be referred to as the longest chord line. An input control parameter IALPHA was incorporated into the NCSU program to allow the user to either specify the airfoil chord line or to allow the program to calculate the longest chord line.

$\text{IALPHA} = 0$  implies that the chord line of the airfoil is parallel to the x-axis of the input reference system of specified airfoil data points. Although it would be more convenient to specify the airfoil coordinates with the chord line as the x-axis of the reference system as shown in Figure 6a, it is only necessary to input the coordinates with the chord line parallel to the x-axis of the reference system as shown in Figure 6b.

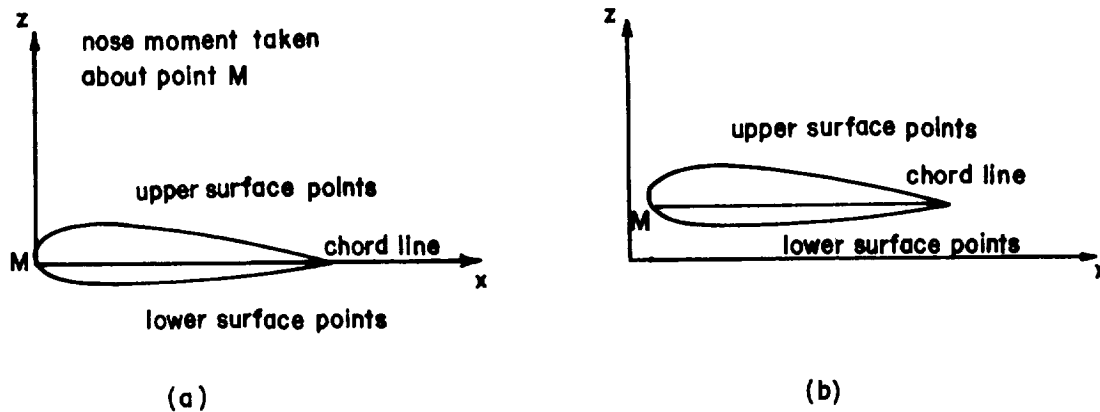


Figure 6. Location of chord line for  $\text{IALPHA} = 0$ .

The authors strongly urge that only the convention in Figure 6a be used. As indicated in the User Instructions of Appendix A, a set of lower surface points and a set of upper surface points are read for the airfoil. The upper and lower surface points are defined as those points above and below the specified chord line respectively as indicated in Figure 6. It should also be noted that when calculating the moment coefficient about the nose, the nose point is taken to be the point where the chord line cuts the leading edge of the airfoil. It should be reemphasized that the above discussion applies only to the  $\text{IALPHA} = 0$  option.

$\text{IALPHA} = 1$  implies that the chord line of the airfoil is the longest chord line calculated by the program. For this particular option the user may choose any convenient reference line for dividing the airfoil into upper and lower surface input points. The only restriction placed on this reference line is that it must go through the trailing edge midpoint. Again however, the authors strongly recommend that this line be the x-axis of the input reference system as shown in Figure 7. After calculating the longest chord line, the program will then rotate and translate the airfoil coordinates so that the longest chord line lies along the x-axis with the nose of the airfoil at the (0,0) point (see Figure 8). The lift and drag coefficients are then calculated with the angle of attack referenced to this longest chord line, while the moment coefficient about the nose is calculated about the (0,0) point. Similarly the moment coefficient about the quarter-chord is calculated using the point (.25C,0), where C is the length of the longest chord line.

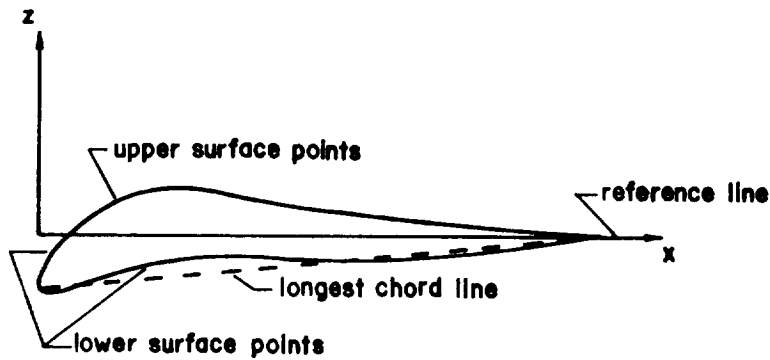


Figure 7. Example airfoil in reference system for IALPHA = 1 option.

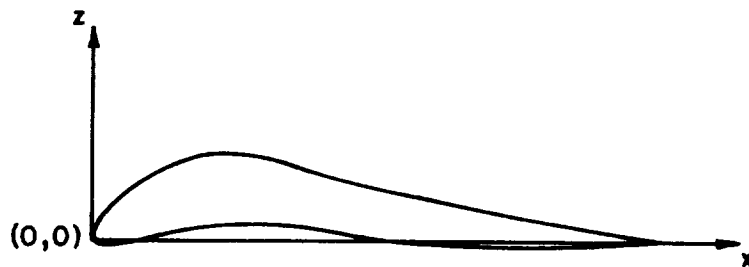


Figure 8. Rotated airfoil after longest chord line has been calculated.

In order to make the NCSU airfoil program compatible with the companion program (given in Appendix C) for calculating three-dimensional aerodynamic coefficients, an input IPUNCH control parameter was added. The control parameter IPUNCH gives the user the option of obtaining punched data (lift, drag, and quarter-chord moment coefficients for each angle of attack) which may be used in the three-dimensional program. IPUNCH = 1 gives punched output while the default IPUNCH = 0 gives none.

Many comment cards were added throughout the entire program to help explain program theory and logic. In general, the purpose of each subroutine is defined at the beginning of the subroutine, and also many of the important areas of the program were denoted using these comment cards.

As a final note to the general program modifications the user is strongly advised to read the User Instructions concerned with input data to the NCSU program since it differs in some respects with that of the NASA program. For example, the input variable RN in the NCSU program denotes the value of the Reynolds number in millions. It does not denote Reynolds number in millions per foot as it did in the NASA program!!!

While many of the revisions of the NASA program could only be classified as general modifications, there were also modifications which were more specific in nature. The revisions which are concerned with airfoil geometry are discussed in the following section.

## CHANGES CONCERNING THE AIRFOIL GEOMETRY SPECIFICATION

In order to compute the lift and drag characteristics of any airfoil, the airfoil coordinates must be specified. The NASA program was designed so that 200 points could be used to specify the shape of the airfoil surface. Since most airfoils can be specified adequately using less than 100 points, the size of the NCSU program was reduced by requiring that the airfoil be specified by 100 points or less. These specified points must be distributed about the airfoil in a manner such that if the airfoil were rotated to the longest chord line system there would be no more than 65 upper or lower surface points (where the upper and lower surface points are defined with respect to the longest chord line). The problem of having more than 65 upper or lower surface points after rotation can usually be avoided if the user specifies no more than 50 input points on either surface. However, if more than 65 points are encountered an appropriate error message will be printed in the program output, and execution of that particular airfoil will be terminated.

As noted under general program modifications the aerodynamic coefficients are calculated based on 65 airfoil solution points. However, these 65 solution points are not specified airfoil input points as such; they are a set of points generated from the specified points by a distribution procedure in subroutine GEOM. Only one call is made to subroutine GEOM since the airfoil can be investigated for several angles of attack and/or Mach numbers using the same set of distributed points. The distribution procedure requires many intermediate arrays for computational purposes, but only two arrays containing the coordinates of the distributed airfoil points are required for the remainder of the program computations. The intermediate arrays are therefore equivalenced to other arrays used in later program computations. This equivalencing procedure gives a reduction of the number of large arrays required by the program.

Subroutine GEOM in the NCSU program is a combination of three of the subroutines in the NASA program (subroutines ROTRAN, GEOM, and DISTP). This subroutine first calculates the longest chord line of the airfoil regardless of the IALPHA option used. It then calculates the angle  $\beta$  between this longest chord line and the x-axis of the input reference system (see Figure 9) and rotates and translates the specified input points so that the longest chord line lies on the x-axis with the nose at the (0,0) point. This is done so that a new set of upper and lower surface points defined with respect to the longest chord line will have monotonic increasing values of x. It was decided that the NASA program could be greatly simplified if the x-values of the distributed upper surface points and the x-values of the distributed lower surface points were the same along the longest chord line. Based on this decision the NCSU program was modified so that it would produce 32 upper and 32 lower surface distributed points along with a common leading edge point (*i.e.* the (0,0) point), giving a total of 65 distributed points.



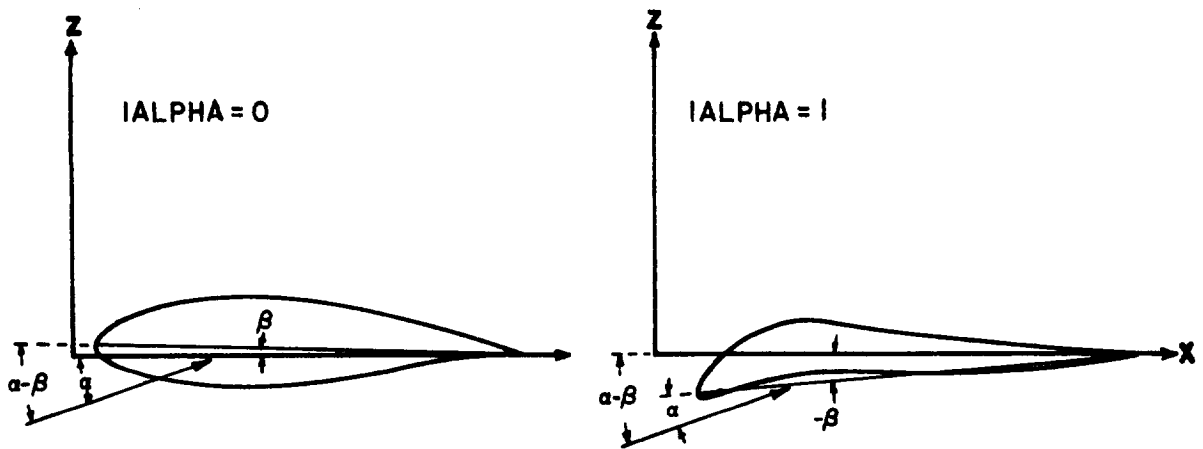


Figure 9. Reference line for the angle of attack for both IALPHA options.

The distribution of the points is made a function of local surface curvature so that more points are distributed in regions of high curvature. The distribution procedure is as follows:

- (1) the program uses the upper surface x-values as a longest chord line scanning array starting with the leading edge point
- (2) the curvatures\* of both the upper and lower surfaces are computed at each of these x-values
- (3) the absolute value of the curvature for both surfaces are compared at each x station, and the maximum curvature is kept
- (4) the Integral  $SUMA_1 = \int_0^{s_1} |K|^{0.25} ds$  is evaluated using the maximum curvatures at the x stations and the corresponding surface arc lengths  $s_1$  along the upper surface (note that a value of this integral is stored for each  $s_1$  station to facilitate backward interpolation)

---

\* In the nose region the curvature K is calculated from

$$K = [cz^2 - (cx + b/2)^2] / [z^2 + (cx + b/2)^2]^{3/2}$$

where c and b are taken from a curve fit of the airfoil points of the form

$$z^2 = a + bx + cx^2 .$$

Note that this curve fit gives a slope  $dz/dx = (cx + b/2)/z$  which becomes infinite when z becomes zero. Because the above curve fit gives an infinite slope when  $z = 0$ , it obviously cannot be used near the trailing edge of the airfoil. Therefore, in the trailing edge region the curvature is calculated from  $K = 2c/[1 + (2cx + b)^2]^{3/2}$ , where c and b are taken from a curve fit of the form  $z = a + bx + cx^2$ .

- (5) the maximum value of the integral is divided into 32 equal portions
- (6) an s value corresponding to each of these increments is found by backwards interpolation between the  $s_j$  array and  $SUMA_j$  array
- (7) similarly an x value corresponding to the s value is found by backward interpolation
- (8) finally corresponding z values for both the upper and lower surfaces are found by backward interpolations.

Although the curve fit formula used in the nose region is designed to approximate an infinite slope, a better value for the curvature integral is achieved when there are more points specified in the nose region of the input data. The better value of the curvature integral will lead to a better set of distributed x's.

In the NASA program the distributed points are rotated and translated back to the reference axis system. For the NCSU program the distributed points remain in the longest chord line system in order to take advantage of the same upper and lower surface x values. For the IALPHA = 1 option the longest chord line system is the ideal system in which to calculate the aerodynamic coefficients. For the IALPHA = 0 option the program calculations are performed using an angle of attack with respect to the longest chord line of  $(\alpha - \beta)$  since this corresponds to an angle  $\alpha$  with respect to the actual airfoil chord line (refer back to Figure 9).

Following this discussion of the specification of the airfoil geometry, the next two sections present the revisions made to the camber, thickness, and boundary layer solutions of the NASA program.

## THICKNESS AND CAMBER SOLUTION MODIFICATIONS

It was pointed out in the section on general program theory that the solution for the complete airfoil is a sum of a thickness solution and a camber solution. The modifications which were made in both the thickness and camber solution portions of the NASA program will now be considered.

Subroutine VOVBT is designed to calculate the  $\gamma$ 's or surface velocities for a symmetric airfoil with the same thickness distribution as the original airfoil plus boundary layer displacement thickness. Remembering that the upper and lower surface x-arrays are the same in the longest chord line system, the upper surface ordinates of the symmetric airfoil are generated from the following equation,

$$(z_{\text{sym.}})_{\text{up}} = \frac{1}{2}((z_{\text{air}})_{\text{up}} - (z_{\text{air}})_{\text{low}}) + \frac{1}{2}((\delta^*)_{\text{up}} + (\delta^*)_{\text{low}}) \quad ,$$

for  $0 \leq x \leq C$  ,

where:

$z_{\text{air}}$  = original airfoil ordinate  
 $\delta^*$  = boundary layer displacement thickness  
 $C$  = length of longest chord line.

It also follows that  $(z_{\text{sym}})_{\text{lower}} = -(z_{\text{sym}})_{\text{upper}}$ . Now, once the boundary layer displacement thicknesses have been added, the symmetric airfoil will have a finite trailing edge thickness which is denoted by  $z_{\text{te}}$ . In the actual physical flow, the wake acts as a displacement body in which the thickness decreases very rapidly from  $z_{\text{te}}$  to a finite value  $z_{\infty} = \frac{1}{2}C_D C$  according to Reference 30, where  $C_D$  is the airfoil drag coefficient based on the chord length  $C$ . In subroutine VOVBT the wake displacement body of the symmetric airfoil is modeled by:

$$(z_{\text{sym}})_{\text{up}} = \frac{1}{2}[(z_{\text{te}} - z_{\infty}) e^{(-6.9XX)} + z_{\infty}](1.0 - XX)$$

where

$$XX = x/C - 1.0 \quad \text{for} \quad C \leq x \leq 2C.$$

Based on actual measurements given in References 72 and 73 the present authors found that the extrapolation function inside the brackets in the equation above closely approximated the boundary layer displacement thickness of the wake in the trailing edge region. The multiplicative term inside the parentheses is included to close the wake displacement body at  $x = 2C$  since the inviscid procedure used for the solution gives best results when applied to closed bodies. The authors feel that this approximation to the wake displacement body gives a better representation of the actual physical flow than does the wake extrapolation procedure in the NASA program while also reducing program size and computation time.

Since the thickness solution is calculated only at a zero angle of attack, the flow field about the symmetric airfoil gives an upper surface  $\gamma$  distribution which is simply the negative of the lower surface  $\gamma$  distribution, *i.e.*  $(\gamma_{up})_{x_i} = -(\gamma_{low})_{x_i}$ , where  $x_i$  denotes a particular  $x$  station of the airfoil along the longest chord line. Thus, only the  $\gamma$ 's for the upper surface of the symmetric airfoil need to be found.

Subroutine CAMBER is designed to calculate the  $\gamma$ 's or surface velocities for an "equivalent" airfoil which has the same thickness distribution as the original airfoil but a modified camber line. This modification is due to the effect of boundary layer displacement thickness on the original airfoil as noted in general program theory. The upper and lower surface ordinates of the "equivalent" airfoil are given by the following equations,

$$(z_{eq})_{up} = (z_{air})_{up} + \frac{1}{2} \Delta z$$

$$(z_{eq})_{low} = (z_{air})_{low} + \frac{1}{2} \Delta z$$

where  $\Delta z = (\delta^*)_{up} - (\delta^*)_{low}$  .

## BOUNDARY LAYER MODIFICATIONS

The NASA program contains four subroutines for boundary layer calculations: LAMNA2, BLTRAN, TURB2, and TURB. LAMNA2 performs the laminar boundary layer calculations on the airfoil surfaces. At each point along the airfoil surface, LAMNA2 calls BLTRAN to determine if either transition from laminar to turbulent boundary layer flow or laminar separation has occurred. If transition has occurred, TURB2 calculates the turbulent boundary layer solution over the remainder of the airfoil surface. After the last iteration between the potential and boundary layer flow calculations is performed, an additional turbulent boundary layer calculation is performed using subroutine TURB. This subroutine performs a refined turbulent boundary layer computation to predict the point of turbulent separation.

A brief description of the methods used in LAMNA2 is given in Reference 31, and they are derived in detail in Reference 32. The method for predicting transition used in BLTRAN is described briefly in Reference 31 and derived in detail in Reference 32, while the method for predicting laminar stall is derived in Reference 31. TURB2 uses Goradia's Turbulent Boundary Layer Method which is derived in Reference 31. Goradia's method is designed to remain stable under the influence of extreme gradients, both favorable and adverse, and provide reasonable momentum and displacement thicknesses downstream of the turbulent separation point. TURB uses Nash's Turbulent Boundary Layer Method which is described briefly in Reference 31. Nash's method provides a prediction of the point of turbulent separation, but his method is too sensitive to adverse gradients to be used in the initial iterations.

The NCSU program retains subroutines LAMNA2, BLTRAN, and TURB2. Subroutine TURB (Nash's method) was removed to reduce program size since it played no active part in the iterative process between the potential and boundary layer flow solutions. However, the user should be able to return it to the NCSU program if he so desires.

The three boundary layer subroutines retained in the NCSU program are virtually identical to the original routines in the NASA program except for some coding clean-up performed mainly in the COMMON statements. However, the authors have made two important changes in subroutine LAMNA2:

- (1) The NASA program input parameter RN specified the Reynolds number in millions per foot. In the NCSU program, the input parameter RN now specifies the Reynolds number in millions. Since subroutine LAMNA2 requires a value for the Reynolds number in millions per foot, the authors have added a variable RNPFT (equal to  $RN/CREF$ ) to LAMNA2. This variable is calculated in statement LAM 61 and is used only in statement LAM 62 (see the listing given in Appendix A).

- (2) The Reynolds number is modified to improve the comparison between calculated and experimental drag coefficients. The modification is justified in the following section of this report (Coefficient Modification). It consists of calculating the boundary layer flow using a Reynolds number which is twice that of the specified Reynolds number. Now the Reynolds number is used only once in LAMNA2 to calculate the kinematic viscosity  $\nu_0$  which is then used in all three of the boundary layer subroutines. Increasing the Reynolds number by a factor of two is equivalent to dividing the kinematic viscosity by a factor of two. Therefore, the Reynolds number modification procedure is carried out in statement LAM 65 by dividing the kinematic viscosity by a factor of two.

## COEFFICIENT MODIFICATION

The various modifications discussed up to this point have resulted in a reduction in both program size and run time. While the authors had hoped that some of the modifications would significantly improve the predicted aerodynamic coefficients, comparison with test results indicated that only slight improvement had been obtained. Since attempts at improving the actual program theory had failed the authors sought to determine whether semi-empirical and empirical corrections might improve the results. The corrections which were incorporated into the program are discussed below.

During the course of the investigation the authors noticed that integration of the pressure coefficients from the inviscid solution gave a non-zero pressure drag. This result was obviously contrary to potential flow theory which says there are no drag forces in inviscid flow. It was first believed that this non-zero pressure drag was the result of round-off and loss of significance in the program computations. Calculations were thus made in both single and double precision arithmetic with various integration procedures to test this hypothesis. The results of these tests demonstrated that the problem was not one of loss of significance in program computations but rather a result of the boundary condition applied at the trailing edge of the airfoil. In true potential flow the Kutta condition requires that a stagnation point be recovered at the trailing edge thus yielding a zero pressure drag. However, the boundary condition employed at the trailing edge in the program's potential flow calculations (subroutines VOVBT and CAMBER) is based on Howarth's criterion that the total flux of vorticity shed into the wake from the upper and lower airfoil surfaces must be zero (References 74 and 75). This condition sometimes referred to as a modified Kutta condition is satisfied by requiring that the upper and lower surface velocities at the trailing edge be equal and thus not necessarily zero as would be the case with a stagnation point at the trailing edge. As a result, a potential flow calculation using this modified Kutta condition yields a velocity distribution which has a non-zero pressure drag.

As discussed in General Program Theory, the superposition technique used in this program implies that the lift forces are represented by the camber solution while the pressure drag due to boundary layer displacement effects is represented by the difference of the two thickness solutions. The difference in the thickness solutions should contain all of the pressure drag; however, because the camber solution is calculated using the modified Kutta condition, it also has an inherent pressure drag. As a result, when the three separate velocity distributions are superimposed, the resulting velocity distribution has, in effect, an "extra" pressure drag in it from the camber solution. The obvious "cure" would be to use a camber solution which has a zero pressure drag. This can be accomplished by using the true Kutta condition as the trailing edge boundary condition for the camber solution while still employing the modified Kutta condition in the two thickness solutions. However, when this procedure was attempted the

program's boundary layer routines were unable to cope with the resulting steeply-rising pressure distribution and failed. The next most obvious "cure" would be to try to estimate this "extra" drag and subtract it from the final drag. The authors found that the best way to estimate this "extra" drag was to integrate the pressure coefficients of the inviscid camber solution calculated in the zeroth\* iteration which contains no boundary layer effects. A modification was therefore incorporated into the NCSU program to calculate the pressure drag of the zeroth iteration and then subtract this pressure drag from the final predicted drag coefficient.

The modified drag coefficients compared much more favorably with experimental data than did the unmodified coefficients, however they were still a little too large. While computing the aerodynamic coefficients for several airfoil sections, the authors noticed that if the coefficients were calculated using a Reynolds number twice as large as the experimental value an even greater improvement in drag coefficient could be achieved. For example, it was found that if the coefficients of the 23012 airfoil were computed at a Reynolds number of 6,000,000 the predicted drag coefficient compared very well with experimental tests at a Reynolds number of 3,000,000. The trend observed with the 23012 airfoil was also evident in the other airfoils which were investigated; thus, it was decided that a modification would be made so that the aerodynamic coefficients would be calculated using a Reynolds number which is twice that of the specified Reynolds number. This procedure can be justified at least qualitatively by the fact that momentum integral boundary layer methods such as that used here give boundary layer thicknesses which are somewhat large when compared with exact results. Using larger Reynolds numbers tend to reduce the boundary layer thickness.

The effect of both of the modifications discussed above is illustrated in the graph on the following page.

Up to this point none of the modifications have affected the lift coefficients to any extent; they still remained in general 3 to 8 percent too high with the larger errors occurring at the larger angles of attack. For some of the thicker airfoils the lift coefficients may differ from experiment by as much as 10 to 12 percent at high angles of attack. One reason for the large lift coefficients resides in the fact that the effect of the wake on the circulation about the airfoil is not included in the theory. In the actual physical situation the presence of the wake tends to reduce the circulation about the airfoil leading to a reduction of its lift coefficient (Ref. 76). In Reference 77 Spence and Beasley developed an expression which gives the reduction of the lift coefficient due to the wake. This expression, incorporated into the NCSU program, is

$$(C_L)_{\text{with wake}} = (1.0 - 0.214 \sqrt{C_D}) (C_L)_{\text{without wake}}$$

In the NASA program the lift and drag coefficients were calculated using the normal axial force coefficients obtained by integrating the pressure and skin friction coefficients over the surface of the airfoil.

---

\* In the program the initial or first iteration is referred to as the zeroth iteration.



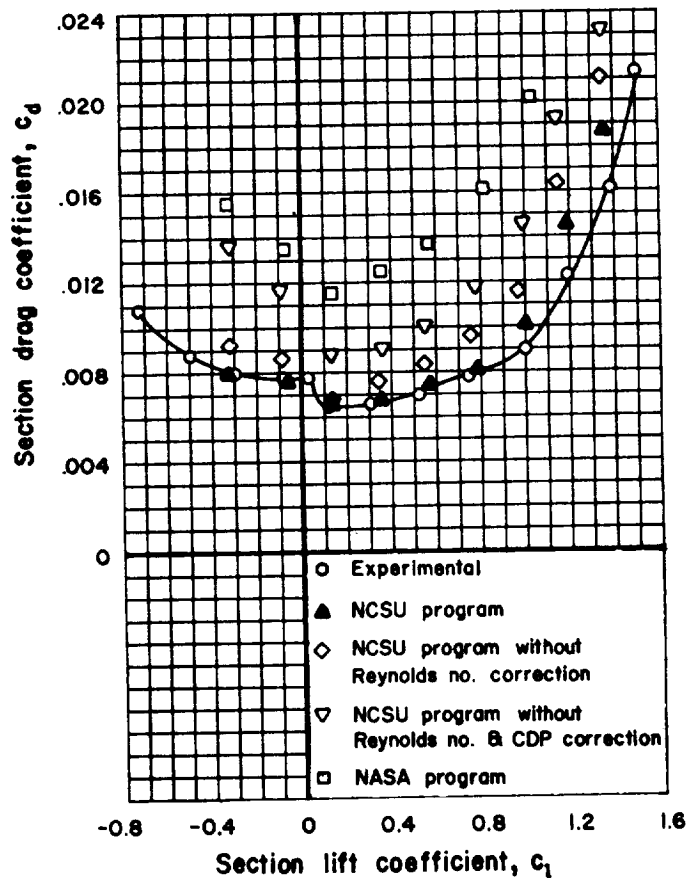


Figure 10. Effect of each of the drag modifications on the drag coefficients of the 23012 airfoil at a Reynolds number of 3.0 million.

In the NCSU program the lift and drag coefficients were calculated in the same manner and then corrected using the modifications discussed above. In order to make the normal and axial force coefficients consistent with these new lift and drag coefficients, the force coefficients were re-computed using the following relations:

$$C_N = C_L \cos \alpha + C_D \sin \alpha$$

$$C_A = -C_L \sin \alpha + C_D \cos \alpha$$

It is important to note that while the aerodynamic and force coefficients can be modified to give values which agree better with experimental data, a similar correction procedure cannot be applied to modify the pressure coefficients, and therefore they are printed as calculated.

The results of these program modifications when applied to the calculation of the aerodynamic characteristics of a number of airfoils are discussed in the next section.

## DISCUSSION OF PROGRAM RESULTS

This section is concerned with quantitative comparisons between the predicted coefficients of both the NASA program and the NCSU program and experimental data (taken for the most part from Ref. 19). In order to obtain generally valid comparisons, fifteen airfoils of various thickness and camber distributions were included in the investigation. The fifteen airfoil contours are depicted in Figure 11. The reader can see by examining Figures 12 through 30 that the lift coefficients predicted by each program are quite similar while the drag coefficients are quite different. (Although the plots show only lift and drag coefficient, the reader is reminded that the normal force, axial force, and moment coefficients for any airfoil investigated may also be obtained from the program if desired.) For most of the airfoils the comparisons are self-explanatory and require little discussion; however, some of the more interesting results warrant individual identification.

In general, the lift and drag coefficients obtained using the NCSU program compare very well with experimental data at the lower angles of attack for airfoils with thickness ratios of less than 18 percent. The drag coefficients for the lower angles of attack are slightly high and therefore conservative. For the higher angles of attack the lift is over-predicted, and the drag coefficient is usually under-predicted, because the boundary layer routines used cannot treat flows with large adverse pressure gradients, separated flows, or large wakes such as are present when the airfoil approaches stall.

For the thicker airfoils (thickness ratios of 18 percent or greater) the lift predicted by the NCSU program is more optimistic than for the thinner airfoils. For example, the 2424 airfoil really has a non-linear lift-curve slope which tends to reduce the lift, but the predicted lift curve slope is quite linear, resulting in the over-prediction of lift. The drag coefficients for the thicker airfoils are also seen to agree less well with experimental data than the drag coefficients of the thinner airfoils.

The NASA program usually gave a slightly higher predicted lift coefficient than did the NCSU program. The predicted drag coefficients for the NASA program, however, are in very poor agreement with experimental data. While the comparisons are generally poor, the NASA program drag coefficients do match experimental data better for the thicker airfoils than for the thinner airfoils.

Neither program does a very good job of predicting the aerodynamic characteristics with leading edge surface roughness as can be seen in the case of the 4412 airfoil (Figure 17). The roughness used in the test condition was approximated in the programs by specifying fixed transition at the leading edge for both the upper and lower surfaces of the airfoil. While both programs did a fairly good job of predicting the lift coefficient at the lower angles of attack, neither program did well for the drag

coefficient; the NASA program over-predicted the drag coefficient by 25 to 40 percent while the NCSU program under-predicted the drag by 20 to 40 percent.

The reader will notice that there are no predicted NASA coefficients for the 63<sub>2</sub>-615 airfoil (Figure 23). While the NCSU program prediction is very good the NASA program was not able to produce an acceptable set of distributed solution points for this airfoil, and thus no correlation can be shown. In a similar situation, the NCSU program was not able to produce a set of distributed points for the 63<sub>3</sub>-618 airfoil until two extra points were added in the nose region to those specified for the airfoil in TR 824 (Ref. 19). The extra points were needed because some of the specified points were extremely close together, leaving a large portion of the airfoil nose with no points to specify its shape. The same procedure was used for the 2424 airfoil whose coefficients are shown in Figures 13 and 14. For the 2424 four extra points were added in the region of the nose. As mentioned above, it is important to specify regions of high airfoil curvature properly. While there were a few exceptions, in most cases the ordinates given in TR 824 were sufficient to define the shape of the airfoil.

The Whitcomb airfoil which is currently being investigated by NASA Langley for possible application to general aviation craft is another airfoil which deserves some special mention. While the drawing of this airfoil in Figure 11 does not show it, the Whitcomb airfoil has its minimum thickness slightly ahead of the trailing edge. While the comparison of the NCSU program with experimental data is good for a Reynolds number of 1.9 million, this unusual trailing edge shape is probably one reason for the poor comparison with the previously unpublished experimental data at a Reynolds number of 9.2 million (Figure 29). The poor comparison at 9.2 million may also be due to the erratic nature of the experimental data at this Reynolds number.

In order to investigate another of the latest airfoil designs, that presented in TN D-7071 (Ref. 52) was investigated using the two computer programs. The airfoil (referred to as the TN D-7071 airfoil) was originally designed to optimize the maximum lift coefficient. Experimental results are given for the pressure coefficients and the lift coefficients in Reference 52, but no drag data is presented. This airfoil was of particular interest because of its unusual shape (see Figure 11) and because the original NASA program was used in Reference 52 for a theoretical correlation with the experimental results. Figure 30 indicates that the lift coefficients for the TN D-7071 airfoil obtained from the NCSU program match the experimental values a little better than do the NASA program values. The drag coefficients for both programs are also included for the sake of completeness even though no experimental drag coefficients are available. Figures 31, 32, and 33 give the pressure distributions over the airfoil for experimental measurement, the NASA program, and the NCSU program for this airfoil at angles of attack of 3.4, 12.4, and 18.7 degrees respectively. These pressure coefficients were included to show that the pressure coefficients obtained from the NCSU program

are still basically the same as those predicted by the NASA program. As indicated in Reference 31 the computed pressure coefficients for conventional airfoils usually compared quite well with experimental data.

In order to study some of the bounds of the computational methods presented herein, an attempt was made to predict the aerodynamic characteristics of the last airfoil shown in Figure 11. This is a very thin, highly cambered airfoil recently tested by Milgram (Ref. 108) over a very wide range in Reynolds Numbers and angles of attack. The very non-linear lift curve and high drag coefficients evident in the experimental data indicate extensive flow separation which changes radically with the changes in angle of attack. Figure 34 compares the predictions with the experimental data. The lift predictions are close to experimental values only for an angle of attack of 2-3°. At large angles of attack where the thin nose of the airfoil points into the wind, more or less, there is extensive separation over the aft portion of the upper surface so that the predicted lift does not materialize. The best that can be said for the drag predictions are that the NCSU program is qualitatively correct but predicts only 25% of the actual drag. This experience leads one to suggest extreme caution in applying the program to airfoils which possess regions of surface concavity. Not only does the boundary layer routine used here fail for what in these circumstances will usually be a separated flow, but the inviscid method also has difficulty with such geometries.

As received from Langley, the program contained a provision to modify both the inviscid and viscous computations of the pressure distribution and aerodynamic force coefficients for the effects of changes in free stream Mach number. This capability was retained although it is expected to be of limited utility for most light aircraft designs. For this reason, the applicability to varied airfoils and the accuracy limits of the routine were not investigated extensively. Plotted in Figure 35 are the results for a 23012 airfoil obtained with the original Langley version and the modified NCSU version. It will be seen that for this case and for  $\alpha = 0$ , at least, the NCSU version gives qualitatively reasonable lift results for all Mach numbers while the original version is reliable to about  $M \approx 0.50$ . The reasons for the apparent superiority of the NCSU version were not examined in detail. No explanation for this behavior can, therefore, be offered. Experimental data for the 23012 airfoil were not at hand for comparison, but one may note that generally the Prandtl-Glauert rule under-predicts the increase in  $C_L$  near  $M_{CR}$  by about 10%. Thus, the NCSU prediction may yield results quantitatively below those found experimentally for  $M > 0.5$ . The user should therefore approach results for  $M > 0.5$  cautiously.

The results of the drag predictions are shown in Figure 36. The Langley results appear to be completely meaningless. Again, the reason for this is not known. The NCSU predictions, on the other hand, appear to be qualitatively correct for all Mach numbers. Quantitatively, the Squire-Young formula seems to give the more reasonable results for  $M > 0.55$ .

Based on the airfoils investigated the authors conclude that:

- (1) the NCSU program gives about the same pressure distribution over the airfoil as does the NASA program
- (2) the lift coefficients for the NCSU program while still a little too large for some airfoils, compare more favorably with experimental data than do the NASA program coefficients
- (3) the predicted drag coefficients using the NCSU program compare much better with experimental data than the drag coefficients obtained from the NASA program.

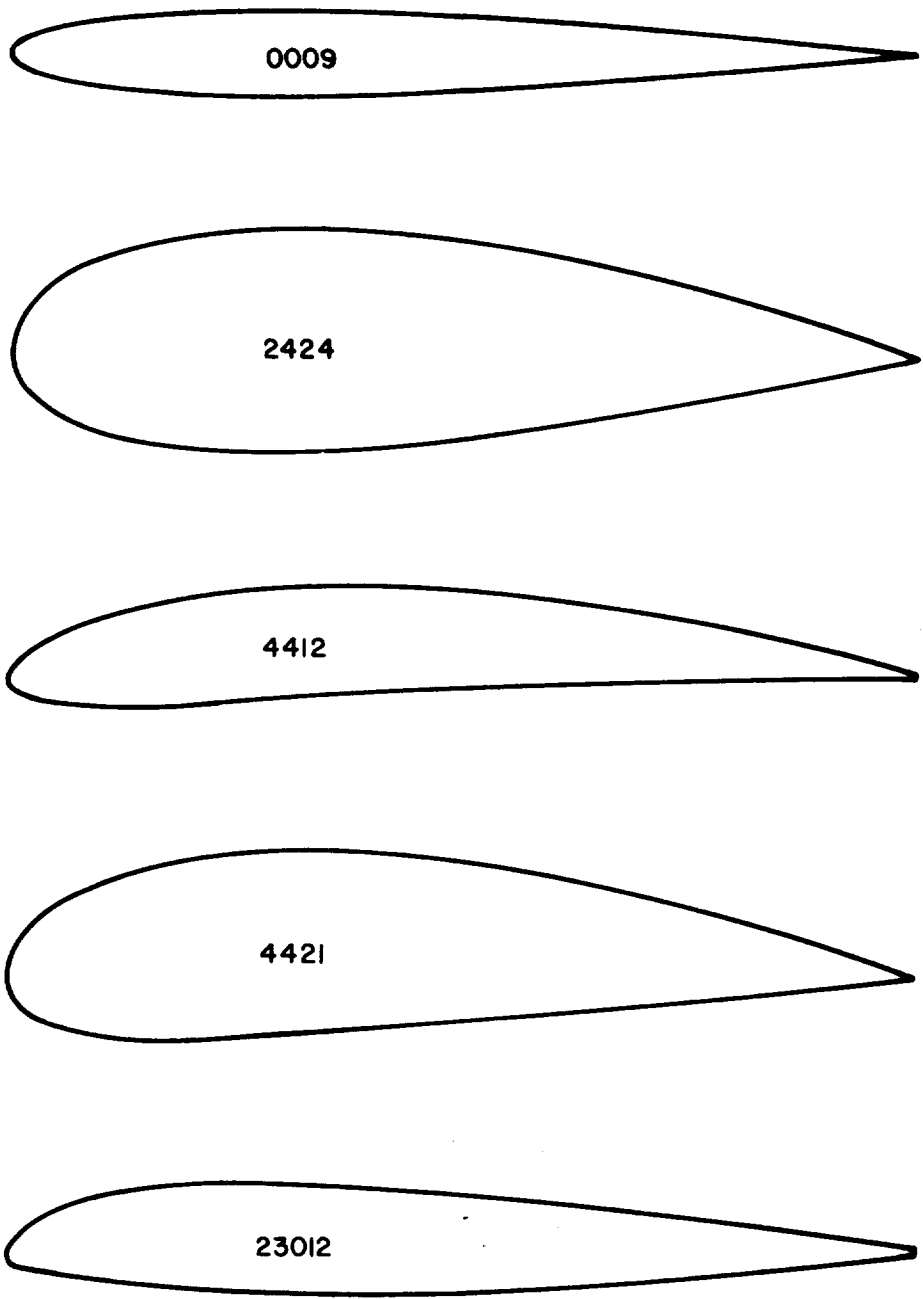


Figure 11. General shape of the 15 airfoils investigated for lift and drag characteristics.

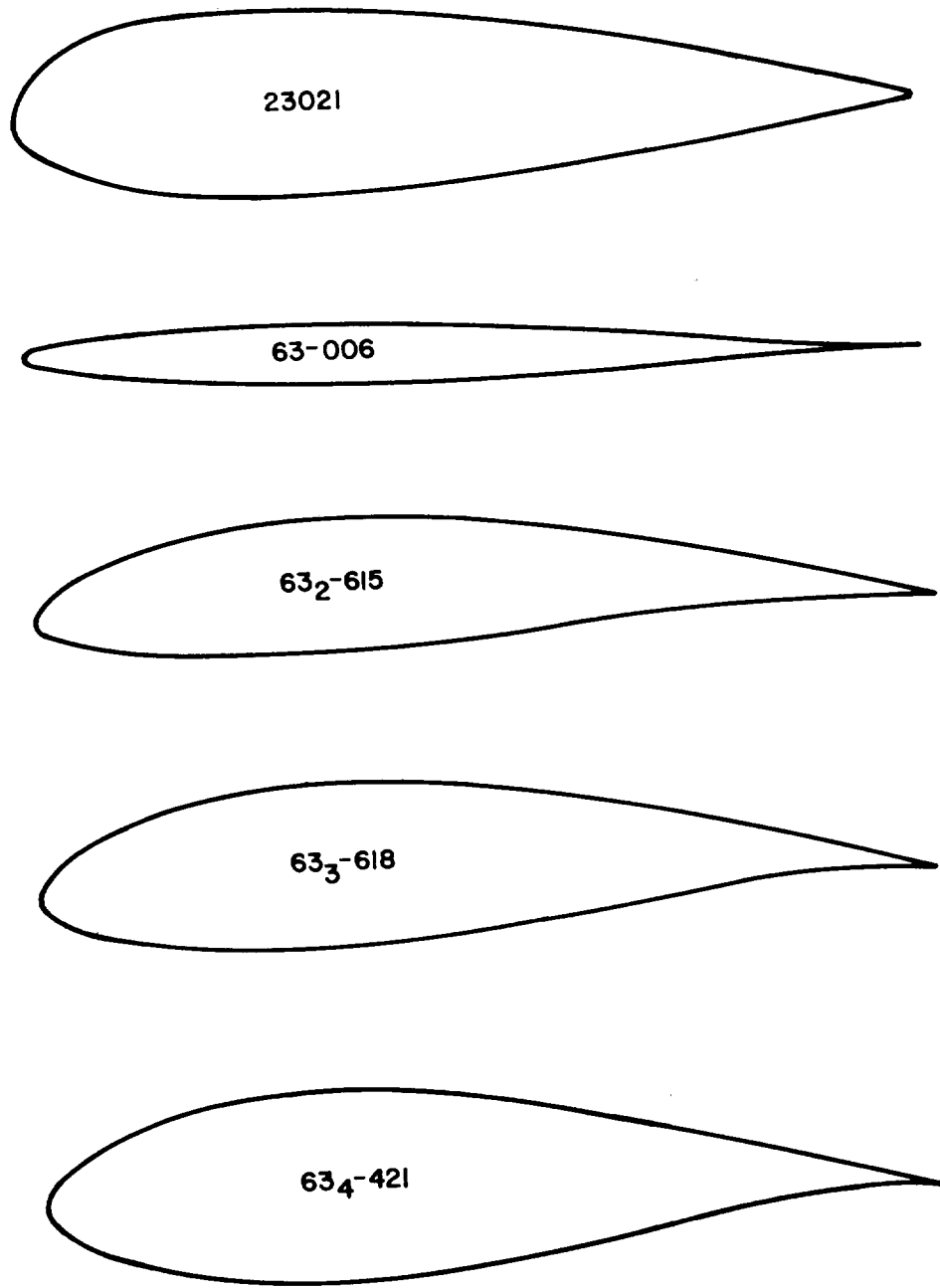


Figure 11. Continued.

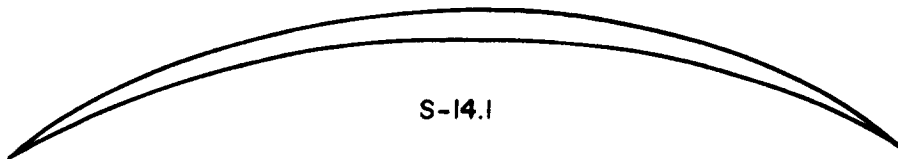
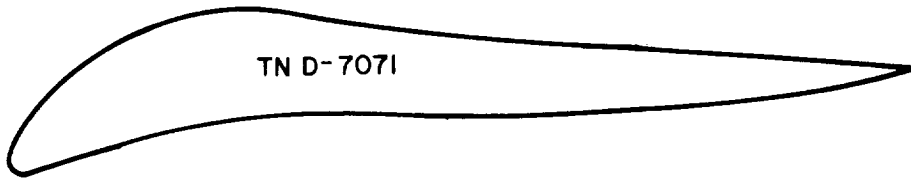
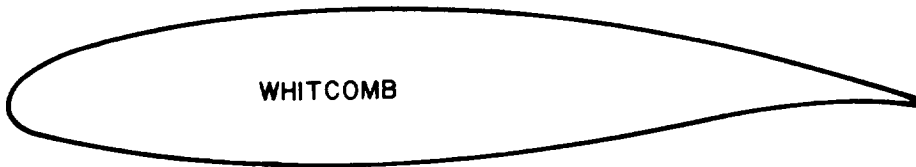
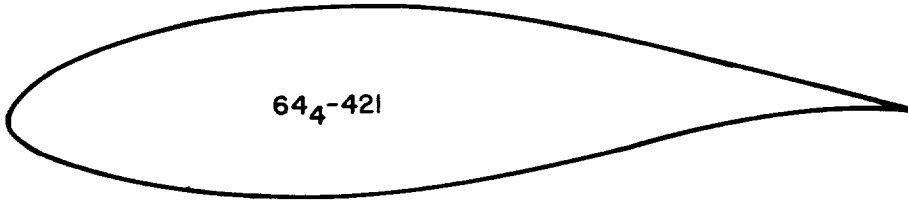
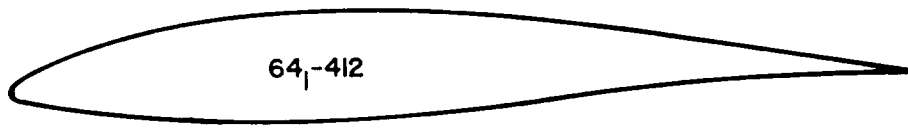


Figure 11. Continued.



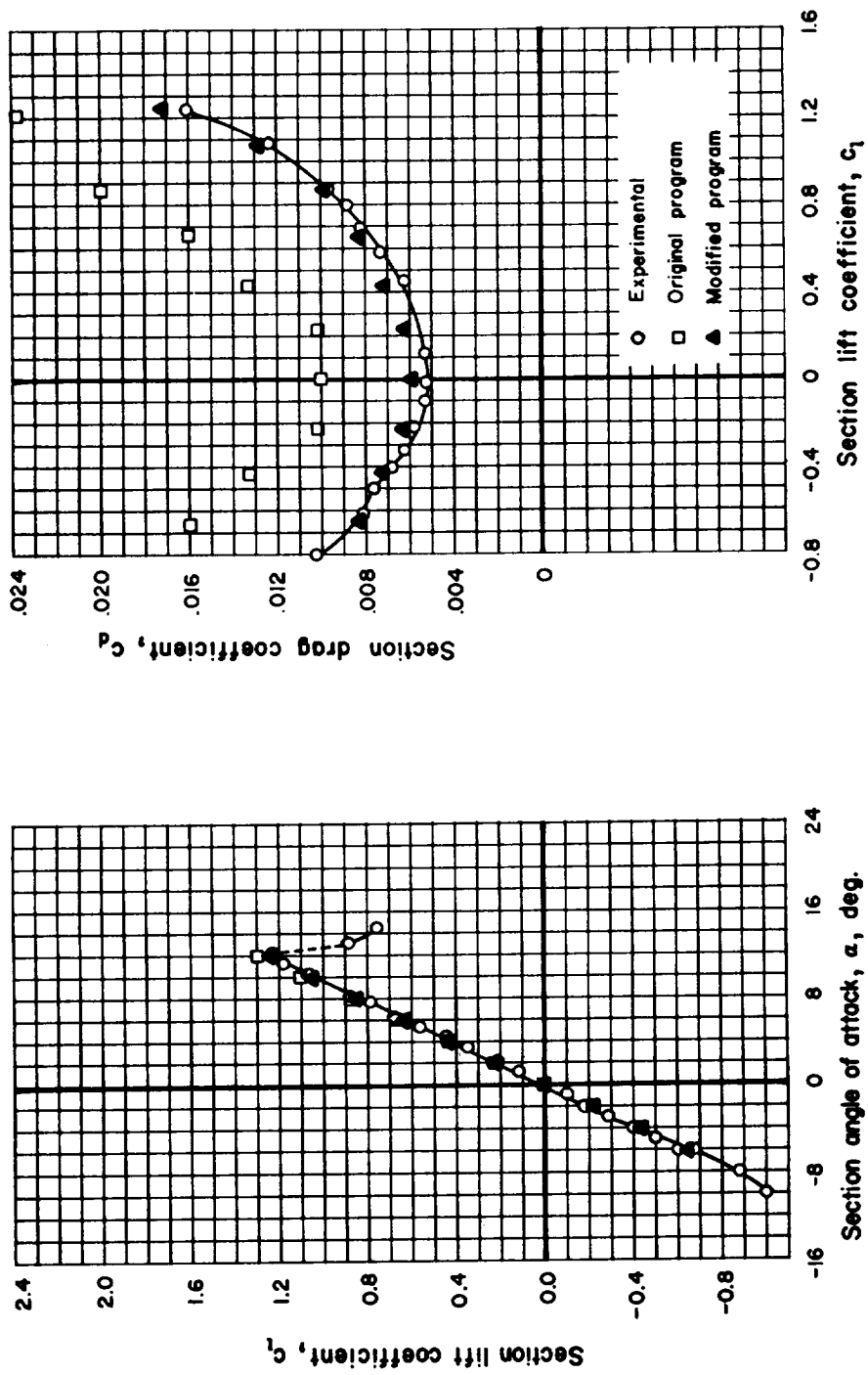


Figure 12. Comparison of 2-D lift and drag coefficients of the 0009 airfoil at a Reynolds number of 3,000,000.

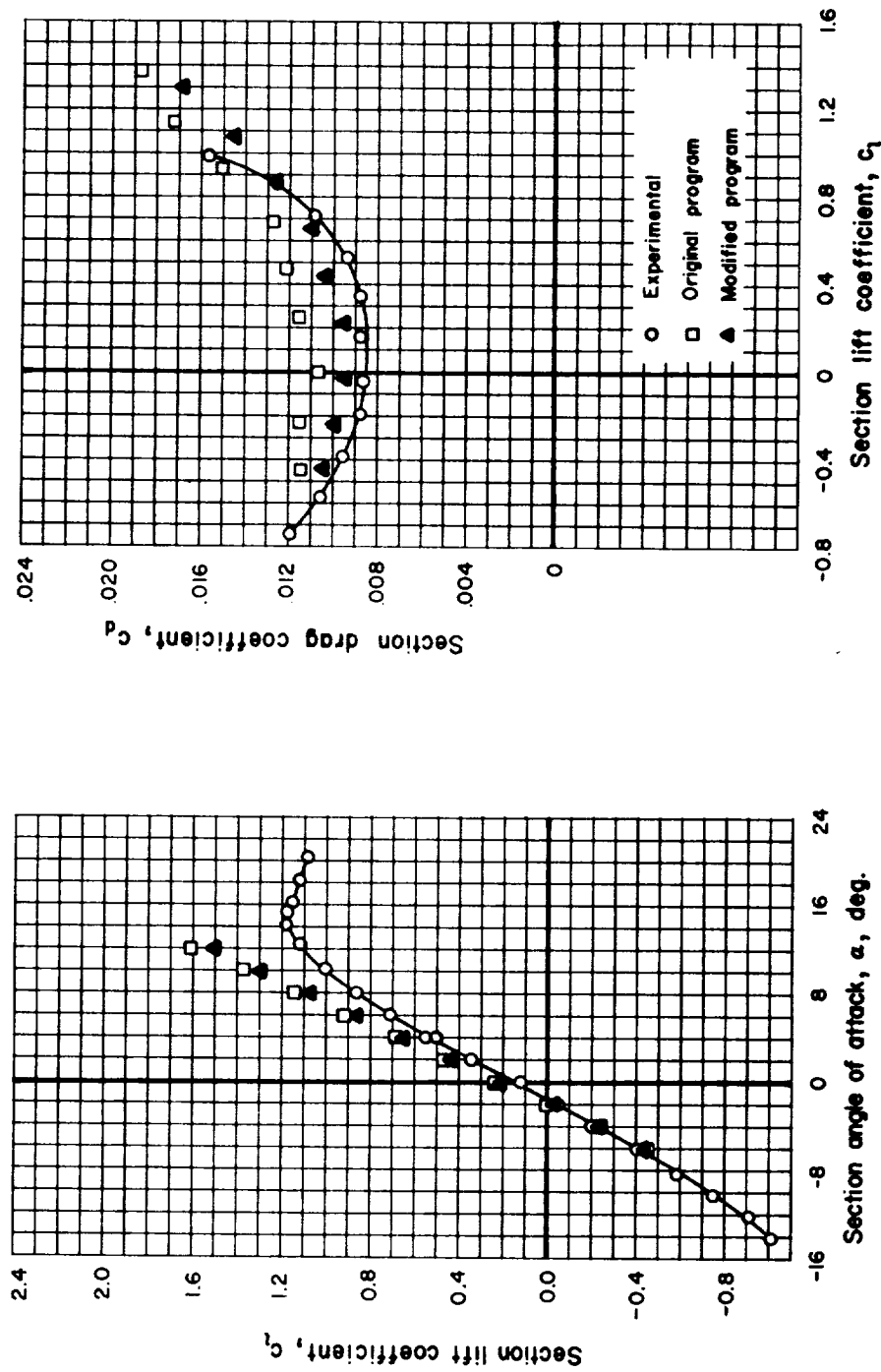


Figure 13. Comparison of 2-D lift and drag coefficients of the 2424 airfoil at a Reynolds number of 2,900,000.

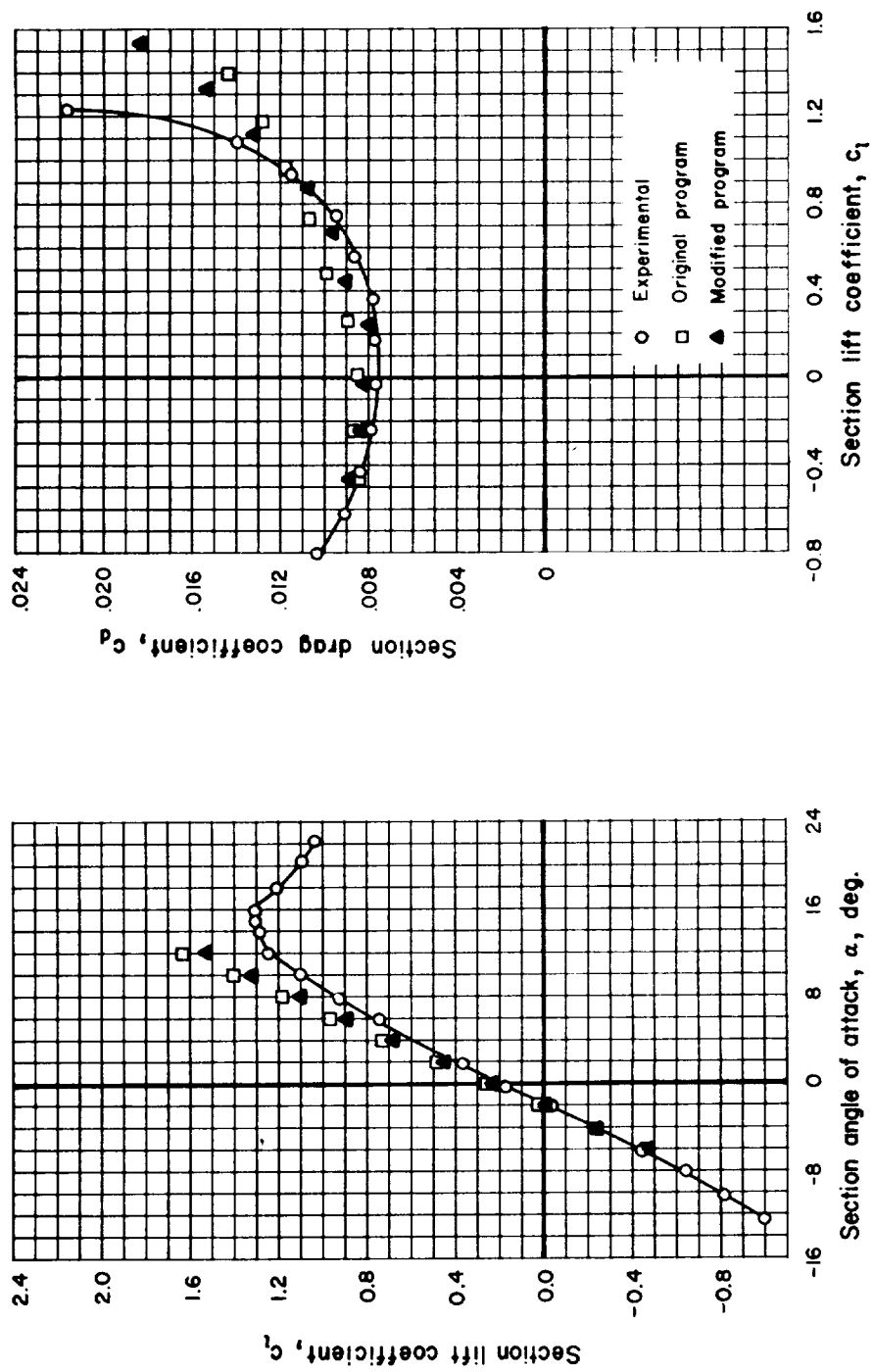


Figure 14. Comparison of 2-D lift and drag coefficients of the 2424 airfoil at a Reynolds number of 9,000,000.

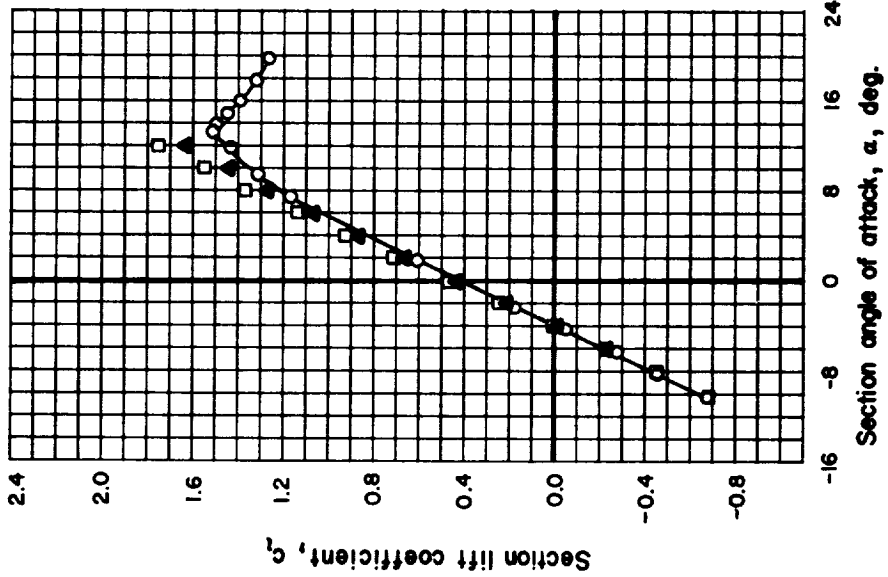
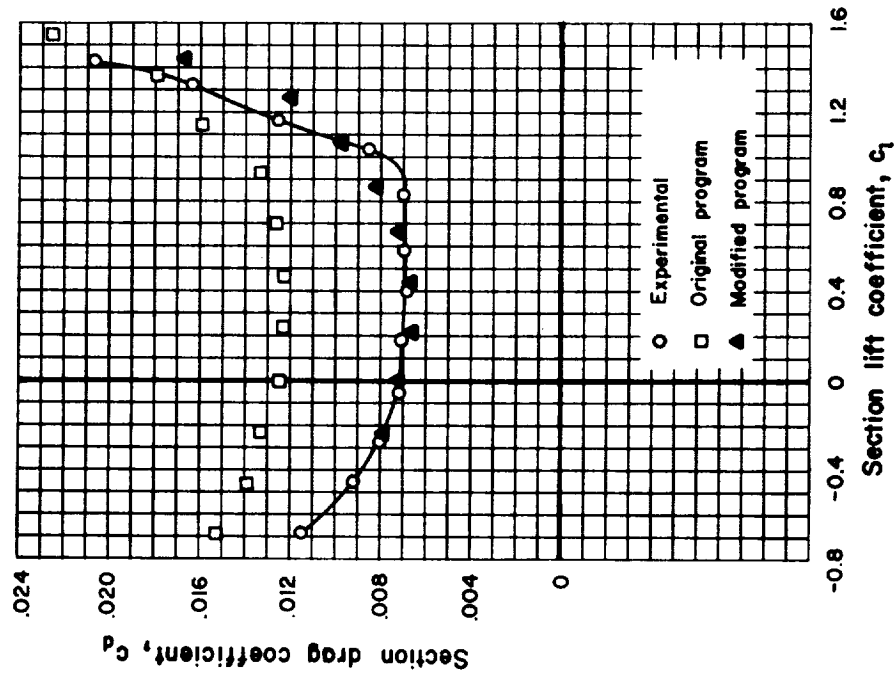


Figure 15. Comparison of 2-D lift and drag coefficients of the 4412 airfoil at a Reynolds number of 3,000,000.

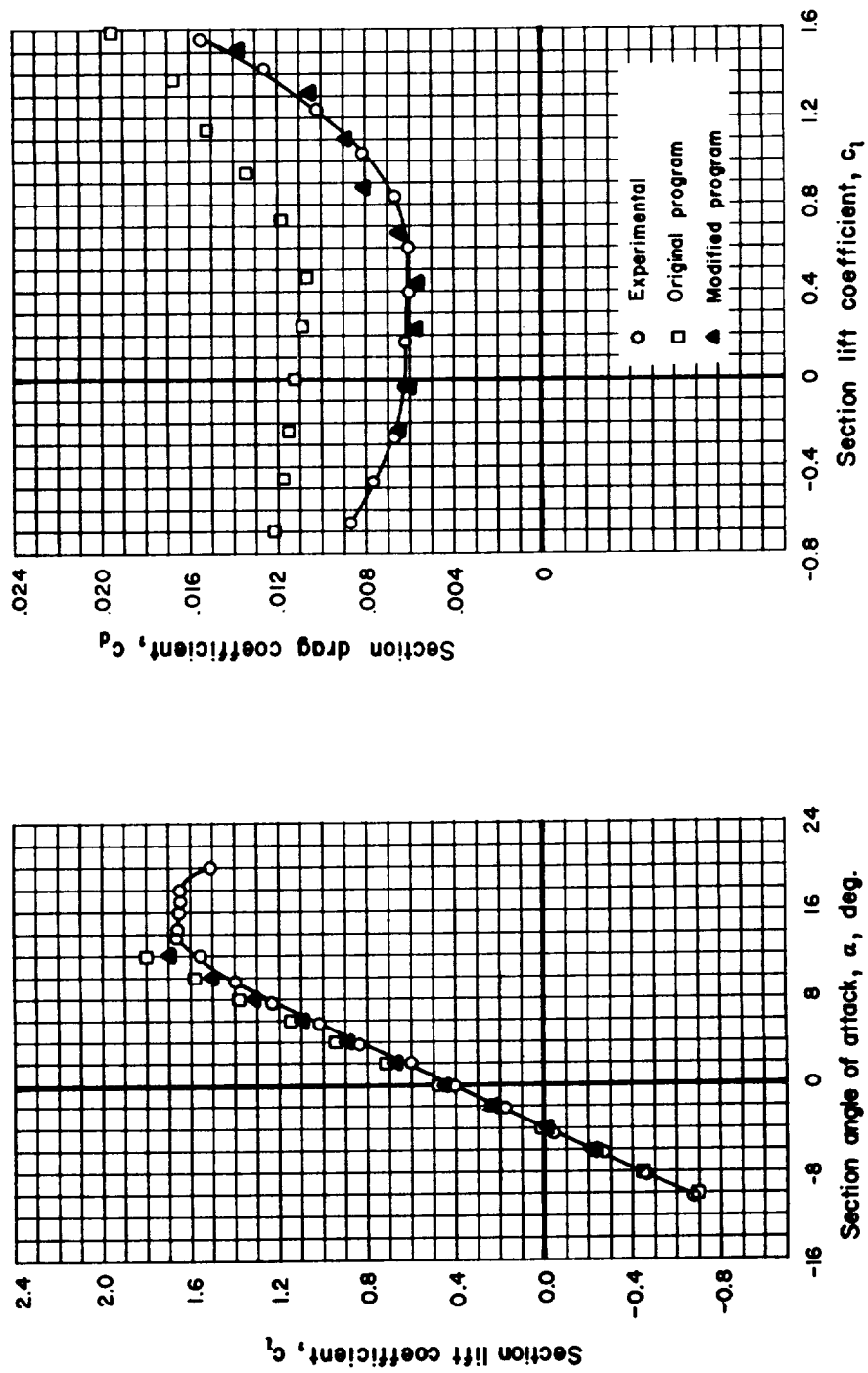


Figure 16. Comparison of 2-D lift and drag coefficients of the 4412 airfoil at a Reynolds number of 9,000,000.

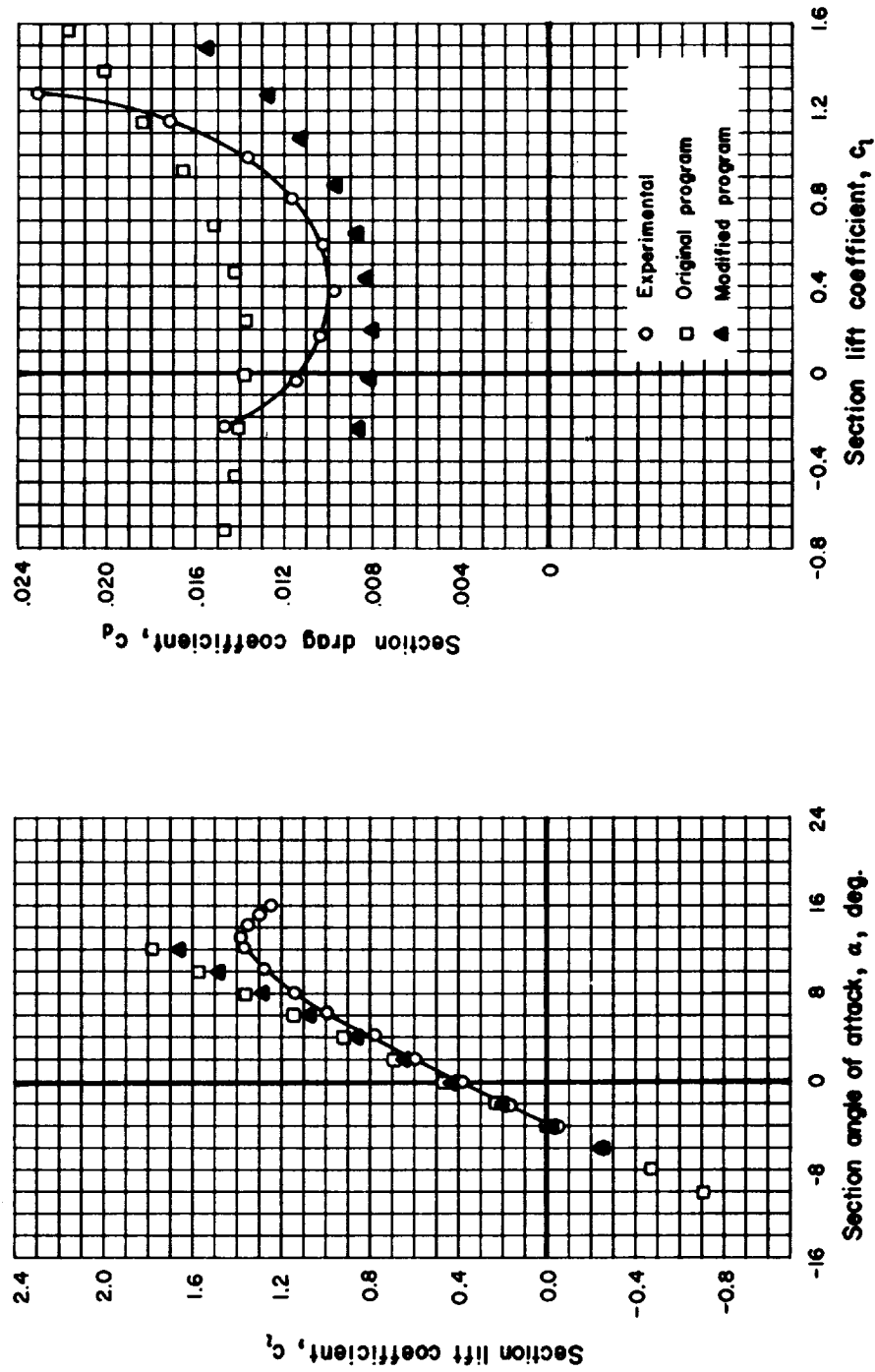


Figure 17. Comparison of 2-D lift and drag coefficients of the 4412 airfoil at a Reynolds number of 6,000,000 with fixed upper and lower surface leading edge transition to approximate standard roughness.

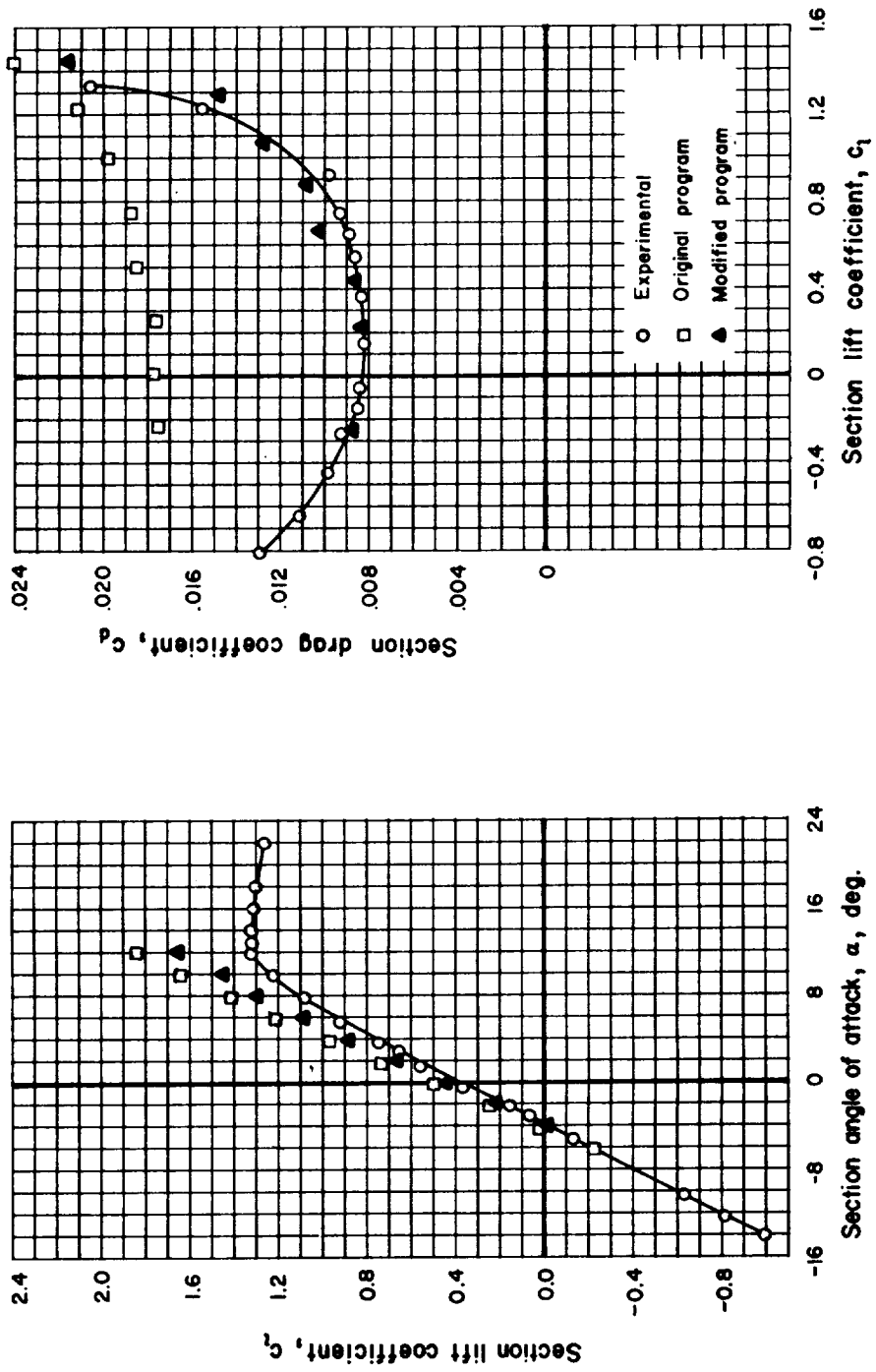


Figure 18. Comparison of 2-D lift and drag coefficients of the 4421 airfoil at a Reynolds number of 3,000,000.

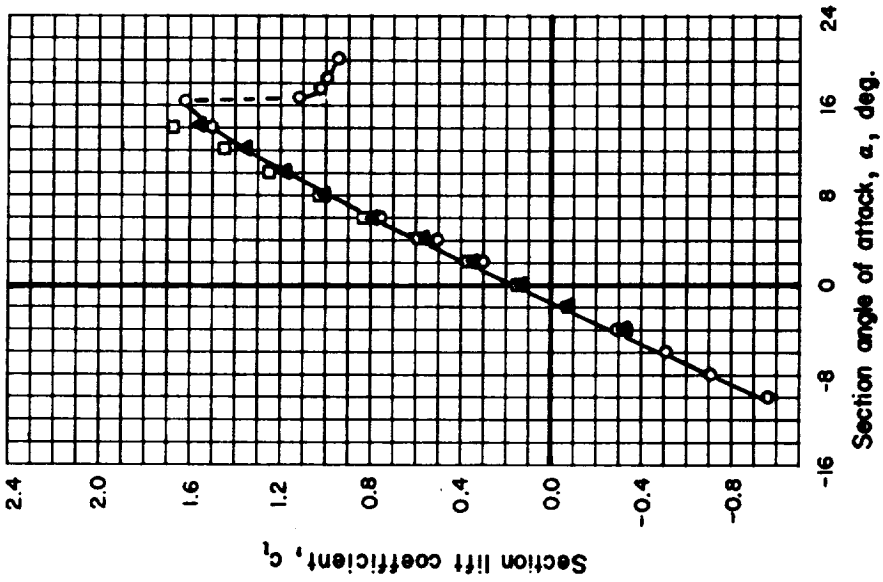
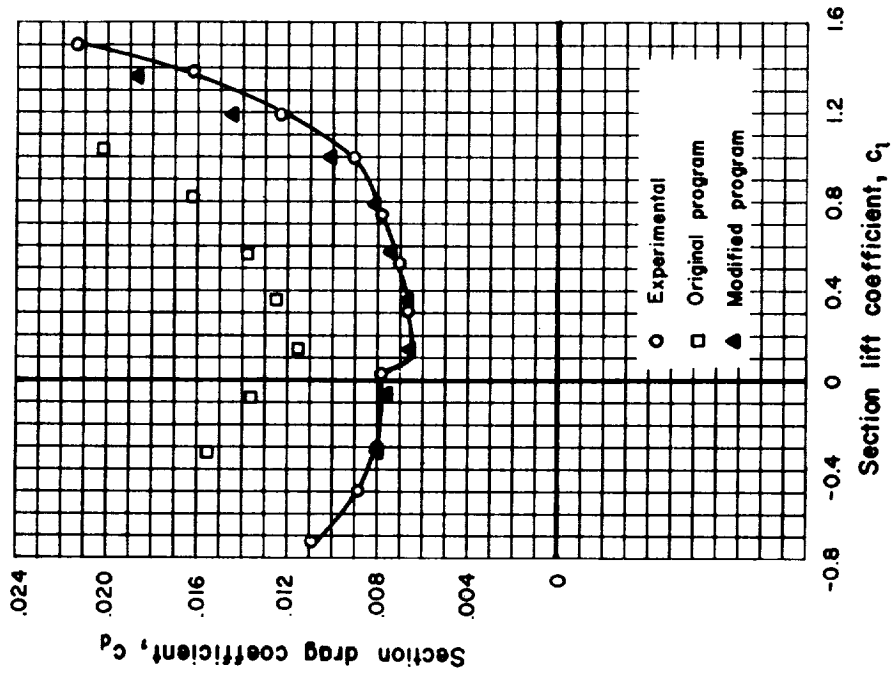


Figure 19. Comparison of 2-D lift and drag coefficients of the 23012 airfoil at a Reynolds number of 3,000,000.



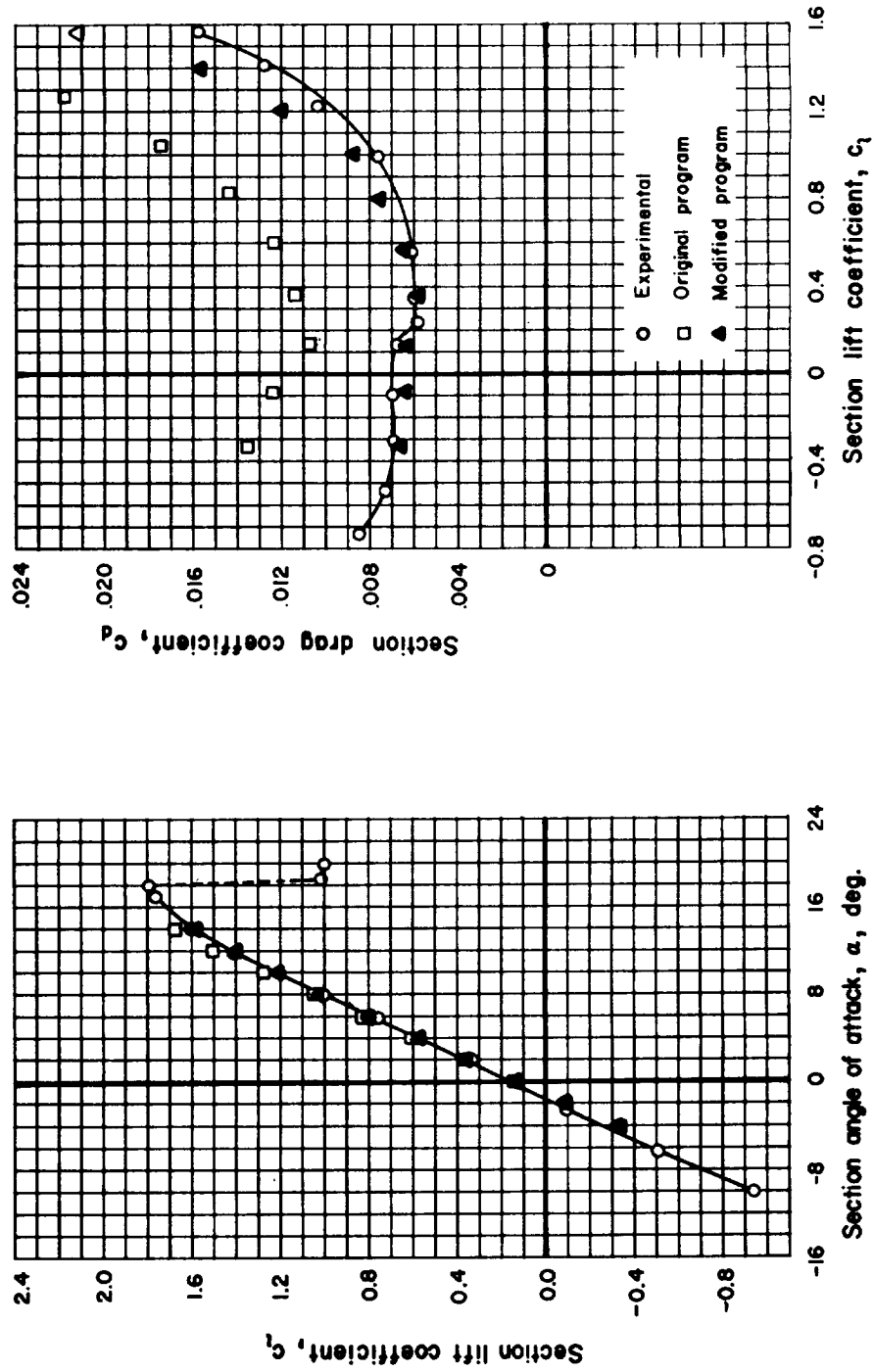


Figure 20. Comparison of 2-D lift and drag coefficients of the 23012 airfoil at a Reynolds number of 8,800,000.

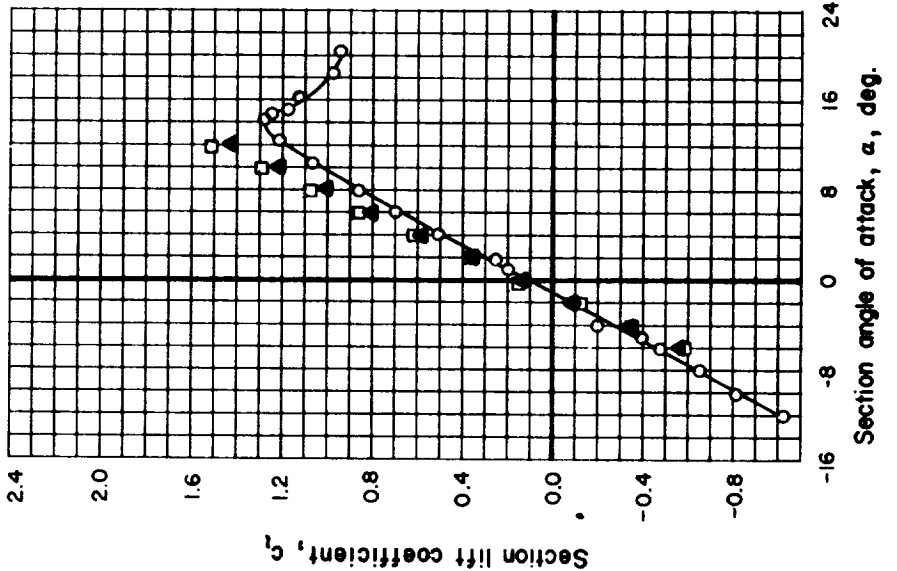
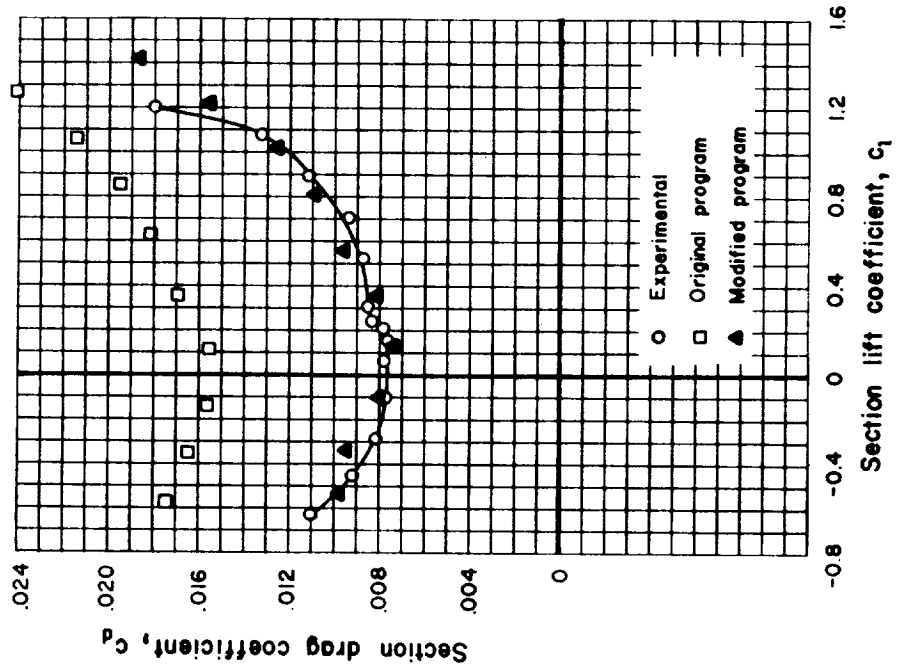


Figure 21. Comparison of 2-D lift and drag coefficients of the 23021 airfoil at a Reynolds number of 3,000,000.

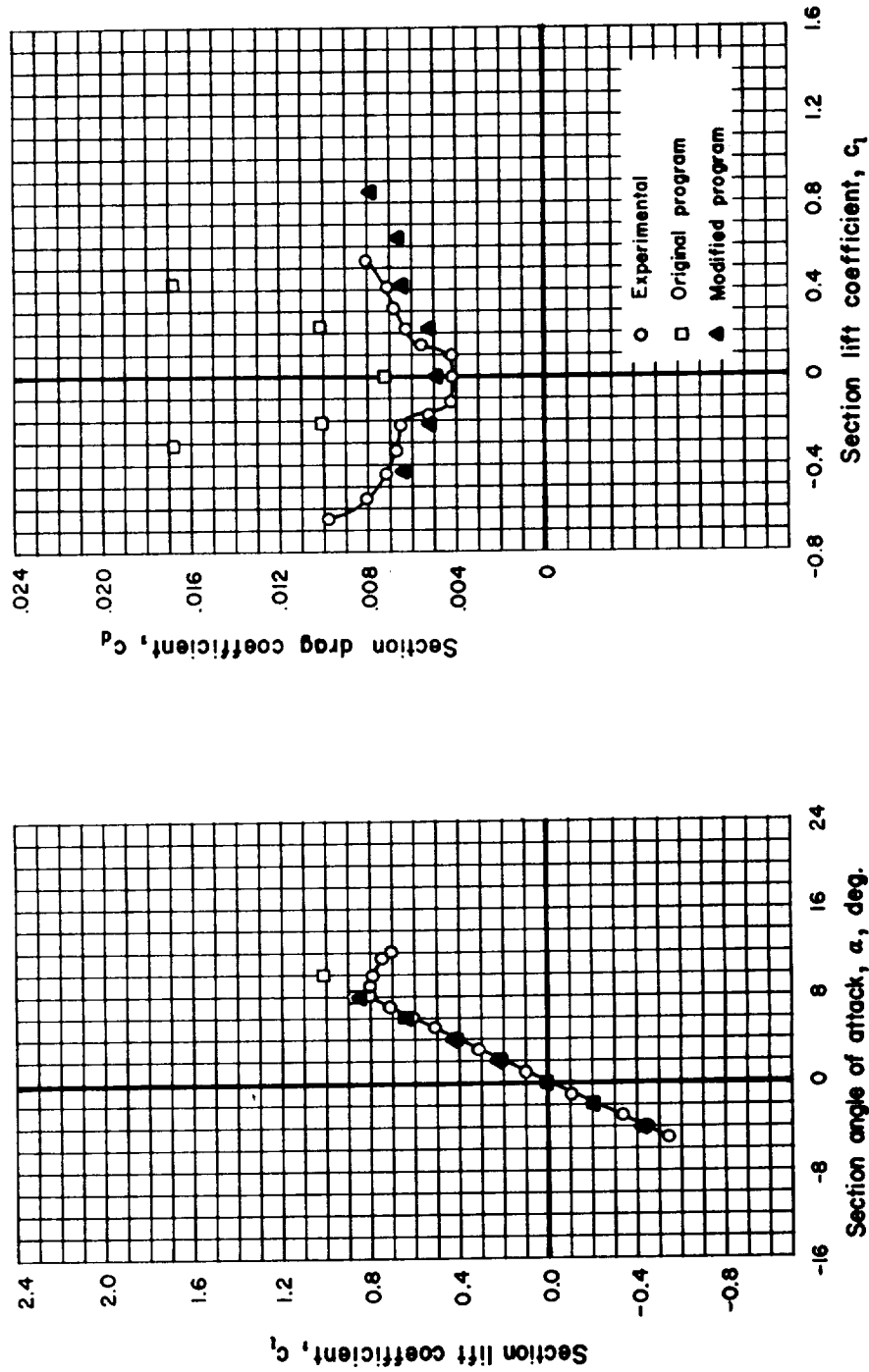


Figure 22. Comparison of 2-D lift and drag coefficients of the 63-006 airfoil at a Reynolds number of 3,000,000.

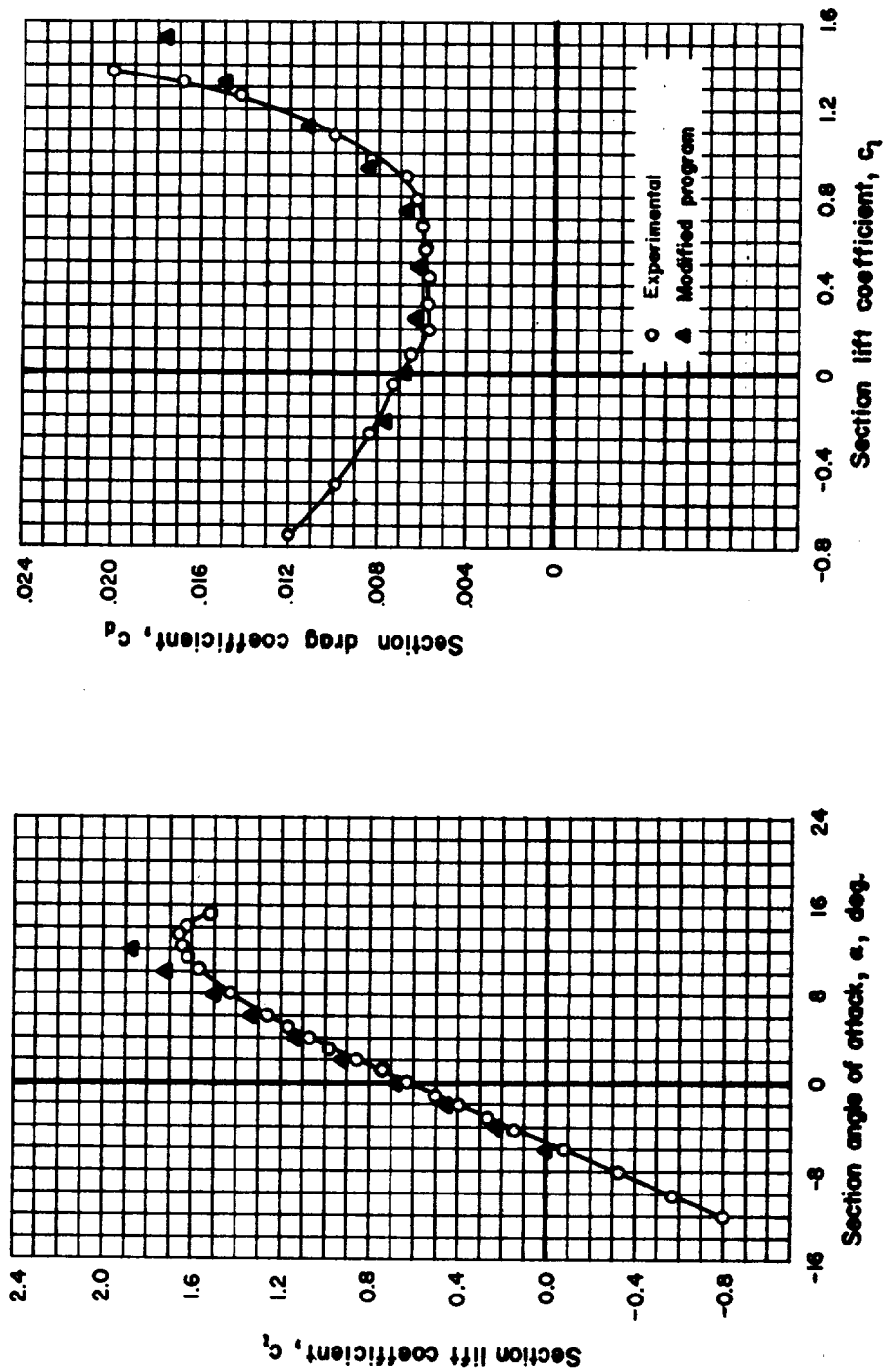


Figure 23. Comparison of 2-D lift and drag coefficients of the 63<sub>2</sub>-615 airfoil at a Reynolds number of 3,000,000.

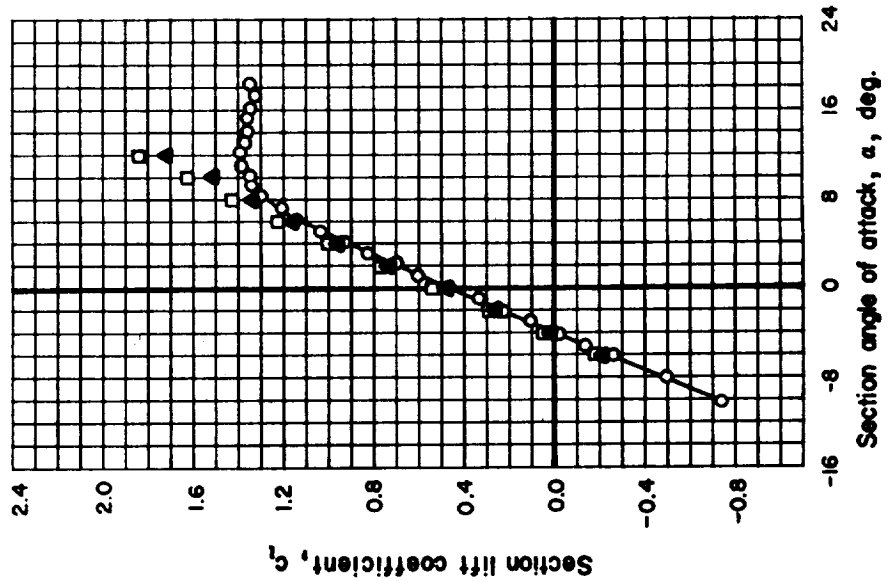
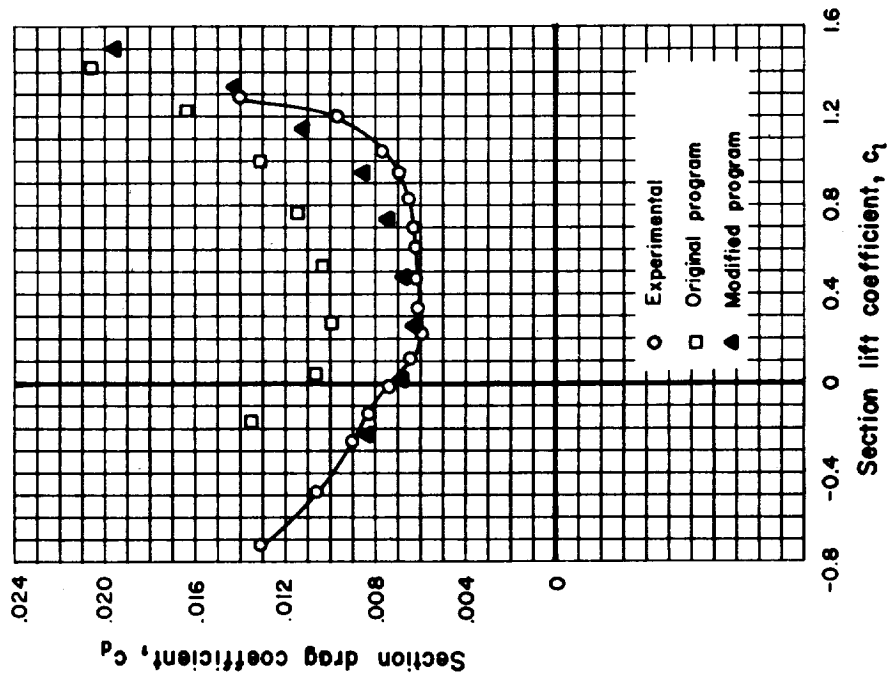


Figure 24. Comparison of 2-D lift and drag coefficients of the 63<sub>3</sub>-618 airfoil at a Reynolds number of 3,000,000.

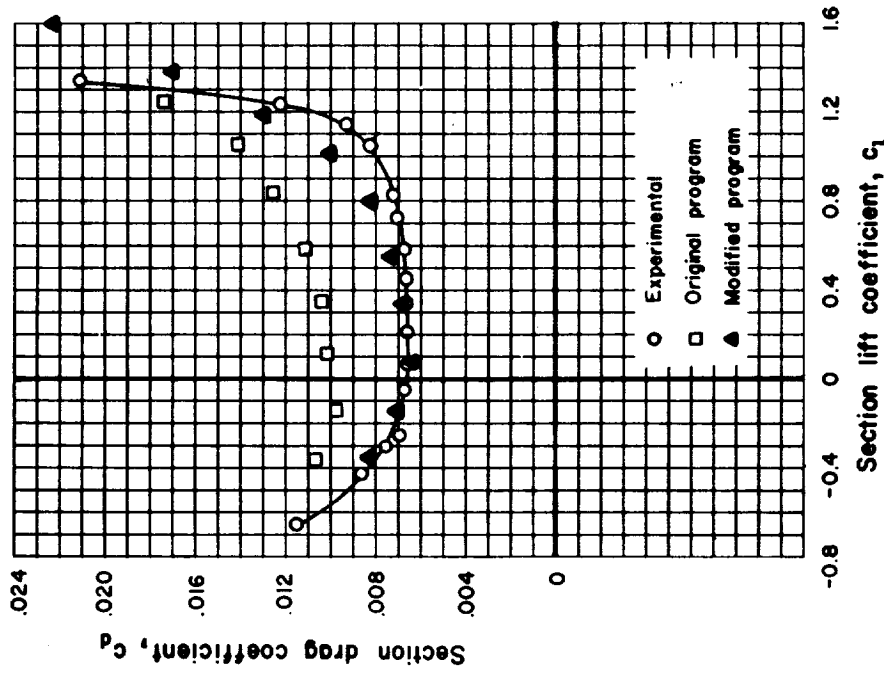
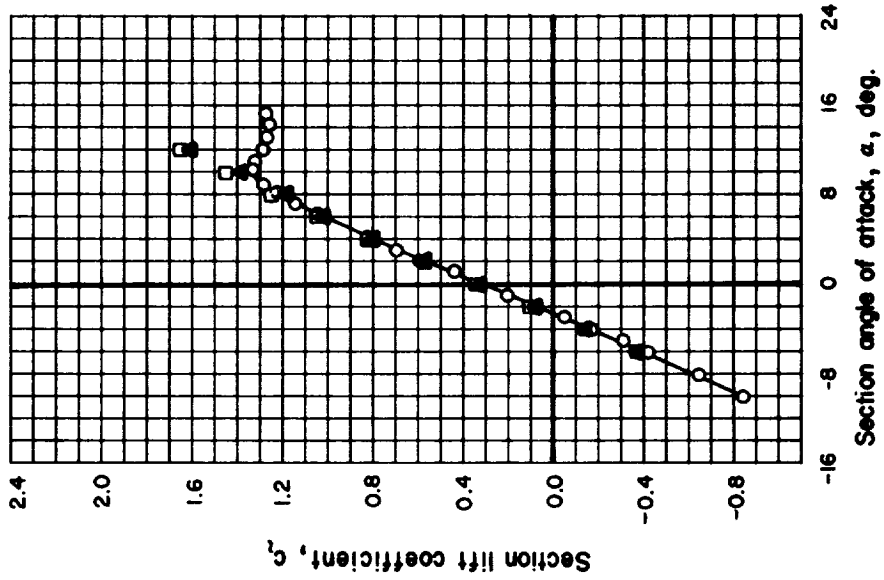


Figure 25. Comparison of 2-D lift and drag coefficients of the 63<sub>4</sub>-421 airfoil at a Reynolds number of 3,000,000.

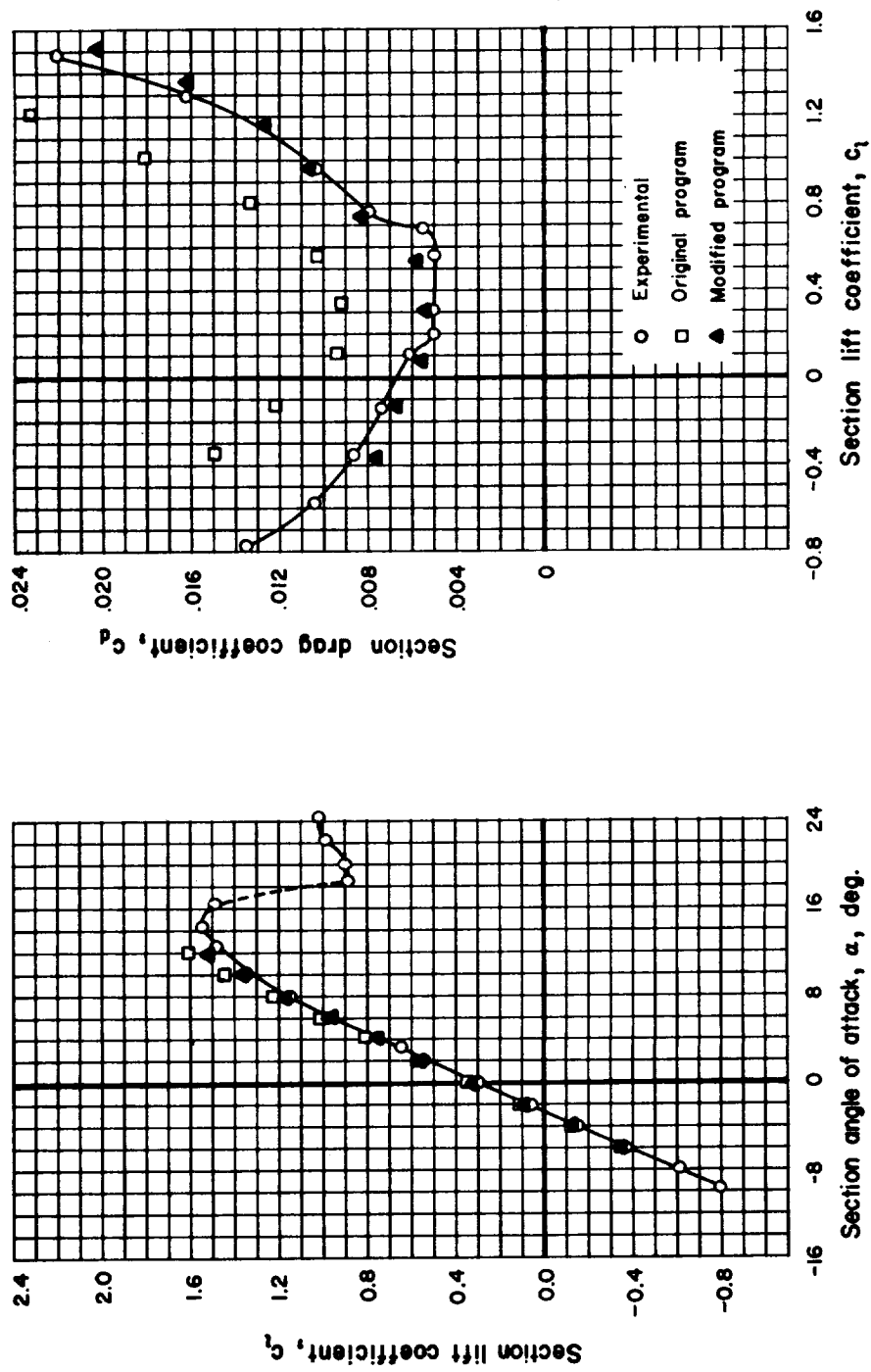


Figure 26. Comparison of 2-D lift and drag coefficients of the 64, -412 airfoil at a Reynolds number of 3,000,000.

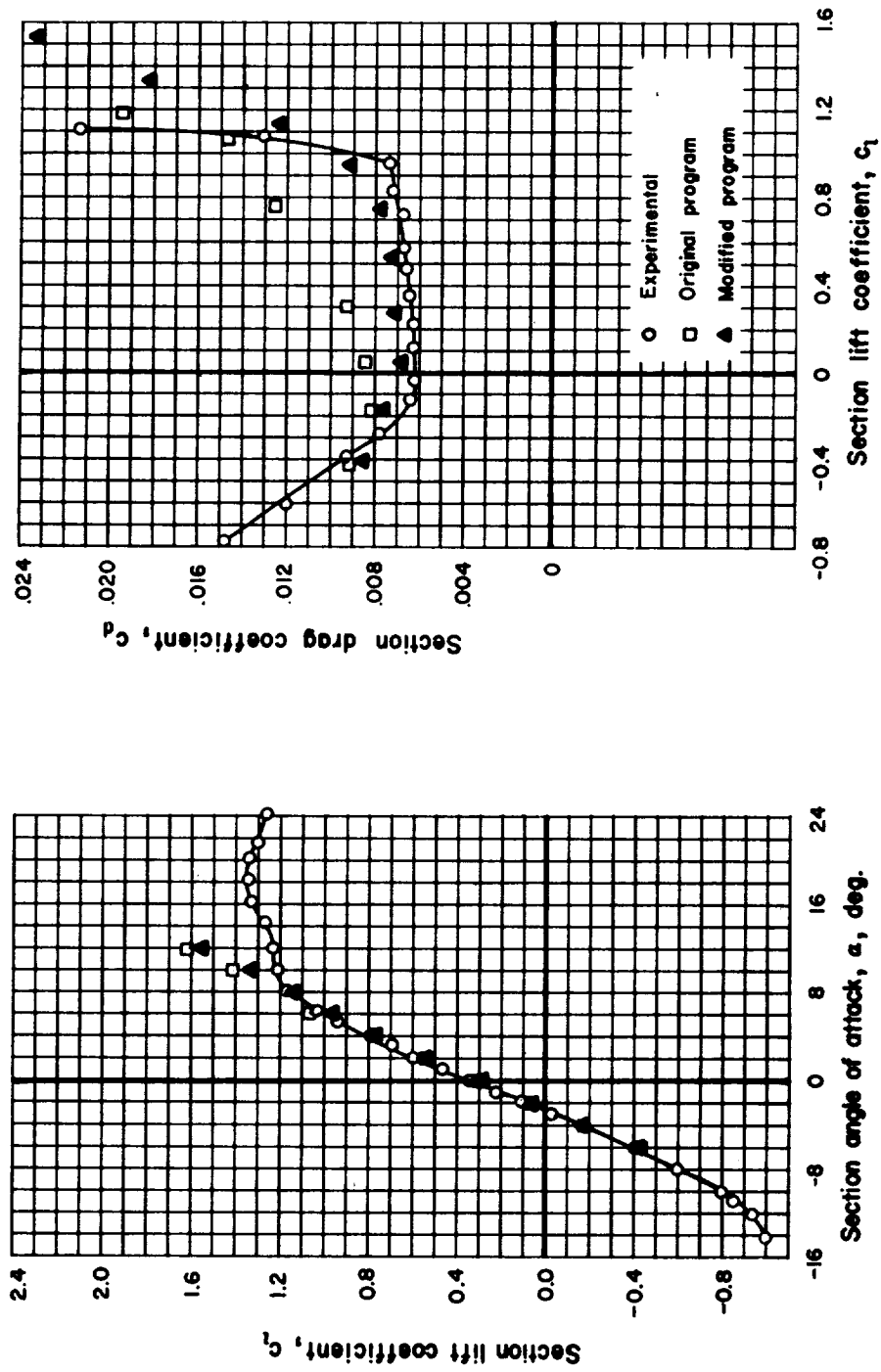


Figure 27. Comparison of 2-D lift and drag coefficients of the 64<sub>4</sub>-421 airfoil at a Reynolds number of 3,000,000.



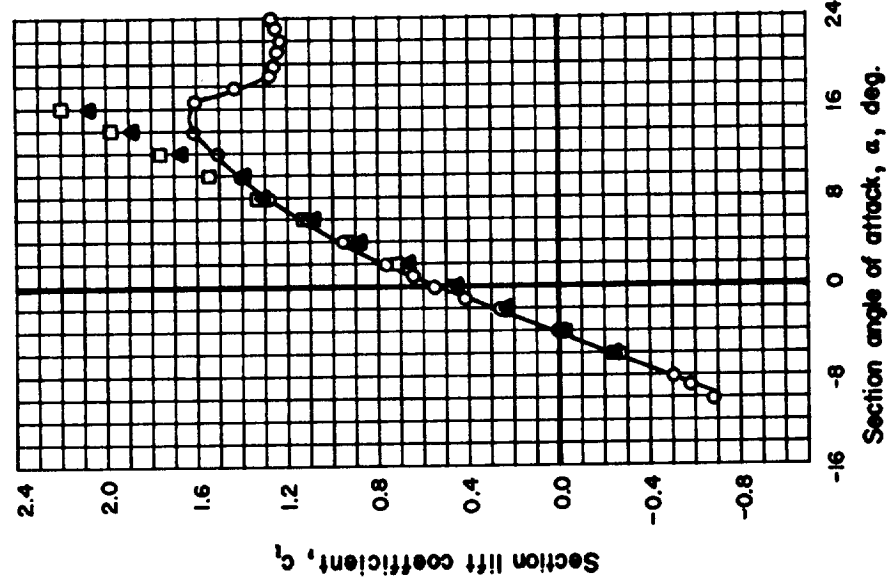
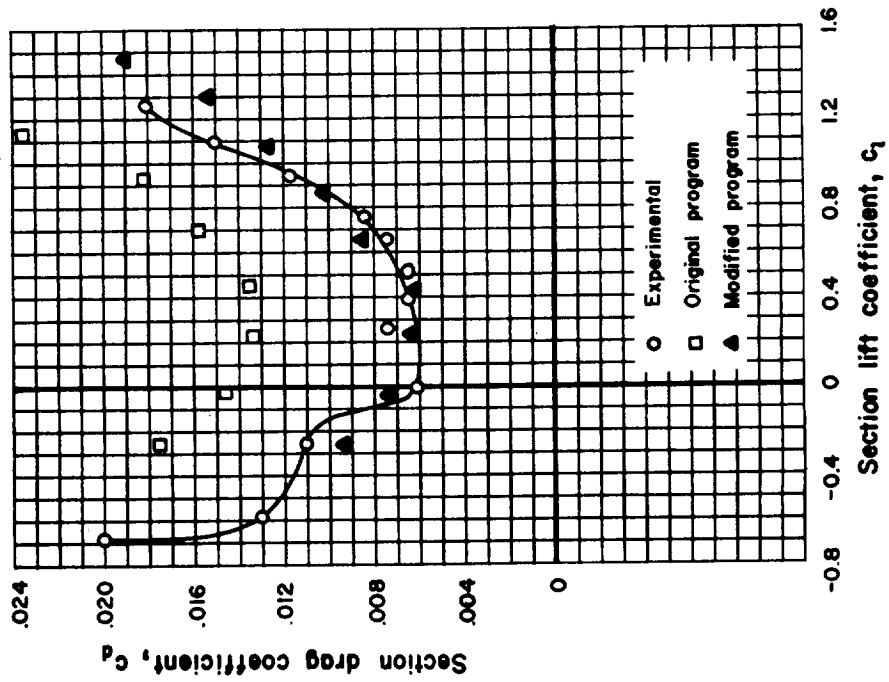


Figure 28. Comparison of 2-D lift and drag coefficients of the Whitcomb airfoil at a Reynolds number of 1,900,000.

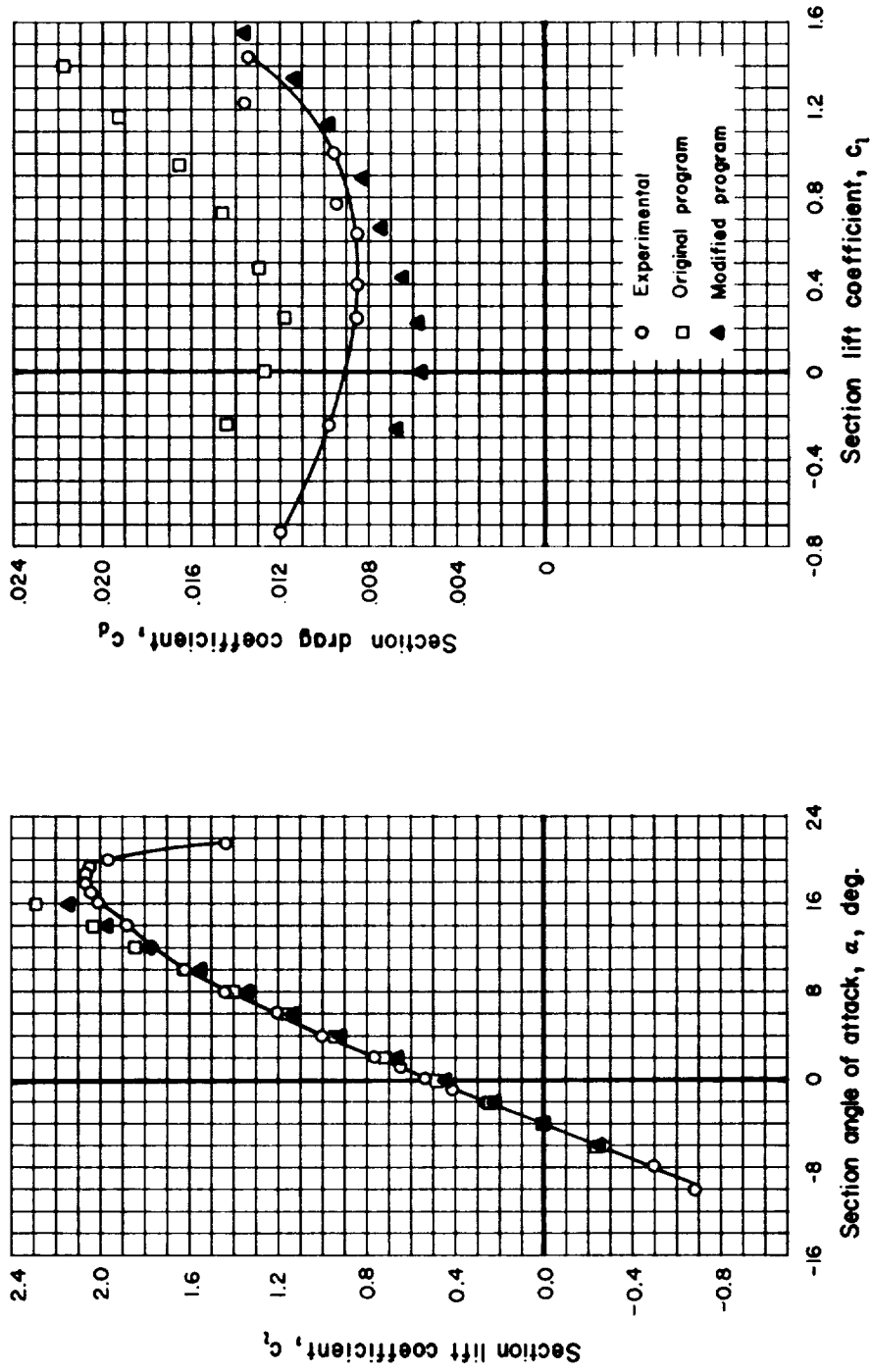


Figure 29. Comparison of 2-D lift and drag coefficients of the Whitcomb airfoil at a Reynolds number of 9,200,000.

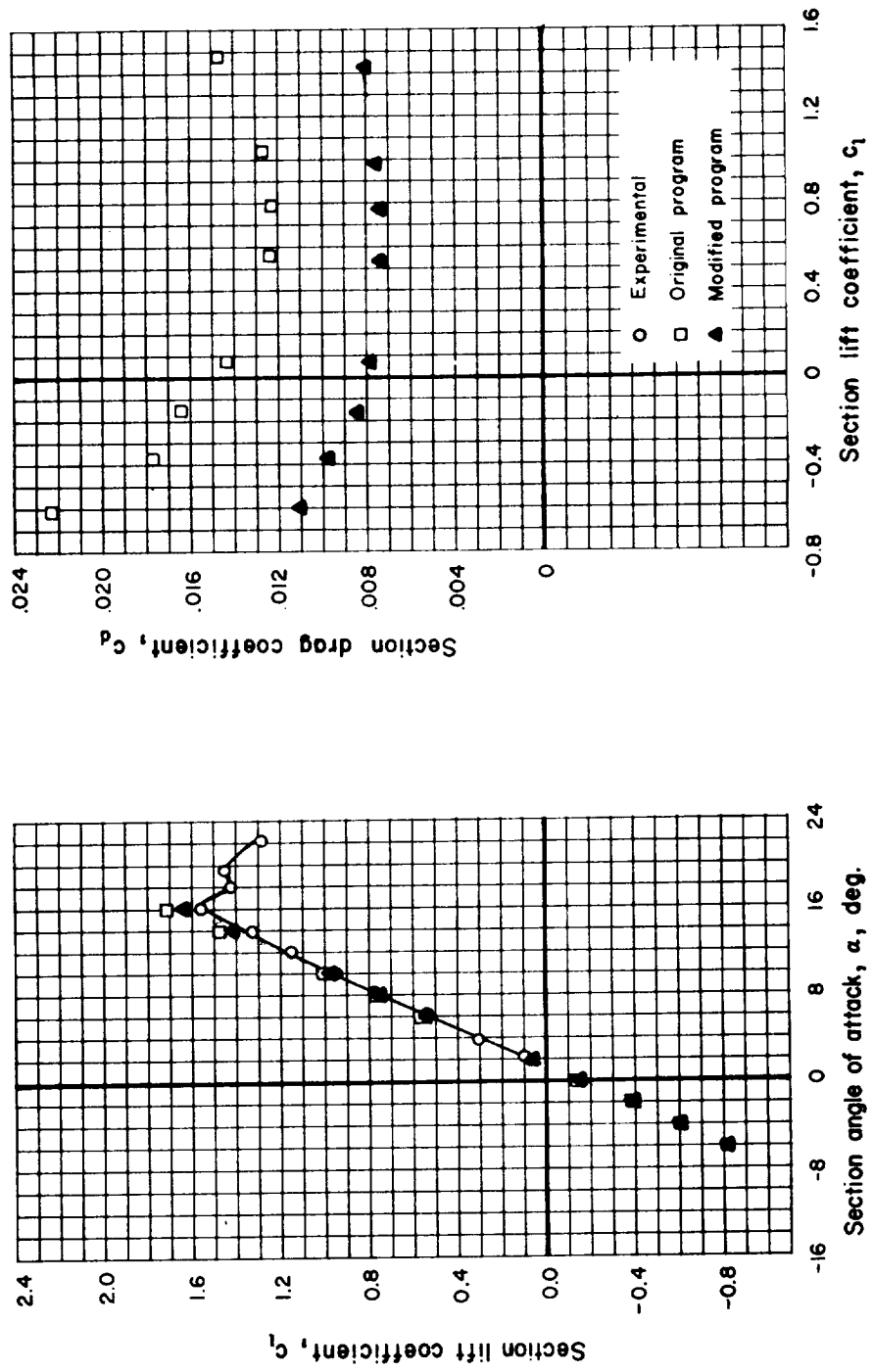


Figure 30. Comparison of 2-D lift and drag coefficients of the TN D-7071 airfoil at a Reynolds number of 9,000,000 (note experimental drag coefficients are not available).

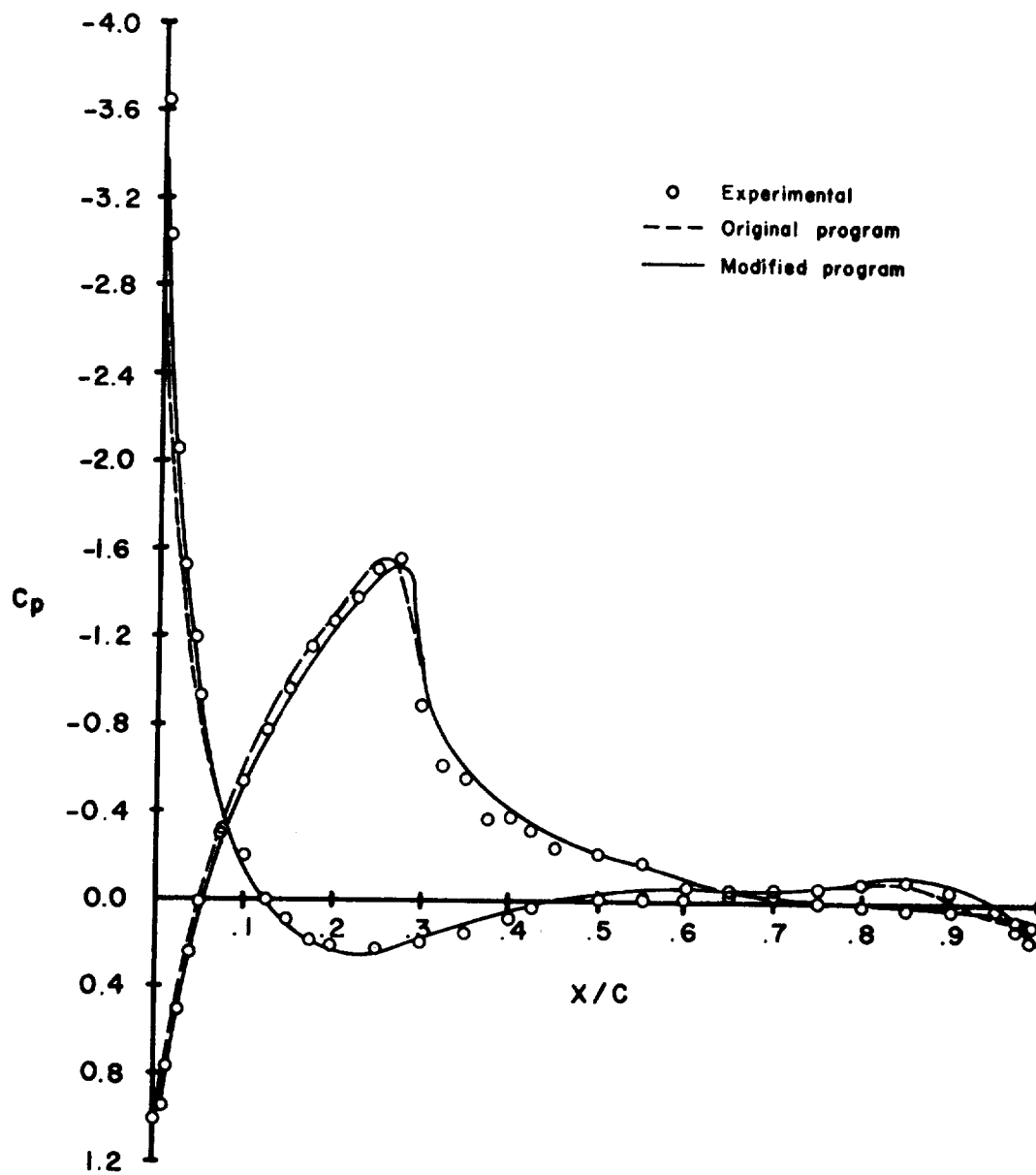


Figure 31. Comparison of pressure coefficients of the TN D-7071 airfoil at a Reynolds number of 9,000,000 and angle of attack of 3.4 degrees.

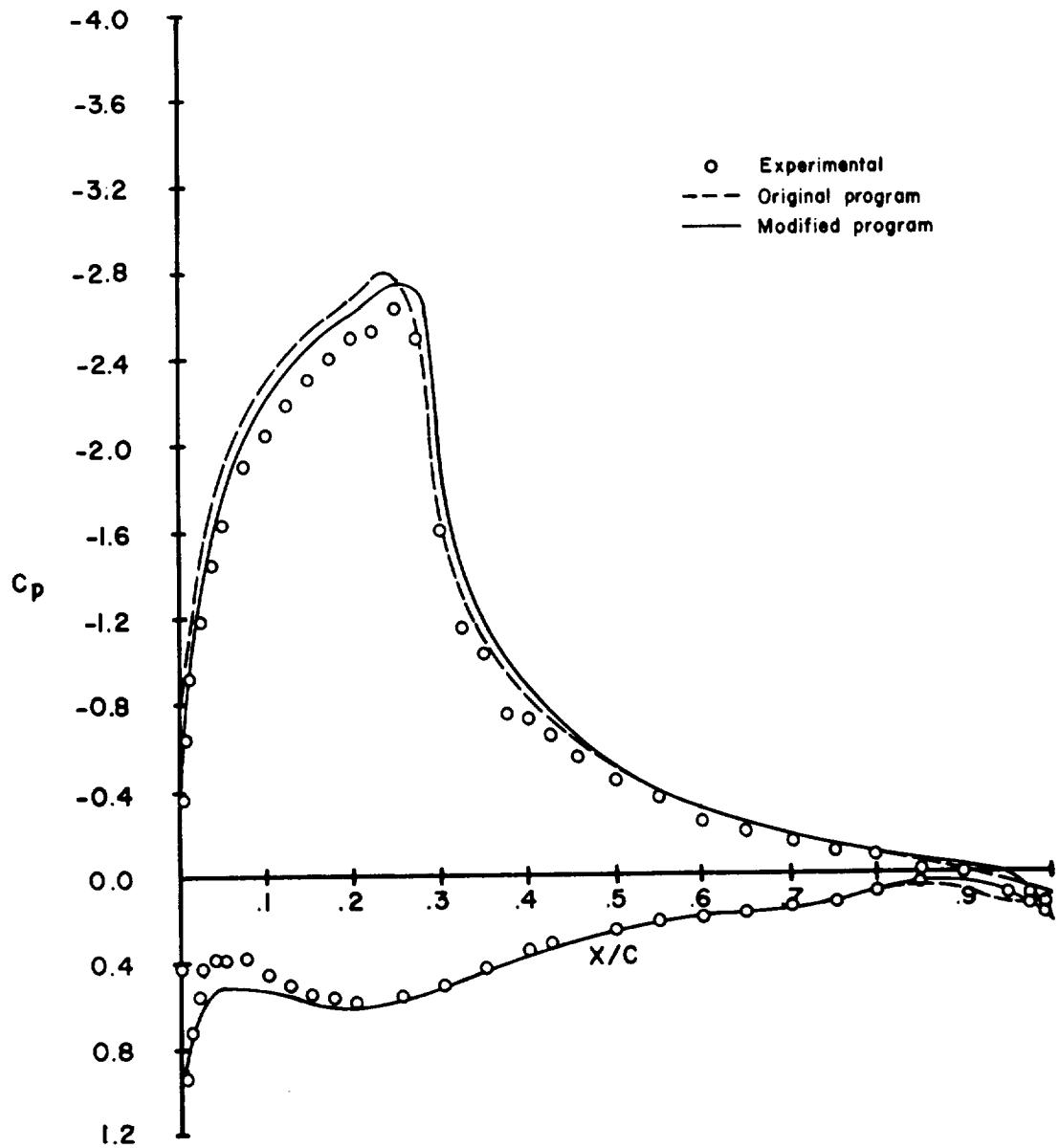


Figure 32. Comparison of pressure coefficients of the TN D-7071 airfoil at a Reynolds number of 9,000,000 and angle of attack of 12.4 degrees.

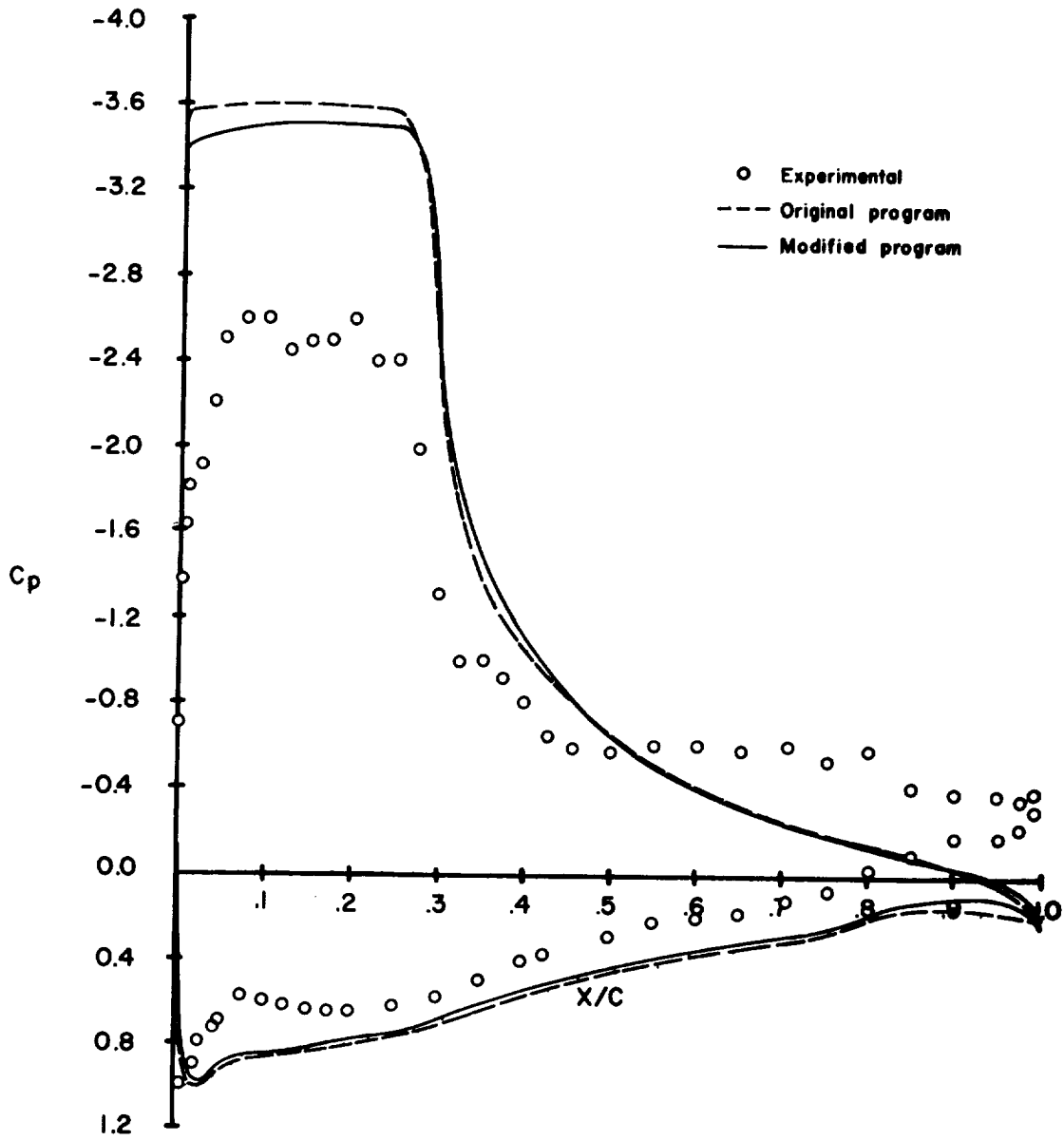


Figure 33. Comparison of pressure coefficients of the TN D-7071 airfoil at a Reynolds number of 9,000,000 and angle of attack of 18.7 degrees.



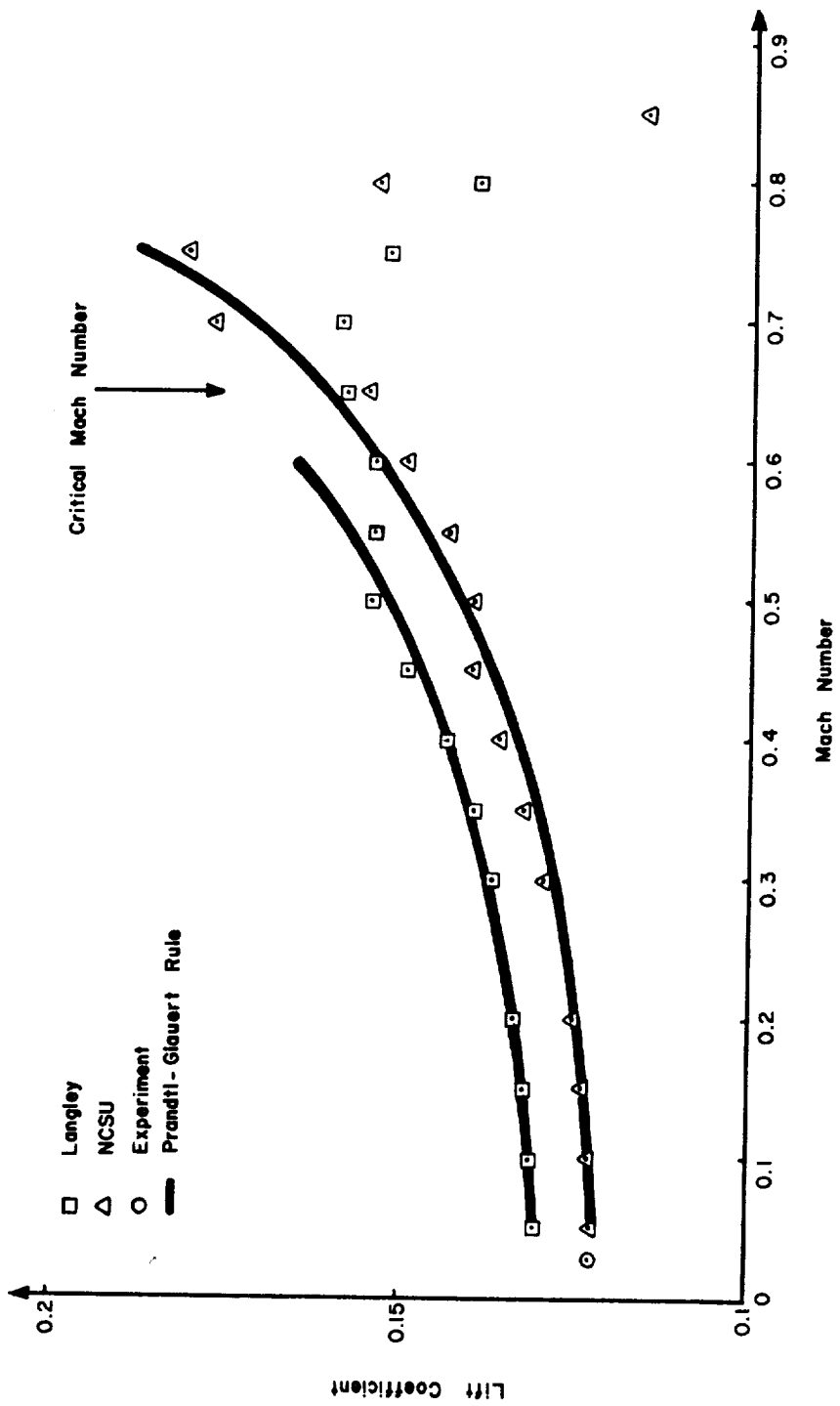


Figure 35. Predictions of  $C_L$  variation with Mach Number at  $\alpha = 0^\circ$  and a Reynolds Number of 3,000,000 for the 23012 airfoil.



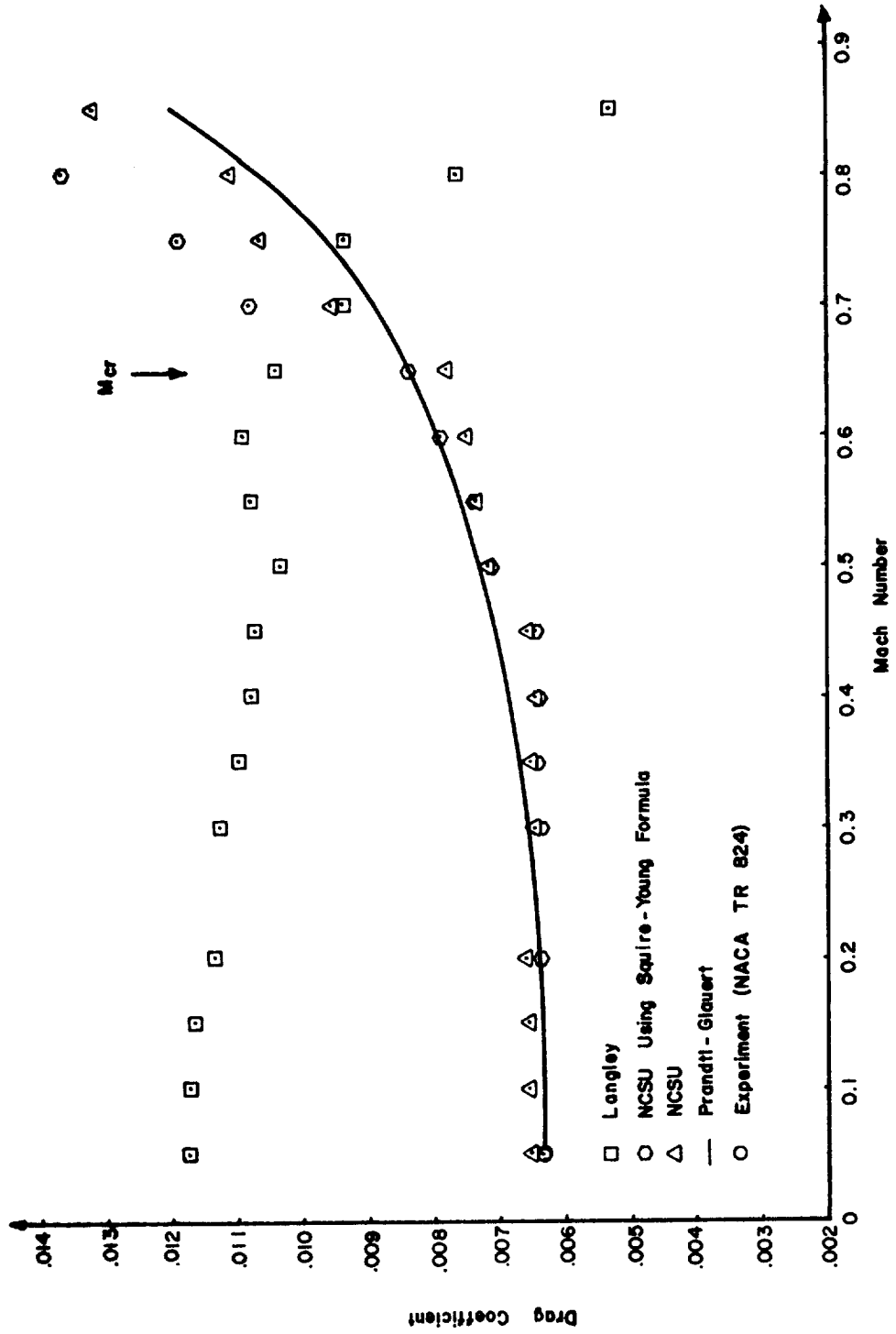


Figure 36. Predictions of  $C_D$  variation with Mach Number at  $\alpha = 0^\circ$  and a Reynolds Number of 3,000,000 for the 23012 airfoil.



## EXTENSION TO THREE DIMENSIONS

## INTRODUCTION

As elaborated in the theory section of the present work, one may employ lifting line theory to find the effective angle of attack at every point along the span of straight, moderately high-aspect-ratio wings. This effective angle of attack in conjunction with two-dimensional lift and drag data may subsequently be used to calculate three-dimensional lift and drag distributions. Integrating these distributions then gives the perceived lift and drag characteristics of the complete wing. A computer program utilizing this theory to predict stall characteristics of straight wing aircraft presently exists and is published in NASA CR-1646 (Ref. 36). It was selected to serve as the basis of a program for generalizing two-dimensional data to three dimensions in order to take advantage of the very considerable effort which went into its development. The program, however, contains many features which are not needed in the present work. Only that portion of the program pertaining to the prediction of the three-dimensional lift, drag, and pitching moment of a wing-fuselage combination is of immediate interest.

Originally written in FORTRAN IV for the CDC-6600 series computer, the program required substantial changes in order to execute effectively on North Carolina State University's IBM 370-165 machine. A list and discussion of the necessary changes is given on page 223.

The program in its original version was written to predict the angle of attack at which a wing-fuselage combination stalls and to aid the designer of a new or modified aircraft in stall-proofing his flight vehicle. This feature of the program cannot be utilized in the present effort because of the inability of the current two-dimensional program to predict boundary layer separation and therefore section aerodynamic characteristics in the near-stall region adequately. As a result, all portions of the program pertaining to the stalling wing, the iterative calculation of the value of the stall angle of attack, and location of the initial stall point were deleted. The resulting program is therefore applicable only to the linear portion of the lift curve.

Since the two-dimensional program treats only unflapped configurations, that portion of the program concerned with prediction of three-dimensional characteristics of flapped airfoils was deleted. Major reductions were also realized in the storage of airfoil data files. Tables of the two-dimensional aerodynamic characteristics were stored in the form of sets of polynomial coefficients with the Reynolds number inherent in the root and tip data sets in order to reduce input-output time and eliminate the need for nine peripheral storage devices which in the original program were used to store the airfoil data in a detailed table-look-up form. (The tables were constructed from the experimental data in NACA TR 824.)

In this modified form, the NCSU program, called FUNC, operates totally within the machine core. It will produce a three-dimensional table of lift, profile drag, induced drag, total drag and moment coefficients for

nine angles of attack (see Figure C-3) in six seconds with sixty thousand bytes of core, considerably less than the 60 seconds and 104 thousand bytes plus ten peripheral storage devices required by the original program, STALL. The specific changes are discussed in detail below.

The only obvious danger in using this fast and efficient polynomial coefficient technique is that the fit may exceed some tolerable level of error. A least squares routine, FITIT, has been provided to determine the polynomial coefficients. With it the fit error encountered on smooth two-dimensional data, as measured by the average mean square deviation, was normally between  $10^{-3}$  and  $10^{-5}$ , certainly less than three percent of the aerodynamic coefficient value. This may be seen in Figure B-3 which gives the fit coefficients and plots of fitted curves for the various aerodynamic coefficient functions of a 23012 airfoil. Although the fits provided by FITIT have always been within an acceptable tolerance for all runs performed to date, it is suggested that one always check the plot of the curve fit before proceeding to supply FUNC with the fitted data. FITIT performs a run of curve fits for the two-dimensional aerodynamic coefficients at nine angles of attack in eight seconds and fifty-four thousand bytes of core storage.

In order to insure that this fit error and the methods employed in modifying the original program were valid, a test case was run which compared the three-dimensional lift and drag produced by STALL using experimental two-dimensional data and the three-dimensional lift and drag as predicted by FITIT and FUNC using experimental two-dimensional data. The results of the test case is shown in Figure 37. This drag error noted is directly attributable to the inability of FITIT to fit the "drag bucket" of these airfoils using only a fourth degree polynomial. Generally, this routine as used with the two-dimensional predictions of the previous chapter do not encounter these "drag buckets" and, as mentioned earlier, operate with much higher accuracy.

Additional test cases were run to compare the three-dimensional data produced by experiment and that produced by the FITIT-and-FUNC-combination using two-dimensional data supplied from the program of the previous chapter. Results of these tests are reported below. Generally, the errors encountered were less than five percent for lift and eight percent for drag (Figure 38 through Figure 40) when compared with experiment. The experimental data and geometric configuration used in these calculations were taken from Reference 78. A drawing of this planform is given in Figure 41.

In the following the reader will find a brief explanation of the theory upon which the programs are based, and a discussion of the modifications implemented in the NCSU program.

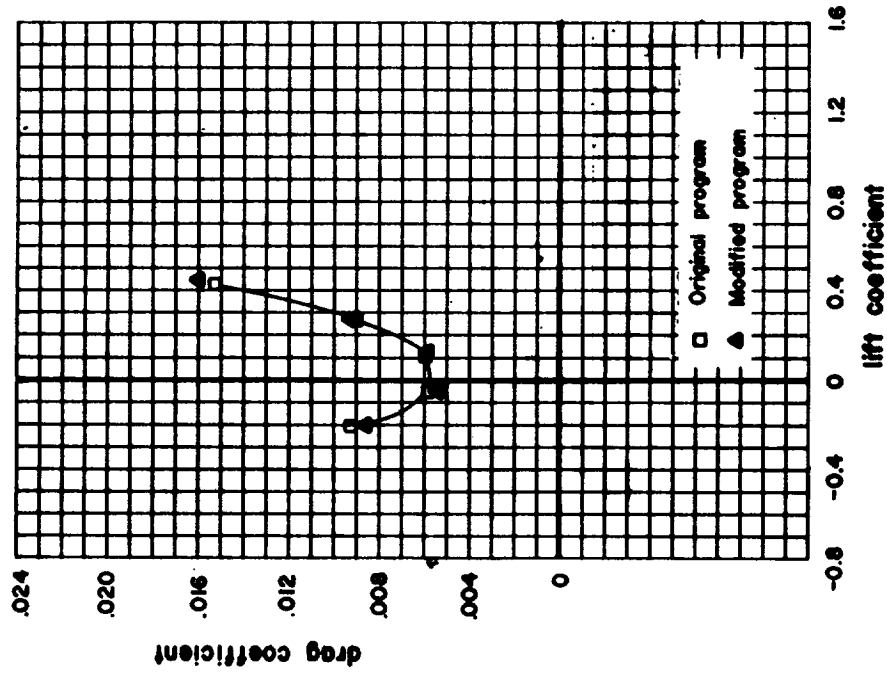
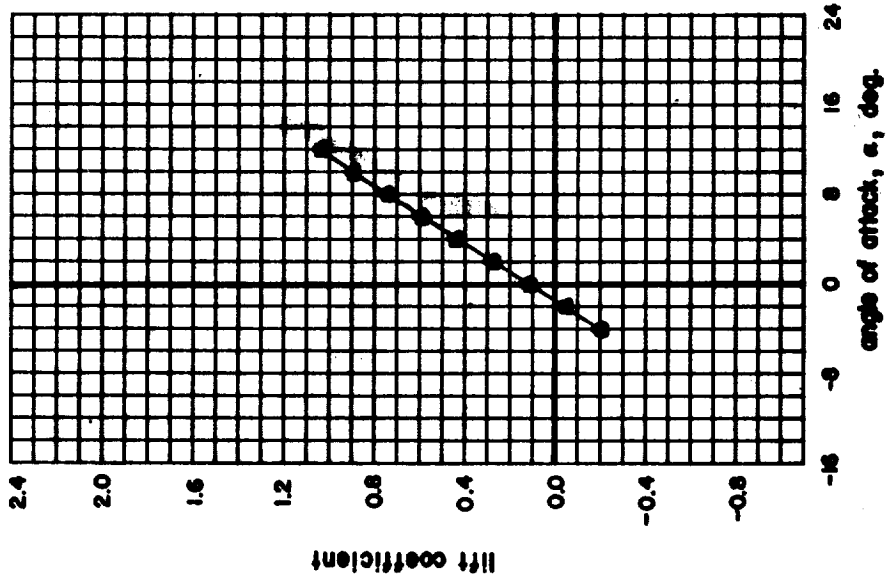


Figure 37. Comparison of original and modified program three-dimensional coefficient values for the 64216 root-64412 tip case.

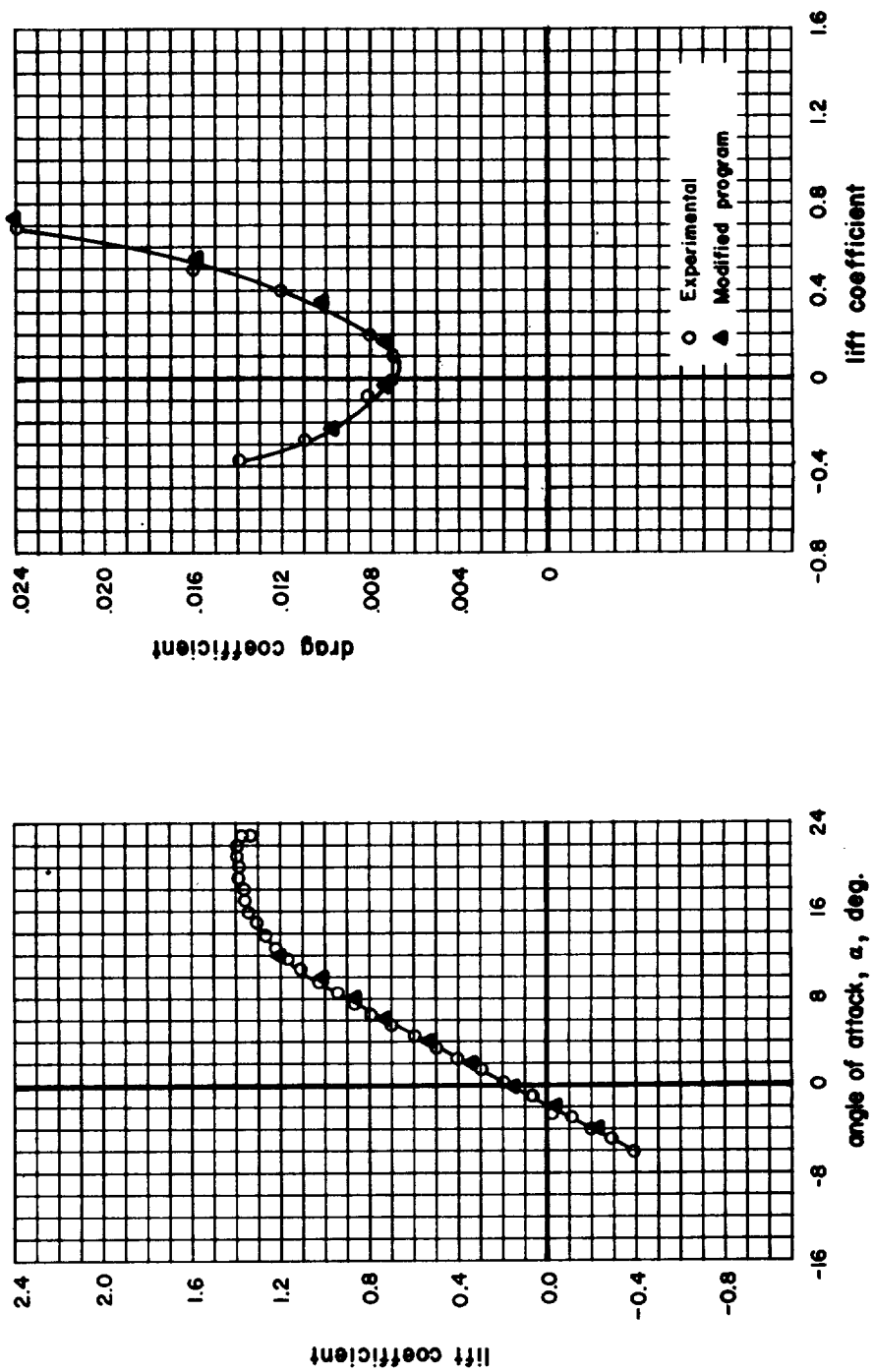


Figure 38. Comparison of experimental and calculated three-dimensional coefficient values for the 64420 root-64412 tip case.

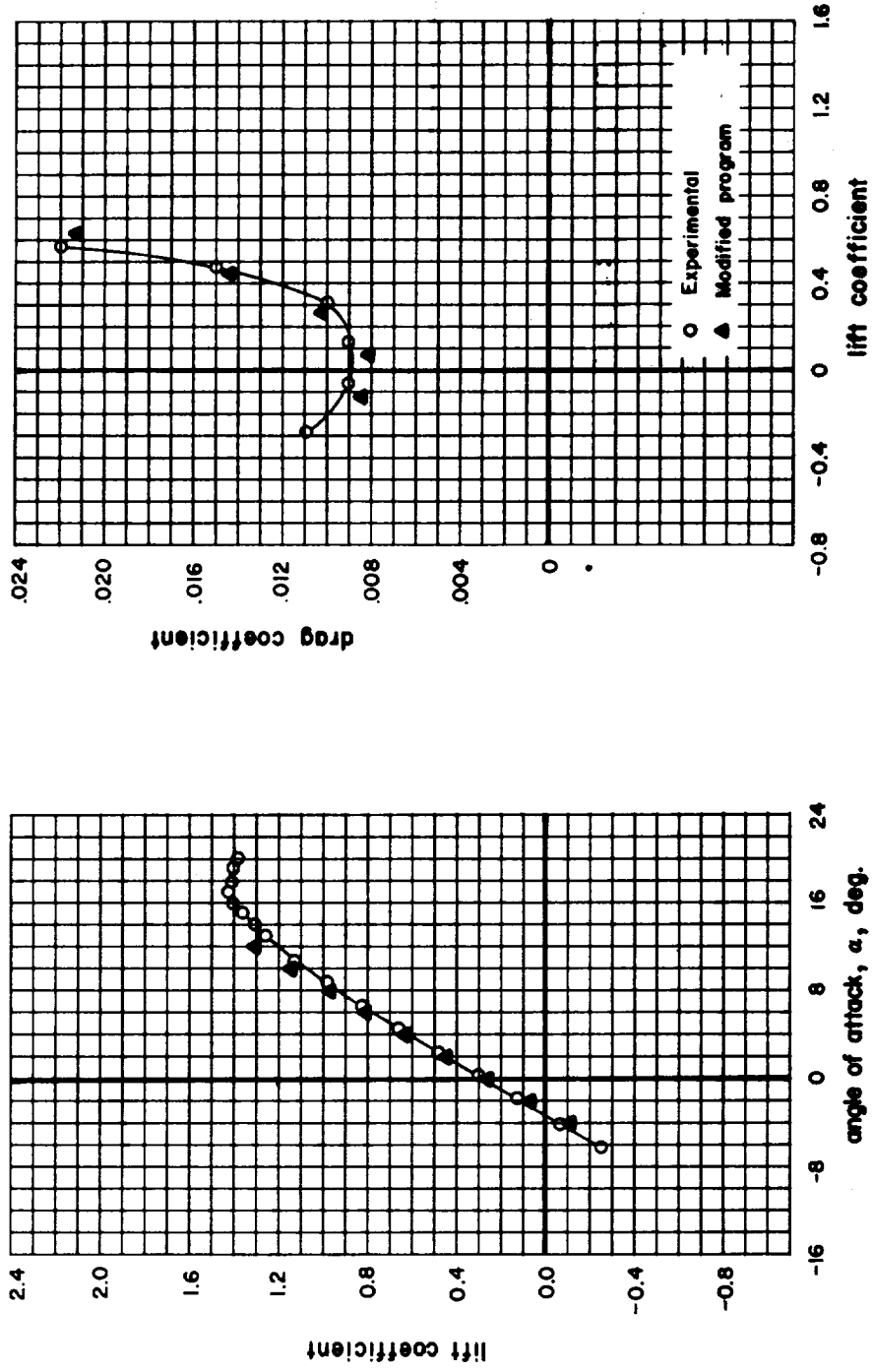


Figure 39. Comparison of experimental and calculated three-dimensional coefficient values for the 4420 root-4412 tip case.



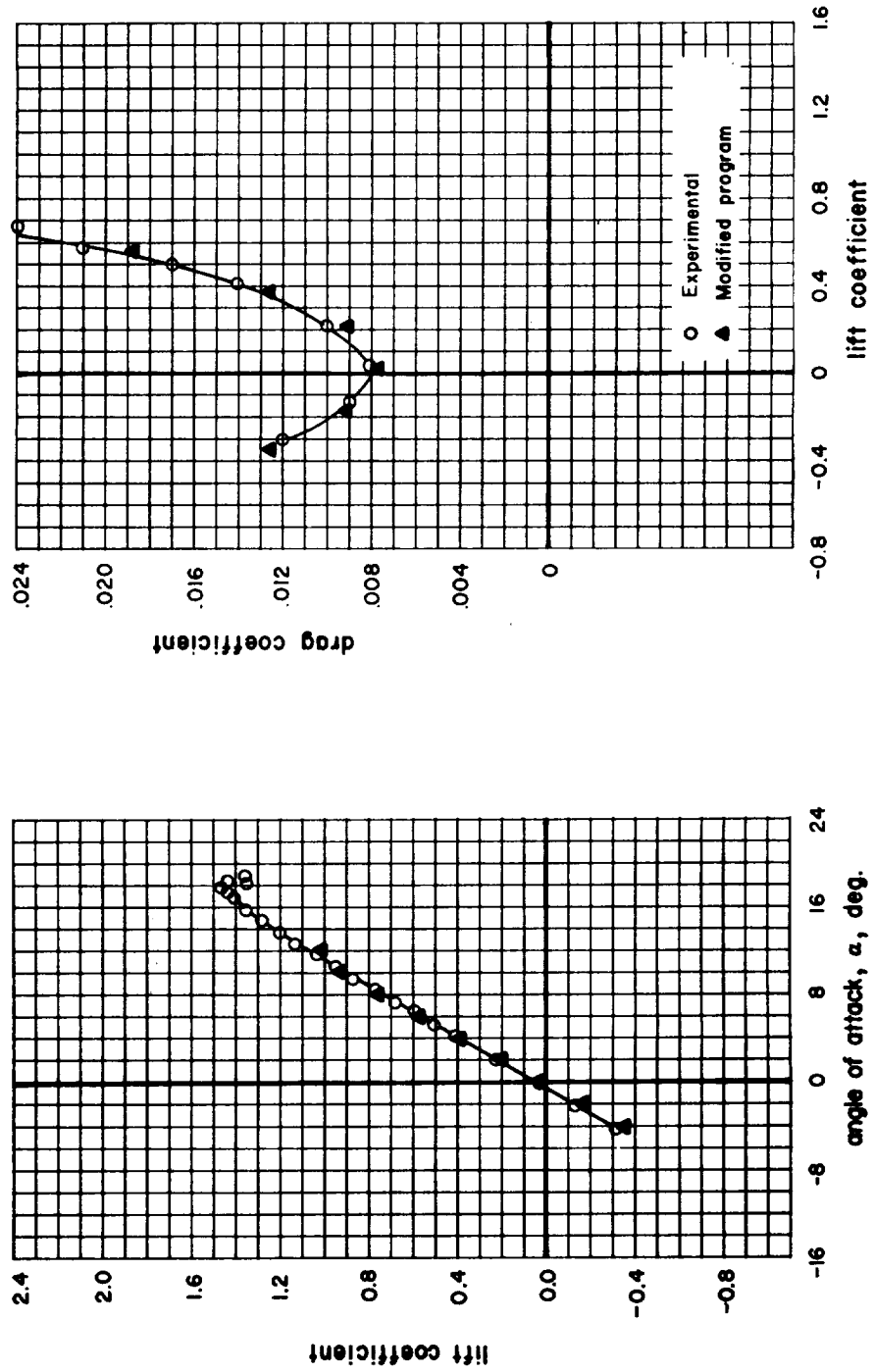


Figure 40. Comparison of experimental and calculated three-dimensional coefficient values for the 23020 root-23012 tip case.

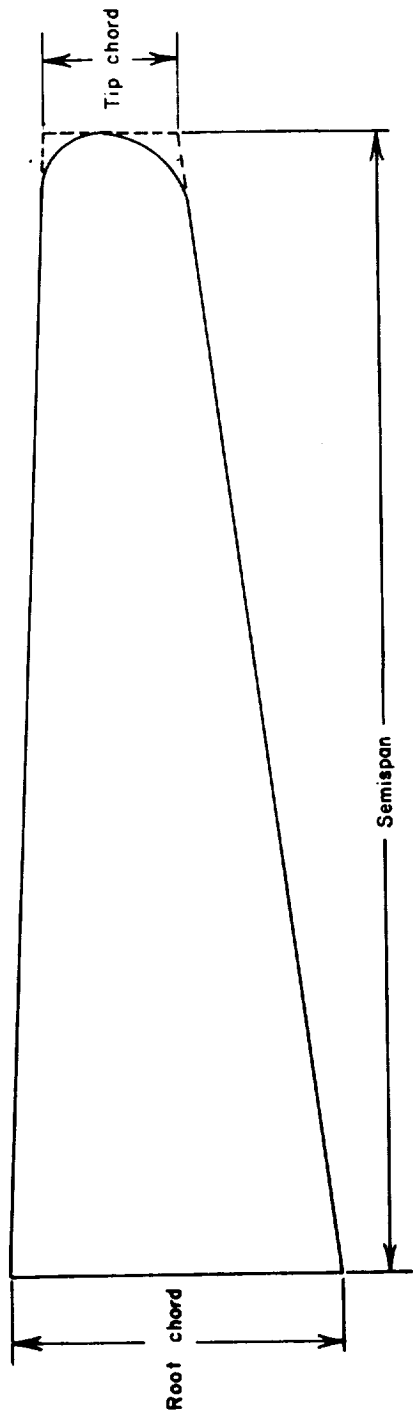


Figure 41. Planform of the three-dimensional test cases from Reference 78.

## GENERAL PROGRAM THEORY AND OPERATION

The mathematical technique for extending two-dimensional data to three dimensions, presented in detail in the theory section of this report, is performed by a modified version of the program (listed in NASA CR-1646) known as STALL. The following is a description of the basic logic of the modified version, FUNC, and its support program FITIT. FUNC is supplied with two-dimensional data in the form of polynomial coefficients by a special program called FITIT. Two-dimensional data (experimental or calculated by two-dimensional programs in the previous chapter) for a specific airfoil is generally given in the form of tables of lift coefficient versus angle of attack, drag coefficient versus lift coefficient, and pitching moment versus lift coefficient for a given Reynolds number. FITIT is designed to take these tables (see Figure B-2) and produce polynomial coefficients (see Figure B-3) for this specific airfoil by a least squares curve-fitting technique (see Figure 42). The polynomial coefficients are then punched into the form acceptable to FUNC. After sufficient data sets have been generated in this fashion, the execution of FUNC is ready to be initiated.

At this point the perceptive reader might suspect that FITIT should be incorporated as a preliminary routine within the program FUNC. This was not done because: (1) The fits should always be checked for intolerable error; (2) The core requirements of FUNC would probably be extended to an intolerable level; and (3) Once a set of data for a given airfoil is run and polynomial coefficients obtained, the set need not be run again, allowing the engineer to run many geometric variations within FUNC without recalculating these polynomial coefficients each time.

As can be seen by the flow chart in Figure 43 operation of FUNC is initiated by reading in (see Figure C-2) all geometric parameters associated with the configuration under consideration. Appropriate polynomial coefficient data are then read in\* and calculation of the geometric quantities associated with the transformation from the  $u$  to the  $\pi$  plane is initiated. If the option to read in irregular geometric shapes has not been initiated, the program proceeds to calculate the chord, thickness, camber, geometric twist and Reynolds number distributions for a wing with linear taper in both chord and thickness. Next, the multipliers  $\beta_{mk}$  from Equation 105, the multiplier employed in Simpson's rule enclosed in brackets in Equation 117 through Equation 120, and the inverted G matrix of Equation 114 are calculated. At this point the values of body angle of attack are read, the first value selected and a case heading printed. After a first approximation to the lift distribution has been estimated by Equation 115, the basic iterative loop searching for a convergent lift distribution is entered.

---

\* Note from Figure C-2 that the thickness ratio of each airfoil data set has been inserted so that FUNC will have explicit knowledge of its value.

The first step in the search for convergence is to calculate the corresponding values of induced angles of attack and determine the effective wing angles of attack in the real plane. Now the equivalent angles of attack from Equation 116 are computed for use with the two-dimensional data. Using the section data, the values of lift coefficient corresponding to these equivalent angles of attack are obtained. If the value of  $C_{\ell c}/\bar{b}$  using these values of lift coefficient is not sufficiently close to the initial estimate of  $C_{\ell c}/\bar{b}$ , the correction factor given by Equation 114 is calculated and added. The process discussed in this paragraph is followed until the calculated values are sufficiently close to the previous values of  $C_{\ell c}/\bar{b}$ .

Having obtained the lift distribution, section values for the profile drag coefficient, the induced drag coefficient, and the pitching moment coefficient are obtained. These are then integrated using Equation 117 through Equation 120.

At this point in the execution, another value of body angle of attack is assumed and the program reenters the search for the convergent lift distribution associated with this body angle of attack. The program continues in this cycle until a body angle of attack of 99.0 is encountered at which time control is returned to the beginning of the program and the next set of geometric parameters is read.

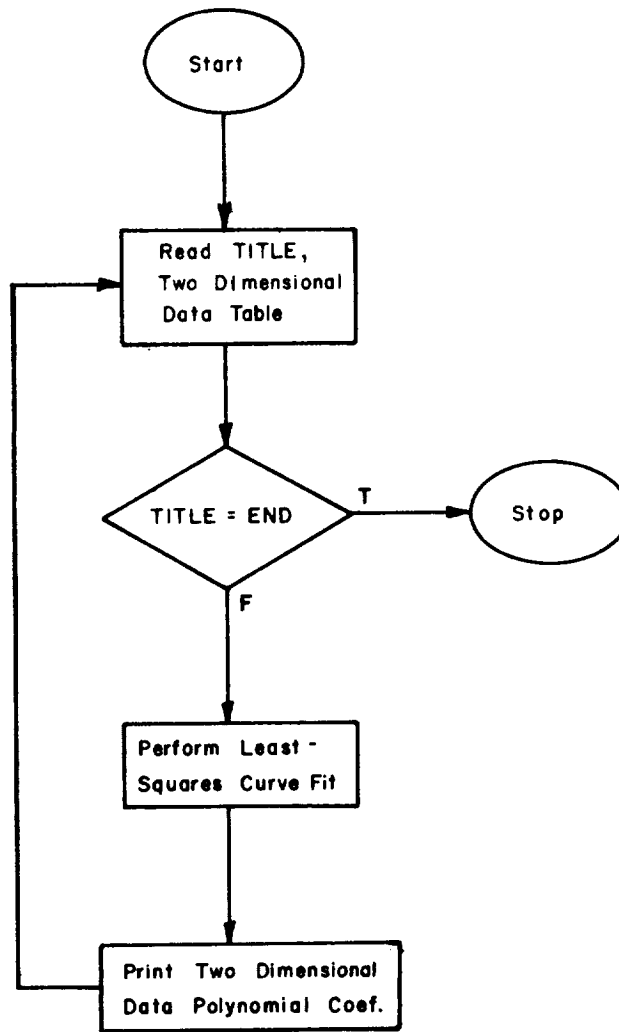


Figure 42. Flow chart of major logic in FITIT.

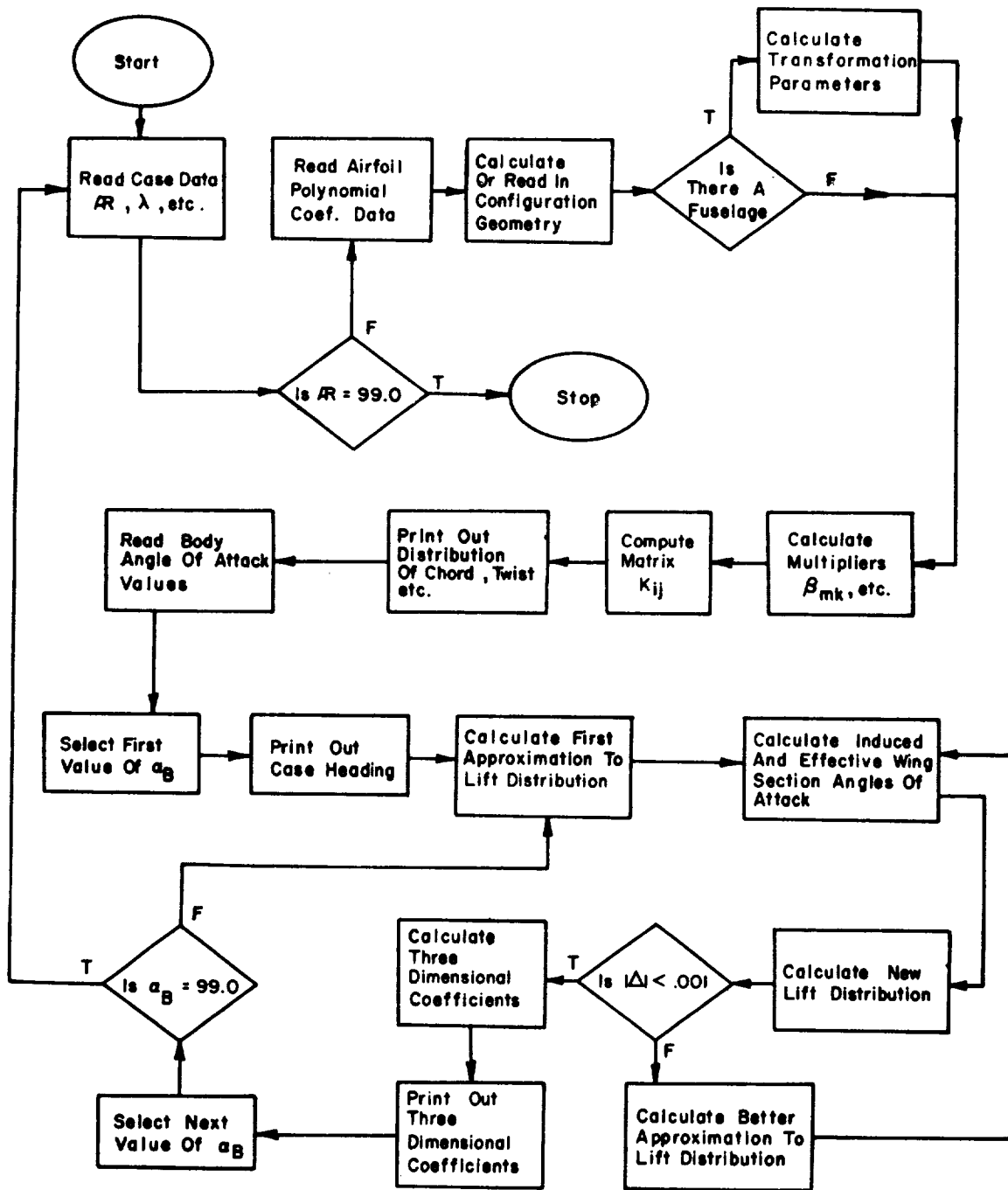


Figure 43. Flow chart of major logic in FUNC.

# MODIFICATIONS REQUIRED TO ADAPT THE CDC "STALL" PROGRAM TO IBM EQUIPMENT

The following changes were necessary in the original program STALL as published in NASA CR-1646 in order to insure effective execution on the NCSU IBM 370-165:

- (1) Eliminate the overlay structure by changing programs STALL, ONE, TWO, and THREE into subroutines STALL, ONE, TWO, and THREE.
- (2) Run with NOSUBCHK option on Fortran IV G-LEVEL compiler.
- (3) Set the variable INNOW equal to zero after logical unit numbers are set in routine MAIN.
- (4) Set ATMP (vector) to zero at statement 40 in BRIDGE.

```
40 KGO = 1
   ATMP(1) = XX(1)
   DO 41 J = 2, NP
41 ATMP(J) = 0.0 .
```

- (5) Insert the following statement immediately preceding the statements setting logical unit numbers in MAIN.

```
ACOS(X) = ARCOS(X)
```

- (6) Prevent illegal entry into a DO loop in LOOK by inserting at statement 60,

```
60 LOCR = 3
61 IF(REYN-A(LVL,1,LOCR)70,70,610
```

and statements 600 to 620 should read

```
600 GO TO 630
610 LOCR = LOCR+1
   IF(LOCR.LE.MAXC)GO TO 61
611 IE = 1
   GO TO 630
620 REYN = 999.0 .
```

- (7) Enclose the variable YY in the argument list of BRIDG in slashes to insure call by name.

## GENERAL PROGRAM MODIFICATIONS

It was mentioned in the Introduction to this chapter that the original program STALL consisted of approximately 1700 executable statements. This section serves as a guide to the systematic dismantling and conversion of the program to its modified form. The program as supplied to NCSU operated in the overlay mode with a main overlay and three additional overlays of the same sublevel. Since total operation within the core of the IBM 370-165 is less expensive than the time to call in overlays, the program was taken out of the overlay mode and compiled and executed as a unit. Some IBM-CDC incompatibilities noted in the previous section were then removed in order to execute the program on the NCSU 370-165. These changes resulted in a significant reduction in execution time at the expense of increased core requirements. As mentioned previously this trade is quite cost-effective.

A second major modification occurred when portions of the program unneeded for the present investigation were removed. These included all portions associated with stall calculations as well as those portions having to do with flaps. These routines are THREE, MAIN3, and MAIN5. See Table 2. These changes reduced the number of executable statements by 550 to approximately 1150, a substantial reduction.

ORIGINAL PROGRAM (STALL)	MODIFIED NCSU PROGRAM (FUNC)
STALL	
MINV	MINV
DAGET	
AAA	AAA
ZZZ	
SSS	SSS
TERP	TERP
SETSW	SETSW
DATSW	DATSW
AERDA	
BRIDG	BRIDG
ARC	
LOOK	
ONE	
MAIN	MAIN
MAIN1	MAIN1
TWO	
MAIN2	MAIN2
MAIN4	MAIN4
THREE	
MAIN3	
MAIN5	
	FUNX
	FUN

Table 2. Comparison of routines contained in the original and modified programs.



A further major reduction was realized by making the Reynolds number of interest inherent in the two-dimensional data. An in-depth look at what is involved with this assumption may be found in the next section of this chapter. Use of this assumption, however, resulted in a decrease in executable statements by 250 to approximately 900.

Still another reduction was made by changing the location of data storage. In addition to saving a tremendous amount of input-output time by expurgating the nine peripheral storage devices associated with the table look-up procedure and storing the polynomial coefficients within core, the move reduced the number of executable statements by 100 to a remaining 800.

Reductions to the existing less-than-700 executable statements can be attributed to the clean-up of unused variables and to common block reorganization.

## CHANGES CONCERNING REYNOLDS NUMBER

In order to locate the two-dimensional value of a given aerodynamic coefficient, say  $C_l$ , in the original program, three separate interpolations were made. Linear interpolation was performed first for the required value of Reynolds number, then for thickness ratio, and finally for camber. Because of the amount of data being searched, an investigation into a possible deletion of one of these variables was initiated. Deletion of any one of the variables would cut the number of interpolations by forty percent. Since the present investigation had excluded the stall region because of the inability of the two-dimensional program to predict boundary layer separation effects adequately, a reduction in dependence of the results on Reynolds number was established. Changes in Reynolds number at low angles of attack produce very little variation in lift coefficient and only slight variation in drag coefficient (Ref. 79). These variations were so slight that it was decided to either calculate the two-dimensional characteristics for both tip and root airfoil families at the Reynolds number of the mean aerodynamic chord or, at the most, enter the characteristics at only the root and tip values.

Error encountered by the use of the mean aerodynamic Reynolds number is low because of the averaging effect of the camber interpolation and eventual integration. Error encountered by the use of root and tip families at their respective Reynolds number should be even less since this effort gives the coefficient data an implicit relationship in Reynolds number.

The calculation of the spanwise Reynolds number distribution was left in as a check for the designer. It is suggested that designs using high taper ratios resulting in wide Reynolds number variation employ the root-tip implicit method. Removal of the Reynolds number interpolation allowed the deletion of two routines, ARC and LOOK, from the original program (see Table 2).

## CHANGES CONCERNING AIRFOIL DATA STORAGE

With the transfer of the Reynolds number to an implicit dependence, half of the minimum data sets were no longer necessary; furthermore, the remaining portions of the data sets could be stored in core, resulting in a substantial reduction in operating time since the comparatively long time required to transfer data from tape or disc files could be eliminated. Adopting this philosophy removed nine external data files, decreased the execution time further, and eliminated approximately 100 executable statements among these being the two routines DAGET and AERDA of the original program.

A further reduction in execute time was realized by storing the two-dimensional data not as tables of points but as polynomial function coefficients and thus eliminating tabular interpolation.\*

A schematic diagram of the storage and evaluation procedure is given in Figure 44. Note that for a geometric configuration with root and tip families different, evaluation of any given aerodynamic coefficient has been reduced to four functional evaluations, two thickness interpolations, and one final camber interpolation.

---

\* Note from Figure C-2 that the angle of attack versus coefficient of lift polynomial was added in order to predict the angles of zero lift without solving for the zeros of a fourth degree polynomial function.

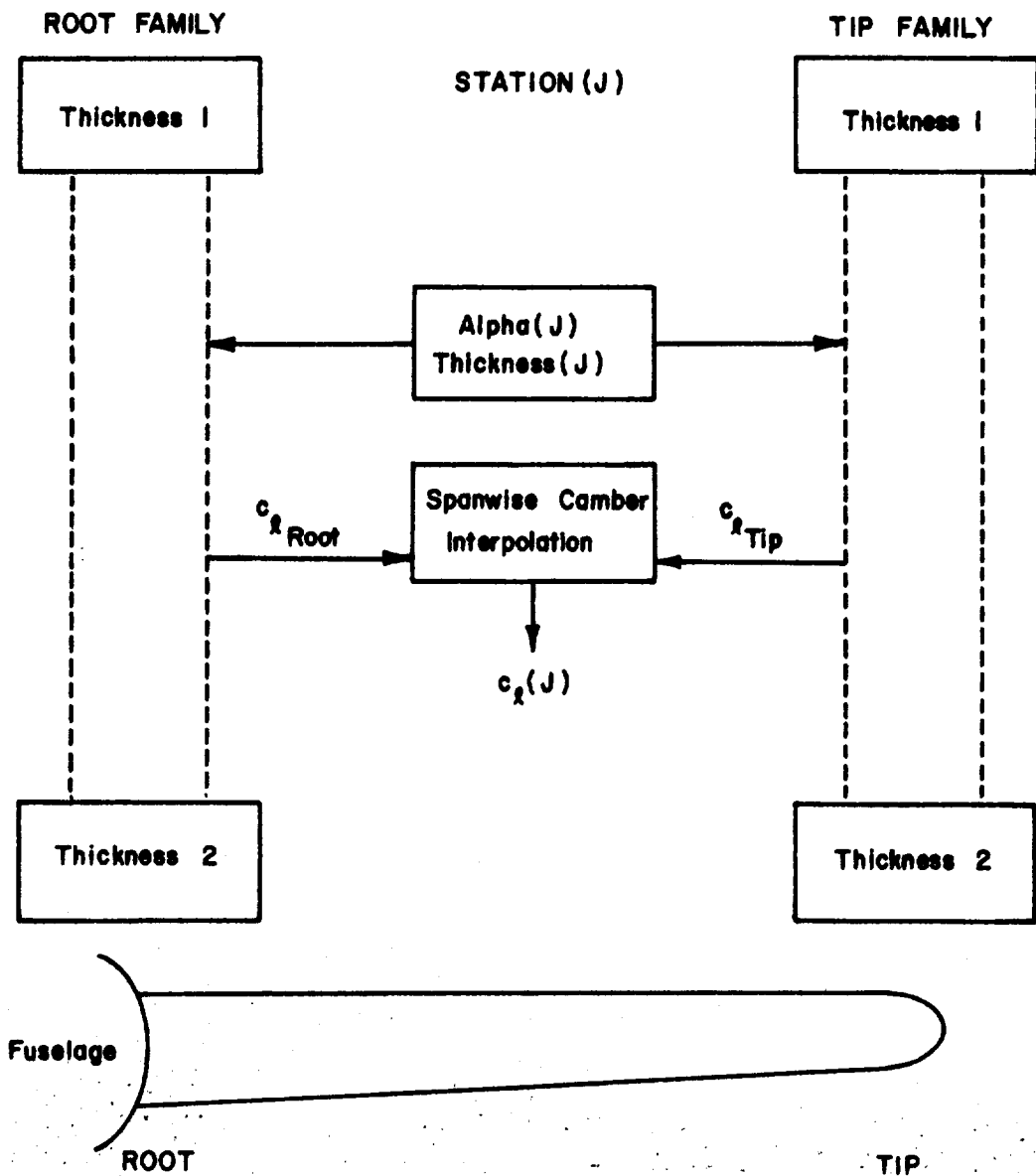


Figure 44. Schematic representation of the modified data look up procedure.

## DISCUSSION OF PROGRAM RESULTS

Results of computations of the three-dimensional lift and drag of a wing using two-dimensional section data as input are shown in Figure 37 for both the reduced NCSU program and for STALL. Agreement with STALL is very good for the lift and quite reasonable for the drag, especially when one considers that drag "buckets" found experimentally on 6-series airfoils and used in STALL cannot be fit satisfactorily with just a fourth order polynomial. This fourth order representation was judged adequate, however, because the airfoil aerodynamic characteristics program inherently predicts relatively smooth drag curves. Since such results were always to be the input to the three-dimensional program, the authors saw no need to increase the program complexity.

A comparison of the results of predictions of the entire computation procedure with experiment is shown in Figures 38, 39, and 40. The lift data for the 6-series airfoils, shown in Figure 38, shows excellent agreement up to a  $C_L$  value of 1.2. The drag data is quite acceptable to a  $C_L$  value of 0.8. The wing data for the four digit airfoils indicates that, particularly for lift coefficients above 0.4, the viscous effects on these thick airfoils are not properly accounted for. The same behavior is noted for other thick airfoils of the same family. (See Figures 13, 14, and 15.) The prediction is, however, much better on the wing constructed of 230-series airfoils (Figure 40). Here, the lift results agree well with experiment for  $C_L < 1.0$  and the drag predictions are in reasonable agreement for  $C_L < 0.6$ . It seems reasonable to conclude therefore that for  $C_L < 1.0$ , the program will provide wing lift data as reliable as the two-dimensional data supplied as input. Wing drag predictions made by the program also seem to be as reliable as the section characteristics used as input, at least for  $C_L < 0.8$ . Thus, for low-to-moderate lift coefficients and moderate-to-high-aspect-ratio, unswept wings this procedure is far simpler computationally and of equal accuracy as compared with the more complex vortex lattice or lifting surface methods.



**PROGRAMS FOR THE CALCULATION OF BODY  
AERODYNAMIC COEFFICIENTS**

## INTRODUCTION

The problem of accurately estimating the lift and drag coefficients of arbitrary three-dimensional bodies in a rigorous fashion will certainly be recognized as an extremely difficult task. The word arbitrary, for example, implies that the routine or procedure for estimating these coefficients must be general enough to handle a variety of bodies including bluff ones to be useful to those to whom this work is directed; yet the procedure cannot require an excessively large number of computations. In order to yield the most reasonable solution within the constraints of small computer run times and small computer storage requirements the present authors chose to use the following procedure:

- (1) A program to calculate the inviscid flow about arbitrary three-dimensional bodies was obtained from the Naval Ship Research and Development Center at Bethesda, Maryland. One important reason for selecting this program was the fact that it was equipped with the capability of computing on-body streamlines. Another was the fact that it was already limited to bodies alone. Two other programs which the authors acquired in the process of developing this procedure would have required removing the wing characteristics calculation portion of the programs.
- (2) The program was reduced in size as much as possible and specialized to calculate the inviscid flow over bodies at zero angles of attack and sideslip. (As received, it permitted one to calculate the inviscid flow field with onset flow components along all three axes.)
- (3) The skin friction drag was estimated by applying a two-dimensional boundary layer technique to the on-body streamlines and integrating the resultant wall shear over the body surface.
- (4) The viscous form or pressure drag was estimated by considering the body wake to be representable within the framework of an inviscid flow solution in much the same manner as the complete airfoil solution was achieved.

The reasons for choosing this procedure are quite straightforward:

- (1) It relies heavily on existing programs or procedures whose applicability and computational problems have been well charted. The time and effort required for program development is thus reduced to a minimum.
- (2) The procedure is step-like so that if necessary it can be done in pieces on a small machine with limited storage capacity. In contrast, it would be very difficult to segment an attempt to solve the general three-dimensional Navier-Stokes equations for a complex boundary shape.



Theoretical justifications for some of the steps in the procedure are given at length in earlier sections of the present work.

Of course, in order to obtain shorter running times and smaller storage requirements, it has been necessary, as is always the case, to limit flexibility and employ certain assumptions which are not uniformly valid. The restriction to  $\alpha = 0$  cases has already been mentioned. In addition, the boundary layer routine used is a two-dimensional one so that stagnation point flows are not well described nor are cases where cross flows are present. Further, the boundary layer procedure does not permit one to consider flow separation, *i. e.*, it assumes separation does not exist. Although body wakes are included in the analysis it has been necessary to assume, in the absence of an understanding at the proper criteria, that they all develop according to the same simplified rules. As a result of these limitations, some discretion should be exercised in applying the results of the computation and in selecting cases for computation so that the governing assumptions are not greatly violated.

The discussion below outlines the computational procedure employed. The original program is described in general so as to provide the reader or user with a reference for understanding the modifications made to it. The modifications are then discussed in detail. Also discussed in detail are the locally developed elements of the program, in particular the boundary layer and wake-body computation procedures. We begin with a presentation of a very effective means to identify errors in the input data. The section concludes with a discussion of the results obtained using the program to compute the drag of three bodies: a sphere, a 3:1 prolate spheroid, and a Cessna 182 aircraft fuselage.

## SPECIFICATION OF INPUT DATA WITH VERIFICATION BY PLOTTING

When calculating the potential flow over a three-dimensional body, one is confronted with the problem of how to specify the shape of the body surface. Obviously, one would like to have an analytical expression for the body surface; however, for general three-dimensional bodies practical analytical representations are usually impossible to obtain. The general practice is therefore to approximate the body surface by a large number of quadrilateral-shaped panels defined by a finite number of points in space; each point is presumably exactly on the body surface. If a computer is to be used to solve for the potential flow over these bodies, someone must input the three coordinates of each point; this is a laborious and error-prone task. In addition, each point must be indexed in such a way that the four corner points of each panel are defined in a clockwise fashion. Checking the input for errors is also a tedious process since detecting errors by simply scanning a list of the input data points is extremely difficult. To minimize such errors one would like a simplified, orderly procedure for inputting the data, and an effective procedure of finding errors before lengthy potential flow calculations are made. Probably the simplest procedure for inputting the data is to specify the shape of the body cross section at various stations along the longitudinal body axis. Among the most effective procedures for detecting input errors is to graph the points as viewed from various directions (See Figure 45).

While the above is true for any arbitrary body, in this report we are concerned only with aircraft fuselages which have a plane of symmetry along the longitudinal axis. In 1970 NASA, aware of the problems of specifying and checking numerical data, developed a computer program to generate the necessary instructions for automatic plotting of an airplane model in numerical form (Ref. 113). The plotting capability of this program along with its simplified data input procedure makes it ideal for producing a final, verified numerical data set describing an aircraft fuselage. The program also has the capability of displaying the complete aircraft configuration including wings, pods, fins, and canards. Using it one may draw three-view and oblique orthographic projections, as well as perspective projections of an airplane. The program even has the capability of plotting stereo frames of the aircraft suitable for viewing in a stereoscope. Because of its versatility the authors chose to use this NASA program to verify aircraft input data. A copy of the program, written for the CDC 6000 computer, was obtained from NASA Langley Research Center and then modified so that it would run on the IBM 370-165 computer at N. C. State University. User instructions, plotting software modification procedures, a program listing, and several sample output plots for the modified plot program are given in Appendix D.

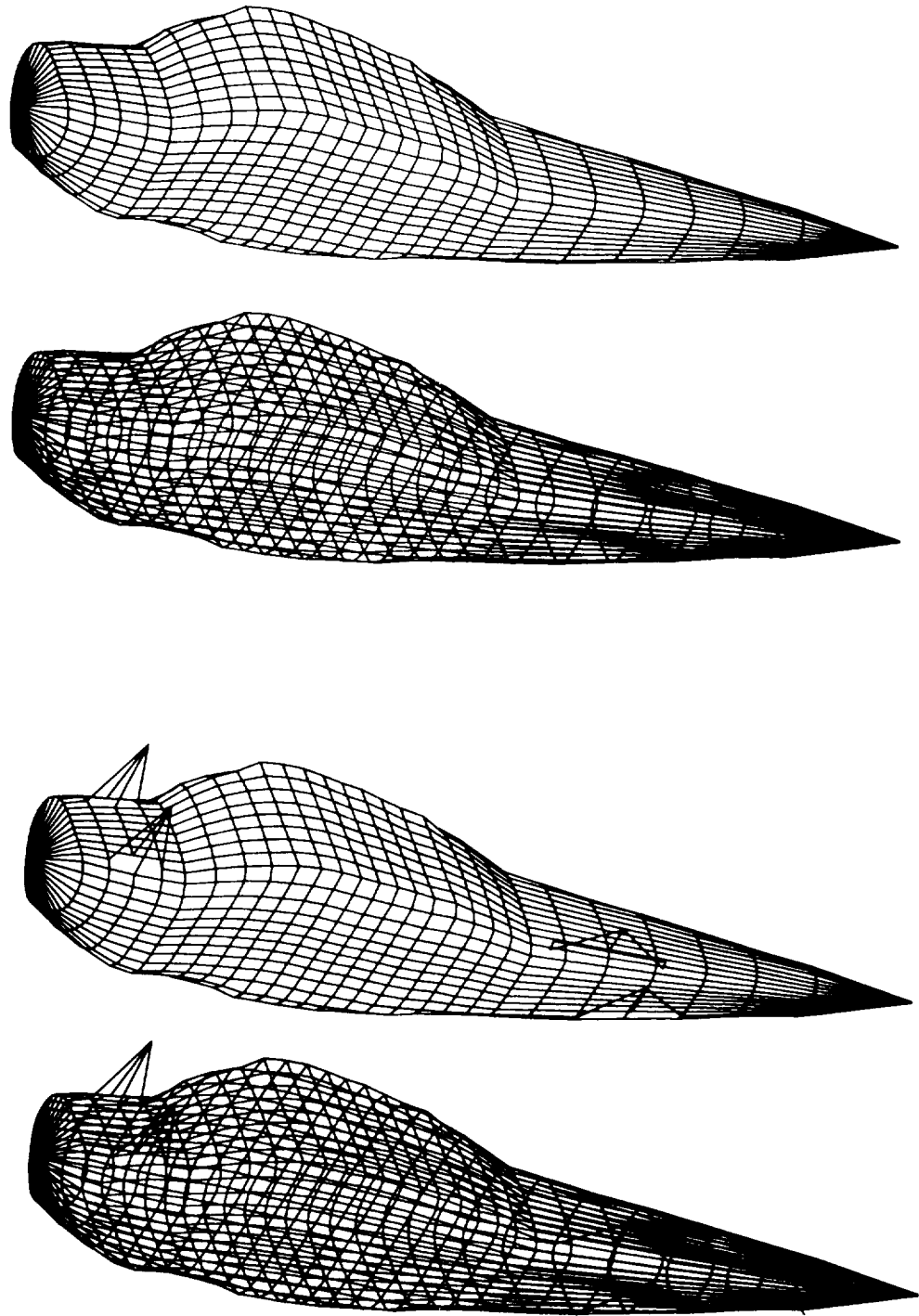


Figure 45. Example of a correct and an incorrect data set for the Cessna 182 fuselage.

It should be noted that most of the modifications made to the original program were those necessary to enable the program to run on the NCSU IBM computer. These modifications included:

- (1) changing the DECODE form of program input to ordinary READ input
- (2) removing the OVERLAY procedure used to reduce program size during execution at NASA
- (3) adding subroutines which could call IBM software plotting instructions which were equivalent to the specified CDC software instructions<sup>†</sup>
- (4) assigning variable names to the input and output file unit numbers as well as to data storage file unit numbers (the user must therefore only specify the appropriate file unit number required at his computing facility).

For more information concerning the basic program the reader is advised to consult Reference 113 which provides a detailed description of much of the program as well as flow charts of each important program section.

While the input to the PLOT program is as concise as possible, the input to the NCSU BODY program (as well as the XYZ potential flow program) is both lengthy and time consuming since three coordinates and two indexes are specified on each point input card. Accordingly, a program which converts a data set for the PLOT program into a properly indexed data set for the NCSU BODY program was developed; thus, once the plot data set is verified, a correct data set for the NCSU BODY program may be generated. As discussed in General Program Theory, one criteria for obtaining a reasonable potential flow solution is that adjacent body panels must generally have areas which differ by less than 50 percent. Therefore, the CONVERT program was also designed to compute the area of each body panel and display these areas in an orderly fashion. Also, the program displays the ratio of the area of each panel to the area of the panel below it and the panel to its right. These ratios simplify the procedure of checking panel areas to see if they meet the criteria described above. It should be noted that while the CONVERT program produces a data set for the fuselage, it will accept the input of a data set for a complete aircraft configuration and ignore the unnecessary information. The program input is obviously the same as the input for the PLOT program and its description is therefore not repeated in Appendix E; however, the program listing and a

---

<sup>†</sup>Since plotting software is different at almost every computing facility, the user must either provide the original CalComp plotting software for which the program was designed or provide three equivalent dummy subroutines as was necessary at the N. C. State facility. See the Plotting Software Modifications section of Appendix D for detailed instructions.

sample output depicting the capabilities described above are given in the appendix.

By inspecting Figure D-1 and Figure F-1, the reader will discover that the body orientations, with respect to the input axis system, are different for the PLOT program and the NCSU BODY program. In order to overcome this difficulty the CONVERT program also contains the instructions required to invert the body with respect to the X-axis and approximately center the body about the origin. These instructions are necessary since the flow is in the direction of the negative X-axis for the NCSU BODY program.

In order to calculate the boundary layer over the body the NCSU BODY program must have the properties of the flow field as well as the body geometry. The CONVERT program was designed specifically for any plot data set as described in the original PLOT program, and these data sets describe only the body shape. It is therefore necessary to insert a flow field parameter card into the data set created by the CONVERT program before the data set is input into the NCSU BODY program. The card (described in Appendix F), which is inserted behind the first card (identification card), specifies the free stream velocity, density, and kinematic viscosity of the flow field as well as the reference area upon which the coefficients are based and an output control parameter. Failure to include this card in the NCSU BODY program input will result in an invalid program execution.

## GENERAL PROGRAM THEORY FOR INVISCID BODY PROGRAM

The XYZ potential flow program, obtained from the Naval Ship Research and Development Center (Ref. 94) is a computer program for the computation of irrotational, incompressible potential flow about three-dimensional bodies of arbitrary shape. The solution method is essentially that developed by Douglas Aircraft Company in References 23 and 83. For a detailed description of the program theory the reader is advised to consult these references; however, an excellent brief description of the method is given in Reference 94, major portions of which are excerpted below.

The body surface is approximated by a set of plane quadrilaterals, and the solution is constructed in terms of a source density on the surface of the body. Based on the assumption that the source density is constant on each quadrilateral, a system of algebraic equations is used to approximate the integral equation for the source density over the body. The source density in each quadrilateral is chosen so that the normal component of the velocity is zero at one point in the quadrilateral. The matrix equation is solved by a simultaneous displacement iteration scheme with a two-eigenvalue extrapolation procedure to speed up convergence.

The XYZ program received at N. C. State is divided into five basic sections. Section 1 reads the input cards, computes the descriptive parameters for each quadrilateral, and checks for errors. Section 2 computes the matrix elements in the equations for the source density and the velocity for points on the body. Section 3 solves the matrix equation for the source density. Section 4 computes and edits the velocity and pressure coefficient on each quadrilateral. Section 5 computes the coordinates of the streamlines on the body surface.

The program actually solves a problem involving a stationary, three-dimensional body in a moving ideal fluid. The fluid is assumed to have a uniform velocity at infinity ( $V_\infty$ ) which is parallel with the x-axis of the body. The velocity potential  $\phi$  satisfies the following equations:

$$\nabla^2 \phi = 0 \quad \text{in the fluid} \quad (1)$$

$$\frac{\partial \phi}{\partial n} = 0 \quad \text{on the surface of the body} \quad (2)$$

$$\phi = -x \cdot V_\infty_x - y \cdot V_\infty_y - z \cdot V_\infty_z \quad \text{at infinity} \quad (3)$$

where  $n$  indicates the direction normal to the surface. A solution to these equations is constructed in the form of a source density ( $S$ ) on the surface of the body,

$$\phi(p) = \iint_{\text{Body Surface}} S(q) \frac{1}{r(p,q)} dA_q - x \cdot V_{\infty x} - y \cdot V_{\infty y} - z \cdot V_{\infty z} \quad (4)$$

where  $r(p,q)$  is the distance between the point  $p$  at which we are interested in finding the potential and some other point  $q$  on the body, and  $A_q$  denotes the area of the quadrilateral containing the point  $q$ . Note that Equations (1) and (3) are satisfied by  $\phi$  as defined by Equation (4). The boundary condition on the body, Equation (2), can be applied to obtain an equation for the source density ( $S$ ).

$$0 = \frac{\partial \phi}{\partial n_p} = -2 S(p) + \iint_{\text{Body Surface}} S(q) \frac{\partial}{\partial n_p} \frac{1}{r(p,q)} dA_q - n_{px} \cdot V_{\infty x} - n_{py} \cdot V_{\infty y} - n_{pz} \cdot V_{\infty z} \quad (5)$$

Since the surface of the body is approximated by a set of plane quadrilaterals which are generated from input points (See Figure 46 ), in the limit the above equation requires that the body surface be represented by an infinite number of panels at each of which the flow normal to the surface is zero. It is important to obtain satisfactory results with a finite number of panels and to properly size and position these panels on the body surface. In Reference 23 Hess and Smith state that the proper distribution of elements over the body surface is largely a matter of intuition and experience. Panels should be concentrated in regions where the flow properties, particularly the source density, are expected to vary rapidly. The method gives correct results for convex corners, but concave corners cause difficulty that may or may not be serious. Accordingly, they recommend that panels should not be concentrated near unrounded concave corners; but if the corner is extreme enough to require rounding, a very great concentration of panels is necessary in that region. The panel sizes also play an important role in determining the validity of the solution. Hess and Smith note that if several small panels are in the vicinity of a large one, the accuracy is that associated with the large panel. Thus, the size of panels should change gradually when going from a region of highly concentrated small panels to a region of sparsely concentrated panels. They recommend that the characteristic dimensions of a panel should usually be no more than 50 percent greater than those of adjacent elements.

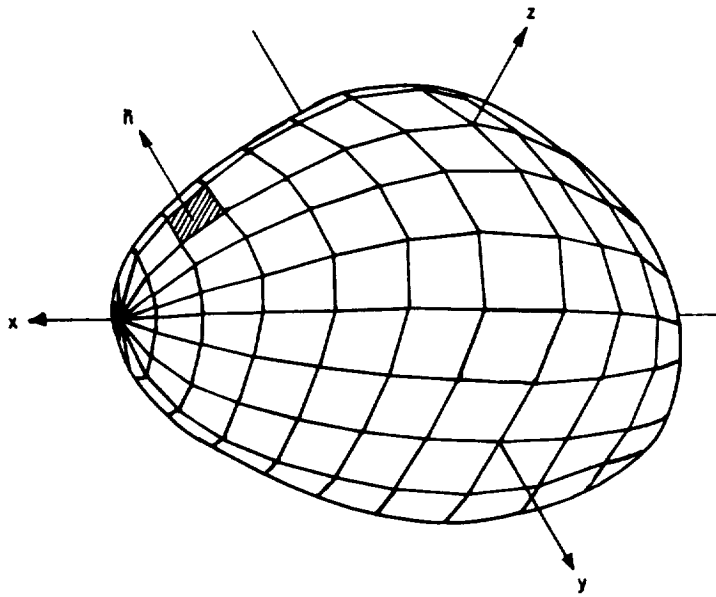


Figure 46. The approximate representation of the body surface.

The source density is assumed to be constant in each of the body panels and is computed by satisfying Equation (5) at one point in each of the quadrilaterals. The point chosen is the panel centroid point. Thus, the integral Equation (5) is approximated by a matrix equation

$$S_i = \sum_j C_{ij} S_j + V_i \quad (6)$$

where

$$C_{ij} = \frac{1}{2\pi} \iint_{\text{Quad. } j} \frac{\partial}{\partial n_i} \left( \frac{1}{r_{ij}} \right) dA$$

$$C_{ii} = 0, \text{ and}$$

$$V_i = -\frac{1}{2\pi} (n_x \cdot V_{\infty x} + n_y \cdot V_{\infty y} + n_z \cdot V_{\infty z}).$$



Equation (6) is solved for  $S_i$  by the iterative procedure mentioned above (see Reference 83 for more detail). The velocity components at each centroid point are then computed from the following equations:

$$VX_i = \sum_j V1_{ij} S_j + V_{\infty x} \quad (7)$$

$$VY_i = \sum_j V2_{ij} S_j + V_{\infty y} \quad (8)$$

$$VZ_i = \sum_j V3_{ij} S_j + V_{\infty z} \quad (9)$$

where

$$V1_{ij} = - \iint_{\text{Quad. } j} \frac{\partial}{\partial x} \left( \frac{1}{r_{ij}} \right) dA$$

$$V2_{ij} = - \iint_{\text{Quad. } j} \frac{\partial}{\partial y} \left( \frac{1}{r_{ij}} \right) dA, \text{ and}$$

$$V3_{ij} = - \iint_{\text{Quad. } j} \frac{\partial}{\partial z} \left( \frac{1}{r_{ij}} \right) dA$$

The pressure coefficient is then computed from these velocity components.

An integral over a quadrilateral is evaluated by one of three methods, depending upon the ratio of the distance of the  $i^{\text{th}}$  point from the quadrilateral to the maximum dimension of the quadrilateral. If the ratio is greater than 4.0, the quadrilateral is approximated by a monopole (as if it were concentrated at one point). If the ratio is greater than 2.0 and less than or equal to 4.0, the quadrilateral is approximated by a quadrupole. If the ratio is less than or equal to 2.0, the integrals are evaluated exactly. The approximate methods are used because they require much less time than the exact method. The evaluation of the integrals is extensively discussed in References 23 and 83.

The on-body streamlines are computed once the velocities are known at each quadrilateral centroid. The streamline computation procedure used in the XYZ program is discussed in some detail in a report to be published by Charles W. Dawson and Janet S. Dean of the Naval Ship Research and Development Center in late 1975. This procedure may be outlined in the following manner:

- (1) The coordinates of a starting point within a particular quadrilateral are specified.
- (2) The two points at which the streamline, passing through the starting point, intersects the sides of the starting quadrilateral are found.
- (3) The intersection point which is in the upstream flow direction is retained.
- (4) A search is made of the adjacent quadrilaterals to determine which quadrilateral the streamline is entering in the upstream direction.
- (5) Using this quadrilateral as a starting quadrilateral the point at which the streamline leaves this new quadrilateral in the upstream direction is determined.
- (6) The above procedure, steps (4) and (5), is continued until the streamline reaches the nose of the body.
- (7) The upstream portion of the streamline so traced is now defined by the coordinates of its intersection points on the sides of the quadrilaterals through which it passes.
- (8) It should be noted that as each point on the streamline is found, the velocity at that point and the distance from that point to the previous streamline point are calculated.
- (9) After returning to the original starting quadrilateral the same procedure is used to trace the streamline in the downstream direction to the body tail.
- (10) The arc lengths computed from point to point in (8) are then all referenced to the nose of the body so that the distance of any point on a streamline from the nose of the body is known.

## GENERAL PROGRAM MODIFICATIONS

Many of the changes made in the XYZ potential flow program as obtained from the Naval Ship Research and Development Center may be classified as general program modifications applicable to the entire program rather than a particular subroutine; these general modifications are discussed below. Throughout the remainder of the text the program as received at N. C. State will be referred to as the XYZ program while the modified viscous flow program will be referred to as the NCSU BODY program.

The XYZ program required only minor modifications in order to execute on the IBM 370-165 computer at N. C. State. Four of the five separate sections of the program were changed to subroutines all of which were called by the first section which was designated as the mainline. It was also necessary to modify the input and output file numbers as well as some of the data storage files.

In the interest of saving scratch file space, several of the files in the XYZ program were eliminated or reduced in size. In some cases the information stored on these files was put into a COMMON statement and thus made available to all five sections of the program. Table 3 gives a list of both the original file numbers used in the XYZ program and, if the information on these files was not commoned or deleted, the new file numbers used in the NCSU BODY program. Variable names were assigned to the input and output file unit numbers (JREAD-input, JWRITE-output) and to each scratch file unit number used in the NCSU BODY program. The values of the unit numbers are assigned by specification statements at the beginning of the mainline of the NCSU BODY program (JREAD=1, JWRITE=3, KFILE1=7, KFILE2=8, KFILE3=9, KFILE4=10, and KFILE5=11). For installations having different input/output unit numbers and file numbers these specifications may be easily changed. The addition of a wake body to the original body required more body panels and therefore more panel geometry storage space on file KFILE1. To prevent recalculating original panel geometry, the appropriate information for the new quadrilaterals was calculated and then added to the original information by using a second file (KFILE2) for panel geometry information. The original panel geometry which was unchanged was copied from file KFILE1 to KFILE2, and the new information was then added to file KFILE2. This two-file procedure is used to prevent file READ-WRITE incompatibilities at other computing facilities.

In an effort to reduce the size of the XYZ program by specializing it to the problem of interest, several modifications were made. Since the program was to be used for bodies at zero angles of attack and sideslip, those portions of the XYZ program which calculate the contributions to the flow and pressure over the body resulting from the Y-flow and Z-flow components were removed when the NCSU BODY program was created. Thus, the free stream velocity in the NCSU BODY program was specified as -1.0 in the X-direction, 0.0 in the Y-direction and 0.0 in the Z-direction. While the potential flow calculations are correctly made using just this unit velocity, the viscous part of the program

requires the specification of the magnitude of the free stream velocity or the Reynolds Number in order to make the boundary layer calculations. The magnitude of the free stream velocity must therefore be specified (see last paragraph in this section).

XYZ Program	NCSU BODY Program	
File Number	File Name	File Number
1	KFILE3	9
2	KFILE4	10
3	Information Commoned	
4	KFILE KFILE1 KFILE2	7 8
5 (Input)	JREAD	1 (input)
6 (output)	JWRITE	3 (output)
7	File Deleted	
8	File Deleted	
9	File Deleted	
11	KFILE5	11
12	File Deleted	
16	File Deleted	

Table 3. Data file comparison for the XYZ and NCSU BODY Programs.

The maximum array size for the quadrilateral input arrays and geometry storage arrays was set at 650. This maximum input array size coupled with the addition of the wake body, which uses part of the geometry storage arrays, means that the user should specify the original body using less than 600 panels. The coefficients of local quadratic representation of the body surface, which were stored on a scratch file as quadrilateral geometry information in the XYZ program,

were deleted from file storage in the NCSU BODY program, thereby reducing the file storage space and the size of the file input array B. The WS array contained in the XYZ program was also deleted from the NCSU BODY program, and the required control variables originally held in this array were commoned or placed in subroutine argument lists.

The addition of the wake body to the original body and the assumption of a plane of symmetry necessitated two important restrictions on specifying data for the NCSU BODY program. First, the line of reference with respect to which the Y-coordinates of the body are specified must be the  $Y=0$  line. Second, the line of reference with respect to which the X-coordinates of the body are specified must be a line parallel to a line from the nose of the body to the tail of the body (see Figure 47 ). This last restriction was incorporated in order to determine the direction in which the wake body should be added onto the original body.

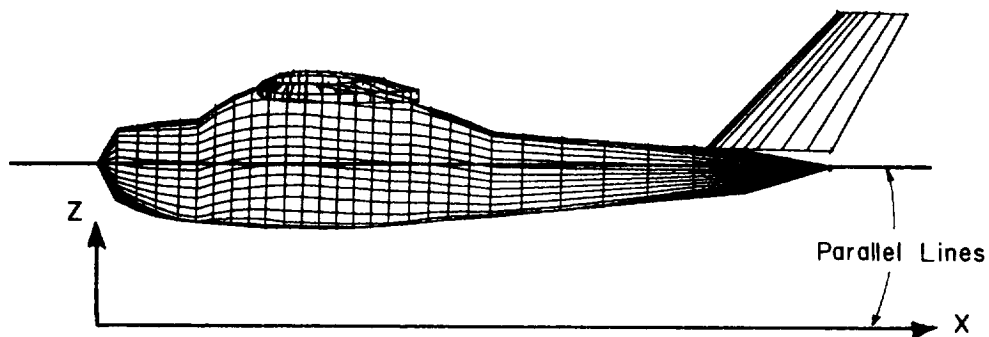


Figure 47. Orientation of body with respect to reference line.

In addition to those mentioned above, there were also other input and output modifications made to the XYZ program. Many of the input integers in the XYZ program were just specified as constant values in the NCSU BODY program:  $NSE=1$ ,  $MIX=150$ ,  $ISM=1$ ,  $EPS=0.0001$ , and  $ISP=0$ . The other input integers  $MIY$ ,  $MIZ$ ,  $IUCT$ ,  $IPS$ , and  $IPF$  were deleted. While the above input variables were deleted, it was also necessary to add the variables  $VINF$  (free stream velocity),  $VO$  (kinematic viscosity),  $ROE$  (density),  $REFA$  (reference area), and  $IWRITE$  to the NCSU BODY program input. The first three were added to supply the boundary layer routines with the necessary information

to compute the Reynolds Number of the body. REFA was added to provide a reference area for normalizing the lift and drag coefficients. IWRITE was added as an output control parameter which has the value 0, 1, or 2. IWRITE=0 gives maximum output while IWRITE=2 gives minimum output. For an exact description of the input required for the NCSU BODY program the reader is referred to the User Instructions in Appendix F.

## STREAMLINE MODIFICATION AND BOUNDARY LAYER CALCULATION

The only practical method for predicting the viscous flow field about an arbitrary three-dimensional body involves the same procedure as that used for the viscous flow about two-dimensional airfoils. The basic steps for this procedure are: (1) obtain an inviscid flow solution for the basic arbitrary body, (2) obtain a boundary layer solution based on the inviscid flow solution, (3) construct a modified body by adding a wake body to the original body, and (4) obtain an inviscid flow solution for the body plus wake body to obtain the final pressures and force coefficients on the physical body. These steps represent an outline of the procedure used in the NCSU BODY program.

The basic method for obtaining the inviscid flow solution has already been discussed in the section General Program Theory For Inviscid Body Program. Present methods available for obtaining a three-dimensional boundary layer solution over arbitrary bodies are very time consuming, require a large amount of computer storage, and are therefore beyond the scope of this report. As an alternative, the authors chose to use two-dimensional boundary layer calculations along streamlines to approximate the actual three-dimensional case. Justification for this procedure has already been discussed in detail beginning on page 113 of the theory section. This method is ideally suited for use with XYZ since the program already provides the capability for computing on-body streamlines. Further, the streamline procedure calculates the absolute velocity and surface length from the nose for each streamline point. Considering the approximate nature of two-dimensional boundary layer solutions along streamlines as applied to this problem, it is appropriate to employ relatively simple laminar and turbulent boundary layer calculation procedures. The boundary layer displacement thickness  $\delta^*$  and wall shear  $\tau_w$  are calculated at each of the panel centroid points. Assuming  $\tau_w$  in each panel is constant over that panel area, and given (1) the axial (X-direction) component of velocity from the potential flow solution, (2) the absolute velocity for each panel, and (3) the area of each panel, the skin friction drag coefficient is found by integrating the axial component of  $\tau_w$  over the body surface. The values of  $\delta^*$  at the panel centroids are used to construct a wake body which is added to the original body. As in the case of the airfoil, the purpose of the wake body is to model the relief of the stagnation condition at the body tail accompanying the presence of the boundary layer (see page 128). The construction of the wake body is discussed in the next section of this report. Once the wake body is generated, a new inviscid solution for the body plus wake body is found; this solution represents the viscous flow solution over the original body. There is no iterative procedure as was the case with the airfoil because of the large amount of computer time required for each solution.

Thus far this section has presented a brief summary of how the viscous flow solution over an arbitrary body can be obtained by modifying the inviscid flow solution. Attention will now be directed to (1) the actual modifications made in the streamline section of the XYZ program and (2) the addition of the two-dimensional boundary layer calculation procedures.

Since the inviscid solution calculates the velocities at the panel centroid points, the appropriate boundary layer parameters are also estimated at these centroids. This is accomplished by the following procedure:

(1) For a given panel a streamline is traced, using the centroid point as the starting point, from the body nose to three points downstream of the panel centroid. The reader should note that this represents two modifications of the original streamline procedure provided in the XYZ program. First, in the XYZ program, the coordinates for a streamline starting point were read in by the user, while in the NCSU BODY program the streamline starting points are automatically specified as the panel centroid points; thus, the user no longer has the option of inputting the starting coordinates for streamlines. Second, the XYZ program traced a streamline from the nose of the body to the body tail; however, since the boundary layer information is needed only at the panel centroid, computation time is simply wasted by continuing to trace a streamline far downstream of a panel centroid. In the NCSU BODY program at most only three points are traced downstream of the panel centroid point.

(2) A cubic spline curve of streamline velocity versus arc length is fitted to the streamline points. This curve is used to generate a more finely spaced set of velocity versus arc length points as well as the derivative of the velocity with respect to arc length. This information is required by the boundary layer computation procedure. The cubic spline curve was used because it may be differentiated to give smooth first derivatives from tabulated data.

(3) A boundary layer is computed along each streamline with transition fixed at the point on the streamline where the arc length is 5 percent of the total length of the body. If laminar separation arises before this point is reached, the program assumes that turbulent reattachment occurs at the point of laminar separation. The laminar boundary layer is computed using the Holstein-Bohlen formulation of the Kármán-Pohlhausen momentum Integral method (Ref. 65). If the velocity for the first point on the streamline is zero then the laminar routine assumes stagnation point starting conditions; however, if a nonzero velocity is found then flat plate starting conditions are used. These two types of starting conditions are necessary since the potential flow program does not always achieve a stagnation point (zero velocity) at the nose of the body. The turbulent boundary layer method, derived by Goradia in Reference 31, is a shortened version of the one used in the airfoil program (Appendix A). Goradia's method is designed to remain stable under the influence of extreme gradients, both favorable and adverse, and provide reasonable momentum and displacement thicknesses downstream of the turbulent separation point. Consequently, turbulent separation is never predicted with this method.



(4) The streamline values of  $\delta^*$  and  $\tau_w$  at the point corresponding to the streamline starting point (panel centroid point) are retained. These quantities are later used for the construction of the wake body and the calculation of the skin friction drag coefficient.

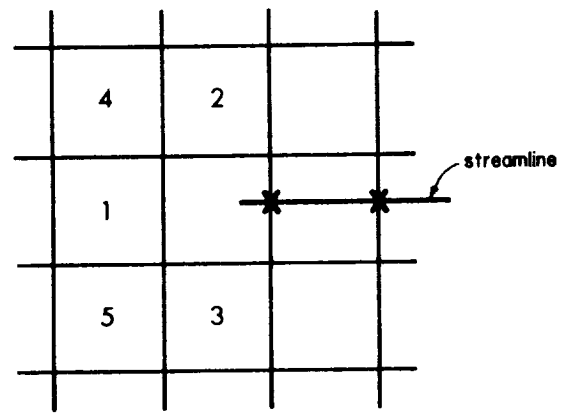
The above procedure, steps (1) through (4) are repeated for each panel centroid point except for the triangular panels at the nose and tail of the body. Initiating streamlines from the centroids of triangular panels is omitted because it was found that the streamline tracing procedure experiences great difficulty in the region where apexes of several triangular panels come together (i.e. in the region of the nose or tail). Thus, it is necessary to approximate the values of  $\delta^*$  and  $\tau_w$  at the centroids of the panels using the following procedure:

(1) For the triangular panels at the nose of the body, the values of  $\delta^*$  and  $\tau_w$  are taken to be one-third of their respective values in the quadrilateral immediately aft of each triangle.

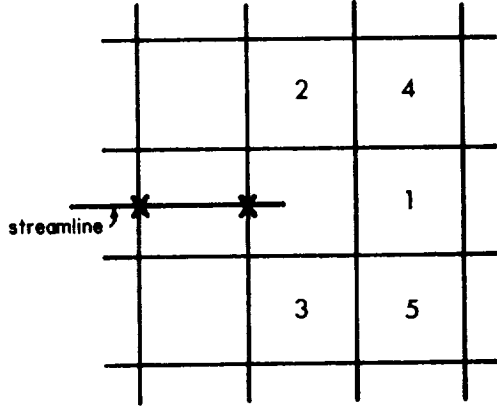
(2) For triangular panels at the tail of the body the values of  $\delta^*$  and  $\tau_w$  are taken to be equal to their respective values in the quadrilateral immediately preceding each triangle.

The streamline procedure was modified in one final way which has not been referred to as of yet. In the XYZ program a search is made of all quadrilaterals to determine the next quadrilateral into which a streamline is traced. In actuality, a streamline traced in either the upstream or downstream direction must enter one of five quadrilaterals adjacent to the quadrilateral it is leaving. Consequently, only these five quadrilaterals need to be checked to see which quadrilateral the streamline will enter. To reduce program execution time this modified search procedure is incorporated in the NCSU BODY program. Figure 48 illustrates the order in which each of the five quadrilaterals are searched when tracing in either the upstream or downstream direction.

It should also be mentioned that in the original XYZ program the streamline variables were dimensioned large enough to provide for tracing 650 streamline points. This is well in excess of the number needed for the NCSU BODY program. The array sizes of the appropriate streamline variables were therefore reduced in the NCSU BODY program in order to reduce overall program size.



tracing in the up-stream direction



tracing in the down-stream direction

Figure 48. New panel identification procedure for tracing streamlines.

## ADDITION OF WAKE BODY

In order to predict the drag of an arbitrary three-dimensional body both the skin friction drag and pressure drag must be calculated. As seen in the previous section, the skin friction drag coefficient is calculated by integrating the wall shear over the body surface. Unfortunately, estimating the pressure drag using an inviscid flow solution technique is not quite as simple. Actually, the pressure or form drag is a relief of the rear stagnation condition caused by the presence of the boundary layer. Thus, in order to estimate the pressure drag this viscous phenomenon must be correctly modeled in the inviscid flow solution. The authors chose to model this effect with the addition of a wake body. A detailed discussion of the effect of the wake on the pressure drag, the modeling of the wake with a wake body, and the procedure chosen to construct the wake body is given beginning on page 128 in the theory section and is therefore not repeated here. Accordingly, in this section, attention will be directed toward the programming aspect of adding the wake body to the inviscid solution.

- (1) The authors chose to define the wake body as the last two sets of panels (modified to some extent) on the original body plus two additional sets of panels downstream of the original body (See Figure 49).

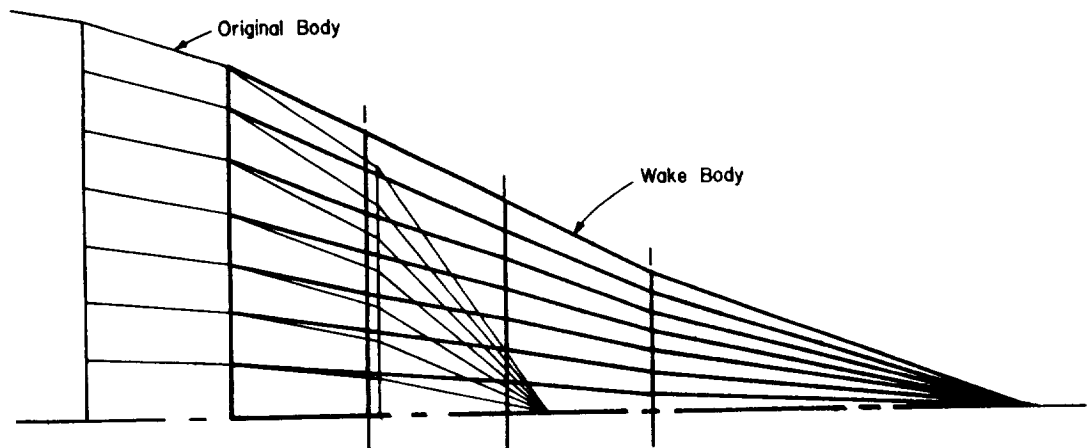


Figure 49. Definition of wake body.

- (2) For simplicity's sake, the wake body is chosen as a body of revolution with its axis on the line joining the nose and tail of the original body as shown in Figure 47. The reader should note that the original body must therefore be input using a reference line parallel to the line between the nose and tail of the original body.

(3) The radius of the wake body is chosen to decrease exponentially from the beginning of the wake body to the end. The particular exponential shape is calculated using the average radius and initial slope at the beginning of the wake body as well as the total length of the wake body.

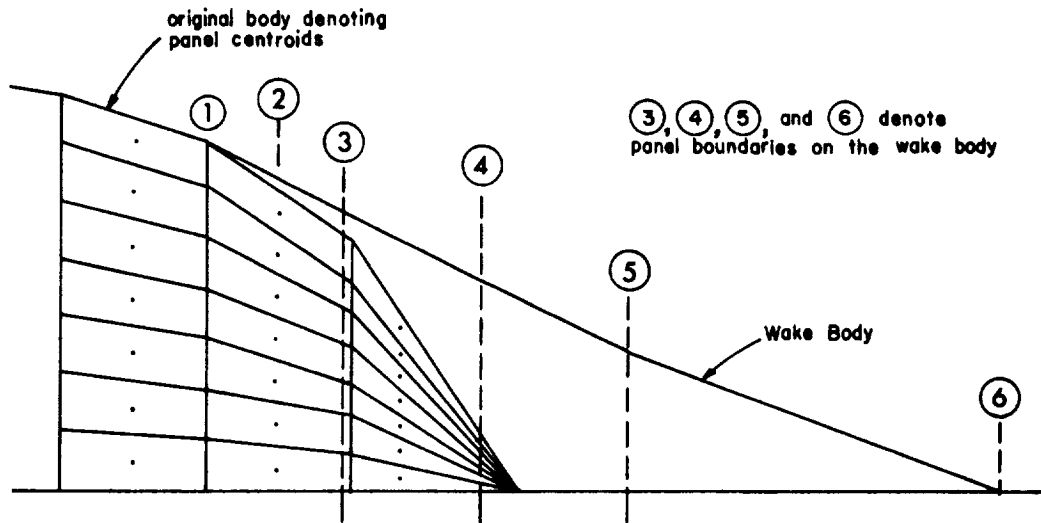


Figure 50. Panel boundaries on the original body and the wake body.

(4) Noting Figure 50, the average radius of the original body is computed for the X-coordinate of the panel centroids at station 2 and is denoted by AVXCG. The average value is computed for the boundary layer displacement thickness of the panels at station 2 and is denoted by AVDELS.

(5) The actual radius is computed for each body input point at station 1 and is denoted by R1. The radius corresponding to each body input point is computed for each panel at station 2 and is denoted by R2. Twice the average boundary layer displacement thickness is then added to each of the R2 values computed.

(6) A value for the slope (denoted as SLOPE) at each panel around the circumference of the body is then computed from the equation below:

$$\text{SLOPE} = (R2 - R1) / (\text{XHOLD1} - \text{AVXCG})$$

where XHOLD1 is the X-coordinate of station 1.

(7) The average slope (denoted by AVSLOP) is computed by summing each slope previously calculated and dividing this sum by the number of points at station 1. This slope is taken to be the initial slope of the exponential.

(8) The location of the end of the wake body, XINF, is then computed from the following equation:

$$XINF = XHOLD1 - AREAT / (3.14159*RAV)$$

where AREAT = 4.0\*AREAAV\*2.0\*MMAHQD and MMAHQD is the total number of points around the half body.

(9) Since all the parameters needed to determine the exponential curve have been found, the X-stations at 3, 4, and 5 are chosen to give panel areas on the surface of the wake body which are approximately equal to AREAAV. The radii corresponding to these X-stations are then calculated using the exponential curve.

(10) It should be noted that if a non-negative average slope is calculated for the initial slope of the exponential, the average slope is calculated from the following equation:

$$AVSLOP = - \text{Absolute Value} (RAV / (XINF - XHOLD1) ).$$

(11) Using the radii values at stations 3 through 6, the X, Y, and Z-coordinate values are generated for surface points on the wake body.

(12) Since the geometric information for the panels on the original body ahead of station 1 need not be changed, this information is copied from KFILE1 to KFILE2 (see page 243) in General Program Modifications). The geometric information for the wake body panels is then calculated and this information is added to KFILE2 in such a manner that body plus wake body appears as one large pseudo-body.

(13) The pressure coefficients for the panels on the pseudo-body are calculated by finding a new inviscid solution over this body. These pressure coefficients are then applied to the corresponding panels on the original physical body along the normals of the original panels (see pages 127 - 132). The appropriate components of these pressure coefficients are then integrated over the body surface to yield a pressure drag coefficient and a pressure lift coefficient.

As an illustration of the shape and location of the wake body with respect to the original body Figures 51 and 52 are included. Figure 51 depicts a 3-1 ellipsoid before and after a wake body is added, while Figure 52 shows the Cessna 182 which has an arbitrary cross-section.

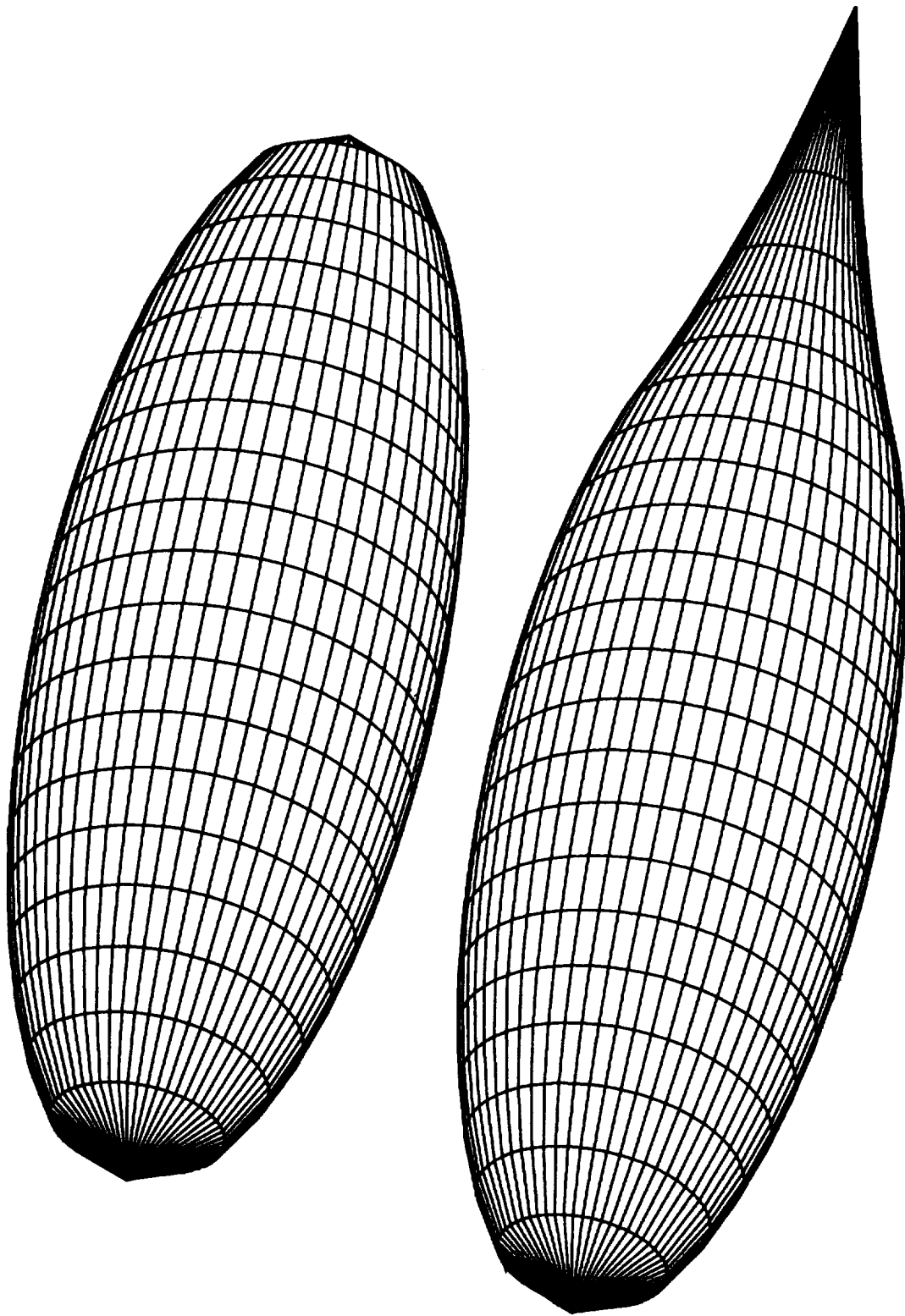


Figure 51. 3-1 ellipsoid with and without a wake body.

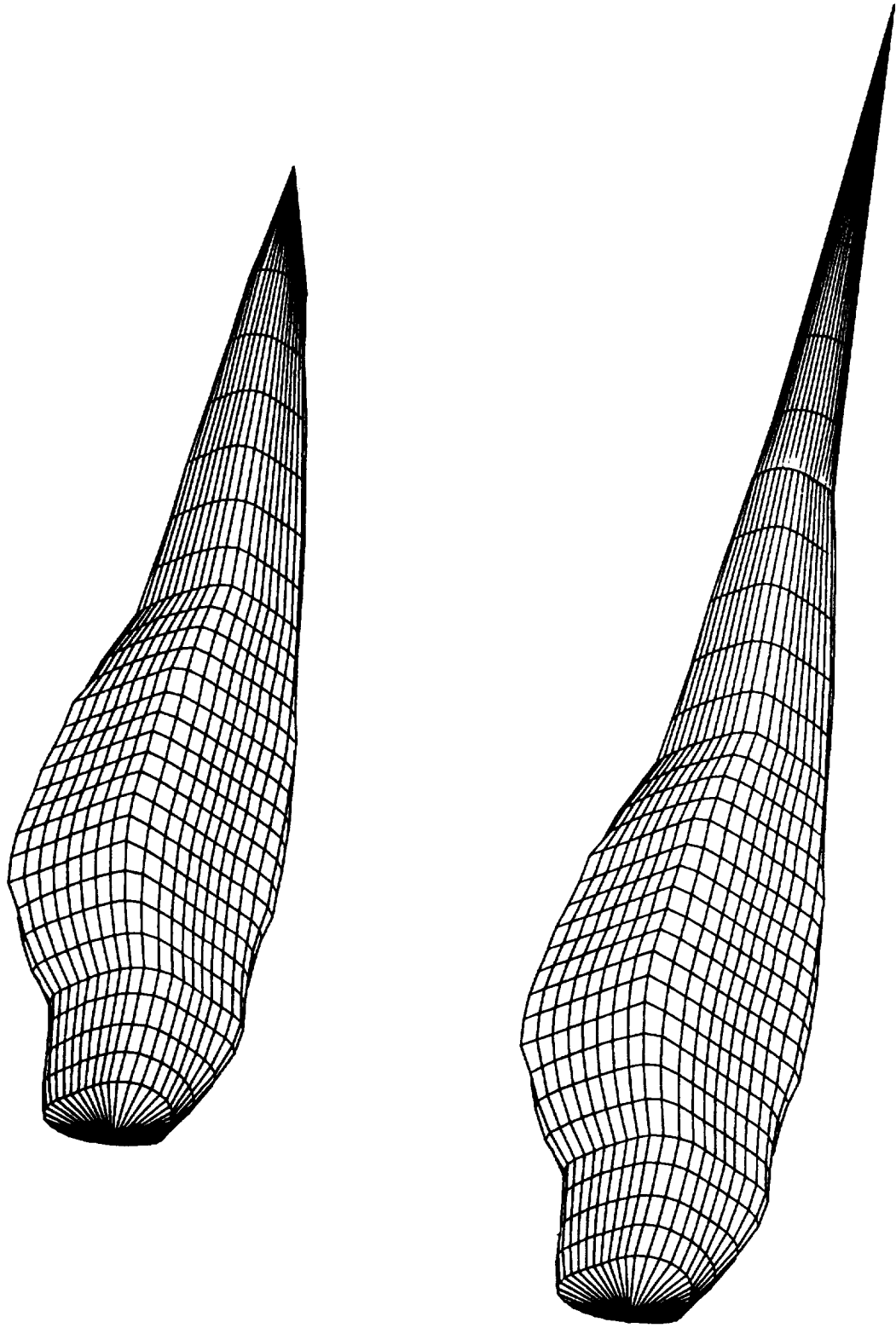


Figure 52. Cessna 182 Fuselage with and without a wake body.

## DISCUSSION OF PROGRAM RESULTS

To the time of the present writing it has not been possible to investigate the applicability of the NCSU BODY program to as many test cases as the authors would have liked. The greater geometric variability and intricacy characteristic of fuselages (in contrast to relatively simple geometry of airfoil families at least), the paucity of reliable experimental data, the extended development time required for the program, and finally, the cost of running the program (more than 10 times as much as the airfoil program) all served to limit the number of runs made using the final version of the program. Three bodies, however, were studied.

The first was a sphere. For a Reynolds Number of 2 million (based on sphere diameter) a drag coefficient of 0.041 was computed. This is about 1/5 the commonly accepted value for the sphere at such Reynolds Numbers. The reason for the low drag value, however, is easy to explain. It may be recalled that the computer program adds the wake body only behind the last two sets of surface panels in the X-direction. For a sphere the wake obviously emanates from a much larger area than the last two sets of panels if one uses a reasonably large number of quadrilaterals to represent the body. During the course of program development it was readily demonstrated that beginning the wake body at the point where separation is observed experimentally does in fact yield the correct value of drag. However, most streamlined bodies produce proportionately smaller separated flow regions; since the program is intended for use primarily with streamlined bodies, it was felt that the wake body formation procedure should attempt to model closely only the wakes of such bodies. One might also point out that if one better understood the relationships among the direction of and location of the flow separation from the body and the body geometry and flow Reynolds Number, then one could include analytical versions of these relationships in the system of equations used to calculate the flow; the appropriate wake body would then come out as part of the solution. In the absence of such knowledge, we can do little more than choose a model representative of one class of bodies.

The second body against which the program predictions were tested was a 3:1 prolate spheroid. In this case a Reynolds Number of 6 million was used in the computations. With 560 panels the calculated drag coefficient was 0.094. With only 100 panels the drag coefficient was 0.109 indicating the effect which a poorer representation of the body has on the computed drag value. No direct experimental data was found for this case but a 2:1 ellipsoid was found (Ref. 117) to give  $C_D = .07$ . There is also some evidence that the 3:1 ellipsoid should have a slightly higher drag because the surface area (skin friction) increases faster than the wake size, and hence, the form drag, diminishes. At any rate, the drag coefficient computed by the program for prolate spheroids with fineness ratios of 3 to 10 appears to be approximately correct.



The final test case was the Cessna 182 fuselage. It was found quite difficult to represent such a body with 560 or fewer panels of nearly equal area. As a result, while the rule of keeping adjacent panel areas within a ratio of 1:1.5 was honored, there is substantial variation in panel areas between the nose region (where many panels are needed to represent the geometry satisfactorily) and the aft cabin region (where large panels are adequate). This variation, it is felt, could be responsible for some error in the computation. The computed drag coefficient value, based on wing area and a length Reynolds Number of 30 million, was .01245. The body lift coefficient at the same condition was 0.00444. The computation, it may be noted, also assumes a turbulent boundary layer for most of the fuselage. It is therefore applicable primarily to the higher speed portions of the flight envelope.

Of course no test data were available against which to compare these figures, but a computation using the  $C_{D\pi}$  method (Ref. 2) gives a drag coefficient .00876, about 30% less than the value given by the NCSU BODY program. The  $C_{D\pi}$  method is probably the method most often used for preliminary design in the light aircraft industry. It does not differentiate between laminar and turbulent boundary layers but nevertheless it seems to yield drag values which match measured performance reasonably well. Thus it is to be expected that the drag value given by the NCSU BODY program is approximately correct. A more detailed test of the ability of the NCSU BODY program and the other programs discussed in the present work to predict the aerodynamic characteristics of actual aircraft is planned for early 1975. A light twin with an advanced wing design is being carefully instrumented for a series of performance and stability tests. It will be among the objectives of these tests to develop lift and drag flight test data against which to compare the prediction of the programs given in the present work. Until the results of this and other comparisons are available, the authors suggest that potential users of the NCSU BODY program employ its predictions cautiously until its range of validity is better defined.



## REFERENCES

1. Smetana, F. O.; Summey, D. C.; and Johnson, W. D.: "Point and Path Performance of Light Aircraft - A Review and Analysis". NASA CR-2272, June 1973, 131 pages.
2. Smetana, F. O.; Summey, D. C.; and Johnson, W. D.: "Riding and Handling Qualities of Light Aircraft - A Review and Analysis". NASA CR-1975, March 1972, 409 pages.
3. Smetana, F. O.; Summey, D. C.; and Johnson, W. D.: "Flight Testing for the Evaluation of Light Aircraft Stability Derivatives - A Review and Analysis". NASA CR-2016, May 1972, 110 pages.
4. von Helmholtz, H.: "Über discontinuirliche Flüssingheitsbewegungen". Monatsberichte der Königlichen Academic der Wissenschaften zu Berlin, 1868, pp. 215-228.
5. Kirchhoff, G.: "Zur Theorie freier Flüssigkeitsstrahlen". Journal für die reine und angewandte Mathematik, 1869, pp. 289-298.
6. Lamb, Horace: Hydrodynamics. Cambridge University Press, First Edition 1879, Sixth Edition 1932.
7. Kutta, M. W.: "Auftriebskräfte in strömenden Flüssigkeiten". Illustrierte aeronautische Mitteilungen, Vol. 6, 1902, pp. 133-135.  
  
Kutta, M. W.: "Über eine mit den Grundlagen des Flugproblems in Beziehung stehende zwei dimensionale Strömung". Sitzungsberichte der Bayerischen Akademie der Wissenschaften, 1910, pp. 1-58.
8. von Karman, Theodore: Aerodynamics. Cornell University Press, 1954.
9. Joukowski, N.: "Über die Konturen der Tragflächen der Drachenflieger". ZFM, 1910, pp. 281-284.
10. von Karman, T.; and Trefftz, E.: "Potentialströmung um gegebene Tragflächenquerschnitte". ZFM, 1918.
11. von Mises, R.: "Zur Theorie des Tragflächenauftriebes". Zeitschrift für Flugtechnik und Motorluftschiffahrt (ZFM) Vol. 11, p. 68, 1920.
12. Müller, W.: "Zur Konstruktion von Tragflächenprofilen". ZAMM, 1924.
13. Theodorsen, T.: "Theory of Wing Sections of Arbitrary Shape". NACA Report No. 411, 1932.
14. Munk, Max M.: "General Theory of Wing Sections". NACA Report 142, 1922.

15. Birnbaum: "Die tragende Wirbelfläche als Hilfsmittel zur Behandlung des ebenen Problems der Tragflügel Theorie". ZAMM, 1923.
16. Glauert, H.: "Theory of Thin Aerofoils". A.R.C. R & M 910 1224.  
Glauert, H.: The Elements of Aerofoil and Airscrew Theory. Cambridge University Press, 1966.
17. Karamcheti, K.: Principles of Ideal-Fluid Aerodynamics. John Wiley and Sons, New York, 1966.
18. Abbott, Ira H.; and von Doenhoff, Albert E.: Theory of Wing Sections. Dover Publications, Inc., New York, 1959, 693 pages.
19. Abbott, Ira H.; von Doenhoff, Albert E.; and Stivers, Louis S.: "Summary of Airfoil Data". NACA TR No. 824, 1945.
20. Weber, J.: "The Calculation of the Pressure Distribution over the Surface of Two-Dimensional and Swept Wings with Symmetrical Airfoil Sections". A.R.C. R & M 2918, July 1953.
21. Weber, J.: "The Calculation of the Pressure Distribution on the Surface of Thick Cambered Wings and the Design of Wings with Given Pressure Distribution". A.R.C. R & M 3026, June 1955.
22. Bridgewater, J.; and Whitlery, M. D.: "An Algol Program for Calculating the Inviscid Subsonic Pressure Distribution on Airfoils by the Weber-Küchemann Method". NPL Aero Note 1062, July 1967, N68-15738.
23. Hess, J. L.; and Smith, A. M. O.: "Calculation of Potential Flow about Arbitrary Bodies". Progress in Aeronautical Sciences, Vol. 8, pp. 1-138, Pergamon Press, 1967.
24. Martensen, E.: "Berechnung der Druckverteilung an Gitterprofilen in ebener Potentialströmung mit einer Fredholmscher Integralgleichung". Arch. Rational Mech. Anal, Vol 3, No. 3, 1959, pp. 235-270.
25. Jacob, K.; and Riegels, F. W.: "Berechnung der Druckverteilung endlich dicker Profile ohne und mit Kapper und Vorflügeln". Zeitschrift für Flugwissenschaften, Vol. 11, No. 9, Sept. 1963, pp. 357-367.
26. Oellers, H. J.: "Die Inkompressible Potentialströmung in der Ebener Gitterstufe". Jahrbuch 1962 der Wissenschaftlichen Gesellschaft für Luft und Raumfahrt, e.v., pp. 349-353.
27. Chen, A. Wen-Shin: "The Determination of the Geometries of Multiple-Element Airfoil Optimized for Maximum Lift Coefficient". Ph.D. Thesis, University of Illinois at Urbana-Champaign, 1971.

28. Lighthill, M. J.: "A New Method of Two-Dimensional Aerodynamic Design". A.R.C. R & M 2112, April 1945.
29. Sato, J.: "An Exact Two-Dimensional Incompressible Potential Flow Theory of Airfoil Design with Specified Velocity Distributions". Transactions Japan Society Aero. Space Sciences, Vol. 9, No. 14, pp. 11-18, 1966.
30. Powell, B. J.: "The Calculation of the Pressure Distribution on a Thick Cambered Aerofoil at Subsonic Speeds, Including the Effects of the Boundary Layer". A.R.C. CP. 1005, June 1967, N69-13421.
31. Stevens, W. A.; Goradia, S. H.; and Braden, J. A.: "Mathematical Model for Two-Dimensional Multi-Component Airfoils in Viscous Flow". NASA CR-1843, July 1971, 181 pages.
32. Bennett, J. A.; and Goradia, S. H.: "Methods for Analysis of Two-Dimensional Airfoils - With Subsonic and Transonic Applications". Lockheed Georgia Company Report CR 8591, July 1966.
33. Van Dyke, Milton D.: "Second-Order Subsonic Airfoil Theory Including Edge Effects". NACA Report 1274, 1956.
34. Lanchester, F. W.: Aerodynamics. London Constable & Co. Ltd., 1907; Aerodanetics, London, 1908.
35. Prandtl, Ludwig: "Tragflügeltheorie". Göttinger Nachrichten, 1918, pp. 451-477.
36. McVeigh, M. A.; and Kisielowski, E.: "A Design Summary of Stall Characteristics of Straight Wing Aircraft". NASA CR-1646, June 1971, 209 pages.
37. Margason, R. J.; and Lamar, J. E.: "Vortex-Lattice Fortran Program for Estimating Subsonic Aerodynamic Characteristics of Complex Planforms". NASA TND-6142, February 1971, 139 pages.
38. Jordan, Peter F.: "Remarks on Applied Lifting Surface Theory". Research Institute for Advanced Studies, Baltimore, Md., August 1967. Available from NTIS as N68-32042.
39. Coote, Ian: "A Fortran Program for Determining the Subsonic Lift Distribution on a Wing Using Lifting-Surface Theory". Department of Aeronautical Engineering, Sydney University. Available from NTIS as N71-33220.
40. Yager, P. M.; Holland, C. H.; and Strand, T.: "Modified Weissinger Lifting-Surface Method for Calculating Aerodynamic Parameters of Arbitrary Wing-Canard Configurations". Air Vehicle Corporation Report No. 354, August 1967, AD660423.

41. Garner, H. C.: "Numerical Appraisal of Multhopp's Low-Frequency Subsonic Lifting Surface Theory". A.R.C. R & M No. 3634, 1970.
42. James, R. M.: "On the Remarkable Accuracy of the Vortex Lattice Discretization in Thin Wing Theory". McDonnell-Douglas Aircraft, Inc., Report No. DAC-67211, February 1969, N69-37939.
43. Garner, H. C.; Hewitt, B. L.; and Labrujere, T. E.: "Comparison of Three Methods for the Evaluation of Subsonic Lifting-Surface Theory". A.R.C. 30 324, June 1968, N69-19965.
44. Coote, Ian: "Note on the Spanwise Integration of the Kernel Function in Subsonic Lifting-Surface Theory". Sydney University Department of Aeronautical Engineering, Aero Tech Note 6093, November 1969, N71-33219.
45. Margason, Richard, J.; and Lamar, John E.: "Vortex-Lattice Fortran Program for Estimating Subsonic Aerodynamic Characteristics of Complex Planforms". NASA TND-6142, February 1971.
46. Hess, J. L.; and Faulkner, Suzanne M.: "Determination of Low Speed Interference Effects by Superposition". Available from NTIS as N71-19377.
47. Anon: "Analytical Methods in Aircraft Aerodynamics". NASA SP-228, 1970. A collection of 31 papers by various authors.
48. Carmichael, Ralph L.: "Recent Experience In Using Finite Element Methods for the Solution of Problems in Aerodynamic Interference". NASA TMX-66884, 1971.
49. Timman, R.: "The Potential Flow About a Yawed Ellipsoid at Zero Incidence". National Aerospace Laboratory NLR, The Netherlands, Report F74. N68-34853 from NTIS.
50. Loeve, W.: "Computer Programs In Use at NLR for the Calculation of Stationary Subsonic Flow around Wing-Body Combinations". Report AT-69-12. Available from NTIS as N70-18119.
51. Multhopp, H.: "Aerodynamics of the Fuselage". NACA TM 1036, December 1942.
52. Bingham, Gene J.; and Chen, Allen Wen-shin: "Low Speed Aerodynamic Characteristics of an Airfoil Optimized for Maximum Lift Coefficient". NASA TND-7071, December 1972, 53 pages.
53. Roskam, Jan: Methods for Estimating Drag Polars of Subsonic Aircraft. Published by the author, Lawrence, Kansas, 1971.
54. Cebeci, Tuncer; Mosinskis, G. J.; and Smith, A. M. O.: "Boundary Layer Separation on Two-Dimensional and Axisymmetric Bodies In Incompressible Flows". McDonnell-Douglas Corp. Report No. MDC-J0973-01, November 1970, N71-25868.

55. Lundry, J. L.: "A Numerical Solution for the Minimum Induced Drag, and the Corresponding Loading, of Non-Planar Wings". McDonnell-Douglas Corp. Report DAC-66900, NASA CR-1218.
56. Liepmann, H. W.; and Puckett, A. E.: Aerodynamics of a Compressible Fluid. John Wiley and Sons, New York, 1947, 262 pages.
57. Liepmann, H. W.; and Roshko, A.: Elements of Gasdynamics. John Wiley and Sons, New York, 1957, 439 pages.
58. Mercer, J. E.; Weber, J. A.; and Lesferd, E. P.: "Aerodynamic Influence Coefficient Method Using Singularity Splines". AIAA Paper No. 73-123, 7 pages.
59. Lamar, John E.: "A Modified Multhopp Approach for Predicting Lifting Pressures and Camber Shape for Composite Planforms in Subsonic Flow". NASA TND-4427, July 1968.
60. Multhopp, H.: "Methods for Calculating the Lift Distribution on Wings (Subsonic Lifting Surface Theory)". A.R.C. R & M No. 2884, January 1950.
61. Garner, H. C.; and Fox, D. A.: "Algol 60 Programme for Multhopp's Low-Frequency Subsonic Lifting-Surface Theory". A.R.C. R & M No. 3517, 1968.
62. Wolowicz, Chester H.; and Yancey, Roxanah B.: "Longitudinal Aerodynamic Characteristics of Light, Twin-Engine Propeller-Driven Airplanes". NASA TND-6800, June 1972, 361 pages.
63. McNally, William D.: "Fortran Program for Calculating Compressible Laminar and Turbulent Boundary Layers in Arbitrary Pressure Gradients". NASA TND-5681, May 1970, 107 pages.
64. Küchemann, D.; and Weber, J.: "The Subsonic Flow Past Swept Wings at Zero Lift without and with Body". A.R.C. R & M No. 2908, March 1953.
65. Schlichting, H.: Boundary Layer Theory. New York, McGraw-Hill Book Co. Inc., Fourth Edition, 1960.
66. Durand, W. F., editor: Aerodynamic Theory. Dover Publications, Inc., Vol. I Division C, 1963, reprint of 1934 edition.
67. Nicolai, L. M. and Sanchez, F.: "Correlation of Wing-Body Combination Lift Data". Journal of Aircraft, Vol. 10, No. 2, 1973, pp. 126-128.
68. Angelucci, S. B.: "Multivortex Model for Bodies of Arbitrary Cross-Sectional Shapes". AIAA Paper No. 73-104.

69. Callaghan, J. G. and Beatty, T. D.: "A Theoretical Method for the Analysis and Design of Multi-Element Airfoils". Journal of Aircraft, Vol. 9, No. 12, December 1972, pp. 844-848.
70. Spence, D. A.: "Wake Curvature and the Kutta Condition". Journal of Fluid Mechanics, Vol. 44, 1970, part 4, pp. 625-636.
71. Riley, N.; and Stewartson K.: "Trailing Edge Flows". Journal of Fluid Mechanics, Vol. 39, 1969, part 1, pp. 193-207.
72. Preston, J. H.; and Sweeting, N. E.: "The Experimental Determination of the Boundary Layer and Wake Characteristics of a Simple Joukowski Aerofoil, with Particular Reference to the Trailing Edge Region". A.R.C. R & M No. 1998, March 1943.
73. Preston, J. H.; Sweeting, N. E.; and Cox, Miss D. K.: "The Experimental Determination of the Boundary Layer and Wake Characteristics of a Piercy 12/40 Aerofoil, with Particular Reference to the Trailing Edge Region". A.R.C. R & M No. 2013, February 1945.
74. Howarth, L.: "The Theoretical Determination of the Lift Coefficient of a Thin Elliptic Cylinder". Proc. Roy. Soc. A, 149, pp. 558-586, 1935.
75. Preston, J. H.: "The Calculation of Lift Taking Account of the Boundary Layer". A.R.C. R & M No. 2725, November 1949.
76. Preston, J. H.: "Note on the Circulation in Circuits which Cut the Streamlines in the Wake of an Aerofoil at Right-Angles". A.R.C. R & M No. 2957, March 1954.
77. Spence, D. A.; and Beasley, J. A.: "The Calculation of Lift Slopes Allowing for Boundary Layer, with Applications to the RAE 101 and 104 Aerofoils". A.R.C. R & M No. 3137, February 1958.
78. Bollech, Thomas V.: "Experimental and Calculated Characteristics of Several High-Aspect-Ratio Tapered Wings Incorporating NACA 44-Series, 230-Series, and Low-Drag 64-Series Airfoil Sections". NACA TN 1677, September 1948, 37 pages.
79. Dommasch, Daniel O.; Sherby, Sydney S.; and Connolly, Thomas F.: Airplane Aerodynamics. Pitman Publishing Corporation, 1967.
80. Bhateley, Ishwar C.; and McWhirter, Jack W.: "Development of Theoretical Method for Two-Dimensional Multi-Element Airfoil Analysis and Design". AFFDL-TR-72-96, Part 1, August 1972, 366 pages.



81. Hess, J. L.: "Numerical Solution of the Integral Equation for the Neumann Problem with Applications to Aircraft and Ships". SIAM Symposium on Numerical Solution of Integral Equations with Physical Applications, Madison, Wisconsin, October 1971, 108 pages. Also Douglas Aircraft Co. Engineering Paper No. 5987.
82. Hess, J. L.: "Higher Order Numerical Solution of the Integral Equation for the Two-Dimensional Neumann Problem". Computer Methods in Applied Mechanics and Engineering, Vol. 2, 1973, pp. 1-15.
83. Hess, John L.; and Smith, A. M. O.: "Calculation of Non-Lifting Potential Flow about Arbitrary Three-Dimensional Bodies". Douglas Aircraft Co. Report No. E. S. 40622, March 15, 1962, 177 pages.
84. Labrujere, T. E.; Loeve, W.; and Slooff, J. W.: "An Approximate Method for the Calculation of the Pressure Distribution on Wing Body Combinations at Subcritical Speeds". Publication of the National Aeronautical Laboratory (NLR), Amsterdam, Netherlands.
85. Loeve, W.; and Slooff, J. W.: "On the Use of Panel Methods for Predicting Subsonic Flow about Aerofoils and Aircraft Configurations". NLR MP 71018 U, June 10, 1971.
86. Keith, J. S.; Ferguson, D. R.; Merkle, C. L.; Heck, P. H.; and Lahti, D. J.: "Analytical Method for Predicting the Pressure Distribution about a Nacelle at Transonic Speeds". NASA CR-2217, July 1973.
87. Hess, J. L.: "Calculation of Potential Flow about Arbitrary Three-Dimensional Lifting Bodies". Douglas Aircraft Company Report MDC-J5679-01, October 1972.
88. Glesing, J. P.; Kálmán, T. P.; and Rodden, W. P.: "Subsonic Steady and Oscillatory Aerodynamics for Multiple Interfering Wings and Bodies", Journal of Aircraft, Vol. 9, No. 10, October 1972, pp. 693-702.
89. Woodward, F. A.: "An Improved Method for the Aerodynamic Analysis of Wing-Body-Tail Configurations in Subsonic and Supersonic Flow. Part I - Theory and Application. Part II - Computer Program Description". NASA CR-2228, May 1973, 126 pages and 315 pages.
90. Widnall, Sheila: "Subsonic Aerodynamics". Aeronautics and Astronautics, April 1973, pp. 14, 21, and 28.
91. Otto, H.: "Calculation of Nonlinear Lift and Pitching Moment Coefficients for Slender Wind-Body Combinations". Journal of Aircraft, Vol. 11, No. 8, August 1974, pp. 489-491.

92. Roskam, Jan; and Lan, C.: "A Parametric Study of Planform and Aeroelastic Effects on Aerodynamic Center,  $\alpha$ - and  $q$ -Stability Derivatives". NASA CR-2117, April 1973.
93. Bleekrode, A. L.: "A Survey of Current Collocation Methods in Inviscid Subsonic Lifting Surface Theory. Part II - Computational Aspects of Solving the Large Systems of Linear Algebraic Equations on a Digital Computer". Publication of NLR Amsterdam, Netherlands.
94. Dawson, Charles W.; and Dean, Janet S.: "The XYZ Potential Flow Program". Naval Ship Research and Development Center, Bethesda, Maryland, Report 3892, June 1972, 65 pages.
95. Hopkins, E. J.: "A Semi-Empirical Method for Calculating the Pitching Moment of Bodies of Revolution at Low Mach Numbers". NACA RM A51C14. 1951.
96. Goodson, K. W.: "Effect of Nose Length, Fuselage Length, and Nose Fineness Ratio on the Longitudinal Aerodynamic Characteristics of Two Complete Models at High Subsonic Speeds". NASA Memo 10-10-58L. 1958.
97. Pitts, W.; Nielsen, J.; and Kaattari, G.: "Lift and Center of Pressure of Wing-Body-Tail Combinations at Subsonic, Transonic, and Supersonic Speeds". NACA TR 1307. 1957.
98. Donovan, A. F., and Lawrence, H. R., editors, Aerodynamic Components of Aircraft at High Speeds, Section C: "Interaction Problems" by C. Ferrari. Princeton University Press, 1957. pp. 281-552.
99. Cebeci, Tuncer; Kaups, Kalle; Mosinskis, G. J.; and Rehn, J. A.: "Some Problems of the Calculation of Three-Dimensional Boundary-Layer Flows on General Configurations". NASA CR-2285. July 1973. 56 pp.
100. Henrici, Peter: Elements of Numerical Analysis, John Wiley, New York, 1964. 336 pp.
101. Allen, H. J., and Perkins, E. W.: "A Study of Viscosity on Flow over Slender Inclined Bodies of Revolution". NACA TR 1048. 1951.
102. Smetana, F. O.: "Investigation of Free Stream and Stagnation Pressure Measurement from Transonic and Supersonic Aircraft. Final Report." WADC TR-55-238. April 1958.
103. Smetana, F.O., and Knepper, D.P.: "Toward Simpler Prediction of Transonic Airfoil Lift, Drag, and Moment". Journal of Aircraft, Vol. 10, No. 2, Feb. 1973. pp. 124-126.
104. Truitt, R.W.: "Shockless Transonic Airfoils," AIAA Paper 70-187, New York. 1970.

105. Sinnott, C. S.; and Osborne, J.: "Review and Extension of Transonic Airfoil Theory". A.R.C. R & M 3156. 1958.
106. Thompson, N.; and Wilby, P. G.: "Transonic Aerodynamics". AGARD Conference Proceedings No. 35 (AD-685270). September 1968.
107. Riger, D. D.; and Rose, N. J.: Differential Equations with Applications, McGraw Hill Book Co., New York, 1968, pp. 545.
108. Milgram, Jerome H.: "Section Data for Thin, Highly Cambered Airfoils in Incompressible Flow". NASA CR-1767, July 1971, pp. 72.
109. Cebeci, T.; Mosinskis, G. J.; and Smith, A. M. O.: "Calculation of Viscous Drag of Two-Dimensional and Axisymmetric Bodies in Incompressible Flows". AIAA Paper 72-1, pp. 11.
110. Cebeci, T.; Mosinskis, G. J.; and Smith, A. M. O.: "Calculation of Separation Points in Incompressible Turbulent Flows". Journal of Aircraft, Vol. 9, No. 9, pp. 618-624, September 1972.
111. Granville, P. S.: "The Calculation of Viscous Drag of Bodies of Revolution". The David Taylor Model Basin Report 849. July 1953.
112. Von Mises, Richard: Theory of Flight, McGraw-Hill Book Co., New York. 1945.
113. Craidon, Charlotte B.: "Description of a Digital Computer Program for Airplane Configuration Plots", NASA TM X-2374, September 1970, pp. 84.
114. Klunker, E. B.; and Newman, P. A.: "Computation of Transonic Flow about Lifting Wing-Cylinder Combinations". Journal of Aircraft, Vol. 11, No. 4, April 1974, pp. 254-256.
115. Ahlberg, J. H.; Nilson, Edwin N.; and Walsh, Joseph L.: The Theory of Splines and Their Applications. Academic Press, New York, 1967.
116. Marshall, F. J.; and Deffenbaugh, F. D.: "Separated Flow Over Bodies of Revolution Using an Unsteady Discrete-Vorticity Cross Wake: Part I - Theory and Application; Part II - Computer Program Description". NASA CR-2414 & 2415, June, 1974. Part I - pp. 89. Part II - pp. 152.
117. Rouse, Hunter: Elementary Mechanics of Fluids. John Wiley and Sons, New York, 1947.



## APPENDICES

# APPENDIX A - Two-Dimensional Wing Aerodynamic Characteristics Program

## User Instructions

The program is written in FORTRAN IV and is designed to run in single precision on an IBM 370-165 computer with an average execution time of 20 to 25 seconds for each angle of attack. The program calculates the two-dimensional viscous flow solution of an arbitrary airfoil and evaluates its aerodynamic force and moment coefficients. The program requires the specification of the following input data:

- (1) The 80 characters of the array TITLE which are used as a header for identifying output. Since the program allows more than one airfoil to be analyzed in a given run, TITLE is used as a control variable to end execution. Termination of execution is achieved by following the last set of airfoil data to be analyzed by a title card having only the word END in the first three spaces (see last card of the sample data set in Figure A-2).
- (2) The number NXU of specified upper surface airfoil coordinates, the number NXL of specified lower surface airfoil coordinates, the control parameter IWRITE, the control parameter IALPHA, and the control parameter IPUNCH. The largest allowed value of either NXU or NXL is 65 and no more than 100 total airfoil points may be specified ( $NXU + NXL \leq 100$ ). The control parameter IWRITE (either 0, 1, 2, or 3) determines the amount of output desired for each set of airfoil data. IWRITE = 0 yields the maximum amount of output while IWRITE = 3 yields the minimum (examples of all the IWRITE options are given in Figure A-3 through Figure A-6). The control parameter IALPHA specifies the line of reference for the angle of attack. The line of reference is the x-axis of the reference system of the input data points. For IALPHA = 1 the line of reference is the longest chord line of the airfoil. Thus, if the user knows the location of the chord line of the airfoil and specifies the airfoil data points so that the chord line is parallel to the x-axis of the reference system of the input data points, he should use IALPHA = 0. If the user is unsure of the position of the airfoil chord line with respect to the x-axis of the input data system, he may choose IALPHA = 1, in which case, the program calculates the longest chord line and references the angle of attack to this line. The user will find that for most cases he will want to use the IALPHA = 0 option. For further explanation of this option see page 112. The control parameter IPUNCH gives the user the option of obtaining punched data (lift, drag, and quarter-chord moment coefficients for each angle of attack) which may be used in the program designed to estimate three dimensional aerodynamic characteristics of wings (see Appendix C). IPUNCH = 1 gives punched output while the default IPUNCH = 0 gives none.

- (3) The NXU values of the abscissa XU for the upper surface input points. The XU array should be monotonic increasing from airfoil leading to trailing edge with 8 points per data card.
- (4) The NXU values of the upper surface ordinate ZU which correspond to the XU values. The ZU array is specified with 8 data points per card.
- (5) The NXL values of the abscissa XL for the lower surface input points. The XL array should be monotonic increasing from airfoil leading to trailing edge with 8 points per data card.
- (6) The NXL values of the lower surface ordinate ZL which correspond to the XL values. The ZL array is specified with 8 data points per card.
- (7) The number NA of angles of attack to be read for which a solution is desired. NA must be less than or equal to 10.
- (8) The NA values of angle of attack, ALPHA, given in degrees, 8 values per data card.
- (9) The number NM of free stream Mach numbers to be read for which a solution is given at each of the NA angles of attack. NM must be less than or equal to 5.
- (10) The NM values of free stream Mach number, FSMACH, 5 values per data card.
- (11) The reference chord CREF in feet and the scale factor SF. The reference chord is used to non-dimensionalize all of the output. The scale factor is a multiplicative constant used to convert the values of XU, ZU, XL, ZL, XTRAN, and ZTRAN to feet. It would be advantageous for the user to input the airfoil coordinates as percentages of the reference chord so that CREF and SF will have the same numerical values.
- (12) The stagnation temperature T0 in degrees Rankine, the Reynolds number RN in millions, the Prandtl number PR, and the heat transfer factor KF. Reynolds number should be calculated based on CREF, and since it is read in millions, RN = 3.0 corresponds to a Reynolds number of 3,000,000. (It should be noted that this Reynolds number specification differs from that used in the NASA program which used millions per foot.) It is recommended that a value of 1.0 be used for the heat transfer factor. For cases where heat transfer effects may be important, the user should consult Reference 32 to determine an appropriate value for KF.
- (13) The control variable LTRAN which determines whether boundary layer transition is free (LTRAN = 0) or fixed (LTRAN = 1), the x location for transition XTRAN, and the z location for

transition ZTRAN. If free transition (LTRAN = 0) is used both XTRAN and ZTRAN should be specified as 0.0, and the program will predict the location of the transition points. It should be noted that if the fixed transition option is used the program will still use its own predicted point of transition if it occurs before the specified transition point. Since transition must be specified on both surfaces, two transition cards must be read (upper surface card first).

Statements (1) through (13) represent a complete set of data for a particular airfoil. The format specification for this data is given in Figure A-1. A sample data set of the 23012 airfoil with IWRITE = 3 option is shown in Figure A-2. The output of this particular data set is shown in Figure A-3, and in addition, examples of the other IWRITE options are given in Figures A-4, A-5, and A-6.



TITLE							
20A4							
NXU	NXL	IWRITE	IALPHA	IPUNCH	/		
I5	I5	I5	I5	I5	/		
XU(1)	XL(2)			etc.			
F10.0	F10.0			etc.			
ZU(1)	ZU(2)			etc.			
F10.0	F10.0			etc.			
XL(1)	XL(2)			etc.			
F10.0	F10.0			etc.			
ZL(1)	ZL(2)			etc.			
F10.0	F10.0			etc.			
NA	/						
I5	/						
ALPHA(1)	ALPHA(2)			etc.			
F10.6	F10.0			etc.			
NR	/						
I5	/						
FSMACH(1)	FSMACH(2)			etc.			
F10.0	F10.0			etc.			
CRFP	SP	/					
F10.0	F10.0	/					
TO	RN	PR	KP	/			
F10.0	F10.0	F10.0	F10.0	/			
LTRAN(1)	XTRAN(1)	ZTRAN(1)	/				
I10	F10.0	F10.0	/				
LTRAN(2)	XTRAN(2)	ZTRAN(2)	/				
I10	F10.0	F10.0	/				

Figure A-1. Format specification of input data for the 2-D characteristics program.



Program Listing

```

COMMON KCT(100),ZCT(100),THETA(65),S(65),OV(65),CP(65),GV(65),CFI
1 1(65),DLTAS(65),GVBT(65),DLTASPI(65),GVBDP(65),TITLE(20),XT
2 1RAN(2),ZTRAN(2),TTRAN(2),ALFA,FSMCH,PO,TO,RN,PR,KF,CREP,C,XSTAG,ZS
3 1TAG,TSSTAG,SSSTAG,BETA,LTRAN(2),IWRITE,MAXK,IALPHA
4 1COMMON /OUTPUT/CL(10),CDI(10),CMI(10),CMI4(10),NALPHA
5 1DIMENSION ALPHA(10),FSMACH(5),XTRSV(2),ZTRSV(2),LTRSV(2)
6 1REAL KF
7 1COMMON /TEMP/ATEMP(100),ZTEMP(100)
8 1COMMON /DRAG/THUP,HUP,THYLG,HLD,CDSY1
9 1COMMON /INOUT/JREAD,JWRITE
10 1JREAD=1
11 1JPUNCH=2
12 1JWRITE=3
13 1IERR=0
14 15 ***** READ THE SPECIFIED AIRFOIL GEOMETRY AND OTHER PERTINENT DATA
15 1***** OBTAIN A SET IF 65-DISTRIBUTED POINTS FROM INPUT AIRFOIL POINTS
16 1***** CALL GEOMTERR,XNOSE,ZNOSE)
17 1IF (IERR.NE.0) GO TO 5
18 1IFLAG=0
19 1DO 10 IJ=1,65
20 1DLTASPI(IJ)=0.0
21 1DLTASPI(IJ)=0.0
22 1DO 5 JJ=1,2
23 1IERR=0
24 1IWRITE=0
25 1IWRITE=0
26 1IWRITE=0
27 1IWRITE=0
28 1IWRITE=0
29 1***** SOLVE FOR THE GVBT'S, AIRFOIL BASIC THICKNESS GAMMA DISTRIBUTION
30 1***** CALL VOVBT(IERR,IFLAG)
31 1IF (IERR.NE.0) GO TO 5
32 1DO 20 I=1,65
33 1***** LOOP ON ALPHA'S (MAX=10) INSIDE LOOP ON MACH NUMBERS (MAX=5)
34 1DO 90 I=1,NM
35 1FSMCH=FSMA*H(1)
36 1NALPHA=J
37 1ALFA=ALPHA(I)/57.2957795
38 1DO 25 L=1,65
39 1CFIL)=0.
40 1DLTASPI)=0.
41 1DLTASPI)=0.
42 1GVBDP(1)=0.
43 1GVBDP(1)=0.
44 1CDSY1)=0.0
45 1MAX=5
46 1***** LOOP FOR ITERATION BETWEEN POTENTIAL AND VISCOUS FLOW SOLUTIONS
47 1DO 30 JJ=1,2
48 1IWRITE=0
49 1IWRITE=0
50 1IWRITE=0
51 1IWRITE=0
52 1IWRITE=0
53 1***** OBTAIN POTENTIAL SOLUTION (MAIN2) AND VISCOUS SOLUTION (MAIN3)
54 1***** CALL MAIN2(IERR,K)
55 1IF (IERR.NE.0) GO TO 95
56 1CALL MAIN3(K)
57 1***** CONTINUE
58 1IF (IWRITE.GT.-2) GO TO 95
59 1***** WRITE (JWRITE,5) TITLE
60 1***** WRITE (JWRITE,40)

```

```

40 1***** FORMAT (//,2X,50HLONGEST CHORDLINE SYSTEM BASIC REFERENCE SYSTE
61 1M,7,7X,3H7/C,9X,3H7/C,12X,3H7/C,9X,3H5/C,7X,2HCP,8X,2HCF,
62 15X,7HDELTA5/C,4X,4HVV/VO,/)
63 1CALL TRANS(ATEMP,ZTEMP,XNOSE,ZNOSE,XCT,ZCT,-BETA,0.0,0.,.65)
64 1DO 45 JJ=1,65
65 1XOC=ZCT(IJ)/CREP
66 1ZOC=ZCT(IJ)/CREP
67 1XREF=ATEMP(IJ)/CREP
68 1ZREF=ATEMP(IJ)/CREP
69 1SOC=SIJJ/CREP
70 1DOC=DLTASPI(IJ)/CREP
71 1CFC=ABS(CFI(IJ))
72 1VOC=SQRT(ABS(1.-CPI(IJ)))
73 1***** WRITE (JWRITE,50) KOC,ZOC,XREF,ZREF,SOC,CPI(IJ),CFC,C,DOC,VVOC
74 150 1***** FORMAT (1A,7F11.5,3F12.5,3F13.5,2F12.5,4F10.5)
75 1***** COMMON /INOUT/JWRITE,5) TITLE
76 1***** WRITE (JWRITE,60) TITLE,FSMCH
77 1***** WRITE (//,5X,20A,/,30X,BHFSMACH *,F9.5,/,4X,77(1H*),/AX,1H*,AX
78 1***** WRITE (//,5X,20A,/,13X,2HCD,10X,BHCMIN(5E1)4X,13HCD(1/4-CHORD),2X,1
79 1***** WRITE (//,4X,1H*,75X,1H*)
80 1***** WRITE (JWRITE,65) (ALPHA(I),CMI(I),CMI4(I),CMI4(I),JK=1
81 1***** WRITE (JWRITE,70)
82 1***** WRITE (JWRITE,70)
83 1***** WRITE (JWRITE,70)
84 1***** PUNCH TABLE OF ANGLE OF ATTACK, LIFT COEFF., DRAG COEFF., AND
85 1***** PUNCH CHORD MOMENT COEFF. FOR Z-D TO 3-D PROGRAM
86 1***** IF (JPUNCH.EQ.0) GO TO 90
87 1***** WRITE (JPUNCH,75) TITLE
88 1***** WRITE (JPUNCH,80) NA
89 1***** WRITE (JPUNCH,80) NA
90 1***** WRITE (JPUNCH,85) (ALPHA(I),CMI(I),CMI4(I),CMI4(I),I=1,NA)
91 1***** WRITE (JPUNCH,85)
92 1***** GO TO 5
93 1***** GO TO 5
94 1***** GO TO 5
95 1***** WRITE (JWRITE,100) KKK
96 1***** WRITE (JWRITE,100) KKK
97 1***** WRITE (JWRITE,100) KKK
98 1***** WRITE (JWRITE,100) KKK
99 1***** WRITE (JWRITE,100) KKK
100 1***** WRITE (JWRITE,100) KKK
101 1***** WRITE (JWRITE,100) KKK
102 1***** WRITE (JWRITE,100) KKK

```









```

1665)DLTAS(65),GVT(65),DVT(65),DLTASP(65),GVBDP(65),GVBDP(65),TITLE(20),XT
ITAG,1,STAG,SSSTAG,BETA,LTRAM(2),ALFA,FSMCM,PO,TO,RN,PR,KF,CREF,C,XSTAG,ZS
COMMON /TEMP/ZTEMP(100),ZTEMP(100)
COMMON /COEF/AA(65),G5)
DIMENSION /IMOU/JREAD,JWRITE
REAL*8 DUMX(133),DUMX(33),A(4)
C***
SMOOTH UPPER AND LOWER BOUNDARY LAYER DISPLACEMENT THICKNESSES
DO 5 IJ=1,33
DUMT(IJ)=THETA(IJ)
5 DUMX(IJ)=DLTAS(IJ)
DO 10 K=1,3
DO 15 IJ=1,33
15 DLTAS(IJ)=DUMX(IJ)
DO 20 IJ=1,33
IA=66-IJ
DUMT(IJ)=THETA(IA)
20 DUMX(IJ)=DLTAS(IA)
DO 25 K=1,3
DO 30 IJ=1,33
IA=66-IJ
30 DLTAS(IA)=DUMX(IJ)
DO 35 J=1,33
JZ=66-J
DZC=2./3.-D(LTAS(J)-DLTAS(J))*(DLTAS(J)-DLTAS(J))/3.
C***
GENERATE Z'S FOR CAMBER SOLUTION BY ADDING THE DIFFERENCE OF UPPER
AND LOWER BOUNDARY LAYER DISPLACEMENT THICKNESSES TO ORIGINAL Z'S
ZTEMP(IJ)=ZC(IJ)+DZC
SINA=SIN(ALFA+BETA)
COSA=COS(ALFA+BETA)
SINLPH=EQ(0) GO TO 40
COSLPH=COS(ALFA)
COSA=COS(ALFA)
SRATIO=Z(31)/S(65)-S(64))
DO 60 I=1,64
XC=XC(I)+XC(I+1))/2.0
ZC=ZTEMP(I)+ZTEMP(I+1))/2.0
DO 50 J=1,64
CALL CHEMIX,ZC,XC(I),ZTEMP(I),XC(I+1),I,J,COEFF)
IF (J-64) 30,45,50
45 AA(I,J)=AA(I,1)-COEFF*SRATIO
AA(I,J)=L.0
GO TO 55
50 AA(I,J)=COEFF
55 GV(I,J)=COSA*ZC+SINA*XC
60 CONTINUE
CALL SIMSOL(GV,64,IERR)
IF (IERR,NE.0) GO TO 70
GV(64)=GV(1)+SRATIO
GVTE=(ABSG(VI(64)))/ABSG(VI(1)))*SRATIO/(L.0*SRATIO)
GV(65)=SIGM(GVTE*GV(64))
DO 65 I=2,64
J=66-I
GV(I)=GV(J)+S(J-1)*GV(J-1)+S(J-1)*S(J-1))/S(J+1)-S(J-1)
65 CONTINUE
GV(I)=GV(65)

```

```

RETURN
70 WRITE (JWRITE,75)
75 FORMAT (/,45H0IN SUBROUTINE CAMBER A SINGULAR COEFFICIENT MATRIX M
IAS GENERATED)
RETURN
END
C***
SUBROUTINE CHEMIX,ZC,XI,Z2,ZZ,ZZ,I,J,COEFF)
ROUTINE TO CALCULATE THE COEFFICIENTS OF THE INFLUENCE MATRIX
REAL*8 DZ,DS,DS1,Z2,Z3,Z4,Z5,Z6,Z7,Z8,DATAN2,DSQRT,DBLE
D=DBLE(IZ-Z1)
DZ=DBLE(ZZ-Z1)
DS=DSQRT(DX*DX+DZ*DZ)
DZ=DS/DZS
DZ=DS/DZS
I1=EQ(J) GO TO 5
I1=EQ(J) GO TO 5
I2=DL(I1-Z1)
I3=DL(I1-Z1)
I4=DL(I1-Z1)
I5=DL(I1-Z1)
I6=DL(I1-Z1)
I7=DL(I1-Z1)
I8=DL(I1-Z1)
I9=DL(I1-Z1)
I10=DL(I1-Z1)
COEF=SMGL(I1,500*(TS*DLG(15)+TS*DLG(16)+TS*DLG(17)+TS*DLG(18)+TS*DLG(19)+TS*DLG(20)+TS*DLG(21)+TS*DLG(22)+TS*DLG(23)+TS*DLG(24)+TS*DLG(25)+TS*DLG(26)+TS*DLG(27)+TS*DLG(28)+TS*DLG(29)+TS*DLG(30)+TS*DLG(31)+TS*DLG(32)+TS*DLG(33)+TS*DLG(34)+TS*DLG(35)+TS*DLG(36)+TS*DLG(37)+TS*DLG(38)+TS*DLG(39)+TS*DLG(40)+TS*DLG(41)+TS*DLG(42)+TS*DLG(43)+TS*DLG(44)+TS*DLG(45)+TS*DLG(46)+TS*DLG(47)+TS*DLG(48)+TS*DLG(49)+TS*DLG(50)+TS*DLG(51)+TS*DLG(52)+TS*DLG(53)+TS*DLG(54)+TS*DLG(55)+TS*DLG(56)+TS*DLG(57)+TS*DLG(58)+TS*DLG(59)+TS*DLG(60)+TS*DLG(61)+TS*DLG(62)+TS*DLG(63)+TS*DLG(64)+TS*DLG(65))
RETURN
5 COEF=SMGL(DS*(DLG(10.500*DS)-1.000)/6.263185400)
RETURN
END
C***
SUBROUTINE COMPRTPLAG,XM,IN)
ROUTINE TO CONVERT INCOMPRESSIBLE VELOCITY DISTRIBUTION TO
COMPRESSIBLE VELOCITY DISTRIBUTION
REAL KF
COMMON XCT(100),THETA(65),S(65),VOV(65),CP(65),GV(65),CFI
L(65),DLTAS(65),GVT(65),DLTASP(65),GVBDP(65),GVBDP(65),TITLE(20),XT
ITAG,1,STAG,SSSTAG,BETA,LTRAM(2),ALFA,FSMCM,PO,TO,RN,PR,KF,CREF,C,XSTAG,ZS
COMMON /IMOU/JREAD,JWRITE
DIMENSION ML(65)
REAL*8 A(4)
REAL ML,S
DATA GAMMA/1.,4/
ML=1
ML=1
ML=2/(1.-XNO*Z1)+XNO*Z1**2
DO 40 I=1,65
VOV(I)=ABSG(VI(I))*I*(1.-ML)/L*(1.-XNO*GV(I)**2)
IF (VOV(I)) 5,10,10
5 VOV(I)=0.
10 CONTINUE
IF (IM) 25,25,15
15 VOVS=ML/S/XNO*SOAT(1+(GAMMA-1)/2.*XNO*XI)/L*(1+(GAMMA-1)/2.*ML*S*ML
153)
IF (VOV(I)=VOVS) 25,25,20
20 VOV(I)=VOVS
ML=ML*S*0.-1
25 ML=1+(2*XNO*VOV(I))/SOAT(1)

```

CAM 65  
CAM 66  
CAM 67  
CAM 68  
CAM 69  
CAM 70

CAM 1  
CAM 2  
CAM 3  
CAM 4  
CAM 5  
CAM 6  
CAM 7  
CAM 8  
CAM 9  
CAM 10  
CAM 11  
CAM 12  
CAM 13  
CAM 14  
CAM 15  
CAM 16  
CAM 17  
CAM 18  
CAM 19  
CAM 20  
CAM 21  
CAM 22  
CAM 23  
CAM 24  
CAM 25  
CAM 26  
CAM 27  
CAM 28  
CAM 29  
CAM 30  
CAM 31  
CAM 32  
CAM 33  
CAM 34  
CAM 35  
CAM 36  
CAM 37  
CAM 38  
CAM 39  
CAM 40  
CAM 41  
CAM 42  
CAM 43  
CAM 44  
CAM 45  
CAM 46  
CAM 47  
CAM 48  
CAM 49  
CAM 50  
CAM 51  
CAM 52  
CAM 53  
CAM 54  
CAM 55  
CAM 56  
CAM 57  
CAM 58  
CAM 59  
CAM 60  
CAM 61  
CAM 62  
CAM 63  
CAM 64







```

62 VINF=AMEI*IMP/ANPFT/1.E06
LAM 63 VOTRUE=VINF/VKAT/RHOMAT
LAM 64 P0=176.02*2*YOT002-591.E-8/(TO+198.61)/VOTRUE
LAM 65 V0=0.5*VOTRUE
LAM 66 A=AI-C1*CNSTAG**2-2.*D1*CNSTAG**3
LAM 67 B=AI*2.*C1*CNSTAG**3+.5*D1*CNSTAG**2
LAM 68 D0=30.K-1*IMP
LAM 69 D1=AME(K)/10
LAM 70 D2=(K-1)*D0
LAM 71 UET1(K)=D0*AME(K)
LAM 72 UET1(K)=D0*SLO(K)*1.+0.2*AME(K)**2)**4/AMUC
LAM 73 UET2(K)=AD*UET1.+2*AME(K)**2)**3/AMU**2*ODMDS(K)*C
LAM 74 K=MP
LAM 75 UET2(K)=UET2(K)*1.-6*AD*UET1.+2*AME(K)**2)**7/AMU**2*AME(K)*SLO(K)**
LAM 76 L2*CO**2
LAM 77 K=2
LAM 78 D0=135.I-3.*MP
LAM 79 IF (K.NE.2) GO TO 35
LAM 80 CN(K)=1.-A*SLO(K)/AME(K)*SUMS(K)/Z.
LAM 81 DELCUT=0.
LAM 82 GO TO 40
LAM 83
LAM 84
LAM 85
LAM 86
LAM 87
LAM 88
LAM 89
LAM 90
LAM 91
LAM 92
LAM 93
LAM 94
LAM 95
LAM 96
LAM 97
LAM 98
LAM 99
LAM 100
LAM 101
LAM 102
LAM 103
LAM 104
LAM 105
LAM 106
LAM 107
LAM 108
LAM 109
LAM 110
LAM 111
LAM 112
LAM 113
LAM 114
LAM 115
LAM 116
LAM 117
LAM 118
LAM 119
LAM 120
LAM 121

```

```

2 ROUTINE TO CALCULATE LAMINAR BOUNDARY LAYER AND TRANSITION POINT
LAM 3 COMMON XCT(100),ZCT(100),THETA(65),S(65),YOV(65),CP(65),GV(65),CFI
LAM 4 (65),DLTAS(65),GVBT(65),DLTASP(65),GVBD(65),GVBDP(65),TITLIZ(20),RT
LAM 5 ITRAK(2),ITRAN(2),TALFA*FSMCH,PO*TO*RN,PR,KF,CREF,CXSTAG,ZS
LAM 6 ITAG,ISTAG,SSTAG,BETA,LTRAN(2),IMRITE*MAKR,IALPHA
LAM 7 COMMON /TURBTR/SCRIT,RECRT,STRAN,ATRAN,THETA1,HINIT,AMETA, SLOTRM
LAM 8
LAM 9 REAL*8 AAI(4)
LAM 10 COMMON /VISCOS/SUMS(43),AME(43),SLO(43),UE(43),ODMDS(43),X(43),ZTE
LAM 11 IMP(43),IMPX,ITERP(43),ISURF
LAM 12 COMMON /LAMTR/H(43),AMTK(43),REMI(43),UET1(43),UET2(43),CN(43),UET
LAM 13 I(43),KBAR(43),RTHTR(43),RENDR(43),SG(43),SH*AO,VO,SEP,AMU,SG,P,MLT
LAM 14 I(43),K,KON
LAM 15 COMMON /PLBLK/DISP
LAM 16 COMMON /INDUT/JREAD,JWRITE
LAM 17
LAM 18 DEHL=K*ME
LAM 19 ITRAN(2)=ELAG(61)-COUCBE(41)-DISP(43)-AMTKOC(43)-DISPOC(43)-SSG(43)
LAM 20 ITRAN(2)=AL(43),TANI(43),CEMU(43),AMUORE(43),SKINFR(43),REMI(43),
LAM 21 ITRAN(2)=CFBAR(43),CRODI(61)
LAM 22 EQUIVALENCE (CNSTAG,CN(111)),HLESTG,ML(111)),(HSTAG,H(11))
LAM 23 IF (LTRAN(J5).NE.1)XTRAN(J5)=-CREF
LAM 24 FACT=1.0
LAM 25 AMEIF=FSMCH
LAM 26 IF (FSMCH=-.01) 5*5,10
LAM 27 DO 15 I=1,6
LAM 28 IFLAG(I)=0
LAM 29 KON=0
LAM 30 SW=KF*(1.+2*PR**2)/(1.+2*AMEIF**2)-1.
LAM 31 SEP=-.06961058-.0395712*SW+.0671724*SW**2
LAM 32 CNSTAG=-.1064*.0172505*SW-.375*SW**2
LAM 33 TMLL=TO*(1.+SW)
LAM 34 COUCBE(4)=.7312+.4.32497*SW+12.251*SW**2+21.8919*SW**3+.0.92805*SW
LAM 35 104
LAM 36 COUCBE(3)=-1.-227599-1.-662198*SW-9.193*SW**2-13.-197*SW**3-17.78015*
LAM 37 15SW**4
LAM 38 COUCBE(2)=-.088925+.309889*SW+1.1802*SW**2+.990225*SW**3+1.-21953
LAM 39 12*SW**4
LAM 40 B8=-10.8327-3.2*SW+2.9611*SW**2-41.298*SW**3
LAM 41 C8=23.4933*292.9871*SW+18.1659*SW**2
LAM 42 D8=-1740.-859-8973.-683*SW-13346.3*SW**2
LAM 43 E8=-6334.05-34314.45*SW-49800*.8745*SW**2
LAM 44 A1=.44
LAM 45 D1=5.28003+2.5138*SW
LAM 46 C1=3.19394+1.0807*SW
LAM 47 D1=-6.39857+1.067*SW
LAM 48 USTAG=1.1139*CNSTAG-11./12.*CNSTAG/(LEP*CNSTAG*(CNSTAG-SEP))
LAM 49 HLESTG=HSTAG/(1.+SW)
LAM 50 RT=-C*CNSTAG/(1.+SW)
LAM 51 AMU=(170+198.61)/(TO*(1.+SW)+198.61)**SQRT(1.+SW)
LAM 52 TIME=TO/(1.+2*AMEIF**2)
LAM 53 AIMP=49.02*SQRT(TIME)
LAM 54 VROT=TIME/TO**3.5*(TO+198.61)/(TIME+198.61)
LAM 55 RHOMAT=(1.+2*AMEIF**2)**2.5
LAM 56 A CORRECTION TO KINEMATIC VISCOSITY HAS BEEN MADE TO IMPROVE DRAG
LAM 57 CORRELATION WITH TEST DATA. THE VARIABLES INVOLVED IN CORRECTION
LAM 58 ARE VO (CORRECTED KINEMATIC VISCOSITY) = 0.5 VOTRUE (TRUE K.V.)
LAM 59 ANPFT=RM/CREF
LAM 60
LAM 61

```







```

T82 26
T82 27
T82 28
T82 29
T82 30
T82 31
T82 32
T82 33
T82 34
T82 35
T82 36
T82 37
T82 38
T82 39
T82 40
T82 41
T82 42
T82 43
T82 44
T82 45
T82 46
T82 47
T82 48
T82 49
T82 50
T82 51
T82 52
T82 53
T82 54
T82 55
T82 56
T82 57
T82 58
T82 59
T82 60
T82 61
T82 62
T82 63
T82 64
T82 65
T82 66
T82 67
T82 68
T82 69
T82 70
T82 71
T82 72
T82 73
T82 74
T82 75
T82 76
T82 77
T82 78
T82 79
T82 80
T82 81
T82 82
T82 83
T82 84
T82 85

IF (LSUMR-EQ.1) WRITE (JWRITE,5) TITLE,JM
IF (LSUMR-EQ.1) GO TO 15
WRITE (JWRITE,10) TITLE,JM
5 FORMAT (I10,2A1,5SHTURBULENT BOUNDARY LAYER SUMMARY FOR EQUIVALENT T82 29
1 AIRFOIL,5X,16H(GORADIA METHOD)//25X,20A4,5X,13MUPPER SURFACE//10X T82 30
1,1AITERATION NUMBER,13,/)
10 FORMAT (I10,2A1,5SHTURBULENT BOUNDARY LAYER SUMMARY FOR EQUIVALENT T82 32
1 AIRFOIL,5X,16H(GORADIA METHOD)//25X,20A4,5X,13MLCHER SURFACE//10X T82 33
1,1AITERATION NUMBER,13,/)
15 SOC=STRAN/CREF
TH=THETA1/CREF
ANGL=ALFA*57.2957795
WRITE (JWRITE,20) TO,PO,F5MCH,C,AM,PR,AF,SOC,TH,HIMIT,ANGL
20 FORMAT (I20,2A1,20H TEMPERATURE,9X,1H+,F8.2,4,19HOGREES,8A1M1 T82 38
1H+,7X,10HSTAGNATION PRESSURE,8X,1H+,F9.3,3X,BHL0/SC FT/23H PRES ST82 39
LEARN MACH NUMBER,9X,1H+,F8.5,23X,13H AIRFOIL CHORD,10A1,1H+,4HPR,8M T82 40
15,3H FT/10H REYNOLDS NUMBER,16X,1H+,F8.5,23X,13H AIRFOIL CHORD,10A1,1H+,4HPR,8M T82 41
1DTL NUMBER,13X,1H+,F8.5,23X,13H AIRFOIL CHORD,10A1,1H+,4HPR,8M T82 42
1,5,23X,21HTRANSITION POINT,5/C,8X,1H+,F8.5,23X,13H AIRFOIL CHORD,10A1,1H+,4HPR,8M T82 43
1UM THICKNESS//C,1X,1H+,F8.5,23X,13H AIRFOIL CHORD,10A1,1H+,4HPR,8M T82 44
1,1H+,F8.5,23X,13H AIRFOIL CHORD,10A1,1H+,4HPR,8M T82 45
1EES)
WRITE (JWRITE,25)
25 FORMAT (I10,4A1,3X,C,13X,3MS/C,13X,1HM,8X,BHOM/(S/C),8X,1HM,10X,7H T82 47
1THETA/C,8X,1HM,8X,BHOM/(S/C),8X,2MCP,10X,2MCP/)
XTR=STRAN/CREF
RND=SL0TR/CREF
DPRN=THE TAINIMIT/CREF
WRITE (JWRITE,30) XTR,STR,AMETR,DMDX,HIMIT,TH,DPRN
30 FORMAT (1H, F10.6,2X,6F13.6,13X,F13.6)
35 C1=0.36
C2=0.1667
C3=1.65
C4=0.246
C5=0.678
C6=0.268
NI=N4-1
UEINI=UEINI*(STRAN-SUMSINI)/(SUMSINI*1)-SUMSINI*1)*UEINI*1-UEINI T82 49
11)
THOLD=TTA(R1)
XHOLD=SUMSINI
UHOLD=UEINI
RHOLD=ARE(R1)
TTAINI=THETA1
IF (XINI-(SUMSINI*1)-.00001) 45,65,60
40 XINI=(SUMSINI*1)-.00001
45 SUMSINI=XINI
UEINI=UEINI
AMEINI=HIMIT
HMEINI=HIMIT
XNUXI=1+.0.25XME*21*0.1.75*VO
E1=3.+.2.+.02
E2=1.+.02
E3=3.+.3.+.02
T1=0.020C1/C3*E2
IBEG=N1+1
DO 90 I=IBEG,MP
JSAVE=I

```

```

MREANI(1)=0.0
MVEANI(1)=0.0
XNUX2=(1+.0.25XME(1)*0.21*0.1.75*VO
IF (I.EQ.NP) GO TO 50
DUEDX=(UEINI-UEI(1))/(SUMSINI-SUMS(I-1))*UEI(1)-UEI(1)/(SUMSINI
1,1)-SURS(I))*0.5
50 CONTINUE
UETR=UEI(1-1)/UEI(1)*0.05
UEINI=0.5XSUMSINI*0.05+UETR*(XNUX2/XNUXI)*0.02+1*XNUX2*0.02/UEI(1)*0.05
1THALEINI=UEI(1)*0.21
TERMCO=0.020C1/(UEI(1)*TTA(1)+XNUX2)*0.02+1.1
T2=TTA(1)/UEI(1)*0.05X
MVEANI(1-1)
MVEANI(1)
DO 75 J=1,M1
TERMB=HVC*4*0.001-C5*MMI*(UEI(1)*TTA(1)+XNUX2)*0.02-C6)
TERMC=TERMB/2.
TERMP=(HNI-1.1)*HVAI2
DMDX=(TERMA*TERMB+TERMC)/TTA(1-1)
HVIIR=MVEANI(1-1)+DMDX*(SUMS(I-1)-SUMS(I))
IF (HVIIR-1.85) 60,55,85
55 HVIIR=1.85
60 IF (HVIIR-1.55) 65,65,70
65 HVIIR=1.55
70 P-ITR=0.379*HVIIR/(HVIIR-1.269)
MVEANI(1)=HVEANI(1)+HVIIR
HMEANI(1)=HMEANI(1)+HTR
PV=HVIIR
75 HVEANI(1)=HVEANI(1)/M1
HMEANI(1)=HMEANI(1)/M1
DSTR1=TTA(1)*HMEANI(1)
DEL21=0.0049713*89*TTA(1)*191.64*TTA(1)*0.02
CELOC(1)=C4*10.0001-C5*HMEANI(1)*UEI(1)*TTA(1)+XNUX2)*0.02-C6)
XNUX1=XNUX2
XOC=XI(1)/CREF
SOC=SUMSINI/CREF
DMDX=SL0(1)/CREF
TH=TTA(1)/CREF
DEL=DEL(1)/CREF
DEL=DEL(1)/CREF
IF (IMRITE-EQ.1.AND.JM.EQ.0) GO TO 85
IF (IMRITE-CT.1) GO TO 85
IF ((JM-CT.0).AND.(JM.LT.MAXR-1)) GO TO 85
MHH=ITEMP(1)
CFLOC=CFLOC*(1+((1.-CP(MHH)))
WRITE (JWRITE,80) XDC,SOC,AME(1),DMDX,HMEANI(1),TH,DEL,CFLOC,
1CP(MHH)
80 FORMAT (1H, F10.6,2X,9(1X,F12.6))
85 IF (SEND-SUMS(1)) 95,95,90
90 CONTINUE
95 DO 100 I=IBEG,JSAVE
IA=ITEMP(1)
DLTASTA(1)=OSTR(1)
DLTALJ(1)=DEL(1)*IA
DLTALJ(1)=DEL(1)*IA
MVALJ(1)=HVAI(1)
RETURN N1 ELEMENTS TO THEIR ARRAYS

```

```

TIA(N1)=THOLD
SUMS(N1)=RHOLD
UE(N1)=RHOLD
ARE(N1)=RHOLD
IF (LSURF.NE.1) GO TO 105
THUP=TTA(JSAVE)
MUP=HMEAN(JSAVE)
GO TO 110
105 THLO=TTA(JSAVE)
MLD=HMEAN(JSAVE)
110 RETURN
END
    
```

```

C*** SUBROUTINE LOAD(NP,CMP,CME,CAP,CAP,CMP,CME)
ROUTINE TO INTEGRATE VISCOS AND PRESSURE FORCES
REAL KF
COMMON XCT(100),ZCT(100),THETA(65),S(65),VOR(65),CP(65),CV(65),CEI
1(65),DLTAS(65),GMR(65),ONTAS(65),GVDR(65),GVDRP(65),TITLE,201,ET
IRAN(2),ZTRAM(2),VTRAM(2),ALFA,FSMCH,PO,TO,PH,PR,KF,CREF,CV,STAG,ES
ITAG,ISTAG,SSTAG,BETA,ALTRAM(2),WRITE,MARK,ALPHA
CMP=0.0
CAP=0.0
CME=0.0
CVP=0.0
CNP=0.0
CNP=0.0
CNP=0.0
CNP=0.0
DO 5 I=2,65
ISTAG=I
IF (GV(I).GE.0.) GO TO 10
5 CONTINUE
10 DO 15 I=2,ISTAG
15 CF(I)=1-CF(I-1)
X1=XC(I)-1
Z1=ZC(I)
Z1=ZC(I)-1
CAP=CAP+(CF(I)+CF(I-1))/2*(Z2-Z1)
CNP=CNP+(CF(I)+CF(I-1))/2*(Z2-Z1)
CME=CME+(CF(I)+CF(I-1))/2*(Z2-Z1)
X3=CF(I)+CF(I-1)
CVP=CVP+X3*(Z2-Z1)/2.0
CAF=CAF+X3*(Z2-Z1)
20 CVP=CVP+X3*(Z2-Z1)-(Z2-Z1)*(X2-X1)/4.0
CAP=CAP/CREF
CNP=CNP/CREF
CME=CME/CREF**2
CAF=CAF/CREF
CVP=CVP/CREF
CNP=CNP/CREF**2
RETURN
END
    
```

```

SUBROUTINE LSQ(F,X,NP,C)
LEAST SQUARES CURVE FIT ROUTINE. FX IS THE DEPENDENT VARIABLE,
C*** X IS THE INDEPENDENT VARIABLE, NP IS THE NUMBER OF OBSERVATIONS,
LSQ 1
LSQ 2
LSQ 3
    
```

```

C*** AND N IS THE ORDER OF THE FITTED POLYNOMIAL.
FIX=MC(1)+C(2)*MC(3)+MC(4)+...+C(N)*MC(N)
DIMENSION A(1),Z(1),C(4),X(NP),F(NP)
REAL*8 A,T1,T2
N2=1
N2=1
C*** SET UP MINIMIZING MATRIX
DO 5 I=1,N1
DO 5 J=1,N2
5 A(I,J)=0.
DO 15 K=1,NP
T1=1.
DO 15 J=1,N1
T2=11
DO 10 I=1,N1
A(I,J)=A(I,J)+T2
10 T2=T2*F(K)
15 T1=T1*F(K)
C*** SOLVE FOR COEFFICIENT VECTOR
DO 20 K=1,NP
DO 20 J=1,N1
T1=A(I,J)*F(K)/A(I,K)
DO 20 I=1,N2
C(I,J)=A(I,J)-T1/A(I,K)
L=K+1
DO 25 J=L,N1
25 C(I,J)=C(I,J)+A(I,K)*J/A(I,K,K)
RETURN
END
    
```

LSQ 4  
LSQ 5  
LSQ 6  
LSQ 7  
LSQ 8  
LSQ 9  
LSQ 10  
LSQ 11  
LSQ 12  
LSQ 13  
LSQ 14  
LSQ 15  
LSQ 16  
LSQ 17  
LSQ 18  
LSQ 19  
LSQ 20  
LSQ 21  
LSQ 22  
LSQ 23  
LSQ 24  
LSQ 25  
LSQ 26  
LSQ 27  
LSQ 28  
LSQ 29  
LSQ 30  
LSQ 31  
LSQ 32  
LSQ 33  
LSQ 34  
LSQ 35  
LSQ 36  
LSQ 37

```

SUBROUTINE TRANS(XTRANS,ZTRANS,XMS,ZMS,X,Z,DELTA,XP,ZP,MPT)
ROUTINE WHICH TRANSLATES AND ROTATES (THROUGH ANGLE DELTA) A SET
OF MPT POINTS (X'S AND Z'S) TO A NEW SET OF POINTS (XTRANS'S AND
ZTRANS'S) SUCH THAT THE POINT (XP,ZP) BECOMES THE POINT (XMS,ZMS).
DIMENSION XTRANS(MPT),ZTRANS(MPT),X(MPT),Z(MPT)
COSD=COS(DELTA)
SIND=SIN(DELTA)
DO 5 I=1,MPT
XSAVE=X(I)
ZSAVE=Z(I)
XTRANS(I)=XMS+(X(I)-XP)*COSD+(Z(I)-ZP)*SIND
ZTRANS(I)=ZMS+(Z(I)-ZP)*COSD-(XSAVE-XP)*SIND
5 RETURN
END
    
```

TRN 1  
TRN 2  
TRN 3  
TRN 4  
TRN 5  
TRN 6  
TRN 7  
TRN 8  
TRN 9  
TRN 10  
TRN 11  
TRN 12  
TRN 13

```

C*** SUBROUTINE PROOTIA,X)
ROUTINE FOR SOLVING A CUBIC POLYNOMIAL
DIMENSION A(4),Z(6),X(6)
DIMENSION U(6),V(6)
REAL IM
PI=3.1415927
M=13*(A(4)+A(2)-A(3)**2)/(9.*M(4)**2)
PRD 1
PRD 2
PRD 3
PRD 4
PRD 5
PRD 6
PRD 7
    
```

PRD 1  
PRD 2  
PRD 3  
PRD 4  
PRD 5  
PRD 6  
PRD 7



```

35 IF (NM2-(N2+2)) 40,45,45
40 N2=NM2-2
45 XP=XPINT-X(N2+1)
DO 30 K=1,3
  L=2*K-1
  W=(1-L)*X(N2+1)
  A2=(Y(1)+W*(31-XP(1)))/XP(1)
  A3=(Y(1)+W*(31-XP(1)))/XP(1)
  A1=(Y(N2+1)+A2*(N2+1)+A3*(N2+1))
  A12=A2-2*A3*(N2+1)
  A13=A3
  RETURN
55 YINT=Y(NM1)
  A11=YINT
  A12=0.0
  A13=0.0
  RETURN
60 A12=(Y(NM2)-Y(NM1))/(X(NM2)-X(NM1))
  A13=Y(NM1)-A12*X(NM1)
  YINT=A11+A12*XINT
  RETURN
END

```

```

PRO 8
PRO 9
PRO 10
PRO 11
PRO 12
PRO 13
PRO 14
PRO 15
PRO 16
PRO 17
PRO 18
PRO 19
PRO 20
PRO 21
PRO 22
PRO 23
PRO 24
PRO 25
PRO 26
PRO 27
PRO 28
PRO 29
PRO 30
PRO 31
PRO 32
PRO 33
PRO 34
PRO 35
PRO 36
PRO 37
PRO 38
PRO 39
PRO 40
PRO 41

```

```

SUBROUTINE SMOOTH(X,Y,N)
  TIME FOR LINEAR LEAST SQUARES SMOOTHING OF THE N POINTS OF
  THE I AND Y ARRAYS
  DIMENSION X(N),Y(N)
  SF=0.5
  IF (N.LE.3) RETURN
  A=0.
  B=0.
  NE=N-3
  DO 15 J=1,NE
    AP=A
    BP=B
    SX=0.
    SY=0.
    SKY=0.
    SK2=0.
    J3=J+3
    DO 5 I=J,J3
      SX=SKX+X(I)*Y(I)
      SY=SY+Y(I)
      SKY=SKY+X(I)*Y(I)
      SK2=SK2+X(I)*X(I)
      A=(SKX*SY-SX*SY)/(SKX*X-4.*S2Z)
      B=(SKY*SY-SX*SY)/(SKX*X-4.*S2Z)
      Y(J)=A+1.0*(Y(J)-SF*(Y(J+1)+SF*(A+BP*(B+BP)*X(J+1))/2.
    CONTINUE
  15 CONTINUE
  Y(N-1)=L-SF*(Y(N-1)+SF*(A+BP*(B+BP)*X(N-1))
  RETURN
END

```

```

PDT 1
PDT 2
PDT 3
PDT 4
PDT 5
PDT 6
PDT 7
PDT 8
PDT 9
PDT 10
PDT 11
PDT 12
PDT 13
PDT 14
PDT 15
PDT 16
PDT 17
PDT 18
PDT 19
PDT 20
PDT 21
PDT 22
PDT 23

```

```

C=((-2.*A(3)+3.*A(4)+A(5)+A(2)+27.*A(4)+2*A(1))/(27.*A(4)+A(5))
TEST=C**2+4.*A(4)
IF (TEST) 5,15,15
5 IM=SQRT(ABS(TEST))/2.
RE=C-672.
RESORT(RE**2,IM**2)
THETAN(I)/RE)
IF (THETA) 10,30,30
10 THETA=THETA*PI
15 IF (C**2) 20,25,25
20 THETA=PI
R=N
GO TO 30
25 THETA=0.
30 R13=R**3/3.
DO 35 K=1,6,2
  T=THETA/3.-*(K-1)*PI/3.
  CT=COS(T)
  ST=SIN(T)
  UK1=R13*CT
  UK2=R13*ST
  V1=-H/(UK1**2+UK2**2)
  VIK=V1/UK1
  DO 40 K=1,6
    ZK=UK1+V(K)
    R=A13/(ZK**4)
    DO 45 I=1,6,2
      X(I)=Z(I)*I
      X(I)=Z(I)*R
  RETURN
END

```

```

SUBROUTINE POINT(X,Y,XINT,YINT,NM1,NM2,A)
  ROUTINE FOR PARABOLIC OR LINEAR INTERPOLATION, GIVEN X AND Y
  ARRAYS THE ROUTINE CALCULATES THE VALUE YINT AT THE GIVEN VALUE
  XINT. IT ALSO RETURNS THE COEFFICIENTS OF THE FIT IN ARRAY A.
  IMPORTANT NOTE: THE X ARRAY MUST BE MONOTONIC INCREASING.
  REAL*8 A2,A3,A
  DIMENSION X(NM2),Y(NM2),A(4)
  NP=NM2-NM1+1
  IF (NP-2) 55,60,5
  DO 10 I=NM1,NM2
    KK=I
    IF (XINT-X(I)) 15,25,10
  10 CONTINUE
  15 XX=KK-K-1*(X(KK)-X(KK-1))/2.
  IF (XINT-XX) 20,25,25
  20 KK=KK-1
  IF (KK.LT.NM1) KK=NM1
  A(4)=KK
  N2=KK-1
  IF (N2=NM1) 30,30,35
  30 N2=NM1
  GO TO 45

```

```

85 I1(L1)=1
RETURN
END

SUBROUTINE SIMSOLB(M,IERR)
ROUTINE SOLVES THE LINEAR SIMULTANEOUS EQUATION AX=B IN M UNKNOWN'S
AND RETURNS THE SOLUTIONS IN B
COMMON /CDEF/AL(65,65)
DIMENSION B(65)
CHECK FOR SINGULARITY
DO 55 J=1,M
  JJ=J+1
  IF (AL(J,J)) 35,5,35
  5 IF (J-M) 10,20,20
  10 DO 15 I=J+M
  IF (AL(I,J)) 25,15,25
  15 CONTINUE
  20 IERR=1
RETURN
C*** AIJ-J = 0 INTERCHANGE ROWS
25 DO 30 L=J,M
  T=AIJ(L)
  AIJ(L)=AI(I,L)
  30 AI(L)=T
  T=B(I)
  B(I)=B(L)
  35 DO 40 K=J,M
  40 AIJ(K)=AI(K,J)+T
C*** GET AI(I,J) = 0. I=1,.....,J-1,J+1,.....,M
DO 55 I=1,M
  IF (I-J) 45,55,45
  45 T=AI(I,J)
  50 AI(I,K)=AI(I,K)-T*AI(J,K)
  B(I)=B(I)-T*B(J)
  55 CONTINUE
RETURN
END

```

```

FTL 1
FTL 2
FTL 3
FTL 4
FTL 5
FTL 6
FTL 7
FTL 8
FTL 9
FTL 10
FTL 11
FTL 12
FTL 13
FTL 14
FTL 15
FTL 16
FTL 17
FTL 18
FTL 19
FTL 20
FTL 21
FTL 22
FTL 23
FTL 24
FTL 25
FTL 26
FTL 27
FTL 28
FTL 29
FTL 30
FTL 31
FTL 32
FTL 33
FTL 34
FTL 35
FTL 36
FTL 37
FTL 38
FTL 39
FTL 40
FTL 41
FTL 42
FTL 43
FTL 44
FTL 45
FTL 46
FTL 47
FTL 48
FTL 49
FTL 50
FTL 51
FTL 52
FTL 53
FTL 54
FTL 55
FTL 56
FTL 57

SUBROUTINE FTFLUP(X,M,N,VARI,VARD)
ROUTINE FOR LINEAR OR PARABOLIC INTERPOLATION. IT CALCULATES THE
VALUE Y AT POINT X (INDEPENDENT) FROM ARRAYS WARI (INDEPENDENT)
AND VARD. N IS THE NUMBER OF POINTS IN THE WARI ARRAYS.
PARABOLIC INTERPOLATION WHILE M=2 GIVES A LINEAR INTERPOLATION.
COMMON /PROD/JREAR,JBRITE
DIMENSION WARI(1,13)
DATA I1(4),I2(3),I3(2)
M=INT(M)
N=INT(N)
M=ABS(M)
L1=1
I=I1(L1)
IF (I.EQ.0 OR M.LT.2) GO TO 35
IF (VARI(I2)-VARI(I1)) 15,15,25
5 R=VARI(I)
S=VARD(I)
WRITE (JBRITE,10) R,S,(VARI(I),J=1,M),(VARD(J),J=1,M)
10 FORMAT (1H1,52HOTABLE BELOW OUT OF ORDER FOR FTFLUP AT ELEMENT VARI
1,(I3,4H) = ,G15.8,6H VARD(,I3,4H) = ,G15.8,/(8C15.8))
STOP
15 DO 20 J=2,M
IF (VARI(I2)-VARI(I1)) 20,5,5
20 CONTINUE
GO TO 35
25 DO 30 J=2,M
IF (VARI(I2)-VARI(I1)) 5,5,30
30 CONTINUE
35 IF (I.LE.0) I=1
IF (I.GE.N) I=M-1
IF (M.LE.1) GO TO 40
IF (M.EQ.0) GO TO 45
40 T=VARD(I)
GO TO 65
45 U=VARD(I1)
50 T=SIGM(I1)*(VARI(I1)-VARI(I1))+(X-VARI(I1))
55 IF (I=1) I.E. 0) GO TO 60
IF (I=I1) I.E. N) GO TO 60
I=I+1
IF (VARI(I1)-X)+(VARI(I1)-X) 60,60,55
60 IF (M.EQ.2) GO TO 65
V=(VARD(I1)+(VARI(I1)-X)-(VARD(I1)+X))/(VARI(I1)-VARI(I1)
)
GO TO 85
65 IF (M.EQ.2) GO TO 5
IF (I.EQ.(M-1)) GO TO 75
IF (I.EQ.1) GO TO 70
Sk=VARI(I1)-VARI(I1)
IF ((Sk*(X-VARI(I1)))-LT.(Sk*(VARI(I2)-X))) GO TO 75
70 L=1
GO TO 80
75 L=L+1
80 V(L)=VARI(I1)-X
V(L2)=VARI(I1)+X
V(L3)=VARI(I1)+X
V(L4)=VARD(I1)+V(L2)-VARD(L1)+V(L3)-VARD(L2)+V(L4)-VARD(L1)
V(L5)=VARD(L1)+V(L3)-VARD(L2)+V(L4)-VARD(L1)
V(L6)=VARD(L1)+V(L3)-VARD(L2)+V(L4)-VARD(L1)

```

```

58
FTL 59
FTL 60
SIM 1
SIM 2
SIM 3
SIM 4
SIM 5
SIM 6
SIM 7
SIM 8
SIM 9
SIM 10
SIM 11
SIM 12
SIM 13
SIM 14
SIM 15
SIM 16
SIM 17
SIM 18
SIM 19
SIM 20
SIM 21
SIM 22
SIM 23
SIM 24
SIM 25
SIM 26
SIM 27
SIM 28
SIM 29
SIM 30
SIM 31
SIM 32
SIM 33
SIM 34
SIM 35
SIM 36
SIM 37
SIM 38

```

# Sample Output

```

***** CASE INPUT *****
NACA 23012 AIRFOIL/ALPHA=0/RN=3.0/MACH NO.=0.2/IWRITE=0
NHU  NHX  IWRITE  IALPHA  IPUNCH
10  11  0          0          0
XU = 0.0      0.125000E-01 0.250000E-01 0.500000E-01 0.750000E-01 0.100000E 00 0.150000E 00 0.200000E 00
0.250000E 00 0.300000E 00 0.400000E 00 0.500000E 00 0.600000E 00 0.700000E 00 0.800000E 00 0.900000E 00
0.950000E 00 0.100000E 01
ZU = 0.0      0.247000E-01 0.361000E-01 0.491000E-01 0.580000E-01 0.642999E-01 0.719000E-01 0.750000E-01
0.740000E-01 0.750000E-01 0.714000E-01 0.614000E-01 0.547000E-01 0.456000E-01 0.308000E-01 0.189000E-01
0.420000E-02 0.130000E-02
XL = 0.0      0.125000E-01 0.250000E-01 0.500000E-01 0.750000E-01 0.100000E 00 0.150000E 00 0.200000E 00
0.250000E 00 0.300000E 00 0.400000E 00 0.500000E 00 0.600000E 00 0.700000E 00 0.800000E 00 0.900000E 00
0.950000E 00 0.100000E 01
ZL = 0.0      -0.123000E-01 -0.171000E-01 -0.224000E-01 -0.241000E-01 -0.242000E-01 -0.230000E-01 -0.216000E-01 -0.197000E-01
-0.428000E-01 -0.448000E-01 -0.448000E-01 -0.417000E-01 -0.367000E-01 -0.300000E-01 -0.216000E-01 -0.123000E-01
-0.700000E-02 -0.130000E-02
NA = 1  ANGLES OF ATTACK W.R.T. REFERENCE LINE (IALPHA=C) OR W.R.T. LONGEST CHORDLINE (IALPHA=1)
0.0
NM = 1  FSNACH = 0.200000E 00
CREP = 0.100000E 01  SF = 0.100000E 01  TO = 0.518690E 03  RN = 0.300000E 01  PR = 0.770000E 00  RF = 0.100000E 01
LTRAN  XTRAN  ZTRAN
UPPER SURFACE  0  0.0  0.0
LOWER SURFACE  0  0.0  0.0

NACA 23012 AIRFOIL/ALPHA=0/RN=3.0/MACH NO.=0.2/IWRITE=0
INPUT AIRFOIL POINTS
UPPER SURFACE  LOWER SURFACE
XU  ZU  XL  ZL
0.0  0.0  0.0  0.0
0.012500  0.024700  0.012500  -0.012300
0.025000  0.036100  0.025000  -0.017100
0.037500  0.049100  0.050000  -0.022600
0.050000  0.058000  0.075000  -0.026100
0.075000  0.064300  0.100000  -0.029200
0.100000  0.071900  0.150000  -0.033500
0.150000  0.074000  0.200000  -0.039700
0.200000  0.075000  0.250000  -0.042800
0.250000  0.075500  0.300000  -0.044600
0.300000  0.071400  0.400000  -0.044800
0.400000  0.041400  0.500000  -0.041700
0.400000  0.054700  0.600000  -0.036700
0.700000  0.043600  0.700000  -0.030000
0.800000  0.030800  0.800000  -0.021600
0.900000  0.016800  0.900000  -0.012300
0.950000  0.009200  0.950000  -0.007000
1.000000  0.001300  1.000000  -0.001300

NACA 23012 AIRFOIL/ALPHA=0/RN=3.0/MACH NO.=0.2/IWRITE=0
DISTRIBUTED AIRFOIL POINTS
UPPER SURFACE  LOWER SURFACE
XU  ZU  XL  ZL
0.001562  0.004283  0.999994  -0.001301
0.005084  0.012968  0.995937  -0.004610
0.011934  0.025865  0.907505  -0.011530
0.024014  0.035987  0.860744  -0.016157
0.039488  0.044376  0.812696  -0.020469
0.057324  0.052210  0.764640  -0.024471
0.077592  0.058774  0.715153  -0.028836
0.099321  0.064163  0.671088  -0.032112
0.122524  0.068949  0.632349  -0.034717
0.147233  0.071997  0.592982  -0.037186
0.173675  0.073929  0.554524  -0.039185
0.202774  0.075110  0.517126  -0.040978
0.234705  0.075893  0.480190  -0.042645
0.268279  0.075991  0.444215  -0.043836
0.303436  0.075427  0.408438  -0.044466
0.338303  0.074418  0.373269  -0.045190
0.373269  0.072901  0.338303  -0.045212
0.408438  0.070786  0.303436  -0.044482
0.444215  0.067706  0.268279  -0.043609
0.480190  0.063119  0.234705  -0.041990
0.517126  0.060018  0.202774  -0.039914
0.554524  0.058292  0.173675  -0.037363
0.592982  0.055314  0.147233  -0.034708
0.632349  0.051589  0.122524  -0.031879
0.671088  0.046984  0.099321  -0.029121
0.715153  0.041770  0.077592  -0.026440
0.764640  0.035461  0.057524  -0.023864
0.812696  0.029089  0.039488  -0.020993
0.860744  0.022487  0.024014  -0.016994
0.907505  0.015678  0.011934  -0.011905
0.953537  0.008651  0.005084  -0.005908
0.999994  0.001562  0.001562  -0.001948
0.0  0.0

```

Figure A-3. Sample output of the 2-D characteristics program with IWRITE=0 (note that only upper surface inviscid and boundary layer solution information is shown here).

INVISCID FLOW SOLUTION  
 NACA 23012 AIRFOIL/ $\alpha=0^\circ/\text{RN}=3.0/\text{MACH NO.}=0.2/\text{WRITE}=0$   
 MACH NUMBER = 0.20000 ANGLE OF ATTACK = 0.0 DEG.

UPPER SURFACE					
ITERATION NUMBER 0					
X	Z	UV/VOIINC.	UV/VOICONPR.	ML	CP
0.00156	0.00420	0.04319	0.04275	0.00682	1.00014
0.00508	0.01295	0.44200	0.45836	0.09138	0.79618
0.01193	0.02586	0.84240	0.83989	0.16778	0.29543
0.02461	0.03956	1.09424	1.09647	0.21967	-0.20184
0.03949	0.04450	1.18249	1.18739	0.23786	-0.40015
0.05752	0.05221	1.23555	1.24229	0.24900	-0.54034
0.07795	0.05677	1.26977	1.27784	0.25422	-0.62087
0.09932	0.05816	1.28923	1.29810	0.26033	-0.68036
0.12252	0.05855	1.29938	1.30346	0.26142	-0.72413
0.14723	0.07160	1.28650	1.29473	0.25965	-0.75177
0.17368	0.07393	1.26901	1.27704	0.25606	-0.76286
0.20277	0.07511	1.24493	1.25203	0.25098	-0.75636
0.23471	0.07585	1.22385	1.23223	0.24696	-0.74157
0.26828	0.07595	1.21233	1.21823	0.24412	-0.72043
0.30344	0.07543	1.19901	1.20444	0.24132	-0.69413
0.33932	0.07416	1.18387	1.19390	0.23920	-0.66440
0.37527	0.07290	1.16794	1.18179	0.23779	-0.63207
0.40944	0.07078	1.17445	1.17906	0.23618	-0.59867
0.44421	0.06771	1.14380	1.14745	0.22978	-0.56561
0.47919	0.06412	1.09372	1.09564	0.21936	-0.50949
0.51373	0.06002	1.02252	1.02444	0.21704	-0.44173
0.54852	0.05829	1.10649	1.10904	0.22201	-0.36293
0.58298	0.05531	1.11455	1.11732	0.22369	-0.28777
0.61727	0.05155	1.10234	1.10479	0.22115	-0.22007
0.65109	0.04698	1.02224	1.02415	0.21698	-0.17507
0.68515	0.04177	1.06417	1.06563	0.21324	-0.13938
0.71848	0.03546	1.04739	1.04844	0.20977	-0.09911
0.75176	0.02908	1.02870	1.02932	0.20591	-0.05949
0.78474	0.02249	1.00898	1.00917	0.20185	-0.01841
0.81751	0.01568	0.98317	0.98263	0.19654	0.03399
0.85054	0.00865	0.94344	0.94230	0.18839	0.11199
0.88399	0.00130	0.92171	0.92028	0.18394	0.15330

LAMINAR BOUNDARY LAYER SUMMARY  
 NACA 23012 AIRFOIL/ $\alpha=0^\circ/\text{RN}=3.0/\text{MACH NO.}=0.2/\text{WRITE}=0$   
 UPPER SURFACE  
 ITERATION NUMBER 0

STAGNATION TEMPERATURE = 518.69 DEGREES RANKINE STAGNATION PRESSURE = 4478.688 LB/SQ FT  
 FREESTREAM MACH NUMBER = 0.20000 AIRFOIL CHORD = 1.00000 FT  
 REYNOLDS NUMBER = 3.00000 MILLION PRANDTL NUMBER = 0.77000  
 HEAT TRANSFER FACTOR K = 1.00000 SEPARATION CORRELATION NO. = 0.049637  
 SPEED OF SOUND = 1114.419 FEET/SECOND KINEMATIC VISCOSITY = 0.0000743 SQ FT/SEC  
 ANGLE OF ATTACK (ALPHA) = 0.0 DEGREES STAGNATION AT X/C = 0.0013655

X/C	S/C	H	DM/DIS/C	H	THETA/C	DELS/C	DELTAS/C	CP	CP
0.001362	0.000697	0.008516	11.982385	2.500737	0.000017	0.000063	0.000003	1.00014	0.000003
0.005080	0.010090	0.041384	7.442142	2.506800	0.000022	0.000055	0.000006	0.79618	0.000006
0.011934	0.024471	0.167739	4.240956	2.499599	0.000026	0.000064	0.000007	0.29543	0.000007
0.024614	0.040430	0.219472	2.224568	2.489263	0.000029	0.000069	0.000008	0.000001	0.000008
0.039490	0.050127	0.237043	0.813860	2.464534	0.000039	0.000096	0.000010	-0.40015	0.000010
0.057524	0.077711	0.249800	0.459911	2.442024	0.000047	0.000117	0.000011	-0.54034	0.000011
0.077952	0.090829	0.254217	0.285159	2.437791	0.000056	0.000137	0.000013	-0.62087	0.000013
0.099321	0.121212	0.260333	0.116874	2.448259	0.000064	0.000157	0.000015	-0.68036	0.000015
0.122524	0.144825	0.261424	-0.010993	2.431297	0.000073	0.000178	0.000018	-0.72413	0.000018
0.147233	0.169721	0.259698	-0.103307	2.409275	0.000084	0.000202	0.000020	-0.75177	0.000020
0.173678	0.194265	0.254056	-0.193993	2.385263	0.000096	0.000229	0.000022	-0.76286	0.000022
0.202774	0.225388	0.250977	-0.151215	2.369837	0.000110	0.000261	0.000026	-0.75636	0.000026
0.234709	0.257327	0.246959	-0.105716	2.375357	0.000123	0.000293	0.000029	-0.74157	0.000029
0.268279	0.290980	0.244118	-0.082107	2.377635	0.000134	0.000322	0.000034	-0.72043	0.000034

SCRIT/C = 0.11799729 RECRIT = 456.51 STRAN/C = 0.2850159 RTRAN = 920.40 THETA1/C = 0.0001359  
 INSTABILITY TRANSITION HAS OCCURRED AT X/C = 0.262390 S/C = 0.285012

TURBULENT BOUNDARY LAYER SUMMARY FOR EQUIVALENT AIRFOIL (GORADIA METHOD)  
 NACA 23012 AIRFOIL/ $\alpha=0^\circ/\text{RN}=3.0/\text{MACH NO.}=0.2/\text{WRITE}=0$   
 UPPER SURFACE  
 ITERATION NUMBER 0

STAGNATION TEMPERATURE = 518.69 DEGREES RANKINE STAGNATION PRESSURE = 4478.688 LB/SQ FT  
 FREESTREAM MACH NUMBER = 0.20000 AIRFOIL CHORD = 1.00000 FT  
 REYNOLDS NUMBER = 3.00000 MILLION PRANDTL NUMBER = 0.77000  
 HEAT TRANSFER FACTOR K = 1.00000 TRANSLATION POINT, S/C = 0.26501  
 INITIAL MOMENTUM THICKNESS/ $\delta^*$  = 0.00013 INIT. INCOMP. FORM FACTOR = 1.35474  
 ANGLE OF ATTACK (ALPHA) = 0.0 DEGREES

X/C	S/C	H	DM/DIS/C	H	THETA/C	DELS/C	DELTAS/C	CP	CP
0.262390	0.289012	0.244684	-0.082987	1.354743	0.000134	0.000181	0.000128	0.006670	-0.461733
0.268279	0.290980	0.244118	-0.082107	1.366482	0.000147	0.000201	0.001298	0.004584	-0.448644
0.303463	0.326661	0.241324	-0.070153	1.532023	0.000226	0.000346	0.001644	0.001596	-0.423725
0.373269	0.360943	0.239199	-0.051209	1.617521	0.000300	0.000449	0.002097	0.001945	-0.406886
0.408438	0.395942	0.237747	-0.042940	1.515099	0.000371	0.000563	0.002747	0.001945	-0.388667
0.443415	0.431179	0.236181	-0.110713	1.391617	0.000443	0.000616	0.003764	0.001945	-0.368647
0.478392	0.467083	0.234701	-0.232464	1.370185	0.000547	0.000749	0.004798	0.001945	-0.346267
0.513369	0.503399	0.213344	-0.176170	1.369901	0.000645	0.000944	0.006191	0.001945	-0.320672
0.548346	0.540415	0.217041	0.034563	1.332398	0.000781	0.001040	0.007297	0.001945	-0.292680
0.583323	0.577952	0.222012	0.089749	1.311459	0.000788	0.001033	0.007670	0.001945	-0.262933
0.618300	0.616426	0.212864	-0.009642	1.305990	0.000832	0.001086	0.008206	0.001945	-0.232772
0.653277	0.655988	0.221132	-0.005451	1.308728	0.000926	0.001210	0.009098	0.001945	-0.202607
0.688254	0.694979	0.216982	-0.096342	1.308531	0.001044	0.001344	0.010221	0.001945	-0.172505
0.723231	0.734951	0.213241	-0.077358	1.307171	0.001171	0.001531	0.011485	0.001945	-0.142403
0.758208	0.774923	0.209500	-0.074661	1.306560	0.001308	0.001719	0.012862	0.001945	-0.112301
0.793185	0.817714	0.205759	-0.081703	1.307045	0.001459	0.001907	0.014324	0.001945	-0.082199
0.828162	0.864213	0.202018	-0.092553	1.310473	0.001623	0.002127	0.015830	0.001945	-0.052097
0.863139	0.913468	0.198277	-0.143903	1.322367	0.001831	0.002421	0.017443	0.001945	-0.021995
0.898116	0.965033	0.194536	-0.194970	1.334883	0.002132	0.002872	0.019228	0.001945	0.111999
0.933093	1.022067	0.190794	-0.054105	1.348401	0.002381	0.003211	0.021643	0.001945	0.153303

Figure A-3. Continued.

LOAD SUMMARY SHEET--ITERATION NUMBER 0

NACA 23012 AIRFOIL/ALPHA=0/RN=3.0/MACH NO.=0.2/ITERATE=0

MACH NUMBER = 0.20000 REFERENCE CHORD (BASIS FOR ALL COEFFICIENT NORMALIZATION) = 1.00000 FT.  
 REYNOLDS NO. = 3.00000 MILLION ANGLE OF ATTACK (VALUE OF ALPHA = 0) = 0.0 DEG.  
 LONGEST CHORDLINE = 1.00000 FEET (ALPHA=0--ANGLE DEFINED W.R.T. REFERENCE LINE)  
 (ALPHA=1--ANGLE DEFINED W.R.T. LONGEST CHORDLINE)

ANGLE BETWEEN LONGEST CHORDLINE AND REFERENCE LINE = 0.0 DEG. (POSITIVE FOR REFERENCE LINE BELOW THE LONGEST CHORDLINE)

NORMAL FORCE COEFFICIENTS  
 (CN)PRESS. = 0.13344  
 (CN)SHEAR = -0.00003  
 CN = 0.13341

AXIAL FORCE COEFFICIENTS  
 (CA)PRESS. = 0.0  
 (CA)SHEAR = 0.00374  
 CA = 0.00374

MOMENT COEFFICIENTS  
 (ABOUT NOSE) (CM)PRESS. = -0.04252  
 (CM)SHEAR = 0.00015  
 CM = -0.04237

LIFT COEFFICIENTS  
 (CL)PRESS. = 0.13344  
 (CL)SHEAR = -0.00003  
 CL = 0.13341

DRAG COEFFICIENTS  
 (CD)PRESS. = 0.0  
 (CD)SHEAR = 0.00374  
 CD = 0.00374

MOMENT COEFFICIENTS  
 (CM)ABOUT NOSE = -0.04237  
 (CM)QUARTER CHORD = -0.00902

DRAG COEFFICIENT COMPUTED BY SQUIRE-YOUNG FORMULA = 0.00637  
 ZEROETH ITERATION PRESSURE DRAG = 0.00194  
 TRANSITION POINTS: X/(LOWER) = 0.39225 X/(UPPER) = 0.26239

LAMINAR BOUNDARY LAYER SUMMARY

NACA 23012 AIRFOIL/ALPHA=0/RN=3.0/MACH NO.=0.2/ITERATE=0

UPPER SURFACE  
 ITERATION NUMBER 4

STAGNATION TEMPERATURE = 518.69 DEGREES RANKINE STAGNATION PRESSURE = 4478.688 LB/SQ FT  
 FREESTREAM MACH NUMBER = 0.20000 AIRFOIL CHORD = 1.00000 FT  
 REYNOLDS NUMBER = 3.00000 MILLION PRANDTL NUMBER = 0.77000  
 HEAT TRANSFER FACTOR K = 1.00000 SEPARATION CORRELATION NO. = 0.049637  
 SPEED OF SOUND = 1116.419 FEET/SECOND KINEMATIC VISCOSITY = 0.000743 SQ FT/SEC  
 ANGLE OF ATTACK (ALPHA) = 0.0 DEGREES  
 STAGNATION AT X/C = 0.0013330 STAGNATION AT Z/C = 0.0037539

X/C	S/C	H	DN/D(S/C)	H	THETA/C	DELS/C	DELTA S/C	CF	CP
0.001562	0.000570	0.006945	11.988713	2.500720	0.000017	0.000043	-0.000002	1.00075	
0.005084	0.003923	0.040079	7.458247	2.506625	0.000022	0.000055	0.000943	0.80221	
0.011934	0.024544	0.164428	4.240575	2.496690	0.000024	0.000064	0.002726	0.30671	
0.024014	0.040303	0.218224	2.232097	2.480362	0.000029	0.000073	0.004725	-0.18838	
0.039488	0.058001	0.236769	0.822852	2.464285	0.000039	0.000096	0.004079	-0.39545	
0.057524	0.077584	0.248006	0.483543	2.461936	0.000047	0.000117	0.003690	-0.52832	
0.077592	0.098694	0.252523	0.267674	2.457661	0.000056	0.000137	0.003289	-0.61729	
0.099321	0.121085	0.259439	0.118551	2.448127	0.000064	0.000157	0.002800	-0.664913	
0.122524	0.144698	0.260567	-0.009007	2.431306	0.000073	0.000178	0.002191	-0.68332	
0.147233	0.169594	0.258853	-0.099894	2.409523	0.000084	0.000202	0.001541	-0.66176	
0.173675	0.194138	0.255324	-0.192524	2.385482	0.000095	0.000229	0.000937	-0.61179	
0.202774	0.225261	0.250257	-0.153313	2.368759	0.000110	0.000260	0.000351	-0.55559	
0.234705	0.257200	0.246084	-0.111010	2.372191	0.000124	0.000293	0.000323	-0.50521	
0.268279	0.290773	0.243049	-0.083411	2.376044	0.000136	0.000323	0.000517	-0.46903	

SCRIT/C = 0.11828900 RECRIT = 456.30 STRAN/C = 0.26427839 RTRAN = 919.04 THETA1/C = 0.00013387  
 INSTABILITY TRANSITION HAS OCCURRED AT X/C = 0.261784 S/C = 0.284278

TURBULENT BOUNDARY LAYER SUMMARY FOR EQUIVALENT AIRFOIL (GORADIA METHOD)

NACA 23012 AIRFOIL/ALPHA=0/RN=3.0/MACH NO.=0.2/ITERATE=0

UPPER SURFACE  
 ITERATION NUMBER 4

STAGNATION TEMPERATURE = 518.69 DEGREES RANKINE STAGNATION PRESSURE = 4478.688 LB/SQ FT  
 FREESTREAM MACH NUMBER = 0.20000 AIRFOIL CHORD = 1.00000 FT  
 REYNOLDS NUMBER = 3.00000 MILLION PRANDTL NUMBER = 0.77000  
 HEAT TRANSFER FACTOR K = 1.00000 TRANSITION POINT, S/C = 0.28428  
 (INITIAL MOMENTUM THICKNESS)/C = 0.0013 ANGLE OF ATTACK (ALPHA) = 0.0 DEGREES  
 (INIT. INCOMP. FDM FACTOR = 1.35291)

X/C	S/C	H	DN/D(S/C)	H	THETA/C	DELS/C	DELTA S/C	CF	CP
0.261784	0.284278	0.243600	-0.086115	1.352907	0.000134	0.000181	0.001314	0.006604	-0.469033
0.268279	0.290773	0.243049	-0.083411	1.345986	0.000149	0.000203	0.001602	0.004902	-0.437479
0.303434	0.325934	0.223734	-0.063882	1.326860	0.000227	0.000347	0.001662	0.004502	-0.437479
0.338303	0.360816	0.238560	-0.043746	1.611190	0.000301	0.000484	0.002069	0.003615	-0.416360
0.373249	0.395815	0.237319	-0.039436	1.511736	0.000371	0.000561	0.002752	0.003954	-0.401831
0.408438	0.431067	0.235867	-0.106623	1.390843	0.000442	0.000615	0.003761	0.004509	-0.385038
0.444215	0.466956	0.229644	-0.227090	1.369104	0.000545	0.000746	0.004787	0.004214	-0.314093
0.480190	0.503222	0.219438	-0.171304	1.359771	0.000691	0.000940	0.006165	0.003712	-0.201474
0.517126	0.540288	0.211125	0.031501	1.332047	0.000776	0.001034	0.007269	0.003690	-0.176594
0.554924	0.577725	0.221856	0.082490	1.311176	0.000786	0.001032	0.007650	0.003958	-0.227728
0.593462	0.616299	0.223110	-0.012178	1.305539	0.000833	0.001080	0.008206	0.003959	-0.243649
0.632349	0.655861	0.220756	-0.084437	1.306490	0.000877	0.001122	0.009105	0.003764	-0.215750
0.671088	0.696452	0.216700	-0.082814	1.308351	0.001044	0.001365	0.010222	0.003525	-0.172051
0.710153	0.738224	0.213149	-0.072805	1.306945	0.001188	0.001526	0.011469	0.003332	-0.134391
0.749440	0.781131	0.208921	-0.069186	1.305591	0.001301	0.001698	0.012819	0.003162	-0.100683
0.812694	0.837587	0.204355	-0.075554	1.305115	0.001444	0.001885	0.014243	0.002986	-0.065975
0.860744	0.886086	0.202594	-0.092798	1.307891	0.001601	0.002094	0.015694	0.002802	-0.025907
0.907589	0.935361	0.197507	-0.137808	1.318851	0.001800	0.002376	0.017275	0.002556	0.024557
0.953537	0.985904	0.189549	-0.132586	1.330118	0.002125	0.002800	0.019253	0.002345	0.099625
0.999444	1.026940	0.185130	-0.081677	1.342957	0.002334	0.003135	0.021416	0.002053	0.142362

Figure A-3. Continued.





TURBULENT BOUNDARY LAYER SUMMARY FOR EQUIVALENT AIRFOIL (GORADIA METHOD)

NACA 23012 AIRFOIL/ALPHA=0/RN=3.0/MACH NO.=0.2/ITER=1

UPPER SURFACE  
ITERATION NUMBER 6

STAGNATION TEMPERATURE = 510.49 DEGREES RANKINE		STAGNATION PRESSURE = 4470.400 LB/50 FT							
FORESTREAM MACH NUMBER = 0.20000		AIRFOIL CHORD = 1.00000 FT							
REYNOLDS NUMBER = 1.00000 MILLION		PRANDTL NUMBER = 0.77000							
HEAT TRANSFER FACTOR K = 1.00000		TRANSITION POINT, S/C = 0.20420							
INITIAL MOMENTUM THICKNESS/S/C = 0.0010		INIT. INCOMP. FORM FACTOR = 1.35291							
ANGLE OF ATTACK (ALPHA) = 0.0 DEGREES									
X/C	S/C	H	DM/D(S/C)	H	THETA/C	DELS/C	DELTA S/C	CP	CP
0.201784	0.201784	0.243600	-0.000115	1.352907	0.000134	0.000181	0.001314	0.000604	-0.449083
0.202775	0.202775	0.243049	-0.000411	1.345986	0.000189	0.000203	0.001462	0.000502	-0.437479
0.203830	0.203830	0.242376	-0.000882	1.320840	0.000227	0.000347	0.001642	0.000365	-0.416360
0.204933	0.204933	0.241560	-0.001484	1.271150	0.000281	0.000464	0.001850	0.000214	-0.385821
0.206093	0.206093	0.240600	-0.002254	1.191736	0.000371	0.000591	0.002082	0.000079	-0.346928
0.207317	0.207317	0.239500	-0.003237	1.090042	0.000442	0.000619	0.002336	0.000000	-0.299828
0.208603	0.208603	0.238176	-0.004463	1.000000	0.000494	0.000646	0.002600	0.000000	-0.245400
0.209950	0.209950	0.236630	-0.005960	0.925000	0.000528	0.000664	0.002870	0.000000	-0.184400
0.211360	0.211360	0.234870	-0.007760	0.865000	0.000544	0.000674	0.003140	0.000000	-0.118000
0.212830	0.212830	0.232900	-0.009900	0.815000	0.000544	0.000674	0.003410	0.000000	-0.048000
0.214360	0.214360	0.230730	-0.012400	0.775000	0.000528	0.000664	0.003680	0.000000	0.024000
0.215950	0.215950	0.228370	-0.015280	0.740000	0.000500	0.000646	0.003950	0.000000	0.094000
0.217600	0.217600	0.225830	-0.018460	0.710000	0.000464	0.000619	0.004220	0.000000	0.158000
0.219310	0.219310	0.223130	-0.021860	0.685000	0.000428	0.000591	0.004490	0.000000	0.212000
0.221080	0.221080	0.220280	-0.025400	0.665000	0.000395	0.000564	0.004760	0.000000	0.252000
0.222910	0.222910	0.217290	-0.029000	0.645000	0.000359	0.000537	0.005030	0.000000	0.278000
0.224800	0.224800	0.214170	-0.032600	0.630000	0.000323	0.000510	0.005300	0.000000	0.294000
0.226750	0.226750	0.210930	-0.036200	0.615000	0.000287	0.000483	0.005570	0.000000	0.298000
0.228760	0.228760	0.207580	-0.039800	0.605000	0.000251	0.000456	0.005840	0.000000	0.288000
0.230830	0.230830	0.204130	-0.043400	0.595000	0.000215	0.000429	0.006110	0.000000	0.268000
0.232960	0.232960	0.200590	-0.047000	0.585000	0.000179	0.000402	0.006380	0.000000	0.238000
0.235150	0.235150	0.196970	-0.050600	0.575000	0.000143	0.000375	0.006650	0.000000	0.198000
0.237400	0.237400	0.193270	-0.054200	0.565000	0.000107	0.000348	0.006920	0.000000	0.148000
0.239710	0.239710	0.189500	-0.057800	0.555000	0.000071	0.000321	0.007190	0.000000	0.088000
0.242080	0.242080	0.185670	-0.061400	0.545000	0.000035	0.000294	0.007460	0.000000	0.018000
0.244510	0.244510	0.181780	-0.065000	0.535000	0.000000	0.000267	0.007730	0.000000	-0.052000
0.247000	0.247000	0.177840	-0.068600	0.525000	0.000000	0.000240	0.008000	0.000000	-0.122000
0.249550	0.249550	0.173860	-0.072200	0.515000	0.000000	0.000213	0.008270	0.000000	-0.182000
0.252160	0.252160	0.169840	-0.075800	0.505000	0.000000	0.000186	0.008540	0.000000	-0.232000
0.254830	0.254830	0.165780	-0.079400	0.495000	0.000000	0.000159	0.008810	0.000000	-0.272000
0.257560	0.257560	0.161690	-0.083000	0.485000	0.000000	0.000132	0.009080	0.000000	-0.298000
0.260350	0.260350	0.157570	-0.086600	0.475000	0.000000	0.000105	0.009350	0.000000	-0.312000
0.263200	0.263200	0.153430	-0.090200	0.465000	0.000000	0.000078	0.009620	0.000000	-0.312000
0.266110	0.266110	0.149270	-0.093800	0.455000	0.000000	0.000051	0.009890	0.000000	-0.298000
0.269080	0.269080	0.145090	-0.097400	0.445000	0.000000	0.000024	0.010160	0.000000	-0.272000
0.272110	0.272110	0.140890	-0.101000	0.435000	0.000000	0.000000	0.010430	0.000000	-0.232000
0.275200	0.275200	0.136670	-0.104600	0.425000	0.000000	0.000000	0.010700	0.000000	-0.178000
0.278350	0.278350	0.132430	-0.108200	0.415000	0.000000	0.000000	0.010970	0.000000	-0.112000
0.281560	0.281560	0.128170	-0.111800	0.405000	0.000000	0.000000	0.011240	0.000000	-0.032000
0.284830	0.284830	0.123890	-0.115400	0.395000	0.000000	0.000000	0.011510	0.000000	0.052000
0.288160	0.288160	0.119590	-0.119000	0.385000	0.000000	0.000000	0.011780	0.000000	0.122000
0.291550	0.291550	0.115270	-0.122600	0.375000	0.000000	0.000000	0.012050	0.000000	0.182000
0.295000	0.295000	0.110930	-0.126200	0.365000	0.000000	0.000000	0.012320	0.000000	0.232000
0.298510	0.298510	0.106570	-0.129800	0.355000	0.000000	0.000000	0.012590	0.000000	0.272000
0.302080	0.302080	0.102190	-0.133400	0.345000	0.000000	0.000000	0.012860	0.000000	0.298000
0.305710	0.305710	0.097790	-0.137000	0.335000	0.000000	0.000000	0.013130	0.000000	0.312000
0.309400	0.309400	0.093370	-0.140600	0.325000	0.000000	0.000000	0.013400	0.000000	0.312000
0.313150	0.313150	0.088930	-0.144200	0.315000	0.000000	0.000000	0.013670	0.000000	0.298000
0.316960	0.316960	0.084470	-0.147800	0.305000	0.000000	0.000000	0.013940	0.000000	0.272000
0.320830	0.320830	0.080000	-0.151400	0.295000	0.000000	0.000000	0.014210	0.000000	0.232000
0.324760	0.324760	0.075540	-0.155000	0.285000	0.000000	0.000000	0.014480	0.000000	0.178000
0.328750	0.328750	0.071080	-0.158600	0.275000	0.000000	0.000000	0.014750	0.000000	0.112000
0.332800	0.332800	0.066630	-0.162200	0.265000	0.000000	0.000000	0.015020	0.000000	0.032000
0.336910	0.336910	0.062190	-0.165800	0.255000	0.000000	0.000000	0.015290	0.000000	-0.048000
0.341080	0.341080	0.057760	-0.169400	0.245000	0.000000	0.000000	0.015560	0.000000	-0.118000
0.345310	0.345310	0.053340	-0.173000	0.235000	0.000000	0.000000	0.015830	0.000000	-0.182000
0.349600	0.349600	0.048930	-0.176600	0.225000	0.000000	0.000000	0.016100	0.000000	-0.232000
0.353950	0.353950	0.044530	-0.180200	0.215000	0.000000	0.000000	0.016370	0.000000	-0.272000
0.358360	0.358360	0.040140	-0.183800	0.205000	0.000000	0.000000	0.016640	0.000000	-0.298000
0.362830	0.362830	0.035760	-0.187400	0.195000	0.000000	0.000000	0.016910	0.000000	-0.312000
0.367360	0.367360	0.031390	-0.191000	0.185000	0.000000	0.000000	0.017180	0.000000	-0.312000
0.371950	0.371950	0.027030	-0.194600	0.175000	0.000000	0.000000	0.017450	0.000000	-0.298000
0.376600	0.376600	0.022680	-0.198200	0.165000	0.000000	0.000000	0.017720	0.000000	-0.272000
0.381310	0.381310	0.018340	-0.201800	0.155000	0.000000	0.000000	0.017990	0.000000	-0.232000
0.386080	0.386080	0.014010	-0.205400	0.145000	0.000000	0.000000	0.018260	0.000000	-0.178000
0.390910	0.390910	0.009690	-0.209000	0.135000	0.000000	0.000000	0.018530	0.000000	-0.112000
0.395800	0.395800	0.005380	-0.212600	0.125000	0.000000	0.000000	0.018800	0.000000	0.032000
0.400750	0.400750	0.001080	-0.216200	0.115000	0.000000	0.000000	0.019070	0.000000	0.092000
0.405760	0.405760	0.000000	-0.219800	0.105000	0.000000	0.000000	0.019340	0.000000	0.142000

LAMINAR BOUNDARY LAYER SUMMARY

NACA 23012 AIRFOIL/ALPHA=0/RN=3.0/MACH NO.=0.2/ITER=1

LOWER SURFACE  
ITERATION NUMBER 6

STAGNATION TEMPERATURE = 510.49 DEGREE RANKINE		STAGNATION PRESSURE = 4470.400 LB/50 FT							
FORESTREAM MACH NUMBER = 0.20000		AIRFOIL CHORD = 1.00000 FT							
REYNOLDS NUMBER = 1.00000 MILLION		PRANDTL NUMBER = 0.77000							
HEAT TRANSFER FACTOR K = 1.00000		SEPARATION CORRELATION NO. = 0.04047							
SPEED OF SOUND = 1114.419 FEET/SECOND		KINEMATIC VISCOSITY = 0.0000745 SQ FT/SEC							
ANGLE OF ATTACK (ALPHA) = 0.0 DEGREES		STAGNATION AT X/C = 0.0037539							
X/C	S/C	H	DM/D(S/C)	H	THETA/C	DELS/C	DELTA S/C	CP	CP
0.0	0.0037539	0.000177	25.227127	2.906629	0.000012	0.000030	0.001002	0.00170	
0.001562	0.000483	0.137352	20.029299	2.433303	0.000011	0.000020	0.000960	0.20173	
0.002904	0.011702	0.156437	0.929864	2.445904	0.000010	0.000007	0.000409	0.13081	
0.011930	0.022809	0.212044	2.678944	2.470644	0.000014	0.000004	0.000702	0.00702	
0.024811	0.023997	0.273964	3.390342	2.430220	0.000033	0.000004	0.000414	-0.34248	
0.039400	0.029609	0.280126	-0.311020	2.397600	0.000049	0.000009	0.000104	-0.21952	
0.057024	0.040230	0.222880	-0.339214	2.373723	0.000069	0.000013	0.000033	-0.23901	
0.077902	0.049071	0.213472	-0.312159	2.362360	0.000090	0.000021	0.000117	0.00104	
0.099321	0.110360	0.219446	-0.043394	2.413507	0.000069	0.000010	0.000009	-0.10091	
0.122324	0.133731	0.217034	0.005121	2.437544	0.000097	0.000024	0.000126	-0.17503	
0.147330	0.150601	0.210187	0.005767	2.447654	0.000103	0.000025	0.001137	-0.20850	
0.174370	0.105170	0.221447	0.043048	2.430796	0.000115	0.000020	0.001029	-0.24303	
0.202775	0.214387	0.224106	0.010309	2.427714	0.000123	0.000020	0.000904	-0.25240	
0.232400	0.244305	0.224106	0.010309	2.427714	0.000123	0.000020	0.000904	-0.25240	
0.263170	0.270								



LOAD SUMMARY SHEET--ITERATION NUMBER 4

NACA 23012 AIRFOIL/ALPHA=0/Re=3.0/RACH NO.=0.2/WRITE=1

RACH NUMBER = 0.20000 REFERENCE CHORD (BASIS FOR ALL COEFFICIENT NORMALIZATION) = 1.00000 FT.  
 REYNOLDS NO. = 3.00000 MILLION ANGLE OF ATTACK (VALUE OF ALPHA = 0) = 0.0 DEG.  
 LONGEST CHORDLINE = 1.00000 FEET (ALPHA=0--ANGLE DEFINED U.R.T. REFERENCE LINE)  
 (ALPHA=1--ANGLE DEFINED U.R.T. LONGEST CHORDLINE)

ANGLE BETWEEN LONGEST CHORDLINE AND REFERENCE LINE = 0.0 DEG. (POSITIVE FOR REFERENCE LINE BELOW THE LONGEST CHORDLINE)

NORMAL FORCE COEFFICIENTS  
 (CNI)PRESS. = 0.12541 (CL)PRESS. = 0.12541  
 (CNI)SHEAR = 0.00000 (CL)SHEAR = 0.00000  
 CN = 0.12536 CL = 0.12536

AXIAL FORCE COEFFICIENTS  
 (CAI)PRESS. = 0.00000 (COI)PRESS. = 0.00000  
 (CAI)SHEAR = 0.00000 (COI)SHEAR = 0.00000  
 CA = 0.00000 CO = 0.00000

MOMENT COEFFICIENTS  
 (CMI)PRESS. = -0.04000 (CMI)ABOUT NOSE = -0.03485  
 (CMI)SHEAR = 0.00000 (CMI)QUARTER CHORD = -0.00050  
 CM = -0.03965

DRAG COEFFICIENT COMPUTED BY SQUARE-ROOTS FORMULA = 0.00643

ZEROTH ITERATION PRESSURE DRAG = 0.00194

TRANSITION POINTS: X/CL(LOWER) = 0.30373 X/CL(UPPER) = 0.26170

LONGEST CHORDLINE SYSTEM		BASIC REFERENCE SYSTEM		S/C	CP	CF	DELTA/C	V/VD
X/C	Z/C	X/C	Z/C					
0.00000	-0.00130	0.00000	-0.00130	0.0	0.14230	0.00226	0.00233	0.92612
0.00354	-0.00661	0.00354	-0.00661	0.04676	0.09004	0.00247	0.00213	0.94000
0.00708	-0.01193	0.00708	-0.01193	0.09365	0.03639	0.00275	0.00194	0.96002
0.01062	-0.01725	0.01062	-0.01725	0.14004	0.00672	0.00305	0.00174	0.98002
0.01416	-0.02257	0.01416	-0.02257	0.18228	-0.02467	0.00310	0.00154	1.01250
0.01770	-0.02789	0.01770	-0.02789	0.22468	-0.05101	0.00324	0.00133	1.03250
0.02124	-0.03321	0.02124	-0.03321	0.26619	-0.08004	0.00343	0.00113	1.03925
0.02478	-0.03853	0.02478	-0.03853	0.30871	-0.11212	0.00359	0.00100	1.05034
0.02832	-0.04385	0.02832	-0.04385	0.35123	-0.14861	0.00380	0.00086	1.05613
0.03186	-0.04917	0.03186	-0.04917	0.39375	-0.18962	0.00393	0.00070	1.05613
0.03540	-0.05449	0.03540	-0.05449	0.43627	-0.23419	0.00407	0.00062	1.07732
0.03894	-0.05981	0.03894	-0.05981	0.47879	-0.28104	0.00419	0.00064	1.09041
0.04248	-0.06513	0.04248	-0.06513	0.52131	-0.33040	0.00428	0.00064	1.09344
0.04602	-0.07045	0.04602	-0.07045	0.56383	-0.38229	0.00434	0.00060	1.10132
0.04956	-0.07577	0.04956	-0.07577	0.60635	-0.43671	0.00436	0.00058	1.10920
0.05310	-0.08109	0.05310	-0.08109	0.64887	-0.49369	0.00434	0.00054	1.11708
0.05664	-0.08641	0.05664	-0.08641	0.69139	-0.55317	0.00428	0.00050	1.12496
0.06018	-0.09173	0.06018	-0.09173	0.73391	-0.61515	0.00419	0.00046	1.13284
0.06372	-0.09705	0.06372	-0.09705	0.77643	-0.68063	0.00407	0.00042	1.14072
0.06726	-0.10237	0.06726	-0.10237	0.81895	-0.74971	0.00393	0.00038	1.14860
0.07080	-0.10769	0.07080	-0.10769	0.86147	-0.82229	0.00376	0.00034	1.15648
0.07434	-0.11301	0.07434	-0.11301	0.90400	-0.89837	0.00359	0.00030	1.16436
0.07788	-0.11833	0.07788	-0.11833	0.94652	-0.97785	0.00343	0.00026	1.17224
0.08142	-0.12365	0.08142	-0.12365	0.98904	-1.06073	0.00324	0.00022	1.18012
0.08496	-0.12897	0.08496	-0.12897	1.03156	-1.14701	0.00305	0.00018	1.18800
0.08850	-0.13429	0.08850	-0.13429	1.07408	-1.23669	0.00287	0.00014	1.19588
0.09204	-0.13961	0.09204	-0.13961	1.11660	-1.32977	0.00268	0.00010	1.20376
0.09558	-0.14493	0.09558	-0.14493	1.15912	-1.42625	0.00249	0.00006	1.21164
0.09912	-0.15025	0.09912	-0.15025	1.20164	-1.52613	0.00229	0.00002	1.21952
0.10266	-0.15557	0.10266	-0.15557	1.24416	-1.62941	0.00209	0.00000	1.22740
0.10620	-0.16089	0.10620	-0.16089	1.28668	-1.73609	0.00189	0.00000	1.23528
0.10974	-0.16621	0.10974	-0.16621	1.32920	-1.84617	0.00169	0.00000	1.24316
0.11328	-0.17153	0.11328	-0.17153	1.37172	-1.95965	0.00149	0.00000	1.25104
0.11682	-0.17685	0.11682	-0.17685	1.41424	-2.07753	0.00129	0.00000	1.25892
0.12036	-0.18217	0.12036	-0.18217	1.45676	-2.19981	0.00109	0.00000	1.26680
0.12390	-0.18749	0.12390	-0.18749	1.49928	-2.32649	0.00089	0.00000	1.27468
0.12744	-0.19281	0.12744	-0.19281	1.54180	-2.45757	0.00069	0.00000	1.28256
0.13098	-0.19813	0.13098	-0.19813	1.58432	-2.59305	0.00049	0.00000	1.29044
0.13452	-0.20345	0.13452	-0.20345	1.62684	-2.73293	0.00029	0.00000	1.29832
0.13806	-0.20877	0.13806	-0.20877	1.66936	-2.87721	0.00009	0.00000	1.30620
0.14160	-0.21409	0.14160	-0.21409	1.71188	-3.02589	0.00000	0.00000	1.31408
0.14514	-0.21941	0.14514	-0.21941	1.75440	-3.17907	0.00000	0.00000	1.32196
0.14868	-0.22473	0.14868	-0.22473	1.79692	-3.33675	0.00000	0.00000	1.32984
0.15222	-0.23005	0.15222	-0.23005	1.83944	-3.49893	0.00000	0.00000	1.33772
0.15576	-0.23537	0.15576	-0.23537	1.88196	-3.66561	0.00000	0.00000	1.34560
0.15930	-0.24069	0.15930	-0.24069	1.92448	-3.83679	0.00000	0.00000	1.35348
0.16284	-0.24601	0.16284	-0.24601	1.96700	-4.01247	0.00000	0.00000	1.36136
0.16638	-0.25133	0.16638	-0.25133	2.00952	-4.19265	0.00000	0.00000	1.36924
0.16992	-0.25665	0.16992	-0.25665	2.05204	-4.37733	0.00000	0.00000	1.37712
0.17346	-0.26197	0.17346	-0.26197	2.09456	-4.56641	0.00000	0.00000	1.38500
0.17700	-0.26729	0.17700	-0.26729	2.13708	-4.75989	0.00000	0.00000	1.39288
0.18054	-0.27261	0.18054	-0.27261	2.17960	-4.95777	0.00000	0.00000	1.40076
0.18408	-0.27793	0.18408	-0.27793	2.22212	-5.16005	0.00000	0.00000	1.40864
0.18762	-0.28325	0.18762	-0.28325	2.26464	-5.36673	0.00000	0.00000	1.41652
0.19116	-0.28857	0.19116	-0.28857	2.30716	-5.57781	0.00000	0.00000	1.42440
0.19470	-0.29389	0.19470	-0.29389	2.34968	-5.79329	0.00000	0.00000	1.43228
0.19824	-0.29921	0.19824	-0.29921	2.39220	-6.01317	0.00000	0.00000	1.44016
0.20178	-0.30453	0.20178	-0.30453	2.43472	-6.23745	0.00000	0.00000	1.44804
0.20532	-0.30985	0.20532	-0.30985	2.47724	-6.46613	0.00000	0.00000	1.45592
0.20886	-0.31517	0.20886	-0.31517	2.51976	-6.69921	0.00000	0.00000	1.46380
0.21240	-0.32049	0.21240	-0.32049	2.56228	-6.93669	0.00000	0.00000	1.47168
0.21594	-0.32581	0.21594	-0.32581	2.60480	-7.17957	0.00000	0.00000	1.47956
0.21948	-0.33113	0.21948	-0.33113	2.64732	-7.42785	0.00000	0.00000	1.48744
0.22302	-0.33645	0.22302	-0.33645	2.68984	-7.68153	0.00000	0.00000	1.49532
0.22656	-0.34177	0.22656	-0.34177	2.73236	-7.94061	0.00000	0.00000	1.50320
0.23010	-0.34709	0.23010	-0.34709	2.77488	-8.20509	0.00000	0.00000	1.51108
0.23364	-0.35241	0.23364	-0.35241	2.81740	-8.47507	0.00000	0.00000	1.51896
0.23718	-0.35773	0.23718	-0.35773	2.85992	-8.75045	0.00000	0.00000	1.52684
0.24072	-0.36305	0.24072	-0.36305	2.90244	-9.03123	0.00000	0.00000	1.53472
0.24426	-0.36837	0.24426	-0.36837	2.94496	-9.31741	0.00000	0.00000	1.54260
0.24780	-0.37369	0.24780	-0.37369	2.98748	-9.60899	0.00000	0.00000	1.55048
0.25134	-0.37901	0.25134	-0.37901	3.02999	-9.90597	0.00000	0.00000	1.55836
0.25488	-0.38433	0.25488	-0.38433	3.07251	-10.20835	0.00000	0.00000	1.56624
0.25842	-0.38965	0.25842	-0.38965	3.11503	-10.51613	0.00000	0.00000	1.57412
0.26196	-0.39497	0.26196	-0.39497	3.15755	-10.82941	0.00000	0.00000	1.58200
0.26550	-0.40029	0.26550	-0.40029	3.20007	-11.14819	0.00000	0.00000	1.58988
0.26904	-0.40561	0.26904	-0.40561	3.24259	-11.47247	0.00000	0.00000	1.59776
0.27258	-0.41093	0.27258	-0.41093	3.28511	-11.80225	0.00000	0.00000	1.60564
0.27612	-0.41625	0.27612	-0.41625	3.32763	-12.13753	0.00000	0.00000	1.61352
0.27966	-0.42157	0.27966	-0.42157	3.37015	-12.47831	0.00000	0.00000	1.62140
0.28320	-0.42689	0.28320	-0.42689	3.41267	-12.82459	0.00000	0.00000	1.62928
0.28674	-0.43221	0.28674	-0.43221	3.45519	-13.17637	0.00000	0.00000	1.63716
0.29028	-0.43753	0.29028	-0.43753	3.49771	-13.53365	0.00000	0.00000	1.64504
0.29382	-0.44285	0.29382	-0.44285	3.54023	-13.89643	0.00000	0.00000	1.65292
0.29736	-0.44817	0.29736	-0.44817	3.58275	-14.26471	0.00000	0.00000	1.66080
0.30090	-0.45349	0.30090	-0.45349	3.62527	-14.63849	0.00000	0.00000	1.66868
0.30444	-0.45881	0.30444	-0.45881	3.66779	-15.01777	0.00000	0.00000	1.67656
0.30798	-0.46413	0.30798	-0.46413	3.71031	-15.40255	0.00000	0.00000	1.68444
0.31152	-0.46945	0.31152	-0.46945	3.75283	-15.79283	0.00000	0.00000	1.69232
0.31506	-0.47477	0.31506	-0.47477	3.79535	-16.18861	0.00000	0.00000	1.70020
0.31860	-0.48009	0.31860	-0.48009	3.83787	-16.58989	0.00000	0.00000	1.70808
0.32214	-0.48541	0.32214	-0.48541	3.88039	-16.99667	0.00000	0.00000	1.71596
0.32568	-0.49073	0.32568	-0.49073	3.92291	-17.40895	0.00000	0.00000	1.72384
0.32922	-0.49605	0.32922	-0.49605	3.96543	-17.82673	0.00000	0.00000	1.73172
0.33276	-0.50137	0.33276	-0.50137	4.00795	-18.25001	0.00000	0.00000	1.73960
0.33630	-0.50669	0.33630	-0.50669	4.05047	-18.67879	0.00000	0.00000	1.74748
0.33984	-0.51201	0.33984	-0.51201	4.09299	-19.11307	0.00000	0.00000	1.75536
0.34338	-0.51733	0.34338	-0.51733	4.13551	-19.55285	0.00000	0.00000	1.76324
0.34692	-0.52265	0.34692	-0.52265	4.17803	-20.00000	0.00000	0.00000	1.77112
0.35046	-0.52797	0.35046	-0.52797	4.22055	-20.45458	0.00000	0.00000	1.77



```

***** CASE INPUT *****
NACA 23012 AIRFOIL/ALPHA=0.2,4,6,8,10,12,14/RN=3.0/MACH NO.=0.2/IWRITE=3
NXU NXL IWRITE IALPHA IPUNCH
18 18 3 0 0
XU = 0.0 0.125000E-01 0.250000E-01 0.500000E-01 0.750000E-01 0.100000E 00 0.150000E 00 0.200000E 00
0.250000E 00 0.300000E 00 0.400000E 00 0.500000E 00 0.600000E 00 0.700000E 00 0.800000E 00 0.900000E 00
0.550000E 00 0.100000E 01
ZU = 0.0 0.267000E-01 0.361000E-01 0.491000E-01 0.580000E-01 0.642999E-01 0.719000E-01 0.750000E-01
0.760000E-01 0.750000E-01 0.714000E-01 0.614000E-01 0.547000E-01 0.436000E-01 0.308000E-01 0.168000E-01
0.920000E-02 0.130000E-02
XL = 0.0 0.125000E-01 0.250000E-01 0.500000E-01 0.750000E-01 0.100000E 00 0.150000E 00 0.200000E 00
0.250000E 00 0.300000E 00 0.400000E 00 0.500000E 00 0.600000E 00 0.700000E 00 0.800000E 00 0.900000E 00
0.950000E 00 0.100000E 01
ZL = 0.0 -0.123000E-01 -0.171000E-01 -0.226000E-01 -0.261000E-01 -0.292000E-01 -0.350000E-01 -0.397000E-01
-0.428000E-01 -0.446000E-01 -0.448000E-01 -0.417000E-01 -0.367000E-01 -0.300000E-01 -0.216000E-01 -0.123000E-01
-0.700000E-02 -0.130000E-02
NA = 8 ANGLES OF ATTACK W.R.T. REFERENCE LINE (IALPHA=0) OR W.R.T. LONGEST CHORDLINE (IALPHA=1)
C-0 0.200000E 01 0.400000E 01 0.600000E 01 0.800000E 01 0.100000E 02
C-120000E 02 0.140000E 02
NM = 1 FSMACH = 0.200000E 00
CREF = 0.100000E 01 SF = 0.100000E 01 TO = C.518690E 03 RN = 0.300000E 01 PR = 0.770000E 00 KF = 0.100000E 01
UPPER SURFACE 0 0.0 0.0
LOWER SURFACE 0 0.0 0.0
LTRAN XTRAN ZTRAN
*****
NACA 23012 AIRFOIL/ALPHA=0.2,4,6,8,10,12,14/RN=3.0/MACH NO.=0.2/IWRITE=3
FSMACH = 0.200000
***** ALPHA CL CD CM(NOSE) CM(1/4-CHORD) *****
* 0.0 0.125380 C.006621 -0.039847 -0.008502 *
* 2.00000 0.348239 0.006935 -0.097525 -0.010458 *
* 4.00000 0.570817 0.007488 -0.154459 -0.011972 *
* 6.00000 0.788949 C.008154 -0.209180 -0.012810 *
* 8.00000 1.004408 0.010101 -0.263183 -0.014173 *
* 10.00000 1.178342 0.014641 -0.302996 -0.012251 *
* 12.00000 1.354321 0.018874 -0.342340 -0.010178 *
* 14.00000 1.562696 C.025908 -0.397864 -0.017228 *
*****

```

Figure A-6. Sample output of the 2-D characteristics program with IWRITE=3.

## APPENDIX B - Polynomial Fit of Two Dimensional Data

### User Instructions

This program is written in Fortran IV and is designed to run in single precision on an IBM 370-165 computer. Execution requires 54,000 bytes of core storage and approximately six seconds to fit one set of two-dimensional airfoil data giving four polynomial curve fits of degree four. For each airfoil the program requires the following input data:

- (1) The 80 characters of the array TITLE which are used as a header for identifying output. Since the program allows more than one airfoil to be analyzed in a given run, TITLE is used as a control variable to end execution. Termination of execution is achieved by following the last set of airfoil data to be analyzed by a title card having only the word END in the first three spaces (see the last card of the sample data set in Figure B-2).
- (2) The number NUM. The largest allowable value of NUM is 20. This variable specifies the number of angles of attack which follow.
- (3) The first element values of the arrays AL, CL, CD, CM. These are the angle of attack and the two-dimensional coefficients of lift, drag, and pitching moment for that angle of attack. Similar cards with successive array elements follow until the number of points specified by NUM are read in.

In addition to the previous input data specification an internal switch is provided to suppress the plot of the input points and the curve fit function. When SWITCH is set to zero, plots are produced; however, when SWITCH is set to one, the plots are suppressed. Another internal switch PUNCH which operates similarly allows for the fitted coefficients to be punched into card form for use with other programs.

Statements (1) through (3) represent a complete data set for a particular airfoil. The format specification for this data is given in Figure B-1. A sample data set of the 23012 airfoil is shown in Figure B-2. The output of this particular data set is shown in Figure B-3.







```

C THIS SUBROUTINE SETS UP DATA FOR THE LEAST SQUARES CURVE FIT
C WRITTEN BY KEVIN R. JONES AND AVAILABLE FROM NCSU COMP. CENTER
C
REAL*8 PLY
INTEGER I, J, ZH, /, SWITCH, N
COMMON /INOUT/JREAD, JPUNCH, JWRITE
DIMENSION Y(500), C(N), X(N), Y(I), TITLE(4)
COMMON /DATA/ V(2, 500), M(2, 500), NK(2)
XLOW=X(1)
XHIGH=X(1)
YLOW=Y(1)
YHIGH=Y(1)
DC 5 I=2, M
IF (X(I)-LT-XLOW) XLOW=X(I)
IF (X(I)-GT-XHIGH) XHIGH=X(I)
IF (Y(I)-LT-YLOW) YLOW=Y(I)
IF (Y(I)-GT-YHIGH) YHIGH=Y(I)
DO 10 KK=1, 3
IF (FLP(KK)=0)
10 IF (SWITCH=EQ.1) GO TO 30
NK(1)=131
IF ((XHIGH-EQ-XLOW).OR.(YHIGH-EQ-YLOW)) GO TO 25
IF (XHIGH-GT-XLOW) GO TO 15
XXX=XHIGH
XHIGH=XLOW
XLOW=XXX
XXX=YHIGH
YHIGH=YLOW
YLOW=XXX
20 XXX=120./ABS(XHIGH-XLOW)
YYY=60./ABS(YHIGH-YLOW)
ZSCALE=DKR*20.
YSCALE=10./YYY
XINCH=DKR*10.
GC TO 30
25 SWITCH=1
IF (FLP(1))=1
30 NK(2)=M
IF (M=EQ.500)IF (LP(2))=1
DO 35 J=1, M
V(2, J)=XXX*(X(J)-XLOW)
W(2, J)=YYY*(Y(J)-YLOW)
WRITE (JWRITE, 100) TITLE
IF (FLP(1)-EQ.1) WRITE (JWRITE, 70)
IF (FLP(2)-EQ.1) WRITE (JWRITE, 115)
WRITE (JWRITE, 90) M, M
CALL LSG(X, Y, M, C, N)
SUM=0.0
DO 45 J=1, M
Y(I)=POLY(X(J), M, C, N)
IF (Y(I)-NE.0) SUM=SUM+Y(I)-Y(I)**2/Y(J)**2
45 CONTINUE
SUM=SUM/(M-1)
WRITE (JWRITE, 110) SUM
WRITE (JWRITE, 80)
DO 50 K=1, NPI
KMI=K-1
50 WRITE (JWRITE, 85) (0, KMI, C(K))
WRITE (JWRITE, 120)
M1=M/2+1
M2=M/2+1
DO 55 I=1, M1
WRITE (JWRITE, 95) X(I), Y(I), Y(I)*X(M2), Y(I)*Y(M2)
IF ((2*M/2)-M1) NE.0) WRITE (JWRITE, 95) X(M1), Y(M1), Y(M1)
IF (SWITCH=EQ.1) WRITE (JWRITE, 135)
IF (SWITCH) 140, 60, 140
60 T=XLOW
WRITE (JWRITE, 125)
DO 65 J=1, 131
W(1, J)=POLY(X(J), M, C, N)-YLOW
Y(1, J)=XXX*(W(1, J)-XLOW)
65 W(1, J)=DKR
WRITE (JWRITE, 130) TITLE, YHIGH, XSCALE, XINCH, YSCALE, YINCH
CALL PLOT
WRITE (JWRITE, 105) XLOW, XHIGH
70 FORMAT (//)
75 IF (XHIGH-XLOW) NE.0) WRITE (JWRITE, 105) XLOW, XHIGH
75 IF (YHIGH-YLOW) NE.0) WRITE (JWRITE, 105) YLOW, YHIGH
75 IF (XHIGH-XLOW) NE.0) WRITE (JWRITE, 105) XLOW, XHIGH
75 IF (YHIGH-YLOW) NE.0) WRITE (JWRITE, 105) YLOW, YHIGH
80 FORMAT (//)
85 FORMAT (A2, 2M, (12, 2M), 613, 2M, //)
90 FORMAT (//)
95 FORMAT (3I4, 614, 71, 8X, 2M1, 2I4, 614, 71)
100 FORMAT (1H1, T49, 444)
105 FORMAT (1X, 2M, Y=, G13, 6, 6M, X=, G13, 6, 6, T118, 2M, G13, 6, 6)
110 FORMAT (1X, MOVARIANCE=, G12, 6)
115 FORMAT (//)
120 FORMAT (//)
125 FORMAT (//)
130 FORMAT (//)
135 FORMAT (//)
140 RETURN
END
SUBROUTINE LSG(X, Y, M, C, N)
C THIS SUBROUTINE PERFORMS A LEAST SQUARES CURVE FIT ON M POINTS
C CONTAINED IN X VERSUS Y INTO A POLYNOMIAL OF DEGREE N AND
C COEFFICIENTS C.
C
REAL*8 A(21, 22), B(500), YSUM, SUM
DIMENSION C(M), X(M), Y(M)
COMMON /INOUT/JREAD, JPUNCH, JWRITE
N=N+1
L1=2
NPI=N+1
NPI=N+1
NMI=N-1
N2M=2*N-1
DO 5 J=1, M
5 B(1, J)=L.0
L1=1
DO 25 L=1, M2N
LSO 1
LSO 2
LSO 3
LSO 4
LSO 5
LSO 6
LSO 7
LSO 8
LSO 9
LSO 10
LSO 11
LSO 12
LSO 13
LSO 14
LSO 15
LSO 16
LSO 17
LSO 18
LSO 19

```







CD VERSUS CL

DEGREE= 4  
 NUMBER OF DATA POINTS= 4  
 VARIANCE= 0.107926E-02

THE FIT COEFFICIENTS ARE

C1 0)= 0.107623E-02  
 C1 1)= 0.201755E-02  
 C1 2)= 0.193333E-02  
 C1 3)= 0.573362E-03  
 C1 4)= 0.265209E-02

K-VALUE	Y-VALUE	Y-FIT		X-VALUE	Y-VALUE	Y-FIT
-0.3196300	0.787330E-02	0.7930178E-02		0.5732100	0.7086098E-02	0.69600 08E-02
-0.9459300E-01	0.7548098E-02	0.7285213E-02		0.7916400	0.8077399E-02	0.80451 28E-02
0.1256500	0.8444801E-02	0.885320E-02		1.0056000	0.9952899E-02	0.1035 837E-01
0.3456200	0.8843600E-02	0.8674223E-02		1.1850000	0.1404800E-01	0.1349 076E-01
1.3580000	0.184340E-01	0.1852990E-01				

PLOT OF Y...(X'S) AND Y-FIT...(X'S) FOLLOWS:

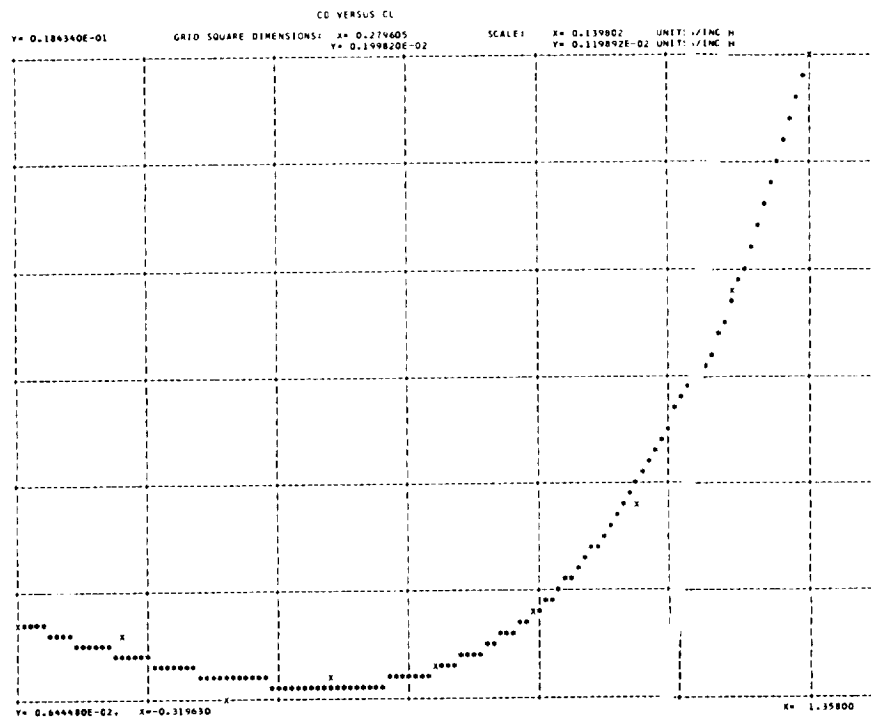


Figure B-3. Continued.

CM VERSUS CL

DEGREE= 4  
 NUMBER OF DATA POINTS= 9  
 VARIANCE= 0.276015E-03

THE FIT COEFFICIENTS ARE

C( 0)=-0.751330E-12  
 C( 1)=-0.764033E-12  
 C( 2)=-0.694403E-13  
 C( 3)=-0.209011E-02  
 C( 4)= 0.424931E-01

X-VALUE	Y-VALUE	Y-FIT	X-VALUE	Y-VALUE	Y-FIT
-0.3196300	-0.5046750 E-02	-0.5041113E-02	0.5792100	-0.1213900E-01	-0.1219019E-01
-0.4499500E-01	-0.4445800 E-02	-0.4789356E-02	0.7916900	-0.1317200E-01	-0.135210E-01
0.1254500	-0.8504301 E-02	-8.8497734E-02	1.005000	-0.1425900E-01	-0.1391044E-01
0.3496200	-0.1054800 E-01	-0.1034226E-01	1.185000	-0.1282500E-01	-0.1292013E-01
1.358000	-0.1025500 E-01	-0.1026347E-01			

PLOT OF Y... (X'S) AND Y-FIT... (S) FOLLOWS:

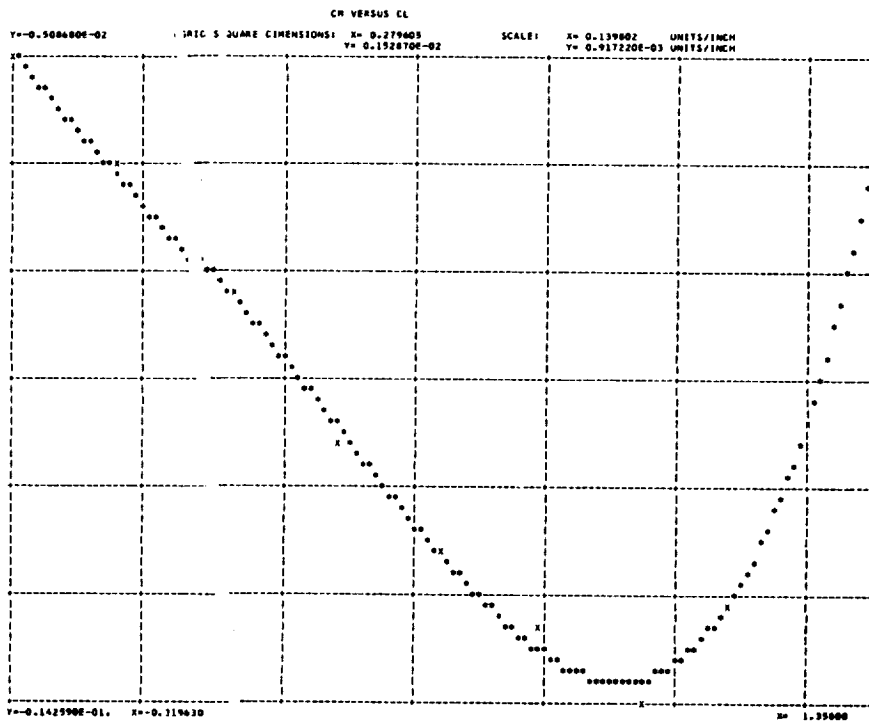


Figure B-3. Continued.

ALPHA VERSUS CL

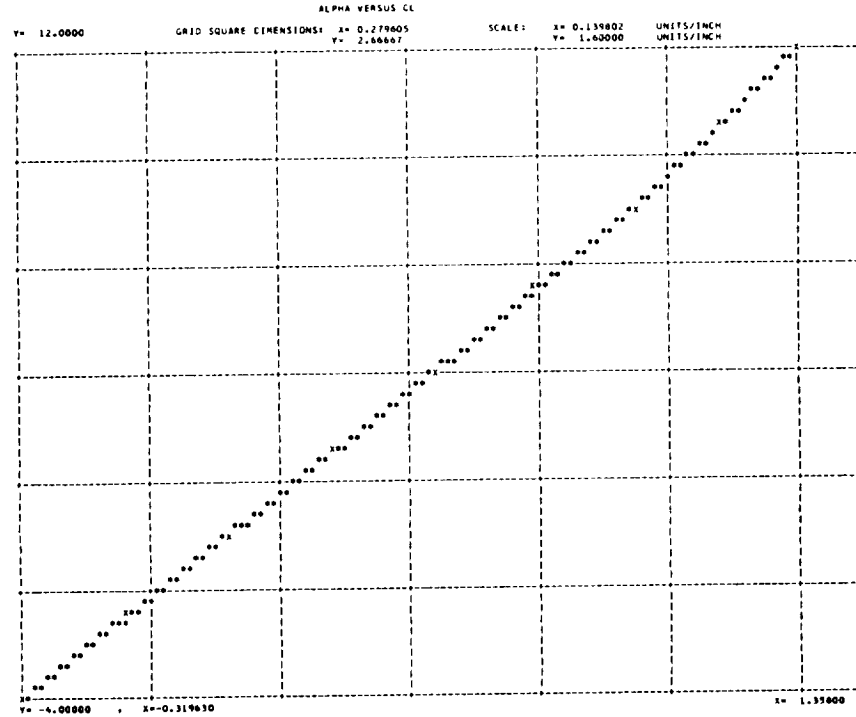
DEGREE= 4  
 NUMBER OF DATA POINTS= 5  
 VARIANCE= 0.105174E-04

THE FIT COEFFICIENTS ARE

C(0)= -1.13585  
 C(1)= 9.02351  
 C(2)= -0.558624E-01  
 C(3)= -0.497165  
 C(4)= 0.059838

X-VALUE	Y-VALUE	Y-FIT	X-VALUE	Y-VALUE	Y-FIT
-0.3196308	-4.000000	-4.002621	0.5732100	4.000000	3.995767
-0.9499388E-01	-2.000000	-1.993043	0.7916900	4.000000	5.985488
0.1256500	0.000000	-0.3748405E-02	1.005600	8.000000	8.050905
0.3496200	2.000000	2.000735	1.185000	10.00000	9.952623
1.358000	12.00000	12.01409			

PLOT OF Y..(R\*S) AND Y-FIT..(R\*S) FOLLOWS:



```

*****
*                               *
* TWO DIMENSIONAL CURVE FIT FUNCTION DATA *
* OF THE FORM Y=C(0)+C(1)*X+C(2)*X**2+... *
*                               *
* 23012 SERIES AIRFOIL / ALPHA=-2.0,2.4,6.8,10.12 / RN=3.49 / MACH NO.=.2 *
*                               *
* C(0) C(1) C(2) C(3) C(4) *
* CL VERSUS ALPHA 0.12631 0.11213 0.00014 -0.00003 -0.00000 *
* CD VERSUS CL 0.00708 -0.00102 0.00193 0.00057 0.00289 *
* CH VERSUS CL -0.00731 -0.00169 -0.00093 -0.00205 0.00429 *
* ALPHA VERSUS CL -1.13585 9.02351 -0.05786 -0.49714 0.05984 *
*                               *
*****
    
```

Figure B-3. Continued.

## APPENDIX C - Airfoil-to-Complete-Wing Program

### User Instructions

This program is written in Fortran IV and is designed to run in single precision on an IBM 370-165 computer. Execution requires 60,000 bytes of core storage and approximately eight seconds to produce the three-dimensional lift, drag, and pitching moment for a given wing-body configuration. For each configuration the program requires the following input data:

- (1) The aspect ratio ASPEC, the thickness ratio of the tip TAUT, the thickness ratio of the root TAUR, the taper ratio TAPER, the geometric twist TWIST in degrees (If geometric twist is specified, the aerodynamic twist TWISA must be set to a value of 100.), the number of spanwise stations R (R must be less than or equal to 20.), Reynolds number in millions based on wing mean aerodynamic chord REYND, and a criterion for convergence of the lift distribution DISCR.
- (2) Fuselage height to wing span ratio A, fuselage width to wing span ratio B, the height of the wing above the fuselage centerline H, again as a ratio to wing span, wing-body incidence angle ALPHR in degrees, x-coordinate of the moment reference point X, z-coordinate of the moment reference point Z, the aerodynamic twist TWISA in degrees (If aerodynamic twist is specified, the geometric twist TWIST must be set to a value of 100.).
- (3) The number of airfoil families (two tables per family) to be read in with this configuration IFAM, a control parameter for reading in wing geometric parameters ISWIT(1), a control parameter for printing out intermediate calculations as they are performed ISWIT(2), a control parameter for printing out matrices ISWIT(3), and an indicator that the tip airfoil is or is not of the same family as the root IRT. A yes action is implied when the control parameter or indicator is set to one; otherwise, the appropriate space is filled with a zero.
- (4) The 80 characters of the array NAME which are used as a header for identifying output.
- (5) The 80 characters of the array TITLE1 which serve as identification for the first airfoil table.
- (6) The thickness ratio of the airfoil in the first table RT1.
- (7) The five coefficients of the lift polynomial CCLRT1 for the airfoil in the first table.
- (8) The domain for which the coefficients of CCLRT1 are valid XLO(1) and XHI(1).

- (9) The five coefficients of the drag polynomial CCDRT1 for the airfoil in the first table.
- (10) The domain for which coefficients of CCDRT1 are valid XLO(2) and XHI(2).
- (11) The five coefficients of the moment polynomial CCMRT1 for the airfoil in the first table.
- (12) The domain for which the coefficients of CCMRT1 are valid XLO(3) and XHI(3).
- (13) The five coefficients of the alpha polynomial CALRT1 for the airfoil in the first table.
- (14) The domain for which the coefficients of CALRT1 are valid XLO(4) and XHI(4).
- (15) A duplication of (4) through (14) for each additional airfoil until the correct number of airfoil coefficient tables are stored.
- (16) The 20 elements of the array ALPHB representing the angles of attack for which three-dimensional lift, drag, and moment coefficients are to be calculated. One element of this array must contain the value 99.0 to insure a later return to the main portion of the program.

The program allows for additional configurations to be calculated during the same run. This may be accomplished simply by repeating the previous input. The program will continue execution until it encounters an ASPEC value of 99.0 followed by a blank card.

Statements (1) through (16) represent a complete data set for a particular configuration. The format specification for this data is given in Figure C-1. A sample data set using a 23020 root-23012 tip wing is shown in Figure C-2. The output of this particular data set is given in Figure C-3.

ASPEC	TAUT	TAUR	TAPER	TWIST	R	REYND	DISCR		
F10.2	F10.2	F10.2	F10.2	F10.2	F10.2	F10.2	F10.2		
A	B	H	ALPHR	X	Z	TWISA			
F10.2	F10.2	F10.2	F10.2	F10.2	F10.2	F10.2			
IFAM	ISWIT(1)	ISWIT(2)	ISWIT(3)	IRT					
I10	I10	I10	I10	I10					
NAME									
20A4									
TITLE1									
20A4									
RT1	/								
Q16.5	/								
CCLRT1(1)								CCLRT1(3)	
Q16.5	Q16.5	Q16.5	Q16.5	Q16.5	Q16.5	Q16.5	Q16.5	Q16.5	Q16.5
XLO(1)	XHI(1)	/							
Q16.5	Q16.5	/							
CCDR1(1)								CCDR1(3)	
Q16.5	Q16.5	Q16.5	Q16.5	Q16.5	Q16.5	Q16.5	Q16.5	Q16.5	Q16.5
XLO(2)	XHI(2)	/							
Q16.5	Q16.5	/							
CCMR1(1)								CCMR1(3)	
Q16.5	Q16.5	Q16.5	Q16.5	Q16.5	Q16.5	Q16.5	Q16.5	Q16.5	Q16.5
XLO(3)	XHI(3)	/							
Q16.5	Q16.5	/							
CALRT1(1)								CALRT1(3)	
Q16.5	Q16.5	Q16.5	Q16.5	Q16.5	Q16.5	Q16.5	Q16.5	Q16.5	Q16.5
XLO(4)	XHI(4)	/							
Q16.5	Q16.5	/							
ADDITIONAL AIRFOIL COEFFICIENT TABLES									
ALPHV(1)									
F8.0	F8.0	F8.0	F8.0	F8.0	F8.0	F8.0	F8.0	F8.0	F8.0
F8.0	F8.0	F8.0	F8.0	F8.0	F8.0	F8.0	F8.0	F8.0	ALPHV(20)
F8.0	F8.0	F8.0	F8.0	F8.0	F8.0	F8.0	F8.0	F8.0	F8.0

Figure C-1. Format specification of input data for the airfoil-to-complete-wing program.











```

C      CALL DATSM(3,JUNK)
      GO TO (25,30),JUNK
      25 WRITE (JWRITE,170)
         CALL AAALALPG(NP)
C
C      FIND CL(K)
C
C      30 CALL BRIDG(CVAL,1,NP,1,ALPG)
      DO 40 K=1,NP
      AC=K
      40 CDBG(K)=CVAL*(N1+ASPEC/(ASPEC+1.0))*(C(K)+CDB*(10.5*(1.0-TAPER)*SINIAK
         10PIER/(13.14399C(K)))
C
C      CHECK FOR DUMP
C
C      CALL DATSM(3,JUNK)
      GO TO (45,50),JUNK
      45 WRITE (JWRITE,175)
         CALL AAALALPG(NP)
C
C      LOOK UP ALPHA VALUE FOR ZERO LIFT
C
C      50 CALL BRIDG(ALPHZ,1,NP,4,CLO)
      DO 60 K=1,NP
      SIG=0.
      60 SIG=CDB(K)*BETA*(K)*SIG
      ALPHU(K)=SIG*(1.0+TFAC*TRANS(K)-1.0)
      ALPHE(K)=ALPG(K)-ALPHU(K)
      65 CONTINUE
C
C      LOOK UP CL VALUES FOR A LIST OF ALPHA
      VALUES
C
C      CALL BRIDG(CVAL,1,NP,1,ALPHE)
      DO 75 K=1,NP*(K)+C(K)+CDB/BHX
      DELTA(K)=CDB*(K)-CDB*(K)
C
C      CHECK FOR DUMP
C
C      CALL DATSM(3,JUNK)
      GO TO (80,85),JUNK
      80 WRITE (JWRITE,180)
         CALL AAALCBG(NP)
         WRITE (JWRITE,185)
         CALL AAALALPHU(NP)
         WRITE (JWRITE,190)
         CALL AAALALPHE(NP)
         WRITE (JWRITE,175)
         CALL AAALALPG(NP)
         WRITE (JWRITE,195)
         CALL AAALCBG(NP)
         WRITE (JWRITE,200)
         CALL AAALDELTA(NP)
C
C      CHECK TOLERANCE
C
C      85 DO 95 K=1,NP
      IF (ABS(DELTA(K))-DISCR) 90,90,100
      90 IF (K=NP) 95,130,130
      95 CONTINUE

```

```

M1 77
M1 78
M1 79
M1 80
M1 81
M1 82
M1 83
M1 84
M1 85
M1 86
M1 87
M1 88
M1 89
M1 90
M1 91
M1 92
M1 93
M1 94
M1 95

M2 1
M2 2
M2 3
M2 4
M2 5
M2 6
M2 7
M2 8
M2 9
M2 10
M2 11
M2 12
M2 13
M2 14
M2 15
M2 16
M2 17
M2 18
M2 19
M2 20
M2 21
M2 22
M2 23
M2 24
M2 25
M2 26
M2 27
M2 28
M2 29
M2 30
M2 31
M2 32
M2 33
M2 34
M2 35
M2 36
M2 37
M2 38
M2 39
M2 40
M2 41
M2 42

C      CALL AAALTAU(NP)
      WRITE (JWRITE,130)
      CALL AAALREV(NP)
      WRITE (JWRITE,135)
      CALL AAALC(NP)
      WRITE (JWRITE,140)
      CALL AAALEPS(NP)
      CALL MAIN2
      RETURN
C
C      105 FORMAT (10X,11MATRIX BETA)
      110 FORMAT (10X,11MATRIX TRI)
      115 FORMAT (1X/10/35X,20A/1X)
      120 FORMAT (1X/10/17MSPANNISE STATIONS)
      125 FORMAT (10X,30THICKNESS / CHORD DISTRIBUTION)
      130 FORMAT (10X,18CHORD REYNOLDS NUMBERS)
      135 FORMAT (10X,18CHORD DISTRIBUTION)
      140 FORMAT (10X,18TWIST DISTRIBUTION)
      148 END
C
C      SUBROUTINE MAIN2
C
C      SUBROUTINE FOR THE CASE WITHOUT A FLAP
C
C      DIMENSION CDB(19),ALPG(19),ALPH(19),ALPHZ(19),DELTA(19),ALPHU(19),
      1CLO(19)
      COMMON ISMT(3),C(19),EPS(19),TRANS(19),REV(19),ETA(19),Y(19),BETA
      119,19),TFAC,TRIX(19),TAU(19),ASPEC,TAPER,REYND,DISCR,PIER,CDB,
      110,EDGE,ALPHE,NP,A,B,M,TAUT,TAUM,TWIST,R,BHX,TMISA,K,Z,ACC,NAME(20)
      1,CVAL(19),ALPHU(19),CBC(19),ALPHE(19),ALPHB,YC
      COMMON /IINPUT/JREAD,WRITE
      DATA CLO/1900./
      WRITE (JWRITE,140) NAME
      WRITE (JWRITE,145) A,B,ASPEC,M,ALPHB,TAUT
      WRITE (JWRITE,150) TAUM,TWIST,R,TMISA,TAPER,REYND,K,Z,DISCR
      WRITE (JWRITE,155)
      WRITE (JWRITE,220)
      WRITE (JWRITE,215)
      WRITE (JWRITE,210)
      WRITE (JWRITE,160)
      WRITE (JWRITE,210)
      WRITE (JWRITE,210)
      WRITE (JWRITE,165)
C
C      IKT=1
C
C      READ (JREAD,135) ALPH
      5 ALPH=ALPH(IKT)
C
C      TEST FOR END OF ALPHA VALUES
C
C      IF (ALPH=99.) 15,10,15
      10 WRITE (JWRITE,210)
      WRITE (JWRITE,215)
      RETURN
      15 ITR=0
      20 ALPG(K)=ALPHB+ALPHE+EPS*(K)+ALPH*TFAC*TRANS(K)-1.0
C
C      SWITCH NUMBER 3 IS USED FOR AM INTERNAL
      DUMP DF ARRAYS COMPUTED DURING ITERATION
      PROCESS
C
C
C

```





```

J1=J1+J
A1=AL(J1)
110 A1(J1)=HOLD
115 J=J+1
IF (J-K) 95,95,120
120 K1=K-N
DO 125 J=1,N
K1=K1+N
HOLD=A1(K1)
J1=K1-K+J
A1(K1)=A1(J1)
125 A1(J1)=HOLD
GC TO 95
130 RETURN
END
    
```

```

MIN 104
MIN 107
MIN 108
MIN 109
MIN 110
MIN 111
MIN 112
MIN 113
MIN 114
MIN 115
MIN 116
MIN 117
MIN 118
MIN 119
MIN 120
    
```

SUBROUTINE SETSM  
SUBROUTINE CHECKS SWITCH SETTINGS ON DATA  
CARD AND LISTS OPTIONS SELECTED

```

C
C
C
C
COMMON /INOUT/JREAD,JWRITE
K=0
WRITE (.WRITE,65)
IF (.ISMIT(1)) 10,10,5
5 K=K+1
WRITE (.WRITE,50)
10 IF (.ISMIT(2)) 20,20,15
15 K=K+1
WRITE (.WRITE,55)
20 IF (.ISMIT(3)) 30,30,25
25 K=K+1
WRITE (.WRITE,60)
30 IF (K) 40,35,40
35 WRITE (.WRITE,65)
40 RETURN
C
45 FORMAT (1H0/1M0,50X,2H)SPECIAL FEATURES FOR THIS RUN(1M0)
50 FORMAT (51X,1,4HREAD IN VALUES(1M0))
55 FORMAT (51X,34HTRACE (OUTPUT OF KEY CALCULATIONS)/1M0)
60 FORMAT (51X,20HPRINT MATRICES BETA AND TRIA(1M0))
65 FORMAT (51X,31M0 SWITCH SETTINGS REGULAR RUN)
END
    
```

```

SET 1
SET 2
SET 3
SET 4
SET 5
SET 6
SET 7
SET 8
SET 9
SET 10
SET 11
SET 12
SET 13
SET 14
SET 15
SET 16
SET 17
SET 18
SET 19
SET 20
SET 21
SET 22
SET 23
SET 24
SET 25
SET 26
SET 27
SET 28
    
```

```

C
C
C
C
SUBROUTINE AAA(CLIST,MV)
SUBROUTINE TO OUTPUT A ONE DIMENSIONAL
ARRAY
C
C
C
DIMENSION CLIST(MV)
COMMON /INOUT/JREAD,JWRITE
WRITE (.WRITE,5) (J,CLIST(J),J=1,MV)
WRITE (.WRITE,10)
RETURN
C
5 FORMAT (5(1X,1M,12,2M),610,8)
10 FORMAT (211M,1)
END
    
```

```

AAA 1
AAA 2
AAA 3
AAA 4
AAA 5
AAA 6
AAA 7
AAA 8
AAA 9
AAA 10
AAA 11
AAA 12
AAA 13
AAA 14
    
```

```

C
C
C
C
SUBROUTINE SSS(A,NP)
SUBROUTINE TO OUTPUT A SQUARE TWO
DIMENSIONAL ARRAY
C
C
C
DIMENSION A1(9,19)
COMMON /INOUT/JREAD,JWRITE
WRITE (.WRITE,5) ((J,K,A(J,K),K=1,NP),J=1,NP)
WRITE (.WRITE,10)
RETURN
C
5 FORMAT (5(1X,1M,12,1M,12,2M),E16,8)
10 FORMAT (3(1M,7))
END
    
```

```

SSS 1
SSS 2
SSS 3
SSS 4
SSS 5
SSS 6
SSS 7
SSS 8
SSS 9
SSS 10
SSS 11
SSS 12
SSS 13
SSS 14
    
```

```

C
C
C
FUNCTION TERP(R1,R2,R3,C1,C3)
INTERPOLATION FUNCTION
C
C
IF (R1-R3) 10,9,10
5 TERP=C1
RETURN
10 TERP=C1+(C3-C1)*((R2-R1)/(R3-R1))
RETURN
END
    
```

```

TER 1
TER 2
TER 3
TER 4
TER 5
TER 6
TER 7
TER 8
TER 9
TER 10
    
```

```

C
C
C
C
SUBROUTINE DATSM(MP,ICOND/1)
SUBROUTINE MAKES DECISION BASED ON THE
SETTING OF THE SWITCH SET=1,NOT SET=0
ICOND=1 IF SWITCH IS SET
ICOND=2 IF SWITCH IS NOT SET
C
C
COMMON /SMIT(3)
IP (M-3) 5,10,15
5 IF (.ISMIT(1)) 20,20,25
10 IF (.ISMIT(2)) 20,20,25
15 IF (.ISMIT(3)) 20,20,25
20 ICOND=2
RETURN
25 ICOND=1
RETURN
END
    
```

```

DAT 1
DAT 2
DAT 3
DAT 4
DAT 5
DAT 6
DAT 7
DAT 8
DAT 9
DAT 10
DAT 11
DAT 12
DAT 13
DAT 14
DAT 15
DAT 16
DAT 17
    
```

```

C
C
C
SUBROUTINE BRIDGE(CCL1,NS,MP,LDW,XXI)
SUBROUTINE TO INTERPOLATE BETWEEN TABLES
C
C
DIMENSION XK(19),CCZ(19),CCZ2(19)
COMMON /SMIT(3),C(19),EPS(19),TRANS(19),REV(19),ETAL(9),Y(19),BETA
119,19),TFAC,TR1(19),TAU(19),ASPEC,TAPER,REYMO,DISCR,PIER,CBB,
10,EDGE,ALPHR,MO,A,B,M,TAUT,TMR,THIST,R,BUS,TMISA,K,Z,ACC,NAME(20)
1-CVAL(19),ALPHU(19),CBC(19),ALPHE(19),ALPHB,VO
COMMON /FUNC/CCLAT(5),CCDAT2(5),CCDAT1(5),CCDAT2(5),CCDAT1(5),CCM
LAT2(5),CALAT1(5),CALAT2(5),CCLT1(5),CCLT2(5),CCDT1(5),CCDT2(5)
1-CGATT1(5),CGATT2(5),CALT1(5),CALT2(5),ICAM,IRT,RTI,RT2,TT1,TT2
    
```

```

BOG 1
BOG 2
BOG 3
BOG 4
BOG 5
BOG 6
BOG 7
BOG 8
BOG 9
BOG 10
BOG 11
BOG 12
    
```





# Sample Output

```

.....
*
*
*          TWO DIMENSIONAL CURVE FIT FUNCTION DATA
*          OF THE FORM Y=C(1)+C(2)*X+C(3)*X**2+...
*
*
*          Z 012 SERIES AIRFOIL / ALPHA=-4,-2,0,2,4,6,8,10,12 / RN=3.49 / MACH NO.=.2
*          THICKNESS RATIO= 0.12
*
*          C(1)  C(2)  C(3)  C(4)
* CL VERSUS ALPHA  0.12631  0.11233  0.00014  -0.00000
* CD VERSUS CL     0.00708  -0.00202  0.00195  0.00057
* CM VERSUS CL     -0.00751  -0.00769  -0.00095  -0.00205
* ALPHA VERSUS CL  -1.13580  0.02350  -0.05586  -0.49714
*
*          DOMAIN= -4.0000 TO 12.0000
*          DOMAIN= -0.3196 TO 1.3580
*          DOMAIN= -0.3196 TO 1.3580
*
*
*          Z3021 SERIES AIRFOIL / ALPHA=-4,-2,0,2,4,6,8,10,12 / RN=3.49 / MACH NO.=.2
*          THICKNESS RATIO= 0.21
*
*          C(1)  C(2)  C(3)  C(4)
* CL VERSUS ALPHA  0.13324  0.11788  -0.00015  -0.00001
* CD VERSUS CL     0.00715  -0.00047  0.00338  0.00154
* CM VERSUS CL     -0.00176  -0.01808  -0.00624  0.01679
* ALPHA VERSUS CL  -1.12880  0.48720  -0.32278  1.16880
*
*          DOMAIN= -4.0000 TO 12.0000
*          DOMAIN= -0.3295 TO 1.4306
*          DOMAIN= -0.3295 TO 1.4306
*
*
*          SPECIAL FEATURES FOR THIS RUN
*
*          MD SWITCH SETTINGS  REGULAR RUN
*
*
*          Z3020 ROOT SERIES - Z3012 SERIES TIP
*
*          SPANWISE STATIONS
* ( 1)  0.98788862  ( 2)  0.95105666  ( 3)  0.89100677  ( 4)  0.80901762  ( 5)  0.70710737
* ( 6)  0.58778608  ( 7)  0.45399171  ( 8)  0.30901825  ( 9)  0.15643688  (10)  0.22214408E-05
* (11) -0.19643227  (12) -0.30901492  (13) -0.45398778  (14) -0.58778286  (15) -0.70710674
* (16) -0.80901533  (17) -0.89100486  (18) -0.95100557  (19) -0.98788783  (
*
*          THICKNESS / CHORD DISTRIBUTION
* ( 1)  0.12241757  ( 2)  0.12911910  ( 3)  0.13873547  ( 4)  0.14969081  ( 5)  0.16069812
* ( 6)  0.17094332  ( 7)  0.18003339  ( 8)  0.18786055  ( 9)  0.19447541  (10)  0.19999987
* (11) 0.19447559  (12) 0.18786073  (13) 0.18003362  (14) 0.17094358  (15) 0.16069835
* (16) 0.14969105  (17) 0.13873571  (18) 0.12911928  (19) 0.12241769  (
*
*          SECTION REYNOLDS NUMBERS
* ( 1)  1.9141284  ( 2)  2.0173960  ( 3)  2.1866866  ( 4)  2.4178228  ( 5)  2.7051210
* ( 6)  3.0415030  ( 7)  3.4180869  ( 8)  3.8273869  ( 9)  4.2575340  (10)  4.6985426
* (11) 4.2575444  (12) 3.8273954  (13) 3.4180974  (14) 3.0415125  (15) 2.7051287
* (16) 2.4178295  (17) 2.1866903  (18) 2.0173998  (19) 1.9141293  (
*
*          CHORD DISTRIBUTION
* ( 1)  0.40738694  ( 2)  0.42936599  ( 3)  0.46539593  ( 4)  0.51458955  ( 5)  0.57573557
* ( 6)  0.64732838  ( 7)  0.72760499  ( 8)  0.81458908  ( 9)  0.90613800  (10)  0.99999869
* (11) 0.90614089  (12) 0.81459105  (13) 0.72760737  (14) 0.64733028  (15) 0.57573718
* (16) 0.51459080  (17) 0.46539712  (18) 0.42936671  (19) 0.40738732  (
*
*          TWIST DISTRIBUTION
* ( 1)  -3.3942242  ( 2)  -3.1010373  ( 3)  -2.8803169  ( 4)  -2.2010231  ( 5)  -1.7196519
* ( 6)  -1.2712250  ( 7)  -0.87353442  ( 8)  -0.53109466  ( 9)  -0.24169743  (10)  -0.31100199E-05
* (11) -0.24168992  (12) -0.53108948  (13) -0.87352425  (14) -1.2712145  (15) -1.7194414
* (16) -2.2010117  (17) -2.8803036  (18) -3.1010256  (19) -3.3942194  (
*
*
*          Z3020 ROOT SERIES - Z3012 SERIES TIP
*
*          /-----/
*
*          BODY HEIGHT / SPAN . . . . .  0.0          BODY WIDTH / SPAN . . . . .  0.0
* ASPECT RATIO . . . . .  10.05          WING HEIGHT / SPAN . . . . .  0.0
* WING BODY INCIDENCE, DEG . . . . .  0.0          TIP THICKNESS CHORD . . . . .  0.12
* ROOT THICKNESS CHORD . . . . .  0.20          GEOMETRIC TWIST, DEG . . . . .  -3.50
* NUMBER OF SPANWISE STATIONS. = 20.00          AERODYNAMIC TWIST, DEG . . . . .  -3.49
* TAPER RATIO . . . . .  0.40          REYNOLDS NUMBER . . . . .  3.49
* COORDINATES OF MOMENT REFERENCE POINT          X= 0.0          Z= 0.0
* VALUE OF DISCRIMINANT. . . . .  0.001000
*
*          /-----/
*
*          THREE DIMENSIONAL LIFT, DRAG, AND MOMENT DATA
*
*          ALPHA  CL  CDP  CDI  CD  CM
* -4.000000 -0.351687  0.008190  0.004400  0.012590  0.000474
* -2.000000 -0.180874  0.007779  0.003111  0.009090 -0.001481
* 0.0 0.015495  0.007519  0.000352  0.007870 -0.004108
* 2.000000 0.202082  0.007467  0.001606  0.009073 -0.004987
* 4.000000 0.383778  0.007686  0.003057  0.012743 -0.009734
* 6.000000 0.570164  0.008247  0.010000  0.018846 -0.012090
* 8.000000 0.748508  0.009229  0.018074  0.027305 -0.013931
* 10.000000 0.921770  0.010713  0.027294  0.038007 -0.015250
* 12.000000 1.089635  0.012778  0.038080  0.050858 -0.016131
*
*

```

Figure C-3. Sample output of the airfoil-to-complete-wing program.

## APPENDIX D - PLOT Program

### User Instructions

This program was originally written for a CDC 6000 computer (Ref. 113) and was then modified to run in single precision on an IBM 370-165. Given a set of input data the program generates the necessary instructions for automatic plotting of an airplane numerical model and can be used to draw three-view and oblique orthographic projections, as well as perspective projections. These plots are very useful in checking the validity of numerical model data. The program has an average execution time of 3 minutes and 20 seconds for a job yielding 8 different views of the same aircraft.

In order to be compatible with the potential flow program used in this report (see Appendix F), the body coordinates are specified with the body nose at, or near the origin of the coordinate system, and the body's longitudinal axis is extended along the X-axis (see Figure D-1). The origin of the Y-axis must lie in the XZ-plane of symmetry, and the Z-axis must be the vertical axis of the body.

Reference 113 does an excellent job of describing the input data cards; therefore, the data specification given below is taken directly from that description. Additional information on this program is available in the cited reference.

### Configuration Cards

Since the airplane has to be symmetrical about the XZ-plane, only half of the airplane need be described to the computer. The convention used in presenting the input data is that the half of the airplane on the positive Y-side of the XZ-plane is presented. The program then uses this information to construct the complete airplane. The number of input cards depends on the number of components used to describe the configuration, whether a component has been described previously, and the amount of detail used to describe each component. The method of input is by FORTRAN "READ" statements.

Columns	FORTRAN Name	Description
01 to 03	J0	If J0=0, no reference area If J0=1, reference area to be read If J0=2, reference area same as previously read

Columns	FORTRAN Name	Description
04 to 06	J1	If J1=0, no wing data If J1=1, cambered wing data to be read If J1=-1, uncambered wing data to be read If J1=2, wing data same as previously read
07 to 09	J2	If J2=0, no fuselage data If J2=1, data for arbitrarily shaped fuselage to be read If J2=-1, data for circular fuselage to be read (with J6=0, fuselage will be cambered; with J6=-1, fuselage will be symmetrical with XY-plane; with J6=1, entire configuration will be symmetrical with XY-plane) If J2=2, fuselage data same as previously read
10 to 12	J3	If J3=0, no pod data If J3=1, pod data to be read If J3=2, pod data same as previously read
13 to 15	J4	If J4=0, no fin data If J4=1, fin data to be read If J4=2, fin data same as previously read
16 to 18	J5	If J5=0, no canard data If J5=1, canard data to be read If J5=2, canard data same as previously read
19 to 21	J6	Simplification code:  If J6=0, Indicates a cambered circular or arbitrary fuselage if J2 ≠ 0 If J6=1, complete configuration is symmetrical with respect to XY-plane, which implies uncambered circular fuselage if there is a fuselage If J6=-1, Indicates uncambered circular fuselage with J2 ≠ 0
22 to 24	NWAF	Number of airfoil sections used to describe the wing; $2 \leq \text{NWAF} \leq 20$
25 to 27	NWAFOR	Number of ordinates used to define each wing airfoil section; $3 \leq \text{NWAFOR} \leq 30$

Columns	FORTRAN Name	Description
28 to 30	NFUS	Number of fuselage segments; $1 \leq NFUS \leq 4$
31 to 33	NRADX(1)	Number of points used to represent half-section of first fuselage segment; if fuselage is circular, the program computes indicated number of y- and z-ordinates; $3 \leq NRADX(1) \leq 30$
34 to 36	NFORX(1)	Number of stations for first fuselage segment; $4 \leq NFORX(1) \leq 30$
37 to 39 40 to 42	NRADX(2) NFORX(2)	Same as NRADX(1) and NFORX(1), but for second fuselage segment
43 to 45 46 to 48	NRADX(3) NFORX(3)	Same as NRADX(1) and NFORX(1), but for third fuselage segment
49 to 51 52 to 54	NRADX(4) NFORX(4)	Same as NRADX(1) and NFORX(1), but for fourth fuselage segment
55 to 57	NP	Number of pods described; $NP \leq 9$
58 to 60	NPODOR	Number of stations at which pod radii are to be specified; $4 \leq NPODOR \leq 30$
61 to 63	NF	Number of fins (vertical tails) described; $NF \leq 6$
64 to 66	NFINOR	Number of ordinates used to define each fin airfoil section; $3 \leq NFINOR \leq 10$
67 to 69	NCAN	Number of canards (horizontal tails) described; $NCAN \leq 2$
70 to 72	NCANOR	Number of ordinates used to define each canard airfoil section; $3 \leq NCANOR \leq 10$ ; if NCANOR is given a negative sign, the program will expect to read lower ordinates also; otherwise, airfoil is assumed to be symmetrical

Cards 3, 4, . . . - remaining data input cards. - The remaining data input contain a detailed description of each component of the airplane. Each card contains up to 10 values, each value punched in a 7-column field with a decimal and may be identified in columns 73 to 80. The cards are arranged in the following order: reference area, wing data cards, fuselage data cards, pod (or nacelle) data cards, fin (vertical tail) data cards, and canard (or horizontal tail) data cards.

Reference area card: The reference area value is punched in columns 1 to 7 and may be identified as REFA in columns 73 to 80.

Wing data cards: The first wing data card (or cards) contains the locations in percent chord at which the ordinates of all the wing airfoils are to be specified. There will be exactly NWAFFOR locations in percent chord given. Each card may be identified in columns 73 to 80 by the symbol XAFj where j denotes the number of the last location in percent chord given on that card. For example, if NWAFFOR=16, there are 16 ordinates to be specified for every airfoil, and two data cards will be required. The first XAF card is identified as XAF 10 and the second as XAF 16.

The next wing data cards (there will be NWAFF cards) each contain four numbers which give the origin and chord length of each of the wing airfoils that is to be specified. The cards representing the most inboard airfoil are given first, followed by the cards for successive airfoils. The information is arranged on each card as follows:

Columns	Description
1 to 7	x-ordinate of airfoil leading edge
8 to 14	y-ordinate of airfoil leading edge
15 to 21	z-ordinate of airfoil leading edge
22 to 28	airfoil streamwise chord length
73 to 80	card identification, WAFORGj where j denotes the particular airfoil; for example, WAFORG1 denotes first (most inboard) airfoil

If a cambered wing has been specified, the next set of wing data cards is the mean camber line (TZORD) cards. The first card contains up to 10  $\Delta z$  values, referenced to the z-ordinate of the airfoil leading edge, at each of the specified percents of chord for the first airfoil. If more than 10 values are to be specified for each airfoil (there will be NWAFFOR values), the remaining values are continued on successive cards. The remaining airfoils are described in the same manner, data for each airfoil starting on a new card, and the cards arranged in the order which begins with the most inboard airfoil and proceeds to the outboard. Each card may be identified in columns 73 to 80 as TZORDj, where j denotes the particular airfoil.

Next are the wing airfoil ordinate (WAFORD) cards. The first card contains up to 10 half-thickness ordinates of the first airfoil expressed as percent chord. If more than 10 ordinates are to be specified for each airfoil (there will be NWAFFOR values), the remaining ordinates are continued on successive cards. The remaining airfoils are each described in the same

manner, and the cards are arranged in the order which begins with the most inboard airfoil and proceeds to the outboard. Each card may be identified in columns 73 to 80 as WAFORDj, where j denotes the particular airfoil.

Fuselage data cards: The first card (or cards) specifies the x values of the fuselage stations of the first segment. There will be NFORX(1) values and the cards may be identified in columns 73 to 80 by the symbol XFUSj where j denotes the number of the last fuselage station given on that card.

If the fuselage is circular and cambered, the next set of cards specifies the z locations of the center of the circular sections. There will be NFORX(1) values and the cards may be identified in columns 73 to 80 by the symbol ZFUSj where j denotes the number of the last fuselage station given on that card.

If the fuselage is circular, the next card (or cards) gives the fuselage cross-sectional areas, and may be identified in columns 73 to 80 by the symbol FUSARDj where j denotes the number of the last fuselage station given on that card. If the fuselage is of arbitrary shape, the y-ordinates for a half-section are given (NRADX(1) values) and identified in columns 73 to 80 as Yi where i is the station number. Following these are the corresponding z-ordinates (NRADX(1) values) for the half-section identified in columns 73 to 80 as Zi where i is the station number. Each station will have a set of Y and Z cards and the convention of ordering the ordinates from bottom to top is observed.

For each fuselage segment a new set of cards as described must be provided. The segment descriptions should be given in order of increasing values of x.

Pod data cards: The first pod or nacelle data card specifies the location of the origin of the first pod. The information is arranged on the card as follows:

Columns	Description
1 to 7	x-ordinate of origin of first pod
8 to 14	y-ordinate of origin of first pod
15 to 21	z-ordinate of origin of first pod
73 to 80	card identification, PODORGj where j denotes pod number

The next pod input data card (or cards) contains the x-ordinates, referenced to the pod origin, at which the pod radii (there will be NPODOR of them)

are to be specified. The first x-value must be zero, and the last x-value is the length of the pod. These cards may be identified in columns 73 to 80 by the symbol XPODj where j denotes the pod number. For example, XPOD1 represents the first pod.

The next pod input data cards give the pod radii corresponding to the pod stations that have been specified. These cards may be identified in columns 73 to 80 as PODRj where j denotes the pod number.

For each additional pod, new PODORG, XPOD, and PODR cards must be provided. Only single pods are described but the program assumes that if the y-ordinate is not zero an exact duplicate is located symmetrically with respect to the XZ-plane; a y-ordinate of zero implies a single pod.

Fin data cards: Exactly three data input cards are used to describe a fin. The information presented on the first fin data input card is as follows:

Columns	Description
1 to 7	x-ordinate of lower airfoil leading edge
8 to 14	y-ordinate of lower airfoil leading edge
15 to 21	z-ordinate of lower airfoil leading edge
22 to 28	chord length of lower airfoil
29 to 35	x-ordinate of upper airfoil leading edge
36 to 42	y-ordinate of upper airfoil leading edge
43 to 49	z-ordinate of upper airfoil leading edge
50 to 56	chord length of upper airfoil
73 to 80	card identification, FINORGj where j denotes fin number

The second fin data input card contains up to 10 locations in percent chord (exactly NFINOR of them) at which the fin airfoil ordinates are to be specified. The card may be identified in columns 73 to 80 as XFINj where j denotes the fin number.

The third fin data input card contains the fin airfoil half-thickness ordinates expressed in percent chord. Since the fin airfoil must be symmetrical,



only the ordinates on the positive y side of the fin chord plane are specified. The card identification, FINORDj, may be given in columns 73 to 80, where j denotes the fin number.

For each fin, new FINORG, XFIN, and FINORD cards must be provided.

Only single fins are described but the program assumes that if the y-ordinate is not zero an exact duplicate is located symmetrically with respect to the XZ-plane; a y-ordinate of zero implies a single fin.

Canard data cards: If the canard (or horizontal tail) airfoil is symmetrical, exactly three cards are used to describe a canard, and the input is given in the same manner as for the fin. If, however, the canard airfoil is not symmetrical (Indicated by a negative value of NCANOR), a fourth canard data input card will be required to give the lower ordinates. The information presented on the first canard data input card is as follows:

Columns	Description
1 to 7	x-ordinate of inboard airfoil leading edge
8 to 14	y-ordinate of inboard airfoil leading edge
15 to 21	z-ordinate of inboard airfoil leading edge
22 to 28	chord length of inboard airfoil
29 to 35	x-ordinate of outboard airfoil leading edge
36 to 42	y-ordinate of outboard airfoil leading edge
43 to 49	z-ordinate of outboard airfoil leading edge
50 to 56	chord length of outboard airfoil
73 to 80	card identification, CANORGj where j denotes the canard number

The second canard data input card contains up to 10 locations in percent chord (exactly NCANOR of them) at which the canard airfoil ordinates are to be specified. The card may be identified in columns 73 to 80 as XCANj where j denotes the canard number.

The third canard data input card contains the upper half-thickness ordinates, expressed in percent chord, of the canard airfoil. This card may be identified in columns 73 to 80 as CANORDj where j denotes the canard number. If the canard

airfoil is not symmetrical, the lower ordinates are presented on a second CANORD card. The program expects both upper and lower ordinates to be punched as positive values in percent chord.

For another canard, new CANORG, XCAN, and CANORD cards must be provided.

### Plot Cards

A single card contains all the necessary information for one plot. The available options and the necessary input for each are described in the succeeding sections.

Orthographic projections. - For orthographic projections, the card should be set up as follows (See Figure D-5):

Columns	FORTRAN Name	Description
1	HORZ	"X", "Y", or "Z" for horizontal axis
3	VERT	"X", "Y", or "Z" for vertical axis
5 to 7	TEST1	Word "OUT" for deletion of hidden lines; otherwise, leave blank
8 to 12	PHI	Roll angle, degrees (See Figure D-1)
13 to 17	THETA	Pitch angle, degrees (See Figure D-1)
18 to 22	PSI	Yaw angle, degrees (See Figure D-1)
48 to 52	PLOTSZ	PLOTSZ determines the size of plot (scale factor is computed using PLOTSZ and maximum dimension of configuration)
53 to 55	TYPE	Word "ORT"
72	KODE	If KODE=0, continue reading plot cards If KODE=1, after processing this plot, read new configuration description

An attempt is made to center the given configuration within the specified field. If the desired plot size is greater than 28 inches, centering is attempted within 28 inches so care must be taken in choosing the view. Minimum values are adjusted so that body axis lines with no rotation angles coincide with grid lines on the plotter paper. Therefore, the plotter pen should always be positioned exactly 1 inch from the side of the plotting space and on the intersection of heavy grid lines at the start of plotting.

Plan, front, and side views (stacked). - For plan, front, and side views, the card should be set up as follows (See Figure D-4):

Columns	FORTRAN Name	Description
8 to 12	PHI	y-origin on paper of plan view, inches
13 to 17	THETA	y-origin on paper of side view, inches
18 to 11	PSI	y-origin on paper of front view, inches
48 to 52	PLOTSZ	PLOTSZ determines size of plot (a scale factor is computed using PLOTSZ and maximum dimension of configuration)
53 to 55	TYPE	Word "VU3"
72	KODE	If KODE=0, continue reading plot cards If KODE=1, after processing this plot, read new configuration description

Perspective views. - For perspective views, the card should be set up as follows (See Figure D-10):

Columns	FORTRAN Name	Description
8 to 12	PHI	x of view point (location of viewer) in data coordinate system
13 to 17	THETA	y of view point in data coordinate system
18 to 22	PSI	z of view point in data coordinate system
23 to 27	XF	x of focal point (determines direction and focus) in data coordinate system
28 to 32	YF	y of focal point in data coordinate system
33 to 37	ZF	z of focal point in data coordinate system
38 to 42	DIST	Distance from eye to viewing plane, inches
43 to 47	FMAG	Viewing-plane magnification factor; it controls size of projected image

Columns	FORTRAN Name	Description
48 to 52	PLOTSZ	Diameter of viewing plane, inches; DIST and PLOTSZ together determine a cone which is field of vision; PLOTSZ value is also relative to type of viewer which is to be used.
53 to 55	TYPE	Word "PER"
72	KODE	If KODE=0, continue reading plot cards If KODE=1, after processing this plot, read new configuration description.

Stereo frames suitable for viewing in a stereoscope. - For stereo frames suitable for viewing in a stereoscope, the input is identical to that for the perspective views except that the word "STE" is used in columns 53 to 55.

Specification of the cards above represent a complete set of data for a particular body. The format specification for this data is given in the above text. A sample data set of a Cessna 182 light aircraft is shown in Figure D-2. The output of this particular data set, with different plot cards, is shown in Figures D-3 through D-14.

## Plotting Software Modifications

Since plotting software is different at almost every computing facility, this section of the appendix is included to help the user specify the appropriate software plotting instructions expected by the plot program. To institute a plotting procedure at any computing facility the user's program must first be linked with the plotter. In the original plot program linkage was established by the statement: CALL CALCOMP. The user must provide the necessary instructions to produce the same result at his facility. This instruction is given on card C00 35 in the Program Listing presented in the next section of this appendix. In addition, at most installations an instruction must also be given to close the plotter data set (i.e. turn the plotter off) after plotting has been completed. In the original plot program this was accomplished by the statement: CALL CALPLT(0.,0.,999). The user must provide an equivalent instruction for his installation as seen on card C00 67 in the Program Listing.

The actual plotting in the program is accomplished using three basic subroutines (CALPLT, NOTATE, and LINE) from the CalComp software package. For the program to operate properly, the user must either provide the original CalComp routines or provide three equivalent dummy subroutines as was necessary at the N. C. State computing facility. Given below is a description of the arguments to, and the results produced by these subroutines. Also included are listings of the equivalent dummy subroutines used at N. C. State to produce the same results as the original CalComp subroutines.

### Subroutine CALPLT

Purpose:

To move the plotter pen to a new location with the pen either up or down, and to turn off the plotter.

Use:

CALL CALPLT(X,Y,IPEN)

where

X,Y        are the floating point values for pen movement.

IPEN=2     pen is moved in a lowered position.  
=3         pen is moved in a raised position.

Negative IPEN (-2 or -3) will assign X = 0, Y = 0 as the location of the pen after moving the pen to X,Y (create a new reference point or origin).

IPEN=999 Turns the plotter off, the X and Y values are ignored.

Restrictions:

All X and Y coordinates must be expressed as floating point inches (actual page dimensions) in deflection from the origin.

(Equivalent N. C. State Routine)

```
SUBROUTINE CALPLT(A,B,I)
  DIMENSION A(1),B(1)
  IF (I.LT.0) GO TO 5
  J=I-2
  CALL PLOT(A,B,J)
  RETURN
5 J=IABS(I)
  J=J-2
  CALL PLOT(A,B,J)
  CALL ORIGIN(A,B,1.0)
  RETURN
END
```

Subroutine NOTATE

Purpose:

To draw alphanumeric information for annotation and labeling.

Use:

CALL NOTATE(X,Y,HEIGHT,BCD,THETA,N)

where

X,Y are the floating point page coordinates of the first character.

For alphanumeric characters, the coordinates of the lower left-hand corner of the characters are specified.

HEIGHT specifies the height in floating point inches for a full-size character.

BCD is the string of characters to be drawn and is usually written in the form: nHXXX--- (the same way an alpha message is written using FORTRAN for-

BCD con't

mat statements). Instead of specifying alpha information as above, one may give the beginning storage location of an array containing alphanumeric information.

THETA is the angle in floating point degrees at which the information is to be drawn. Zero degrees will print horizontally reading from left to right,  $90^\circ$  will print the line vertically reading from bottom to top,  $180^\circ$  will print the line horizontally reading from right to left (i.e., upside down), and  $270^\circ$  will print vertically reading from top to bottom.

N is the number of characters, including blanks, in the label.

(Equivalent N. C. State Routine)

```
SUBROUTINE NOTATE(A,B,C,D,E,I)
DIMENSION D(1),DD(21)
DATA STOP/4H _/
J=1/4
XI=1
XR=XI/4
IF ((XR-J).GT.0.1)J=J+1
DO 5 K=1,J
5 DD(K)=D(K)
DD(J+1)=STOP
CALL SYMBOL(A,B,C,DD,E)
RETURN
END
```

#### Subroutine LINE

Purpose:

To draw a continuous line through a set of successive data points where the minimum values and scale factors are stored at the end of the data arrays.

Use:

CALL LINE(XARRAY,YARRAY,N,K,J,L,S)

where

XARRAY and YARRAY are the names of arrays containing the X values and Y values, respectively, to be plotted. Values must be in floating point.

- N is the number of points to be plotted.
- K = 1 this value of K is constant in the plot program.
- J = 0 for line plot. Only line plots are used in the plot program.
- L is an integer describing symbol to be used. This variable is not used but a space for it in the calling sequence must be provided.
- S is the desired symbol height. This variable is not used but a space for it in the calling sequence must be provided.

Restrictions:

LINE expects the adjusted minimums and scale factors. These two parameters (two for the XARRAY and two for the YARRAY) are automatically calculated and provided by the plotting program at the ends of the XARRAY and YARRAY respectively. The points actually plotted by LINE are

$$(XARRAY(J) - XARRAY(N+1))/XARRAY(N+2) \quad \text{for } J=1,N$$

and

$$(YARRAY(J) - YARRAY(N+1))/YARRAY(N+2) \quad \text{for } J=1,N.$$

(Equivalent N. C. State Routine)

```
SUBROUTINE LINE(A,B,I,J,K,L,S)
DIMENSION A(1),B(1),X(31),Y(31)
XMIN=A(I+1)
XSCALE=A(I+2)
YMIN=B(I+1)
YSCALE=B(I+2)
DO 5 I1=1,I
X(I1)=(A(I1)-XMIN)/XSCALE
```



```
5 Y(11)=(B(11)-YMIN)/YSCALE  
CALL PLOT(X,Y,I)  
RETURN  
END
```

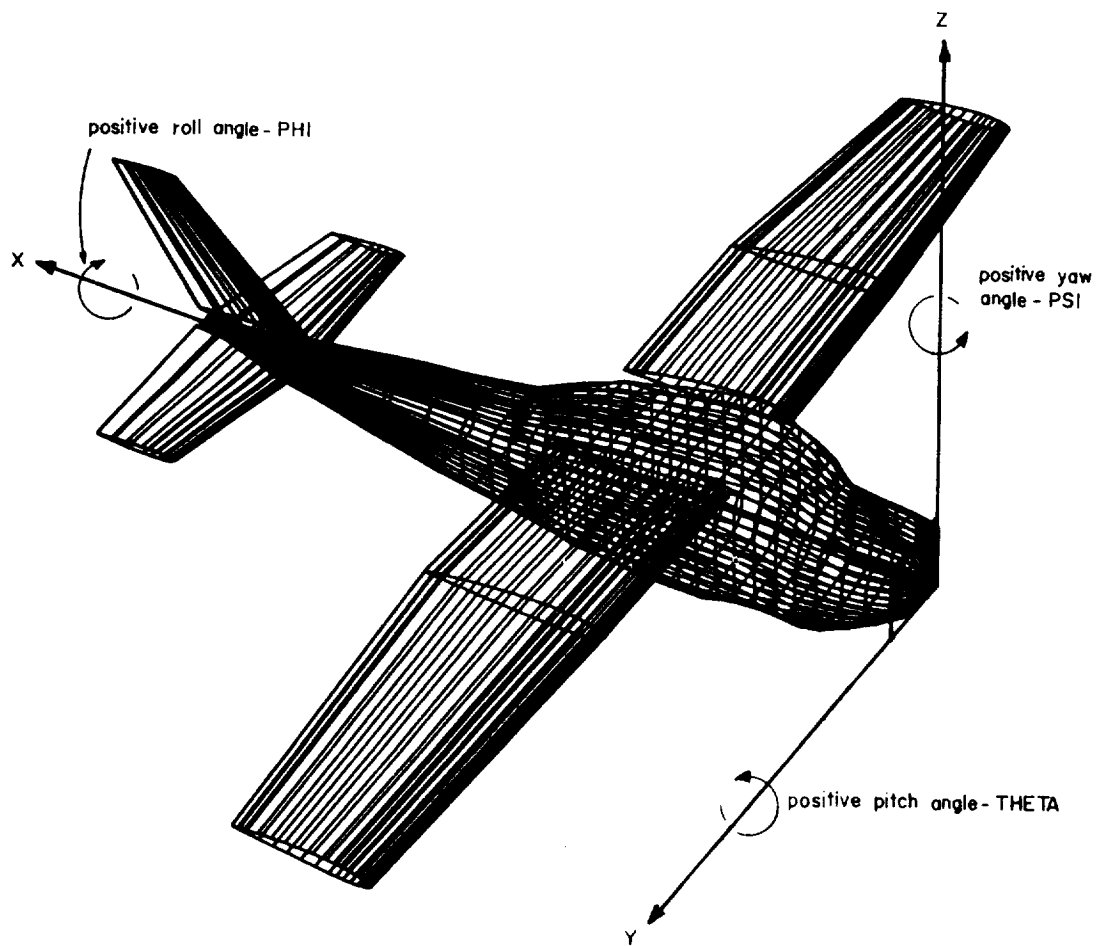


Figure D-1. Orientation of body with respect to body reference axes for the PLOT programs.



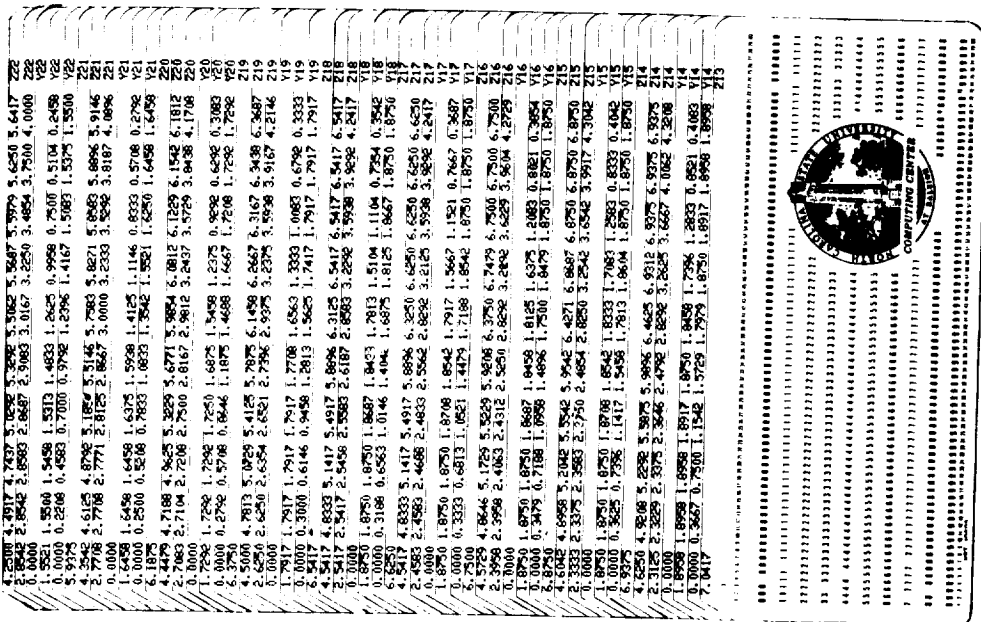
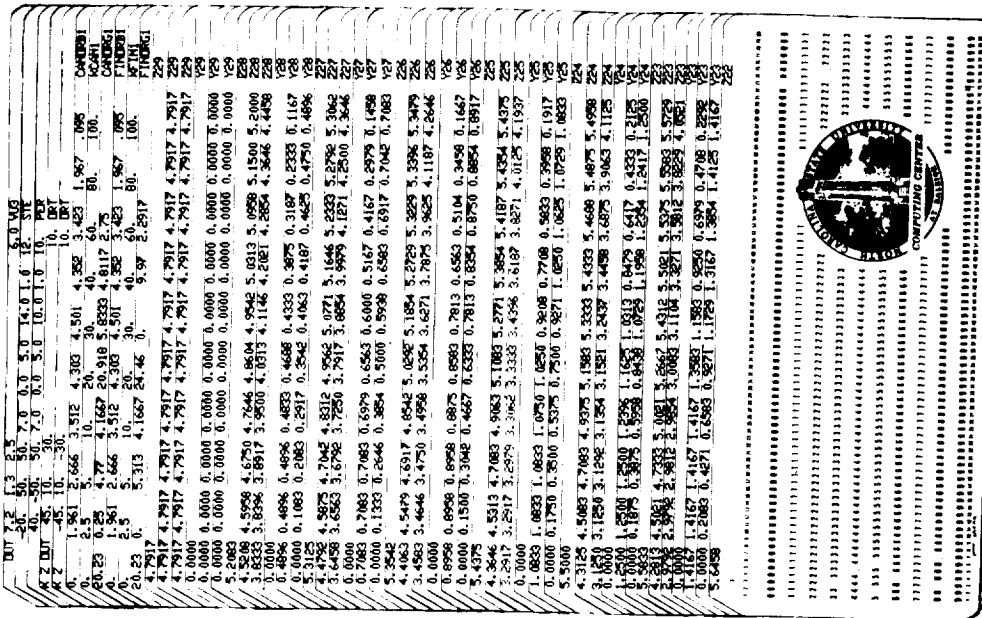


Figure D-2. Continued.



Program Listing

```

C000 THIS PLOT PROGRAM WAS OBTAINED FROM MASA LANGLEY TO GIVE
C001 M.C. STATE THE CAPABILITY TO GRAPHICALLY DISPLAY LIGHT AIRCRAFT.
C002 THE ONLY MODIFICATIONS EMPLOYED WERE THOSE REQUIRED TO TURN THE
C003 PROGRAM ON AN IBM COMPUTER. AS A TOOL THIS PLOT PROGRAM IS
C004 AVAILABLE FOR FINDING INPUT ERRORS IN OUR MODIFIED INVTSC TO BODY
C005 PROGRAM. WE WOULD LIKE TO THANK MR. CHARLES M. FOX JR. OF MASA
C006 LANGLEY FOR HIS HELP IN OBTAINING THE PROGRAM.
C007
C008 REFERENCE: DESCRIPTION OF A DIGITAL COMPUTER PROGRAM FOR AIRPLANE
C009 CONFIGURATION PLOTS
C010 CHARLOTTE B. CRAIGTON
C011 MASA TN 8-2076
C012 SEPTEMBER, 1970
C013
C014 AIRCRAFT CONFIGURATION PLOTS
C015 COMMON ABC(20),JO,J1,J2,J3,J4,J5,J6,J7,J8,J9,J10,J11,J12,J13,J14,J15,
C016 IRT(4),MP,MPDODR,MF,NFINOR,NCANOR,JZTEST,MM,NC,ABCDEI(20),HORZ,Y
C017 IERT,TEST1,PHI,THETA,PSI,XF,YF,ZF,DIST,FMAG,PLOTSZ,TYPE,KODE,MMIN,X
C018 IMAX,YMIN,YMAX,ZMIN,ZMAX,XMID,YMID,ZPID,BIGD,ISP
C019 COMMON /INOUT/JREAD,JWRITE,JMWRITE,KFILE1,KFILE2,KFILE3,KFILE4
C020 JREAD=1
C021 JWRITE=5
C022 KFILE1=9
C023 KFILE2=10
C024 KFILE3=11
C025 KFILE4=12
C026
C027 IMPORTANT???
C028
C029 CALL PICSI(99,0,11,0) IS THE APPROPRIATE CALL TO TURN THE PLOTTER
C030 ON FOR THE M. C. STATE PLOTTING SOFTWARE. THE CALL FOR THE
C031 ORIGINAL CALCOMP PLOTTER SOFTWARE WAS CALL CALPL(10,0,999).
C032 PROVIDE THE APPROPRIATE CALL FOR HIS INSTALLATION.
C033
C034 CALL PICSI(99,0,11,0)
C035 WRITE (JWRITE,5)
C036 5 FORMAT (11H17XTHPROGRAM D2290 PLOTS OF AIRCRAFT CONFIGURATION//
C037 1)
C038 DO 10 I=1,6
C039 10 WRITE (KFILE4,IDUM
C040 INPUT LIST TWO CARDS
C041 15 FORMAT (20A4)
C042 WRITE (JREAD,15,END=55) ABC
C043 WRITE (JWRITE,30) ABC
C044 30 FORMAT (28X25MCONFIGURATION DESCRIPTION//1X20A4/)
C045 READ (JREAD,35) JO,J1,J2,J3,J4,J5,J6,J7,J8,J9,J10,J11,J12,J13,J14,J15,
C046 IRT(4),MP,MPDODR,MF,NFINOR,NCANOR,JZTEST,MM,NC,ABCDEI(20),HORZ,Y
C047 IERT,TEST1,PHI,THETA,PSI,XF,YF,ZF,DIST,FMAG,PLOTSZ,TYPE,KODE,MMIN,X
C048 IMAX,YMIN,YMAX,ZMIN,ZMAX,XMID,YMID,ZPID,BIGD,ISP
C049 WRITE (JWRITE,40) JO,J1,J2,J3,J4,J5,J6,J7,J8,J9,J10,J11,J12,J13,J14,J15,
C050 IRT(4),MP,MPDODR,MF,NFINOR,NCANOR,JZTEST,MM,NC,ABCDEI(20),HORZ,Y
C051 IERT,TEST1,PHI,THETA,PSI,XF,YF,ZF,DIST,FMAG,PLOTSZ,TYPE,KODE,MMIN,X
C052 40 FORMAT (11X,24I3)
C053 INPUT CONFIGURATION DESCRIPTION AND INITIALIZE
C054 CALL CBC10
C055 PLOT CONFIGURATION
C056 WRITE (JWRITE,45)
C057 45 FORMAT (77X64MPLLOT DATA//)
C058 READ (JREAD,15,END=55) ABCDE
C059 GO TO 60
C060
C061 ***** IMPORTANT???
C062
C063 CALL PICSI(10,0,0,0) IS THE APPROPRIATE CALL TO TURN THE PLOTTER
C064 OFF FOR THE M. C. STATE PLOTTING SOFTWARE. THE CALL FOR THE
C065 ORIGINAL CALCOMP PLOTTER SOFTWARE WAS CALL CALPL(10,0,999).
C066 THE USER MUST PROVIDE THE APPROPRIATE CALL FOR HIS INSTALLATION.
C067
C068 55 CALL PICSI(10,0,0,0)
C069 STOP
C070 60 WRITE (KFILE3,15) ABCDE
C071 REWIND KFILE3
C072 READ (KFILE3,65) HORZ,VERT,TEST1,PHI,THETA,PSI,XF,YF,ZF,DIST,FMAG,
C073 PLOTSZ,TYPE,KODE
C074 REWIND KFILE3
C075 65 FORMAT (2A2,A3,9F5,0,A3,16X,11)
C076 WRITE (JWRITE,70) HORZ,VERT,TEST1,PHI,THETA,PSI,XF,YF,ZF,DIST,FMAG
C077 1,PLOTSZ,TYPE,KODE
C078 70 FORMAT (11X,ZAZ,A3,9(I1X,F10,5),A3,16X,11)
C079 CALL CBC20
C080 IF (KODE.EQ.0) GO TO 50
C081 WRITE (JWRITE,75)
C082 75 FORMAT (1M1)
C083 GO TO 20
C084 END
C085
C086 ***** SUBROUTINE CBC10
C087 ***** INPUTS AND INITIALIZES CONFIGURATION DESCRIPTION
C088 COMMON ABC(20),JO,J1,J2,J3,J4,J5,J6,J7,J8,J9,J10,J11,J12,J13,J14,J15,
C089 IRT(4),MP,MPDODR,MF,NFINOR,NCANOR,JZTEST,MM,NC,ABCDEI(20),HORZ,Y
C090 IERT,TEST1,PHI,THETA,PSI,XF,YF,ZF,DIST,FMAG,PLOTSZ,TYPE,KODE,MMIN,X
C091 IMAX,YMIN,YMAX,ZMIN,ZMAX,XMID,YMID,ZPID,BIGD,ISP
C092 COMMON /INOUT/JREAD,JWRITE,KFILE1,KFILE2,KFILE3,KFILE4
C093 DIMENSION BLOCK(7500)
C094 DIMENSION XAF(30),WAFORG(20,4),WAFORD(20,3,30),TZORD(20,30)
C095 EQUIVALENCE (BLOCK,XAF),(BLOCK(31),WAFORG),(BLOCK(111),WAFORD),(BL
C096 CK(191),TZORD)
C097 DIMENSION XFUS(30,4),ZFUS(30,4),FUSARD(30,4),FUSRADI(30,4),SFUS(30,
C098 130,8)
C099 EQUIVALENCE (BLOCK,XFUS),(BLOCK(121),ZFUS),(BLOCK(241),FUSARD),(BL
C100 CK(361),FUSRADI),(BLOCK(241),SFUS),(BLOCK(111),WAFORD),(BL
C101 CK(191),TZORD)
C102 DIMENSION PODORG(9,3),APOD(9,30),PODORD(9,30),XP0D(19,30)
C103 EQUIVALENCE (BLOCK,PODORG),(BLOCK(28),APOD),(BLOCK(298),PODORD),(B
C104 CK(158),XP0D)
C105 DIMENSION FIMORG(6,2,4),FIM(6,10),FIMORD(6,2,10),FINX(2,6,2,10),FI
C106 NORD(2,2)
C107 EQUIVALENCE (BLOCK,FIMORG),(BLOCK(49),FIM),(BLOCK(109),FINORD),(B
C108 CK(129),FINX),(BLOCK(349),FINX)
C109 DIMENSION CAMORG(2,2,4),CAM(2,10),CAMORD(2,2,10),CAMOR(12,2,10),C
C110 AMOR(2,2)
C111 EQUIVALENCE (BLOCK,CAMORG),(BLOCK(171),CAM),(BLOCK(37),CAMORD),(BL
C112 CK(177),CAMOR),(BLOCK(117),CAMORX)
C113 DIMENSION ALRT(31,3,2),VECRT(30,3,1),ANSIMI(30),AMCS(30)
C114 DIMENSION ABCD(8)
C115 DATA NAMZ/24/
C116 DATA PI/3.14159265/
C117 REWIND KFILE1
C118 REWIND KFILE2
C119 REWIND KFILE4
C120 5 FORMAT (8A10)
C121
C122 ***** SUBROUTINE CBC10
C123 ***** INPUTS AND INITIALIZES CONFIGURATION DESCRIPTION
C124 COMMON ABC(20),JO,J1,J2,J3,J4,J5,J6,J7,J8,J9,J10,J11,J12,J13,J14,J15,
C125 IRT(4),MP,MPDODR,MF,NFINOR,NCANOR,JZTEST,MM,NC,ABCDEI(20),HORZ,Y
C126 IERT,TEST1,PHI,THETA,PSI,XF,YF,ZF,DIST,FMAG,PLOTSZ,TYPE,KODE,MMIN,X
C127 IMAX,YMIN,YMAX,ZMIN,ZMAX,XMID,YMID,ZPID,BIGD,ISP
C128 COMMON /INOUT/JREAD,JWRITE,KFILE1,KFILE2,KFILE3,KFILE4
C129 DIMENSION BLOCK(7500)
C130 DIMENSION XAF(30),WAFORG(20,4),WAFORD(20,3,30),TZORD(20,30)
C131 EQUIVALENCE (BLOCK,XAF),(BLOCK(31),WAFORG),(BLOCK(111),WAFORD),(BL
C132 CK(191),TZORD)
C133 DIMENSION XFUS(30,4),ZFUS(30,4),FUSARD(30,4),FUSRADI(30,4),SFUS(30,
C134 130,8)
C135 EQUIVALENCE (BLOCK,XFUS),(BLOCK(121),ZFUS),(BLOCK(241),FUSARD),(BL
C136 CK(361),FUSRADI),(BLOCK(241),SFUS),(BLOCK(111),WAFORD),(BL
C137 CK(191),TZORD)
C138 DIMENSION PODORG(9,3),APOD(9,30),PODORD(9,30),XP0D(19,30)
C139 EQUIVALENCE (BLOCK,PODORG),(BLOCK(28),APOD),(BLOCK(298),PODORD),(B
C140 CK(158),XP0D)
C141 DIMENSION FIMORG(6,2,4),FIM(6,10),FIMORD(6,2,10),FINX(2,6,2,10),FI
C142 NORD(2,2)
C143 EQUIVALENCE (BLOCK,FIMORG),(BLOCK(49),FIM),(BLOCK(109),FINORD),(B
C144 CK(129),FINX),(BLOCK(349),FINX)
C145 DIMENSION CAMORG(2,2,4),CAM(2,10),CAMORD(2,2,10),CAMOR(12,2,10),C
C146 AMOR(2,2)
C147 EQUIVALENCE (BLOCK,CAMORG),(BLOCK(171),CAM),(BLOCK(37),CAMORD),(BL
C148 CK(177),CAMOR),(BLOCK(117),CAMORX)
C149 DIMENSION ALRT(31,3,2),VECRT(30,3,1),ANSIMI(30),AMCS(30)
C150 DIMENSION ABCD(8)
C151 DATA NAMZ/24/
C152 DATA PI/3.14159265/
C153 REWIND KFILE1
C154 REWIND KFILE2
C155 REWIND KFILE4
C156 5 FORMAT (8A10)
C157

```

```

10 FORMAT (1XGALO)
15 FORMAT (10F7.0)
C***
C
IF (J0.NE.2) GO TO 20
READ (KFILE4)REFA
WRITE (KFILE1)REFA
GO TO 35
20 IF (J0.EQ.0) GO TO 30
READ (JREAD15) REFA
WRITE (JWRITE25) REFA
30 WRITE (KFILE1)REFA
READ (KFILE4)DUM
C***
35 IF (J1.NE.2) GO TO 40
NMAFOR=IABS(NMAFOR)
MM=NMAFOR
READ (KFILE4)BLOCK
WRITE (KFILE1)BLOCK
GO TO 110
40 N=IABS(NMAFOR)
MREC=(N+9)/10
I1=-9
I2=0
DO 55 NN=1,MREC
I3=I1+10
I2=I2+10
READ (JREAD15) (XAF(I),I=I1,I2)
WRITE (JWRITE25) (XAF(I),I=I1,I2)
45 CONTINUE
DO 50 I=1,NMAF
READ (JREAD15) (MAFOR(I),J=1,4)
WRITE (JWRITE25) (MAFOR(I),J=1,4)
50 CONTINUE (I=1,0) GO TO 65
DO 60 NN=1,NMAF
I1=-9
I2=0
DO 55 N1=1,MREC
I3=I1+10
I2=I2+10
READ (JREAD15) (TZORD(NN,I),I=1,12)
WRITE (KFILE2) ((ALRT(N,N3,2),N=1,NM),N3=1,3)
60 CONTINUE
GO TO 75
65 DO 70 I=1,NMAF
DO 70 K=1,M
TZORD(I,K)=0.
75 L=1
IF (NMAFOR.LT.0) L=2
DO 85 MM=1,NMAF
MM 85 K=1,L
I1=-9
I2=0
DO 90 M1=1,MREC
I3=I1+10
I2=I2+10
70 CALL SURCLIN(M,ALRT,VECTR)
149 CALL SURCLIN(M,ALRT,VECTR)
190 CONTINUE
WRITE (KFILE2) ((VECTR(N,N3),N=1,MM),N3=1,3)
C10 95
C10 96
C10 97
C10 98
C10 99
C10 100
C10 101
C10 102
C10 103
C10 104
C10 105
C10 106
C10 107
C10 108
C10 109
C10 110
C10 111
C10 112
C10 113
C10 114
C10 115
C10 116
C10 117
C10 118
C10 119
C10 120
C10 121
C10 122
C10 123
C10 124
C10 125
C10 126
C10 127
C10 128
C10 129
C10 130
C10 131
C10 132
C10 133
C10 134
C10 135
C10 136
C10 137
C10 138
C10 139
C10 140
C10 141
C10 142
C10 143
C10 144
C10 145
C10 146
C10 147
C10 148
C10 149
C10 150
C10 151
C10 152
C10 153
C10 154
C10 155
C10 156
C10 157
C10 158
C10 159
C10 160
C10 161
C10 162
C10 163
C10 164
C10 165
C10 166
C10 167
C10 168
C10 169
C10 170
C10 171
C10 172
C10 173
C10 174
C10 175
C10 176
C10 177
C10 178
C10 179
C10 180
C10 181
C10 182
C10 183
C10 184
C10 185
C10 186
C10 187
C10 188
C10 189
C10 190
C10 191
C10 192
C10 193
C10 194
C10 195
C10 196
C10 197
C10 198
C10 199
C10 200
C10 201
C10 202
C10 203
C10 204
C10 205
C10 206
C10 207
C10 208
C10 209
C10 210
C10 211
C10 212
C10 213
C10 214
C10 215
C10 216
C10 217
C10 218
C10 219
C10 220
C10 221
C10 222
C10 223
C10 224
C10 225
C10 226
C10 227
C10 228
C10 229
C10 230
C10 231
C10 232
C10 233
C10 234
C10 235
C10 236
C10 237
C10 238
C10 239
C10 240
C10 241
C10 242
C10 243
C10 244
C10 245
C10 246
C10 247
C10 248
C10 249
C10 250
C10 251
C10 252
C10 253
C10 254
C10 255
C10 256
C10 257
C10 258
C10 259
C10 260
C10 261
C10 262
C10 263
C10 264
C10 265
C10 266
C10 267
C10 268
C10 269
C10 270
C10 271
C10 272
C10 273
C10 274
C10 275
C10 276
C10 277
C10 278
C10 279
C10 280
C10 281
C10 282
C10 283
C10 284
C10 285
C10 286
C10 287
C10 288
C10 289
C10 290
C10 291
C10 292
C10 293
C10 294
C10 295
C10 296
C10 297
C10 298
C10 299
C10 300
C10 301
C10 302
C10 303
C10 304
C10 305
C10 306
C10 307
C10 308
C10 309
C10 310
C10 311
C10 312
C10 313
C10 314
C10 315
C10 316
C10 317
C10 318
C10 319
C10 320
C10 321
C10 322
C10 323
C10 324
C10 325
C10 326
C10 327
C10 328
C10 329
C10 330
C10 331
C10 332
C10 333
C10 334
C10 335
C10 336
C10 337
C10 338
C10 339
C10 340
C10 341
C10 342
C10 343
C10 344
C10 345
C10 346
C10 347
C10 348
C10 349
C10 350
C10 351
C10 352
C10 353
C10 354
C10 355
C10 356
C10 357
C10 358
C10 359
C10 360
C10 361
C10 362
C10 363
C10 364
C10 365
C10 366
C10 367
C10 368
C10 369
C10 370
C10 371
C10 372
C10 373
C10 374
C10 375
C10 376
C10 377
C10 378
C10 379
C10 380
C10 381
C10 382
C10 383
C10 384
C10 385
C10 386
C10 387
C10 388
C10 389
C10 390
C10 391
C10 392
C10 393
C10 394
C10 395
C10 396
C10 397
C10 398
C10 399
C10 400
C10 401
C10 402
C10 403
C10 404
C10 405
C10 406
C10 407
C10 408
C10 409
C10 410
C10 411
C10 412
C10 413
C10 414
C10 415
C10 416
C10 417
C10 418
C10 419
C10 420
C10 421
C10 422
C10 423
C10 424
C10 425
C10 426
C10 427
C10 428
C10 429
C10 430
C10 431
C10 432
C10 433
C10 434
C10 435
C10 436
C10 437
C10 438
C10 439
C10 440
C10 441
C10 442
C10 443
C10 444
C10 445
C10 446
C10 447
C10 448
C10 449
C10 450
C10 451
C10 452
C10 453
C10 454
C10 455
C10 456
C10 457
C10 458
C10 459
C10 460
C10 461
C10 462
C10 463
C10 464
C10 465
C10 466
C10 467
C10 468
C10 469
C10 470
C10 471
C10 472
C10 473
C10 474
C10 475
C10 476
C10 477
C10 478
C10 479
C10 480
C10 481
C10 482
C10 483
C10 484
C10 485
C10 486
C10 487
C10 488
C10 489
C10 490
C10 491
C10 492
C10 493
C10 494
C10 495
C10 496
C10 497
C10 498
C10 499
C10 500
C10 501
C10 502
C10 503
C10 504
C10 505
C10 506
C10 507
C10 508
C10 509
C10 510
C10 511
C10 512
C10 513
C10 514
C10 515
C10 516
C10 517
C10 518
C10 519
C10 520
C10 521
C10 522
C10 523
C10 524
C10 525
C10 526
C10 527
C10 528
C10 529
C10 530
C10 531
C10 532
C10 533
C10 534
C10 535
C10 536
C10 537
C10 538
C10 539
C10 540
C10 541
C10 542
C10 543
C10 544
C10 545
C10 546
C10 547
C10 548
C10 549
C10 550
C10 551
C10 552
C10 553
C10 554
C10 555
C10 556
C10 557
C10 558
C10 559
C10 560
C10 561
C10 562
C10 563
C10 564
C10 565
C10 566
C10 567
C10 568
C10 569
C10 570
C10 571
C10 572
C10 573
C10 574
C10 575
C10 576
C10 577
C10 578
C10 579
C10 580
C10 581
C10 582
C10 583
C10 584
C10 585
C10 586
C10 587
C10 588
C10 589
C10 590
C10 591
C10 592
C10 593
C10 594
C10 595
C10 596
C10 597
C10 598
C10 599
C10 600
C10 601
C10 602
C10 603
C10 604
C10 605
C10 606
C10 607
C10 608
C10 609
C10 610
C10 611
C10 612
C10 613
C10 614
C10 615
C10 616
C10 617
C10 618
C10 619
C10 620
C10 621
C10 622
C10 623
C10 624
C10 625
C10 626
C10 627
C10 628
C10 629
C10 630
C10 631
C10 632
C10 633
C10 634
C10 635
C10 636
C10 637
C10 638
C10 639
C10 640
C10 641
C10 642
C10 643
C10 644
C10 645
C10 646
C10 647
C10 648
C10 649
C10 650
C10 651
C10 652
C10 653
C10 654
C10 655
C10 656
C10 657
C10 658
C10 659
C10 660
C10 661
C10 662
C10 663
C10 664
C10 665
C10 666
C10 667
C10 668
C10 669
C10 670
C10 671
C10 672
C10 673
C10 674
C10 675
C10 676
C10 677
C10 678
C10 679
C10 680
C10 681
C10 682
C10 683
C10 684
C10 685
C10 686
C10 687
C10 688
C10 689
C10 690
C10 691
C10 692
C10 693
C10 694
C10 695
C10 696
C10 697
C10 698
C10 699
C10 700
C10 701
C10 702
C10 703
C10 704
C10 705
C10 706
C10 707
C10 708
C10 709
C10 710
C10 711
C10 712
C10 713
C10 714
C10 715
C10 716
C10 717
C10 718
C10 719
C10 720
C10 721
C10 722
C10 723
C10 724
C10 725
C10 726
C10 727
C10 728
C10 729
C10 730
C10 731
C10 732
C10 733
C10 734
C10 735
C10 736
C10 737
C10 738
C10 739
C10 740
C10 741
C10 742
C10 743
C10 744
C10 745
C10 746
C10 747
C10 748
C10 749
C10 750
C10 751
C10 752
C10 753
C10 754
C10 755
C10 756
C10 757
C10 758
C10 759
C10 760
C10 761
C10 762
C10 763
C10 764
C10 765
C10 766
C10 767
C10 768
C10 769
C10 770
C10 771
C10 772
C10 773
C10 774
C10 775
C10 776
C10 777
C10 778
C10 779
C10 780
C10 781
C10 782
C10 783
C10 784
C10 785
C10 786
C10 787
C10 788
C10 789
C10 790
C10 791
C10 792
C10 793
C10 794
C10 795
C10 796
C10 797
C10 798
C10 799
C10 800
C10 801
C10 802
C10 803
C10 804
C10 805
C10 806
C10 807
C10 808
C10 809
C10 810
C10 811
C10 812
C10 813
C10 814
C10 815
C10 816
C10 817
C10 818
C10 819
C10 820
C10 821
C10 822
C10 823
C10 824
C10 825
C10 826
C10 827
C10 828
C10 829
C10 830
C10 831
C10 832
C10 833
C10 834
C10 835
C10 836
C10 837
C10 838
C10 839
C10 840
C10 841
C10 842
C10 843
C10 844
C10 845
C10 846
C10 847
C10 848
C10 849
C10 850
C10 851
C10 852
C10 853
C10 854
C10 855
C10 856
C10 857
C10 858
C10 859
C10 860
C10 861
C10 862
C10 863
C10 864
C10 865
C10 866
C10 867
C10 868
C10 869
C10 870
C10 871
C10 872
C10 873
C10 874
C10 875
C10 876
C10 877
C10 878
C10 879
C10 880
C10 881
C10 882
C10 883
C10 884
C10 885
C10 886
C10 887
C10 888
C10 889
C10 890
C10 891
C10 892
C10 893
C10 894
C10 895
C10 896
C10 897
C10 898
C10 899
C10 900
C10 901
C10 902
C10 903
C10 904
C10 905
C10 906
C10 907
C10 908
C10 909
C10 910
C10 911
C10 912
C10 913
C10 914
C10 915
C10 916
C10 917
C10 918
C10 919
C10 920
C10 921
C10 922
C10 923
C10 924
C10 925
C10 926
C10 927
C10 928
C10 929
C10 930
C10 931
C10 932
C10 933
C10 934
C10 935
C10 936
C10 937
C10 938
C10 939
C10 940
C10 941
C10 942
C10 943
C10 944
C10 945
C10 946
C10 947
C10 948
C10 949
C10 950
C10 951
C10 952
C10 953
C10 954
C10 955
C10 956
C10 957
C10 958
C10 959
C10 960
C10 961
C10 962
C10 963
C10 964
C10 965
C10 966
C10 967
C10 968
C10 969
C10 970
C10 971
C10 972
C10 973
C10 974
C10 975
C10 976
C10 977
C10 978
C10 979
C10 980
C10 981
C10 982
C10 983
C10 984
C10 985
C10 986
C10 987
C10 988
C10 989
C10 990
C10 991
C10 992
C10 993
C10 994
C10 995
C10 996
C10 997
C10 998
C10 999
C10 1000

```

```

C10 155      WRITE (KFILE2)((ALRTIN,M3,2),M=1,NM),M3=1,3)
C10 156
C10 157      155 CONTINUE
C10 158      160 CONTINUE
C10 159      MI=MMAF-1
C10 160      DO 200 I=1,2
C10 161      DO 165 M=1,MMAF
C10 162      DO 170 N3=1,3
C10 163      ALRTIN,1,2)=MAFORDIN,3,1)
C10 164      ALRTIN,2,2)=MAFORDIN,2,1)
C10 165      ALRTIN,3,2)=MAFORDIN,1,1)
C10 166      165 CONTINUE
C10 167      WRITE (KFILE2)((ALRTIN,M3,2),M=1,NMAF),M3=1,3)
C10 168      DO 195 NM=2,NM
C10 169      DO 170 N3=1,3
C10 170      ALRTIN,M3,1)=ALRTIN,M3,2)
C10 171      170 CONTINUE
C10 172      DO 175 N=1,NMAF
C10 173      ALRTIN,1,2)=MAFORDIN,3,MM)
C10 174      ALRTIN,2,2)=MAFORDIN,2,MM)
C10 175      ALRTIN,3,2)=MAFORDIN,1,MM)
C10 176      175 CONTINUE
C10 177      DO 180 I=1,185,1)
C10 178      180 CALL SURC(INMAF,ALRT,VECRT)
C10 179      GO TO 190
C10 180      185 CALL SURC(INMAF,ALRT,VECRT)
C10 181      190 CONTINUE
C10 182      WRITE (KFILE2)((VECRT(M,M3),M=1,NL),M3=1,3)
C10 183      WRITE (KFILE2)((ALRTIN,M3,2),M=1,NMAF),M3=1,3)
C10 184      195 CONTINUE
C10 185      200 CONTINUE
C10 186      IF (J1.EQ.2) GO TO 210
C10 187      205 WRITE (KFILE1)BLOCK
C10 188      READ (KFILE1)DUM
C10 189      210 IF (J2.NE.2) GO TO 215
C10 190      FUSELAGE
C10 191      READ (KFILE1)BLOCK
C10 192      WRITE (KFILE1)BLOCK
C10 193      GO TO 280
C10 194      215 IF (J2.EQ.0) GO TO 425
C10 195      JZTEST=3
C10 196      IF (J2.EQ.-1.AND.J6.EQ.-1)JZTEST=1
C10 197      IF (J2.EQ.-1.AND.J6.EQ.0)JZTEST=2
C10 198      IF (J6.EQ.1)JZTEST=1
C10 199      225 MFI=1,MMFUS
C10 200      MMAD=MMOZIMEU
C10 201      MMUSOM=MMOZIMEU
C10 202      MMFUSOR
C10 203      MREC=(M+9)/10
C10 204      11=-9
C10 205      12=0
C10 206      DO 220 M1=1,MREC
C10 207      11=11*10
C10 208      READ (JREAD,15) (MFUS(I,MFU),I=1,12)
C10 209      WRITE (JWRITE,25) (MFUS(I,MFU),I=1,12)
C10 210      220 CONTINUE
C10 211      IF (JZTEST.NE.2) GO TO 230
C10 212      11=-9
C10 213
C10 214

```

```

C10 155      WRITE (KFILE2)((ALRTIN,M3,2),M=1,NM),M3=1,3)
C10 156
C10 157      155 CONTINUE
C10 158      160 CONTINUE
C10 159      MI=MMAF-1
C10 160      DO 200 I=1,2
C10 161      DO 165 M=1,MMAF
C10 162      DO 170 N3=1,3
C10 163      ALRTIN,1,2)=MAFORDIN,3,1)
C10 164      ALRTIN,2,2)=MAFORDIN,2,1)
C10 165      ALRTIN,3,2)=MAFORDIN,1,1)
C10 166      165 CONTINUE
C10 167      WRITE (KFILE2)((ALRTIN,M3,2),M=1,NMAF),M3=1,3)
C10 168      DO 195 NM=2,NM
C10 169      DO 170 N3=1,3
C10 170      ALRTIN,M3,1)=ALRTIN,M3,2)
C10 171      170 CONTINUE
C10 172      DO 175 N=1,NMAF
C10 173      ALRTIN,1,2)=MAFORDIN,3,MM)
C10 174      ALRTIN,2,2)=MAFORDIN,2,MM)
C10 175      ALRTIN,3,2)=MAFORDIN,1,MM)
C10 176      175 CONTINUE
C10 177      DO 180 I=1,185,1)
C10 178      180 CALL SURC(INMAF,ALRT,VECRT)
C10 179      GO TO 190
C10 180      185 CALL SURC(INMAF,ALRT,VECRT)
C10 181      190 CONTINUE
C10 182      WRITE (KFILE2)((VECRT(M,M3),M=1,NL),M3=1,3)
C10 183      WRITE (KFILE2)((ALRTIN,M3,2),M=1,NMAF),M3=1,3)
C10 184      195 CONTINUE
C10 185      200 CONTINUE
C10 186      IF (J1.EQ.2) GO TO 210
C10 187      205 WRITE (KFILE1)BLOCK
C10 188      READ (KFILE1)DUM
C10 189      210 IF (J2.NE.2) GO TO 215
C10 190      FUSELAGE
C10 191      READ (KFILE1)BLOCK
C10 192      WRITE (KFILE1)BLOCK
C10 193      GO TO 280
C10 194      215 IF (J2.EQ.0) GO TO 425
C10 195      JZTEST=3
C10 196      IF (J2.EQ.-1.AND.J6.EQ.-1)JZTEST=1
C10 197      IF (J2.EQ.-1.AND.J6.EQ.0)JZTEST=2
C10 198      IF (J6.EQ.1)JZTEST=1
C10 199      225 MFI=1,MMFUS
C10 200      MMAD=MMOZIMEU
C10 201      MMUSOM=MMOZIMEU
C10 202      MMFUSOR
C10 203      MREC=(M+9)/10
C10 204      11=-9
C10 205      12=0
C10 206      DO 220 M1=1,MREC
C10 207      11=11*10
C10 208      READ (JREAD,15) (MFUS(I,MFU),I=1,12)
C10 209      WRITE (JWRITE,25) (MFUS(I,MFU),I=1,12)
C10 210      220 CONTINUE
C10 211      IF (JZTEST.NE.2) GO TO 230
C10 212      11=-9
C10 213
C10 214

```

```

C10 215      12=0
C10 216      DO 225 M1=1,MREC
C10 217      11=11*10
C10 218      READ (JREAD,15) (MFUS(I,MFU),I=1,12)
C10 219      WRITE (JWRITE,25) (MFUS(I,MFU),I=1,12)
C10 220      225 CONTINUE
C10 221      DO 230 I=1,N
C10 222      DO 235 L=1,N
C10 223      230 ZRUS(I,MFI)=0.
C10 224      235 ZRUS(I,MFI)=0.
C10 225      240 IF (JZTEST.NE.3) GO TO 260
C10 226      MCARD=(NRAD*9)/10
C10 227      DO 255 LM=1,M
C10 228      DO 230 K=1,2
C10 229      KK=K*(MFU-1)+2
C10 230      11=10
C10 231      11=-9
C10 232      12=C
C10 233      DO 245 NM=1,MCARD
C10 234      IF (NM.EC.MCARD)I=MC0(NRAD,10)
C10 235      IF (I1.EQ.0)I1=10
C10 236      11=11*10
C10 237      12=12*11
C10 238      READ (JREAD,15) (SFUS(I,LM,MM),I=1,12)
C10 239      WRITE (JWRITE,25) (SFUS(I,LM,MM),I=1,12)
C10 240      245 CONTINUE
C10 241      250 CONTINUE
C10 242      255 CONTINUE
C10 243      GO TO 275
C10 244      260 11=-9
C10 245      12=265
C10 246      11=11*10
C10 247      12=12*10
C10 248      READ (JREAD,15) (FUSARD(I,MFU),I=1,12)
C10 249      WRITE (JWRITE,25) (FUSARD(I,MFU),I=1,12)
C10 250      265 CONTINUE
C10 251      DO 270 I=1,M
C10 252      DO 275 FUSARD(I,MFU)=SORT(FUSARD(I,MFU)/P)
C10 253      275 CONTINUE
C10 254      280 IF (J1.NE.0) GO TO 290
C10 255      FUSELAGE MIN AND MAX
C10 256      MMIN=MFUS(1,1)
C10 257      MMAX=MFUS(1,1)
C10 258      IF (JZTEST.EQ.3) GO TO 285
C10 259      YMAX=FUSARD(1,1)
C10 260      ZMIN=FUSARD(1,1)+ZFUS(1,1)
C10 261      ZMAX=FUSARD(1,1)+ZFUS(1,1)
C10 262      285 YMAX=SFUS(1,1)
C10 263      ZMIN=SFUS(1,1)
C10 264      ZMAX=SFUS(1,1)
C10 265      290 DO 310 M1=MMFUS
C10 266      MMAD=MMOZIMEU
C10 267      MMUSOM=MMOZIMEU
C10 268      MMFUSOR
C10 269      MREC=(M+9)/10
C10 270      11=11*10
C10 271      READ (JREAD,15) (MFUS(I,MFU),I=1,12)
C10 272      WRITE (JWRITE,25) (MFUS(I,MFU),I=1,12)
C10 273      220 CONTINUE
C10 274      IF (JZTEST.NE.3) GO TO 295
C10 275      YMAX=MMAX(YMAX,FUSARD(MN,M))

```





```

C10 495
C10 496
C10 497
C10 498
C10 499
C10 500
C10 501
C10 502
C10 503
C10 504
C10 505
C10 506
C10 507
C10 508
C10 509
C10 510
C10 511
C10 512
C10 513
C10 514

C000 SETUP LIST LINE AROUND PODS
NL1=MANGL-1
DO 530 NP1=1,MP
DO 510 N=1,MANGL
N=N
ALRT(N,1,2)=XPOD(NP1,1)+PODORG(NP1,1)
ALRT(N,2,2)=PODORG(NP1,1)+ANCSIN(N)+PODORG(NP1,2)
ALRT(N,3,2)=PODORG(NP1,1)+ANCSIN(N)+PODORG(NP1,3)
510 CONTINUE
WRITE (KFLE2)((ALRT(N,M3,2),N=1,MANGL,M3=1,3)
DO 525 NN=2,NPODOR
DO 515 NN=1,3
CONTINUE
515 DO 520 N=1,MANGL
N=N
ALRT(N,1,2)=XPOD(NP1,NN)+PODORG(NP1,1)
ALRT(N,2,2)=PODORG(NP1,NN)+ANCSIN(N)+PODORG(NP1,2)
ALRT(N,3,2)=PODORG(NP1,NN)+ANCSIN(N)+PODORG(NP1,3)
520 CONTINUE
CALL SURCC(INANG1,ALRT,VECTR)
WRITE (KFLE2)((ALRT(N,M3),N=1,ML1,M3=1,3)
WRITE (KFLE2)((ALRT(N,M3,2),N=1,MANGL,M3=1,3)
525 CONTINUE
530 CONTINUE
IF (J3.EQ.2) GO TO 540
535 WRITE (KFLE1)BLOCK
535 READ (KFLE4)IDUM
C000 FINS
540 IF (JA,NE.2) GO TO 545
WRITE (KFLE4)BLOCK
GO TO 565
545 IF (JA,EG.0) GO TO 660
N=NOR
DO 570 M=1,MP
WRITE (JWRITE,25) ((FINDORG(M,1),J)=1,4),(-1,2)
WRITE (JWRITE,25) ((FINDORG(M,1),J)=1,4),(-1,2)
READ (JREAD,15) (XFIND(NM,1),I=1,M)
WRITE (JWRITE,25) (XFIND(NM,1),I=1,M)
READ (JREAD,15) (FINDORG(M,1),J)=1,M)
WRITE (JWRITE,25) (FINDORG(M,1),J)=1,M)
550 CONTINUE
C000 CHANGE TO ACTUAL UNITS, COMPUTE MINIMUMS AND MAXIMUMS
DO 560 LQ=1,MP
DO 560 I=1,2
J=3-I
E=0.01*FINDORG(LQ,J,4)
E2=FINDORG(LQ,J,2)
DO 555 K=1,NFINDOR
E2=FINDORG(LQ,K)*E
FINDORG(LQ,J,K)=E2+E
FINZ(LQ,J,K)=E2-E
555 FINZ(LQ,J,K)=FINDORG(LQ,J,1)+E*XFIND(LQ,K)
560 CONTINUE
565 IF (JJ,NE.0,OR,J2,NE.0,OR,J3,NE.0) GO TO 570
XIN=FINDORG(1,1,1)
MAX=FINDORG(1,1,1)
MIN=FINDORG(1,1,2)

```

```

C10 395
C10 396
C10 397
C10 398
C10 399
C10 400
C10 401
C10 402
C10 403
C10 404
C10 405
C10 406
C10 407
C10 408
C10 409
C10 410
C10 411
C10 412
C10 413
C10 414
C10 415
C10 416
C10 417
C10 418
C10 419
C10 420
C10 421
C10 422
C10 423
C10 424
C10 425
C10 426
C10 427
C10 428
C10 429
C10 430
C10 431
C10 432
C10 433
C10 434
C10 435
C10 436
C10 437
C10 438
C10 439
C10 440
C10 441
C10 442
C10 443
C10 444
C10 445
C10 446
C10 447
C10 448
C10 449
C10 450
C10 451
C10 452
C10 453
C10 454

READ (JREAD,15) (XPOD(NM,1),I=1,1,12)
WRITE (JWRITE,25) (XPOD(NM,1),I=1,1,12)
440 CONTINUE
I1=9
I2=0
DO 445 N1=1,NREC
I1=I1+10
I2=I2+10
READ (JREAD,15) (PODORG(NM,1),I=1,1,12)
WRITE (JWRITE,25) (PODORG(NM,1),I=1,1,12)
445 CONTINUE
450 CONTINUE
C000 COMPUTE ACTUAL X,MINIMUM,MAXIMUM
DO 440 NN=1,NPODOR
XIN=XPOD(1,1)
MAX=XPOD(1,1)+NPODOR
YIN=XPOD(1,2)
YMAX=XPOD(1,2)+NPODOR(1,1)
ZIN=XPOD(1,3)
ZMAX=XPOD(1,3)+NPODOR(1,1)
445 DO 475 N=1,MP
YIN=MAX(XIN,YIN,XPOD(N,1))
YMAX=MAX(XMAX,YMAX,XPOD(N,1)+NPODOR)
DO 470 NN=1,NPODOR
YIN=MAX(XIN,YIN,XPOD(N,NN)+PODORG(N,2))
YMAX=MAX(XMAX,YMAX,XPOD(N,NN)+PODORG(N,2))
470 ZIN=MAX(XIN,ZIN,XPOD(N,3)+PODORG(N,MM))
ZMAX=MAX(XMAX,ZMAX,XPOD(N,3)+PODORG(N,MM))
475 CONTINUE
NAME1=MANZ+1
FANG=MANZ
DELE=6.2831853/FANG
DO 480 N=1,MANGL
E=N-1
ANCSIN(I)=SINE*DELE
ARCSIN(I)=COSIE*DELE
C000 SETUP LIST LINE IN STREAMWISE DIRECTION
DO 505 NP1=1,MP
ALRT(N,1,2)=XPOD(NP1,N)+PODORG(NP1,1)
ALRT(N,2,2)=PODORG(NP1,N)+ANCSIN(I)+PODORG(NP1,2)
ALRT(N,3,2)=PODORG(NP1,N)+ANCSIN(I)+PODORG(NP1,3)
485 CONTINUE
WRITE (KFLE2)((ALRT(N,M3,2),N=1,NPODOR,M3=1,3)
DO 500 NN=2,NPODOR
DO 490 NN=1,3
ALRT(N,1,2)=XPOD(NP1,NN)+PODORG(NP1,1)
ALRT(N,2,2)=PODORG(NP1,NN)+ANCSIN(I)+PODORG(NP1,2)
ALRT(N,3,2)=PODORG(NP1,NN)+ANCSIN(I)+PODORG(NP1,3)
490 CONTINUE
DO 495 N=1,NPODOR
ALRT(N,2,2)=PODORG(NP1,N)+ANCSIN(I)+PODORG(NP1,2)
ALRT(N,3,2)=PODORG(NP1,N)+ANCSIN(I)+PODORG(NP1,3)
495 CONTINUE
CALL SURCC(INPODOR,ALRT,VECTR)
WRITE (KFLE2)((ALRT(N,M3),N=1,ML1,M3=1,3)
WRITE (KFLE2)((ALRT(N,M3,2),N=1,NPODOR,M3=1,3)
500 CONTINUE
505 CONTINUE

```

```

ZRM=FINORG(1,1,3)
ZMAX=FINORG(1,1,3)
570 DO 575 N=1,NF
ZRM=ARMI(ZRM,FINORG(N,1,3))
ZMAX=MAX(ZMAX,FINORG(N,2,3))
DO 575 N2=1,2
ZRM=ARMI(ZRM,FINORG(N,N2,3))
ZMAX=MAX(ZMAX,FINORG(N,N2,3))
DO 575 NM=1,NFINOR
ZMAX=MAX(ZMAX,FINORG(N,N2,NM))
CONTINUE
575 ML=SEFINOR-1
C***
DO 580 N2=1,NF
DO 580 N=1,NFINOR
ALRT(N,1,N2)=FINORG(N,1,N2,N)
ALRT(N,2,N2)=FINORG(N,1,N2,N)
ALRT(N,3,N2)=FINORG(N,1,N2,3)
580 CONTINUE
CALL SURCL(NFINOR,ALRT,VECTR)
WRITE (KFILE2)((ALRT(N,N3,1),N=1,NFINOR),N3=1,3)
WRITE (KFILE2)((ALRT(N,N3),N=1,NL1),N3=1,3)
WRITE (KFILE2)((ALRT(N,N3,2),N=1,NFINOR),N3=1,3)
CHANGE Y FOR INSIDE LINES
C***
DO 585 N2=1,2
DO 585 N=1,NFINOR
ALRT(N,2,N2)=FINXZ(N,1,N2,N)
585 CONTINUE
CALL SURCC(NFINOR,ALRT,VECTR)
WRITE (KFILE2)((ALRT(N,N3,1),N=1,NFINOR),N3=1,3)
WRITE (KFILE2)((ALRT(N,N3),N=1,NL1),N3=1,3)
WRITE (KFILE2)((ALRT(N,N3,2),N=1,NFINOR),N3=1,3)
590 CONTINUE
SETUP LINES IN VERTICAL DIRECTION
C***
DO 595 N2=1,2
DO 595 N=1,NFINOR
ALRT(N,2,N2)=FINXZ(N,1,N2,1)
IF (NM2.EQ.2) GO TO 595
ALRT(N2,2,2)=FINXZ(N,1,N2,1)
GO TO 600
595 ALRT(N2,2,2)=FINXZ(N,1,N2,1)
600 CONTINUE
ALRT(N2,3,2)=FINORG(N,1,N2,3)
605 CONTINUE
WRITE (KFILE2)((ALRT(N,N3,2),N=1,2),N3=1,3)
DO 610 N3=1,3
DO 610 N2=1,2
ALRT(N2,N3,1)=ALRT(N2,N3,2)
610 CONTINUE
DO 625 N2=1,2
ALRT(N2,1,2)=FINXZ(N,1,N2,NH)
IF (NM2.EQ.2) GO TO 615
ALRT(N2,2,2)=FINXZ(N,1,N2,NH)
GO TO 620
615 ALRT(N2,2,2)=FINXZ(N,1,N2,NH)
620 CONTINUE
ALRT(N2,3,2)=FINXZ(N,1,N2,3)

```

```

C10 516
C10 517
C10 518
C10 519
C10 520
C10 521
C10 522
C10 523
C10 524
C10 525
C10 526
C10 527
C10 528
C10 529
C10 530
C10 531
C10 532
C10 533
C10 534
C10 535
C10 536
C10 537
C10 538
C10 539
C10 540
C10 541
C10 542
C10 543
C10 544
C10 545
C10 546
C10 547
C10 548
C10 549
C10 550
C10 551
C10 552
C10 553
C10 554
C10 555
C10 556
C10 557
C10 558
C10 559
C10 560
C10 561
C10 562
C10 563
C10 564
C10 565
C10 566
C10 567
C10 568
C10 569
C10 570
C10 571
C10 572
C10 573
C10 574

```

```

625 CONTINUE
CALL TO (M30,635),NM2
630 CALL SURCC(Z,ALRT,VECTR)
635 CALL SURCL(Z,ALRT,VECTR)
640 CONTINUE
WRITE (KFILE2)((ALRT(N2,N3,2),N2=1,2),N3=1,3)
645 CONTINUE
650 CONTINUE
655 CONTINUE
IF (JA.EQ.2) GO TO 665
660 WRITE (KFILE1)BLOCK
C***
CANARDS
READ (KFILE4)DUM
665 IF (J5.NE.2) GO TO 670
NC=NCANOR
NCANOR=TABS(NCANOR)
READ (KFILE4)BLOCK
WRITE (KFILE1)BLOCK
GO TO 705
670 IF (J5.EQ.0) GO TO 820
N=TABS(NCANOR)
DO 685 NM=1,NCAN
WRITE (KFILE2)((CANORG(NM,1,J),J=1,4),J=1,2)
READ (KFILE2)((CANORG(NM,1,J),J=1,4),J=1,2)
WRITE (KFILE2)((CANORG(NM,1,J),J=1,N)
READ (KFILE2)((CANORG(NM,1,J),J=1,N)
WRITE (KFILE2)((CANORG(NM,1,J),J=1,N)
IF (NCANOR.LT.0) GO TO 680
DO 675 J=1,N
CANOR(NM,1,J)=CANOR(NM,1,J)
GO TO 685
680 READ (KFILE2)((CANORG(NM,1,J),J=1,N)
WRITE (KFILE2)((CANORG(NM,1,J),J=1,N)
685 CONTINUE
NCANOR=TABS(NCANOR)
C***
CHANGE TO ACTUAL UNITS, COMPUTE MINIMUMS AND MAXIMUMS
DO 700 NM=1,NCAN
DO 695 K=1,2
I=3-K
E=-01*CANORG(NM,1,4)
E3=CANORG(NM,1,3)
DO 690 J=1,NCANOR
CANOR(NM,1,J)=E+CANOR(NM,1,J)+E3
CANOR(NM,1,J)=E+CANOR(NM,1,J)+E3
695 CONTINUE
700 CONTINUE
705 IF (J1.NE.0,OR,J2.NE.0,OR,J3.NE.0,OR,J4.NE.0) GO TO 710
ZMAX=CANOR(1,1)
ZRM=CANOR(1,1)
YMAX=CANOR(1,2)
ZRM=CANOR(1,2)
ZRM=CANOR(1,1,1)
ZMAX=CANOR(1,1,1)
ZMAX=CANOR(1,1,1)
DO 725 NCA=1,NCAN
710 YMAX=MAX(YMAX,CANORG(NCA,2,2))
DO 720 N2=1,2

```

```

C10 575
C10 576
C10 577
C10 578
C10 579
C10 580
C10 581
C10 582
C10 583
C10 584
C10 585
C10 586
C10 587
C10 588
C10 589
C10 590
C10 591
C10 592
C10 593
C10 594
C10 595
C10 596
C10 597
C10 598
C10 599
C10 600
C10 601
C10 602
C10 603
C10 604
C10 605
C10 606
C10 607
C10 608
C10 609
C10 610
C10 611
C10 612
C10 613
C10 614
C10 615
C10 616
C10 617
C10 618
C10 619
C10 620
C10 621
C10 622
C10 623
C10 624
C10 625
C10 626
C10 627
C10 628
C10 629
C10 630
C10 631
C10 632
C10 633
C10 634

```

```

C10 695      XMIN=AMIN(XMIN,CANORX(INCA,N2,1))
C10 696      XMAX=AMAX(XMAX,CANORX(INCA,N2,MCANOR))
C10 697      DO 715 NN=1,MCANOR
C10 698      ZMIN=AMIN(ZMIN,CANOR1(INCA,N2,NN))
C10 699      ZMAX=AMAX(ZMAX,CANORD(INCA,N2,NN))
C10 700      715 CONTINUE
C10 701      720 CONTINUE
C10 702      725 CONTINUE
C10 703      MLI=MC-1
C10 704      C***  SETUP TWO LINES IN STREAMWISE DIRECTION FOR UPPER AND LOWER
C10 705      DO 760 MCA=1,MCAN
C10 706      DO 755 I=1,I2
C10 707      DO 735 N2=1,2
C10 708      MLI=MLI+1
C10 709      CANORX(INCA,N2,N)
C10 710      CANORD(INCA,N2,2)
C10 711      IF (I.EQ.2) GO TO 730
C10 712      ALRT(N3,N2)=CANORD(INCA,N2,N)
C10 713      GO TO 735
C10 714      730 ALRT(N3,N2)=CANOR1(INCA,N2,N)
C10 715      735 CONTINUE
C10 716      GO TO (740,745),I
C10 717      740 CALL SURCL(INC,ALRT,VECRT)
C10 718      GO TO 750
C10 719      745 CALL SURCL(INC,ALRT,VECRT)
C10 720      750 CONTINUE
C10 721      WRITE (KFILE2)((VECRT(N3),N=1,ML),N3=1,3)
C10 722      WRITE (KFILE2)((ALRT(N3,2),N=1,NC),N3=1,3)
C10 723      755 CONTINUE
C10 724      760 CONTINUE
C10 725      C***  SETUP LINES IN SPANNWISE DIRECTION
C10 726      DO 815 MCA=1,MCAN
C10 727      DO 810 I=1,I2
C10 728      DO 770 N2=1,2
C10 729      ALRT(N3,2)=CANORX(INCA,N2,1)
C10 730      ALRT(N3,2)=CANORD(INCA,N2,2)
C10 731      IF (I.EQ.2) GO TO 785
C10 732      ALRT(N3,2)=CANORD(INCA,N2,1)
C10 733      GO TO 790
C10 734      765 ALRT(N3,2)=CANOR1(INCA,N2,1)
C10 735      770 CONTINUE
C10 736      WRITE (KFILE2)((ALRT(N3,2),N2=1,2),N3=1,3)
C10 737      DO 805 NN=2,MC
C10 738      DO 775 M2=1,3
C10 739      ALRT(N3,1)=ALRT(N2,N3,2)
C10 740      775 CONTINUE
C10 741      DO 785 M2=1,2
C10 742      ALRT(N3,2)=CANORX(INCA,N2,NN)
C10 743      ALRT(N3,2)=CANORD(INCA,N2,2)
C10 744      IF (I.EQ.2) GO TO 780
C10 745      ALRT(N3,2)=CANORD(INCA,N2,NN)
C10 746      GO TO 785
C10 747      780 ALRT(N3,2)=CANOR1(INCA,N2,NN)
C10 748      785 CONTINUE
C10 749      GO TO (790,795),I
C10 750      790 CALL SURCL(2,ALRT,VECRT)
C10 751      GO TO 800
C10 752      795 CALL SURCL(2,ALRT,VECRT)
C10 753      800 CONTINUE

```

```

C10 636      XMIN=AMIN(XMIN,CANORX(INCA,N2,1))
C10 637      XMAX=AMAX(XMAX,CANORX(INCA,N2,MCANOR))
C10 638      DO 715 NN=1,MCANOR
C10 639      ZMIN=AMIN(ZMIN,CANOR1(INCA,N2,NN))
C10 640      ZMAX=AMAX(ZMAX,CANORD(INCA,N2,NN))
C10 641      715 CONTINUE
C10 642      720 CONTINUE
C10 643      725 CONTINUE
C10 644      MLI=MC-1
C10 645      C***  SETUP TWO LINES IN STREAMWISE DIRECTION FOR UPPER AND LOWER
C10 646      DO 760 MCA=1,MCAN
C10 647      DO 755 I=1,I2
C10 648      DO 735 N2=1,2
C10 649      MLI=MLI+1
C10 650      CANORX(INCA,N2,N)
C10 651      CANORD(INCA,N2,2)
C10 652      IF (I.EQ.2) GO TO 730
C10 653      ALRT(N3,N2)=CANORD(INCA,N2,N)
C10 654      GO TO 735
C10 655      730 ALRT(N3,N2)=CANOR1(INCA,N2,N)
C10 656      735 CONTINUE
C10 657      GO TO (740,745),I
C10 658      740 CALL SURCL(INC,ALRT,VECRT)
C10 659      GO TO 750
C10 660      745 CALL SURCL(INC,ALRT,VECRT)
C10 661      750 CONTINUE
C10 662      WRITE (KFILE2)((VECRT(N3),N=1,ML),N3=1,3)
C10 663      WRITE (KFILE2)((ALRT(N3,2),N=1,NC),N3=1,3)
C10 664      755 CONTINUE
C10 665      760 CONTINUE
C10 666      C***  SETUP LINES IN SPANNWISE DIRECTION
C10 667      DO 815 MCA=1,MCAN
C10 668      DO 810 I=1,I2
C10 669      DO 770 N2=1,2
C10 670      ALRT(N3,2)=CANORX(INCA,N2,1)
C10 671      ALRT(N3,2)=CANORD(INCA,N2,2)
C10 672      IF (I.EQ.2) GO TO 785
C10 673      ALRT(N3,2)=CANORD(INCA,N2,1)
C10 674      GO TO 790
C10 675      765 ALRT(N3,2)=CANOR1(INCA,N2,1)
C10 676      770 CONTINUE
C10 677      WRITE (KFILE2)((ALRT(N3,2),N2=1,2),N3=1,3)
C10 678      DO 805 NN=2,MC
C10 679      DO 775 M2=1,3
C10 680      ALRT(N3,1)=ALRT(N2,N3,2)
C10 681      775 CONTINUE
C10 682      DO 785 M2=1,2
C10 683      ALRT(N3,2)=CANORX(INCA,N2,NN)
C10 684      ALRT(N3,2)=CANORD(INCA,N2,2)
C10 685      IF (I.EQ.2) GO TO 780
C10 686      ALRT(N3,2)=CANORD(INCA,N2,NN)
C10 687      GO TO 785
C10 688      780 ALRT(N3,2)=CANOR1(INCA,N2,NN)
C10 689      785 CONTINUE
C10 690      GO TO (790,795),I
C10 691      790 CALL SURCL(2,ALRT,VECRT)
C10 692      GO TO 800
C10 693      795 CALL SURCL(2,ALRT,VECRT)
C10 694      800 CONTINUE

```

```

C10 695      WRITE (KFILE2)((VECRT(N3),N=1,ML),N3=1,3)
C10 696      805 CONTINUE
C10 697      810 CONTINUE
C10 698      815 CONTINUE
C10 699      IF (J5.EQ.2) GO TO 825
C10 700      820 WRITE (KFILE1)BLOCK
C10 701      READ (KFILE4)DUM
C10 702      REWIND KFILE4
C10 703      825 REWIND KFILE1
C10 704      READ (KFILE1)REFA
C10 705      WRITE (KFILE4)REFA
C10 706      DD 830,K=1,5
C10 707      READ (KFILE1)BLOCK
C10 708      830 WRITE (KFILE4)BLOCK
C10 709      C***  FIND MAXIMUM DISTANCE AND MIDPOINT
C10 710      YMIN=YMAX=XMIN
C10 711      XDIS=YMAX-XMIN
C10 712      YDIS=YMAX-YMIN
C10 713      ZDIS=ZMAX-ZMIN
C10 714      @IGD=MAX(1,XDIS,YDIS,ZDIS)
C10 715      XMID=.5*(XMAX+XMIN)+XMIN
C10 716      YMID=.5*(YMAX+YMIN)
C10 717      ZMID=.5*(ZMAX+ZMIN)+ZMIN
C10 718      RETURN
C10 719      840 CONTINUE
C10 720      845 CONTINUE

```

```

C10 695      SUBROUTINE SURCLINPT,FLINE,FVEC)
C10 696      COMPUTES SURFACE UNIT NORMALS
C10 697      DIMENSION FLINE(3),FVEC(3)
C10 698      DO 10 N=2,NPT
C10 699      T1X=FLINE(N,2)-FLINE(N-1,1)
C10 700      T2X=FLINE(N-1,2)-FLINE(N,1)
C10 701      T1Y=FLINE(N,2)-FLINE(N-1,2)
C10 702      T2Y=FLINE(N-1,2)-FLINE(N,2)
C10 703      T1Z=FLINE(N,3)-FLINE(N-1,3)
C10 704      T2Z=FLINE(N-1,3)-FLINE(N,3)
C10 705      YN=X-T1X-T2X
C10 706      YN=X-T1Y-T2Y
C10 707      ZN=X-T1Z-T2Z
C10 708      FMSOR(T1X**2+YNY**2+ZMZ**2)
C10 709      IF (FN.EQ.0.) GO TO 5
C10 710      FVEC(N-1,1)=XN/FM
C10 711      FVEC(N-1,2)=YNY/FM
C10 712      FVEC(N-1,3)=ZMZ/FM
C10 713      GO TO 10
C10 714      5 FVEC(N-1,1)=0.
C10 715      FVEC(N-1,2)=0.
C10 716      FVEC(N-1,3)=0.
C10 717      10 CONTINUE
C10 718      RETURN
C10 719      840 CONTINUE
C10 720      845 CONTINUE

```

```

DO 10 N=2,NPT
  TLX=PLINE(N,1,2)-FLINE(N-1,1,1)
  TZK=PLINE(N,1,1)-FLINE(N-1,1,2)
  TLY=PLINE(N,2,1)-FLINE(N-1,2,1)
  T1Y=PLINE(N,2,2)-FLINE(N-1,2,1)
  T1Z=PLINE(N,2,1)-FLINE(N-1,2,2)
  T2Z=PLINE(N,3,1)-FLINE(N-1,3,1)
  T2Z=PLINE(N,3,1)-FLINE(N-1,3,1)
  XNR=TZ*TLZ-T1Y*T1Z
  YNY=TL*TYZ-T1X*TYZ
  ZNZ=TZ*TY-T1X*TYZ
  FN=SQRT(XNR**2+YNY**2+ZNZ**2)
  IF (FN.EQ.0.) GO TO 5
  FVEC(N-1,1)=XNR/FN
  FVEC(N-1,2)=YNY/FN
  FVEC(N-1,3)=ZNZ/FN
  GO TO 10
5 FVEC(N-1,1)=0.
  FVEC(N-1,2)=0.
  FVEC(N-1,3)=0.
10 CONTINUE
  RETURN
  END

SUBROUTINE CIRC20
  CONTROL ROUTINE FOR VARIOUS TYPES OF PLOTS OF AN AIRCRAFT
  COMMON ABC(20),JO,J1,J2,J3,J4,J5,J6,MWAF,MWAFOR,MFUS,MAAD(4),MFOR
  IX(4),MPODDOR,MF,FMOR,MCAN,MCANOR,MZTEST,MH,MC,ABCDE(20),MORZ,V
  IER,TESTI,PHI,THETA,PSI,KF,YF,ZF,DI,ST,FRAG,PLOTSZ,TYPE,KODE,XMIN,X
  IMAX,YMIN,YMAX,ZMIN,ZMAX,XMID,YMID,ZMID,BIGD,ISP
  COMMON /IMOUT/IMOUT,JWRITE,JWRITE,KFILE1,KFILE2,KFILE3,KFILE4
  DIMENSION ORG(3)
  DATA TYPED/SHORT/,TYPEP/SHPER/,TYPES/3MSTE/,TYPEV/3MVU3/
  DATA XI/IMX/YI/IMY/ZI/IMZ/
  REMIND KFILEZ
  XSAV=XMIN
  YSAV=YMIN
  ZSAV=ZMIN
  XMSAV=XMAX
  YMSAV=YMAX
  ZMSAV=ZMAX
  IF (TYPE.EQ. TYPEV) GO TO 25
  SCALE=BIGD/PLOTSZ
  ORG(1)=PHI
  ORG(2)=THETA
  ORG(3)=PSI
  PH=0.
  PI=3.141592653589793
  P=PI.
  Y1G=ORG(1)
  Y1G=FLOAT(IFIX(YMAX/SCALE))+ORG(1)
  IF (Y1G.GT.ORG(2)) GO TO 5
  Y1G=ORG(2)
  Y1G=FLOAT(IFIX(ZMAX/SCALE))+ORG(2)
  Y1G=FLOAT(IFIX(ZMAX/SCALE)) GO TO 10
5 Y1G=ORG(3)
  Y1G=FLOAT(IFIX(ZMAX/SCALE))+ORG(3)
10 CALL CALPLT(2,0,YORG,-3)

```

```

C***
  NOTATE ON 3VIEW PLOTS
  MCNAR=IFIX(6.*PLOTSZ)
  IF (MCNAR.GT.80) GO TO 15
  X=0.
  GO TO 20
15 CONTINUE
  MDIF=(MCNAR-80)/2
  X=FLOAT(MDIF)/6.
  MCNAR=80
  20 CALL NOTATE(X,0.,.2,ABC,0.,MCNAR)
  XMIN=0.
  YMIN=0.
  ZMIN=0.
  MORZ=XI
  VERT=YI
  YORG=ORG(1)-YORG-1
  CALL CALPLT(0.,YORG,-3)
  CALL CIRC21
  REMIND KFILEZ
  YORG=ORG(2)-ORG(1)
  CALL CALPLT(0.,YORG,-3)
  CALL CIRC21
  REMIND KFILEZ
  MORZ=YI
  YORG=ORG(3)-ORG(2)
  YMIN=FLOAT(IFIX(YSAV/SCALE))+SCALE
  CALL CALPLT(0.,YORG,-3)
  CALL CIRC21
  X=FLOAT(IFIX(PLOTSZ+6.))
  Y1=-ORG(3)
  GO TO 45
25 CONTINUE
  IF (TYPE.EQ. TYPES) GO TO 35
  IF (TYPE.EQ. TYPEP) GO TO 35
  X=0.
  MCNAR=IFIX(11.*PLOTSZ)+3
  IF (MCNAR.LE.80) GO TO 30
  MDIF=(MCNAR-80)/2
  X=FLOAT(MDIF)/11.
  MCNAR=80
  30 CALL NOTATE(X,.5,-1,ABC,0.,MCNAR)
  35 CONTINUE
  CALL CALPLT(0.,-3)
  IF (TYPE.EQ. TYPEP-OR. TYPE.EQ. TYPES) GO TO 40
  CALL CIRC21
  X=FLOAT(IFIX(PLOTSZ+2.))
  Y=-0.
  GO TO 45
40 ISP=1
  IF (TYPE.EQ. TYPES) ISP=2
  PEASPECTIVE OR STEREO
  CALL CIRC22
  X=PLOTSZ+2.
  IF (TYPE.EQ. TYPES) X=PLOTSZ
  Y=-0.
  45 CONTINUE
C***

```

C20 36  
C20 37  
C20 38  
C20 39  
C20 40  
C20 41  
C20 42  
C20 43  
C20 44  
C20 45  
C20 46  
C20 47  
C20 48  
C20 49  
C20 50  
C20 51  
C20 52  
C20 53  
C20 54  
C20 55  
C20 56  
C20 57  
C20 58  
C20 59  
C20 60  
C20 61  
C20 62  
C20 63  
C20 64  
C20 65  
C20 66  
C20 67  
C20 68  
C20 69  
C20 70  
C20 71  
C20 72  
C20 73  
C20 74  
C20 75  
C20 76  
C20 77  
C20 78  
C20 79  
C20 80  
C20 81  
C20 82  
C20 83  
C20 84  
C20 85  
C20 86  
C20 87  
C20 88  
C20 89  
C20 90  
C20 91  
C20 92  
C20 93  
C20 94  
C20 95





```

DO 15 NN=1,NVEC
DO 10 M3=1,3
VECT(FIN,M3,1)=VECT(IN,M3,2)
VECL(FIN,M3,1)=VECL(IN,M3,2)
10 CONTINUE
20 READ (KFILEZ)((ALINE(MN,M3),NN=1,MPT),M3=1,3)
IF (N.NE.NL) GO TO 25
K1=1
K2=1
GO TO 35
DO 30 NN=1,NVEC
DO 40 MM=1,MPT
ALINE(MN,2)=ALINE(MN,2)
45 IF (ITEST1.EQ.1) GO TO 70
45 IF (ITEST2.EQ.1) GO TO 85
C*** NO ROTATION OR VISIBILITY TEST
DO 50 MN=1,MPT
XLINE(MN,1)=ALINE(MN,IMORZ)
50 XLINE(MN,2)=ALINE(MN,IVERT)
GO TO 65
C*** ROTATE BUT NO VISIBILITY TEST
DO 60 MM=1,MPT
XLINE(MN,M2)=ALINE(MN,2)
60 CONTINUE
C*** SCALE AND PLOT
DO 65 XLINE(MPT,1)=MMIN
XLINE(MPT,2)=MMIN
XLINE(MPT,3)=SCALE
XLINE(MPT,2)=SCALE
CALL LINE(XLINE(1,1),XLINE(1,2),MPT,1,0,0)
70 IF (ITEST2.EQ.1) GO TO 95
GO TO 150
C*** CHECK VISIBILITY BUT NO ROTATION
DO 75 MN=1,MPT
RLINE(MN,1)=ALINE(MN,IMORZ)
RLINE(MN,2)=ALINE(MN,IVERT)
75 CONTINUE
DO 90 NN=1,NVEC
DO 85 N2=1,2
IF (NN2.EQ.2) GO TO 80
RVEC(MN,M2)=VECT(MN,ITEST,M2)
GO TO 85
80 RVEC(MN,M2)=VECL(MN,ITEST,M2)
90 CONTINUE
GO TO 115
C*** ROTATE AND CHECK VISIBILITY
95 CALL PLOT(MPT,ALINE,RLINE)
IF (NN2.EQ.2) GO TO 105

```

```

PLT 18
PLT 19
PLT 20
PLT 21
PLT 22
PLT 23
PLT 24
PLT 25
PLT 26
PLT 27
PLT 28
PLT 29
PLT 30
PLT 31
PLT 32
PLT 33
PLT 34
PLT 35
PLT 36
PLT 37
PLT 38
PLT 39
PLT 40
PLT 41
PLT 42
PLT 43
PLT 44
PLT 45
PLT 46
PLT 47
PLT 48
PLT 49
PLT 50
PLT 51
PLT 52
PLT 53
PLT 54
PLT 55
PLT 56
PLT 57
PLT 58
PLT 59
PLT 60
PLT 61
PLT 62
PLT 63
PLT 64
PLT 65
PLT 66
PLT 67
PLT 68
PLT 69
PLT 70
PLT 71
PLT 72
PLT 73
PLT 74
PLT 75
PLT 76
PLT 77

```

```

DO 100 N2=K1,K2
CALL VECROT(MEC,C,VECT(1,1,N2),RVEC(1,N2))
100 CONTINUE
GO TO 115
105 DO 110 N2=K1,K2
CALL VECROT(MEC,C,VECL(1,1,N2),RVEC(1,N2))
110 CONTINUE
C*** FIND VISIBLE LINES
115 IF (ITEST.NE.2) GO TO 125
DO 120 N2=K1,K2
DO 120 M1,NVEC
120 RVEC(M,N2)=RVEC(M,N2)
125 CALL VISTIKODE,MPT,MSET,MMUM,RLINE,RVEC,PLINE)
IF (ITEST.NE.2) GO TO 135
DO 130 N2=K1,K2
DO 130 M1,NVEC
130 RVEC(M,N2)=RVEC(M,N2)
135 CONTINUE
C*** IF INSET.EQ.0) GO TO 150
140 CONTINUE
XLINE(MN,1)=MMIN
XLINE(MN,2)=MMIN
XLINE(MN,1)=MMIN
XLINE(MN,2)=MMIN
CALL LINE(XLINE(1,1),XLINE(1,2),MM,1,0,0)
145 CONTINUE
150 CONTINUE
155 RETURN
END

```

```

PLT 78
PLT 79
PLT 80
PLT 81
PLT 82
PLT 83
PLT 84
PLT 85
PLT 86
PLT 87
PLT 88
PLT 89
PLT 90
PLT 91
PLT 92
PLT 93
PLT 94
PLT 95
PLT 96
PLT 97
PLT 98
PLT 99
PLT 100
PLT 101
PLT 102
PLT 103
PLT 104
PLT 105
PLT 106
PLT 107
PLT 108
PLT 109
PLT 110
PLT 111
PLT 112
PLT 113
PLT 114
PLT 115

```

```

SUBROUTINE VISTIKODE,MPT,MSET,MMUM,RLINE,RVEC,PLINE)
TESTS A LINE OF POINTS FOR VISIBILITY
DIMENSION MMUM(4),XLINE(3,2),RVEC(30,2),PLINE(31,2)
RVEC=MPT-1
MSET=0
ICOUNT=0
GO TO (5,10,15),KODE
5 M1=1
M2=2
GO TO 20
10 M1=1
M2=1
GO TO 20
15 M1=2
M2=2
20 DO 65 N=1,MPT
IF (N.EQ.1) GO TO 30
IF (N.EQ.MPT) GO TO 40

```

```

VIS 1
VIS 2
VIS 3
VIS 4
VIS 5
VIS 6
VIS 7
VIS 8
VIS 9
VIS 10
VIS 11
VIS 12
VIS 13
VIS 14
VIS 15
VIS 16
VIS 17
VIS 18
VIS 19

```

```

DO 25 MM=M1,M2
IF (RVECT(N)=MM).GT.0.1.OR.(RVECT(N,MM).GT.0.1) GO TO 60
25 CONTINUE
DO 30 MM=M1,M2
IF (RVECT(N,MM).GT.0.1) GO TO 60
35 CONTINUE
GO TO 50
DO 45 MM=M1,M2
IF (RVECT(N,MM).GT.0.1) GO TO 60
45 CONTINUE
POINT NOT VISIBLE
50 IF (ICOUNT.LE.1) GO TO 55
MMUM(MM)=ICOUNT
55 ICOUNT=0
GO TO 65
C*** POINT IS VISIBLE
60 MPLT=MPLT+1
ICOUNT=ICOUNT+1
PLINE(MPLT,1)=RLINE(N,1)
PLINE(MPLT,2)=RLINE(N,2)
65 CONTINUE
IF (ICOUNT.LE.1) GO TO 70
MMUM(MM)=ICOUNT
70 RETURN
END

SUBROUTINE PTROT(MPT,A,ALINE,RLINE)
DIMENSION A(2,3),ALINE(3),RLINE(3),2
DO 10 MM=1,MPT
RLINE(MM)=0.
DO 5 J=1,2
DO 5 J=1,3
5 RLINE(M,1)=RLINE(N,1)+A(1,J)*ALINE(N,J)
10 CONTINUE
RETURN
END

SUBROUTINE VECROT(IVEC,C,FVEC,RVEC)
TRANSFORMS VECTORS
DIMENSION C(3),FVEC(30),RVEC(30)
DO 10 M=1,NVEC
SUM=0.
DO 5 MM=1,3
5 SUM=SUM+C(MM)*FVEC(M,MM)
10 RVEC(M)=SUM
RETURN
END

SUBROUTINE COC22

```

VIS 20  
VIS 21  
VIS 22  
VIS 23  
VIS 24  
VIS 25  
VIS 26  
VIS 27  
VIS 28  
VIS 29  
VIS 30  
VIS 31  
VIS 32  
VIS 33  
VIS 34  
VIS 35  
VIS 36  
VIS 37  
VIS 38  
VIS 39  
VIS 40  
VIS 41  
VIS 42  
VIS 43  
VIS 44  
VIS 45  
VIS 46  
VIS 47

PTR 1  
PTR 2  
PTR 3  
PTR 4  
PTR 5  
PTR 6  
PTR 7  
PTR 8  
PTR 9  
PTR 10  
PTR 11  
PTR 12

VEC 1  
VEC 2  
VEC 3  
VEC 4  
VEC 5  
VEC 6  
VEC 7  
VEC 8  
VEC 9  
VEC 10

C22 1

```

C*** CONTROL ROUTINE FOR PERSPECTIVE AND STEREO
COMMON ABC(20),JO,J1,J2,J3,JA,J5,JB,JMAF,MMAFOR,MFOR,MKAD(4),MFOR
1X(4),MP,MPODOR,MF,MFOR,MKAN,MKANOR,MJTEST,MN,NC,ABCDE(20),MORL,V
IERT,TESTI,PHI,THETA,PSI,XF,YF,ZF,DIST,FRAG,PLOT,SIZE,TYPE,KODE,MNIN,X
IMAX,YMIN,YMAX,ZMIN,ZMAX,MID,VMID,ZMID,BIGD,ISP
COMMON /INDUT/JREAD,JWRITE,KFILE1,KFILE2,KFILE3,KFILE4
DIMENSION XINIT(2),YINIT(2),ZINIT(2)
DATA MARZ/24/
XINIT(1)=PHI
YINIT(1)=XF
ZINIT(1)=ZF
XINIT(2)=THETA
YINIT(2)=PSI
ZINIT(2)=DIST
CALL STEREO(XINIT,YINIT,ZINIT,0.1,0.3,PLOT,SIZE,DIST,FRAG)
C*** LOOP FOR RIGHT AND LEFT FRAMES
DO 95 IC=1,ISP
REWINO KFILE2
NC1=IC
C*** BEGIN PLOTTING LINES
C*** WING
IF (J1.EQ.0) GO TO 20
DO 10 I=1,2
10 CALL PLTITS(MNMF,MN,PHI,THETA,PSI,XF,YF,ZF,PLOT,SIZE,DIST,FRAG,NC1)
DO 15 I=1,2
15 CALL PLTITS(MN,MNMF,PHI,THETA,PSI,XF,YF,ZF,PLOT,SIZE,DIST,FRAG,NC1)
C*** FUSELAGE
20 IF (J2.EQ.0) GO TO 35
DO 25 MF=1,MFUS
MANG1=MKAD(MFU)
MFUSOR=MFORX(MFU)
CALL PLTITS(MANG1,MFUSOR,PHI,THETA,PSI,XF,YF,ZF,PLOT,SIZE,DIST,FRAG,M
IC1)
25 CONTINUE
DO 30 MF=1,MFUS
MANG1=MKAD(MFU)
MFUSOR=MFORX(MFU)
CALL PLTITS(MFUSOR,MANG1,PHI,THETA,PSI,XF,YF,ZF,PLOT,SIZE,DIST,FRAG,M
IC1)
30 CONTINUE
MANG1=MANG1
DO 40 MP1=1,MP
CALL PLTITS(MANG1,MPODOR,PHI,THETA,PSI,XF,YF,ZF,PLOT,SIZE,DIST,FRAG,M
IC1)
40 CONTINUE
DO 45 MP1=1,MP
CALL PLTITS(MPODOR,MANG1,PHI,THETA,PSI,XF,YF,ZF,PLOT,SIZE,DIST,FRAG,M
IC1)
45 CONTINUE
50 IF (JA.EQ.0) GO TO 65
DO 55 MF1=1,MF
CALL PLTITS(MF1,MFOR,PHI,THETA,PSI,XF,YF,ZF,PLOT,SIZE,DIST,FRAG,NC1)
55 CALL PLTITS(MFOR,MF1,PHI,THETA,PSI,XF,YF,ZF,PLOT,SIZE,DIST,FRAG,NC1)
DO 60 MF1=1,MF
CALL PLTITS(MF1,MFOR,2,PHI,THETA,PSI,XF,YF,ZF,PLOT,SIZE,DIST,FRAG,NC1)
60 CALL PLTITS(MFOR,2,PHI,THETA,PSI,XF,YF,ZF,PLOT,SIZE,DIST,FRAG,NC1)
C*** CAMMID

```

C22 2  
C22 3  
C22 4  
C22 5  
C22 6  
C22 7  
C22 8  
C22 9  
C22 10  
C22 11  
C22 12  
C22 13  
C22 14  
C22 15  
C22 16  
C22 17  
C22 18  
C22 19  
C22 20  
C22 21  
C22 22  
C22 23  
C22 24  
C22 25  
C22 26  
C22 27  
C22 28  
C22 29  
C22 30  
C22 31  
C22 32  
C22 33  
C22 34  
C22 35  
C22 36  
C22 37  
C22 38  
C22 39  
C22 40  
C22 41  
C22 42  
C22 43  
C22 44  
C22 45  
C22 46  
C22 47  
C22 48  
C22 49  
C22 50  
C22 51  
C22 52  
C22 53  
C22 54  
C22 55  
C22 56  
C22 57  
C22 58  
C22 59  
C22 60  
C22 61



```

45 IF (JS.EQ.0) GO TO 90
DO 75 NCA=1,NCAN
DO 70 I=1,2
TO CALL PLTYSIZ,INC,PHI,THETA,PSI,IF,VF,ZF,PLOTSZ,DIST,FRAG,MC,1)
75 CONTINUE
DO 85 NCA=1,NCAN
DO 80 I=1,2
80 CALL PLTYS(INC,2,PHI,THETA,PSI,IF,VF,ZF,PLOTSZ,DIST,FRAG,MC,1)
90 CONTINUE
95 CONTINUE
RETURN
END

C***
SUBROUTINE STERPT(X,Y,Z,N,R,MC,IP,PAG,PLA,MPR)
PROGNAME = 'GEORGE C. SALLEY'
DIMENSION VP(3),TRAN(3),SANG(3),CANG(3),ADJ(3),PT(4),ZLP(2),ZLP(2)
DIMENSION PLX(6),PLY(6),PLZ(2)
DIMENSION PIX(6),PIY(6),PIZ(2)
DIMENSION ILP(6),IPL(6)
DATA PI,PIZ,PI32,PI62/3.1415926,1.5707963,4.7123889,6.2831852/
DATA PAR/1.125/
DATA MPR/0/
DATA NPT/1/
DATA FRAME/9,80/
DATA TURN/11,01/
ND=1
KK=K
II=IP
IF (MC) 80,5,110
5 MP=MPK+1
MP=MPK
PL=MPAG/2.
SP=MPR
NPL=PLA
DO 10 I=1,6
PLX(I)=0.
PLY(I)=0.
PIX(I)=0.
PIY(I)=0.
IPL(I)=0.
IPL(I)=0.
DO 15 I=1,2
IPL(I)=0.
PLZ(I)=0.
PIZ(I)=0.
15 VPX=K(MP)
VPY=V(MP)
VPZ=Z(MP)
FPX=K(MR)
FPY=V(MR)
FPZ=Z(MR)
VV=VPX-PPX
VY=VPY-PPY
VZ=VPZ-PPZ
VP(3)=SQRT((VX**2)+(VY**2)+(VZ**2))
TRAN(1)=VPX-(VPL*(VX/VP(2)))
STE 45
STE 46
STE 47
STE 48
STE 49
STE 50
STE 51
STE 52
STE 53
STE 54
STE 55
STE 56
STE 57
STE 58
STE 59
STE 60
STE 61
STE 62
STE 63
STE 64
STE 65
STE 66
STE 67
STE 68
STE 69
STE 70
STE 71
STE 72
STE 73
STE 74
STE 75
STE 76
STE 77
STE 78
STE 79
STE 80
STE 81
STE 82
STE 83
STE 84
STE 85
STE 86
STE 87
STE 88
STE 89
STE 90
STE 91
STE 92
STE 93
STE 94
STE 95
STE 96
STE 97
STE 98
STE 99
STE 100
STE 101
STE 102
STE 103
STE 104

TRAN(2)=VPY-(VPL*(VY/VP(2)))
TRAN(3)=VPZ-(VPL*(VZ/VP(2)))
VANG=ATAN((PAR/VP(3)))
20 IF (VX) 55,20,35
25 PANG=PI2
60 TO 75
30 PANG=PI2
35 IF (I) 90,40,45
35 IF (I) 75
40 PANG=0
45 PANG=ATAN(VY/VX)
50 PANG=PI2-ATAN((ABS(VY))/VX)
55 IF (VY) 70,60,65
60 PANG=PI
65 PANG=PI-ATAN((VY/ABS(VX)))
GO TO 75
70 PANG=PI+ATAN((ABS(VY))/ABS(VX)))
75 PANG=PI32-PANG
UANG=PANG-VANG
RANG=UANG+I2.*VANG
SANG(1)=SIN(UANG)
SANG(2)=SIN(RANG)
CANG(1)=COS(UANG)
CANG(2)=COS(RANG)
SANG(3)=VZ/VP(3)
CANG(3)=VP(2)/VP(3)
VPL(I)=0.
ZLP(I)=0.
ZLP(I)=RANG
ZLP(I)=0.
ADJ(I)=PI*IN
ADJ(I)=ADJ(I)+FRAME
IF (IN) 300,300,110
80 M=ABS(INC)
L=M
IF (MPG+MC) 115,85,115
85 IF (Z*MC) 300,95,90
90 MPG=2
GO TO 100
95 MPG=1
100 CONTINUE
DO 105 I=1,L
CALL CALPLT(TURN,0,-3)
105 CONTINUE
CALL CALPLT(ILP(M),ZLP(M),3)
110 M=L
115 DO 205 I=M,L
120 IF (MPC) 300,120,120
125 IF (MPC) 125,125,120
130 IF (MPC+MC) 300,130,130
135 MPT=2
300,140,135
135 MPT=2
STE 105
STE 106
STE 107
STE 108
STE 109
STE 110
STE 111
STE 112
STE 113
STE 114
STE 115
STE 116
STE 117
STE 118
STE 119
STE 120
STE 121
STE 122
STE 123
STE 124
STE 125
STE 126
STE 127
STE 128
STE 129
STE 130
STE 131
STE 132
STE 133
STE 134
STE 135
STE 136
STE 137
STE 138
STE 139
STE 140
STE 141
STE 142
STE 143
STE 144

```







0.0	0.36670	0.75000	1.15420	1.57290	1.79790	1.87500	1.99170	1.99580	1.99580
1.89580	1.89580	1.89580	1.89170	1.87500	1.84580	1.79660	1.20330	0.95210	0.40890
0.0	2.32290	2.33750	2.36448	2.47920	2.82920	3.26250	3.66670	4.00620	4.32000
2.31250	4.92000	5.22920	5.58750	5.98660	6.46250	6.93120	6.93750	6.93750	6.93750
4.62500	0.0	0.36250	0.73960	1.14170	1.54580	1.78130	1.86040	1.87500	1.87500
6.93750	1.87500	1.87500	1.87080	1.85420	1.83330	1.70830	1.25830	0.83330	0.40420
0.0	2.33750	2.35830	2.37500	2.48540	2.82500	3.25420	3.65420	3.99170	4.30420
1.87500	4.89580	5.20420	5.59420	5.99420	6.42710	6.86870	6.87500	6.87500	6.87500
0.0	0.34790	0.71800	1.09580	1.48960	1.75000	1.84790	1.87500	1.87500	1.87500
1.87500	1.87500	1.87500	1.86870	1.84580	1.81250	1.63750	1.20830	0.80210	0.38540
0.0	2.39580	2.40630	2.45120	2.52500	2.87920	3.22920	3.62290	3.96040	4.27290
2.39580	4.86440	5.17290	5.52290	5.92000	6.37500	6.74790	6.75000	6.75000	6.75000
0.0	0.33330	0.68130	1.0210	1.44790	1.71800	1.85420	1.87500	1.87500	1.87500
1.87500	1.87500	1.87500	1.87080	1.85420	1.79170	1.56670	1.15210	0.76670	0.36870
0.0	2.45830	2.46880	2.48330	2.55620	2.82920	3.21250	3.59380	3.92920	4.24170
2.45830	4.83330	5.14170	5.49170	5.89660	6.32900	6.62500	6.62500	6.62500	6.62500
0.0	0.31880	0.65630	1.01460	1.40420	1.68750	1.81250	1.86670	1.87500	1.87500
1.87500	1.87500	1.87500	1.86870	1.84380	1.78130	1.51040	1.11640	0.73540	0.35420
0.0	2.54170	2.54880	2.55830	2.61870	2.85830	3.22920	3.59380	3.92920	4.24170
2.54170	4.83330	5.14170	5.49170	5.89660	6.31250	6.54170	6.54170	6.54170	6.54170
0.0	0.50000	0.81460	0.94580	1.28130	1.56250	1.74170	1.79170	1.79170	1.79170
1.79170	1.79170	1.79170	1.79170	1.77080	1.65630	1.33330	1.00830	0.67920	0.33330
0.0	2.62500	2.62500	2.63940	2.65210	2.73960	2.93750	3.25750	3.59380	4.21460
2.62500	4.78130	5.07290	5.41250	5.78750	6.14580	6.26670	6.31670	6.34380	6.36870
0.0	0.27920	0.37080	0.86660	1.18750	1.46880	1.66470	1.72080	1.72920	1.72920
1.72920	1.72920	1.72920	1.72500	1.68750	1.54980	1.23790	0.92920	0.62920	0.30830
0.0	2.70830	2.71840	2.72880	2.75000	2.81670	2.98120	3.24370	3.57290	4.17080
2.70830	4.64790	4.71880	4.76250	5.32290	5.67710	5.98540	6.00120	6.12290	6.15420
0.0	0.25000	0.32080	0.78330	1.08330	1.35420	1.55210	1.62500	1.64580	1.64580
1.64580	1.64580	1.64580	1.63750	1.59380	1.41250	1.11640	0.83330	0.57080	0.27920
0.0	2.77080	2.77710	2.81250	2.86670	3.00000	3.23330	3.52920	3.81870	4.08960
2.77080	4.35420	4.61250	4.87920	5.18540	5.51460	5.75830	5.82710	5.85830	5.89460
0.0	0.22080	0.45830	0.70000	0.97920	1.23960	1.41670	1.50830	1.53750	1.55000
1.55210	1.55000	1.54580	1.53130	1.48330	1.26250	0.99540	0.75000	0.51040	0.26540
0.0	2.85420	2.85420	2.85830	2.86870	2.90830	3.01670	3.22500	3.48540	3.75000
2.85420	4.25000	4.49170	4.74370	5.02920	5.32920	5.50620	5.56870	5.59790	5.62500
0.0	0.20830	0.42710	0.65830	0.92710	1.17290	1.31670	1.38540	1.41250	1.41670
1.41670	1.41670	1.41670	1.41670	1.39830	1.15830	0.92500	0.69790	0.47080	0.22920
0.0	2.97920	2.97920	2.98120	2.98540	3.00830	3.11040	3.32710	3.58290	4.05210
2.97920	4.28130	4.50210	4.73330	5.00210	5.24670	5.43120	5.50210	5.53750	5.55870
0.0	0.18750	0.38750	0.59580	0.84380	1.07290	1.19580	1.23540	1.24170	1.25000
1.25000	1.25000	1.25000	1.23960	1.16250	0.91330	0.84790	0.64170	0.43330	0.21250
0.0	3.12500	3.12500	3.12920	3.13940	3.15210	3.24370	3.44580	3.68750	4.11250
3.12500	4.31250	4.50830	4.70830	4.93750	5.15830	5.33330	5.43330	5.46880	5.48750
0.0	0.17500	0.35000	0.53750	0.75000	0.92710	1.02500	1.06250	1.07290	1.08330
1.08330	1.08330	1.08330	1.07500	1.02500	0.92080	0.77080	0.58330	0.39580	0.19170
0.0	3.29170	3.29170	3.29790	3.30620	3.33330	3.43960	3.61870	3.82710	4.01250
3.29170	4.36440	4.53130	4.70830	4.90630	5.10830	5.27710	5.38940	5.41670	5.43540
0.0	0.15000	0.30420	0.46870	0.66870	0.83330	0.78130	0.83540	0.87500	0.89170
0.89580	0.89580	0.89580	0.88750	0.85830	0.78130	0.65830	0.51040	0.36580	0.16670
0.0	3.45830	3.46440	3.47500	3.49580	3.53540	3.62710	3.78750	3.96250	4.11870
3.45830	4.40630	4.54790	4.69170	4.85420	5.02920	5.18540	5.27290	5.32290	5.33960
0.0	0.13330	0.26440	0.38540	0.50000	0.59380	0.65830	0.69170	0.70420	0.70830
0.70830	0.70830	0.70830	0.69790	0.65830	0.60000	0.51470	0.41670	0.29790	0.14580
0.0	3.64580	3.65630	3.67920	3.72500	3.79170	3.88540	3.99790	4.12710	4.25000
3.64580	4.47920	4.58750	4.70420	4.83120	4.95620	5.07710	5.16440	5.23330	5.27920
0.0	0.10830	0.20830	0.29170	0.35420	0.40630	0.41870	0.46250	0.47920	0.48960
0.48960	0.48960	0.48960	0.48330	0.46880	0.43330	0.38750	0.31870	0.23330	0.11670
0.0	3.83330	3.83960	3.89170	3.95000	4.03130	4.11440	4.20210	4.28940	4.44580
3.83330	4.52080	4.59580	4.67500	4.76440	4.86040	4.95420	5.03130	5.09580	5.15800
0.0	0.0	0.0	0.0	0.0	0.0	0.0	0.0	0.0	0.0
0.0	0.0	0.0	0.0	0.0	0.0	0.0	0.0	0.0	0.0
0.0	4.79170	4.79170	4.79170	4.79170	4.79170	4.79170	4.79170	4.79170	4.79170
4.79170	4.79170	4.79170	4.79170	4.79170	4.79170	4.79170	4.79170	4.79170	4.79170
0.0	0.0	5.31300	4.16670	24.49990	0.0	9.97080	2.29170	80.00000	100.00000
20.23000	2.50000	3.00000	10.00000	20.00000	30.00000	40.00000	60.00000	80.00000	100.00000
0.0	1.96100	2.66600	3.51200	4.30300	4.98100	6.32200	8.23000	1.96700	0.09500
0.0	0.25000	4.77000	4.16670	20.91800	5.83330	4.81170	2.75000	0.0	0.0
20.23000	0.0	2.50000	5.00000	10.00000	20.00000	30.00000	40.00000	60.00000	80.00000
0.0	1.96100	2.66600	3.51200	4.30300	4.98100	6.32200	8.23000	1.96700	0.09500

PLOT DATA

Y I OUT -45.00000 10.00000 -30.00000 0.0 0.0 0.0 0.0 0.0 0.0 7.5000000T  
 X I OUT 45.00000 10.00000 30.00000 0.0 0.0 0.0 0.0 0.0 0.0 10.000000T

Figure D-3. Continued.

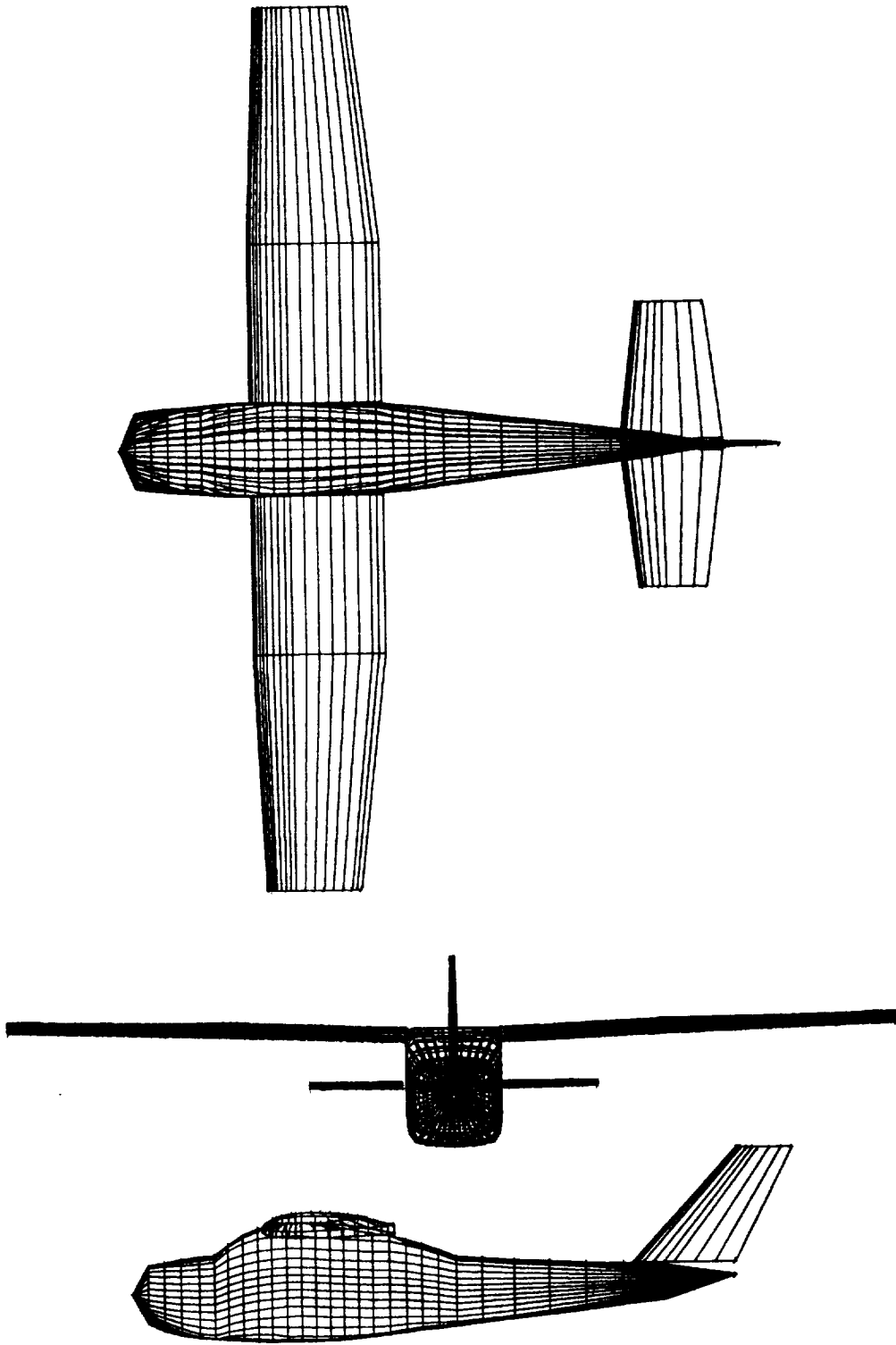
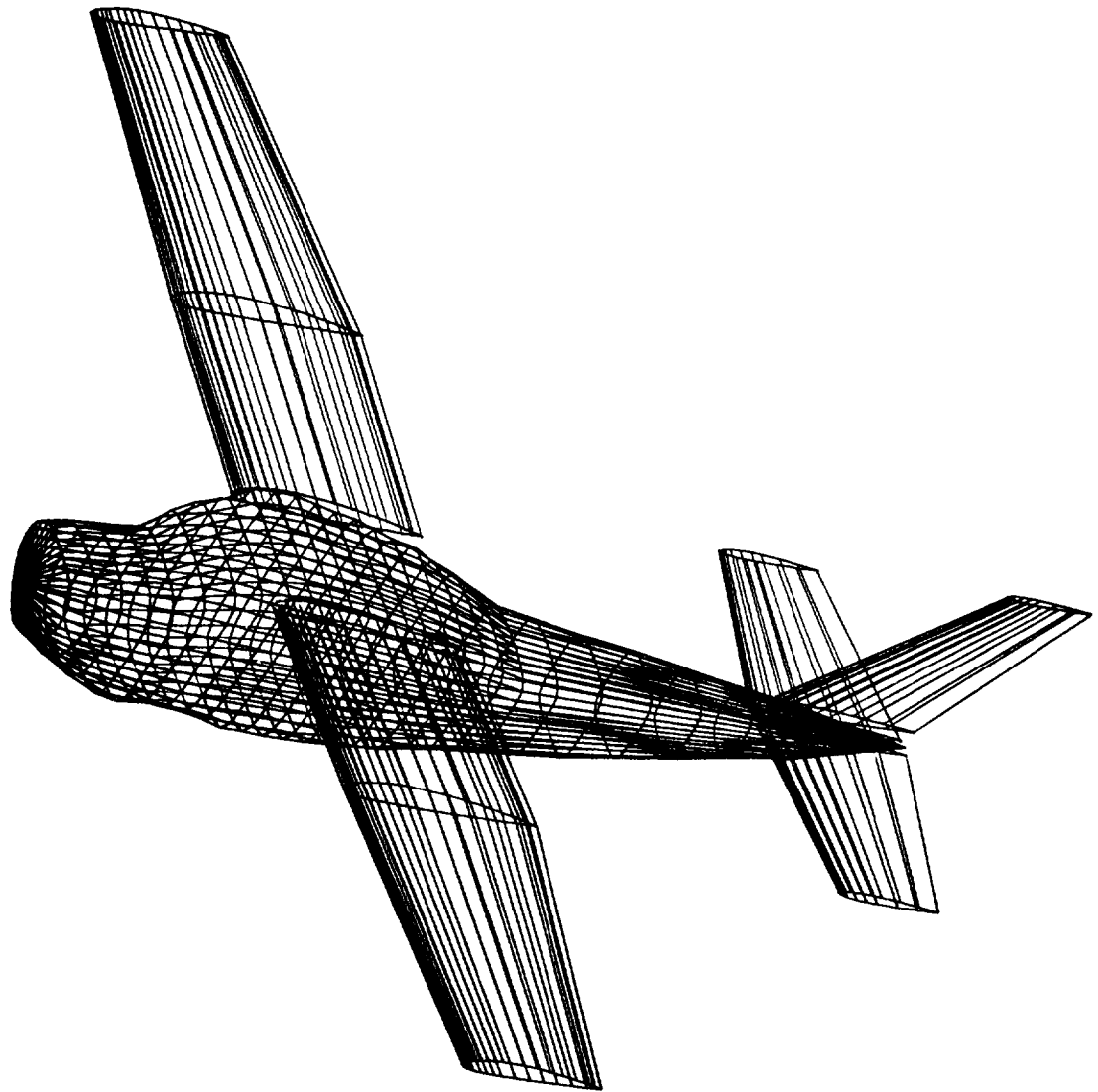


Figure D-4. Plotted 3-view of the Cessna 182.

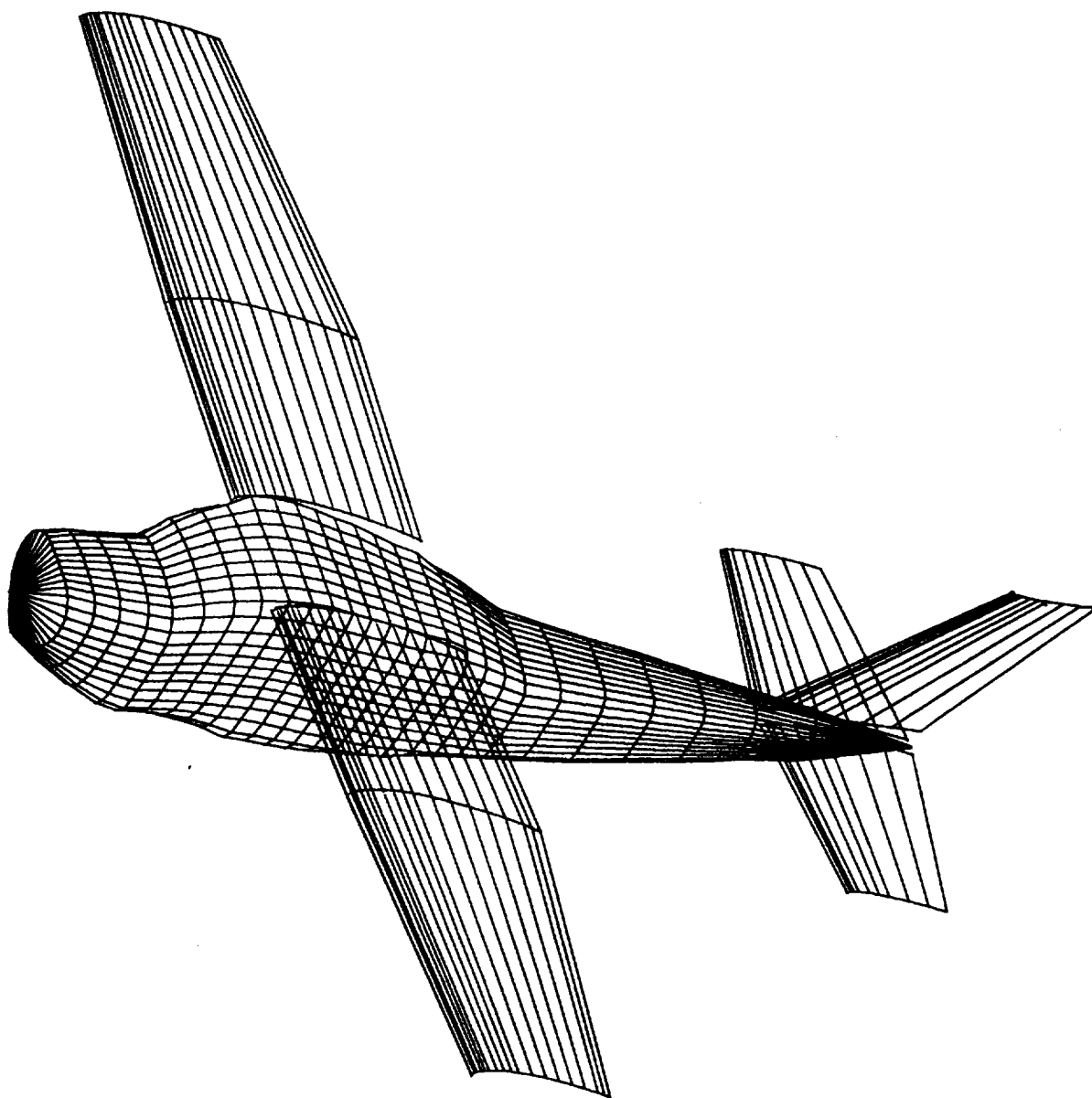


BEST CESSNA 182 WITH M=21 AND N=29 YIELDING 560 PANELS -- COMPLETE AIRPLANE

X Z -45. 10. -30.

8.5 ORT

Figure D-5. Orthographic projection of a Cessna 182 rolled  $-45^\circ$ , pitched  $10^\circ$  and yawed  $-30^\circ$  with respect to the X-Z plane of symmetry.



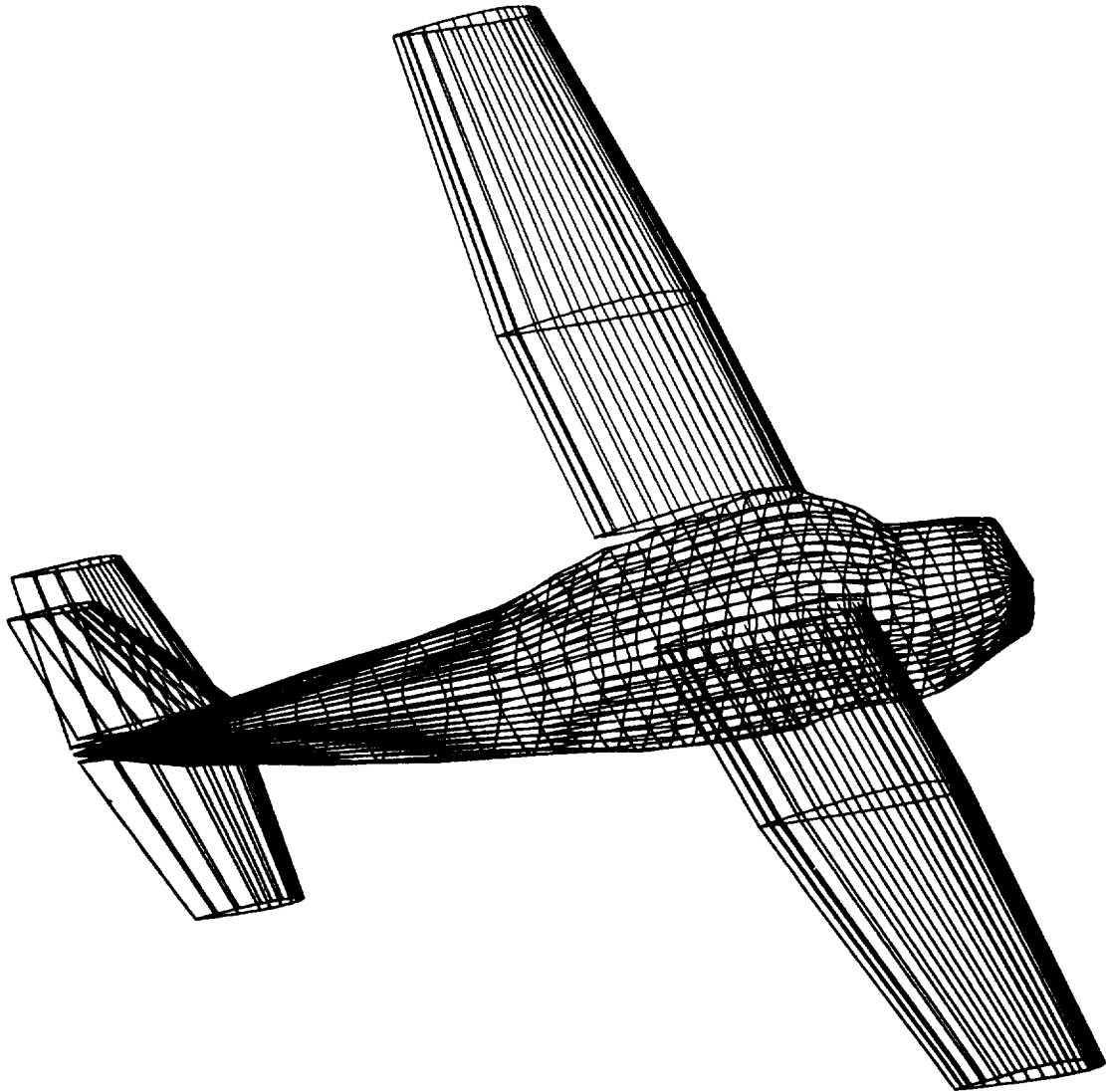
BEST CESSNA 182 WITH M=21 AND N=29 YIELDING 560 PANELS --- COMPLETE AIRPLANE

X Z OUT 45. 10. 30.

9.25 ORT

Figure D-6. Orthographic projection with hidden lines removed of a Cessna 182 rolled  $45^\circ$ , pitched  $10^\circ$ , and yawed  $30^\circ$  with respect to the X-Z plane of symmetry.



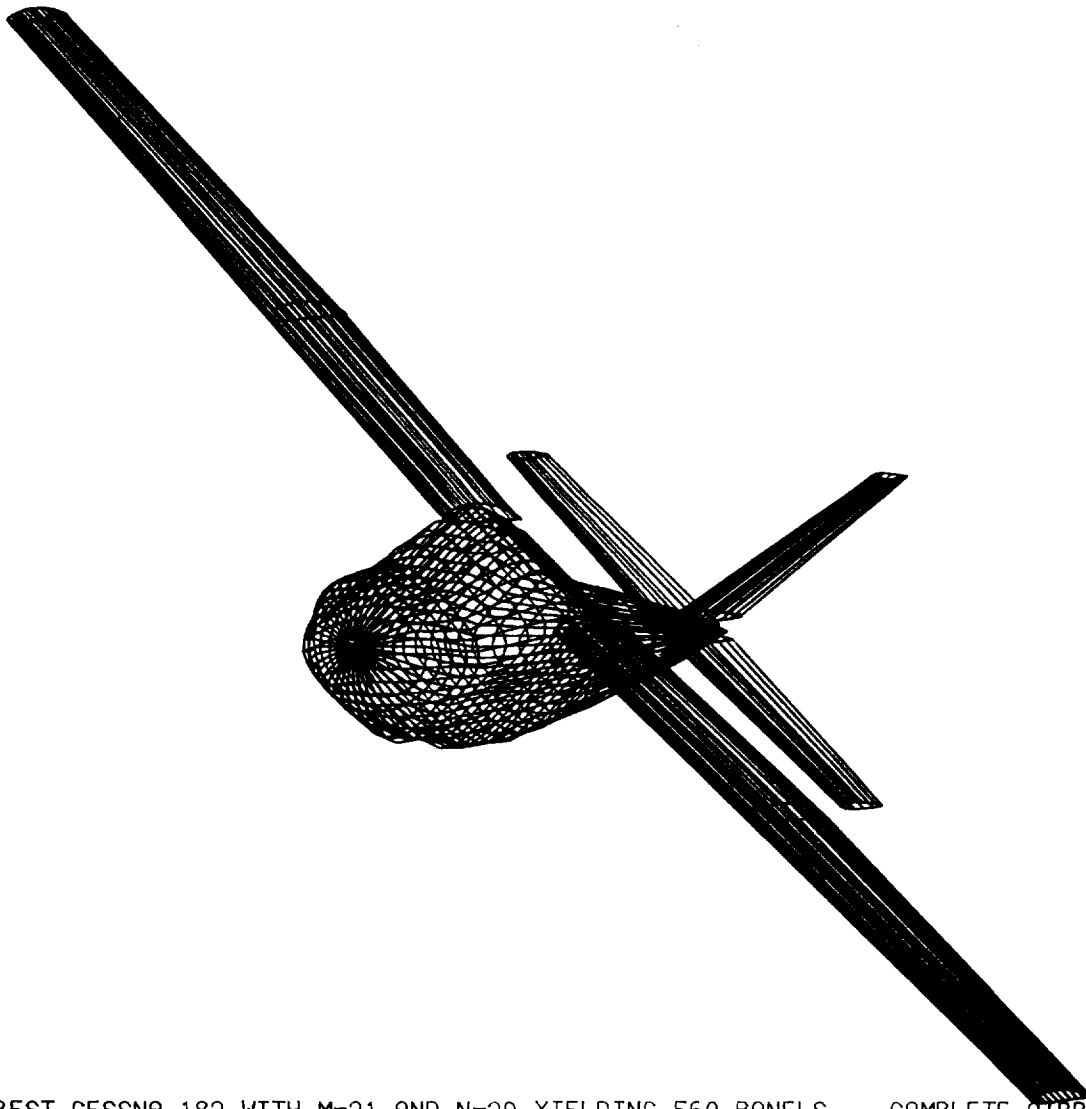


BEST CESSNA 182 WITH M=21 AND N=29 YIELDING 560 PANELS — COMPLETE AIRPLANE

X Z 45. 10. 160.

8.5 ORT

Figure D-7. Orthographic projection of a Cessna 182 rolled  $45^\circ$ , pitched  $10^\circ$ , and yawed  $160^\circ$  with respect to the X-Z plane of symmetry.

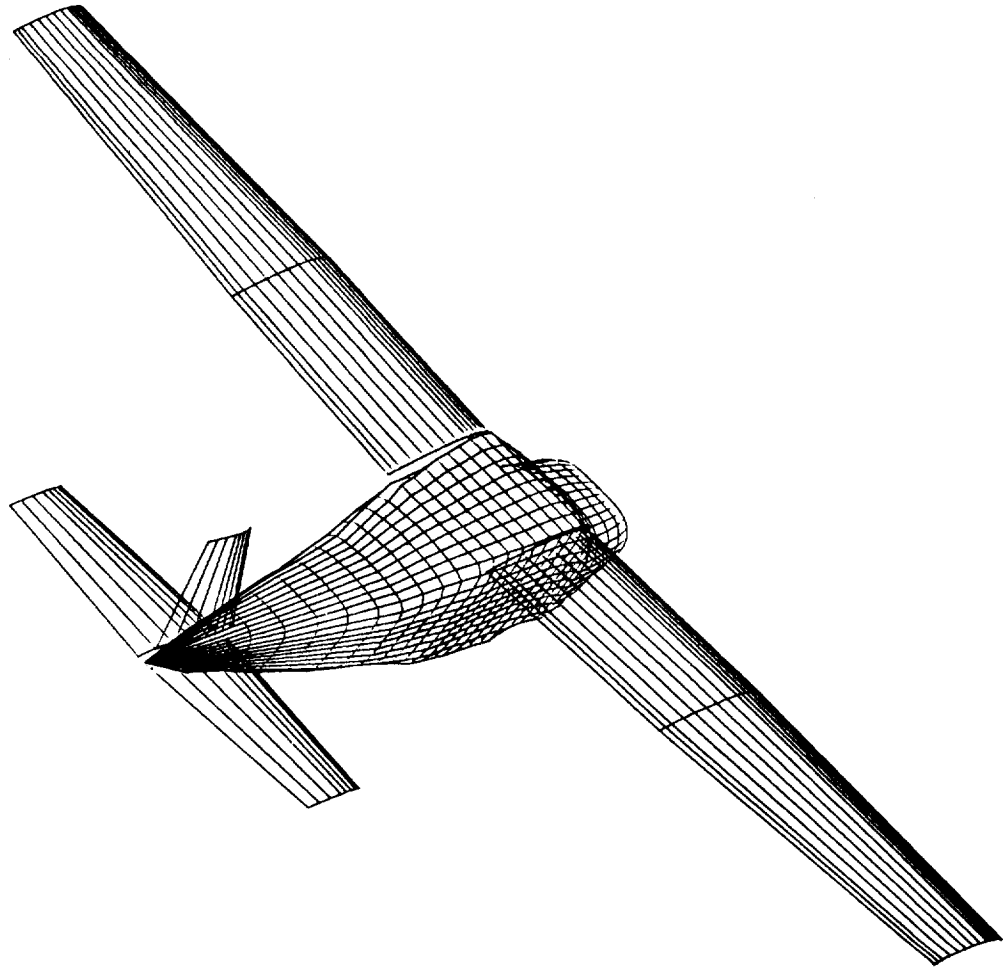


BEST CESSNA 182 WITH M=21 AND N=29 YIELDING 560 PANELS --- COMPLETE AIRPLANE

X Z    -45.    0.    -70.

8.5 ORT

Figure D-8. Orthographic projection of a Cessna 182 rolled  $-45^\circ$  and yawed  $-70^\circ$  with respect to the X-Z plane of symmetry.

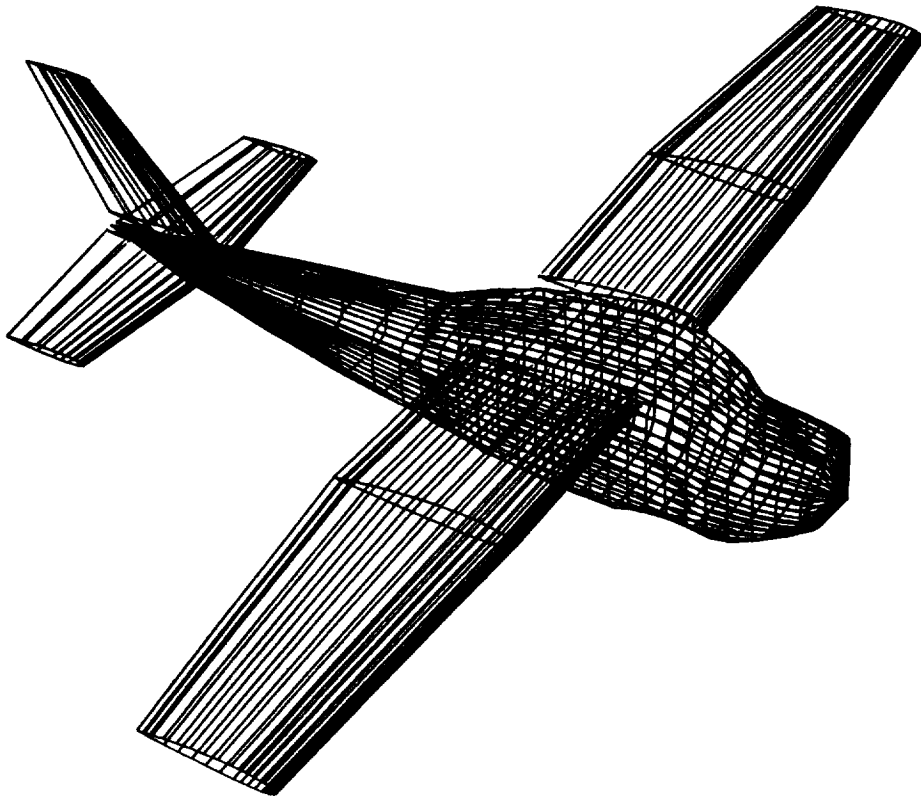


BEST CESSNA 182 WITH M=21 AND N=29 YIELDING 560 PANELS - COMPLETE AIRPLANE

Y Z OUT -45. 10. -30

7.5 ORT

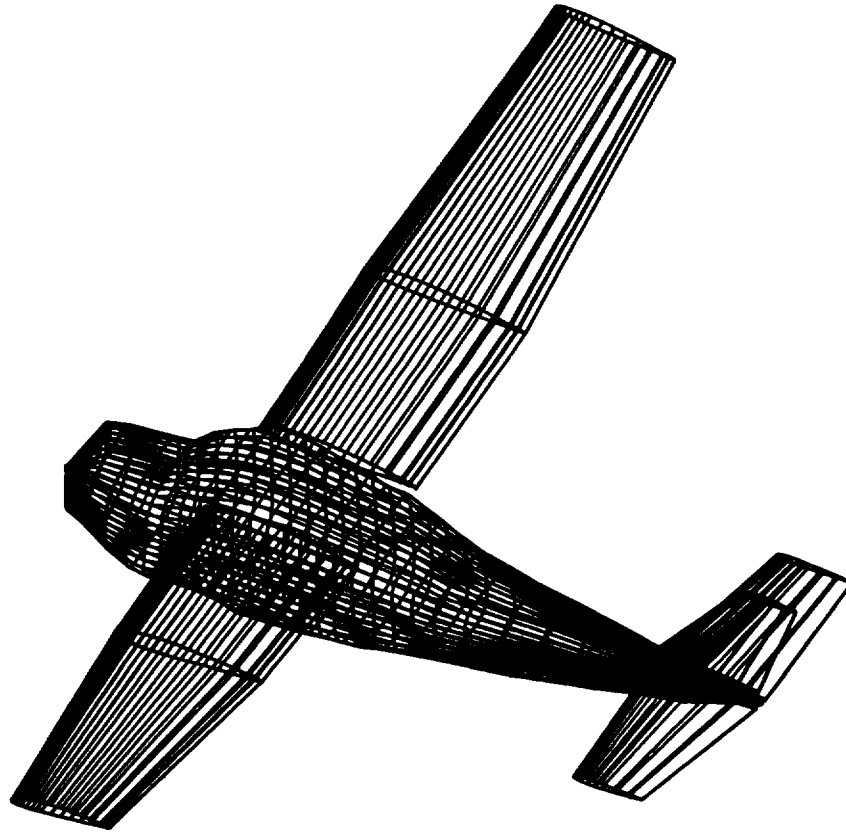
Figure D-9. Orthographic projection of a Cessna 182 rolled  $-45^\circ$ , pitched  $10^\circ$ , and yawed  $-30^\circ$  with respect to the Y-Z plane.



BEST CESSNA 182 WITH M=21 AND N=29 YIELDING 560 PANELS --- COMPLETE AIRPLANE

--20. 50. 50. 7.0 0.0 5.0 14.0 1.0 10. .PER

Figure D-10. Perspective view number 1 of the Cessna 182.



BEST CESSNA 182 WITH M-21 AND N-29 YIELDING 560 PANELS -- COMPLETE AIRPLANE

-20. -50. -50. 7.0 0.0 5.0 14.0 1.0 10. PER

Figure D-11. Perspective view number 2 of the Cessna 182  
(The reader should note that the viewer is  
under the aircraft looking up.)

BEST CESSNA 182 WITH M=21 AND N=29

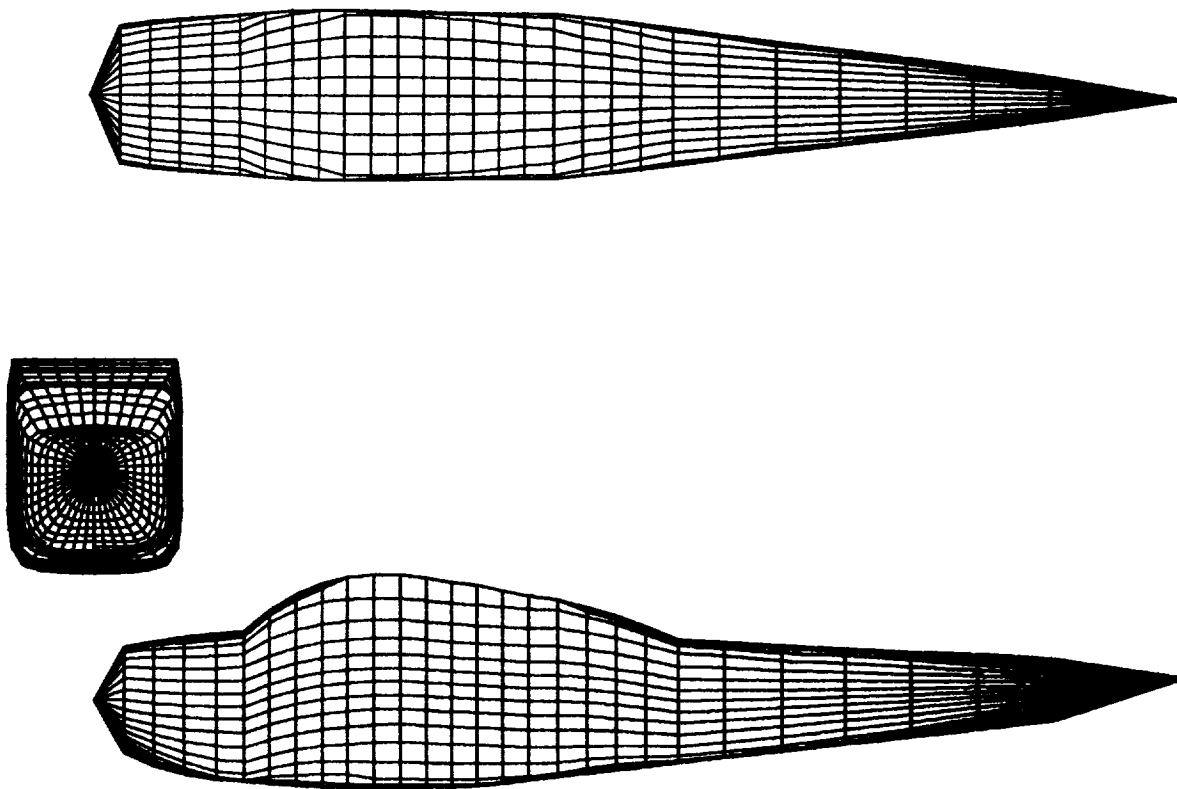
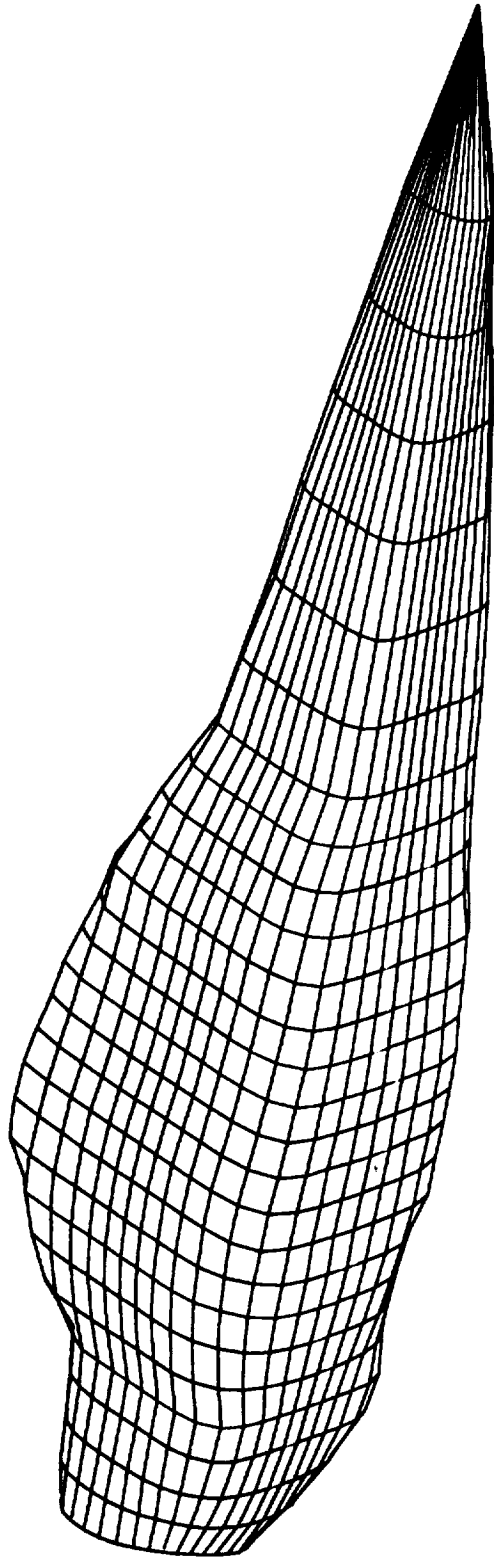
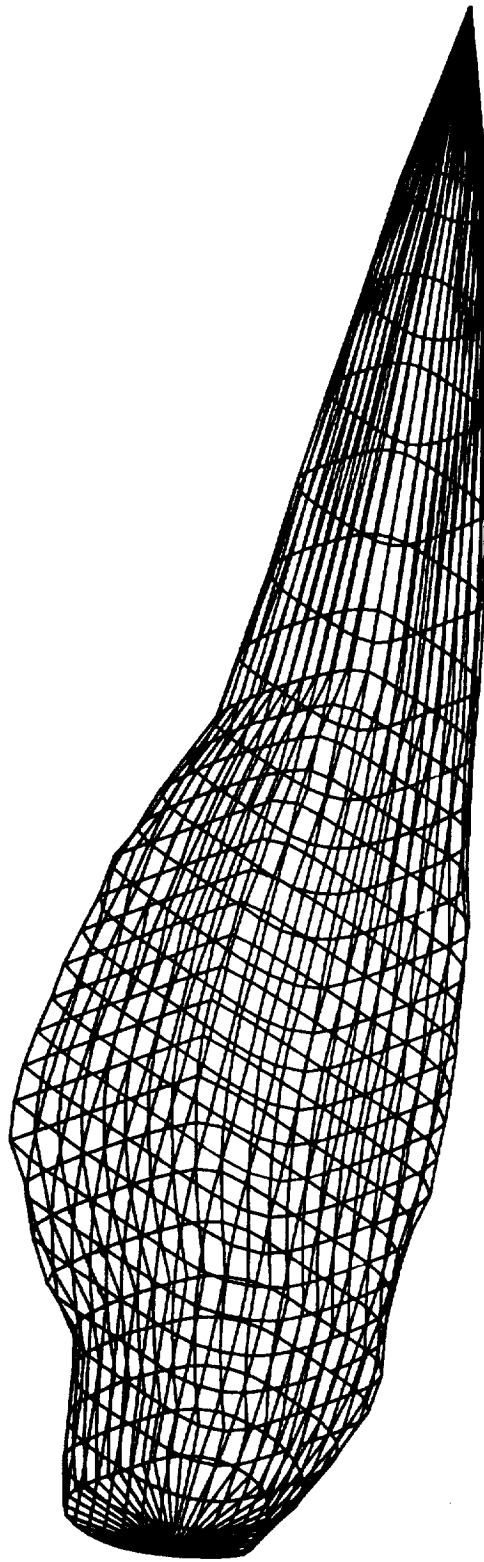


Figure D-12. Plotted 3-view of the Cessna 182 fuselage.



X Z OUT -45. 10. -30.

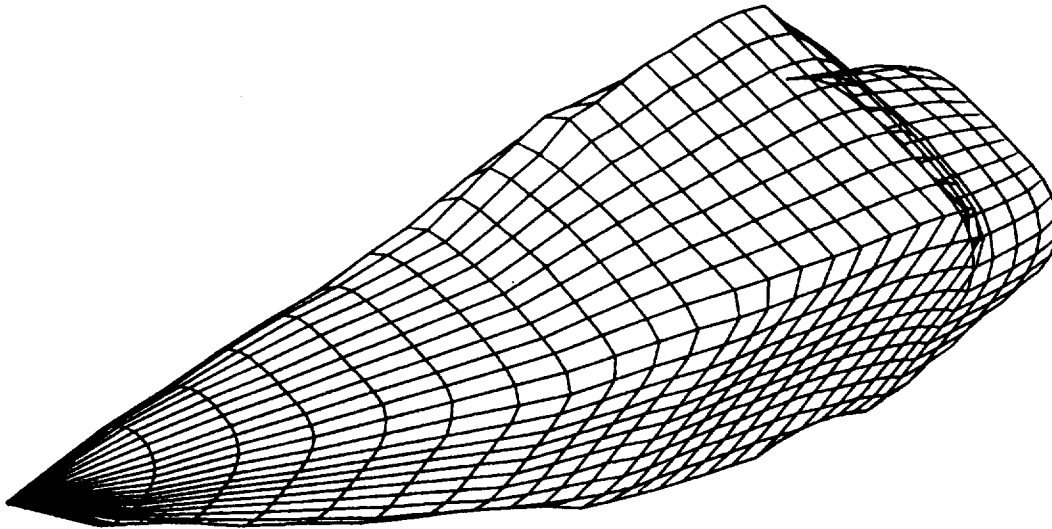
10. ORT



X Z -45. 10. -30.

10. ORT

Figure D-13. Two orthographic projections of a Cessna 182 fuselage rolled  $-45^\circ$ , pitched  $10^\circ$ , and yawed  $-30^\circ$  with respect to the X-Z plane of symmetry. The top view has hidden lines removed.



BEST CESSNA 182 WITH M=21 AND N=29 YIELDING 560 PANELS -- FUSCLAGE ONLY

Y Z OUT -45. 10. -30.

11. ORT

Figure D-14. Orthographic projection with hidden lines removed of a Cessna 182 fuselage rolled  $-45^\circ$ , pitched  $10^\circ$ , and yawed  $-30^\circ$  with respect to the Y-Z plane.



## APPENDIX E - CONVERT Program

### User Instructions

This program is written in FORTRAN IV and is designed to run in single precision on an IBM 370-165 computer. Given a set of plot input data as described in Appendix D, this program (1) produces a properly indexed data set for the NCSU BODY program, (2) computes the area of each body panel described by the input points and displays each area in an orderly fashion, and (3) displays the ratio of the area of each panel to the area of the panel below it and the panel to its right. It should be noted that while the CONVERT program produces a data set for the aircraft body, it will accept the input of a data set for a complete aircraft configuration and ignore the unnecessary information (wing, tail, nacelles, etc.). Execution requires 92,000 bytes of core storage and approximately 15 seconds to run a case with 560 panels specified. A description of the input data cards is not included here since it is the same as that for the PLOT program in Appendix D. The format specification is also the same. The program listing is given in the next section of this appendix and is followed by the sample output (Figure E-1) corresponding to the Cessna 182 data set given in Figure D-3.

## Program Listing

```

C000 THIS PROGRAM CONVERTS A SET OF CRADION INPUT DATA INTO A DATA SET
C000 WHICH CAN BE USED WITH THE XYZ POTENTIAL FLOW PROGRAM FOR A BODY.
C000 DIMENSION DUM(30),DUMRY(30),TITLE(20),IMADR(4),IMFOR(4),EPUS(30),Z
C000 IFUSAR(30),X(1500),Y(1500),Z(1500),XII(1500),YII(1500),ZII(1500),I(150
C000 1,50),AQ(50,30),NRWRITE(50),RATIO(50,30),RATIOI(50,30)
C000 IREAD=1
C000 IPUNCH=2
C000 IWRITE=3
C000 IWRITE=4
C000 IWRITE=5
C000 IWRITE=6
C000 IWRITE=7
C000 IWRITE=8
C000 IWRITE=9
C000 IWRITE=10
C000 IWRITE=11
C000 IWRITE=12
C000 IWRITE=13
C000 IWRITE=14
C000 IWRITE=15
C000 IWRITE=16
C000 IWRITE=17
C000 IWRITE=18
C000 IWRITE=19
C000 IWRITE=20
C000 IWRITE=21
C000 IWRITE=22
C000 IWRITE=23
C000 IWRITE=24
C000 IWRITE=25
C000 IWRITE=26
C000 IWRITE=27
C000 IWRITE=28
C000 IWRITE=29
C000 IWRITE=30
C000 IWRITE=31
C000 IWRITE=32
C000 IWRITE=33
C000 IWRITE=34
C000 IWRITE=35
C000 IWRITE=36
C000 IWRITE=37
C000 IWRITE=38
C000 IWRITE=39
C000 IWRITE=40
C000 IWRITE=41
C000 IWRITE=42
C000 IWRITE=43
C000 IWRITE=44
C000 IWRITE=45
C000 IWRITE=46
C000 IWRITE=47
C000 IWRITE=48
C000 IWRITE=49
C000 IWRITE=50
C000 IWRITE=51
C000 IWRITE=52
C000 IWRITE=53
C000 IWRITE=54
C000 IWRITE=55
C000 IWRITE=56
C000 IWRITE=57
C000 IWRITE=58
C000 IWRITE=59
C000 IWRITE=60
C000 IWRITE=61
C000 IWRITE=62
C000 IWRITE=63
C000 IWRITE=64
C000 IWRITE=65
C000 IWRITE=66
C000 IWRITE=67
C000 IWRITE=68
C000 IWRITE=69
C000 IWRITE=70
C000 IWRITE=71
C000 IWRITE=72
C000 IWRITE=73
C000 IWRITE=74
C000 IWRITE=75
C000 IWRITE=76
C000 IWRITE=77
C000 IWRITE=78
C000 IWRITE=79
C000 IWRITE=80
C000 IWRITE=81
C000 IWRITE=82
C000 IWRITE=83
C000 IWRITE=84
C000 IWRITE=85
C000 IWRITE=86
C000 IWRITE=87
C000 IWRITE=88
C000 IWRITE=89
C000 IWRITE=90
C000 IWRITE=91
C000 IWRITE=92
C000 IWRITE=93
C000 IWRITE=94
C000 IWRITE=95
C000 IWRITE=96
C000 IWRITE=97
C000 IWRITE=98
C000 IWRITE=99
C000 IWRITE=100
C000 IWRITE=101
C000 IWRITE=102
C000 IWRITE=103
C000 IWRITE=104
C000 IWRITE=105
C000 IWRITE=106
C000 IWRITE=107
C000 IWRITE=108
C000 IWRITE=109
C000 IWRITE=110
C000 IWRITE=111
C000 IWRITE=112
C000 IWRITE=113
C000 IWRITE=114
C000 IWRITE=115
C000 IWRITE=116
C000 IWRITE=117
C000 IWRITE=118
C000 IWRITE=119
C000 IWRITE=120

```

```

C000 COMPLETE SYMMETRY W.R.T. XY PLANE IS NOT HANDLED IN THIS PROGRAM
C000 AS IT IS IN THE PROGRAM AS SUPPLIED.
C000 CHECK TO SEE IF FUSELAGE IS CAMBERED (JAM=0)
C000 I=6 GO TO 70
C000 I=7 GO TO 70
C000 I=8 GO TO 70
C000 I=9 GO TO 70
C000 I=10 GO TO 70
C000 I=11 GO TO 70
C000 I=12 GO TO 70
C000 I=13 GO TO 70
C000 I=14 GO TO 70
C000 I=15 GO TO 70
C000 I=16 GO TO 70
C000 I=17 GO TO 70
C000 I=18 GO TO 70
C000 I=19 GO TO 70
C000 I=20 GO TO 70
C000 I=21 GO TO 70
C000 I=22 GO TO 70
C000 I=23 GO TO 70
C000 I=24 GO TO 70
C000 I=25 GO TO 70
C000 I=26 GO TO 70
C000 I=27 GO TO 70
C000 I=28 GO TO 70
C000 I=29 GO TO 70
C000 I=30 GO TO 70
C000 I=31 GO TO 70
C000 I=32 GO TO 70
C000 I=33 GO TO 70
C000 I=34 GO TO 70
C000 I=35 GO TO 70
C000 I=36 GO TO 70
C000 I=37 GO TO 70
C000 I=38 GO TO 70
C000 I=39 GO TO 70
C000 I=40 GO TO 70
C000 I=41 GO TO 70
C000 I=42 GO TO 70
C000 I=43 GO TO 70
C000 I=44 GO TO 70
C000 I=45 GO TO 70
C000 I=46 GO TO 70
C000 I=47 GO TO 70
C000 I=48 GO TO 70
C000 I=49 GO TO 70
C000 I=50 GO TO 70
C000 I=51 GO TO 70
C000 I=52 GO TO 70
C000 I=53 GO TO 70
C000 I=54 GO TO 70
C000 I=55 GO TO 70
C000 I=56 GO TO 70
C000 I=57 GO TO 70
C000 I=58 GO TO 70
C000 I=59 GO TO 70
C000 I=60 GO TO 70
C000 I=61 GO TO 70
C000 I=62 GO TO 70
C000 I=63 GO TO 70
C000 I=64 GO TO 70
C000 I=65 GO TO 70
C000 I=66 GO TO 70
C000 I=67 GO TO 70
C000 I=68 GO TO 70
C000 I=69 GO TO 70
C000 I=70 GO TO 70
C000 I=71 GO TO 70
C000 I=72 GO TO 70
C000 I=73 GO TO 70
C000 I=74 GO TO 70
C000 I=75 GO TO 70
C000 I=76 GO TO 70
C000 I=77 GO TO 70
C000 I=78 GO TO 70
C000 I=79 GO TO 70
C000 I=80 GO TO 70
C000 I=81 GO TO 70
C000 I=82 GO TO 70
C000 I=83 GO TO 70
C000 I=84 GO TO 70
C000 I=85 GO TO 70
C000 I=86 GO TO 70
C000 I=87 GO TO 70
C000 I=88 GO TO 70
C000 I=89 GO TO 70
C000 I=90 GO TO 70
C000 I=91 GO TO 70
C000 I=92 GO TO 70
C000 I=93 GO TO 70
C000 I=94 GO TO 70
C000 I=95 GO TO 70
C000 I=96 GO TO 70
C000 I=97 GO TO 70
C000 I=98 GO TO 70
C000 I=99 GO TO 70
C000 I=100 GO TO 70
C000 I=101 GO TO 70
C000 I=102 GO TO 70
C000 I=103 GO TO 70
C000 I=104 GO TO 70
C000 I=105 GO TO 70
C000 I=106 GO TO 70
C000 I=107 GO TO 70
C000 I=108 GO TO 70
C000 I=109 GO TO 70
C000 I=110 GO TO 70
C000 I=111 GO TO 70
C000 I=112 GO TO 70
C000 I=113 GO TO 70
C000 I=114 GO TO 70
C000 I=115 GO TO 70
C000 I=116 GO TO 70
C000 I=117 GO TO 70
C000 I=118 GO TO 70
C000 I=119 GO TO 70
C000 I=120 GO TO 70

```

```

ZP=Z(11)-ZORG
XX(I)=XP
YY(I)=YP
ZZ(I)=ZP
130 CONTINUE
LL=C
DO 145 I=1,LM
DO 145 J=1,JK
LL=LL+1
C*** PRINT DATA FOR VISCOUS FLOW PROGRAM
135 WRITE (IWRITE,135) XX(1),YY(1),ZZ(1),I,J,NS
135 FORMAT (1X,3F12.7,3I4)
C*** PUNCH DATA FOR VISCOUS FLOW PROGRAM
140 WRITE (IPUNCH,140) XX(1),YY(1),ZZ(1),I,J,NS
140 FORMAT (3P12.7,3I2,4I2)
DO 150 M=1,JK
DO 150 N=1,LM
P1=ID(M,N)
P2=ID(M,N)
P3=ID(M,N)
P4=ID(M,N)
IF (I1.EQ.0) GO TO 150
X1=XX(P3)-XX(P1)
Z2=XX(P4)-XX(P2)
Y1=YY(P3)-YY(P1)
Y2=YY(P4)-YY(P2)
Z1=ZZ(P3)-ZZ(P2)
XN=X1*Z2-Z2*Y1
YN=X1*Z2-Z2*Y1
ZN=X2*Y1-Y1*Y2
R=SQ2(LM,YN,ZN)
150 AQ(N,M)=G.5*R
MOD=LM-1
DO 170 N=1,MOD
DO 170 M=1,MOD
IF (M.EQ.1) GO TO 155
RATIO(N,M)=AQ(N,M)/AQ(N-1,M)
GO TO 160
155 RATIO(N,M)=1.0
160 IF (M.EQ.1) GO TO 165
RATIO(N,M)=AQ(N,M)/AQ(N,M-1)
GO TO 170
165 RATIO(N,M)=1.0
170 CONTINUE
WRITE (IWRITE,225)
LINES=5
NCOUNT=10
NSTART=1
DO 180 I=NSTART,NSTOP
180 WRITE (I1,I)
C*** OUTPUT AREAS AND AREA RATIOS FOR QUADRILATERALS
DO 185 I=1,MOD
WRITE (IWRITE,200) (I,WRITE(I),J=NSTART,NSTOP)
WRITE (IWRITE,205) (AQ(J,I),J=NSTART,NSTOP)

```

```

CVT 121
CVT 122
CVT 123
CVT 124
CVT 125
CVT 126
CVT 127
CVT 128
CVT 129
CVT 130
CVT 131
CVT 132
CVT 133
CVT 134
CVT 135
CVT 136
CVT 137
CVT 138
CVT 139
CVT 140
CVT 141
CVT 142
CVT 143
CVT 144
CVT 145
CVT 146
CVT 147
CVT 148
CVT 149
CVT 150
CVT 151
CVT 152
CVT 153
CVT 154
CVT 155
CVT 156
CVT 157
CVT 158
CVT 159
CVT 160
CVT 161
CVT 162
CVT 163
CVT 164
CVT 165
CVT 166
CVT 167
CVT 168
CVT 169
CVT 170
CVT 171
CVT 172
CVT 173
CVT 174
CVT 175
CVT 176
CVT 177
CVT 178
CVT 179
CVT 180

```

```

185 WRITE (IWRITE,210) (RATIO(I,J),J=NSTART,NSTOP)
WRITE (IWRITE,215) (RATIO(I,J),J=NSTART,NSTOP)
WRITE (IWRITE,220)
IF (NSTOP.EQ.MOD) GO TO 195
NSTART=NSTART+10
NCOUNT=NCOUNT+10
LINES=LINES+MOD*5
IF (LINES.GT.50) GO TO 190
GO TO 175
190 WRITE (IWRITE,225)
LINES=5
GO TO 175
195 CONTINUE
200 FORMAT (/,1X,10I2X,1Z,1M,/,1Z,5X1)
205 FORMAT (1X,10F10.3,2X1)
210 FORMAT (1X,10I1X,9,2,2X1)
215 FORMAT (1X,10I1X,9,2,2X1,/)
220 FORMAT (1X,11I1M-1)
225 FORMAT (1M1,1X,10I1X,9,2,2X1,/,1X,10I2X,4HAREA,6X),/,1X,10I2X,
C*** SEE IF CANNARDS WERE SPECIFIED
230 IF (J5.EQ.0) GO TO 240
DO 235 I=1,JP
J3=EQ-2) GO TO 240
READ (IREAD,30) (OUM(I),I=1,3)
235 READ (IREAD,30) (OUM(I),I=1,NPODDM)
C*** SEE IF FINS WERE SPECIFIED
240 IF (J4.EQ.0) GO TO 250
DO 245 I=1,NF
READ (IREAD,30) (OUM(I),I=1,8)
245 READ (IREAD,30) (OUM(I),I=1,NFINDM)
C*** SEE IF CANNARDS WERE SPECIFIED
250 IF (J5.EQ.0) GO TO 260
NCANI=IABST(CANI)
DO 255 I=1,MCANI
READ (IREAD,30) (OUM(I),I=1,8)
255 IF (I.EQ.1) GO TO 260
READ (IREAD,30) (OUM(I),I=1,MCANOR)
IF (MCAN.LT.0) READ (1,200) (DUM(I),I=1,MCANOR)
255 CONTINUE (IREAD,265, END=275) KODE
260 READ (IREAD,265, END=275) KODE
IF (KODE.NE.1) GO TO 260
WRITE (IPUNCH,270)
270 FORMAT (10X1)
275 WRITE (IPUNCH,270)
END
C*** FUNCTION SQ2(X,Y,Z)
SQ2 = ABS(X)+ABS(Y)+ABS(Z)+.000000000001
R=R+R/R
R=0.25*R+R/R
R=R+R/R
RETURN
END
SQ2 1
SQ2 2
SQ2 3
SQ2 4
SQ2 5
SQ2 6
SQ2 7
SQ2 8
SQ2 9
SQ2 10

```

```

CVT 181
CVT 182
CVT 183
CVT 184
CVT 185
CVT 186
CVT 187
CVT 188
CVT 189
CVT 190
CVT 191
CVT 192
CVT 193
CVT 194
CVT 195
CVT 196
CVT 197
CVT 198
CVT 199
CVT 200
CVT 201
CVT 202
CVT 203
CVT 204
CVT 205
CVT 206
CVT 207
CVT 208
CVT 209
CVT 210
CVT 211
CVT 212
CVT 213
CVT 214
CVT 215
CVT 216
CVT 217
CVT 218
CVT 219
CVT 220
CVT 221
CVT 222
CVT 223
CVT 224
CVT 225
CVT 226
CVT 227
CVT 228
CVT 229
CVT 230

```



(M,N) AREA RATIGN RATIGN	(M,N) AREA RATIGN RATIGN	(M,N) AREA RATIGN RATIGN	(M,N) AREA RATIGN RATIGN	(M,N) AREA RATIGN RATIGN	(M,N) AREA RATIGN RATIGN	(M,N) AREA RATIGN RATIGN	(M,N) AREA RATIGN RATIGN	(M,N) AREA RATIGN RATIGN	(M,N) AREA RATIGN RATIGN	(M,N) AREA RATIGN RATIGN
1, 1 0.127E 00 0.10E 01 0.10E 01	1, 2 0.149E 00 0.10E 01 0.12E 01	1, 3 0.161E 00 0.10E 01 0.11E 01	1, 4 0.184E 00 0.10E 01 0.12E 01	1, 5 0.160E 00 0.10E 01 0.04E 00	1, 6 0.163E 00 0.10E 01 0.10E 01	1, 7 0.199E 00 0.209E 00 0.10E 01	1, 8 0.209E 00 0.209E 00 0.10E 01	1, 9 0.209E 00 0.209E 00 0.10E 01	1, 10 0.229E 00 0.10E 01 0.11E 01	1, 11 0.229E 00 0.10E 01 0.11E 01
2, 1 0.120E 00 0.09E 00 0.10E 01	2, 2 0.156E 00 0.10E 01 0.12E 01	2, 3 0.169E 00 0.10E 01 0.11E 01	2, 4 0.174E 00 0.11E 01 0.12E 01	2, 5 0.169E 00 0.10E 01 0.04E 00	2, 6 0.169E 00 0.10E 01 0.10E 01	2, 7 0.204E 00 0.219E 00 0.11E 01	2, 8 0.219E 00 0.219E 00 0.11E 01	2, 9 0.219E 00 0.219E 00 0.10E 01	2, 10 0.241E 00 0.10E 01 0.11E 01	2, 11 0.241E 00 0.10E 01 0.11E 01
3, 1 0.117E 00 0.09E 00 0.10E 01	3, 2 0.158E 00 0.10E 01 0.11E 01	3, 3 0.174E 00 0.11E 01 0.11E 01	3, 4 0.211E 00 0.11E 01 0.12E 01	3, 5 0.184E 00 0.11E 01 0.07E 00	3, 6 0.174E 00 0.07E 00 0.12E 01	3, 7 0.211E 00 0.224E 00 0.10E 01	3, 8 0.224E 00 0.224E 00 0.10E 01	3, 9 0.224E 00 0.224E 00 0.10E 01	3, 10 0.246E 00 0.10E 01 0.11E 01	3, 11 0.246E 00 0.10E 01 0.11E 01
4, 1 0.120E 00 0.10E 01 0.10E 01	4, 2 0.164E 00 0.11E 01 0.14E 01	4, 3 0.188E 00 0.11E 01 0.11E 01	4, 4 0.244E 00 0.11E 01 0.12E 01	4, 5 0.211E 00 0.11E 01 0.00E 00	4, 6 0.200E 00 0.09E 00 0.11E 01	4, 7 0.222E 00 0.222E 00 0.11E 01	4, 8 0.229E 00 0.229E 00 0.10E 01	4, 9 0.227E 00 0.227E 00 0.10E 01	4, 10 0.243E 00 0.10E 01 0.11E 01	4, 11 0.243E 00 0.10E 01 0.11E 01
5, 1 0.117E 00 0.09E 00 0.10E 01	5, 2 0.157E 00 0.10E 01 0.13E 01	5, 3 0.187E 00 0.11E 01 0.12E 01	5, 4 0.234E 00 0.11E 01 0.13E 01	5, 5 0.209E 00 0.11E 01 0.07E 00	5, 6 0.199E 00 0.09E 00 0.11E 01	5, 7 0.232E 00 0.232E 00 0.11E 01	5, 8 0.239E 00 0.239E 00 0.10E 01	5, 9 0.237E 00 0.237E 00 0.10E 01	5, 10 0.253E 00 0.10E 01 0.12E 01	5, 11 0.253E 00 0.10E 01 0.12E 01
6, 1 0.114E 00 0.11E 01 0.10E 01	6, 2 0.167E 00 0.11E 01 0.13E 01	6, 3 0.194E 00 0.11E 01 0.12E 01	6, 4 0.252E 00 0.12E 01 0.12E 01	6, 5 0.228E 00 0.11E 01 0.04E 00	6, 6 0.218E 00 0.09E 00 0.07E 00	6, 7 0.240E 00 0.240E 00 0.11E 01	6, 8 0.247E 00 0.247E 00 0.10E 01	6, 9 0.245E 00 0.245E 00 0.10E 01	6, 10 0.261E 00 0.10E 01 0.12E 01	6, 11 0.261E 00 0.10E 01 0.12E 01
7, 1 0.120E 00 0.09E 00 0.10E 01	7, 2 0.160E 00 0.09E 00 0.12E 01	7, 3 0.182E 00 0.10E 01 0.12E 01	7, 4 0.242E 00 0.10E 01 0.12E 01	7, 5 0.209E 00 0.09E 00 0.09E 00	7, 6 0.200E 00 0.04E 00 0.04E 00	7, 7 0.222E 00 0.222E 00 0.11E 01	7, 8 0.229E 00 0.229E 00 0.09E 00	7, 9 0.227E 00 0.227E 00 0.10E 01	7, 10 0.243E 00 0.10E 01 0.11E 01	7, 11 0.243E 00 0.10E 01 0.11E 01
8, 1 0.114E 00 0.11E 01 0.10E 01	8, 2 0.167E 00 0.10E 01 0.11E 01	8, 3 0.194E 00 0.11E 01 0.11E 01	8, 4 0.252E 00 0.12E 01 0.12E 01	8, 5 0.228E 00 0.11E 01 0.00E 00	8, 6 0.218E 00 0.04E 00 0.04E 00	8, 7 0.240E 00 0.240E 00 0.11E 01	8, 8 0.247E 00 0.247E 00 0.09E 00	8, 9 0.245E 00 0.245E 00 0.09E 00	8, 10 0.261E 00 0.10E 01 0.12E 01	8, 11 0.261E 00 0.10E 01 0.12E 01
9, 1 0.117E 00 0.12E 01 0.10E 01	9, 2 0.157E 00 0.10E 01 0.10E 01	9, 3 0.187E 00 0.11E 01 0.11E 01	9, 4 0.234E 00 0.11E 01 0.12E 01	9, 5 0.209E 00 0.11E 01 0.04E 00	9, 6 0.199E 00 0.09E 00 0.09E 00	9, 7 0.232E 00 0.232E 00 0.11E 01	9, 8 0.239E 00 0.239E 00 0.10E 01	9, 9 0.237E 00 0.237E 00 0.09E 00	9, 10 0.253E 00 0.10E 01 0.12E 01	9, 11 0.253E 00 0.10E 01 0.12E 01
10, 1 0.114E 00 0.11E 01 0.10E 01	10, 2 0.167E 00 0.10E 01 0.09E 00	10, 3 0.194E 00 0.10E 01 0.10E 01	10, 4 0.252E 00 0.12E 01 0.12E 01	10, 5 0.228E 00 0.11E 01 0.09E 00	10, 6 0.218E 00 0.04E 00 0.04E 00	10, 7 0.240E 00 0.240E 00 0.11E 01	10, 8 0.247E 00 0.247E 00 0.09E 00	10, 9 0.245E 00 0.245E 00 0.09E 00	10, 10 0.261E 00 0.10E 01 0.12E 01	10, 11 0.261E 00 0.10E 01 0.12E 01
11, 1 0.117E 00 0.11E 01 0.10E 01	11, 2 0.157E 00 0.10E 01 0.09E 00	11, 3 0.187E 00 0.10E 01 0.10E 01	11, 4 0.234E 00 0.11E 01 0.11E 01	11, 5 0.209E 00 0.11E 01 0.09E 00	11, 6 0.199E 00 0.09E 00 0.09E 00	11, 7 0.232E 00 0.232E 00 0.11E 01	11, 8 0.239E 00 0.239E 00 0.10E 01	11, 9 0.237E 00 0.237E 00 0.09E 00	11, 10 0.253E 00 0.10E 01 0.12E 01	11, 11 0.253E 00 0.10E 01 0.12E 01
12, 1 0.120E 00 0.12E 01 0.10E 01	12, 2 0.160E 00 0.10E 01 0.09E 00	12, 3 0.182E 00 0.10E 01 0.10E 01	12, 4 0.242E 00 0.10E 01 0.11E 01	12, 5 0.209E 00 0.11E 01 0.04E 00	12, 6 0.200E 00 0.11E 01 0.04E 00	12, 7 0.222E 00 0.222E 00 0.11E 01	12, 8 0.229E 00 0.229E 00 0.09E 00	12, 9 0.227E 00 0.227E 00 0.10E 01	12, 10 0.243E 00 0.10E 01 0.11E 01	12, 11 0.243E 00 0.10E 01 0.11E 01
13, 1 0.114E 00 0.10E 01 0.10E 01	13, 2 0.167E 00 0.10E 01 0.09E 00	13, 3 0.194E 00 0.10E 01 0.11E 01	13, 4 0.252E 00 0.11E 01 0.11E 01	13, 5 0.228E 00 0.11E 01 0.07E 00	13, 6 0.218E 00 0.04E 00 0.04E 00	13, 7 0.240E 00 0.240E 00 0.11E 01	13, 8 0.247E 00 0.247E 00 0.09E 00	13, 9 0.245E 00 0.245E 00 0.09E 00	13, 10 0.261E 00 0.10E 01 0.12E 01	13, 11 0.261E 00 0.10E 01 0.12E 01
14, 1 0.117E 00 0.09E 00 0.10E 01	14, 2 0.157E 00 0.09E 00 0.10E 01	14, 3 0.187E 00 0.10E 01 0.11E 01	14, 4 0.234E 00 0.10E 01 0.11E 01	14, 5 0.209E 00 0.10E 01 0.04E 00	14, 6 0.199E 00 0.09E 01 0.11E 01	14, 7 0.232E 00 0.232E 00 0.11E 01	14, 8 0.239E 00 0.239E 00 0.10E 01	14, 9 0.237E 00 0.237E 00 0.09E 00	14, 10 0.253E 00 0.10E 01 0.12E 01	14, 11 0.253E 00 0.10E 01 0.12E 01
15, 1 0.120E 00 0.09E 00 0.10E 01	15, 2 0.160E 00 0.10E 01 0.09E 00	15, 3 0.182E 00 0.10E 01 0.10E 01	15, 4 0.242E 00 0.10E 01 0.11E 01	15, 5 0.209E 00 0.10E 01 0.04E 00	15, 6 0.200E 00 0.11E 01 0.04E 00	15, 7 0.222E 00 0.222E 00 0.11E 01	15, 8 0.229E 00 0.229E 00 0.09E 00	15, 9 0.227E 00 0.227E 00 0.10E 01	15, 10 0.243E 00 0.10E 01 0.11E 01	15, 11 0.243E 00 0.10E 01 0.11E 01
16, 1 0.114E 00 0.09E 00 0.10E 01	16, 2 0.167E 00 0.09E 00 0.10E 01	16, 3 0.194E 00 0.10E 01 0.11E 01	16, 4 0.252E 00 0.11E 01 0.11E 01	16, 5 0.228E 00 0.10E 01 0.07E 00	16, 6 0.218E 00 0.04E 01 0.11E 01	16, 7 0.240E 00 0.240E 00 0.10E 01	16, 8 0.247E 00 0.247E 00 0.09E 00	16, 9 0.245E 00 0.245E 00 0.09E 00	16, 10 0.261E 00 0.10E 01 0.12E 01	16, 11 0.261E 00 0.10E 01 0.12E 01
17, 1 0.117E 00 0.09E 00 0.10E 01	17, 2 0.157E 00 0.09E 00 0.10E 01	17, 3 0.187E 00 0.09E 00 0.11E 01	17, 4 0.234E 00 0.09E 00 0.04E 00	17, 5 0.209E 00 0.09E 00 0.04E 00	17, 6 0.199E 00 0.09E 01 0.11E 01	17, 7 0.232E 00 0.232E 00 0.11E 01	17, 8 0.239E 00 0.239E 00 0.10E 01	17, 9 0.237E 00 0.237E 00 0.09E 00	17, 10 0.253E 00 0.10E 01 0.12E 01	17, 11 0.253E 00 0.10E 01 0.12E 01
18, 1 0.120E 00 0.09E 00 0.10E 01	18, 2 0.160E 00 0.10E 01 0.10E 01	18, 3 0.182E 00 0.10E 01 0.11E 01	18, 4 0.242E 00 0.10E 01 0.07E 00	18, 5 0.209E 00 0.11E 01 0.04E 00	18, 6 0.200E 00 0.11E 01 0.04E 00	18, 7 0.222E 00 0.222E 00 0.11E 01	18, 8 0.229E 00 0.229E 00 0.09E 00	18, 9 0.227E 00 0.227E 00 0.10E 01	18, 10 0.243E 00 0.10E 01 0.11E 01	18, 11 0.243E 00 0.10E 01 0.11E 01
19, 1 0.114E 00 0.10E 01 0.10E 01	19, 2 0.167E 00 0.10E 01 0.09E 00	19, 3 0.194E 00 0.10E 01 0.11E 01	19, 4 0.252E 00 0.11E 01 0.07E 00	19, 5 0.228E 00 0.10E 01 0.04E 00	19, 6 0.218E 00 0.09E 01 0.11E 01	19, 7 0.240E 00 0.240E 00 0.11E 01	19, 8 0.247E 00 0.247E 00 0.09E 00	19, 9 0.245E 00 0.245E 00 0.09E 00	19, 10 0.261E 00 0.10E 01 0.12E 01	19, 11 0.261E 00 0.10E 01 0.12E 01
20, 1 0.117E 00 0.09E 00 0.10E 01	20, 2 0.157E 00 0.10E 01 0.10E 01	20, 3 0.187E 00 0.10E 01 0.11E 01	20, 4 0.234E 00 0.10E 01 0.07E 00	20, 5 0.209E 00 0.10E 01 0.04E 00	20, 6 0.199E 00 0.09E 00 0.11E 01	20, 7 0.232E 00 0.232E 00 0.11E 01	20, 8 0.239E 00 0.239E 00 0.10E 01	20, 9 0.237E 00 0.237E 00 0.09E 00	20, 10 0.253E 00 0.10E 01 0.12E 01	20, 11 0.253E 00 0.10E 01 0.12E 01

Figure E-1. Continued.



(R,M) AREA RATIGN	(R,M) AREA RATIGN	(R,M) AREA RATIGN	(R,M) AREA RATIGN	(R,M) AREA RATIGN	(R,M) AREA RATIGN	(R,M) AREA RATIGN	(R,M) AREA RATIGN	(R,M) AREA RATIGN	(R,M) AREA RATIGN
1,21	1,22	1,23	1,24	1,25	1,26	1,27	1,28		
0.179E 00	0.229E 00	0.237E 00	0.259E 00	0.262E 00	0.215E 00	0.211E 00	0.164E 00		
0.10E 01	0.10E 01	0.10E 01	0.10E 01	0.10E 01	0.10E 01	0.10E 01	0.10E 01		
0.99E 00	0.13E 01	0.11E 01	0.10E 01	0.94E 00	0.69E 00	0.90E 00	0.78E 00		
2,21	2,22	2,23	2,24	2,25	2,26	2,27	2,28		
0.107E 00	0.259E 00	0.272E 00	0.267E 00	0.266E 00	0.217E 00	0.212E 00	0.170E 00		
0.11E 01	0.11E 01	0.11E 01	0.10E 01	0.10E 01	0.10E 01	0.10E 01	0.10E 01		
0.99E 00	0.13E 01	0.11E 01	0.90E 00	0.92E 00	0.69E 00	0.97E 00	0.90E 00		
3,21	3,22	3,23	3,24	3,25	3,26	3,27	3,28		
0.106E 00	0.260E 00	0.260E 00	0.262E 00	0.262E 00	0.221E 00	0.200E 00	0.153E 00		
0.99E 00	0.10E 01	0.10E 01	0.11E 01	0.11E 01	0.10E 01	0.94E 00	0.90E 00		
0.99E 00	0.13E 01	0.12E 01	0.99E 00	0.93E 00	0.64E 00	0.91E 00	0.76E 00		
4,21	4,22	4,23	4,24	4,25	4,26	4,27	4,28		
0.219E 00	0.209E 00	0.237E 00	0.230E 00	0.260E 00	0.229E 00	0.202E 00	0.152E 00		
0.11E 01	0.12E 01	0.12E 01	0.12E 01	0.11E 01	0.10E 01	0.10E 01	0.10E 01		
0.10E 01	0.13E 01	0.12E 01	0.99E 00	0.87E 00	0.60E 00	0.68E 00	0.75E 00		
5,21	5,22	5,23	5,24	5,25	5,26	5,27	5,28		
0.214E 00	0.207E 00	0.234E 00	0.224E 00	0.259E 00	0.233E 00	0.201E 00	0.149E 00		
0.10E 01	0.99E 00	0.99E 00	0.99E 00	0.99E 00	0.10E 01	0.10E 01	0.99E 00		
0.10E 01	0.13E 01	0.12E 01	0.97E 00	0.89E 00	0.62E 00	0.66E 00	0.72E 00		
6,21	6,22	6,23	6,24	6,25	6,26	6,27	6,28		
0.213E 00	0.217E 00	0.232E 00	0.214E 00	0.252E 00	0.227E 00	0.190E 00	0.129E 00		
0.10E 01	0.97E 00	0.97E 00	0.98E 00	0.98E 00	0.97E 00	0.99E 00	0.69E 00		
0.10E 01	0.13E 01	0.12E 01	0.98E 00	0.68E 00	0.61E 00	0.93E 00	0.69E 00		
7,21	7,22	7,23	7,24	7,25	7,26	7,27	7,28		
0.214E 00	0.203E 00	0.230E 00	0.222E 00	0.252E 00	0.237E 00	0.196E 00	0.139E 00		
0.10E 01	0.10E 01	0.10E 01	0.10E 01	0.11E 01	0.10E 01	0.10E 01	0.11E 01		
0.10E 01	0.13E 01	0.12E 01	0.99E 00	0.90E 00	0.61E 00	0.64E 00	0.70E 00		
8,21	8,22	8,23	8,24	8,25	8,26	8,27	8,28		
0.203E 00	0.260E 00	0.261E 00	0.290E 00	0.259E 00	0.212E 00	0.170E 00	0.117E 00		
0.94E 00	0.97E 00	0.97E 00	0.97E 00	0.97E 00	0.69E 00	0.90E 00	0.69E 00		
0.11E 01	0.13E 01	0.11E 01	0.96E 00	0.69E 00	0.63E 00	0.64E 00	0.64E 00		
9,21	9,22	9,23	9,24	9,25	9,26	9,27	9,28		
0.192E 00	0.252E 00	0.264E 00	0.277E 00	0.244E 00	0.197E 00	0.172E 00	0.121E 00		
0.94E 00	0.94E 00	0.94E 00	0.94E 00	0.94E 00	0.93E 00	0.96E 00	0.10E 01		
0.94E 00	0.13E 01	0.11E 01	0.97E 00	0.80E 00	0.61E 00	0.87E 00	0.70E 00		
10,21	10,22	10,23	10,24	10,25	10,26	10,27	10,28		
0.109E 00	0.252E 00	0.250E 00	0.254E 00	0.253E 00	0.194E 00	0.165E 00	0.109E 00		
0.99E 00	0.10E 01	0.99E 00	0.96E 00	0.93E 00	0.90E 00	0.94E 00	0.91E 00		
0.10E 01	0.13E 01	0.11E 01	0.95E 00	0.60E 00	0.63E 00	0.69E 00	0.64E 00		
11,21	11,22	11,23	11,24	11,25	11,26	11,27	11,28		
0.184E 00	0.263E 00	0.271E 00	0.250E 00	0.250E 00	0.189E 00	0.160E 00	0.109E 00		
0.97E 00	0.97E 00	0.97E 00	0.96E 00	0.96E 00	0.97E 00	0.97E 00	0.16E 01		
0.10E 01	0.13E 01	0.11E 01	0.95E 00	0.69E 00	0.62E 00	0.69E 00	0.68E 00		
12,21	12,22	12,23	12,24	12,25	12,26	12,27	12,28		
0.191E 00	0.254E 00	0.261E 00	0.249E 00	0.239E 00	0.197E 00	0.171E 00	0.119E 00		
0.10E 01	0.10E 01	0.10E 01	0.10E 01	0.10E 01	0.10E 01	0.11E 01	0.11E 01		
0.11E 01	0.13E 01	0.11E 01	0.94E 00	0.69E 00	0.62E 00	0.87E 00	0.68E 00		
13,21	13,22	13,23	13,24	13,25	13,26	13,27	13,28		
0.210E 00	0.261E 00	0.265E 00	0.260E 00	0.269E 00	0.210E 00	0.190E 00	0.131E 00		
0.11E 01	0.11E 01	0.12E 01	0.11E 01	0.11E 01	0.11E 01	0.11E 01	0.11E 01		
0.97E 00	0.13E 01	0.11E 01	0.94E 00	0.68E 00	0.61E 00	0.64E 00	0.69E 00		
14,21	14,22	14,23	14,24	14,25	14,26	14,27	14,28		
0.234E 00	0.260E 00	0.260E 00	0.264E 00	0.267E 00	0.233E 00	0.190E 00	0.141E 00		
0.11E 01	0.10E 01	0.10E 01	0.10E 01	0.11E 01	0.11E 01	0.10E 01	0.11E 01		
0.10E 01	0.13E 01	0.11E 01	0.95E 00	0.91E 00	0.61E 00	0.69E 00	0.71E 00		
15,21	15,22	15,23	15,24	15,25	15,26	15,27	15,28		
0.224E 00	0.264E 00	0.269E 00	0.266E 00	0.277E 00	0.233E 00	0.203E 00	0.146E 00		
0.99E 00	0.94E 00	0.94E 00	0.94E 00	0.97E 00	0.10E 01	0.10E 01	0.10E 01		
0.10E 01	0.13E 01	0.11E 01	0.94E 00	0.94E 00	0.64E 00	0.87E 00	0.72E 00		
16,21	16,22	16,23	16,24	16,25	16,26	16,27	16,28		
0.224E 00	0.271E 00	0.267E 00	0.270E 00	0.251E 00	0.204E 00	0.182E 00	0.131E 00		
0.10E 01	0.95E 00	0.94E 00	0.94E 00	0.91E 00	0.68E 00	0.90E 00	0.69E 00		
0.10E 01	0.12E 01	0.11E 01	0.95E 00	0.90E 00	0.62E 00	0.69E 00	0.72E 00		
17,21	17,22	17,23	17,24	17,25	17,26	17,27	17,28		
0.204E 00	0.269E 00	0.260E 00	0.253E 00	0.259E 00	0.204E 00	0.187E 00	0.137E 00		
0.97E 00	0.92E 00	0.97E 00	0.10E 01	0.10E 01	0.10E 01	0.10E 01	0.11E 01		
0.97E 00	0.12E 01	0.11E 01	0.10E 01	0.90E 00	0.61E 00	0.91E 00	0.73E 00		
18,21	18,22	18,23	18,24	18,25	18,26	18,27	18,28		
0.194E 00	0.249E 00	0.263E 00	0.262E 00	0.262E 00	0.218E 00	0.197E 00	0.147E 00		
0.95E 00	0.96E 00	0.10E 01	0.99E 00	0.10E 01	0.11E 01	0.11E 01	0.11E 01		
0.94E 00	0.12E 01	0.12E 01	0.10E 01	0.93E 00	0.63E 00	0.91E 00	0.74E 00		
19,21	19,22	19,23	19,24	19,25	19,26	19,27	19,28		
0.217E 00	0.265E 00	0.260E 00	0.261E 00	0.264E 00	0.250E 00	0.242E 00	0.184E 00		
0.11E 01	0.11E 01	0.11E 01	0.11E 01	0.11E 01	0.11E 01	0.12E 01	0.13E 01		
0.90E 00	0.12E 01	0.11E 01	0.10E 01	0.91E 00	0.69E 00	0.97E 00	0.76E 00		
20,21	20,22	20,23	20,24	20,25	20,26	20,27	20,28		
0.204E 00	0.240E 00	0.254E 00	0.250E 00	0.264E 00	0.235E 00	0.220E 00	0.170E 00		
0.99E 00	0.94E 00	0.95E 00	0.99E 00	0.93E 00	0.94E 00	0.94E 00	0.92E 00		
0.94E 00	0.12E 01	0.12E 01	0.10E 01	0.93E 00	0.68E 00	0.97E 00	0.75E 00		

Figure E-1. Continued.

## APPENDIX F- NCSU BODY Program

### User Instructions

The program is written in FORTRAN IV and is designed to run in single precision on an IBM 370-165 computer with an execution time of 10-12 minutes for a half-body with 560 panels (1 minute for a half-body with 100 panels). The 560 panel case required 250,000 bytes of core storage. The program calculates an approximate solution of the three-dimensional viscous flow over an arbitrary body and estimates the body lift and drag coefficients. The program was obtained by making major modifications to the XYZ potential flow program (Ref. 94) supplied by the Naval Ship Research and Development Center, Bethesda, Maryland. The data input and program logic modifications were employed to specialize the program for light aircraft fuselages; therefore, this modified program no longer has the design capability of the original XYZ program. Figure F-1 illustrates how the body ordinates should be input to provide the correct body orientation with respect to the flow direction.

The program input data specification is based on the description given in Reference 94 except where changes were made. The input consists of an identification card, two parameter cards, and several body point cards. A description of the program input is given below.

Card 1 - Identification - Card 1 contains any information to identify the problem in columns 1 through 80.

Card 2 - Flow Control Variables - Card 2 contains 3 variables which determine the flow Reynolds Number, the reference area upon which the coefficients are based, and an output control parameter. This is the only card which must be inserted into a data set produced by the CONVERT program in Appendix E.

<u>Parameter</u>	<u>Column</u>	<u>Description</u>
VINF	1-10	Reference free stream velocity in ft./sec. if the body input points are specified in feet (in general it will be units/second where units are the units in which the body input points are specified).
VO	11-20	Kinematic viscosity of the fluid in which the body is moving in ft. <sup>2</sup> /sec. if the velocity is specified in ft./sec.

---

† All of these cards except one (card 2) is supplied by the CONVERT program given in Appendix E.



<u>Parameter</u>	<u>Column</u>	<u>Description</u>
ROE	21-30	The density of the fluid in which the body is moving in slugs/ft. <sup>3</sup>
REFA	31-40	The reference area upon which the aerodynamic coefficients will be based in ft. <sup>2</sup>
IWRITE	45	Control variable which denotes the amount of output the user desires. IWRITE=0 yields maximum output. IWRITE=1 deletes information given for each input point. IWRITE=2 deletes streamline and boundary layer information as well as input point information. (See Sample Output).

Card 3 - Control Integer - Card 3 contains a control integer which must be right justified.

<u>Parameter</u>	<u>Column</u>	<u>Description</u>
NQE	1-4	Number of quadrilateral panels to be specified by the point cards. The value of NQE should generally be less than 600 (see page 244).

Cards 4, 5, . . . - Point Cards - Each point card contains the following information for one point on the body surface. If one section is used for the fuselage there should be P points specified where P is equal to the maximum MI times the maximum NI.

<u>Parameter</u>	<u>Column</u>	<u>Description</u>
XI	1-12	X-coordinate of the input point.
YI	13-24	Y-coordinate of the input point.
ZI	25-36	Z-coordinate of the input point.
NI	39-40	N body station index (see Figure F-2). For plotting purposes NI $\leq$ 30.
MI	43-44	M body station index (see Figure F-2). For plotting purposes MI $\leq$ 30.
NS	45-48	Section identification number. The CONVERT program (Appendix E) supplies a one-section data set with a section number of 1.

Last Card - End of Data Set - The last card is a blank card to signify the last card of a particular data set.

It should be noted that the program can be run for more than one data set; the user must simply put the complete data sets he desires to analyze in consecutive order. For more information about this program the user should see pages 243 - 255 which describe the modifications made to the original program as well as Reference 94 which describes the original program.

Specification of the cards above represent a complete set of data for a particular body. The format specification for this data is given in Figure F-3. A sample data set of a prolate spheroid is shown in Figure F-4. Portions of the sample output for the light aircraft data set shown in Figure D-3 and plotted in Appendix D are given in Figure F-5. The light aircraft data set was not used in Figure F-4 as the sample data set because of the excessive length of the light aircraft data set (in excess of 600 cards).

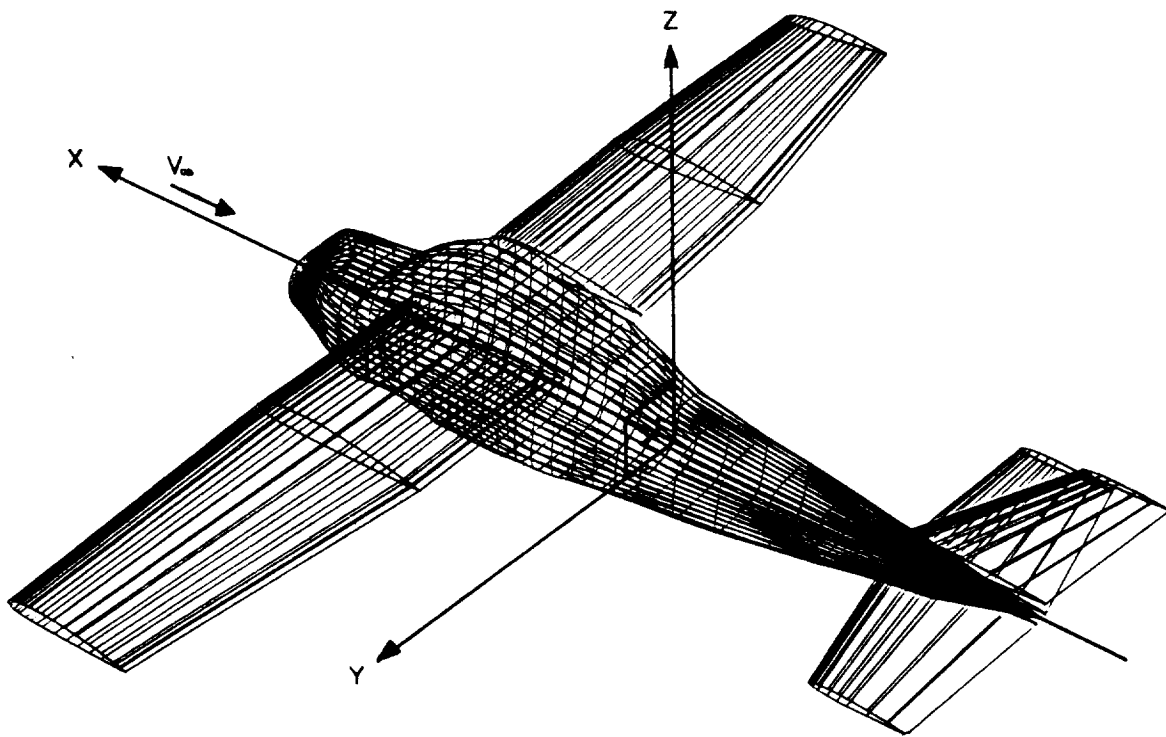


Figure F-1. Orientation of body with respect to body reference axes for the NCSU BODY program.

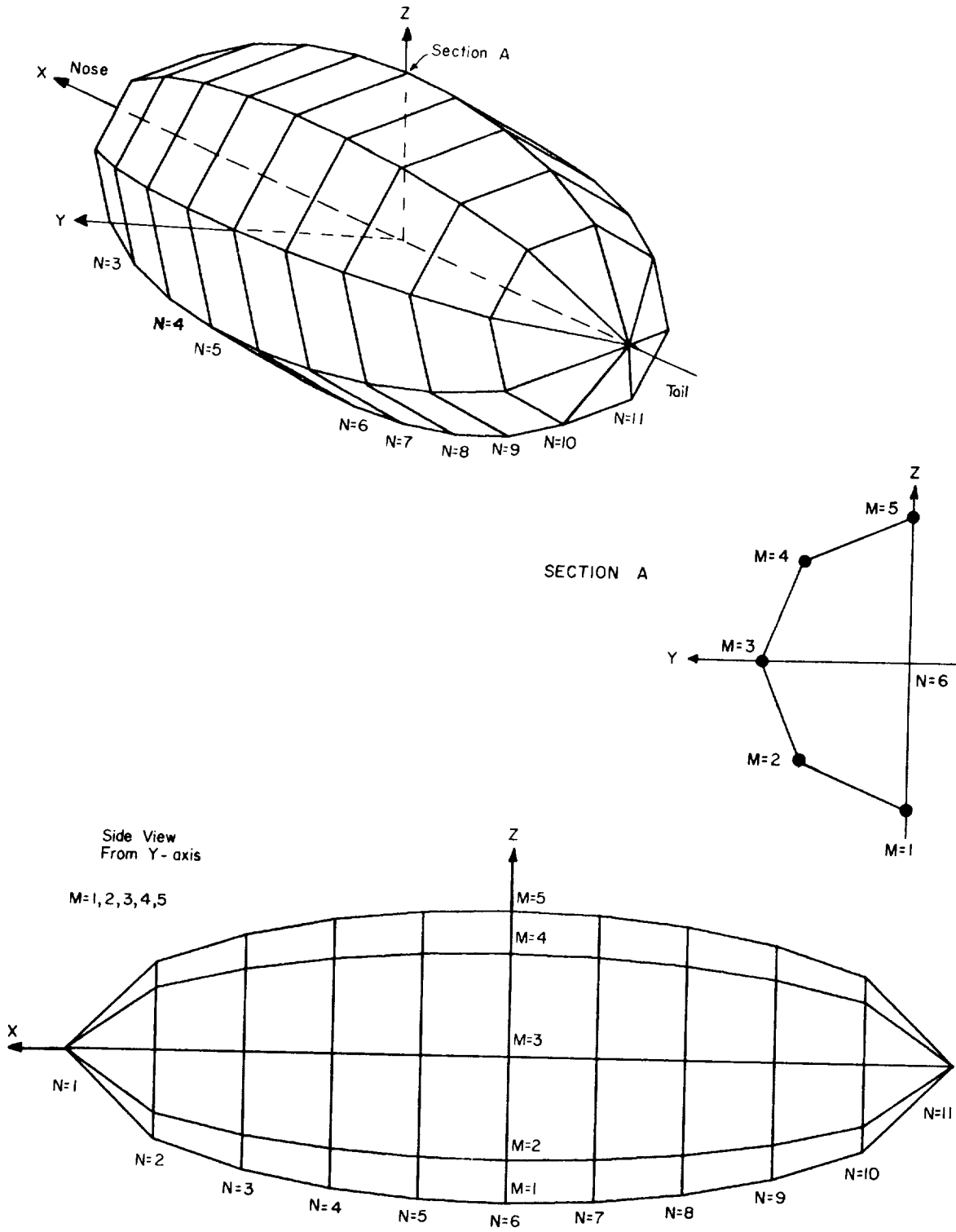


Figure F-2. Schematic of indexing scheme used for a 3-1 ellipsoid with 60 panels describing the half-body.

TITLE										
20A4										
VINF	VO	ROE	REFA	IWRITE						
F10.5	F10.5	F10.5	F10.5	I5						
NOE										
I4										
X1	V1	Z1	N1	M1	NB					
F12.9	F12.9	F12.9	I4	I4	I4					
.	.	.	.	.	.					
.	.	.	.	.	.					
(THIS IS A BLANK CARD AFTER THE LAST POINT CARD)										

Figure F-3. Format specification for the NCSU BODY program.



Program Listing

```

Cooo THIS BASIC PROGRAM WAS OBTAINED FROM THE NAVAL SHIP RESEARCH AND
Cooo DEVELOPMENT CENTER AND WAS THEN EXTENSIVELY MODIFIED FOR USE AT
Cooo M.C. STATE UNIVERSITY. WE WOULD LIKE TO THANK CHARLES W DAMSON FOR
Cooo PROVIDING THE PROGRAM AND FOR HIS HELP IN MAKING SOME OF THE
Cooo MODIFICATIONS.
Cooo
Cooo REFERENCE: CHARLES W. DAMSON & JANET S. DEAN
Cooo REPORT 3892
Cooo NAVAL SHIP RESEARCH & DEVELOPMENT CENTER
Cooo BETHESDA, MARYLAND 20034
Cooo
Cooo POTENTIAL FLOW PROGRAM SECTION 1 OF 5 SECTIONS
Cooo DIMENSION IMDE(9,3),G(9,6),F(9),CZ(9),PI(9),IP(10),VP(10),ZP(10),X(4
Cooo 150),Y(650),Z(150),ID(31,31),O(192),PP(9,1),M(10,11,2),MMEM(150),YM
Cooo 150),ZMEM(150),MK(4),MK(4)
Cooo EQUIVALENCE (MMEM(11),DELS(11)),(YMEM(11),CF(11)),(ZMEM(11),TMT(11)),(C
Cooo 1Z(11),F(11),F(11),F(11))
Cooo COMMON TITLE(20),KCP(650),KCP(650),ZCP(650),YMP(650),ZMP(
Cooo 1650),OP(650),REPA,REBODY,QUAD,TWRITE,MP,KMEM
Cooo COMMON /BL/VO(175),SS(175),VIMP,VO,ROE,DELS(150),CF(150),TMT(150),
Cooo 1SDTAL,XIK
Cooo COMMON /INOUT/IREAD,JWRITE,KFILE,KFILE2,KFILES,KFILES,KFILE4,KFILE
Cooo 15
Cooo INTEGER P,P1,P2,P3,P4,PC,P5,P6,PT,P8,P9
Cooo REAL G,DE
Cooo JWRITE=3
Cooo KELE1=7
Cooo KELE2=8
Cooo KELE3=9
Cooo KELE4=10
Cooo KFILES=11
Cooo KFILE=KFILE1
Cooo 5 READ (JREAD,15,END=440) (TITLE(I),I=1,20)
Cooo WRITE (JWRITE,10)
Cooo
Cooo 10 FORMAT (1M1//,2X,34H POTENTIAL FLOW PROGRAM SECTION 1,/)
Cooo 15 FORMAT (20A4)
Cooo
Cooo KMEM=1
Cooo KWRITE=0
Cooo KHOLD=0
Cooo J=0
Cooo WRITE (JWRITE,20) (TITLE(I),I=1,20)
Cooo 20 FORMAT (1X,20A4)
Cooo
Cooo 25 J=0
Cooo 30 FORMAT (17HNO. OF QUADS. =14/17H NO. OF SECTIONS=,IN/31H PAR. N
Cooo 10. OF ITERATIONS X FLOW ,13)
Cooo 35 DEFINE AND READ PERTINENT GEOMETRIC & FLOW CONTROL PARAMETERS
Cooo 35 READ (JREAD,35) VIMP,VO,ROE,DEFA,TWRITE
Cooo 40 READ (JREAD,40) NOE
Cooo 45 NSE=1
Cooo 50 MIX=150
Cooo 55 ISM=1
Cooo
Cooo 1
Cooo 2
Cooo 3
Cooo 4
Cooo 5
Cooo 6
Cooo 7
Cooo 8
Cooo 9
Cooo 10
Cooo 11
Cooo 12
Cooo 13
Cooo 14
Cooo 15
Cooo 16
Cooo 17
Cooo 18
Cooo 19
Cooo 20
Cooo 21
Cooo 22
Cooo 23
Cooo 24
Cooo 25
Cooo 26
Cooo 27
Cooo 28
Cooo 29
Cooo 30
Cooo 31
Cooo 32
Cooo 33
Cooo 34
Cooo 35
Cooo 36
Cooo 37
Cooo 38
Cooo 39
Cooo 40
Cooo 41
Cooo 42
Cooo 43
Cooo 44
Cooo 45
Cooo 46
Cooo 47
Cooo 48
Cooo 49
Cooo 50
Cooo 51
Cooo 52
Cooo 53
Cooo 54
Cooo 55
Cooo 56
Cooo 57
Cooo 58
Cooo 59
Cooo 60
Cooo
Cooo EPS=0.0001
Cooo ISM=0
Cooo WRITE (JWRITE,30) NOE,NOE,MIX
Cooo 40 FORMAT (//,1X,TWRITE = ,F10.6,3X,VOE,DEFA,TWRITE
Cooo 1X,THEFA = ,F10.6,3X,TWRITE, /,2, /)
Cooo 45 FORMAT (2X,CONVERSION FACTOR = ,F10.6,3X,2M3,12X,2M4,12X,2M5,12X,2M6,12X,2M7,12X,2M8,12X,2M9,12X,2M10,12X,2M11,12X,2M12,12X,2M13,12X,2M14,12X,2M15,12X,2M16,12X,2M17,12X,2M18,12X,2M19,12X,2M20,12X,2M21,12X,2M22,12X,2M23,12X,2M24,12X,2M25,12X,2M26,12X,2M27,12X,2M28,12X,2M29,12X,2M30,12X,2M31,12X,2M32,12X,2M33,12X,2M34,12X,2M35,12X,2M36,12X,2M37,12X,2M38,12X,2M39,12X,2M40,12X,2M41,12X,2M42,12X,2M43,12X,2M44,12X,2M45,12X,2M46,12X,2M47,12X,2M48,12X,2M49,12X,2M50,12X,2M51,12X,2M52,12X,2M53,12X,2M54,12X,2M55,12X,2M56,12X,2M57,12X,2M58,12X,2M59,12X,2M60,12X,2M61,12X,2M62,12X,2M63,12X,2M64,12X,2M65,12X,2M66,12X,2M67,12X,2M68,12X,2M69,12X,2M70,12X,2M71,12X,2M72,12X,2M73,12X,2M74,12X,2M75,12X,2M76,12X,2M77,12X,2M78,12X,2M79,12X,2M80,12X,2M81,12X,2M82,12X,2M83,12X,2M84,12X,2M85,12X,2M86,12X,2M87,12X,2M88,12X,2M89,12X,2M90,12X,2M91,12X,2M92,12X,2M93,12X,2M94,12X,2M95,12X,2M96,12X,2M97,12X,2M98,12X,2M99,12X,2M100,12X,2M101,12X,2M102,12X,2M103,12X,2M104,12X,2M105,12X,2M106,12X,2M107,12X,2M108,12X,2M109,12X,2M110,12X,2M111,12X,2M112,12X,2M113,12X,2M114,12X,2M115,12X,2M116,12X,2M117,12X,2M118,12X,2M119,12X,2M120,12X,2M121,12X,2M122,12X,2M123,12X,2M124,12X,2M125,12X,2M126,12X,2M127,12X,2M128,12X,2M129,12X,2M130,12X,2M131,12X,2M132,12X,2M133,12X,2M134,12X,2M135,12X,2M136,12X,2M137,12X,2M138,12X,2M139,12X,2M140,12X,2M141,12X,2M142,12X,2M143,12X,2M144,12X,2M145,12X,2M146,12X,2M147,12X,2M148,12X,2M149,12X,2M150,12X,2M151,12X,2M152,12X,2M153,12X,2M154,12X,2M155,12X,2M156,12X,2M157,12X,2M158,12X,2M159,12X,2M160,12X,2M161,12X,2M162,12X,2M163,12X,2M164,12X,2M165,12X,2M166,12X,2M167,12X,2M168,12X,2M169,12X,2M170,12X,2M171,12X,2M172,12X,2M173,12X,2M174,12X,2M175,12X,2M176,12X,2M177,12X,2M178,12X,2M179,12X,2M180,12X,2M181,12X,2M182,12X,2M183,12X,2M184,12X,2M185,12X,2M186,12X,2M187,12X,2M188,12X,2M189,12X,2M190,12X,2M191,12X,2M192,12X,2M193,12X,2M194,12X,2M195,12X,2M196,12X,2M197,12X,2M198,12X,2M199,12X,2M200,12X,2M201,12X,2M202,12X,2M203,12X,2M204,12X,2M205,12X,2M206,12X,2M207,12X,2M208,12X,2M209,12X,2M210,12X,2M211,12X,2M212,12X,2M213,12X,2M214,12X,2M215,12X,2M216,12X,2M217,12X,2M218,12X,2M219,12X,2M220,12X,2M221,12X,2M222,12X,2M223,12X,2M224,12X,2M225,12X,2M226,12X,2M227,12X,2M228,12X,2M229,12X,2M230,12X,2M231,12X,2M232,12X,2M233,12X,2M234,12X,2M235,12X,2M236,12X,2M237,12X,2M238,12X,2M239,12X,2M240,12X,2M241,12X,2M242,12X,2M243,12X,2M244,12X,2M245,12X,2M246,12X,2M247,12X,2M248,12X,2M249,12X,2M250,12X,2M251,12X,2M252,12X,2M253,12X,2M254,12X,2M255,12X,2M256,12X,2M257,12X,2M258,12X,2M259,12X,2M260,12X,2M261,12X,2M262,12X,2M263,12X,2M264,12X,2M265,12X,2M266,12X,2M267,12X,2M268,12X,2M269,12X,2M270,12X,2M271,12X,2M272,12X,2M273,12X,2M274,12X,2M275,12X,2M276,12X,2M277,12X,2M278,12X,2M279,12X,2M280,12X,2M281,12X,2M282,12X,2M283,12X,2M284,12X,2M285,12X,2M286,12X,2M287,12X,2M288,12X,2M289,12X,2M290,12X,2M291,12X,2M292,12X,2M293,12X,2M294,12X,2M295,12X,2M296,12X,2M297,12X,2M298,12X,2M299,12X,2M300,12X,2M301,12X,2M302,12X,2M303,12X,2M304,12X,2M305,12X,2M306,12X,2M307,12X,2M308,12X,2M309,12X,2M310,12X,2M311,12X,2M312,12X,2M313,12X,2M314,12X,2M315,12X,2M316,12X,2M317,12X,2M318,12X,2M319,12X,2M320,12X,2M321,12X,2M322,12X,2M323,12X,2M324,12X,2M325,12X,2M326,12X,2M327,12X,2M328,12X,2M329,12X,2M330,12X,2M331,12X,2M332,12X,2M333,12X,2M334,12X,2M335,12X,2M336,12X,2M337,12X,2M338,12X,2M339,12X,2M340,12X,2M341,12X,2M342,12X,2M343,12X,2M344,12X,2M345,12X,2M346,12X,2M347,12X,2M348,12X,2M349,12X,2M350,12X,2M351,12X,2M352,12X,2M353,12X,2M354,12X,2M355,12X,2M356,12X,2M357,12X,2M358,12X,2M359,12X,2M360,12X,2M361,12X,2M362,12X,2M363,12X,2M364,12X,2M365,12X,2M366,12X,2M367,12X,2M368,12X,2M369,12X,2M370,12X,2M371,12X,2M372,12X,2M373,12X,2M374,12X,2M375,12X,2M376,12X,2M377,12X,2M378,12X,2M379,12X,2M380,12X,2M381,12X,2M382,12X,2M383,12X,2M384,12X,2M385,12X,2M386,12X,2M387,12X,2M388,12X,2M389,12X,2M390,12X,2M391,12X,2M392,12X,2M393,12X,2M394,12X,2M395,12X,2M396,12X,2M397,12X,2M398,12X,2M399,12X,2M400,12X,2M401,12X,2M402,12X,2M403,12X,2M404,12X,2M405,12X,2M406,12X,2M407,12X,2M408,12X,2M409,12X,2M410,12X,2M411,12X,2M412,12X,2M413,12X,2M414,12X,2M415,12X,2M416,12X,2M417,12X,2M418,12X,2M419,12X,2M420,12X,2M421,12X,2M422,12X,2M423,12X,2M424,12X,2M425,12X,2M426,12X,2M427,12X,2M428,12X,2M429,12X,2M430,12X,2M431,12X,2M432,12X,2M433,12X,2M434,12X,2M435,12X,2M436,12X,2M437,12X,2M438,12X,2M439,12X,2M440,12X,2M441,12X,2M442,12X,2M443,12X,2M444,12X,2M445,12X,2M446,12X,2M447,12X,2M448,12X,2M449,12X,2M450,12X,2M451,12X,2M452,12X,2M453,12X,2M454,12X,2M455,12X,2M456,12X,2M457,12X,2M458,12X,2M459,12X,2M460,12X,2M461,12X,2M462,12X,2M463,12X,2M464,12X,2M465,12X,2M466,12X,2M467,12X,2M468,12X,2M469,12X,2M470,12X,2M471,12X,2M472,12X,2M473,12X,2M474,12X,2M475,12X,2M476,12X,2M477,12X,2M478,12X,2M479,12X,2M480,12X,2M481,12X,2M482,12X,2M483,12X,2M484,12X,2M485,12X,2M486,12X,2M487,12X,2M488,12X,2M489,12X,2M490,12X,2M491,12X,2M492,12X,2M493,12X,2M494,12X,2M495,12X,2M496,12X,2M497,12X,2M498,12X,2M499,12X,2M500,12X,2M501,12X,2M502,12X,2M503,12X,2M504,12X,2M505,12X,2M506,12X,2M507,12X,2M508,12X,2M509,12X,2M510,12X,2M511,12X,2M512,12X,2M513,12X,2M514,12X,2M515,12X,2M516,12X,2M517,12X,2M518,12X,2M519,12X,2M520,12X,2M521,12X,2M522,12X,2M523,12X,2M524,12X,2M525,12X,2M526,12X,2M527,12X,2M528,12X,2M529,12X,2M530,12X,2M531,12X,2M532,12X,2M533,12X,2M534,12X,2M535,12X,2M536,12X,2M537,12X,2M538,12X,2M539,12X,2M540,12X,2M541,12X,2M542,12X,2M543,12X,2M544,12X,2M545,12X,2M546,12X,2M547,12X,2M548,12X,2M549,12X,2M550,12X,2M551,12X,2M552,12X,2M553,12X,2M554,12X,2M555,12X,2M556,12X,2M557,12X,2M558,12X,2M559,12X,2M560,12X,2M561,12X,2M562,12X,2M563,12X,2M564,12X,2M565,12X,2M566,12X,2M567,12X,2M568,12X,2M569,12X,2M570,12X,2M571,12X,2M572,12X,2M573,12X,2M574,12X,2M575,12X,2M576,12X,2M577,12X,2M578,12X,2M579,12X,2M580,12X,2M581,12X,2M582,12X,2M583,12X,2M584,12X,2M585,12X,2M586,12X,2M587,12X,2M588,12X,2M589,12X,2M590,12X,2M591,12X,2M592,12X,2M593,12X,2M594,12X,2M595,12X,2M596,12X,2M597,12X,2M598,12X,2M599,12X,2M600,12X,2M601,12X,2M602,12X,2M603,12X,2M604,12X,2M605,12X,2M606,12X,2M607,12X,2M608,12X,2M609,12X,2M610,12X,2M611,12X,2M612,12X,2M613,12X,2M614,12X,2M615,12X,2M616,12X,2M617,12X,2M618,12X,2M619,12X,2M620,12X,2M621,12X,2M622,12X,2M623,12X,2M624,12X,2M625,12X,2M626,12X,2M627,12X,2M628,12X,2M629,12X,2M630,12X,2M631,12X,2M632,12X,2M633,12X,2M634,12X,2M635,12X,2M636,12X,2M637,12X,2M638,12X,2M639,12X,2M640,12X,2M641,12X,2M642,12X,2M643,12X,2M644,12X,2M645,12X,2M646,12X,2M647,12X,2M648,12X,2M649,12X,2M650,12X,2M651,12X,2M652,12X,2M653,12X,2M654,12X,2M655,12X,2M656,12X,2M657,12X,2M658,12X,2M659,12X,2M660,12X,2M661,12X,2M662,12X,2M663,12X,2M664,12X,2M665,12X,2M666,12X,2M667,12X,2M668,12X,2M669,12X,2M670,12X,2M671,12X,2M672,12X,2M673,12X,2M674,12X,2M675,12X,2M676,12X,2M677,12X,2M678,12X,2M679,12X,2M680,12X,2M681,12X,2M682,12X,2M683,12X,2M684,12X,2M685,12X,2M686,12X,2M687,12X,2M688,12X,2M689,12X,2M690,12X,2M691,12X,2M692,12X,2M693,12X,2M694,12X,2M695,12X,2M696,12X,2M697,12X,2M698,12X,2M699,12X,2M700,12X,2M701,12X,2M702,12X,2M703,12X,2M704,12X,2M705,12X,2M706,12X,2M707,12X,2M708,12X,2M709,12X,2M710,12X,2M711,12X,2M712,12X,2M713,12X,2M714,12X,2M715,12X,2M716,12X,2M717,12X,2M718,12X,2M719,12X,2M720,12X,2M721,12X,2M722,12X,2M723,12X,2M724,12X,2M725,12X,2M726,12X,2M727,12X,2M728,12X,2M729,12X,2M730,12X,2M731,12X,2M732,12X,2M733,12X,2M734,12X,2M735,12X,2M736,12X,2M737,12X,2M738,12X,2M739,12X,2M740,12X,2M741,12X,2M742,12X,2M743,12X,2M744,12X,2M745,12X,2M746,12X,2M747,12X,2M748,12X,2M749,12X,2M750,12X,2M751,12X,2M752,12X,2M753,12X,2M754,12X,2M755,12X,2M756,12X,2M757,12X,2M758,12X,2M759,12X,2M760,12X,2M761,12X,2M762,12X,2M763,12X,2M764,12X,2M765,12X,2M766,12X,2M767,12X,2M768,12X,2M769,12X,2M770,12X,2M771,12X,2M772,12X,2M773,12X,2M774,12X,2M775,12X,2M776,12X,2M777,12X,2M778,12X,2M779,12X,2M780,12X,2M781,12X,2M782,12X,2M783,12X,2M784,12X,2M785,12X,2M786,12X,2M787,12X,2M788,12X,2M789,12X,2M790,12X,2M791,12X,2M792,12X,2M793,12X,2M794,12X,2M795,12X,2M796,12X,2M797,12X,2M798,12X,2M799,12X,2M800,12X,2M801,12X,2M802,12X,2M803,12X,2M804,12X,2M805,12X,2M806,12X,2M807,12X,2M808,12X,2M809,12X,2M810,12X,2M811,12X,2M812,12X,2M813,12X,2M814,12X,2M815,12X,2M816,12X,2M817,12X,2M818,12X,2M819,12X,2M820,12X,2M821,12X,2M822,12X,2M823,12X,2M824,12X,2M825,12X,2M826,12X,2M827,12X,2M828,12X,2M829,12X,2M830,12X,2M831,12X,2M832,12X,2M833,12X,2M834,12X,2M835,12X,2M836,12X,2M837,12X,2M838,12X,2M839,12X,2M840,12X,2M841,12X,2M842,12X,2M843,12X,2M844,12X,2M845,12X,2M846,12X,2M847,12X,2M848,12X,2M849,12X,2M850,12X,2M851,12X,2M852,12X,2M853,12X,2M854,12X,2M855,12X,2M856,12X,2M857,12X,2M858,12X,2M859,12X,2M860,12X,2M861,12X,2M862,12X,2M863,12X,2M864,12X,2M865,12X,2M866,12X,2M867,12X,2M868,12X,2M869,12X,2M870,12X,2M871,12X,2M872,12X,2M873,12X,2M874,12X,2M875,12X,2M876,12X,2M877,12X,2M878,12X,2M879,12X,2M880,12X,2M881,12X,2M882,12X,2M883,12X,2M884,12X,2M885,12X,2M886,12X,2M887,12X,2M888,12X,2M889,12X,2M890,12X,2M891,12X,2M892,12X,2M893,12X,2M894,12X,2M895,12X,2M896,12X,2M897,12X,2M898,12X,2M899,12X,2M900,12X,2M901,12X,2M902,12X,2M903,12X,2M904,12X,2M905,12X,2M906,12X,2M907,12X,2M908,12X,2M909,12X,2M910,12X,2M911,12X,2M912,12X,2M913,12X,2M914,12X,2M915,12X,2M916,12X,2M917,12X,2M918,12X,2M919,12X,2M920,12X,2M921,12X,2M922,12X,2M923,12X,2M924,12X,2M925,12X,2M926,12X,2M927,12X,2M928,12X,2M929,12X,2M930,12X,2M931,12X,2M932,12X,2M933,12X,2M934,12X,2M935,12X,2M936,12X,2M937,12X,2M938,12X,2M939,12X,2M940,12X,2M941,12X,2M942,12X,2M943,12X,2M944,12X,2M945,12X,2M946,12X,2M947,12X,2M948,12X,2M949,12X,2M950,12X,2M951,12X,2M952,12X,2M953,12X,2M954,12X,2M955,12X,2M956,12X,2M957,12X,2M958,12X,2M959,12X,2M960,12X,2M961,12X,2M962,12X,2M963,12X,2M964,12X,2M965,12X,2M966,12X,2M967,12X,2M968,12X,2M969,12X,2M970,12X,2M971,12X,2M972,12X,2M973,12X,2M974,12X,2M975,12X,2M976,12X,2M977,12X,2M978,12X,2M979,12X,2M980,12X,2M981,12X,2M982,12X,2M983,12X,2M984,12X,2M985,12X,2M986,12X,2M987,12X,2M988,12X,2M989,12X,2M990,12X,2M991,12X,2M992,12X,2M993,12X,2M994,12X,2M995,12X,2M996,12X,2M997,12X,2M998,12X,2M999,12X,2M1000,12X,2M1001,12X,2M1002,12X,2M1003,12X,2M1004,12X,2M1005,12X,2M1006,12X,2M1007,12X,2M1008,12X,2M1009,12X,2M1010,12X,2M1011,12X,2M1012,12X,2M1013,12X,2M1014,12X,2M1015,12X,2M1016,12X,2M1017,12X,2M1018,12X,2M1019,12X,2M1020,12X,2M1021,12X,2M1022,12X,2M1023,12X,2M1024,12X,2M1025,12X,2M1026,12X,2M1027,12X,2M1028,12X,2M1029,12X,2M1030,12X,2M1031,12X,2M1032,12X,2M1033,12X,2M1034,12X,2M1035,12X,2M1036,12X,2M1037,12X,2M1038,12X,2M1039,12X,2M1040,12X,2M1041,12X,2M1042,12X,2M1043,12X,2M1044,12X,2M1045,12X,2M1046,12X,2M1047,12X,2M1048,12X,2M1049,12X,2M1050,12X,2M1051,12X,2M1052,12X,2M1053,12X,2M1054,12X,2M1055,12X,2M1056,12X,2M1057,12X,2M1058,12X,2M1059,12X,2M1060,12X,2M1061,12X,2M1062,12X,2M1063,12X,2M1064,12X,2M1065,12X,2M1066,12X,2M1067,12X,2M1068,12X,2M1069,12X,2M1070,12X,2M1071,12X,2M1072,12X,2M1073,12X,2M1074,12X,2M1075,12X,2M1076,12X,2M1077,12X,2M1078,12X,2M1079,12X,2M1080,12X,2M1081,12X,2M1082,12X,2M1083,12X,2M1084,12X,2M1085,12X,2M1086,12X,2M1087,12X,2M1088,12X,2M1089,12X,2M109
```









```

PF1 461      NI=1
PF1 462      NS=1000
PF1 463      X=(HMAXQD-3)*(HMAXQD-1)
PF1 464      ME=0
PF1 465      MEHNS=2*(HMAXQD-1)
PF1 466      MEHNS=2*(HMAXQD-1)
PF1 467      DO 390, I=1, ILE
PF1 468      READ (NF1LE10, 0(11JK), IJK=1, 192)
PF1 469      WRITE (KF1LE210, 0(11JK), IJK=1, 192)
PF1 470      390 CONTINUE
PF1 471      KFILE=NF ILEZ
PF1 472      J=JHOLD
PF1 473      IF (J.EQ.0) GO TO 400
PF1 474      DO 395, I=1, J
PF1 475      395 0(11)=HOLD(I)
PF1 476      400 Q=QHOLD
PF1 477      JP=JHOLD/16
PF1 478      QADD=QHOLD*.5
PF1 479      P=QADD*JP
PF1 480      ISTART=(HMAXQD-3)*HMAXQD
PF1 481      ISTART+HMAXQD
PF1 482      XHOLD=X(ISTART+1)
PF1 483      XHOLD=X(IST+1)
PF1 484      C*** Y REFERENCE LINE MUST BE 0.0
PF1 485      ZAV=0.0
PF1 486      DO 485, I=1, HMAXQD
PF1 487      XHEM(I)=X(ISTART+I)
PF1 488      ZHEM(I)=Y(ISTART+I)
PF1 489      ZHEM(I)=Y(ISTART+I)
PF1 490      ZHEM(I)=Y(ISTART+I)
PF1 491      405 THETA=90.0*(.14159/180.0)
PF1 492      RAV=0.0
PF1 493      ZAV=ZAV/HMAXQD
PF1 494      DO 410, I=1, HMAXQD
PF1 495      RHEM=SQRT((YHEM(I))**2+(ZHEM(I)-ZAV)**2)
PF1 496      410 RAV=RAV+RHEM
PF1 497      RAV=RAV/HMAXQD
PF1 498      FAC=(AVXCG-HOLD1)/(XHOLD2-HHOLD1)
PF1 499      AVSLOP=0.0
PF1 500      DO 415, I=1, HMAXQD
PF1 501      YCG=YHEM(I)-(YHEM(I)-Y(IST+1))*FAC
PF1 502      ZCG=ZHEM(I)-(ZHEM(I)-Z(IST+1))*FAC
PF1 503      R1=SQRT((YHEM(I))**2+(ZHEM(I)-ZAV)**2)
PF1 504      R2=SQRT((YCG)**2+(ZCG-ZAV)**2)+2.0*AVDELS
PF1 505      SLOPE=(R2-R1)/(HHOLD1-AVXCG)
PF1 506      415 AVSLOP=AVSLOP+SLOPE
PF1 507      AREA=0.0*AREA+Y*Z
PF1 508      XING=HOLD1-AREA/(3.14159*RAV)
PF1 509      CHECK TO MAKE SURE BODY SLOPE IS DECREASING
PF1 510      IF (AVSLOP>0.)AVSLOP=-ABS(RAV/((XING-HOLD1)))
PF1 511      IF (XING<0.)AVSLOP=-ABS(RAV/AVXCG*ZING)
PF1 512      FROM (XING, XING)AVSLOP=GEOMTRY//, 1TH AVERAGE SLOPE =
PF1 513      1 * P 10.5, 31ZERN BEGIN NAME BODY GEOMETRY//, 1TH AVERAGE SLOPE =
PF1 514      1 * P 10.5, 31ZERN END OF BODY AT X = P 10.5)
PF1 515      DELTAZ=0.1
PF1 516      K=1
PF1 517      X1=HHOLD1
PF1 518      Z1Z=0.0
PF1 519      222=0.0
PF1 520      420 FUNCTION SQZ(X,Y,Z)
PF1 521      FUNCTION TO COMPUTE SQUARE ROOT OF X**2
PF1 522      R=ABS(X)+ABS(Y)+ABS(Z)+.000000000001
PF1 523      R=R*.857R
PF1 524      430
PF1 525      435 THETA=THETA+DTMETHA
PF1 526      XI=XHEM(I)
PF1 527      VI=YHEM(I)
PF1 528      ZI=ZHEM(I)
PF1 529      GO TO 310
PF1 530      440 CALL EXIT
PF1 531      END
PF1 532
PF1 533
PF1 534
PF1 535
PF1 536
PF1 537
PF1 538
PF1 539
PF1 540
PF1 541
PF1 542
PF1 543
PF1 544
PF1 545
PF1 546
PF1 547
PF1 548
PF1 549
PF1 550
PF1 551
PF1 552
PF1 553
PF1 554
PF1 555
PF1 556
PF1 557
PF1 558
PF1 559
PF1 560
PF1 561
PF1 562
PF1 563
PF1 564
PF1 565
PF1 566
PF1 567
PF1 568
PF1 569
PF1 570
PF1 571
PF1 572
PF1 573
PF1 574
PF1 575
PF1 576
PF1 577
PF1 578
PF1 579
PF1 580
PF1 581
PF1 582
PF1 583
PF1 584
PF1 585
PF1 586
PF1 587
PF1 588
PF1 589
PF1 590
PF1 591
PF1 592
PF1 593
PF1 594
PF1 595
PF1 596
PF1 597
PF1 598
PF1 599
PF1 600
PF1 601
PF1 602
PF1 603
PF1 604
PF1 605
PF1 606
PF1 607
PF1 608
PF1 609
PF1 610
PF1 611
PF1 612
PF1 613
PF1 614
PF1 615
PF1 616
PF1 617
PF1 618
PF1 619
PF1 620
PF1 621
PF1 622
PF1 623
PF1 624
PF1 625
PF1 626
PF1 627
PF1 628
PF1 629
PF1 630
PF1 631
PF1 632
PF1 633
PF1 634
PF1 635
PF1 636
PF1 637
PF1 638
PF1 639
PF1 640
PF1 641
PF1 642
PF1 643
PF1 644
PF1 645
PF1 646
PF1 647
PF1 648
PF1 649
PF1 650
PF1 651
PF1 652
PF1 653
PF1 654
PF1 655
PF1 656
PF1 657
PF1 658
PF1 659
PF1 660
PF1 661
PF1 662
PF1 663
PF1 664
PF1 665
PF1 666
PF1 667
PF1 668
PF1 669
PF1 670
PF1 671
PF1 672
PF1 673
PF1 674
PF1 675
PF1 676
PF1 677
PF1 678
PF1 679
PF1 680
PF1 681
PF1 682
PF1 683
PF1 684
PF1 685
PF1 686
PF1 687
PF1 688
PF1 689
PF1 690
PF1 691
PF1 692
PF1 693
PF1 694
PF1 695
PF1 696
PF1 697
PF1 698
PF1 699
PF1 700
PF1 701
PF1 702
PF1 703
PF1 704
PF1 705
PF1 706
PF1 707
PF1 708
PF1 709
PF1 710
PF1 711
PF1 712
PF1 713
PF1 714
PF1 715
PF1 716
PF1 717
PF1 718
PF1 719
PF1 720
PF1 721
PF1 722
PF1 723
PF1 724
PF1 725
PF1 726
PF1 727
PF1 728
PF1 729
PF1 730
PF1 731
PF1 732
PF1 733
PF1 734
PF1 735
PF1 736
PF1 737
PF1 738
PF1 739
PF1 740
PF1 741
PF1 742
PF1 743
PF1 744
PF1 745
PF1 746
PF1 747
PF1 748
PF1 749
PF1 750
PF1 751
PF1 752
PF1 753
PF1 754
PF1 755
PF1 756
PF1 757
PF1 758
PF1 759
PF1 760
PF1 761
PF1 762
PF1 763
PF1 764
PF1 765
PF1 766
PF1 767
PF1 768
PF1 769
PF1 770
PF1 771
PF1 772
PF1 773
PF1 774
PF1 775
PF1 776
PF1 777
PF1 778
PF1 779
PF1 780
PF1 781
PF1 782
PF1 783
PF1 784
PF1 785
PF1 786
PF1 787
PF1 788
PF1 789
PF1 790
PF1 791
PF1 792
PF1 793
PF1 794
PF1 795
PF1 796
PF1 797
PF1 798
PF1 799
PF1 800
PF1 801
PF1 802
PF1 803
PF1 804
PF1 805
PF1 806
PF1 807
PF1 808
PF1 809
PF1 810
PF1 811
PF1 812
PF1 813
PF1 814
PF1 815
PF1 816
PF1 817
PF1 818
PF1 819
PF1 820
PF1 821
PF1 822
PF1 823
PF1 824
PF1 825
PF1 826
PF1 827
PF1 828
PF1 829
PF1 830
PF1 831
PF1 832
PF1 833
PF1 834
PF1 835
PF1 836
PF1 837
PF1 838
PF1 839
PF1 840
PF1 841
PF1 842
PF1 843
PF1 844
PF1 845
PF1 846
PF1 847
PF1 848
PF1 849
PF1 850
PF1 851
PF1 852
PF1 853
PF1 854
PF1 855
PF1 856
PF1 857
PF1 858
PF1 859
PF1 860
PF1 861
PF1 862
PF1 863
PF1 864
PF1 865
PF1 866
PF1 867
PF1 868
PF1 869
PF1 870
PF1 871
PF1 872
PF1 873
PF1 874
PF1 875
PF1 876
PF1 877
PF1 878
PF1 879
PF1 880
PF1 881
PF1 882
PF1 883
PF1 884
PF1 885
PF1 886
PF1 887
PF1 888
PF1 889
PF1 890
PF1 891
PF1 892
PF1 893
PF1 894
PF1 895
PF1 896
PF1 897
PF1 898
PF1 899
PF1 900
PF1 901
PF1 902
PF1 903
PF1 904
PF1 905
PF1 906
PF1 907
PF1 908
PF1 909
PF1 910
PF1 911
PF1 912
PF1 913
PF1 914
PF1 915
PF1 916
PF1 917
PF1 918
PF1 919
PF1 920
PF1 921
PF1 922
PF1 923
PF1 924
PF1 925
PF1 926
PF1 927
PF1 928
PF1 929
PF1 930
PF1 931
PF1 932
PF1 933
PF1 934
PF1 935
PF1 936
PF1 937
PF1 938
PF1 939
PF1 940
PF1 941
PF1 942
PF1 943
PF1 944
PF1 945
PF1 946
PF1 947
PF1 948
PF1 949
PF1 950
PF1 951
PF1 952
PF1 953
PF1 954
PF1 955
PF1 956
PF1 957
PF1 958
PF1 959
PF1 960
PF1 961
PF1 962
PF1 963
PF1 964
PF1 965
PF1 966
PF1 967
PF1 968
PF1 969
PF1 970
PF1 971
PF1 972
PF1 973
PF1 974
PF1 975
PF1 976
PF1 977
PF1 978
PF1 979
PF1 980
PF1 981
PF1 982
PF1 983
PF1 984
PF1 985
PF1 986
PF1 987
PF1 988
PF1 989
PF1 990
PF1 991
PF1 992
PF1 993
PF1 994
PF1 995
PF1 996
PF1 997
PF1 998
PF1 999
PF1 1000

```



```

IF (BC11=0) 345,20,345
15 FORMAT (2XNO POINTS OUT OF ORDER B(1)=,IFA,0.4H P=,1P4.0)
20 J=2
25 X1=B(J)
Y1=B(J+1)
X2=B(J+2)
Y2=B(J+3)
X3=B(J+4)
Y3=B(J+5)
X4=B(J+6)
Y4=B(J+7)
X5=B(J+8)
Y5=B(J+9)
X6=B(J+10)
Y6=B(J+11)
X7=B(J+12)
Y7=B(J+13)
X8=B(J+14)
Y8=B(J+15)
X9=B(J+16)
Y9=B(J+17)
X10=B(J+18)
Y10=B(J+19)
X11=B(J+20)
Y11=B(J+21)
X12=B(J+22)
Y12=B(J+23)
X13=B(J+24)
Y13=B(J+25)
X14=B(J+26)
Y14=B(J+27)
X15=B(J+28)
Y15=B(J+29)
X16=B(J+30)
Y16=B(J+31)
X17=B(J+32)
Y17=B(J+33)
X18=B(J+34)
Y18=B(J+35)
X19=B(J+36)
Y19=B(J+37)
X20=B(J+38)
Y20=B(J+39)
X21=B(J+40)
Y21=B(J+41)
X22=B(J+42)
Y22=B(J+43)
X23=B(J+44)
Y23=B(J+45)
X24=B(J+46)
Y24=B(J+47)
X25=B(J+48)
Y25=B(J+49)
X26=B(J+50)
Y26=B(J+51)
X27=B(J+52)
Y27=B(J+53)
X28=B(J+54)
Y28=B(J+55)
X29=B(J+56)
Y29=B(J+57)
X30=B(J+58)
Y30=B(J+59)
X31=B(J+60)
Y31=B(J+61)
X32=B(J+62)
Y32=B(J+63)
X33=B(J+64)
Y33=B(J+65)
X34=B(J+66)
Y34=B(J+67)
X35=B(J+68)
Y35=B(J+69)
X36=B(J+70)
Y36=B(J+71)
X37=B(J+72)
Y37=B(J+73)
X38=B(J+74)
Y38=B(J+75)
X39=B(J+76)
Y39=B(J+77)
X40=B(J+78)
Y40=B(J+79)
X41=B(J+80)
Y41=B(J+81)
X42=B(J+82)
Y42=B(J+83)
X43=B(J+84)
Y43=B(J+85)
X44=B(J+86)
Y44=B(J+87)
X45=B(J+88)
Y45=B(J+89)
X46=B(J+90)
Y46=B(J+91)
X47=B(J+92)
Y47=B(J+93)
X48=B(J+94)
Y48=B(J+95)
X49=B(J+96)
Y49=B(J+97)
X50=B(J+98)
Y50=B(J+99)
X51=B(J+100)
Y51=B(J+101)
X52=B(J+102)
Y52=B(J+103)
X53=B(J+104)
Y53=B(J+105)
X54=B(J+106)
Y54=B(J+107)
X55=B(J+108)
Y55=B(J+109)
X56=B(J+110)
Y56=B(J+111)
X57=B(J+112)
Y57=B(J+113)
X58=B(J+114)
Y58=B(J+115)
X59=B(J+116)
Y59=B(J+117)
X60=B(J+118)
Y60=B(J+119)
X61=B(J+120)
Y61=B(J+121)
X62=B(J+122)
Y62=B(J+123)
X63=B(J+124)
Y63=B(J+125)
X64=B(J+126)
Y64=B(J+127)
X65=B(J+128)
Y65=B(J+129)
X66=B(J+130)
Y66=B(J+131)
X67=B(J+132)
Y67=B(J+133)
X68=B(J+134)
Y68=B(J+135)
X69=B(J+136)
Y69=B(J+137)
X70=B(J+138)
Y70=B(J+139)
X71=B(J+140)
Y71=B(J+141)
X72=B(J+142)
Y72=B(J+143)
X73=B(J+144)
Y73=B(J+145)
X74=B(J+146)
Y74=B(J+147)
X75=B(J+148)
Y75=B(J+149)
X76=B(J+150)
Y76=B(J+151)
X77=B(J+152)
Y77=B(J+153)
X78=B(J+154)
Y78=B(J+155)
X79=B(J+156)
Y79=B(J+157)
X80=B(J+158)
Y80=B(J+159)
X81=B(J+160)
Y81=B(J+161)
X82=B(J+162)
Y82=B(J+163)
X83=B(J+164)
Y83=B(J+165)
X84=B(J+166)
Y84=B(J+167)
X85=B(J+168)
Y85=B(J+169)
X86=B(J+170)
Y86=B(J+171)
X87=B(J+172)
Y87=B(J+173)
X88=B(J+174)
Y88=B(J+175)
X89=B(J+176)
Y89=B(J+177)
X90=B(J+178)
Y90=B(J+179)
X91=B(J+180)
Y91=B(J+181)
X92=B(J+182)
Y92=B(J+183)
X93=B(J+184)
Y93=B(J+185)
X94=B(J+186)
Y94=B(J+187)
X95=B(J+188)
Y95=B(J+189)
X96=B(J+190)
Y96=B(J+191)
X97=B(J+192)
Y97=B(J+193)
X98=B(J+194)
Y98=B(J+195)
X99=B(J+196)
Y99=B(J+197)
X100=B(J+198)
Y100=B(J+199)
X101=B(J+200)
Y101=B(J+201)
X102=B(J+202)
Y102=B(J+203)
X103=B(J+204)
Y103=B(J+205)
X104=B(J+206)
Y104=B(J+207)
X105=B(J+208)
Y105=B(J+209)
X106=B(J+210)
Y106=B(J+211)
X107=B(J+212)
Y107=B(J+213)
X108=B(J+214)
Y108=B(J+215)
X109=B(J+216)
Y109=B(J+217)
X110=B(J+218)
Y110=B(J+219)
X111=B(J+220)
Y111=B(J+221)
X112=B(J+222)
Y112=B(J+223)
X113=B(J+224)
Y113=B(J+225)
X114=B(J+226)
Y114=B(J+227)
X115=B(J+228)
Y115=B(J+229)
X116=B(J+230)
Y116=B(J+231)
X117=B(J+232)
Y117=B(J+233)
X118=B(J+234)
Y118=B(J+235)
X119=B(J+236)
Y119=B(J+237)
X120=B(J+238)
Y120=B(J+239)
X121=B(J+240)
Y121=B(J+241)
X122=B(J+242)
Y122=B(J+243)
X123=B(J+244)
Y123=B(J+245)
X124=B(J+246)
Y124=B(J+247)
X125=B(J+248)
Y125=B(J+249)
X126=B(J+250)
Y126=B(J+251)
X127=B(J+252)
Y127=B(J+253)
X128=B(J+254)
Y128=B(J+255)
X129=B(J+256)
Y129=B(J+257)
X130=B(J+258)
Y130=B(J+259)
X131=B(J+260)
Y131=B(J+261)
X132=B(J+262)
Y132=B(J+263)
X133=B(J+264)
Y133=B(J+265)
X134=B(J+266)
Y134=B(J+267)
X135=B(J+268)
Y135=B(J+269)
X136=B(J+270)
Y136=B(J+271)
X137=B(J+272)
Y137=B(J+273)
X138=B(J+274)
Y138=B(J+275)
X139=B(J+276)
Y139=B(J+277)
X140=B(J+278)
Y140=B(J+279)
X141=B(J+280)
Y141=B(J+281)
X142=B(J+282)
Y142=B(J+283)
X143=B(J+284)
Y143=B(J+285)
X144=B(J+286)
Y144=B(J+287)
X145=B(J+288)
Y145=B(J+289)
X146=B(J+290)
Y146=B(J+291)
X147=B(J+292)
Y147=B(J+293)
X148=B(J+294)
Y148=B(J+295)
X149=B(J+296)
Y149=B(J+297)
X150=B(J+298)
Y150=B(J+299)
X151=B(J+300)
Y151=B(J+301)
X152=B(J+302)
Y152=B(J+303)
X153=B(J+304)
Y153=B(J+305)
X154=B(J+306)
Y154=B(J+307)
X155=B(J+308)
Y155=B(J+309)
X156=B(J+310)
Y156=B(J+311)
X157=B(J+312)
Y157=B(J+313)
X158=B(J+314)
Y158=B(J+315)
X159=B(J+316)
Y159=B(J+317)
X160=B(J+318)
Y160=B(J+319)
X161=B(J+320)
Y161=B(J+321)
X162=B(J+322)
Y162=B(J+323)
X163=B(J+324)
Y163=B(J+325)
X164=B(J+326)
Y164=B(J+327)
X165=B(J+328)
Y165=B(J+329)
X166=B(J+330)
Y166=B(J+331)
X167=B(J+332)
Y167=B(J+333)
X168=B(J+334)
Y168=B(J+335)
X169=B(J+336)
Y169=B(J+337)
X170=B(J+338)
Y170=B(J+339)
X171=B(J+340)
Y171=B(J+341)
X172=B(J+342)
Y172=B(J+343)
X173=B(J+344)
Y173=B(J+345)
X174=B(J+346)
Y174=B(J+347)
X175=B(J+348)
Y175=B(J+349)
X176=B(J+350)
Y176=B(J+351)
X177=B(J+352)
Y177=B(J+353)
X178=B(J+354)
Y178=B(J+355)
X179=B(J+356)
Y179=B(J+357)
X180=B(J+358)
Y180=B(J+359)
X181=B(J+360)
Y181=B(J+361)
X182=B(J+362)
Y182=B(J+363)
X183=B(J+364)
Y183=B(J+365)
X184=B(J+366)
Y184=B(J+367)
X185=B(J+368)
Y185=B(J+369)
X186=B(J+370)
Y186=B(J+371)
X187=B(J+372)
Y187=B(J+373)
X188=B(J+374)
Y188=B(J+375)
X189=B(J+376)
Y189=B(J+377)
X190=B(J+378)
Y190=B(J+379)
X191=B(J+380)
Y191=B(J+381)
X192=B(J+382)
Y192=B(J+383)
X193=B(J+384)
Y193=B(J+385)
X194=B(J+386)
Y194=B(J+387)
X195=B(J+388)
Y195=B(J+389)
X196=B(J+390)
Y196=B(J+391)
X197=B(J+392)
Y197=B(J+393)
X198=B(J+394)
Y198=B(J+395)
X199=B(J+396)
Y199=B(J+397)
X200=B(J+398)
Y200=B(J+399)
X201=B(J+400)
Y201=B(J+401)
X202=B(J+402)
Y202=B(J+403)
X203=B(J+404)
Y203=B(J+405)
X204=B(J+406)
Y204=B(J+407)
X205=B(J+408)
Y205=B(J+409)
X206=B(J+410)
Y206=B(J+411)
X207=B(J+412)
Y207=B(J+413)
X208=B(J+414)
Y208=B(J+415)
X209=B(J+416)
Y209=B(J+417)
X210=B(J+418)
Y210=B(J+419)
X211=B(J+420)
Y211=B(J+421)
X212=B(J+422)
Y212=B(J+423)
X213=B(J+424)
Y213=B(J+425)
X214=B(J+426)
Y214=B(J+427)
X215=B(J+428)
Y215=B(J+429)
X216=B(J+430)
Y216=B(J+431)
X217=B(J+432)
Y217=B(J+433)
X218=B(J+434)
Y218=B(J+435)
X219=B(J+436)
Y219=B(J+437)
X220=B(J+438)
Y220=B(J+439)
X221=B(J+440)
Y221=B(J+441)
X222=B(J+442)
Y222=B(J+443)
X223=B(J+444)
Y223=B(J+445)
X224=B(J+446)
Y224=B(J+447)
X225=B(J+448)
Y225=B(J+449)
X226=B(J+450)
Y226=B(J+451)
X227=B(J+452)
Y227=B(J+453)
X228=B(J+454)
Y228=B(J+455)
X229=B(J+456)
Y229=B(J+457)
X230=B(J+458)
Y230=B(J+459)
X231=B(J+460)
Y231=B(J+461)
X232=B(J+462)
Y232=B(J+463)
X233=B(J+464)
Y233=B(J+465)
X234=B(J+466)
Y234=B(J+467)
X235=B(J+468)
Y235=B(J+469)
X236=B(J+470)
Y236=B(J+471)
X237=B(J+472)
Y237=B(J+473)
X238=B(J+474)
Y238=B(J+475)
X239=B(J+476)
Y239=B(J+477)
X240=B(J+478)
Y240=B(J+479)
X241=B(J+480)
Y241=B(J+481)
X242=B(J+482)
Y242=B(J+483)
X243=B(J+484)
Y243=B(J+485)
X244=B(J+486)
Y244=B(J+487)
X245=B(J+488)
Y245=B(J+489)
X246=B(J+490)
Y246=B(J+491)
X247=B(J+492)
Y247=B(J+493)
X248=B(J+494)
Y248=B(J+495)
X249=B(J+496)
Y249=B(J+497)
X250=B(J+498)
Y250=B(J+499)
X251=B(J+500)
Y251=B(J+501)
X252=B(J+502)
Y252=B(J+503)
X253=B(J+504)
Y253=B(J+505)
X254=B(J+506)
Y254=B(J+507)
X255=B(J+508)
Y255=B(J+509)
X256=B(J+510)
Y256=B(J+511)
X257=B(J+512)
Y257=B(J+513)
X258=B(J+514)
Y258=B(J+515)
X259=B(J+516)
Y259=B(J+517)
X260=B(J+518)
Y260=B(J+519)
X261=B(J+520)
Y261=B(J+521)
X262=B(J+522)
Y262=B(J+523)
X263=B(J+524)
Y263=B(J+525)
X264=B(J+526)
Y264=B(J+527)
X265=B(J+528)
Y265=B(J+529)
X266=B(J+530)
Y266=B(J+531)
X267=B(J+532)
Y267=B(J+533)
X268=B(J+534)
Y268=B(J+535)
X269=B(J+536)
Y269=B(J+537)
X270=B(J+538)
Y270=B(J+539)
X271=B(J+540)
Y271=B(J+541)
X272=B(J+542)
Y272=B(J+543)
X273=B(J+544)
Y273=B(J+545)
X274=B(J+546)
Y274=B(J+547)
X275=B(J+548)
Y275=B(J+549)
X276=B(J+550)
Y276=B(J+551)
X277=B(J+552)
Y277=B(J+553)
X278=B(J+554)
Y278=B(J+555)
X279=B(J+556)
Y279=B(J+557)
X280=B(J+558)
Y280=B(J+559)
X281=B(J+560)
Y281=B(J+561)
X282=B(J+562)
Y282=B(J+563)
X283=B(J+564)
Y283=B(J+565)
X284=B(J+566)
Y284=B(J+567)
X285=B(J+568)
Y285=B(J+569)
X286=B(J+570)
Y286=B(J+571)
X287=B(J+572)
Y287=B(J+573)
X288=B(J+574)
Y288=B(J+575)
X289=B(J+576)
Y289=B(J+577)
X290=B(J+578)
Y290=B(J+579)
X291=B(J+580)
Y291=B(J+581)
X292=B(J+582)
Y292=B(J+583)
X293=B(J+584)
Y293=B(J+585)
X294=B(J+586)
Y294=B(J+587)
X295=B(J+588)
Y295=B(J+589)
X296=B(J+590)
Y296=B(J+591)
X297=B(J+592)
Y297=B(J+593)
X298=B(J+594)
Y298=B(J+595)
X299=B(J+596)
Y299=B(J+597)
X300=B(J+598)
Y300=B(J+599)
X301=B(J+600)
Y301=B(J+601)
X302=B(J+602)
Y302=B(J+603)
X303=B(J+604)
Y303=B(J+605)
X304=B(J+606)
Y304=B(J+607)
X305=B(J+608)
Y305=B(J+609)
X306=B(J+610)
Y306=B(J+611)
X307=B(J+612)
Y307=B(J+613)
X308=B(J+614)
Y308=B(J+615)
X309=B(J+616)
Y309=B(J+617)
X310=B(J+618)
Y310=B(J+619)
X311=B(J+620)
Y311=B(J+621)
X312=B(J+622)
Y312=B(J+623)
X313=B(J+624)
Y313=B(J+625)
X314=B(J+626)
Y314=B(J+627)
X315=B(J+628)
Y315=B(J+629)
X316=B(J+630)
Y316=B(J+631)
X317=B(J+632)
Y317=B(J+633)
X318=B(J+634)
Y318=B(J+635)
X319=B(J+636)
Y319=B(J+637)
X320=B(J+638)
Y320=B(J+639)
X321=B(J+640)
Y321=B(J+641)
X322=B(J+642)
Y322=B(J+643)
X323=B(J+644)
Y323=B(J+645)
X324=B(J+646)
Y324=B(J+647)
X325=B(J+648)
Y325=B(J+649)
X326=B(J+650)
Y326=B(J+651)
X327=B(J+652)
Y327=B(J+653)
X328=B(J+654)
Y328=B(J+655)
X329=B(J+656)
Y329=B(J+657)
X330=B(J+658)
Y330=B(J+659)
X331=B(J+660)
Y331=B(J+661)
X332=B(J+662)
Y332=B(J+663)
X333=B(J+664)
Y333=B(J+665)
X334=B(J+666)
Y334=B(J+667)
X335=B(J+668)
Y335=B(J+669)
X336=B(J+670)
Y336=B(J+671)
X337=B(J+672)
Y337=B(J+673)
X338=B(J+674)
Y338=B(J+675)
X339=B(J+676)
Y339=B(J+677)
X340=B(J+678)
Y340=B(J+679)
X341=B(J+680)
Y341=B(J+681)
X342=B(J+682)
Y342=B(J+683)
X343=B(J+684)
Y343=B(J+685)
X344=B(J+686)
Y344=B(J+687)
X345=B(J+688)
Y345=B(J+689)
X346=B(J+690)
Y346=B(J+691)
X347=B(J+692)
Y347=B(J+693)
X348=B(J+694)
Y348=B(J+695)
X349=B(J+696)
Y349=B(J+697)
X350=B(J+698)
Y350=B(J+699)
X351=B(J+700)
Y351=B(J+701)
X352=B(J+702)
Y352=B(J+703)
X353=B(J+704)
Y353=B(J+705)
X354=B(J+706)
Y354=B(J+707)
X355=B(J+708)
Y355=B(J+709)
X356=B(J+710)
Y356=B(J+711)
X357=B(J+712)
Y357=B(J+713)
X358=B(J+714)
Y358=B(J+715)
X359=B(J+716)
Y359=B(J+717)
X360=B(J+718)
Y360=B(J+719)
X361=B(J+720)
Y361=B(J+721)
X362=B(J+722)
Y362=B(J+723)
X363=B(J+724)
Y363=B(J+725)
X364=B(J+726)
Y364=B(J+727)
X365=B(J+728)
Y365=B(J+729)
X366=B(J+730)
Y366=B(J+731)
X367=B(J+732)
Y367=B(J+733)
X368=B(J+734)
Y368=B(J+735)
X369=B(J+736)
Y369=B(J+737)
X370=B(J+738)
Y370=B(J+739)
X371=B(J+740)
Y371=B(J+741)
X372=B(J+742)
Y372=B(J+743)
X373=B(J+744)
Y373=B(J+745)
X374=B(J+746)
Y374=B(J+747)
X375=B(J+748)
Y375=B(J+749)
X376=B(J+750)
Y376=B(J+751)
X377=B(J+752)
Y377=B(J+753)
X378=B(J+754)
Y378=B(J+755)
X379=B(J+756)
Y379=B(J+757)
X380=B(J+758)
Y380=B(J+759)
X381=B(J+760)
Y381=B(J+761)
X382=B(J+762)
Y382=B(J+763)
X383=B(J+764)
Y383=B(J+765)
X384=B(J+766)
Y384=B(J+767)
X385=B(J+768)
Y385=B(J+769)
X386=B(J+770)
Y386=B(J+771)
X387=B(J+772)
Y387=B(J+773)
X388=B(J+774)
Y388=B(J+775)
X389=B(J+776)
Y389=B(J+777)
X390=B(J+778)
Y390=B(J+779)
X391=B(J+780)
Y391=B(J+781)
X392=B(J+782)
Y392=B(J+783)
X393=B(J+784)
Y393=B(J+785)
X394=B(J+786)
Y394=B(J+787)
X395=B(J+788)
Y395=B(J+789)
X396=B(J+790)
Y396=B(J+791)
X397=B(J+792)
Y397=B(J+793)
X398=B(J+794)
Y398=B(J+795)
X399=B(J+796)
Y399=B(J+797)
X400=B(J+798)
Y400=B(J+799)
X401=B(J+800)
Y401=B(J+801)
X402=B(J+802)
Y402=B(J+803)
X403=B(J+804)
Y403=B(J+805)
X404=B(J+806)
Y404=B(J+807)
X405=B(J+808)
Y405=B(J+809)
X406=B(J+810)
Y406=B(J+811)
X407=B(J+812)
Y407=B(J+813)
X408=B(J+814)
Y408=B(J+815)
X409=B(J+816)
Y409=B(J+817)
X410=B(J+818)
Y410=B(J+819)
X411=B(J+820)
Y411=B(J+821)
X412=B(J+822)
Y412=B(J+823)
X413=B(J+824)
Y413=B(J+825)
X414=B(J+826)
Y414=B(J+827)
X415=B(J+828)
Y415=B(J+829)
X416=B(J+830)
Y416=B(J+831)
X417=B(J+832)
Y417=B(J+833)
X418=B(J+834)
Y418=B(J+835)
X419=B(J+836)
Y419=B(J+837)
X420=B(J+838)
Y420=B(J+839)
X421=B(J+840)
Y421=B(J+841)
X422=B(J+842)
Y422=B(J+843)
X423=B(J+844)
Y423=B(J+845)
X424=B(J+846)
Y424=B(J+847)
X425=B(J+848)
Y425=B(J+849)
X426=B(J+850)
Y426=B(J+851)
X427=B(J+852)
Y427=B(J+853)
X428=B(J+854)
Y428=B(J+855)
X429=B(J+856)
Y429=B(J+857)
X430=B(J+858)
Y430=B(J+859)
X431=B(J+860)
Y431=B(J+861)
X432=B(J+862)
Y432=B(J+863)
X433=B(J+864)
Y433=B(J+865)
X434=B(J+866)
Y434=B(J+867)
X435=B(J+868)
Y435=B(J+869)
X436=B(J+870)
Y436=B(J+871)
X437=B(J+872)
Y437=B(J+873)
X438=B(J+874)
Y438=B(J+875)
X439=B(J+876)
Y439=B(J+877)
X440=B(J+878)
Y440=B(J+879)
X441=B(J+880)
Y441=B(J+881)
X442=B(J+882)
Y442=B(J+883)
X443=B(J+884)
Y443=B(J+885)
X444=B(J+886)
Y444=B(J+887)
X445=B(J+888)
Y445=B(J+889)
X446=B(J+890)
Y446=B(J+891)
X447=B(J+892)
Y447=B(J+893)
X448=B(J+894)
Y448=B(J+895)
X449=B(J+896)
Y449=B(J+897)
X450=B(J+898)
Y450=B(J+899)
X451=B(J+900)
Y451=B(J+901)
X452=B(J+902)
Y452=B(J+903)
X453=B(J+904)
Y453=B(J+905)
X454=B(J+906)
Y454=B(J+907)
X455=B(J+908)
Y455=B(J+909)
X456=B(J+910)
Y456=B(J+911)
X457=B(J+912)
Y457=B(J+913)
X458=B(J+914)
Y458=B(J+915)
X459=B(J+916)
Y459=B(J+917)
X460=B(J+918)
Y460=B(J+919)
X461=B(J+920)
Y461=B(J+921)
X462=B(J+922)
Y462=B(J+923)
X463=B(J+924)
Y463=B(J+925)
X464=B(J+926)
Y464=B(J+927)
X465=B(J+928)
Y465=B(J+929)
X466=B(J+930)
Y466=B(J+931)
X467=B(J+932)
Y467=B(J+933)
X468=B(J+934)
Y468=B(J+935)
X469=B(J+936)
Y469=B(J+937)
X470=B(J+938)
Y470=B(J+939)
X471=B(J+940)
Y471=B(J+941)
X472=B(J+942)
Y472=B(J+943)
X473=B(J+944)
Y473=B(J+945)
X474=B(J+946)
Y474=B(J+947)
X475=B(J+948)
Y475=B(J+949)
X476=B(J+950)
Y476=B(J+951)
X477=B(J+952)
Y477=B(J+953)
X478=B(J+954)
Y478=B(J+955)
X479=B(J+956)
Y479=B(J+957)
X480=B(J+958)
Y480=B(J+959)
X481=B(J+960)
Y481=B(J+961)
X482=B(J+962)
Y482=B(J+963)
X483=B(J+964)
Y483=B(J+965)
X484=B(J+966)
Y484=B(J+967)
X485=B(J+968)
Y485=B(J+969)
X486=B(J+970)
Y486=B(J+971)
X487=B(J+972)
Y487=B(J+973)
X488=B(J+974)
Y488=B(J+975)
X489=B(J+976)
Y489=B(J+977)
X490=B(J+978)
Y490=B(J+979)
X491=B(J+980)
Y491=B(J+981)
X492=B(J+982)
Y492=B(J+983)
X493=B(J+984)
Y493=B(J+985)
X494=B(J+986)
Y494=B(J+987)
X495=B(J+988)
Y495=B(J+989)
X496=B(J+990)
Y496=B(J+991)
X497=B(J+992)
Y497=B(J+993)
X498=B(J+994)
Y498=B(J+995)
X499=B(J+996)
Y499=B(J+997)
X500=B(J+998)
Y500=B(J+999)
X501=B(J+1000)
Y501=B(J+1001)
X502=B(J+1002)
Y502=B(J+1003)
X503=B(J+1004)
Y503=B(J+1005)
X504=B(J+1006)
Y504=B(J+1007)
X505=B(J+1008)
Y505=B(J+1009)
X506=B(J+1010)
Y506=B(J+1011)
X507=B(J+1012)
Y507=B(J+1013)
X508=B(J+1014)
Y508=B(J+1015)
X509=B(J+1016)
Y509=B(J+1017)
X510=B(J+1018)
Y510=B(J+1019)
X511=B(J+1020)
Y511=B(J+1021)
X512=B(J+1022)
Y512=B(J+1023)
X513=B(J+1024)
Y513=B(J+1025)
X514=B(J+1026)
Y514=B(J+1027)
X515=B(J+1028)
Y515=B(J+1029)
X516=B(J+1030)
Y516=B(J+1031)
X517=B(J+1032)
Y517=B(J+1033)
X518=B(J+1034)
Y518=B(J+1035)
X519=B(J+1036)
Y519=B(J+1037)
X520=B(J+1038)
Y520=B(J+1039)
X521=B(J+1040)
Y521=B(J+1041)
X522=B(J+1042)
Y522=B(J+1043)
X
```



```

Cooo WRITE REMAINING COEFFICIENTS ON TAPE
355 WRITE (FILEDIBLK,V1
      REMIND KFILE3
360 REMIND KFILES
365 WRITE (FILES)BLK,V1
370 WRITE (FILES)BLK,V1
375 WRITE (FILES)BLK,C1
      REMIND KFILE4
      REMIND KFILE
      GO TO 385
380 FORMAT (3H L=,15,20X,3H P=,F5.1)
385 CONTINUE
      RETURN
      END

```

```

Cooo FUNCTION SQZF(X1,X2,Y1,Y2,Z1,Z2)
      X=X1-X2
      Y=Y1-Y2
      Z=Z1-Z2
      R=SQRT(Y**2+Z**2)
      R=ABS(Z1+ABS(Y1)*ABS(Z2))+1.0E-20
      R=SQRT(R)
      P=184/R
      SQZF=P*P*RS/R
      RETURN
      END

```

```

Cooo SUBROUTINE PEP3(EPS,MIX)
      WRITE (JWRITE,5)
      DIMENSION VIP(650),S(5,650),COEF(900)
      COMMON TITLE(20),ICP(650),YCP(650),ZCP(650),ZMP(650),ZMP1
      1650),ADP(650),REFA,REBODY,NOUAD,HRRITE,MP,KNEH
      COMMON /INOUT/JREAD,JWRITE,JMWRITE,KFILE1,KFILE2,KFILES,KFILE4,KFILE
      15
      COMMON /SIK/SIK(650)
      WRITE (JWRITE,5)
      5 FORMAT (///,3HPOTENTIAL PLOM PROGRAM SECTION 3)
      10 FORMAT (1H0,20M4)
      KI=1
      K=0
      SET CONDITIONS FOR FLOW OF -1.0 IN X DIRECTION, ZERO IN Y&Z DIRECT
      Cooo
      Cooo COMPUTE INITIAL SOURCE APPROXIMATION & SET PARTIAL SUM VECTOR = 0
      DO 15 K=1,MP
      VIP(K)=VIP(K)*K
      S(5,K)=VIP(K)*.11936
      15 SH(K)=0.
      SH(MP+1)=0.
      SH(MP+2)=0.
      SH(MP+3)=0.
      SH(MP+4)=0.

```

```

PF2 264
PF2 265
PF2 266
PF2 267
PF2 268
PF2 269
PF2 270
PF2 271
PF2 272
PF2 273
PF2 274
PF2 275
PF2 276
PF2 277
PF2 278
PF2 279

```

```

SOF 1
SOF 2
SOF 3
SOF 4
SOF 5
SOF 6
SOF 7
SOF 8
SOF 9
SOF 10
SOF 11
SOF 12
SOF 13

```

```

PF3 1
PF3 2
PF3 3
PF3 4
PF3 5
PF3 6
PF3 7
PF3 8
PF3 9
PF3 10
PF3 11
PF3 12
PF3 13
PF3 14
PF3 15
PF3 16
PF3 17
PF3 18
PF3 19
PF3 20
PF3 21
PF3 22
PF3 23
PF3 24
PF3 25

```

```

WRITE (JWRITE,150) P4
WRITE (JWRITE,20)
20 FORMAT (/,12E,37M)ITERATIVE MATRIX SOLUTION INFORMATION,/,27M)ITERA
      110M SUM OF CHANGES,9X,1M4,10X,2M81,10X,2M82)
      11=1
      IC=5
Cooo START ITERATION,READ FIRST BLOCK OF COEFS.,START LOOP OVER QUADS.
25 READ (KFILE4)IION,COEF
      J=0
Cooo PICK UP SOURCE DENSITY & START LOOP OVER CENTROID POINTS
      DO 40 K=1,MP
      SP=SI(K)
      DO 40 KP=1,MP,5
      IF (J=900) 35,30,30
      30 READ (KFILE4)IION,COEF
      J=0
Cooo COMPUTE PARTIAL SUMS FOR NEXT 5 POINTS
35 SH(KP)=SH(KP)+COEF(I,J)*I*SP
      SH(KP+1)=SH(KP+1)+COEF(I,J)*I*SP
      SH(KP+2)=SH(KP+2)+COEF(I,J)*I*SP
      SH(KP+3)=SH(KP+3)+COEF(I,J)*I*SP
      SH(KP+4)=SH(KP+4)+COEF(I,J)*I*SP
      SH(KP+5)=SH(KP+5)+COEF(I,J)*I*SP
      40 CONTINUE
Cooo REMIND KFILE4
      REMIND KFILE4
      PASS=1,0
      SUM=0.
      DO 45 K=1,K2
      SH(K)=(SH(K)+VIP(K))*(-5/3,1*(19265)
      TEST=ABS(SH(K))-SI(K,R))
      SUM=SUM+TEST
      IF (TEST<GT,EPSPASS)-1,0
      45 CONTINUE
      WRITE (JWRITE,145) IT,SUM
      IF (PASS=EQ,1,0) GO TO 135
      IF (IT=EQ,MIX) GO TO 135
      IT=IT+1
      IC=IC-1
      IF (IC=EQ,0) GO TO 55
      DO 50 K=1,K2
      SI(K)=SH(K)
      50 SH(K)=0.
      55
      R2=0.
      R3=0.
      R4=0.
      O1=0.
      O2=0.
      DO 65 K=1,K2
      B59=2*(SI(K)-SH(K))-SI(2,K)
      IF (O59<GT,0.) GO TO 60
      A=0,SI(2,K)-SI(1,K)
      D=0A-O59
      GO TO 65
      60 A=A+SI(1,K)-SI(2,K)
      B=0A+O59
      65 B51=SI(1,K)-SI(3,K)

```

```

PF3 26
PF3 27
PF3 28
PF3 29
PF3 30
PF3 31
PF3 32
PF3 33
PF3 34
PF3 35
PF3 36
PF3 37
PF3 38
PF3 39
PF3 40
PF3 41
PF3 42
PF3 43
PF3 44
PF3 45
PF3 46
PF3 47
PF3 48
PF3 49
PF3 50
PF3 51
PF3 52
PF3 53
PF3 54
PF3 55
PF3 56
PF3 57
PF3 58
PF3 59
PF3 60
PF3 61
PF3 62
PF3 63
PF3 64
PF3 65
PF3 66
PF3 67
PF3 68
PF3 69
PF3 70
PF3 71
PF3 72
PF3 73
PF3 74
PF3 75
PF3 76
PF3 77
PF3 78
PF3 79
PF3 80
PF3 81
PF3 82
PF3 83
PF3 84
PF3 85

```

```

052-S(2,K1)-S(2,K)
053-S(1,-052)
054-S(2,K1)-S(1,K)
055-S(2,-053)
056-S(1,-054)
057-S(2,K1)-S(1,K)
058-S(2,-055)
059-S(1,-056)
060-S(2,K1)-S(1,K)
061-S(2,-057)
062-S(1,-058)
063-S(2,K1)-S(1,K)
064-S(2,-059)
065-S(1,-060)
066-S(2,K1)-S(1,K)
067-S(2,-061)
068-S(1,-062)
069-S(2,K1)-S(1,K)
070-S(2,-063)
071-S(1,-064)
072-S(2,K1)-S(1,K)
073-S(2,-065)
074-S(1,-066)
075-S(2,K1)-S(1,K)
076-S(2,-067)
077-S(1,-068)
078-S(2,K1)-S(1,K)
079-S(2,-069)
080-S(1,-070)
081-S(2,K1)-S(1,K)
082-S(2,-071)
083-S(1,-072)
084-S(2,K1)-S(1,K)
085-S(2,-073)
086-S(1,-074)
087-S(2,K1)-S(1,K)
088-S(2,-075)
089-S(1,-076)
090-S(2,K1)-S(1,K)
091-S(2,-077)
092-S(1,-078)
093-S(2,K1)-S(1,K)
094-S(2,-079)
095-S(1,-080)
096-S(2,K1)-S(1,K)
097-S(2,-081)
098-S(1,-082)
099-S(2,K1)-S(1,K)
100-S(2,-083)
101-S(1,-084)
102-S(2,K1)-S(1,K)
103-S(2,-085)
104-S(1,-086)
105-S(2,K1)-S(1,K)
106-S(2,-087)
107-S(1,-088)
108-S(2,K1)-S(1,K)
109-S(2,-089)
110-S(1,-090)
111-S(2,K1)-S(1,K)
112-S(2,-091)
113-S(1,-092)
114-S(2,K1)-S(1,K)
115-S(2,-093)
116-S(1,-094)
117-S(2,K1)-S(1,K)
118-S(2,-095)
119-S(1,-096)
120-S(2,K1)-S(1,K)
121-S(2,-097)
122-S(1,-098)
123-S(2,K1)-S(1,K)
124-S(2,-099)
125-S(1,-100)
126-S(2,K1)-S(1,K)
127-S(2,-101)
128-S(1,-102)
129-S(2,K1)-S(1,K)
130-S(2,-103)
131-S(1,-104)
132-S(2,K1)-S(1,K)
133-S(2,-105)
134-S(1,-106)
135-S(2,K1)-S(1,K)
136-S(2,-107)
137-S(1,-108)
138-S(2,K1)-S(1,K)
139-S(2,-109)
140-S(1,-110)
141-S(2,K1)-S(1,K)
142-S(2,-111)
143-S(1,-112)
144-S(2,K1)-S(1,K)
145-S(2,-113)
146-S(1,-114)
147-S(2,K1)-S(1,K)
148-S(2,-115)
149-S(1,-116)
150-S(2,K1)-S(1,K)
151-S(2,-117)
152-S(1,-118)
153-S(2,K1)-S(1,K)
154-S(2,-119)
155-S(1,-120)
156-S(2,K1)-S(1,K)
157-S(2,-121)
158-S(1,-122)
159-S(2,K1)-S(1,K)
160-S(2,-123)
161-S(1,-124)
162-S(2,K1)-S(1,K)
163-S(2,-125)
164-S(1,-126)
165-S(2,K1)-S(1,K)
166-S(2,-127)
167-S(1,-128)
168-S(2,K1)-S(1,K)
169-S(2,-129)
170-S(1,-130)
171-S(2,K1)-S(1,K)
172-S(2,-131)
173-S(1,-132)
174-S(2,K1)-S(1,K)
175-S(2,-133)
176-S(1,-134)
177-S(2,K1)-S(1,K)
178-S(2,-135)
179-S(1,-136)
180-S(2,K1)-S(1,K)
181-S(2,-137)
182-S(1,-138)
183-S(2,K1)-S(1,K)
184-S(2,-139)
185-S(1,-140)
186-S(2,K1)-S(1,K)
187-S(2,-141)
188-S(1,-142)
189-S(2,K1)-S(1,K)
190-S(2,-143)
191-S(1,-144)
192-S(2,K1)-S(1,K)
193-S(2,-145)
194-S(1,-146)
195-S(2,K1)-S(1,K)
196-S(2,-147)
197-S(1,-148)
198-S(2,K1)-S(1,K)
199-S(2,-149)
200-S(1,-150)
201-S(2,K1)-S(1,K)
202-S(2,-151)
203-S(1,-152)
204-S(2,K1)-S(1,K)
205-S(2,-153)
206-S(1,-154)
207-S(2,K1)-S(1,K)
208-S(2,-155)
209-S(1,-156)
210-S(2,K1)-S(1,K)
211-S(2,-157)
212-S(1,-158)
213-S(2,K1)-S(1,K)
214-S(2,-159)
215-S(1,-160)
216-S(2,K1)-S(1,K)
217-S(2,-161)
218-S(1,-162)
219-S(2,K1)-S(1,K)
220-S(2,-163)
221-S(1,-164)
222-S(2,K1)-S(1,K)
223-S(2,-165)
224-S(1,-166)
225-S(2,K1)-S(1,K)
226-S(2,-167)
227-S(1,-168)
228-S(2,K1)-S(1,K)
229-S(2,-169)
230-S(1,-170)
231-S(2,K1)-S(1,K)
232-S(2,-171)
233-S(1,-172)
234-S(2,K1)-S(1,K)
235-S(2,-173)
236-S(1,-174)
237-S(2,K1)-S(1,K)
238-S(2,-175)
239-S(1,-176)
240-S(2,K1)-S(1,K)
241-S(2,-177)
242-S(1,-178)
243-S(2,K1)-S(1,K)
244-S(2,-179)
245-S(1,-180)
246-S(2,K1)-S(1,K)
247-S(2,-181)
248-S(1,-182)
249-S(2,K1)-S(1,K)
250-S(2,-183)
251-S(1,-184)
252-S(2,K1)-S(1,K)
253-S(2,-185)
254-S(1,-186)
255-S(2,K1)-S(1,K)
256-S(2,-187)
257-S(1,-188)
258-S(2,K1)-S(1,K)
259-S(2,-189)
260-S(1,-190)
261-S(2,K1)-S(1,K)
262-S(2,-191)
263-S(1,-192)
264-S(2,K1)-S(1,K)
265-S(2,-193)
266-S(1,-194)
267-S(2,K1)-S(1,K)
268-S(2,-195)
269-S(1,-196)
270-S(2,K1)-S(1,K)
271-S(2,-197)
272-S(1,-198)
273-S(2,K1)-S(1,K)
274-S(2,-199)
275-S(1,-200)

```

```

SUBROUTINE PFA(IGDA,CORAI
POTENTIAL FLOW PROGRAM SECTION 4--COMPUTES VELOCITIES AND PRESSURE
COEFFICIENTS AT THE PANEL CENTROID POINTS
Cooo
DIMENSION CVI(1,000)
COMMON TITLE(20),XCP(650),YCP(650),ZCP(650),XMP(650),YMP(650),ZMP(
1650),AMP(650),RFA,REBODY,INJAD,WRITE,MP,KNEE
COMMON /SIX/S(1,650)
COMMON /HOLD/XMH(650),ZMH(650),ASPH(650)
COMMON /INOUT/READ,WRITE,KFILE1,KFILE2,KFILE3,KFILE4,KFILE
15
5 FORMAT (1H1,33H POTENTIAL FLOW PROGRAM SECTION 4)
WRITE (JWRITE,5)
D=-.5/3.14159265
J=1
K1=1
IF (RMEN.EQ.1)K1HOLD=MP
K2=MP
C0=0.0
C1=0.0
C2=0.0
C3=0.0
C4=0.0
C5=0.0
C6=0.0
C7=0.0
C8=0.0
C9=0.0
C10=0.0
C11=0.0
C12=0.0
C13=0.0
C14=0.0
C15=0.0
C16=0.0
C17=0.0
C18=0.0
C19=0.0
C20=0.0
C21=0.0
C22=0.0
C23=0.0
C24=0.0
C25=0.0
C26=0.0
C27=0.0
C28=0.0
C29=0.0
C30=0.0
C31=0.0
C32=0.0
C33=0.0
C34=0.0
C35=0.0
C36=0.0
C37=0.0
C38=0.0
C39=0.0
C40=0.0
C41=0.0
C42=0.0
C43=0.0
C44=0.0
C45=0.0
C46=0.0
C47=0.0
C48=0.0
C49=0.0
C50=0.0
C51=0.0
C52=0.0
C53=0.0
C54=0.0
C55=0.0
C56=0.0
C57=0.0
C58=0.0
C59=0.0
C60=0.0
C61=0.0
C62=0.0
C63=0.0
C64=0.0
C65=0.0
C66=0.0
C67=0.0
C68=0.0
C69=0.0
C70=0.0
C71=0.0
C72=0.0
C73=0.0
C74=0.0
C75=0.0
C76=0.0
C77=0.0
C78=0.0
C79=0.0
C80=0.0
C81=0.0
C82=0.0
C83=0.0
C84=0.0
C85=0.0
C86=0.0
C87=0.0
C88=0.0
C89=0.0
C90=0.0
C91=0.0
C92=0.0
C93=0.0
C94=0.0
C95=0.0
C96=0.0
C97=0.0
C98=0.0
C99=0.0
C100=0.0
C101=0.0
C102=0.0
C103=0.0
C104=0.0
C105=0.0
C106=0.0
C107=0.0
C108=0.0
C109=0.0
C110=0.0
C111=0.0
C112=0.0
C113=0.0
C114=0.0
C115=0.0
C116=0.0
C117=0.0
C118=0.0
C119=0.0
C120=0.0
C121=0.0
C122=0.0
C123=0.0
C124=0.0
C125=0.0
C126=0.0
C127=0.0
C128=0.0
C129=0.0
C130=0.0
C131=0.0
C132=0.0
C133=0.0
C134=0.0
C135=0.0
C136=0.0
C137=0.0
C138=0.0
C139=0.0
C140=0.0
C141=0.0
C142=0.0
C143=0.0
C144=0.0
C145=0.0
C146=0.0
C147=0.0
C148=0.0
C149=0.0
C150=0.0
C151=0.0
C152=0.0
C153=0.0
C154=0.0
C155=0.0
C156=0.0
C157=0.0
C158=0.0
C159=0.0
C160=0.0
C161=0.0
C162=0.0
C163=0.0
C164=0.0
C165=0.0
C166=0.0
C167=0.0
C168=0.0
C169=0.0
C170=0.0
C171=0.0
C172=0.0
C173=0.0
C174=0.0
C175=0.0
C176=0.0
C177=0.0
C178=0.0
C179=0.0
C180=0.0
C181=0.0
C182=0.0
C183=0.0
C184=0.0
C185=0.0
C186=0.0
C187=0.0
C188=0.0
C189=0.0
C190=0.0
C191=0.0
C192=0.0
C193=0.0
C194=0.0
C195=0.0
C196=0.0
C197=0.0
C198=0.0
C199=0.0
C200=0.0
C201=0.0
C202=0.0
C203=0.0
C204=0.0
C205=0.0
C206=0.0
C207=0.0
C208=0.0
C209=0.0
C210=0.0
C211=0.0
C212=0.0
C213=0.0
C214=0.0
C215=0.0
C216=0.0
C217=0.0
C218=0.0
C219=0.0
C220=0.0
C221=0.0
C222=0.0
C223=0.0
C224=0.0
C225=0.0
C226=0.0
C227=0.0
C228=0.0
C229=0.0
C230=0.0
C231=0.0
C232=0.0
C233=0.0
C234=0.0
C235=0.0
C236=0.0
C237=0.0
C238=0.0
C239=0.0
C240=0.0
C241=0.0
C242=0.0
C243=0.0
C244=0.0
C245=0.0
C246=0.0
C247=0.0
C248=0.0
C249=0.0
C250=0.0
C251=0.0
C252=0.0
C253=0.0
C254=0.0
C255=0.0
C256=0.0
C257=0.0
C258=0.0
C259=0.0
C260=0.0
C261=0.0
C262=0.0
C263=0.0
C264=0.0
C265=0.0
C266=0.0
C267=0.0
C268=0.0
C269=0.0
C270=0.0
C271=0.0
C272=0.0
C273=0.0
C274=0.0
C275=0.0
C276=0.0
C277=0.0
C278=0.0
C279=0.0
C280=0.0
C281=0.0
C282=0.0
C283=0.0
C284=0.0
C285=0.0
C286=0.0
C287=0.0
C288=0.0
C289=0.0
C290=0.0
C291=0.0
C292=0.0
C293=0.0
C294=0.0
C295=0.0
C296=0.0
C297=0.0
C298=0.0
C299=0.0
C300=0.0
C301=0.0
C302=0.0
C303=0.0
C304=0.0
C305=0.0
C306=0.0
C307=0.0
C308=0.0
C309=0.0
C310=0.0
C311=0.0
C312=0.0
C313=0.0
C314=0.0
C315=0.0
C316=0.0
C317=0.0
C318=0.0
C319=0.0
C320=0.0
C321=0.0
C322=0.0
C323=0.0
C324=0.0
C325=0.0
C326=0.0
C327=0.0
C328=0.0
C329=0.0
C330=0.0
C331=0.0
C332=0.0
C333=0.0
C334=0.0
C335=0.0
C336=0.0
C337=0.0
C338=0.0
C339=0.0
C340=0.0
C341=0.0
C342=0.0
C343=0.0
C344=0.0
C345=0.0
C346=0.0
C347=0.0
C348=0.0
C349=0.0
C350=0.0
C351=0.0
C352=0.0
C353=0.0
C354=0.0
C355=0.0
C356=0.0
C357=0.0
C358=0.0
C359=0.0
C360=0.0
C361=0.0
C362=0.0
C363=0.0
C364=0.0
C365=0.0
C366=0.0
C367=0.0
C368=0.0
C369=0.0
C370=0.0
C371=0.0
C372=0.0
C373=0.0
C374=0.0
C375=0.0
C376=0.0
C377=0.0
C378=0.0
C379=0.0
C380=0.0
C381=0.0
C382=0.0
C383=0.0
C384=0.0
C385=0.0
C386=0.0
C387=0.0
C388=0.0
C389=0.0
C390=0.0
C391=0.0
C392=0.0
C393=0.0
C394=0.0
C395=0.0
C396=0.0
C397=0.0
C398=0.0
C399=0.0
C400=0.0
C401=0.0
C402=0.0
C403=0.0
C404=0.0
C405=0.0
C406=0.0
C407=0.0
C408=0.0
C409=0.0
C410=0.0
C411=0.0
C412=0.0
C413=0.0
C414=0.0
C415=0.0
C416=0.0
C417=0.0
C418=0.0
C419=0.0
C420=0.0
C421=0.0
C422=0.0
C423=0.0
C424=0.0
C425=0.0
C426=0.0
C427=0.0
C428=0.0
C429=0.0
C430=0.0
C431=0.0
C432=0.0
C433=0.0
C434=0.0
C435=0.0
C436=0.0
C437=0.0
C438=0.0
C439=0.0
C440=0.0
C441=0.0
C442=0.0
C443=0.0
C444=0.0
C445=0.0
C446=0.0
C447=0.0
C448=0.0
C449=0.0
C450=0.0
C451=0.0
C452=0.0
C453=0.0
C454=0.0
C455=0.0
C456=0.0
C457=0.0
C458=0.0
C459=0.0
C460=0.0
C461=0.0
C462=0.0
C463=0.0
C464=0.0
C465=0.0
C466=0.0
C467=0.0
C468=0.0
C469=0.0
C470=0.0
C471=0.0
C472=0.0
C473=0.0
C474=0.0
C475=0.0
C476=0.0
C477=0.0
C478=0.0
C479=0.0
C480=0.0
C481=0.0
C482=0.0
C483=0.0
C484=0.0
C485=0.0
C486=0.0
C487=0.0
C488=0.0
C489=0.0
C490=0.0
C491=0.0
C492=0.0
C493=0.0
C494=0.0
C495=0.0
C496=0.0
C497=0.0
C498=0.0
C499=0.0
C500=0.0
C501=0.0
C502=0.0
C503=0.0
C504=0.0
C505=0.0
C506=0.0
C507=0.0
C508=0.0
C509=0.0
C510=0.0
C511=0.0
C512=0.0
C513=0.0
C514=0.0
C515=0.0
C516=0.0
C517=0.0
C518=0.0
C519=0.0
C520=0.0
C521=0.0
C522=0.0
C523=0.0
C524=0.0
C525=0.0
C526=0.0
C527=0.0
C528=0.0
C529=0.0
C530=0.0
C531=0.0
C532=0.0
C533=0.0
C534=0.0
C535=0.0
C536=0.0
C537=0.0
C538=0.0
C539=0.0
C540=0.0
C541=0.0
C542=0.0
C543=0.0
C544=0.0
C545=0.0
C546=0.0
C547=0.0
C548=0.0
C549=0.0
C550=0.0
C551=0.0
C552=0.0
C553=0.0
C554=0.0
C555=0.0
C556=0.0
C557=0.0
C558=0.0
C559=0.0
C560=0.0
C561=0.0
C562=0.0
C563=0.0
C564=0.0
C565=0.0
C566=0.0
C567=0.0
C568=0.0
C569=0.0
C570=0.0
C571=0.0
C572=0.0
C573=0.0
C574=0.0
C575=0.0
C576=0.0
C577=0.0
C578=0.0
C579=0.0
C580=0.0
C581=0.0
C582=0.0
C583=0.0
C584=0.0
C585=0.0
C586=0.0
C587=0.0
C588=0.0
C589=0.0
C590=0.0
C591=0.0
C592=0.0
C593=0.0
C594=0.0
C595=0.0
C596=0.0
C597=0.0
C598=0.0
C599=0.0
C600=0.0
C601=0.0
C602=0.0
C603=0.0
C604=0.0
C605=0.0
C606=0.0
C607=0.0
C608=0.0
C609=0.0
C610=0.0
C611=0.0
C612=0.0
C613=0.0
C614=0.0
C615=0.0
C616=0.0
C617=0.0
C618=0.0
C619=0.0
C620=0.0
C621=0.0
C622=0.0
C623=0.0
C624=0.0
C625=0.0
C626=0.0
C627=0.0
C628=0.0
C629=0.0
C630=0.0
C631=0.0
C632=0.0
C633=0.0
C634=0.0
C635=0.0
C636=0.0
C637=0.0
C638=0.0
C639=0.0
C640=0.0
C641=0.0
C642=0.0
C643=0.0
C644=0.0
C645=0.0
C646=0.0
C647=0.0
C648=0.0
C649=0.0
C650=0.0
C651=0.0
C652=0.0
C653=0.0
C654=0.0
C655=0.0
C656=0.0
C657=0.0
C658=0.0
C659=0.0
C660=0.0
C661=0.0
C662=0.0
C663=0.0
C664=0.0
C665=0.0
C666=0.0
C667=0.0
C668=0.0
C669=0.0
C670=0.0
C671=0.0
C672=0.0
C673=0.0
C674=0.0
C675=0.0
C676=0.0
C677=0.0
C678=0.0
C679=0.0
C680=0.0
C681=0.0
C682=0.0
C683=0.0
C684=0.0
C685=0.0
C686=0.0
C687=0.0
C688=0.0
C689=0.0
C690=0.0
C691=0.0
C692=0.0
C693=0.0
C694=0.0
C695=0.0
C696=0.0
C697=0.0
C698=0.0
C699=0.0
C700=0.0
C701=0.0
C702=0.0
C703=0.0
C704=0.0
C705=0.0
C706=0.0
C707=0.0
C708=0.0
C709=0.0
C710=0.0
C711=0.0
C712=0.0
C713=0.0
C714=0.0
C715=0.0
C716=0.0
C717=0.0
C718=0.0
C719=0.0
C720=0.0
C721=0.0
C722=0.0
C723=0.0
C724=0.0
C725=0.0
C726=0.0
C727=0.0
C728=0.0
C729=0.0
C730=0.0
C731=0.0
C732=0.0
C733=0.0
C734=0.0
C735=0.0
C736=0.0
C737=0.0
C738=0.0
C739=0.0
C740=0.0
C741=0.0
C742=0.0
C743=0.0
C744=0.0
C745=0.0
C746=0.0
C747=0.0
C748=0.0
C749=0.0
C750=0.0
C751=0.0
C752=0.0
C753=0.0
C754=0.0
C755=0.0
C756=0.0
C757=0.0
C758=0.0
C759=0.0
C760=0.0
C761=0.0
C762=0.0
C763=0.0
C764=0.0
C765=0.0
C766=0.0
C767=0.0
C768=0.0
C769=0.0
C770=0.0
C771=0.0
C772=0.0
C773=0.0
C774=0.0
C775=0.0
C776=0.0
C777=0.0
C778=0.0
C779=0.0
C780=0.0
C781=0.0
C782=0.0
C783=0.0
C784=0.0
C785=0.0
C786=0.0
C787=0.0
C788=0.0
C789=0.0
C790=0.0
C791=0.0
C792=0.0
C793=0.0
C794=0.0
C795=0.0
C796=0.0
C797=0.0
C798=0.0
C799=0.0
C800=0.0
C801=0.0
C802=0.0
C803=0.0
C804=0.0
C805=0.0
C806=0.0
C807=0.0
C808=0.0
C809=0.0
C810=0.0
C811=0.0
C812=0.0
C813=0.0
C814=0.0
C815=0.0
C816=0.0
C817=0.0
C818=0.0
C819=0.0
C820=0.0
C821=0.0
C822=0.0
C823=0.0
C824=0.0
C825=0.0
C826=0.0
C827=0.0
C828=0.0
C829=0.0
C830=0.0
C831=0.0
C832=0.0
C833=0.0
C834=0.0
C835=0.0
C836=0.0
C837=0.0
C838=0.0
C839=0.0
C840=0.0
C841=0.0
C842=0.0
C843=0.0
C844=0.0
C845=0.0
C846=0.0
C847=0.0
C848=0.0
C849=0.0
C850=0.0
C851=0.0
C852=0.0
C853=0.0
C854=0.0
C855=0.0
C856=0.0
C857=0.0
C858=0.0
C859=0.0
C860=0.0
C861=0.0
C862=0.0
C863=0.0
C864=0.0
C865=0.0
C866=0.0
C867=0.0
C868=0.0
C869=0.0
C870=0.0
C871=0.0
C872=0.0
C873=0.0
C874=0.0
C875=0.0
C876=0.0
C877=0.0
C878=0.0
C879=0.0
C880=0.0
C881=0.0
C882=0.0
C883=0.0
C884=0.0
C885=0.0
C886=0.0
C887=0.0
C888=0.0
C889=0.0
C890=0.0
C891=0.0
C892=0.0
C893=0.0
C894=0.0
C895=0.0
C896=0.0
C897=0.0
C898=0.0
C899=0.0
C900=0.0
C901=0.0
C902=0.0
C903=0.0
C904=0.0
C905=0.0
C906=0.0
C907=0.0
C908=0.0
C909=0.0
C910=0.0
C911=0.0
C912=0.0
C913=0.0
C914=0.0
C915=0.0
C916=0.0
C917=0.0
C918=0.0
C919=0.0
C920=0.0
C921=0.0
C922=0.0
C923=0.0
C924=0.0
C925=0.0
C926=0.0
C927=0.0
C928=0.0
C929=0.0
C930=0.0
C931=0.0
C932=0.0
C933=0.0
C934=0.0
C935=0.0
C936=0.0
C937=0.0
C938=0.0
C939=0.0
C940=0.0
C941=0.0
C942=0.0
C943=0.0
C944=0.0
C945=0.0
C946=0.0
C947=0.0
C948=0.0
C949=0.0
C950=0.0
C951=0.0
C952=0.0
C953=0.0
C954=0.0
C955=0.0
C956=0.0
C957=0.0
C958=0.0
C959=0.0
C960=0.0
C961=0.0
C962=0.0
C963=0.0
C964=0.0
C965=0.0
C966=0.0
C967=0.0
C968=0.0
C969=0.0
C970=0.0
C971=0.0
C972=0.0
C973=0.0
C974=0.0
C975=0.0
C976=0.0
C977=0.0
C978=0.0
C979=0.0
C980=0.0
C981=0.0
C982=0.0
C983=0.0
C984=0.0
C985=0.0
C986=0.0
C987=0.0
C988=0.0
C989=0.0
C990=0.0
C991=0.0
C992=0.0
C993=0.0
C994=0.0
C995=0.0
C996=0.0
C997=0.0
C998=0.0
C999=0.0
C1000=0.0

```







```

Cooo
VM=(VCR(M)+VCR(M+1))/2
PTMO INTERSECTION WITH SIDE OF QUAD.
SP=SQRT((M-U)*M+V*V)
AC=3*(SF(M)+2*SF(M+1)+SF(M+2))/6
IF (AC.EQ.0) GO TO 95
SR=SQRT((M+2)*M+V*V)
TP=(BC-SR)/(2.*AC)
IF (TP.LE.1.-AND.TP.GE.0.) GO TO 100
GO TO 100
TP=(BC-SR)/(2.*AC)
95 IF (BC.EQ.0) GO TO 105
TP=SF(M)/BC
100 XNTP=(1.-TP)*VCR(M)+TP*VCR(M+1)
YNTP=(1.-TP)*VCR(M)+TP*VCR(M+1)
TESTP=((XNTP-XYT)*QU*(YNTP-XYT)/VQ)*DIRTY
IF (TESTP.LE.-TEST) GO TO 105
TEST=TESTP
MNT=MNTP
YNT=YNTP
105 CONTINUE
IF (TEST.EQ.0) GO TO 160
Cooo
AVERAGE LAST VELOCITY AND CURVATURE
UX=(UX+UXP)/2
UY=(UY+UYP)/2
UZ=(UZ+UZP)/2
VQ=(VQ+VQP)/2
CP=1-10*SQRT(1.-CP)
IF (J.LE.VSTOP) GO TO 165
Cooo
COMPUTE VELOCITY AT NEXT POINT
J=J+1
USL=UB*HNT*U+VNT*U2
VSL=VB*HNT*V+VNT*V2
UX=USL*(X3(MQ)+VSL*(X4(MQ)
UY=USL*(Y3(MQ)+VSL*(Y4(MQ)
UZ=USL*(Z3(MQ)+VSL*(Z4(MQ)
V500=USL*(W2+VSL*(W2)
CORD=SQRT((XNT-XYT)**2+(YNT-XYT)**2)*DIRT
STPL(J)=STPL(JL)*CORD
CP=1.-V500
UABS(J)=SQRT(U.-CP)
AF=.5
LMQ=MQ
X(LJ)=XNT*(X3(MQ)+YNT*(X4(MQ)+XCP*(MQ)
Y(LJ)=YNT*(Y3(MQ)+YNT*(Y4(MQ)+YCP*(MQ)
Z(LJ)=ZNT*(Z3(MQ)+YNT*(Z4(MQ)+ZCP*(MQ)
IF (J.LE.MINJ.OR.J.GE.MAXJ) GO TO 245
Cooo
PROCEDURE FOR FINDING NEXT QUAD. WAS MODIFIED SO THAT, DEPENDING
ON THE DIRECTION, THERE ARE ONLY 3 POSSIBLE QUADS. TO TEST
M=MO*(MQ+Z)
MTEST=9
ZF(DIRT) 120,110,135
110 WRITE (LM1,1X,7HD)IRT = ,F10.7,26MPROGRAM TERMINATED IN PFP7)
CALL EXIT
120 IF (MND) 125,130,125
Cooo
LAST QUAD. IS ODD & WE ARE TESTING AGAINST THE STREAM DIRECTION
125 MTEST(1)=MQ-2*(MH-1)*1
MTEST(2)=MQ-2

```

```

MTEST(3)=MQ-2
MTEST(4)=MTEST(1)+2
MTEST(5)=MTEST(1)-2
IF (MQ.EQ.1) GO TO 150
MTEST(2)=MTEST(5)
MTEST=3
GO TO 150
Cooo
LAST QUAD. IS EVEN & WE ARE TESTING AGAINST THE STREAM DIRECTION
130 MTEST(1)=MQ-1
MTEST(2)=MQ+2
MTEST(3)=MQ-2
MTEST(4)=MQ+1
MTEST(5)=MQ-3
IF (MQ.GT.1) GO TO 150
MTEST(1)=MTEST(2)
MTEST(2)=MTEST(3)
MTEST=2
IF (MQ.EQ.2) MTEST=1
GO TO 150
135 IF (MND) 140,145,140
Cooo
LAST QUAD IS ODD & WE ARE TESTING IN THE STREAM DIRECTION
140 MTEST(1)=MQ+1
MTEST(2)=MQ-2
MTEST(3)=MQ+2
MTEST(4)=MQ-1
MTEST(5)=MQ+3
IF (MQ.LT.1) GO TO 150
MTEST=2
MTEST(1)=MTEST(3)
MTEST(2)=MQ+1
MTEST(3)=MQ-2
IF (MQ.EQ.1) MTEST=1
GO TO 150
Cooo
LAST QUAD IS EVEN & WE ARE TESTING IN THE STREAM DIRECTION
145 MTEST(1)=MQ+2*(MH-1)-1
MTEST(2)=MQ+2
MTEST(3)=MQ-2
MTEST(4)=MTEST(1)+2
MTEST(5)=MTEST(1)-2
IF (MQ.EQ.2) GO TO 150
MTEST=4
MTEST(3)=MTEST(5)
150 M=1
155 I=MTEST(M)
MQ=1
TEST=X(LJ)-XCP(1)+Y(LJ)-YCP(1)+Z(LJ)-ZCP(1)+2*DIRX(1)
IF (TEST.GT.0) GO TO 140
O52=(XZ(1)-XCA(1))+2*(YV(1)-YV2(1))+2*Z(1)+2*Z2(1)+2*Z3(1)+2*Z4(1)
O53=(XCA(1)-XCA(1))+2*(YV(1)-YV2(1))+2*Z(1)+2*Z2(1)+2*Z3(1)+2*Z4(1)
O54=(XCA(1)-XCA(1))+2*(YV(1)-YV2(1))+2*Z(1)+2*Z2(1)+2*Z3(1)+2*Z4(1)
M=(X(LJ)-XCP(1))+2*(Y(LJ)-YCP(1))+2*(Z(LJ)-ZCP(1))+2*Z(1)+2*Z2(1)+2*Z3(1)+2*Z4(1)
ZLT=X(LJ)-XCP(1)+Y(LJ)-YCP(1)+Z(LJ)-ZCP(1)+2*Z(1)+2*Z2(1)+2*Z3(1)+2*Z4(1)
160 M=1
155 I=MTEST(M)
Z50=ZLT*2
TEST=Z50-1*DIRX(1)
IF (TEST.GT.0) GO TO 140
AC=1-SQRT(Z50*(XLT-XC1(1))+2*(YLT-YC1(1))+2*Z(1)+2*Z2(1)+2*Z3(1)+2*Z4(1))
AC2=SQRT(Z50*(XLT-XC2(1))+2*(YLT-YC2(1))+2*Z(1)+2*Z2(1)+2*Z3(1)+2*Z4(1))
AC3=SQRT(Z50*(XLT-XC3(1))+2*(YLT-YC3(1))+2*Z(1)+2*Z2(1)+2*Z3(1)+2*Z4(1))
AC4=SQRT(Z50*(XLT-XC4(1))+2*(YLT-YC4(1))+2*Z(1)+2*Z2(1)+2*Z3(1)+2*Z4(1))

```

PFS 243  
PFS 244  
PFS 245  
PFS 246  
PFS 247  
PFS 248  
PFS 249  
PFS 250  
PFS 251  
PFS 252  
PFS 253  
PFS 254  
PFS 255  
PFS 256  
PFS 257  
PFS 258  
PFS 259  
PFS 260  
PFS 261  
PFS 262  
PFS 263  
PFS 264  
PFS 265  
PFS 266  
PFS 267  
PFS 268  
PFS 269  
PFS 270  
PFS 271  
PFS 272  
PFS 273  
PFS 274  
PFS 275  
PFS 276  
PFS 277  
PFS 278  
PFS 279  
PFS 280  
PFS 281  
PFS 282  
PFS 283  
PFS 284  
PFS 285  
PFS 286  
PFS 287  
PFS 288  
PFS 289  
PFS 290  
PFS 291  
PFS 292  
PFS 293  
PFS 294  
PFS 295  
PFS 296  
PFS 297  
PFS 298  
PFS 299  
PFS 300  
PFS 301  
PFS 302



```

Cooo WRITE POINTS, DSTAR, C SKIN FOR EACH CENTROID. COMPUTE FRICTION CD
DO 295 J=1,NP
  WRITE (JWRITE,99) J,VCDF(J),VCF(J),DCPJ(J),DSTAR(J),SKIN(J)
290 FORMAT (A5,13,5F10.5,4X,2E15.7)
  CDF=COF*SKIN(J)/WALL(J)/10.5*VABS(J)
  AREA=AREA+ADP(J)
295 CONTINUE
  AREAAV=AREA/NLIN
  CDF=2.0*CDF
  CDF=CDF/MEFA
300 FORMAT (///,13X,25HFRICITION DRAG COEFFICIENT,/,13X,29(1W9),/17X)
  1=H*FRICTION CD = F11.5/17X+17*REFERENCE AREA = F11.5/13X+18W9Y
  1) HOLDS NUMBER = .611-A/17X+14*BODY LENGTH = F11.5/13X+29(1W9),//
  WRITE (JWRITE,300) CDF,MEFA,REBODY*STOTAL
  REWIND KFILES
  REWIND KFILES
  REWIND KFILES
  SUMA=0.0
  AVXC=0.0
  AVY=0.0
  AVZ=0.0
  DO NLIN=2,NH+4
    CALCULATE AVERAGE DSTAR, AVERAGE PANEL AREA, AND AVERAGE X-ORDINATE
    FOR THE THIRD STATION OF INPUT POINTS FROM THE END OF BODY. THESE
    QUANTITIES ARE USED TO CALCULATE THE WAKE-BODY COORDINATES.
    DO 305 I=1,NLIN
      AVXC=AVXC+DSTAR(I)*XADP(I-1)
      AVY=AVY+DSTAR(I)*YADP(I-1)
      AVZ=AVZ+DSTAR(I)*ZADP(I-1)
      SUMA=SUMA+ADP(I-1)
      AVDEL=AVDEL+AVAREA
      AVXG=AVXG+AVAREA
      AVY=AVY+AVXG/AVAREA
      SUMA=SUMA/(NIN-1)
      AREA=SUMA/(AREA+V*SUMA)
    DO 310 I=1,NLIN
      XMH(I)=XMP(I)
      ZMH(I)=ZMP(I)
    310 ADPH(I)=ADP(I)
  RETURN
  315 WRITE (JWRITE,320) IS,MS
  320 FORMAT (14H TAPE ON ERROR,Z14)
  325 RETURN
  END

```

```

SUBROUTINE BLCONT(NP, IWRITE)
  BOUNDARY LAYER CONTROL ROUTINE WHICH CALLS LAMINR & TURB2, THE
  DIMING AND TURBULENT ROUTINES WHICH USE MOMENTUM INTEGRAL METHOD
  DIMENSION X(150),YDEL(150),DUDX(150)
  COMMON /RNDM/TAM(150),MREAN(150),VCOEF(14,75),MP
  COMMON /BL/VOW(175),SS(175),VIMP,V0,ROE,DELS(150),CF(150),TMT(150),
  1STOTAL,REK
  COMMON /INOUT/JREAD, JWRITE, KFILE1, KFILE2, KFILE3, KFILE4, KFILE
  15
  STRAM=.05
  NP=NP
  Cooo SPLINE IS CALLED TO CURVE FIT THE STREAMLINE VALUES OF ABSOLUTE
  BLC 1
  BLC 2
  BLC 3
  BLC 4
  BLC 5
  BLC 6
  BLC 7
  BLC 8
  BLC 9
  BLC 10
  BLC 11
  BLC 12
  BLC 13
  BLC 14
  BLC 15

```

```

Cooo VELOCITY VERSUS SURFACE DISTANCE FROM THE NOSE OF THE BODY
CALL SPLINE(NP,VOW,SS,VCOEF)
M=NP-1
SEMD=SS(MP)
REK=2
K=1
S(1)=SS(1)
V(1)=VOW(1)
DUDS(1)=VCOEF(3,1)
DO 5 I=1,M
  D(5 I)=S(I)-S(I+1)/KXK
  DO 5 J=1,REK
    S(J)=S(I)+K
    V(J)=V(I)+VCOEF(2,1)*S(I)+VCOEF(3,1)*S(I)+VCOEF(4,1)
    1) DUDS(1)=13.0000*VCOEF(1,1)*S(I)+2.0000*VCOEF(2,1)*S(I)+VCOEF(3,1)
    MP=REK*(M-1)
  5 CONTINUE
  DO 10 I=1,MP
    S(1)=S(1)/STOTAL
    10 DUDS(1)=DUDS(1)*STOTAL
    CALL LAMINR(15,V,DUDS,STRAM,11,MPP,IWRITE)
    IF (111.EQ.MPP) GO TO 15
    CALL TURB2(15,V,DUDS,SEMD,11,MPP)
    15 IF (IWRITE.GT.1) GO TO 25
    WRITE (JWRITE,20)
    20 FORMAT (1/6X,1MS,13X,1W9,10X,4H DUDS,9H,SHMREAN,8X,4HDELTA5,7X,6HNT)
    1) JETAS,8X,ZTAN,9X,ZMCF(1)
    25 DO 30 I=1,MP
      S(1)=S(1)+STOTAL
      V(1)=V(1)+VIMP
      DUDS(1)=DUDS(1)+VIMP/STOTAL
      30 DELS(1)=DELS(1)+STOTAL
      IF (IWRITE.GT.1) RETURN
      DO 35 I=1,MP+REK
        S(I)=S(I)+K
        V(I)=V(I)+VCOEF(2,1)*S(I)+VCOEF(3,1)*S(I)+VCOEF(4,1)
        35 WRITE (JWRITE,40) S(I),V(I),DUDS(1),MREAN(1),DELS(1),TMT(1),TAM(1)
        1) CDF(I)
        40 FORMAT (11X,8F10.5,3X)
      RETURN
    END

```

```

SUBROUTINE LAMINR(X, YDEL, DUDX, ITRAM, II, NPP, IWRITE)
  CALCULATES LAMINAR BOUNDARY LAYER BY MOMENTUM INTEGRAL
  DIMENSION X(150),YDEL(150),DUDX(150)
  COMMON /RNDM/TAM(150),MREAN(150),VCOEF(14,75),MP
  COMMON /BL/VOW(175),SS(175),VIMP,V0,ROE,DELS(150),CF(150),TMT(150),
  1STOTAL,REK
  COMMON /INOUT/JREAD, JWRITE, KFILE1, KFILE2, KFILE3, KFILE4, KFILE
  15
  II=1
  M=X(II)-K(II)
  IF (YDEL(II).LT.LC-0.6) GO TO 5
  5 STARTING CONDITIONS ASSUMING FLAT PLATE
  Z=0.0
  TMT(II)=0.0
  DELS(II)=0.0
  TMT(II)=5000.0
  BLC 1
  BLC 2
  BLC 3
  BLC 4
  BLC 5
  BLC 6
  BLC 7
  BLC 8
  BLC 9
  BLC 10
  BLC 11
  BLC 12
  BLC 13
  BLC 14
  BLC 15

```

```

CF(I)=1000.0
MREAN(I)=2.554
I1=2
GO TO 20
SUBROUTINE FFK(ARD,FD,FID,FZD)
ROUTINE FOR NUMERICAL INTERPOLATION OF LAMINAR O-L. FUNCTIONS
DIMENSION AK(55),F(55),F1(55),F2(55)
COMMON /INOUT/AREAD,WRITE,MPFILE,MPFILE2,MPFILE3,MPFILE4,MPFILE
5
DATA AK/0.094815,0.094632,0.094083,0.093166,0.091872,0.09023,0.08
18223,0.08855,0.083134,0.080068,0.076664,0.072930,0.068877,0.06451
16,0.059857,0.054912,0.049697,0.044223,0.038506,0.032562,0.026405,0
1.020587,0.013524,0.006833,0.000000,0.000000,-0.006957,-0.014021,-0.021170,-
10.028387,-0.035651,-0.042943,-0.050244,-0.057532,-0.064789,-0.0719
195,-0.079129,-0.086171,-0.093104,-0.099906,-0.106559,-0.113093,-0.
119541,-0.125934,-0.131304,-0.136935,-0.142309,-0.147811,-0.152228
12,-0.156759,-0.160927,-0.164789,-0.168300,-0.171470,-0.174287,-0.17
13
DATA F/-0.094815,-0.093915,-0.091177,-0.084562,-0.078963,-0.071100
14
15,-0.060818,-0.048195,-0.033512,-0.018759,0.002048,0.022984,0.04581
16,0.070918,0.097932,0.126938,0.157897,0.190770,0.225508,0.263060,0
17
1.300369,0.340371,0.381999,0.425181,0.469884,0.515896,0.563244,0.61
18
1.1833,0.661571,0.712321,0.764004,0.816516,0.869752,0.923401,0.97785
19
12,-0.032691,1.087700,1.142862,1.198055,1.253157,1.308043,1.362591
20
11259,1.416445,1.470165,1.522902,1.574802,1.625719,1.675522,1.724079,1.77
21
11259,1.816936,1.860975,1.903251,1.943633,1.981997
22
DATA F1/2.250000,2.250666,2.252684,2.255924,2.260349,2.265904,2.27
23
12545,2.280231,2.288928,2.298269,2.309248,2.32028,2.33333,2.34675
24
11,-2.361073,2.376291,2.392406,2.409414,2.427320,2.446130,2.465849,2
25
1-4.86485,2.508572,2.530574,2.550532,2.568518,2.603985,2.630480,2.65
26
18031,2.686666,2.716418,2.747321,2.779412,2.812734,2.847327,2.88324
27
12,-2.920529,2.959246,2.999447,3.041200,3.084570,3.129634,3.176471,3
28
1-2.25166,3.275810,3.328505,3.383357,3.440479,3.498999,3.562056,3.62
29
16788,3.69360,3.764940,3.838720,3.915903/
30
DATA F2/0.355556,0.355293,0.3551,0.3551,0.353236,0.351470,0.349229,0.34
31
16528,0.34380,0.339800,0.335801,0.33197,0.326401,0.32126,0.31589
32
12,0.31000,0.303782,0.297237,0.290340,0.283234,0.275804,0.268107,0
33
1.260156,0.251966,0.243549,0.234921,0.226093,0.217082,0.207899,0.19
34
1853,0.186077,0.176646,0.167306,0.159066,0.149987,0.139995,0.12995
35
11,0.118794,0.109071,0.099350,0.089397,0.079247,0.068912,0.058280,0
36
101765,-0.027914,-0.034496,-0.041284,-0.049286,-0.059486,-0.072867/
37
IF (AKD.LE.AK(1)) GO TO 5
IF (AKD.LE.AK(1)) GO TO 5
FD=F(I)
FID=F(I)
FZD=F(1)
AKD=AK(1)
RETURN
5 IF (AKD.GT.AK(55)) GO TO 10
FD=F(55)
FID=F(55)
FZD=F(55)
AKD=AK(55)
RETURN
10 DO 15 I=1,54
IF (AKD.LE.AK(I))-AND.AND.GT.AK(I+1)) GO TO 25
15 CONTINUE
WRITE (WRITE,20) AND
20 FORMAT (1X,6HAKD = ,E12.5,2XZM EXCEEDS ALLOWED RANGE)
CALL EXIT
25 POMP(I)=F(I)-F(I+1)+F(I+1)*P(I)/(AK(I)-AK(I+1))
P(I)=P(I)+F(I+1)-P(I+1)+P(I+1)*P(I)/(AK(I+1)-AK(I))

```

```

LAM 17
LAM 18
LAM 19
LAM 20
LAM 21
LAM 22
LAM 23
LAM 24
LAM 25
LAM 26
LAM 27
LAM 28
LAM 29
LAM 30
LAM 31
LAM 32
LAM 33
LAM 34
LAM 35
LAM 36
LAM 37
LAM 38
LAM 39
LAM 40
LAM 41
LAM 42
LAM 43
LAM 44
LAM 45
LAM 46
LAM 47
LAM 48
LAM 49
LAM 50
LAM 51
LAM 52
LAM 53
LAM 54
LAM 55
LAM 56
LAM 57
LAM 58
LAM 59
LAM 60
LAM 61
LAM 62
LAM 63
LAM 64
LAM 65
LAM 66
LAM 67
LAM 68
LAM 69
LAM 70
LAM 71
LAM 72
LAM 73
LAM 74
LAM 75
CF(I)=1000.0
MREAN(I)=2.554
I1=2
GO TO 20
STARTING CONDITIONS ASSUMING STAGNATION POINT
DUDX0=2.0*VCDEF(13,1)*STOTAL
DUDX0=2.0*VCDEF(12,1)*STOTAL**2
Z=0.0770/DUDX0
TMT(I)=SQRT(Z*VO)/(VIMP*STOTAL)
DELS(I)=TMT(I)*52.308
CF(I)=0.664*DUDEL(I)/(TMT(I)*VIMP*STOTAL/VO)
TAM(I)=CF(I)*1140.54*ROE*VIMP*VIMP
MREAN(I)=2.308
I1=2
GO TO 15
MREAN(I)=K(I)-1
GO TO 20
15 ANI=ANI-0.0452*DUDX0/(DUDX0**2)
GO TO 25
20 AKD=Z*DUDX(I)-1
CALL FFK(ARD,FD,FID,FZD)
ANI=ANI*FD/DUDEL(I)-1
DUDXP=0.5*(DUDX(I)-1)*DUDEL(I)
AKD=(Z+ANI/2.0)*DUDXP
CALL FFK(ARD,FD,FID,FZD)
ANI=ANI*FD/DUDEL
AM3=ANI*FD/DUDEL
AKD=(Z+AM3)*DUDX(I)
CALL FFK(ARD,FD,FID,FZD)
ANI=ANI*FD/DUDEL(I)
Z=Z*(ANI+2.0)*ANI**2.0*ANI**2.0*ANI**2.0*ANI**2.0*ANI**2.0
AKD=Z*DUDX(I)
CALL FFK(ARD,FD,FID,FZD)
DELS(I)=SQRT(Z*VO)/(VIMP*STOTAL)
CF(I)=0.664*DUDEL(I)/(TMT(I)*VIMP*STOTAL/VO)
TAM(I)=CF(I)*1140.54*ROE*VIMP*VIMP
MREAN(I)=DELS(I)/(TMT(I))
IF (TAM(I).LT.0.0) GO TO 40
IF (X(I)).GE.X(TRANS) GO TO 30
IF (I1.EQ.NP) GO TO 30
GO TO 10
30 IF (IWRITE.GT.1) RETURN
WRITE (IWRITE,35) X(I),I1
35 FORMAT (1X,16HTRANSITION AT X = ,F10.5,17H FOR STEP NUMBER ,I3)
RETURN
40 IF (IWRITE.GT.1) RETURN
IK=I1/IKK
WRITE (IWRITE,45) TAM(I),IK
45 FORMAT (1/27H NEGATIVE VALUE OF TAMST = ,E14.7,21H AT OR AFTER STA
TION ,I3,15H ON THE STREAMLINE,30H FOR MORE INFORMATION ON THE LOCA
TION,7,10H OF LAMINAR SEPARATION USE IWRITE = 0 PRINT OPTION, 7
THE TURBULENT ROUTINE IS CALLED AT THE SEPARATION POINT.)
RETURN
END

```









POTENTIAL FLOW PROGRAM SECTION 3  
 BEST CASESMA 182 WITH N=21 AND N=29 YIELDING 560 PANELS -- PUSELAGE ONLY

X VELOCITY=1.0 Y VELOCITY=0.0 I VELOCITY=0.0  
 ITERATIVE MATRIX SOLUTION INFORMATION

ITERATION	SUM OF CHANGES	A	B1	B2
1	0.49002E 01			
2	0.30909E 01			
3	0.24772E 01			
4	0.20167E 01			
5	0.16831E 01			
6	0.14274E 01	0.549E 00	0.421E 00	0.597E 00
7	0.12204E 01			
8	0.10719E 01			
9	0.09492E 00			
10	0.08946E 00			
A EXTRAPOLATION				
11	0.26799E-01	0.320E 00	0.500E 00	0.201E 00
12	0.34513E-01			
13	0.32543E-01			
14	0.30042E-01			
15	0.27939E-01			
A EXTRAPOLATION				
16	0.95009E-03	0.513E 00	0.499E 00	0.209E 00

POTENTIAL FLOW PROGRAM SECTION 4

BEST CASESMA 182 WITH N=21 AND N=29 YIELDING 560 PANELS -- PUSELAGE ONLY

PAGE = 1

X PLUM	X	Y	Z	VX	VY	VZ	ANG. V	CP	SOURCE	V NORM
PT:										
1	11.76403	0.00110	-1.22013	-0.44399	0.10321	-0.40094	0.07033	0.33907	0.00490	0.210
2	11.20092	0.10202	-1.77742	-0.96556	0.00935	-0.44133	1.06168	-0.12716	0.03070	0.200
3	11.76403	0.10053	-1.18403	-0.44108	0.23701	-0.45003	0.47906	0.33766	0.00413	0.210
4	11.19695	0.30250	-1.73500	-0.92927	0.00342	-0.47920	1.04368	-0.09346	0.04300	0.190
5	11.76403	0.20097	-1.13203	-0.40395	0.23216	-0.46504	0.05020	0.36667	0.09909	0.230
6	11.19695	0.49906	-1.67016	-0.88844	0.14293	-0.48453	1.02196	-0.04441	0.04709	0.180
7	11.76403	0.39513	-1.07360	-0.30390	0.32364	-0.40319	0.43002	0.37768	0.10934	0.210
8	11.19323	0.60437	-1.50009	-0.89990	0.23573	-0.49914	1.00239	-0.00470	0.05437	0.130
9	11.76403	0.49650	-1.00973	-0.40160	0.20190	-0.43246	0.45004	0.37226	0.10960	0.210
10	11.19407	0.89505	-1.47752	-0.89442	0.33213	-0.39107	0.99663	0.00672	0.05469	0.170
11										
12										
13										
14										
15										
16										
17										
18										
19										
20										
21										
22										
23										
24										
25										
26										
27										
28										
29										
30										
31										
32										
33										
34										
35										
36										
37										
38										
39										
40										
41										
42										
43										
44										
45										
46										
47										
48										
49										
50										
51										
52										
53										
54										
55										
56										
57										
58										
59										
60										

PRESSURE LIFT AND DRAG COEFFICIENTS

\*\*\*\*\*  
 PRESSURE CL = 0.00466  
 PRESSURE CD = 0.00400  
 REFERENCE AREA = 174.00000  
 REYNOLDS NUMBER = 0.30000 00  
 \*\*\*\*\*

POTENTIAL FLOW PROGRAM SECTION 5

BEST CASESMA 182 WITH N=21 AND N=29 YIELDING 560 PANELS -- PUSELAGE ONLY  
 PER V INFINITY = -1.0,0.0,0.0. COMPUTE 560 STREAMLINES STARTING AT EACH PANEL CENTROID POINT

LINE PASSING THROUGH QUADRILATERAL 2

I	X	Y	Z	CP	SL	UABS
1	11.50330	0.07060	-1.42204	0.19093	0.0	0.00466
2	11.20092	0.10202	-1.77742	-0.12716	0.37046	1.06168
3	10.87652	0.00400	-1.92773	-0.34735	0.73449	1.16075
4	10.20030	0.00110	-2.11460	-0.27059	1.42011	1.13073
5	0.47936	0.07097	-2.23746	-0.34901	2.16793	1.16101

TRANSITION AT X = 0.05049 FOR STEP NUMBER 7

S	V	DAIS	HREAN	DELTA	THETAS	TAN	CFI
0.0	179.89175	93.11142	2.95400	0.0	0.0	5000.00000	1000.00000
0.37046	200.72560	75.74790	2.41216	0.00073	0.00001	0.07993	0.00165
0.73449	226.20360	26.24503	2.46956	0.00096	0.00002	0.00011	0.00131
1.42011	222.90069	-21.90993	1.45000	0.00093	0.00003	0.02000	0.00044
2.16793	220.41102	90.24440	1.64000	0.00317	0.00000	0.13944	0.00303

Figure F-5. Continued.

LINE PASSING THROUGH QUADRILATERAL 4

I	X	Y	Z	CP	SL	UABS
1	11.54038	0.25242	-1.56896	0.20013	0.0	0.89435
2	11.19693	0.30250	-1.73560	-0.09396	0.38588	1.04569
3	10.87431	0.29672	-1.90791	-0.30112	0.35167	1.14667
4	10.20878	0.29660	-2.11429	-0.27854	1.44751	1.13072
5	9.47874	0.29589	-2.23589	-0.38547	2.18758	1.16662

TRANSITION AT X = 0.05928 FOR STEP NUMBER 7

S	V	DLOS	HMEAN	DELTA	THETAS	TAW	CFI
0.0	175.82773	81.47296	7.55400	0.0	0.0	5000.00000	1000.00000
0.38588	205.59162	88.15516	7.41685	0.00076	0.00001	0.07183	0.00196
0.78167	224.25491	29.85786	7.45881	0.00098	0.00002	0.05803	0.00126
1.44731	222.29994	-14.66576	1.45000	0.00093	0.00003	0.02455	0.00083
2.18758	229.74476	50.78996	7.64668	0.00313	0.00008	0.14129	0.00307
*	*	*	*	*	*	*	*
*	*	*	*	*	*	*	*
*	*	*	*	*	*	*	*
*	*	*	*	*	*	*	*
12.21214	169.03409	-24.48887	1.41431	0.04772	0.00130	0.05336	0.00120
12.99302	185.91722	10.80281	1.36538	0.04996	0.00150	0.05662	0.00123
14.03771	182.20955	15.13150	0.78832	0.03682	0.00118	0.08041	0.00175
15.33162	189.03224	1.41562	1.75374	0.03368	0.00110	0.08251	0.00201
16.74883	194.95903	1.55478	1.23150	0.03258	0.00108	0.10064	0.00219
18.23149	193.09097	-0.70904	1.22348	0.03509	0.00117	0.09881	0.00215
18.69722	192.79828	-0.09471	1.22072	0.03574	0.00120	0.09859	0.00213
19.73271	193.64034	-0.25937	1.21548	0.03716	0.00125	0.09811	0.00213
20.57314	193.26279	-0.72820	1.21228	0.03848	0.00130	0.09729	0.00212
21.46687	192.20120	-1.71849	1.21094	0.04033	0.00136	0.09541	0.00208

LINE PASSING THROUGH QUADRILATERAL 559

I	X	Y	Z	CP	SL	UABS
1	11.94265	0.09419	0.78633	0.01125	0.0	0.99436
2	10.87962	0.03990	0.90574	-0.27022	0.87761	1.12784
3	10.20865	0.04662	1.00875	0.11576	1.35268	0.94034
4	9.47910	0.05386	1.08324	0.30982	2.08594	0.83077
5	8.87325	0.06325	1.12966	0.51722	2.69560	0.69982
6	8.31187	0.08404	1.19076	0.80139	3.42033	0.77370
7	7.70868	0.09266	1.26921	-0.18974	4.13266	1.09733
8	7.12489	0.09784	2.21612	-0.58968	4.76632	1.26083
9	6.56250	0.09979	2.38662	-0.66089	5.34799	1.28878
10	5.95850	0.10097	2.42710	-0.75152	5.95921	1.32345
11	5.37951	0.10111	2.42705	-0.72915	6.53821	1.25644
12	4.79149	0.10061	2.36385	-0.13948	7.12812	1.15736
13	4.22950	0.09914	2.23461	-0.74647	7.69970	1.11644
14	3.68650	0.09722	2.17710	-0.74149	8.24616	1.11422
15	3.08350	0.09671	2.05210	-0.13959	8.86242	1.08487
16	2.50052	0.09175	1.92696	-0.08335	9.45869	1.04084
17	1.83348	0.08877	1.84390	-0.15435	10.13089	1.07441
18	1.18648	0.08840	1.67550	-0.15653	10.81881	1.07542
19	0.52038	0.08554	1.48817	0.00985	11.49193	0.99504
20	-0.14472	0.07453	1.23150	0.28034	12.20452	0.85992
21	-0.87460	0.05506	0.94854	0.79028	12.98756	0.86245
22	-1.91642	0.05208	0.88189	0.14268	14.03152	0.92592
23	-3.20849	0.04864	0.80107	0.06817	15.32612	0.96931
24	-4.62459	0.04673	0.74135	0.01688	16.74347	0.99153
25	-6.10451	0.04881	0.65489	0.02755	18.27591	0.98613
26	-7.60452	0.05782	0.61242	0.02848	19.72655	0.99566
27	-8.43732	0.06591	0.56108	0.03304	20.56097	0.98334
28	-9.33354	0.06529	0.50635	0.04475	21.45886	0.97762

NEGATIVE VALUE OF TAWST = -0.618394E-02 AT 0M AFTER STATION 2 ON THE STREAMLINE. FOR MORE INFORMATION ON THE LOCATION OF LAMINAR SEPARATION USE TWISTE = 0 PRINT OPTION. THE TURBULENT ROUTINE IS CALLED AT THE SEPARATION POINT.

S	V	DLOS	HMEAN	DELTA	THETAS	TAW	CFI
0.0	195.49095	65.61627	7.55400	0.0	0.0	5000.00000	1000.00000
0.47761	221.57565	-15.74668	2.62353	0.00116	0.00002	0.04004	0.00087
1.35266	184.87061	50.57137	1.64868	0.00293	0.00007	0.09873	0.00215
2.08593	163.32964	-37.20828	1.44820	0.00602	0.00017	0.08674	0.00189
2.89360	136.60424	-26.98951	1.54832	0.01300	0.00034	0.04921	0.00098
3.42033	152.10971	69.25374	1.29487	0.00903	0.00028	0.08480	0.00185
4.13244	215.36378	81.32014	1.25156	0.00402	0.00013	0.20391	0.00444
4.76632	247.87802	22.02628	1.27178	0.00382	0.00012	0.25658	0.00598
5.34799	253.34549	10.52014	1.27847	0.00478	0.00015	0.24877	0.00591
5.95521	260.22705	-2.75351	1.27622	0.00558	0.00018	0.25076	0.00594
6.53820	247.04973	-34.51620	1.29871	0.00789	0.00025	0.20260	0.00441
7.12812	227.54654	-25.96162	1.31625	0.01151	0.00036	0.15505	0.00337
7.69949	214.44673	-2.70016	1.29964	0.01374	0.00043	0.14219	0.00308
8.24616	219.05988	-7.68846	1.28346	0.01465	0.00047	0.14227	0.00310
8.86241	209.33728	-16.94574	1.29281	0.01802	0.00057	0.12284	0.00247
9.45868	204.62071	7.89397	1.27913	0.02012	0.00064	0.11680	0.00254
10.13088	211.25720	9.61184	1.25142	0.01843	0.00062	0.13022	0.00283
10.81880	211.42952	-10.79190	1.25007	0.01999	0.00065	0.12878	0.00280
11.49152	195.64638	-36.30284	1.29572	0.02742	0.00087	0.09726	0.00212
12.20491	169.00110	-25.48275	1.41969	0.04815	0.00139	0.05481	0.00119
12.98756	165.59624	10.76632	1.37049	0.05067	0.00151	0.05583	0.00121
14.03152	182.09966	13.11627	1.28881	0.03724	0.00118	0.07983	0.00174
15.32411	189.77525	3.42574	1.25443	0.03388	0.00111	0.09211	0.00200
16.74341	194.93204	1.62446	1.23261	0.03273	0.00109	0.10035	0.00218
18.23583	193.84407	-0.96972	1.22453	0.03975	0.00118	0.09851	0.00214
19.73271	193.78215	-0.10278	1.21583	0.04200	0.00125	0.09816	0.00214
20.56888	193.32541	-0.88039	1.21277	0.04396	0.00130	0.09722	0.00212
21.46587	192.19889	-1.75163	1.21080	0.04606	0.00137	0.09527	0.00207

Figure F-5. Continued.



POTENTIAL FLOW PROGRAM SECTION 2

BEST CESSNA 182 WITH N=21 AND N=29 YIELDING 560 PANELS -- FUSELAGE ONLY

POTENTIAL FLOW PROGRAM SECTION 3

BEST CESSNA 182 WITH N=21 AND N=29 YIELDING 560 PANELS -- FUSELAGE ONLY

X VELOCITY=-1.0 Y VELOCITY= 0.0 Z VELOCITY= 0.0

ITERATIVE MATRIX SOLUTION INFORMATION

ITERATION	SUM OF CHANGES	A	B1	B2
1	0.49780E 01			
2	0.32203E 01			
3	0.26497E 01			
4	0.22521E 01			
5	0.19827E 01			
6	0.17895E 01	0.532E 00	0.420E 00	0.599E 00
7	0.16792E 01			
8	0.16119E 01			
9	0.15901E 01			
10	0.16120E 01	0.497E 00	0.501E 00	0.259E 00
11	0.16777E 01			
12	0.17838E 01			
13	0.19420E 01			
14	0.21290E 01			
15	0.23450E 01	0.476E 00	0.500E 00	0.231E 00
16	0.25928E 01			
17	0.28768E 01			
18	0.32095E 01			
19	0.35924E 01			
20	0.40360E 01			
A EXTRAPOLATION				
		0.471E 00	0.500E 00	0.232E 00
21	0.80136E-01			
22	0.84759E-01			
23	0.90082E-01			
24	0.96259E-01			
25	0.10577E 00			
A EXTRAPOLATION				
		0.475E 00	0.500E 00	0.233E 00
26	0.47522E-02			

POTENTIAL FLOW PROGRAM SECTION 4

BEST CESSNA 182 WITH N=21 AND N=29 YIELDING 560 PANELS -- FUSELAGE ONLY

PAGE = 1

X FLOW	X	Y	Z	VX	VY	VZ	ABS.V	CP	SOURCE	V NORMAL
1	11.76403	0.06110	-1.22013	-0.44360	0.16120	-0.40653	0.67832	0.53988	0.88433	0.170-05
2	11.20092	0.10202	-1.77742	-0.96555	0.00935	-0.44131	1.06166	-0.12713	0.83079	0.888-05
3	11.76403	0.18033	-1.10403	-0.44189	0.23760	-0.43002	0.67499	0.53767	0.88814	0.268-05
4	11.19699	0.30250	-1.73560	-0.92927	0.05341	-0.47526	1.04567	-0.09943	0.84209	0.388-05
5	11.76403	0.25097	-1.13263	-0.40394	0.23214	-0.46509	0.65827	0.54668	0.89299	0.388-05
6	11.19651	0.49906	-1.67816	-0.88843	0.14254	-0.48451	1.02199	-0.04430	0.84704	-0.288-05
7	11.76403	0.39313	-1.07360	-0.39398	0.23263	-0.46310	0.65001	0.53749	0.10934	0.688-05
8	11.19323	0.68437	-1.58009	-0.89330	0.23374	-0.49912	1.00238	-0.00476	0.85437	-0.298-05
9	11.76403	0.49650	-1.00973	-0.40160	0.23189	-0.43264	0.65483	0.53225	0.10968	0.458-05
10	11.19487	0.89845	-1.47752	-0.85442	0.33212	-0.39109	0.99462	0.86675	0.87464	-0.418-05
.	.	.	.	.	.	.	.	.	.	.
.	.	.	.	.	.	.	.	.	.	.
.	.	.	.	.	.	.	.	.	.	.
.	.	.	.	.	.	.	.	.	.	.
590	-15.28517	0.20467	-0.10159	-0.97906	-0.06736	-0.04448	0.98230	0.83493	-0.06676	-0.698-05
591	-12.07821	0.31777	0.07299	-0.97743	-0.06127	-0.05956	0.98093	0.83779	-0.08764	-0.248-05
592	-15.28517	0.17480	-0.15172	-0.97875	-0.06090	-0.05406	0.98211	0.83946	-0.08675	-0.898-05
593	-12.07821	0.29566	0.11012	-0.97702	-0.05909	-0.06680	0.98063	0.83837	-0.08769	-0.248-05
594	-15.28517	0.14063	-0.12690	-0.97828	-0.06088	-0.05776	0.98176	0.83814	-0.08728	-0.698-05
595	-12.07821	0.18725	0.15297	-0.97670	-0.05819	-0.07600	0.98339	0.83883	-0.08798	-0.248-05
596	-15.28517	0.10300	-0.10772	-0.97800	-0.05898	-0.07443	0.98158	0.83658	-0.08728	-0.698-05
597	-12.07821	0.11422	0.17678	-0.97667	-0.05367	-0.08241	0.98023	0.83915	-0.08801	-0.248-05
598	-15.28517	0.06223	-0.09467	-0.97778	-0.05182	-0.08321	0.98199	0.83867	-0.08764	-0.698-05
599	-12.07821	0.03839	0.16871	-0.97636	-0.06001	-0.08571	0.98015	0.83931	-0.08807	-0.248-05
600	-15.28517	0.02112	-0.08806	-0.97763	-0.05929	-0.08463	0.98133	0.83788	-0.08764	-0.698-05

PRESSURE LIFT AND DRAG COEFFICIENTS

\*\*\*\*\*  
 PRESSURE CL = 0.80444  
 PRESSURE CD = 0.08491  
 REFERENCE AREA = 174.00000  
 REYNOLDS NUMBER = 8.3000E 08  
 \*\*\*\*\*

TOTAL BODY COEFFICIENTS

\*\*\*\*\*  
 TOTAL BODY CL = 0.80444  
 TOTAL BODY CD = 0.81249  
 REFERENCE AREA = 174.00000  
 REYNOLDS NUMBER = 8.3000E 08  
 BODY LENGTH = 24.41699  
 \*\*\*\*\*

Figure F-5. Continued.

## APPENDIX G- Theoretical Basis of Oeller's Method

If an inviscid two-dimensional flow is everywhere parallel to the surface of a closed body, then the surface of the body can be represented by a streamline on which the stream function,  $\psi$ , is constant. Oeller (Ref. 26) used this fact to develop a method for obtaining the potential flow about an airfoil. He replaced the airfoil surface by a vortex sheet and required that the sum of the stream function for a uniform stream and the stream function for the vortex sheet be a constant on the airfoil surface. This requirement is represented by the integral equation

$$\psi = z(s) V_{\infty} \cos \alpha - x(s) V_{\infty} \sin \alpha - \frac{1}{2\pi} \oint \gamma(s') \ln [r(s,s')] ds' \quad (G1)$$

where  $\psi$  is the unknown constant stream function value on the airfoil surface,  $V_{\infty}$  is the free stream velocity,  $\alpha$  is the angle between the free stream and the x-axis of the reference system,  $\gamma(s')$  is the vorticity strength at any point  $s'$  on the surface,  $r(s,s')$  is the distance between points  $s$  and  $s'$ , and  $x(s)$  and  $z(s)$  are the coordinates of the point of interest  $s$ .  $s$  and  $s'$  are arc lengths measured along the airfoil surface starting from the trailing edge.  $s$  is any fixed point on the airfoil surface while  $s'$  is the integration variable point which moves from the trailing edge over the airfoil surface back to the trailing edge. (See Figure G-1.)

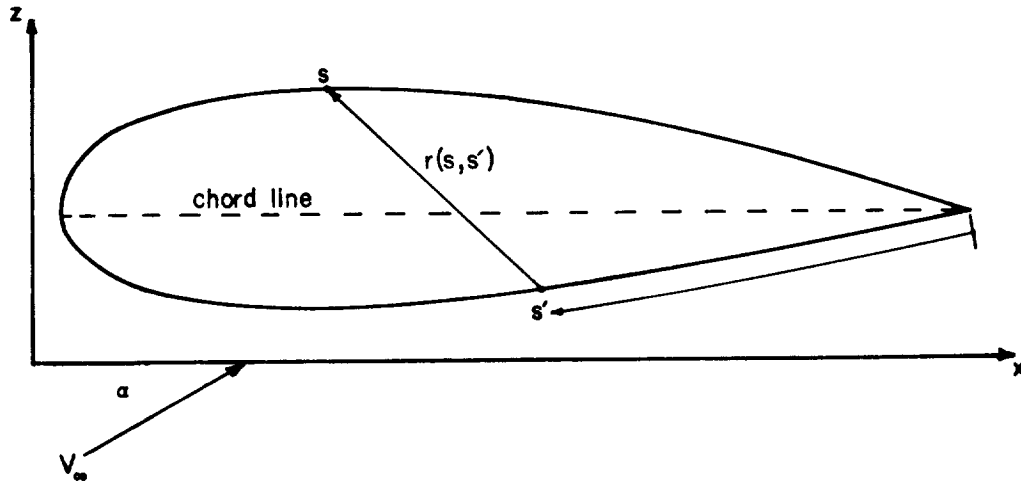


Figure G-1. Geometry for potential flow calculation.

Note that the reference system is chosen with its x-axis parallel to the airfoil chord line so that  $\alpha$  will be the angle of attack of the airfoil.

To solve Equation (G1) for  $\psi$  and  $\gamma(s')$ , the integral is approximated by a summation. The airfoil is divided into  $N$  segments,  $\gamma(s')$  is assumed constant on each segment, and Equation (G1) is applied at the mid-point of

each segment to yield the following system of simultaneous linear equations (see Figure G-2).

$$\psi = z_{c_i} V_\infty \cos \alpha - x_{c_i} V_\infty \sin \alpha - \sum_{j=1}^N K_{ij} \gamma_j \quad (G2)$$

for  $i = 1, 2, \dots, N$

where

$$K_{ij} = \frac{1}{2\pi} \int_{s_j}^{s_{j+1}} \ln [r(s_{c_i}, s')] ds'$$

and

$$x_{c_i} = (x_{i+1} + x_i)/2$$

$$z_{c_i} = (z_{i+1} + z_i)/2$$

are the coordinates of the midpoint of the  $i$ th segment. This point is called control point  $s_{c_i}$ , and it is the point where the requirement that  $\psi$  have a constant value is enforced.

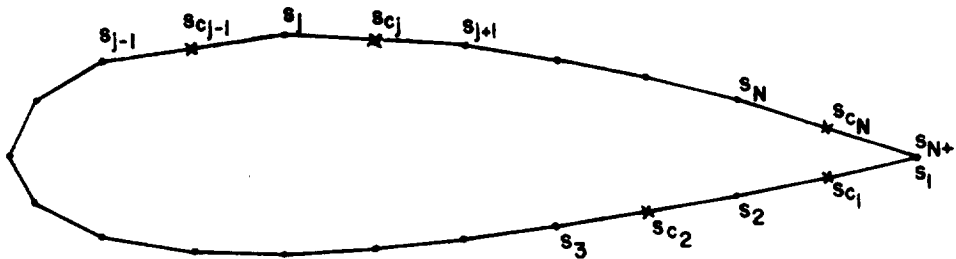


Figure G-2. Airfoil approximation by polygon.

$K_{ij}$  represents the influence coefficient for the effect of the vorticity of line segment  $j$  at the control point  $i$ . The influence of all of the line segments at control point  $i$  is obtained by summing over  $j$  as is done in Equation (G2). To obtain the required expressions for the  $K_{ij}$  we must evaluate the integrals

$$\int_{s_j}^{s_{j+1}} \ln [r(s_{c_i}, s')] ds' .$$

First consider the case where  $i \neq j$ , *i.e.* the  $i$ th control point  $(x_{c_i}, z_{c_i})$  does not lie on the  $j$ th segment of the airfoil as shown in the figure on the following page.

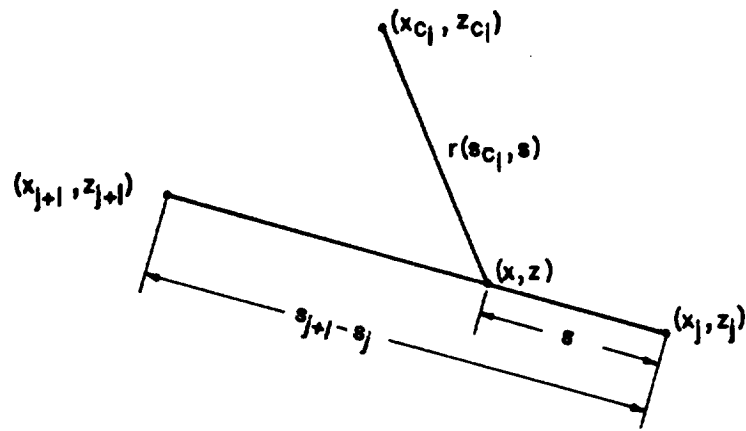


Figure G-3. Geometry for calculation of  $K_{ij}$ ,  $i \neq j$ .

Now with a change in variables from  $s'$  to  $s$  ( $s = s' - s_j$ ),

$$\int_{s_j}^{s_{j+1}} \ln [r(s_{c_1}, s')] ds' = \int_0^{s_{j+1} - s_j} \ln [r(s_{c_1}, s)] ds. \quad (G3)$$

In the above figure,  $x$  and  $z$  are the coordinates of the moving integration variable point  $s$  which moves from point  $(x_j, z_j)$  to point  $(x_{j+1}, z_{j+1})$  as  $s$  changes from 0 to  $s_{j+1} - s_j$ . Since we are considering a straight line segment

$$\begin{aligned} x &= x_j + \frac{(x_{j+1} - x_j)}{(s_{j+1} - s_j)} s \\ z &= z_j + \frac{(z_{j+1} - z_j)}{(s_{j+1} - s_j)} s \\ r^2 &= (x - x_{c_1})^2 + (z - z_{c_1})^2 \\ &= s^2 + \frac{2}{(s_{j+1} - s_j)} \left[ (x_j - x_{c_1})(x_{j+1} - x_j) + (z_j - z_{c_1})(z_{j+1} - z_j) \right] s \\ &\quad + (x_j - x_{c_1})^2 + (z_j - z_{c_1})^2 \\ &= s^2 + bs + a \end{aligned} \quad (G4)$$

for  $0 \leq s \leq s_{j+1} - s_j$ .

Now

$$\begin{aligned} \int \ln [r(s_{c_i}, s)] ds &= \int \ln \{ [r^2(s_{c_i}, s)]^{1/2} \} ds \\ &= \frac{1}{2} \int \ln [r^2(s_{c_i}, s)] ds ; \end{aligned} \quad (G5)$$

therefore

$$\begin{aligned} \int_{s_j}^{s_{j+1}} \ln [r(s_{c_i}, s')] ds' &= \frac{1}{2} \int_0^{s_{j+1}-s_j} \ln [r^2(s_{c_i}, s)] ds \\ &= \frac{1}{2} \int_0^{s_{j+1}-s_j} \ln [s^2 + bs + a] ds \\ &= \frac{1}{2} \left[ \left( s + \frac{b}{2} \right) \ln (s^2 + bs + a) - 2s \right. \\ &\quad \left. + \sqrt{4a - b^2} \tan^{-1} \left( \frac{2s + b}{\sqrt{4a - b^2}} \right) \right]_0^{s_{j+1}-s_j} . \end{aligned} \quad (G6)$$

The integral has this value provided  $4a - b^2 > 0$ . That this is always true for this representation of airfoils can be shown by substituting the expressions for  $a$  and for  $b$  from Equation (G3) into  $4a - b^2$  to obtain

$$\begin{aligned} 4a - b^2 &= 4 \left[ \frac{(x_j - x_{c_i})(z_{j+1} - z_j) - (z_j - z_{c_i})(x_{j+1} - x_j)}{(s_{j+1} - s_j)} \right]^2 \\ &> 0 . \end{aligned}$$

Also

$$\begin{aligned} \sqrt{4a - b^2} &= 2 \left| \frac{(x_j - x_{c_i})(z_{j+1} - z_j) - (z_j - z_{c_i})(x_{j+1} - x_j)}{(s_{j+1} - s_j)} \right| \\ &= 2C \end{aligned} \quad (G7)$$

where the absolute value signs are used to insure that the positive square root is obtained.

To obtain a final expression for Equation (G6) we must evaluate the terms  $s + b/2$  and  $s^2 + bs + a$  for  $s = 0$  and for  $s = s_{j+1} - s_j$ , corresponding to the two ends of the  $j$ th line segment. For  $s = s_{j+1} - s_j = \Delta s$ ,

$$\begin{aligned} s^2 + bs + a &= (x_{j+1} - x_{c_i})^2 + (z_{j+1} - z_{c_i})^2 \\ &= R2 \end{aligned} \quad (G8)$$

$$\begin{aligned} s + b/2 &= \left[ (x_{j+1} - x_{c_i})(x_{j+1} - x_j) + (z_{j+1} - z_{c_i})(z_{j+1} - z_j) \right] / \Delta s \\ &= T2 . \end{aligned}$$



For  $s = 0$

$$\begin{aligned} s^2 + bs + a &= (x_j - x_{c_i})^2 + (z_j - z_{c_i})^2 \\ &= R1 \end{aligned}$$

$$\begin{aligned} s + b/2 &= \left[ (x_j - x_{c_i})(x_{j+1} - x_j) + (z_j - z_{c_i})(z_{j+1} - z_j) \right] / \Delta s \\ &= T1 \end{aligned} \quad (G9)$$

Substituting the above expressions into Equation (G6) and Equation (G2) we obtain

$$K_{ij} = \frac{1}{4\pi} \left[ T2 \ln(R2) - T1 \ln(R1) \right] - \frac{\Delta s}{2\pi} + \frac{C}{2\pi} \left[ \tan^{-1} \left( \frac{T2}{C} \right) - \tan^{-1} \left( \frac{T1}{C} \right) \right] \quad (G10)$$

for  $i \neq j$ .

Now consider the case where  $i = j$ , *i.e.* the *i*th control point lies on the *j*th segment as shown in the figure below.

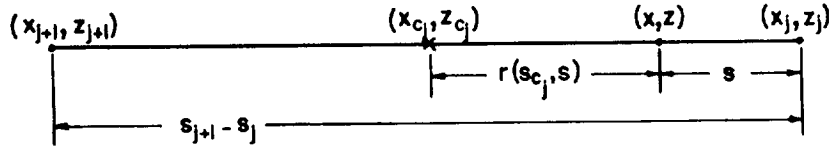


Figure G-4. Geometry for calculation of  $K_{jj}$ .

Here we have (letting  $\Delta s = s_{j+1} - s_j$ )

$$r(s_{c_j}, s) = \frac{\Delta s}{2} - s \quad \text{for} \quad 0 \leq s \leq \frac{\Delta s}{2}$$

and

$$r(s_{c_j}, s) = s - \frac{\Delta s}{2} \quad \text{for} \quad \frac{\Delta s}{2} \leq s \leq \Delta s.$$

Thus for Equation (G3) we have

$$\begin{aligned} \int_0^{s_{j+1} - s_j} \ln[r(s_{c_j}, s)] ds &= \int_0^{\Delta s/2} \ln \left[ \frac{\Delta s}{2} - s \right] ds + \int_{\Delta s/2}^{\Delta s} \ln \left[ s - \frac{\Delta s}{2} \right] ds \\ &= \Delta s \left[ \ln \left( \frac{\Delta s}{2} \right) - 1 \right] \end{aligned} \quad (G11)$$

and therefore

$$K_{jj} = \frac{\Delta s}{2\pi} \left[ \ln \left( \frac{\Delta s}{2} \right) - 1 \right]. \quad (G12)$$

Equation (G2) represents a system of N equations in N + 1 unknowns, *i.e.*  $\gamma_1, \gamma_2, \dots, \gamma_N$  and  $\psi$ . The additional equation needed to close the system is obtained from the Kutta condition which is represented by

$$\gamma_N (s_{N+1} - s_N) = -\gamma_1 (s_2 - s_1) . \quad (G13)$$

Although Equation (G13) appears to be a rather odd way to express the Kutta condition, the discussion below will show that it is indeed correct.

The solution of the system of Equations (G2) plus Equation (G13) gives a set of  $\gamma_j$ 's for the N segments of the airfoil. These vorticity strengths,  $\gamma_j$ 's, are the same as the actual local tangential velocities at the mid-chord control points. Because only the body points are stored in the program and all calculations are referred to these body points, one observes (refer to Figure G-2) that what is actually desired are the local tangential velocities at the body points which are the end points of the line segments. Therefore, some form of an averaging procedure is needed to obtain the vorticity at a body point from the vorticities on the two line segments that join at the body point. Letting  $\bar{\gamma}_j$  denote the vorticity (and thus the local tangential velocity) at body point  $s_j$ , the correct averaging procedure is

$$\begin{aligned} \bar{\gamma}_j &= \left[ \gamma_j (s_{c_j} - s_j) + \gamma_{j-1} (s_j - s_{c_{j-1}}) \right] / (s_{c_j} - s_{c_{j-1}}) \\ &= \left[ \gamma_j (s_{j+1} - s_j) + \gamma_{j-1} (s_j - s_{j-1}) \right] / (s_{j+1} - s_{j-1}) . \end{aligned} \quad (G14)$$

Since  $\gamma$  times a line segment length is the circulation due to a vortex sheet of that length, Equation (G14) is equivalent to requiring the circulation due to  $\bar{\gamma}_j$  on the line segment  $s_{c_j} - s_{c_{j-1}}$  be the same as the circulation due to  $\gamma_{j-1}$  on line segment  $s_j - s_{c_{j-1}}$  plus the circulation due to  $\gamma_j$  on line segment  $s_{c_j} - s_j$ .

Now consider the Kutta condition represented in Equation (G13). Substituting Equation (G13) into Equation (G14) gives

$$\bar{\gamma}_1 = \bar{\gamma}_{N+1} = 0$$

and thus there is a stagnation point at the trailing edge which is the Kutta condition.

As discussed on page 122, the program actually uses a modified Kutta condition which states that the upper and lower surface velocities at the trailing edge are equal but not necessarily zero. For this case, the trailing edge velocities  $\bar{\gamma}_1$  and  $\bar{\gamma}_{N+1}$  are calculated from

$$\bar{\gamma}_1 = \bar{\gamma}_{N+1} = \frac{|\gamma_1|(s_2 - s_1) + |\gamma_N|(s_{N+1} - s_N)}{(s_2 - s_1 + s_{N+1} - s_N)} . \quad (G16)$$

All other body point velocities are calculated using Equation (G14).

## APPENDIX H-Rapid, Inviscid Computation of the Pressure Distribution of Symmetrical Airfoils for Mach Numbers Less Than or Equal To 1.0

Prior to undertaking the present study, the senior author had the occasion to estimate the characteristics of some unusual symmetrical airfoils at Mach numbers from zero to unity. These airfoils were reportedly capable of relatively low drag at transonic speeds. It was the intention of the research to test models of these airfoils and to develop fairly simple, yet reasonably accurate, methods for predicting their behavior. The reader will recognize that the development of such methods usually follows one of two paths: either some new bit of physical or mathematical insight is uncovered which permits one to legitimately simplify the formulation of the problem or its method of solution; or one seeks to find or assemble correlations among empirical results. To pursue the first path—certainly the more elegant and distinctive of the two—requires that the researcher be struck by unusual inspiration, an occurrence that is not always within his power to command, at least during a fixed time interval. For this reason many simple, but reasonably accurate, prediction methods are at least semi-empirical.

In reviewing some of the semi-empirical methods given in the literature for predicting the pressure distribution on airfoils at free stream Mach numbers near unity it was found that they require as a starting condition the pressure distribution at  $M_{CRITICAL}$ . Thus in order for one to investigate the utility of these methods or modifications thereof it would be necessary to have some fairly reliable means of predicting the  $M_{CR}$  pressure distribution. The task of mounting the computer program discussed in NASA CR-1843 (Ref. 34) seemed to be more involved than was warranted by the uncertainties of the final result. For this reason it was decided to obtain the pressure distribution by using the 16-point Weber method (Ref. 20) to which had been added a Kármán-Tsien Mach number correction. This method is easily programmed for computer solution because Weber, by fixing the chordwise location of the 16 points (see Table H-1) at which the pressure is computed, was able to determine, once and for all, coefficients by which the airfoil ordinates at these 16 points could be multiplied and the results summed to find the surface pressures and velocities. One merely supplies these coefficients (which are given in Weber's paper and here in Tables H-2 through H-7) as a permanent data set and the ordinates of the airfoil for which the pressures are desired as a changeable data set. It must be understood, however, that this form of Weber's method is restricted to inviscid flow about symmetrical airfoils. Thus it can be expected to give reasonable lift and moment values only for relatively thin airfoils at moderate-to-small angles of attack. No drag values can be obtained.

Because of its simplicity the method permits the calculations to be carried out very rapidly by even the smallest computer. It therefore seems well suited for use by those who would be satisfied to investigate the characteristics of new symmetrical airfoils in a more qualitative fashion, those whose access to larger machines or computing funds is restricted, or those with limited skill or time to mount foreign programs. The accuracy of the method is quite good except in the immediate vicinity of the leading edge as can be seen in Figure H-1.

The computer program for performing the calculations required by the 16-point Weber method was given the name TRINSON. This program provides the pressure data upon which a second program, COMPR, operates to modify the pressure distribution for Mach numbers other than zero. As noted above, below  $M_{CR}$ , a Kármán-Tsien correction is used. For  $M > M_{CR}$  a series of semi-empirical correlations are used to obtain the pressure distribution over the complete airfoil surface. These are described in more detail in Ref. 103. Essentially, the procedure uses an approximate analytical method (by Truitt, Ref. 104) to locate the shock on the airfoil at  $M = 1$ . The pressure distribution between the shock and the sonic point at  $M = 1.0$  is found from the correlation of Thompson and Wilby (Ref. 106). Sinnott's (Ref. 105) semi-empirical correlation, which gives the pressure distribution aft of the airfoil peak in terms of the pressure distributions at  $M = 1$  and  $M = M_{CR}$ , is used for intermediate Mach numbers. A spline fit of pressure data at the airfoil peak and that near the sonic point plus the idea that the pressure distribution on blunt bodies in supersonic flow "freezes" (does not change with changes in  $M_\infty$ ) are used to represent the airfoil surface pressures between the leading edge and the airfoil peak. The pressure rise through the shockwave is then "smeared out" following the empirical result presented in Schlichting (Ref. 65) that the pressure rise occurs over a streamwise distance of about 50 boundary layer thicknesses for laminar boundary layers and over about 12 boundary layer thicknesses for turbulent boundary layers.

Comparisons between the predictions obtained through the use of TRINSON and COMPR and experimental data for one airfoil obtained in the NCSU transonic wind tunnel are shown in Figure H-2. Note that qualitatively the agreement is quite good; quantitatively, however, the predictions do not match the experimental results as closely as one might expect for Mach numbers just above the critical. In particular, it is evident that for Mach numbers between  $M_{CR}$  ( $\sim 0.77$ ) and  $M_\infty = 0.85$  the pressure rise through the shock is even more "smeared out" than that suggested by the 50 $\delta$  criterion. On the other hand, for  $M > 0.85$  this concept seems to give very good results.

On the basis of these results an effort was made to develop a somewhat more accurate prediction by using the 32-point Weber method, given here as TRANSON, and a more accurate representation of the pressure rise through a shock. Experimental data showing pressures during the interaction of very weak normal shocks with laminar boundary layers seem to be quite scarce as are correlations identifying the governing parameters in a useable fashion.

As a result, it was not possible to find a model analogous to the  $50\delta$  concept which was capable of accurately representing the pressure rise through the shock at all Mach numbers from  $M_{CR}$  to  $M = 1.0$ . Also, the 32-point Weber method does not appear to give results markedly different from those obtained by the 16-point method except for the first 10 percent of the airfoil chord. Apparently, off-body viscous effects, which are of course inadequately described by any potential flow treatment or, for that matter, even by simple boundary layers added to potential flows, are sufficiently prominent in the experimental data to prevent one from achieving a better prediction using this approach.

Since these computer programs have not been previously made available in any form and since they provide comparatively rapid, at least qualitatively accurate, predictions of the pressure distribution on a limited, but highly useable class of airfoils for all Mach numbers less than or equal to unity, it was felt that inclusion of these programs here may prove helpful to many readers: Those who, on occasion, may not wish to incur the expense of running the 65-point airfoil program and who are thereby willing to accept the inherent limitations of the shorter programs; and those who wish at least a qualitative prediction of airfoil lift and moment characteristics at Mach numbers above the applicable range of the 65-point program. The following discussion provides listings of three programs, instructions for entering data, and typical output.

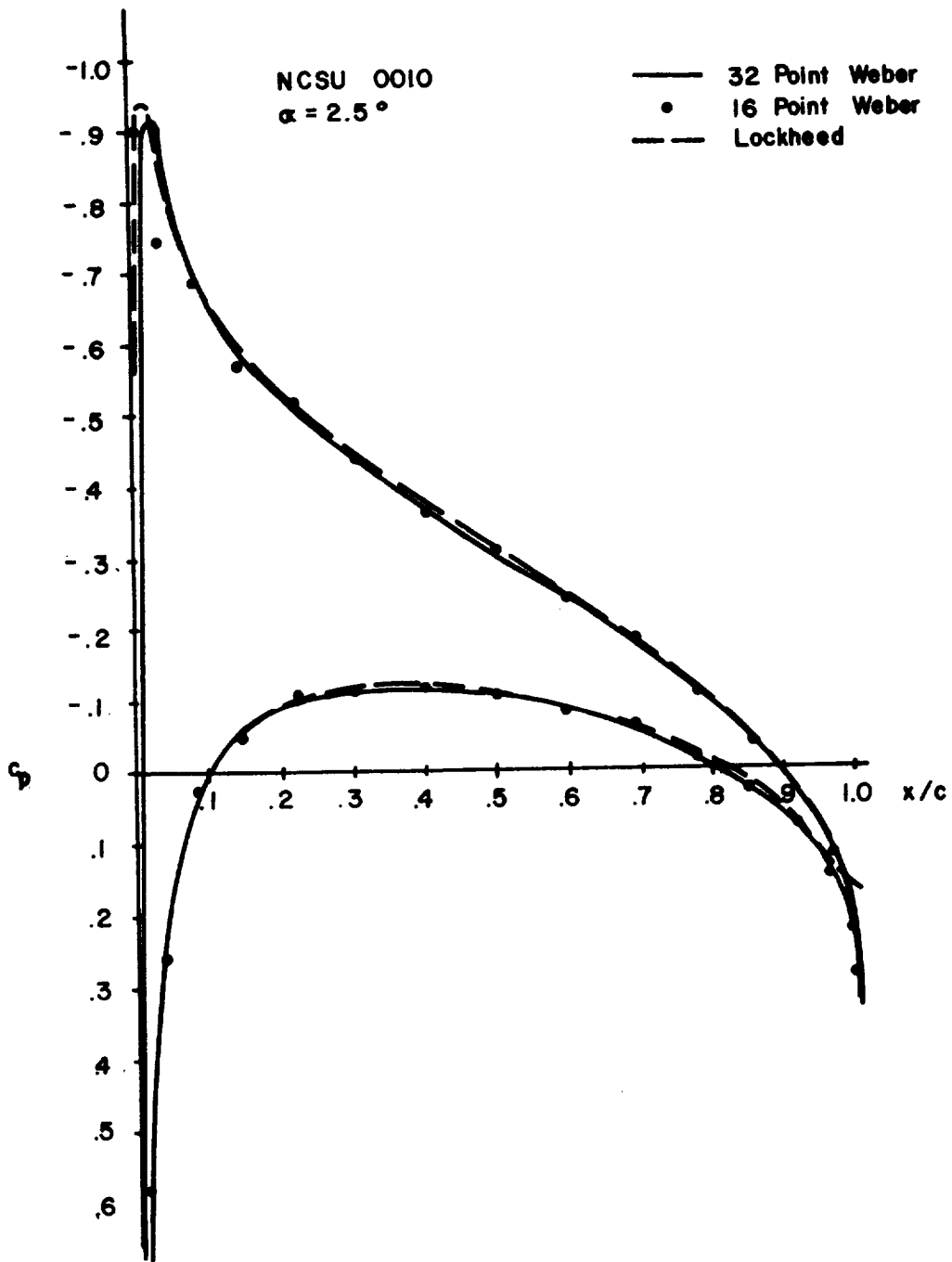


Figure H-1. Comparison of 16 point Weber, 32 point Weber, and 65 point Lockheed methods for predicting airfoil pressure distributions on the NCSU 0010 at  $\alpha = 2.5^\circ$ .

*Position of the Pivotal Points*

N = 8		N = 16		N = 32	
y	x <sub>p</sub>	y	x <sub>p</sub>	y	x <sub>p</sub>
0	1.0000	0	1.0000	0	1.0000
1	0.9619	1	0.9904	1	0.9976
		2	0.9619	2	0.9904
		3	0.9157	3	0.9785
		4	0.8536	4	0.9619
		5	0.7778	5	0.9410
		6	0.6913	6	0.9157
		7	0.5975	7	0.8865
		8	0.5000	8	0.8536
		9	0.4025	9	0.8172
		10	0.3087	10	0.7778
		11	0.2222	11	0.7357
		12	0.1464	12	0.6913
		13	0.08427	13	0.6451
		14	0.03806	14	0.5975
		15	0.00961	15	0.5490
		16	0	16	0.5000
				17	0.4510
				18	0.4025
				19	0.3549
				20	0.3087
				21	0.2643
				22	0.2222
				23	0.1828
				24	0.1464
				25	0.1135
				26	0.08427
				27	0.05904
				28	0.03806
				29	0.02153
				30	0.00961
				31	0.00241
				32	0

Table H-1. Position of the pivotal points.

$s_{\mu}^{(1)}$  for  $N = 16$ 

$\mu$	1	2	3	4	5	6	7	8	9	10	11	12	13	14	15	16
1	82.013	-15.061	0	-0.651	0	-0.136	0	-0.051	0	-0.026	0	-0.017	0	-0.013	0	-0.012
2	-29.544	41.810	-11.203	0	-0.705	0	-0.180	0	-0.076	0	-0.044	0	-0.031	0	-0.026	0
3	0	-16.265	28.799	-8.990	0	-0.690	0	-0.201	0	-0.094	0	-0.059	0	-0.045	0	-0.041
4	-2.360	0	-11.430	22.627	-7.698	0	-0.674	0	-0.217	0	-0.111	0	-0.075	0	-0.062	0
5	0	-1.532	0	-9.052	19.243	-6.954	0	-0.673	0	-0.236	0	-0.130	0	-0.095	0	-0.086
6	-0.646	0	-1.147	0	-7.727	17.318	-6.563	0	-0.692	0	-0.262	0	-0.157	0	-0.124	0
7	0	-0.462	0	-0.935	0	-6.968	16.314	-6.442	0	-0.735	0	-0.301	0	-0.196	0	-0.172
8	-0.280	0	-0.362	0	-0.810	0	-6.569	16.000	-6.569	0	-0.810	0	-0.362	0	-0.280	0
9	0	-0.196	0	-0.301	0	-0.735	0	-6.442	16.314	-6.968	0	-0.935	0	-0.462	0	-0.378
10	-0.124	0	-0.157	0	-0.282	0	-0.692	0	-6.563	17.318	-7.727	0	-1.147	0	-0.646	0
11	0	-0.095	0	-0.130	0	-0.236	0	-0.673	0	-6.954	19.243	-9.052	0	-1.532	0	-1.052
12	-0.062	0	-0.075	0	-0.111	0	-0.217	0	-0.674	0	-7.698	22.627	-11.430	0	-2.360	0
13	0	-0.045	0	-0.059	0	-0.094	0	-0.201	0	-0.690	0	-8.990	28.799	-16.265	0	-4.890
14	-0.026	0	-0.031	0	-0.044	0	-0.076	0	-0.180	0	-0.705	0	-11.203	41.810	-29.544	0
15	0	-0.013	0	-0.017	0	-0.026	0	-0.051	0	-0.136	0	-0.651	0	-15.061	82.013	-132.103

Table H-2. Weber coefficients  $S^{(1)}$  for the 16 point method.



$s_m^m$  for  $N = 16$

$\mu$	1	2	3	4	5	6	7	8	9	10	11	12	13	14	15
1	25.769	17.917	-4.703	2.016	-1.104	0.706	-0.506	0.398	-0.338	0.310	-0.305	0.327	-0.388	0.535	-1.020
2	-68.941	6.309	14.908	-4.983	2.489	-1.531	1.071	-0.828	0.697	-0.634	0.622	-0.664	0.785	-1.082	2.060
3	38.144	-31.420	2.694	12.636	-4.844	2.680	-1.780	1.336	-1.104	0.991	-0.963	1.021	-1.203	1.654	-3.143
4	-26.486	17.048	-20.468	1.414	11.224	-4.718	2.816	-2.000	1.598	-1.405	1.347	-1.414	1.654	-2.266	4.295
5	20.046	-11.798	10.849	-15.519	0.804	10.411	-4.704	2.993	-2.259	1.918	-1.800	1.862	-2.158	2.937	-5.548
6	-15.836	8.922	-7.411	8.054	-12.854	0.448	10.043	-4.828	3.261	-2.613	2.369	-2.396	2.739	-3.696	6.946
7	12.797	-7.033	5.548	-5.418	6.546	-11.318	0.203	10.055	-5.126	3.675	-3.143	3.075	-3.439	4.581	-8.551
8	-10.453	5.657	-4.330	4.000	-4.330	5.657	-10.453	0	10.453	-5.657	4.330	-4.000	4.330	-5.657	10.453
9	8.551	-4.581	3.439	-3.075	3.143	-3.675	5.126	-10.055	-0.203	11.318	-6.546	5.418	-5.548	7.033	-12.797
10	-6.946	3.686	-2.739	2.388	-2.369	2.613	-3.261	4.828	-10.043	-0.448	12.854	-8.054	7.411	-8.922	15.836
11	5.548	-2.937	2.158	-1.862	1.800	-1.918	2.259	-2.993	4.704	-10.411	-0.804	15.519	-10.849	11.798	-20.046
12	-4.295	2.266	-1.654	1.414	-1.347	1.405	-1.598	2.000	-2.816	4.718	-11.224	-1.414	20.468	-17.048	26.486
13	3.143	-1.654	1.203	-1.021	0.963	-0.991	1.104	-1.336	1.780	-2.680	4.844	-4.844	-2.694	31.420	-38.144
14	-2.060	1.082	-0.785	0.664	-0.622	0.634	-0.697	0.828	-1.071	1.531	-2.499	4.993	-4.993	-14.908	68.941
15	1.020	-0.535	0.388	-0.327	0.305	-0.310	0.338	-0.398	0.506	-0.706	1.104	-2.016	4.703	-17.917	-25.769

Table H-3. Weber coefficients  $s(2)$  for the 16 point method.

$s_m^{(3)}$  for  $N = 16$

$\mu$	1	2	3	4	5	6	7	8	9	10	11	12	13	14	15	16
1	82.013	7.458	0	4.031	0	2.006	0	1.256	0	0.914	0	0.742	0	0.659	0	0.635
2	-41.024	41.810	-4.134	0	1.068	0	0.716	0	0.507	0	0.388	0	0.341	0	0.317	0
3	0	-21.134	28.799	-5.362	0	0.313	0	0.340	0	0.276	0	0.234	0	0.211	0	0.204
4	-3.562	0	-14.273	22.627	-5.365	0	0.016	0	0.175	0	0.169	0	0.155	0	0.147	0
5	0	-2.349	0	-11.036	19.243	-5.215	0	-0.132	0	0.084	0	0.108	0	0.108	0	0.107
6	-1.098	0	-1.750	0	-9.293	17.318	-5.121	0	-0.224	0	0.026	0	0.066	0	0.074	0
7	0	-0.811	0	-1.433	0	-8.326	16.314	-5.136	0	-0.293	0	-0.019	0	0.032	0	0.042
8	-0.515	0	-0.662	0	-1.280	0	-7.850	16.000	-5.287	0	-0.360	0	-0.061	0	-0.005	0
9	0	-0.424	0	-0.584	0	-1.176	0	-7.749	16.314	-5.609	0	-0.437	0	-0.112	0	-0.062
10	-0.323	0	-0.380	0	-0.551	0	-1.160	0	-8.006	17.318	-6.162	0	-0.544	0	-0.193	0
11	0	-0.298	0	-0.369	0	-0.557	0	-1.215	0	-8.694	19.243	-7.068	0	-0.716	0	-0.376
12	-0.271	0	-0.305	0	-0.391	0	-0.609	0	-1.365	0	-10.031	22.627	-8.587	0	-1.068	0
13	0	-0.301	0	-0.351	0	-0.465	0	-0.742	0	-1.692	0	-12.599	28.799	-11.385	0	-2.220
14	-0.369	0	-0.403	0	-0.485	0	-0.660	0	-1.076	0	-2.479	0	-18.273	41.810	-18.064	0
15	0	-0.686	0	-0.776	0	-0.966	0	-1.357	0	-2.279	0	-5.334	0	-37.590	82.013	-65.410
16	-0.063	0	-0.068	0	-0.080	0	-0.105	0	-0.155	0	-0.281	0	-0.742	0	-6.505	0

Table H-4. Weber coefficients  $S^{(3)}$  for the 16 point method.

$s_{\mu}^{(1)}$  for  $N = 32$

$\mu$	1	2	3	4	5	6	7	8	9	10	11	12	13	14	15	16
1	326.474	-59.103	0	-2.410	0	-0.457	0	-0.148	0	-0.063	0	-0.033	0	-0.019	0	-0.012
2	-117.636	164.027	-42.889	0	-2.495	0	-0.565	0	-0.203	0	-0.094	0	-0.051	0	-0.031	0
3	0	-63.816	110.237	-33.198	0	-2.305	0	-0.581	0	-0.225	0	-0.110	0	-0.063	0	-0.040
4	-9.409	0	-43.765	83.620	-27.171	0	-2.102	0	-0.571	0	-0.234	0	-0.119	0	-0.070	0
5	0	-6.029	0	-33.470	67.883	-23.149	0	-1.928	0	-0.553	0	-0.236	0	-0.125	0	-0.076
6	-2.591	0	-4.411	0	-27.287	57.599	-20.321	0	-1.788	0	-0.536	0	-0.237	0	-0.129	0
7	0	-1.837	0	-3.484	0	-23.207	50.442	18.258	0	-1.677	0	-0.520	0	-0.237	0	-0.133
8	-1.065	0	-1.416	0	-2.892	0	-20.350	45.255	16.717	0	-1.591	0	-0.509	0	-0.238	0
9	0	-0.805	0	-1.153	0	-2.488	0	-18.275	41.397	-15.552	0	-1.525	0	-0.501	0	-0.240
10	-0.538	0	-0.645	0	-0.976	0	-2.198	0	16.728	38.486	-14.689	0	-1.477	0	-0.496	0
11	0	-0.425	0	-0.538	0	-0.850	0	-1.984	0	-15.560	36.284	-14.008	0	-1.444	0	-0.496
12	-0.308	0	-0.350	0	-0.463	0	-0.758	0	-1.823	0	-14.674	34.637	-13.527	0	-1.425	0
13	0	-0.251	0	-0.298	0	-0.408	0	-0.688	0	-1.700	0	-14.010	33.440	-13.199	0	-1.420
14	-0.192	0	-0.211	0	-0.290	0	-0.367	0	-0.635	0	-1.606	0	-13.529	32.627	-13.010	0
15	0	-0.160	0	-0.182	0	-0.231	0	-0.335	0	-0.594	0	-1.535	0	-13.201	32.155	-12.948
16	-0.126	0	-0.137	0	-0.161	0	-0.209	0	-0.311	0	-0.563	0	-1.483	0	-13.011	32.000
17	0	-0.107	0	-0.119	0	-0.144	0	-0.192	0	-0.291	0	-0.538	0	-1.448	0	-12.948
18	-0.087	0	-0.092	0	-0.106	0	-0.131	0	-0.178	0	-0.276	0	-0.520	0	-1.427	0
19	0	-0.074	0	-0.081	0	-0.095	0	-0.120	0	-0.167	0	-0.264	0	-0.508	0	-1.420
20	-0.061	0	-0.064	0	-0.072	0	-0.086	0	-0.112	0	-0.158	0	-0.255	0	-0.500	0
21	0	-0.052	0	-0.057	0	-0.065	0	-0.079	0	-0.105	0	-0.151	0	-0.248	0	-0.496
22	-0.043	0	-0.045	0	-0.050	0	-0.059	0	-0.073	0	-0.099	0	-0.145	0	-0.243	0
23	0	-0.037	0	-0.040	0	-0.045	0	-0.054	0	-0.068	0	-0.093	0	-0.140	0	-0.240
24	-0.031	0	-0.032	0	-0.035	0	-0.040	0	-0.049	0	-0.064	0	-0.089	0	-0.136	0
25	0	-0.026	0	-0.028	0	-0.031	0	-0.036	0	-0.045	0	-0.059	0	-0.085	0	-0.133
26	-0.021	0	-0.022	0	-0.024	0	-0.027	0	-0.032	0	-0.041	0	-0.055	0	-0.080	0
27	0	-0.017	0	-0.018	0	-0.020	0	-0.023	0	-0.029	0	-0.037	0	-0.051	0	-0.076
28	-0.013	0	-0.013	0	-0.015	0	-0.017	0	-0.020	0	-0.025	0	-0.032	0	-0.046	0
29	0	-0.010	0	-0.010	0	-0.011	0	-0.013	0	-0.016	0	-0.020	0	-0.027	0	-0.040
30	-0.006	0	-0.007	0	-0.007	0	-0.008	0	-0.009	0	-0.012	0	-0.015	0	-0.021	0
31	0	-0.003	0	-0.003	0	-0.004	0	-0.004	0	-0.005	0	-0.007	0	-0.009	0	-0.012

Table H-5. Weber coefficients  $S(1)$  for the 32 point method.

#	17	18	19	20	21	22	23	24	25	26	27	28	29	30	31	32
1	0	-0.009	0	-0.007	0	-0.015	0	-0.004	0	-0.004	0	-0.003	0	-0.003	0	-0.003
2	-0.021	0	-0.015	0	-0.012	0	-0.009	0	-0.008	0	-0.007	0	-0.007	0	-0.006	0
3	0	-0.027	0	-0.020	0	-0.016	0	-0.013	0	-0.011	0	-0.010	0	-0.010	0	-0.009
4	-0.046	0	-0.032	0	-0.025	0	-0.020	0	-0.017	0	-0.015	0	-0.013	0	-0.013	0
5	0	-0.051	0	-0.037	0	-0.029	0	-0.023	0	-0.020	0	-0.018	0	-0.017	0	-0.017
6	-0.080	0	-0.055	0	-0.041	0	-0.032	0	-0.027	0	-0.024	0	-0.022	0	-0.021	0
7	0	-0.085	0	-0.059	0	-0.045	0	-0.036	0	-0.031	0	-0.028	0	-0.026	0	-0.025
8	-0.136	0	-0.089	0	-0.064	0	-0.049	0	-0.040	0	-0.035	0	-0.032	0	-0.031	0
9	0	-0.140	0	-0.083	0	-0.068	0	-0.054	0	0.045	0	-0.040	0	-0.037	0	-0.036
10	-0.243	0	-0.145	0	-0.089	0	-0.073	0	-0.059	0	-0.050	0	-0.045	0	-0.043	0
11	0	-0.248	0	-0.151	0	-0.105	0	-0.079	0	-0.065	0	-0.057	0	-0.052	0	-0.051
12	-0.500	0	-0.255	0	-0.158	0	-0.112	0	-0.086	0	-0.072	0	-0.064	0	-0.061	0
13	0	-0.508	0	-0.264	0	-0.167	0	-0.120	0	-0.095	0	-0.081	0	-0.074	0	-0.072
14	-1.427	0	-0.520	0	-0.276	0	-0.178	0	-0.131	0	-0.106	0	-0.092	0	-0.087	0
15	0	-1.448	0	-0.538	0	-0.291	0	-0.192	0	-0.144	0	-0.119	0	-0.107	0	-0.103
16	-13.011	0	-1.483	0	-0.563	0	-0.311	0	-0.209	0	-0.161	0	-0.137	0	-0.126	0
17	32.155	-13.201	0	1.535	0	-0.584	0	-0.335	0	-0.231	0	-0.182	0	-0.160	0	-0.153
18	-13.010	32.627	-13.529	0	1.606	0	-0.635	0	-0.367	0	-0.260	0	-0.211	0	-0.192	0
19	0	-13.199	33.440	14.010	0	-1.700	0	-0.688	0	-0.408	0	-0.298	0	-0.251	0	-0.237
20	-1.425	0	-13.527	34.037	14.674	0	1.823	0	-0.758	0	-0.463	0	-0.350	0	-0.308	0
21	0	-1.444	0	-14.008	36.284	15.560	0	-1.884	0	-0.850	0	-0.538	0	-0.425	0	-0.395
22	-0.496	0	-1.477	0	-14.689	38.486	16.728	0	-2.198	0	-0.976	0	-0.645	0	-0.538	0
23	0	-0.501	0	1.525	0	-15.552	41.897	18.275	0	-2.488	0	-1.153	0	-0.805	0	-0.723
24	-0.238	0	-0.509	0	-1.591	0	16.717	45.255	20.350	0	-2.882	0	-1.416	0	-1.065	0
25	0	-0.237	0	-0.520	0	-1.677	0	18.258	50.442	23.207	0	-3.484	0	-1.837	0	-1.539
26	-0.129	0	-0.237	0	-0.536	0	-1.788	0	20.321	57.584	27.287	0	-4.411	0	-2.591	0
27	0	-0.125	0	-0.236	0	-0.553	0	1.928	0	23.149	67.883	33.470	0	-6.029	0	-4.226
28	-0.070	0	-0.119	0	-0.234	0	-0.571	0	-2.102	0	-27.171	83.620	43.765	0	-9.409	0
29	0	-0.063	0	-0.110	0	-0.225	0	-0.581	0	-2.305	0	-33.198	110.237	63.816	0	-19.572
30	-0.031	0	-0.051	0	-0.084	0	-0.203	0	-0.565	0	-2.485	0	-42.869	164.027	117.636	0
31	0	-0.019	0	-0.033	0	-0.083	0	-0.148	0	-0.457	0	-2.410	0	-59.103	326.474	-528.400

Table H-5. Continued.

$s_{\mu}^{(2)}$  for  $N = 32$

$\mu$	1	2	3	4	5	6	7	8	9	10	11	12	13	14	15	16
1	103.596	69.783	-17.658	7.184	-3.671	2.155	-1.391	0.962	-0.703	0.536	-0.424	0.346	-0.291	0.250	-0.220	0.197
2	-276.452	25.769	56.370	-17.917	8.372	-4.703	2.960	-2.016	1.457	-1.104	0.869	-0.706	0.590	-0.508	0.444	-0.398
3	154.876	-124.802	11.356	45.888	-16.417	8.329	-4.976	3.286	-2.328	1.740	-1.356	1.094	-0.910	0.777	-0.679	0.607
4	-109.508	68.941	-79.750	6.309	38.696	-14.908	7.997	-4.983	3.420	-2.499	1.918	-1.531	1.262	-1.071	0.931	-0.828
5	84.923	-48.880	43.293	-58.716	3.969	33.636	-13.645	7.627	-4.927	3.474	-2.604	2.044	-1.665	1.400	-1.209	1.069
6	-69.243	38.144	-30.507	31.420	-46.720	2.694	29.961	-12.635	7.293	-4.844	3.499	-2.680	2.146	-1.780	1.522	-1.336
7	58.263	-31.301	23.764	-21.976	24.713	-39.066	1.921	27.227	-11.841	7.018	-4.770	3.518	-2.747	2.238	-1.889	1.641
8	-50.084	26.487	-19.500	17.048	-17.161	20.469	-33.826	1.414	25.160	-11.224	6.803	-4.718	3.546	-2.816	2.333	-2.000
9	43.717	-22.878	16.512	-13.956	13.250	-14.120	17.581	-30.069	1.062	23.589	-10.755	6.648	-4.685	3.588	-2.896	2.437
10	-38.592	20.046	-14.273	11.798	-10.809	10.849	-12.055	15.519	-27.292	0.804	22.401	-10.411	6.551	-4.704	3.652	-2.993
11	34.356	-17.749	12.514	-10.186	9.115	-8.817	9.218	-10.583	13.999	-25.202	0.606	21.521	-10.177	6.509	-4.747	3.742
12	-30.778	15.836	-11.084	8.922	-7.851	7.411	-7.462	8.055	9.496	12.854	-23.617	0.448	20.898	-10.043	6.522	-4.828
13	27.700	-14.207	9.890	-7.893	6.862	-6.365	6.250	-5.418	5.776	6.545	-8.050	11.318	-21.533	0.203	20.305	-10.055
14	-25.013	12.797	-8.866	7.033	-6.059	5.548	-5.350	5.418	-5.776	6.545	-8.050	11.318	-21.533	0.203	20.305	-10.055
15	22.634	-11.557	7.983	-6.298	5.386	-4.885	4.648	-4.621	4.800	-5.232	6.044	-7.568	10.818	-20.905	0.099	20.306
16	-20.503	10.453	-7.200	5.657	-4.811	4.330	-4.078	4.000	-4.078	4.330	-4.811	5.657	-7.200	10.453	-20.503	0
17	18.575	-9.457	6.499	-5.090	4.309	-3.854	3.602	-3.496	3.516	-3.663	3.963	-4.482	5.356	-6.924	10.202	-20.306
18	-16.813	8.551	-5.866	4.581	-3.864	3.439	-3.193	3.075	-3.059	3.142	-3.337	3.675	-4.223	5.126	-6.725	10.055
19	15.190	-7.718	5.286	-4.119	3.464	-3.071	2.837	-2.714	2.678	-2.721	2.849	-3.078	3.445	-4.020	4.953	-6.593
20	-13.682	6.946	-4.752	3.696	-3.100	2.739	-2.520	2.398	-2.350	2.369	-2.453	2.613	-2.869	3.261	-3.862	4.828
21	12.270	-6.228	4.254	-3.303	2.765	-2.437	2.234	-2.117	2.063	-2.066	2.121	-2.235	2.420	-2.698	3.113	-3.742
22	-10.940	5.548	-3.788	2.937	-2.454	2.158	-1.973	1.863	-1.808	1.800	-1.836	1.918	-2.054	2.259	-2.557	2.993
23	9.679	-4.906	3.347	-2.593	2.163	-1.898	1.732	-1.630	1.576	-1.563	1.585	-1.645	1.747	-1.900	2.121	-2.437
24	-8.476	4.295	-2.928	2.266	-1.888	1.654	-1.506	1.414	-1.364	1.347	-1.361	1.405	-1.482	1.596	-1.765	2.000
25	7.321	-3.708	2.527	-1.954	1.626	-1.423	1.294	-1.212	1.166	-1.149	1.156	-1.188	1.247	-1.336	1.464	-1.641
26	-6.206	3.143	-2.140	1.654	-1.376	1.203	-1.091	1.021	-0.981	0.963	-0.967	0.991	-1.035	1.104	-1.201	1.336
27	5.124	-2.594	1.766	-1.364	1.134	-0.990	0.898	-0.839	0.804	-0.789	0.790	-0.807	0.840	-0.893	0.967	-1.069
28	-4.069	2.060	-1.402	1.062	-0.899	0.785	-0.711	0.664	-0.635	0.622	-0.622	0.634	-0.659	0.697	-0.753	0.828
29	3.034	-1.536	1.045	-0.807	0.670	-0.594	0.529	-0.493	0.472	-0.462	0.461	-0.469	0.486	-0.514	0.553	-0.607
30	-2.015	1.020	-0.694	0.535	-0.444	0.388	-0.351	0.327	-0.313	0.305	-0.305	0.310	-0.321	0.336	-0.363	0.386
31	1.005	-0.509	0.346	-0.266	0.222	-0.194	0.175	-0.163	0.156	-0.152	0.152	-0.154	0.159	-0.167	0.180	-0.197

Table H-6. Weber coefficients  $S^{(2)}$  for the 32 point method.

#	17	18	19	20	21	22	23	24	25	26	27	28	29	30	31
1	-0.180	0.167	-0.159	0.154	-0.152	0.152	-0.156	0.163	-0.175	0.194	-0.222	0.266	-0.346	0.509	-1.005
2	0.363	-0.338	0.321	-0.310	0.305	-0.305	0.313	-0.327	0.351	-0.388	0.444	-0.535	0.694	-1.020	2.015
3	-0.553	0.514	-0.486	0.469	-0.461	0.462	-0.472	0.493	-0.529	0.584	-0.670	0.807	-1.045	1.536	-3.034
4	0.753	-0.697	0.659	-0.634	0.622	-0.622	0.635	-0.664	0.711	-0.785	0.899	-1.082	1.402	-2.060	4.069
5	-0.967	0.893	-0.840	0.807	-0.790	0.789	-0.804	0.839	-0.898	0.990	-1.134	1.364	-1.766	2.594	-5.124
6	1.201	-1.104	1.035	-0.991	0.967	-0.963	0.981	-1.021	1.091	-1.203	1.376	-1.654	2.140	-3.143	6.206
7	-1.464	1.336	-1.247	1.188	-1.156	1.149	-1.166	1.212	-1.294	1.423	-1.626	1.954	-2.527	3.708	-7.321
8	1.765	-1.598	1.482	-1.405	1.361	-1.347	1.364	-1.414	1.506	-1.654	1.888	-2.266	2.928	-4.295	8.476
9	-2.121	1.900	-1.747	1.645	-1.585	1.563	-1.576	1.630	-1.732	1.898	-2.163	2.593	-3.347	4.906	-9.679
10	2.557	-2.259	2.054	-1.918	1.836	-1.800	1.808	-1.863	1.973	-2.158	2.454	-2.937	3.788	-5.548	10.940
11	-3.113	2.698	-2.420	2.235	-2.121	2.066	-2.063	2.117	-2.234	2.437	-2.765	3.303	-4.254	6.226	-12.270
12	3.862	-3.261	2.869	-2.613	2.453	-2.369	2.350	-2.398	2.520	-2.739	3.100	-3.696	4.752	-6.946	13.682
13	-4.953	4.020	-3.445	3.078	-2.849	2.721	-2.678	2.714	-2.837	3.071	-3.464	4.119	-5.286	7.718	-15.190
14	6.725	-5.126	4.223	-3.675	3.337	-3.142	3.059	-3.075	3.193	-3.439	3.864	-4.581	5.866	-8.551	16.813
15	-10.202	6.924	-5.126	4.223	-3.675	3.337	-3.142	3.059	-3.075	3.193	-3.439	3.864	-4.581	5.866	-8.551
16	20.503	-10.453	7.200	-5.657	4.811	-4.330	4.078	-4.000	4.078	-4.330	4.811	-5.657	7.200	-10.453	20.503
17	-0.099	20.905	-10.818	7.568	-6.044	5.232	-4.800	4.621	-4.648	4.885	-5.386	6.298	-7.983	11.557	-22.634
18	-20.305	-0.203	21.533	-11.318	8.050	-6.545	5.776	-5.418	5.350	-5.548	6.059	-7.033	8.866	-12.797	25.013
19	10.002	-20.499	0.317	-22.420	-11.982	8.677	-7.195	6.493	-6.250	6.365	-6.862	7.893	-9.890	14.207	-27.700
20	-6.522	10.043	-20.898	-0.448	23.617	-12.854	9.496	-8.055	7.462	-7.411	7.851	-8.922	11.084	-15.836	30.778
21	4.747	-6.509	10.177	-21.521	-0.606	25.202	-13.999	10.583	-9.218	8.817	-9.115	10.186	-12.514	17.749	-34.356
22	-3.652	4.704	-6.551	10.411	-22.401	-0.804	27.292	-15.519	12.055	-10.849	10.809	-11.798	14.273	-20.046	38.592
23	2.896	-3.588	4.695	-6.648	10.755	-23.589	-1.062	30.069	-17.581	14.120	-13.250	13.956	-16.512	22.878	-43.717
24	-2.333	2.816	-3.546	4.718	-6.803	11.224	-25.160	-1.414	33.826	-20.469	17.161	-17.048	19.500	-26.487	50.084
25	1.889	-2.238	2.747	-3.518	4.770	-7.018	11.841	-27.227	-1.921	39.066	-24.713	21.976	-23.764	31.301	-58.263
26	-1.522	1.780	-2.146	2.680	-3.499	4.844	-7.293	12.635	-29.961	-2.694	46.720	-31.420	30.507	-38.144	69.243
27	1.209	-1.400	1.665	-2.044	2.604	-3.474	4.927	-7.627	13.645	-33.636	-3.969	58.716	-43.293	48.880	-84.923
28	-0.931	1.071	-1.262	1.531	-1.918	2.499	-3.420	4.993	-7.997	14.908	-38.696	-6.309	79.750	-68.941	109.508
29	0.679	-0.777	0.910	-1.094	1.356	-1.740	2.328	-3.286	4.976	-8.329	16.417	-45.888	-11.356	124.802	-154.876
30	-0.444	0.506	-0.590	0.706	-0.869	1.104	-1.457	2.016	-2.960	4.703	-8.372	17.917	-56.370	25.769	-276.452
31	0.220	-0.250	0.291	-0.346	0.424	-0.536	0.703	-0.962	1.391	-2.155	3.671	-7.184	17.658	-69.783	-103.586

Table H-6. Continued.

$s_{\mu}^{(3)}$  for  $N = 32$

$\mu$	1	2	3	4	5	6	7	8	9	10	11	12	13	14	15	16
1	326.474	29.462	0	15.475	0	7.333	0	4.279	0	2.838	0	2.049	0	1.575	0	1.269
2	-162.133	164.027	-16.018	0	3.986	0	2.519	0	1.647	0	1.164	0	0.877	0	0.685	0
3	0	-81.875	110.237	-20.176	0	1.127	0	1.143	0	0.648	0	0.640	0	0.502	0	0.410
4	-13.980	0	-53.644	83.620	-19.386	0	0.063	0	0.557	0	0.488	0	0.397	0	0.326	0
5	0	-8.711	0	-39.790	67.883	-17.883	0	-0.411	0	0.280	0	0.295	0	0.261	0	0.225
6	-3.965	0	-6.204	0	-31.747	57.589	-16.472	0	-0.646	0	0.089	0	0.179	0	0.178	0
7	0	-2.785	0	-4.790	0	-26.578	50.442	-15.289	0	-0.771	0	-0.015	0	0.104	0	0.122
8	-1.679	0	-2.124	0	-3.903	0	-23.032	45.255	-14.286	0	-0.841	0	-0.085	0	0.051	0
9	0	-1.272	0	-1.712	0	-3.309	0	-20.499	41.397	-13.501	0	-0.883	0	-0.133	0	0.015
10	-0.880	0	-1.020	0	-1.437	0	-2.889	0	-18.635	38.486	-12.883	0	-0.910	0	-0.167	0
11	0	-0.703	0	-0.851	0	-1.244	0	-2.585	0	-17.244	36.284	-12.410	0	-0.931	0	-0.195
12	-0.529	0	-0.586	0	-0.734	0	-1.105	0	-2.361	0	-16.199	34.637	-12.063	0	-0.950	0
13	0	-0.440	0	-0.478	0	-0.649	0	-2.001	0	-2.192	0	-15.424	33.440	-11.827	0	-0.970
14	-0.351	0	-0.378	0	-0.446	0	-0.588	0	-1.848	0	-2.067	0	-14.968	32.627	-11.697	0
15	0	-0.302	0	-0.334	0	-0.402	0	-1.641	0	-1.726	0	-1.976	0	-14.495	32.155	-11.667
16	-0.252	0	-0.268	0	-0.303	0	-0.371	0	-1.508	0	-1.628	0	-1.914	0	-14.286	32
17	0	-0.223	0	-0.242	0	-0.279	0	-1.348	0	-1.483	0	-1.799	0	-1.877	0	-14.229
18	-0.194	0	-0.203	0	-0.224	0	-0.263	0	-1.232	0	-1.467	0	-1.783	0	-1.862	0
19	0	-0.177	0	-0.189	0	-0.211	0	-1.125	0	-1.321	0	-1.458	0	-1.777	0	-1.870
20	-0.159	0	-0.165	0	-0.179	0	-0.203	0	-1.025	0	-1.316	0	-1.456	0	-1.781	0
21	0	-0.150	0	-0.159	0	-0.174	0	-0.199	0	-1.023	0	-1.317	0	-1.461	0	-1.797
22	-0.140	0	-0.144	0	-0.155	0	-0.172	0	-0.199	0	-1.024	0	-1.323	0	-1.473	0
23	0	-0.137	0	-0.144	0	-0.156	0	-0.175	0	-1.024	0	-1.252	0	-1.335	0	-1.495
24	-0.135	0	-0.138	0	-0.146	0	-0.159	0	-0.181	0	-1.021	0	-1.266	0	-1.357	0
25	0	-0.138	0	-0.144	0	-0.154	0	-0.169	0	-1.023	0	-1.229	0	-1.289	0	-1.388
26	-0.144	0	-0.148	0	-0.155	0	-0.167	0	-0.185	0	-1.021	0	-1.256	0	-1.322	0
27	0	-0.159	0	-0.165	0	-0.175	0	-0.190	0	-1.021	0	-1.247	0	-1.297	0	-1.377
28	-0.183	0	-0.187	0	-0.196	0	-0.209	0	-0.230	0	-1.025	0	-1.301	0	-1.366	0
29	0	-0.232	0	-0.239	0	-0.252	0	-0.272	0	-1.021	0	-1.341	0	-1.400	0	-1.490
30	-0.300	0	-0.338	0	-0.351	0	-0.373	0	-0.406	0	-1.025	0	-1.519	0	-1.615	0
31	0	-0.648	0	-0.668	0	-0.702	0	-0.753	0	-0.827	0	-0.933	0	-1.080	0	-1.283
32	-0.031	0	-0.032	0	-0.033	0	-0.035	0	-0.038	0	-0.042	0	-0.048	0	-0.057	0

Table H-7. Weber coefficients  $s_{\mu}^{(3)}$  for the 32 point method.

$\mu$	17	18	19	20	21	22	23	24	25	26	27	28	29	30	31	32
1	0	1.062	0	0.920	0	0.818	0	0.745	0	0.694	0	0.662	0	0.642	00	0.636
2	0.573	0	0.489	0	0.429	0	0.388	0	0.357	0	0.337	0	0.324	0	0.318	0
3	0	0.346	0	0.301	0	0.269	0	0.246	0	0.230	0	0.219	0	0.212	0	0.211
4	0.274	0	0.237	0	0.209	0	0.190	0	0.175	0	0.166	0	0.161	0	0.157	0
5	0	0.195	0	0.173	0	0.155	0	0.144	0	0.135	0	0.129	0	0.125	0	0.124
6	0.162	0	0.146	0	0.132	0	0.121	0	0.113	0	0.107	0	0.104	0	0.102	0
7	0	0.119	0	0.111	0	0.103	0	0.097	0	0.092	0	0.088	0	0.086	0	0.086
8	0.084	0	0.088	0	0.086	0	0.083	0	0.079	0	0.076	0	0.074	0	0.073	0
9	0	0.055	0	0.066	0	0.068	0	0.067	0	0.065	0	0.064	0	0.063	0	0.063
10	-0.013	0	0.033	0	0.047	0	0.053	0	0.054	0	0.055	0	0.054	0	0.054	0
11	0	-0.035	0	0.015	0	0.033	0	0.041	0	0.044	0	0.045	0	0.046	0	0.045
12	-0.219	0	-0.054	0	0	0	0.021	0	0.031	0	0.035	0	0.037	0	0.037	0
13	0	-0.239	0	-0.070	0	-0.013	0	0.011	0	0.021	0	0.027	0	0.029	0	0.029
14	-0.992	0	-0.257	0	-0.085	0	-0.024	0	0.001	0	0.012	0	0.019	0	0.020	0
15	0	-1.019	0	-0.277	0	-0.099	0	-0.036	0	-0.009	0	0.004	0	0.009	0	0.011
16	-11.736	0	-1.052	0	-0.298	0	-0.114	0	-0.047	0	-0.019	0	-0.006	0	0	0
17	32.155	-11.907	0	-1.094	0	-0.319	0	-0.129	0	-0.060	0	-0.030	0	-0.018	0	-0.014
18	-14.324	32.627	-12.190	0	-1.145	0	-0.344	0	-0.146	0	-0.074	0	-0.044	0	-0.033	0
19	0	-14.571	33.440	-12.596	0	-1.206	0	-0.375	0	-0.167	0	-0.092	0	-0.062	0	-0.053
20	-1.900	0	-14.991	34.637	-13.149	0	-1.285	0	-0.411	0	-0.192	0	-0.114	0	-0.067	0
21	0	-1.957	0	-15.606	36.294	-13.876	0	-1.383	0	-0.456	0	-0.225	0	-0.147	0	-0.126
22	-0.825	0	-2.044	0	-16.455	38.496	-14.821	0	-1.507	0	-0.515	0	-0.270	0	-0.196	0
23	0	-0.869	0	-2.167	0	-17.603	41.997	-16.051	0	-1.667	0	-0.594	0	-0.336	0	-0.281
24	-0.528	0	-0.933	0	-2.341	0	-19.148	45.255	-17.668	0	-1.881	0	-0.708	0	-0.451	0
25	0	-0.578	0	-1.025	0	-2.583	0	-21.247	50.442	-19.836	0	-2.178	0	-0.889	0	-0.671
26	-0.436	0	-0.653	0	-1.161	0	-2.930	0	-24.170	57.599	-22.827	0	-2.618	0	-1.217	0
27	0	-0.511	0	-0.767	0	-1.366	0	-3.445	0	-28.405	67.883	-27.150	0	-3.347	0	-1.981
28	-0.466	0	-0.635	0	-0.956	0	-1.689	0	-4.287	0	-34.9568	83.620	-33.891	0	-4.828	0
29	0	-0.628	0	-0.860	0	-1.298	0	-2.305	0	-5.737	0	-46.220	110.237	-45.757	0	-9.569
30	-0.757	0	-0.979	0	-1.352	0	-2.053	0	-3.649	0	-8.976	0	-69.760	164.027	-73.139	0
31	0	-1.613	0	-2.115	0	-2.964	0	-4.575	0	-8.247	0	-20.295	0	-147.688	326.474	-263.566
32	-0.069	0	-0.088	0	-0.118	0	-0.171	0	-0.275	0	-0.529	0	-1.451	0	-12.979	0

Table H-7. Continued.



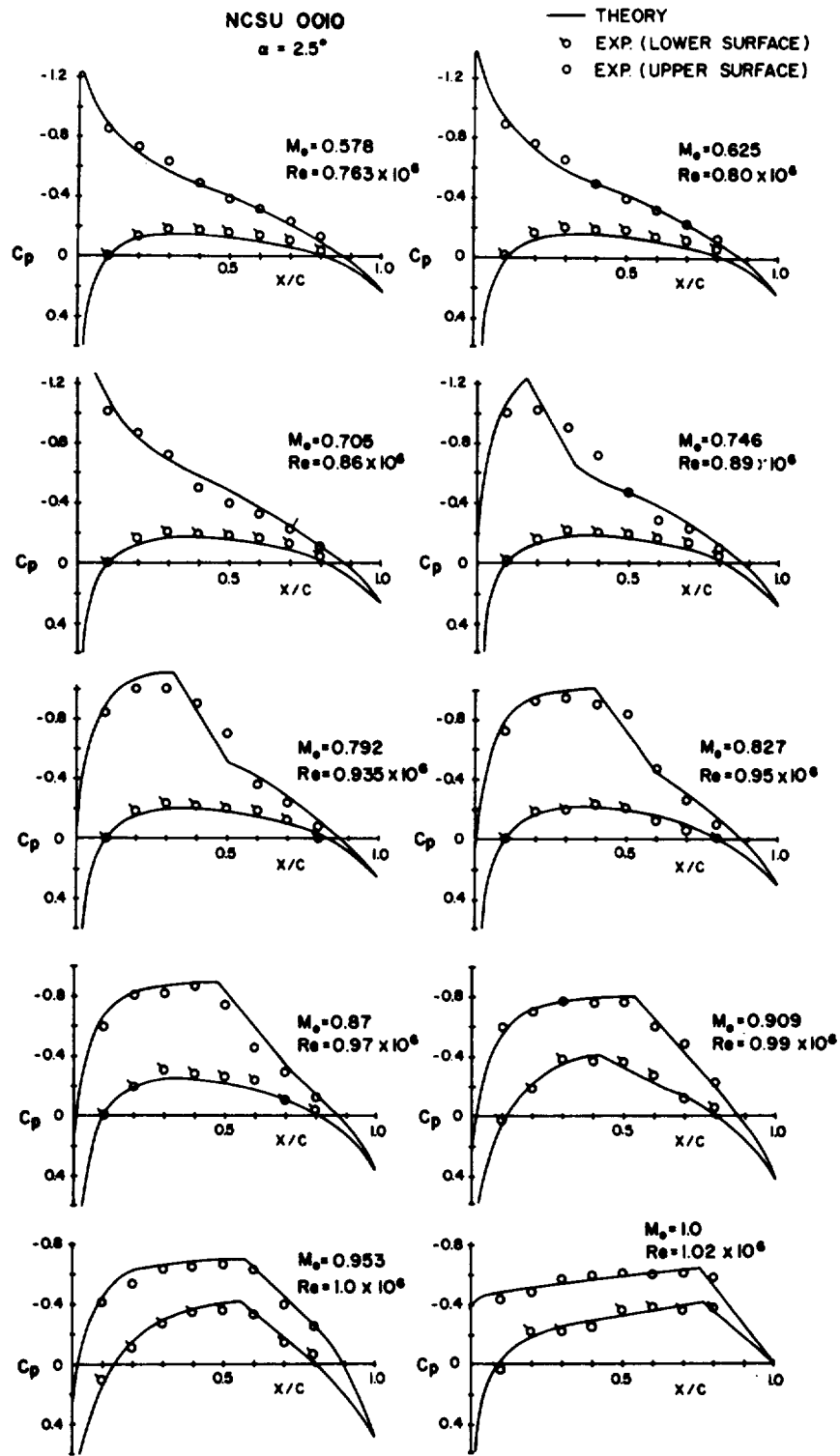


Figure H-2. Comparison of theory and experiment for one airfoil.

## User Instructions - TRINSON

This program is written in FORTRAN IV and is designed to run in single precision on an IBM 370-165 computer. Execution requires 32,000 bytes of core storage and approximately 3 seconds to produce the two-dimensional zero Mach number pressure distribution for an airfoil at six angles of attack by the 16-point Weber method. For a given run, the program requires the following input data:

(1) The 240 elements of the Matrix S1 given in A.R.C. R&M 2918 and listed herein as Table H-2.

(2) The 240 elements of the Matrix S2 also given in A.R.C. R&M 2918 and listed herein as Table H-3.

(3) The 256 elements of Matrix S3 also given in A.R.C. R&M 2918 and listed herein as Table H-4.

(4) The 72 characters of the array TITLE which are used as a header for identifying output. It is an alphameric array and usually contains information about the type of airfoil, run number, and any other such information desired by the programmer as a header.

(5) The values of X, the x-coordinates (given as X/C of the airfoil to be considered) from Table H-1.

(6) The values of Y (the normalized y-coordinate of the airfoil to be considered) corresponding to the values of X.

(7) The values of angle of attack, A, and airfoil leading edge radius, RHO, for a given airfoil, followed by a last card indicator giving A a value of greater than 15.

(8) Additional data sets containing information from item (4) through item (7), for another airfoil, if needed. Only two airfoils may be considered per run.

Format specifications for these variables may be found in Figure H-3. A sample data set of the NCSU 0010 may be found in Figure H-4 and the output for that data set is given in Figure H-5.

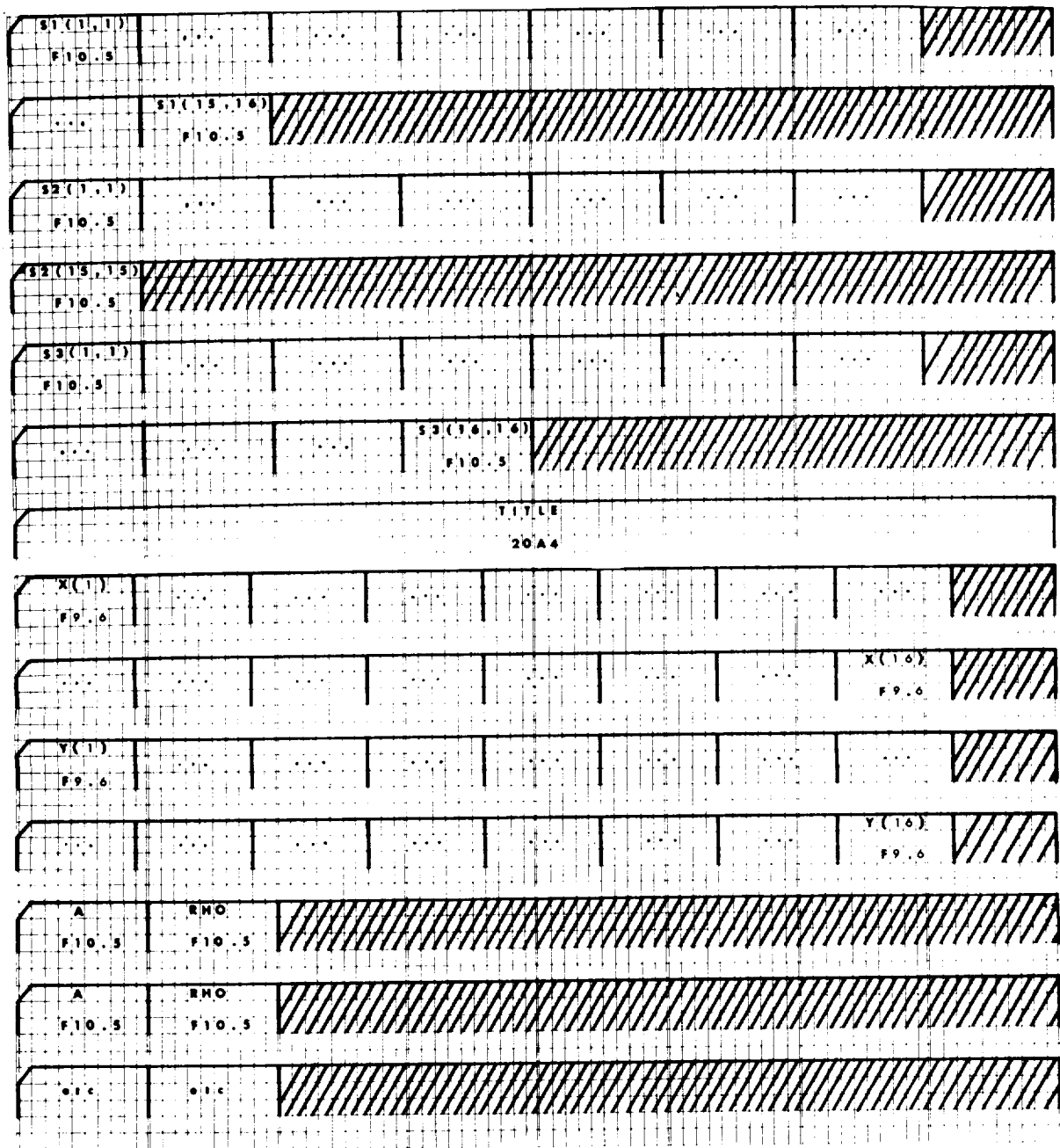


Figure H-3. Format specification of input data for TRINSON.





# Sample Output - TRINSON

INCOMPRESSIBLE PRESSURE COEFFICIENT			INCOMPRESSIBLE PRESSURE COEFFICIENT		
NCSU 0010			NCSU 0010		
ANGLE OF ATTACK= 1.000000			ANGLE OF ATTACK= 1.000000		
X/C	Y/C	CP-UPPER	X/C	Y/C	CP-LOWER
0.990000	0.001300	0.231837	0.990000	0.001300	0.236393
0.961900	0.004800	0.127022	0.961900	0.004800	0.137808
0.915000	0.010400	0.040493	0.915000	0.010400	0.058998
0.853600	0.017300	-0.018052	0.853600	0.017300	0.008959
0.777800	0.025200	-0.079037	0.777800	0.025200	-0.042096
0.691300	0.033300	-0.146583	0.691300	0.033300	-0.097166
0.597500	0.040300	-0.197896	0.597500	0.040300	-0.129807
0.500000	0.045800	-0.244597	0.500000	0.045800	-0.164456
0.402500	0.049000	-0.284382	0.402500	0.049000	-0.188161
0.308700	0.049900	-0.337182	0.308700	0.049900	-0.209759
0.222200	0.047800	-0.389627	0.222200	0.047800	-0.225881
0.146400	0.042200	-0.401874	0.146400	0.042200	-0.191769
0.084270	0.034400	-0.458526	0.084270	0.034400	-0.169070
0.038060	0.023800	-0.400694	0.038060	0.023800	0.001869
0.009610	0.012600	-0.379138	0.009610	0.012600	0.279523

INCOMPRESSIBLE PRESSURE COEFFICIENT			INCOMPRESSIBLE PRESSURE COEFFICIENT		
NCSU 0010			NCSU 0010		
ANGLE OF ATTACK= 1.730000			ANGLE OF ATTACK= 1.730000		
X/C	Y/C	CP-UPPER	X/C	Y/C	CP-LOWER
0.990000	0.001300	0.230637	0.990000	0.001300	0.238915
0.961900	0.004800	0.123577	0.961900	0.004800	0.162332
0.915000	0.010400	0.034281	0.915000	0.010400	0.010624
0.853600	0.017300	-0.027378	0.853600	0.017300	0.019289
0.777800	0.025200	-0.092056	0.777800	0.025200	-0.028072
0.691300	0.033300	-0.166194	0.691300	0.033300	-0.078736
0.597500	0.040300	-0.215624	0.597500	0.040300	-0.106523
0.500000	0.045800	-0.273753	0.500000	0.045800	-0.135163
0.402500	0.049000	-0.321191	0.402500	0.049000	-0.167879
0.308700	0.049900	-0.384461	0.308700	0.049900	-0.184111
0.222200	0.047800	-0.451107	0.222200	0.047800	-0.167905
0.146400	0.042200	-0.481902	0.146400	0.042200	-0.118599
0.084270	0.034400	-0.571242	0.084270	0.034400	-0.070690
0.038060	0.023800	-0.563684	0.038060	0.023800	0.132413
0.009610	0.012600	-0.471492	0.009610	0.012600	0.487542

INCOMPRESSIBLE PRESSURE COEFFICIENT			INCOMPRESSIBLE PRESSURE COEFFICIENT		
NCSU 0010			NCSU 0010		
ANGLE OF ATTACK= 2.500000			ANGLE OF ATTACK= 2.500000		
X/C	Y/C	CP-UPPER	X/C	Y/C	CP-LOWER
0.990000	0.001300	0.229642	0.990000	0.001300	0.241019
0.961900	0.004800	0.120244	0.961900	0.004800	0.147330
0.915000	0.010400	0.028048	0.915000	0.010400	0.076236
0.853600	0.017300	-0.036893	0.853600	0.017300	0.030916
0.777800	0.025200	-0.105446	0.777800	0.025200	-0.013013
0.691300	0.033300	-0.182501	0.691300	0.033300	-0.059087
0.597500	0.040300	-0.259498	0.597500	0.040300	-0.081843
0.500000	0.045800	-0.304420	0.500000	0.045800	-0.104280
0.402500	0.049000	-0.360113	0.402500	0.049000	-0.109676
0.308700	0.049900	-0.434727	0.308700	0.049900	-0.116511
0.222200	0.047800	-0.516876	0.222200	0.047800	-0.107897
0.146400	0.042200	-0.568230	0.146400	0.042200	-0.043974
0.084270	0.034400	-0.694113	0.084270	0.034400	0.028751
0.038060	0.023800	-0.744757	0.038060	0.023800	0.260498
0.009610	0.012600	-1.009651	0.009610	0.012600	0.635264

Figure H-5. Sample output for TRINSON.

## User Instructions - COMPR

This program is written in FORTRAN IV and designed to run in single precision on an IBM 370-165 computer. Execution requires 23 seconds and 68,000 bytes of core to produce complete pressure distributions about a two-dimensional airfoil with a round leading edge for ten Mach numbers from zero to one at one angle of attack. The calculations are carried out first for the upper surface and then the lower. For each airfoil the program requires the following input:

(1) The 72 characters of the array TITLE. This array, which should contain an accurate description of the airfoil, is printed at the first of the output for identification.

(2) The variable NNN and the value of JPRINT, an integer from 2 to 10 which specifies the print information. NNN should first take on the value 1, which implies that the data to follow is that of the upper surface and later, the value 2, which implies that the data to follow is that of the lower surface. The number of points printed may be calculated by  $(10 + 90/JPRINT)$ .

(3) The 28 values of the array X, the x-coordinate (given in fraction of chord) as measured from the leading edge. These values must be specified at every one percent chord starting from  $x/c = 0.01$  to  $x/c = 0.10$ . From  $x/c = 0.10$  to  $x/c = 1.00$  values at each five percent chord are sufficient.

(4) The 28 corresponding values of the array Y, the absolute value of a y-coordinate of either the upper or lower surface according to the value of NNN previously specified.

(5) The 28 values of the array CPI. These are the incompressible pressure coefficients (for the angle of attack of interest) corresponding to X and Y above. Note from (2) and (3) above that these values of CPI are not given at the same points as specified by TRINSON or TRANSON (the 16-point or 32-point incompressible pressure distribution programs respectively, from which this information is supplied). The data from these programs must be plotted, smoothed, and the correct values of CPI read off at the specific coordinate locations of (2) and (3).

(6) The angle of attack A in degrees, the airfoil maximum thickness in fraction of chord, the airfoil slope, E, given at  $x/c = 0.01$ , the airfoil slope, G, given at  $x/c = 1.0$ , the maximum y-coordinate above the chord line ZMAX in fraction of chord, and CREST, the x-position of the maximum y-coordinate given in percent chord.

(7) The value of N1N, the number of free stream Mach numbers for which the calculations are to be made.

(8) The values of a free stream Mach number  $X_M$ , a Reynolds Number,  $RE$ , corresponding to that Mach number, and  $KTPE$  which takes on the value one to specify the type of boundary layer as laminar and the value zero to indicate a turbulent boundary layer. Item (8) is repeated until  $N1N$  Mach numbers have been entered.

(9) Items (2) through (8) should be entered now for the lower surface. Only one airfoil may be considered for each run.

Format specification for these variables may be found in Figure H-6. A sample data set of the NCSU 0010 may be found in Figure H-7 and the output of that data set is given in Figure H-8.



TITLE						
10A4						
NNN	JPRINT					
I10	I10					
X(1)	/					
D15.6	/					
X(28)	/					
D15.6	/					
Y(1)	/					
D15.6	/					
Y(28)	/					
D15.6	/					
CP1(1)	/					
CP1(28)	/					
D15.6	/					
A	TMIC	B	Q	ZMAX	CREST	
F12.6	F12.6	F12.6	F12.6	F12.6	F12.6	
N12	/					
I2	/					
RM	RE	RTPE				
F10.5	E20.5	I2				

Figure H-6. Format specification of Input data for COMPR.







```

225 FORMAT (I2,
DO 360 I=1,MIN
READ (JREAD,30) XM,RE,KTPE
230 FORMAT (F10.2,E20.5,I2)
IF (LN,LE,KMC) GO TO 235
GO TO 250
235 WRITE (JWRITE,240) XM
240 FORMAT (I4,/,/,304,13MACH NUMBER=,F10.5,/)
WRITE (JWRITE,135)
DO 245 I=1,99
PHI=(1+.2*(XMOE2))**(-3.5)
BETA=SQRT(1.-XMOE2)
BE=2.*BETA*1.
CP(1)=CP(1)/(BETA*(CP(1)+XMOE2))/BE)
PHI(1)=CP(1)/(1+.7*PHI)*XMOE2)
XMH(1)=SQRT(5.*PHI(1))**(-2.857)-1.1)
245 IF (LOG(1)) WRITE (JWRITE,140) XX(1),YY(1),PHI(1),XMH(1)
1,CP(1)
GO TO 360
C
C THE FOLLOWING SECTION USES THE PRANDTL GLAUERT RULE TO FIND THE
C PRESSURE DISTRIBUTION FROM THE CREST OF THE AIRFOIL TO THE
C TRAILING EDGE
C
250 BM=(YM-KMC)/(1.-KMC)
PIPSR=(-.430821)*BM**5+(1.32859)*BM**4+(-1.6355)*BM**3+(1.06519)*B
1M**2+(-.428408)*BM**1.00895*(1.-BM)**(1.117)*A
PCRPSR=(-.49244)*BM**5+(1.49793)*BM**4+(-1.7943)*BM**3+(1.1174)*BM
1**2+(-.408045)*BM**1.0791467
PHI=(1+.2*(XMOE2))**(-3.5)
DO 255 K=1,100
CPG(K)=CP(1)/SQRT(1.-XMOE2)
PG(K)=CPG(K)*(1+.7*PHI)*XMOE2)
IF (PG(K).LT.0.0) GO TO 255
XMLG(K)=(5.*PG(K))**(-2.857)-1.1)
IF (XMLG(K).LT.0.1) GO TO 255
XMLG(K)=SQRT(XMLG(K))
PIPO=PIPSR*PSIK
P2P=1-(63.1078)*PIPO**3+(-75.3377)*PIPO**2+(26.4082)*PIPO+(-1.2277
13)
255 P2GPO(K)=P2P*PIPO
DO 260 I=1,100
IF (PG(1))=BE-P2GPO(1)) GO TO 265
260 CONTINUE
265 RES=RE*XX(1)
C
C CALCULATION OF THE INCOMPRESSIBLE BOUNDARY LAYER THICKNESS
C
IF (KTPE=EQ.1)DEL=(256.*XX(1))/SQRT(RES)
IF (KTPE=NE.1)DEL=(1.-85*XX(1))/(RES**2)
XMA=100.*XB
WRITE (JWRITE,240) XM
WRITE (JWRITE,270) I,XM
270 FORMAT (/,/,134,13MACH NUMBER LOCATED AT ,F3.32M PERCENT CHORD FOR MACH
1 NUMBER=,F6.3,/)
IF (KTPE=EQ.1) WRITE (JWRITE,275) RE
275 FORMAT (/,/,144,13MACH NUMBER LOCATED AT ,F3.32M PERCENT CHORD FOR MACH
1)

```

```

280 FORMAT (/,/,144,13MACH NUMBER LOCATED AT ,F3.32M PERCENT CHORD FOR MACH
1)
WRITE (JWRITE,135)
PCR=PCRPSR*PSIJ)
JRR=J+1
DO 305 L=1,JRR
IF (L=J) GO TO 285
DO 295 I=1,99
PHI=(1+.2*(XMOE2))**(-3.5)
BETA=SQRT(1.-XMOE2)
BE=2.*BETA*1.
CP(1)=CP(1)/(BETA*(CP(1)+XMOE2))/BE)
PHI(1)=CP(1)/(1+.7*PHI)*XMOE2)
XMH(1)=SQRT(5.*PHI(1))**(-2.857)-1.1)
295 IF (LOG(1)) WRITE (JWRITE,140) XX(1),YY(1),PHI(1),XMH(1)
1,CP(1)
GO TO 360
300 XXX=XX(1)-XX(J)/(XX(1)-XX(J))
PPSRPO=PCRPSR*(PIPSR-PCRPSR)*XXX
PPQ(1)=PPSRPO*PSIL)
305 CONTINUE
AK=PPOLJ)
AK=IPPO(JRR)-PPOLJ)/(XX(JRR)-XX(J))
CCC=0.9-(0.05*AK)
AAA=(2./XX(J))**5)*AK3-AK*XX(J)-CCC)
BBB=AK*(1.7*XX(J))**5)*AK3-AK*XX(J)-CCC)
JRR=J-1
PHI=(1+.2*(XMOE2))**(-3.5)
DO 310 J=1,JRR
PHI(J)=AAA*SQRT(XX(J))-BBB*XX(J)+CCC)
IF (PHI(J).LE.0.1) GO TO 310
PHI(J)=15.*0.1/PHI(J)**(-2.857)-1.1)
XMH(J)=SQRT(XMH(J))
CP(J)=11.4285/(XMOE2)*PHI(J)
310 CONTINUE
IF (LN,LE-J) GO TO 315
GO TO 325
315 DO 320 J=1,IXA
320 IF (LOG(J)) WRITE (JWRITE,140) XX(J),YY(J),PHI(J),XMH(J),CP(J
1)
GO TO 335
325 DO 330 J=1,JR
330 IF (LOG(J)) WRITE (JWRITE,140) XX(J),YY(J),PHI(J),XMH(J),CP(J
1)
335 IF (IXA=LE-J) GO TO 345
XXX=XX(1)-XX(J)/(XX(1)-XX(J))
PPSRPO=PCRPSR*(PIPSR-PCRPSR)*XXX
PPQ(1)=PPSRPO*PSIL)
XMH(L)=SQRT(5.*PHI(L))**(-2.857)-1.1)
XMH(L)=11.4285/(XMOE2)*PHI(L)
340 IF (LOG(L)) WRITE (JWRITE,140) XX(L),YY(L),PHI(L),XMH(L),CP(L)
345 IF (IXA=LE-J) GO TO 355
PPQ(IXA)=PPQ(1)
IXA=IXA-1

```

```

DO 350 IS=IX,II
IF (IXA.LE.JJ)PPOIIS=SL*(XX(IIS)-XX(IXA))+PMM(IXA)
IF (IXA.GT.JJ)PPOIIS=SL*(XX(IIS)-XX(IXA))+PPOIIXA
XRL(IIS)=SORTIS.*((I./PPOIIS))*.28571-1.1)
CPIIS=(1.-4285/(MHPX))*(PPOIIS/PMMI)-1.1)
350 IF (LOG(IIS)) WRITE (JWRITE,140) XRL(IIS),YX(IIS),PPOIIS),XRL(IIS),CPII
15)
MM=I+1
DO 355 MM=1,100
355 IF (LOG(M)) WRITE (JWRITE,140) X(M),Y(M),PG(M),XRL(M),CPG(M)
360 CEN(M)=1.0) GO TO 365
365 IF (MM.EQ.1) GO TO 15
CALL EXIT
STOP
END

C SUBROUTINES 'SPLINE', 'FUNCT', AND 'FIRST' CALCULATE THE SLOPE
C OF THE AIRFOIL SURFACE
SUBROUTINE SPLINE(M,X,AA,IKEY,YPI,YPN)
IMPLICIT REAL*8(A-H,O-Z)
DIMENSION AA(100),Q(99),U(99),X(99),Y(99)
C THIS SUBROUTINE PERFORMS A SPLINE FIT ON THE TABULATED
C DATA Y VS. X. THE SPLINE FIT PROVIDES A CURVE FIT OF THE
C TABULATED DATA THAT HAS A SMOOTH FIRST DERIVATIVE. THE
C FORM OF THE CURVE FIT IS
C 
$$Y = AA(1,1) + x^{003} + AA(2,1) x^{002} + AA(3,1) x + AA(4,1)$$

C FOR  $X(1) <= X <= X(1+1)$ .
C
C N - NUMBER OF TABULATED DATA POINTS
C Y - TABULATED FUNCTION VALUES
C X - TABULATED ARGUMENT VALUES
C AA - ARRAY OF COEFFICIENTS OF THE CUBIC POLYNOMIAL
C IKEY - SPLINE FIT DIMENSIONS OF AA ARE 4 BY N+1
C YPI - CONTROL PARAMETERS THAT SPECIFY THE TYPE OF
C END CONDITION TO BE USED IN THE SPLINE FIT.
C IKEY = 1 -> LEAST-SQUARE END CONDITION
C IKEY = 2 -> SECOND DERIVATIVE OF Y(X) SET
C TO ZERO AT END POINTS
C IKEY = 3 -> FIRST DERIVATIVE OF Y(X) IS
C SPECIFIED AT BOTH END POINTS.
C IF IKEY=3, THEN THE CALLING
C PROGRAM MUST SUPPLY VALUES
C FOR YPI AND YPN.
C
C YPI - FIRST DERIVATIVE OF Y(X) AT THE LEFT
C END POINT X(1)
C YPN - FIRST DERIVATIVE OF Y(X) AT THE RIGHT
C END POINT X(N)
C
C THE EQUATION NUMBERS REFERRED TO IN THE COMMENTS BELOW ARE FROM
C THE THEORY OF SPLINES AND THEIR APPLICATIONS

```

```

CHAPTER II, PAGES 9 - 15
J.H. AHLBERG, ET AL, ACADEMIC PRESS, NEW YORK, 1967
SOLVE EQ.(2.1.8) USING THE ALGORITHM GIVEN BY EQ.(2.1.20)
AND EQ.(2.1.21). GENERATE Q(I) AND U(I) OF EQ.(2.1.20) USING
THE APPROPRIATE END CONDITION SPECIFIED BY IKEY.
MM=1
M1=X(2)-X(1)
GO TO (5,10,15),IKEY
5 Q(1)=1-1.000/16.000
M2=X(3)-X(2)
M3=X(4)-X(3)
U(1)=Y(1)+132.000*M1+42.000*M2+21.000*M3/(M1+M2)/(M1+M2+M3)-Y(2)*
111.000*M1+42.000*M2+21.000*M3/(M2+Y(3)+M1*(111.000*M1+21.0
100*(M2+M3))/(M1+M2)/(M2+Y(4)+M1*(111.000*M1+21.000*M2)/(M2+M3)/(M
11+M2+M3)/M3
U(1)=3.000*U(1)/M1/8.000
GO TO 20
IKEY=2 -> SECOND DERIVATIVE OF Y(X) SET TO ZERO AT X(1).
THIS IMPLIES M(O)=0 OR LAMDA(O) & D(O) OF
EQ.(2.1.6) ARE ZERO.
10 Q(1)=0.000
U(1)=0.000
GO TO 20
IKEY=3 -> FIRST DERIVATIVE OF Y(X) SET EQUAL TO YPI AT X(1).
LAMDA(O) & D(O) OF EQ.(2.1.6) DETERMINED BY EQ.(2.1.55)
15 Q(1)=3.000*(Y(2)-Y(1))/(M1-YPI)/M1
U(1)=0.000
GO TO 20
GENERATE U(K), K=2,N-1, OF EQ.(2.1.20) USING DEFINITIONS OF
LAMDA(I), M(I), AND D(I) GIVEN BY EQ.(2.1.7)
20 MM=M1
YPI=Y(2)
YPN=Y(1)
DO 25 I=2,MM1
MM=X(I+1)-X(I)
YPI=Y(I+1)
D=6.000*(YI-YI)/MM-(YI-YI)/MM/(MM+MM)
C=MM/(MM+MM)
A=1.000-C
P=A*Q(I-1)+2.000
Q(I)=C/P
U(I)=(D-A*U(I-1))/P
MM=MM
YPI=YI
25 YPI=YI
GENERATE U(M) OF EQ.(2.1.20) USING THE APPROPRIATE END
CONDITION SPECIFIED BY IKEY
GO TO (30,35,40),IKEY
IKEY=1 -> LEAST-SQUARE RIGHT END CONDITION

```

```

MM 361
MM 362
MM 363
MM 364
MM 365
MM 366
MM 367
MM 368
MM 369
MM 370
MM 371
MM 372
MM 373
MM 374
MM 375
MM 376
SPL 1
SPL 2
SPL 3
SPL 4
SPL 5
SPL 6
SPL 7
SPL 8
SPL 9
SPL 10
SPL 11
SPL 12
SPL 13
SPL 14
SPL 15
SPL 16
SPL 17
SPL 18
SPL 19
SPL 20
SPL 21
SPL 22
SPL 23
SPL 24
SPL 25
SPL 26
SPL 27
SPL 28
SPL 29
SPL 30
SPL 31
SPL 32
SPL 33
SPL 34
SPL 35
SPL 36
SPL 37
SPL 38
SPL 39
SPL 40
SPL 41

```

```

SPL 42
SPL 43
SPL 44
SPL 45
SPL 46
SPL 47
SPL 48
SPL 49
SPL 50
SPL 51
SPL 52
SPL 53
SPL 54
SPL 55
SPL 56
SPL 57
SPL 58
SPL 59
SPL 60
SPL 61
SPL 62
SPL 63
SPL 64
SPL 65
SPL 66
SPL 67
SPL 68
SPL 69
SPL 70
SPL 71
SPL 72
SPL 73
SPL 74
SPL 75
SPL 76
SPL 77
SPL 78
SPL 79
SPL 80
SPL 81
SPL 82
SPL 83
SPL 84
SPL 85
SPL 86
SPL 87
SPL 88
SPL 89
SPL 90
SPL 91
SPL 92
SPL 93
SPL 94
SPL 95
SPL 96
SPL 97
SPL 98
SPL 99
SPL 100
SPL 101

```







ANGLE OF ATTACK= 2.50 DEGREES

PRESSURE DISTRIBUTION BETWEEN SONIC POINT AND TRAILING EDGE FOR P=1

LOWER SURFACE  
THE AIRFOIL COORDINATES AND INCOMPRESSIBLE PRESSURE DISTRIBUTION

X/C	Y/C	CP
0.010000	0.011300	0.505000
0.020000	0.011000	0.400000
0.030000	0.020800	0.310000
0.040000	0.024500	0.241000
0.050000	0.027500	0.180000
0.060000	0.029500	0.143000
0.070000	0.031400	0.108000
0.080000	0.033500	0.078000
0.090000	0.035000	0.500000
0.100000	0.036000	0.430000
0.150000	0.042700	-0.050000
0.200000	0.046400	-0.094000
0.250000	0.048700	-0.110000
0.300000	0.049800	-0.111000
0.350000	0.049000	-0.111000
0.400000	0.048200	-0.110000
0.450000	0.047000	-0.108000
0.500000	0.045000	-0.098000
0.550000	0.043300	-0.090000
0.600000	0.042000	-0.080000
0.650000	0.039600	-0.068000
0.700000	0.038000	-0.050000
0.750000	0.028100	-0.030000
0.800000	0.023200	-0.020000
0.850000	0.017900	0.006000
0.900000	0.012300	0.048000
0.950000	0.006300	0.129000
1.000000	0.000000	1.000000

THE CRITICAL MACH NUMBER= 0.898

XX	YY	DIV	THETA
0.010000	0.011300	0.508000	0.470027
0.020000	0.011000	0.500419	0.463983
0.030000	0.020800	0.340323	0.328028
0.040000	0.024500	0.358284	0.344040
0.050000	0.027500	0.236527	0.222294
0.060000	0.029500	0.156272	0.193142
0.070000	0.031400	0.210992	0.207942
0.080000	0.033500	0.160412	0.159097
0.090000	0.035000	0.167361	0.165924
0.100000	0.036000	0.190144	0.187901
0.150000	0.042700	0.079469	0.079303
0.200000	0.046400	0.061979	0.061900
0.250000	0.048700	0.057614	0.052602
0.300000	0.049800	0.011945	0.011945
0.350000	0.049000	-0.006874	-0.006874
0.400000	0.048200	-0.020068	-0.020068
0.450000	0.047000	-0.037932	-0.037932
0.500000	0.045000	-0.046823	-0.046823
0.550000	0.043300	-0.057057	-0.056995
0.600000	0.042000	-0.067249	-0.067148
0.650000	0.036600	-0.075948	-0.075902

X/C	Y/C	P/P0	M-LOCAL	CP
0.150000	0.04270	C.41597	1.15691	-0.24962
0.200000	0.04640	C.44715	1.13700	-0.21999
0.250000	0.04870	C.43114	1.16562	-0.26269
0.300000	0.04980	C.42266	1.18049	-0.28681
0.350000	0.04900	C.41522	1.19472	-0.30572
0.400000	0.04920	C.41246	1.19985	-0.31319
0.450000	0.04790	C.40789	1.20827	-0.32539
0.500000	0.04500	C.40054	1.22222	-0.34542
0.550000	C.04330	C.39589	1.23107	-0.35800
0.600000	C.04020	C.39089	1.24066	-0.37192
0.650000	0.03660	0.38664	1.24866	-0.38700
0.700000	0.03260	0.38087	1.26014	-0.40362
0.750000	0.02810	0.37534	1.27103	-0.41156
0.800000	0.02320	0.37080	1.28005	-0.42583
0.850000	0.01790	0.36614	1.28942	-0.43845
0.900000	C.01230	C.36461	1.29250	-0.44258
0.950000	0.00630	C.35670	1.30863	-0.44397
1.000000	-0.00000	C.35508	1.31196	-0.44836

MACH NUMBER= 0.97800

X/C	Y/C	P/P0	M-LOCAL	CP
0.010000	0.01130	C.90661	0.37688	0.58592
0.020000	0.01710	C.88488	0.42145	0.44903
0.030000	0.02380	C.86587	0.45828	0.36706
0.040000	0.02950	C.84904	0.49560	0.28752
0.050000	0.02750	C.83773	0.50934	0.21419
0.060000	0.02950	0.82958	0.52359	0.17246
0.070000	0.03160	0.82180	0.53649	0.13584
0.080000	0.03350	0.81509	0.54842	0.09475
0.090000	0.03500	C.80878	0.55906	0.06093
0.100000	0.03690	C.80425	0.56863	0.03066
0.150000	0.04270	C.78593	0.59685	-0.01775
0.200000	0.04640	C.77571	0.61143	-0.11462
0.250000	0.04870	C.77197	0.61946	-0.13649
0.300000	0.04980	C.77173	0.61984	-0.13775
0.350000	0.04900	C.77173	0.61984	-0.13775
0.400000	0.04920	C.77197	0.61946	-0.13649
0.450000	0.04790	C.77337	0.61770	-0.12946
0.500000	0.04590	C.77477	0.61494	-0.12143
0.550000	0.04330	C.77664	0.61192	-0.11142
0.600000	0.04020	C.77897	0.60816	-0.09893
0.650000	0.03660	C.78176	0.60363	-0.08397
0.700000	0.03260	C.78593	0.59865	-0.06162
0.750000	0.02810	C.79054	0.59311	-0.03690
0.800000	0.02320	C.79560	0.58749	-0.01490
0.850000	0.01790	C.80334	0.58015	0.01177
0.900000	C.01230	C.81268	0.57272	0.08270
0.950000	0.00630	0.82404	0.52896	0.15582

MACH NUMBER= 0.95700

SHOCK LOCATED AT 76 PERCENT CHORD FOR MACH NUMBER= 0.951

LAMINAR BOUNDARY LAYER--REYNOLDS NUMBER= 0.100E 07

X/C	Y/C	P/P0	M-LOCAL	CP
0.700000	0.03260	-0.084960	-0.084756	
0.750000	0.02810	-0.094212	-0.093435	
0.800000	0.02320	-0.102192	-0.101818	
0.850000	0.01790	-0.109020	-0.108591	
0.900000	0.01230	-0.115728	-0.115215	
0.950000	0.00630	-0.124068	-0.123437	
1.000000	-0.000000	-0.126000	-0.125339	

CALCULATION OF THE LOCAL MACH NUMBER NEAR THE NOSE FOR P=1

X/C	Y/C	P/P0	M-LOCAL	CP
0.010000	0.01130	0.73906	0.67168	0.56996
0.020000	0.01710	C.69072	0.74667	0.43925
0.030000	0.02080	C.65112	C.80750	0.33213
0.040000	0.02450	0.62188	0.85249	0.25311
0.050000	0.02750	0.59682	0.89131	0.18535
0.060000	0.02950	C.58198	0.91448	0.14521
0.070000	0.03160	C.56819	0.93617	0.10791
0.080000	0.03350	0.55649	0.95660	0.07644
0.090000	0.03500	0.54584	0.97168	0.04748
0.100000	0.03690	0.53628	0.98381	0.02705

LOCAL MACH NUMBER HAS EXCEEDED UNITY BEFORE 11 PERCENT CHORD

LAMBDA= 1.458002

X/C	Y/C	P/P0	M-LOCAL	CP
C.10000	C.01130	C.82427	0.53275	0.75236
C.07000	0.01710	C.15134	0.64918	0.55225
C.10000	0.02080	C.10175	0.72658	0.41237
C.04000	0.02450	C.68522	0.78585	0.30368
C.05000	C.02750	C.47376	0.83619	0.21491
C.06000	0.02950	C.40731	0.87503	0.14030
0.07000	0.03160	C.58466	0.91029	0.07961
0.08000	0.03350	C.56502	0.94117	0.02102
C.09000	0.03500	0.54784	0.96847	-0.02744
0.10000	0.03690	0.53273	0.99277	-0.07009
0.15000	0.04270	0.47944	1.08100	-0.22039
0.20000	0.04640	C.45088	1.13078	-0.30096
0.25000	0.04870	C.43787	1.15346	-0.33746
0.30000	0.04980	C.42926	1.16897	-0.36195
0.35000	0.04900	C.42110	1.18386	-0.38498
0.40000	0.04920	C.41790	1.19873	-0.40398
0.45000	0.04790	C.41298	1.19886	-0.40794
0.50000	0.04590	C.40512	1.21353	-0.41604
0.55000	0.04330	C.41233	1.20006	-0.40973
0.60000	0.04020	C.44002	1.19462	-0.33180
0.65000	0.03660	C.46772	1.10106	-0.28447
0.70000	0.03260	0.49541	1.05407	-0.17534
0.75000	C.02810	C.52311	1.00838	-0.09721
0.80000	0.02320	0.55289	0.96042	-0.01320
0.85000	0.01790	C.58799	0.90508	0.05882
0.90000	0.01230	C.63713	0.82900	0.22444
0.95000	C.00630	C.70850	0.71924	C.42579
1.00000	-0.00000	1.72757UUUUUUUUUUUUUUUU		3.30066

Figure H-8. Continued.

## User Instructions - TRANSON

This program is written in FORTRAN IV and is designed to run in single precision on a IBM 370-165 computer. Execution requires 42,000 bytes of core storage and approximately 6 seconds to produce the two-dimensional zero Mach number pressure distribution for an airfoil at six angles of attack by the 32-point Weber method. For a given run the program requires the following input data:

- (1) The 992 elements of the Matrix S1 given in A.R.C. R&M 2918 and listed herein as Table H-5.
- (2) The 992 elements of the Matrix S2 also given in A.R.C. R&M 2918 and listed herein as Table H-6.
- (3) The 1024 elements of Matrix S3 also given in A.R.C. R&M 2918 and listed herein as Table H-7.
- (4) The 72 characters of the array TITLE which are used as a header for identifying output. It is an alphameric array and usually contains information about the type of airfoil, run numbers, and any other such information desired by the programmer as a header..
- (5) The values of X, from Table H-1.
- (6) The values of Y, the y-coordinates (given in fraction of chord) of the airfoil to be considered at the previously specified values of X.
- (7) The values of angle of attack,  $A$ , and airfoil leading edge radius,  $RHO$ , for a given airfoil, followed by a last card indicator giving  $A$  a value of greater than 15.
- (8) Additional data sets containing information from item (4) through item (7), if needed. Only two airfoils may be considered per run.

Format specifications for these variables may be found in Figure H-9. A sample data set of the NCSU 0010 may be found in Figure H-10 and the output for that data set is given in Figure H-11.





Program Listing - TRANSON

```

C C PROGRAM TO CALCULATE THE INCOMPRESSIBLE PRESSURE DISTRIBUTION
C C ABOUT 2-D SYMMETRICAL AIRFOILS (REFERENCE- WEBER, J.- A.R.C. R.G.M.
C C 2918, JULY, 1953.)
C C THE INPUT DATA NEEDED ARE AS FOLLOWS :
C C S1(I,J),S2(I,J),C S3(I,J) ARE COEFFICIENTS LISTED IN R.G.M. 2918
C C TITLE, PRESIDENT INFORMATION TO BE LISTED AT FIRST OF OUTPUT
C C X(1), Y(1) ARE THE PROFILES, ABSCISSA AND ORDINATES (X/C & Y/C)
C C THESE ARE INPUT FROM THE TRAILING EDGE FORWARD FOR THE
C C SPECIFIC LOCATIONS FOR N = 22
C C A= AIRFOIL ANGLE OF ATTACK (DEGREES)
C C RHO= AIRFOIL LEADING EDGE RADIUS (DECIMAL FRACTION OF CHORD)
C C DIMENSION S1(32),S2(32),S3(32),X(32),Y(32),S11(32),S22(32)
C C DIMENSION TITLE(18)
C C COMMON /INOUT/JREAD,JWRITE
C C JREAD=1
C C JWRITE=3
C C READ (JREAD,4) ((S1(I,J),J=1,32),I=1,31)
C C READ (JREAD,5) ((S2(I,J),J=1,31),I=1,31)
C C READ (JREAD,4) ((S3(I,J),J=1,32),I=1,32)
C C FORMAT (BF10.5)
C C READ (JREAD,10) (TITLE(I),I=1,18)
C C FORMAT (18A4)
C C DO 20 JJJ=1,2
C C READ (JREAD,5) (X(I),I=1,32)
C C READ (JREAD,5) (Y(I),I=1,32)
C C FORMAT (BF10.6)
C C READ (JREAD,6) A,RHO
C C FORMAT (ZF10.5)
C C A=ATP15,GO TO 19
C C Y(32)=RHO,GO TO 19
C C WRITE (JWRITE,5)
C C WRITE (JWRITE,32)
C C FORMAT (1H1,/,19X,35HINCOMPRESSIBLE PRESSURE COEFFICIENT)
C C WRITE (JWRITE,13) (TITLE(I),I=1,18)
C C FORMAT (10A4)
C C WRITE (JWRITE,14) A
C C FORMAT (10A4)
C C IF (JJJ.EQ.2) GO TO 91
C C WRITE (JWRITE,12)
C C FORMAT (10A4)
C C GO TO 90
C C WRITE (JWRITE,31)
C C FORMAT (10A4)
C C DO 100 J=1,31
C C S11(J)=0.
C C S22(J)=0.
C C S33(J)=S3(32),J*(Y(32)
C C DO 8 I=1,31
C C S11(J)=S11(J)+S1(I,J)*Y(I)
C C CONTINUE
C C DO 9 I=1,31
C C S22(J)=S22(J)+S2(I,J)*Y(I)
C C CONTINUE
C C DO 10 I=1,31
C C S33(J)=S33(J)+S3(I,J)*Y(I)
C C CONTINUE
C C
C C B=COS(A/57.2958)*L1+S11(J)
C C C=SIN(A/57.2958)*SQRT(1.-X(J)/X(J))*L1+S33(J)
C C D=L1+S22(J)*D2
C C IF (JJJ.EQ.2) GO TO 22
C C CPU(J)=1.-((1B+C)*D2/D)
C C GO TO 107
C C CPU(J)=1.-((1B-C)*D2/D)
C C WRITE (JWRITE,11) X(J),Y(J),CPU(J)
C C FORMAT (3F20.6)
C C CONTINUE
C C WRITE (JWRITE,32)
C C FORMAT (10A4)
C C GO TO 7
C C IF (JJJ.EQ.2,AND,A.GT.15.) CALL EXIT
C C CONTINUE
C C STOP
C C END

```

# Sample Output - TRANSON

INCOMPRESSIBLE PRESSURE COEFFICIENT			INCOMPRESSIBLE PRESSURE COEFFICIENT		
*****			*****		
NCSU 0010 32 POINT			NCSU 0010 32 POINT		
ANGLE OF ATTACK= 1.000000			ANGLE OF ATTACK= 1.000000		
X/C	Y/C	CP-UPPER	X/C	Y/C	CP-LOWER
0.997600	0.000300	0.338278	0.997600	0.000300	0.340111
0.996400	0.001200	0.256765	0.996400	0.001200	0.241133
0.979500	0.002000	0.160352	0.979500	0.002000	0.167868
0.961900	0.004800	0.131678	0.961900	0.004800	0.142446
0.941000	0.007400	0.080033	0.941000	0.007400	0.094474
0.915700	0.010400	0.047191	0.915700	0.010400	0.065578
0.886500	0.013000	0.010094	0.886500	0.013000	0.032629
0.853600	0.017500	-0.018539	0.853600	0.017500	0.007666
0.817200	0.021500	-0.062837	0.817200	0.021500	-0.030996
0.777800	0.025400	-0.080945	0.777800	0.025400	-0.063776
0.735700	0.029400	-0.112421	0.735700	0.029400	-0.086688
0.691300	0.033300	-0.139244	0.691300	0.033300	-0.090072
0.645100	0.037000	-0.169633	0.645100	0.037000	-0.113703
0.597900	0.040410	-0.191290	0.597900	0.040410	-0.128077
0.549000	0.043490	-0.225970	0.549000	0.043490	-0.150091
0.500000	0.045920	-0.241208	0.500000	0.045920	-0.161114
0.451000	0.047890	-0.267856	0.451000	0.047890	-0.170005
0.402500	0.049340	-0.290399	0.402500	0.049340	-0.182999
0.354000	0.049940	-0.315150	0.354000	0.049940	-0.201146
0.308700	0.049890	-0.354826	0.308700	0.049890	-0.207135
0.264300	0.049140	-0.357075	0.264300	0.049140	-0.213676
0.222200	0.047640	-0.379512	0.222200	0.047640	-0.215991
0.182000	0.045350	-0.394442	0.182000	0.045350	-0.210094
0.144400	0.042400	-0.417375	0.144400	0.042400	-0.203590
0.113900	0.038740	-0.439997	0.113900	0.038740	-0.193477
0.084270	0.034220	-0.407974	0.084270	0.034220	-0.124574
0.059040	0.029680	-0.415840	0.059040	0.029680	-0.124634
0.038060	0.024440	-0.523752	0.038060	0.024440	-0.074299
0.021530	0.018600	-0.421732	0.021530	0.018600	0.006618
0.009610	0.012400	-0.390279	0.009610	0.012400	0.346053
0.002410	0.004500	0.831925	0.002410	0.004500	0.439479

ANGLE OF ATTACK= 2.500000			ANGLE OF ATTACK= 2.500000		
X/C	Y/C	CP-UPPER	X/C	Y/C	CP-LOWER
0.997600	0.000300	0.337994	0.997600	0.000300	0.342522
0.996400	0.001200	0.254471	0.996400	0.001200	0.265579
0.979500	0.002000	0.155970	0.979500	0.002000	0.174967
0.961900	0.004800	0.124993	0.961900	0.004800	0.151842
0.941000	0.007400	0.070590	0.941000	0.007400	0.106705
0.915700	0.010400	0.034495	0.915700	0.010400	0.059648
0.886500	0.013000	-0.005382	0.886500	0.013000	0.050890
0.853600	0.017500	-0.037192	0.853600	0.017500	0.030251
0.817200	0.021500	-0.085829	0.817200	0.021500	-0.005108
0.777800	0.025400	-0.107942	0.777800	0.025400	-0.014587
0.735700	0.029400	-0.143370	0.735700	0.029400	-0.036177
0.691300	0.033300	-0.174986	0.691300	0.033300	-0.052191
0.645100	0.037000	-0.210584	0.645100	0.037000	-0.070901
0.597900	0.040410	-0.237821	0.597900	0.040410	-0.080054
0.549000	0.043490	-0.278641	0.549000	0.043490	-0.099937
0.500000	0.045920	-0.301007	0.500000	0.045920	-0.100983
0.451000	0.047890	-0.335332	0.451000	0.047890	-0.110968
0.402500	0.049340	-0.366810	0.402500	0.049340	-0.114371
0.354000	0.049940	-0.401311	0.354000	0.049940	-0.118361
0.308700	0.049890	-0.432605	0.308700	0.049890	-0.113715
0.264300	0.049140	-0.467877	0.264300	0.049140	-0.109631
0.222200	0.047640	-0.506671	0.222200	0.047640	-0.098258
0.182000	0.045350	-0.539010	0.182000	0.045350	-0.078497
0.144400	0.042400	-0.586824	0.144400	0.042400	-0.057859
0.113900	0.038740	-0.637625	0.113900	0.038740	-0.021944
0.084270	0.034220	-0.630991	0.084270	0.034220	0.008742
0.059040	0.029680	-0.762879	0.059040	0.029680	0.101465
0.038060	0.024440	-0.909543	0.038060	0.024440	0.212848
0.021530	0.018600	-0.886577	0.021530	0.018600	0.409517
0.009610	0.012400	-1.150623	0.009610	0.012400	0.743783
0.002410	0.004500	0.715663	0.002410	0.004500	0.985260

Figure H-11. Sample output for TRANSON.

**APPENDIX I - A Computer Program Providing Rapid Evaluation  
of Closed-Form Solution for the Flow About a  
Prolate Spheroid Moving Along Its X-Axis**

In order to evaluate the accuracy of the method described in the body of this work for predicting potential flow about an arbitrary three-dimensional body, a search was undertaken for a suitable body with a closed-form velocity distribution. The most obvious was the sphere. While the sphere does provide a means for such comparison, it is a very crude approximation of an aircraft fuselage or similar type three-dimensional body. A body which had a higher length-to-width ratio would be more representative; therefore, an analytical method for generating the potential flow about an ellipsoid was examined.

The solution for potential flow about an ellipsoid is well known and can be found in Lamb (Ref. 6) and Munk (Ref. 66). The solution and formulae for generating the velocity distributions are also given in Timman (Ref. 49). The equations in the latter work, originally developed for a yawed ellipsoid, were degenerated to apply to the case of a spheroid (ellipsoid with y and z axes equal) in a uniform flow field of velocity  $U_0$  at zero incidence to the x-axis of the spheroid.

The velocity distribution of the spheroid was calculated by a computer program in the following manner:

Knowing the x-axis (a), the y and z-axes (b) of the spheroid, and the x, y, and z coordinates of the point for which the potential flow is to be evaluated, a series of coefficients is then determined:

$$s = \sqrt{1 - b^2/a^2}$$

$$\alpha_0 = \frac{2 ab^2}{(a^2 - b^2)^{3/2}} [\tanh^{-1}(s) - s]$$

$$P = \frac{2 U_0}{(2 - \alpha_0)}$$

$$G = \frac{x^2}{a^4} + \frac{1}{b^4} (y^2 + z^2)$$

Following Timman, one may manipulate the degenerate form of the equations to obtain the velocity components in terms of these coefficients:

$$u = \frac{-P}{Gb^4} (y^2 + z^2)$$

$$v = \frac{P}{G} \left( \frac{xy}{a^2b^2} \right)$$

$$w = \frac{P}{G} \left( \frac{xz}{a^2b^2} \right)$$

Given the dimensions of the spheroid and the free stream velocity, the program then computes  $u$ ,  $v$ , and  $w$  at a specified  $x$ ,  $y$ , and  $z$  on the surface of the spheroid by means of the relations above.

From the equations it can be seen that the potential flow about a sphere may also be generated by letting  $a$  be equal to  $b$ . Because of the indeterminate form of the solution for this case, it is necessary to obtain a solution for a sphere by letting  $a = 1.01b$ .

Because of its speed and accuracy this program was most helpful in establishing when the general three-dimensional body potential flow program was running correctly and how many panels were required and in what distribution to represent a body adequately. It is presented here so that the reader may use it for that purpose or as a direct solution for a special class of fuselages. The latter case may be of special interest to those with limited computing facilities or those who wish to demonstrate the design concepts related herein without incurring the large computing expenses of the general three-dimensional body program. The following discussion provides a listing, instructions for entering data, and typical output.



# Sample Output

## 3-1 SPHEROID

### THE THEORETICAL VELOCITY SOLUTION FOR A SPHEROID

A= 3.00000  
B= 1.00000  
U0= 1.00000

I	X	Y	Z	U	V	W	CP
1	3.00000	0.00000	0.00000	-0.00000	0.00000	0.00000	1.00000
2	2.98000	0.00000	0.35177	-0.89511	0.00000	0.45062	-0.00428
3	2.00000	0.00000	0.74417	-1.03011	0.00000	0.30761	-0.19979
4	1.50000	0.00000	0.86603	-1.00190	0.00000	0.20021	-0.21909
5	1.00000	0.00000	0.94258	-1.10659	0.00000	0.13044	-0.24154
6	0.50000	0.00000	0.98413	-1.11842	0.00000	0.08301	-0.25409
7	0.00000	0.00000	1.00000	-1.12197	0.00000	0.00000	-0.25891

## SPHERE

### THE THEORETICAL VELOCITY SOLUTION FOR A SPHEROID

A= 1.00100  
B= 1.00000  
U0= 1.00000

I	X	Y	Z	U	V	W	CP
1	1.00100	0.00000	0.00104	-0.00000	0.00000	0.00155	1.00000
2	1.00000	0.00000	0.04472	-0.00301	0.00000	0.06706	0.99549
3	0.99900	0.00000	0.06322	-0.00601	0.00000	0.09470	0.99100
4	0.99800	0.00000	0.07741	-0.00900	0.00000	0.11584	0.98650
5	0.99700	0.00000	0.08736	-0.01200	0.00000	0.13350	0.98201
6	0.99599	0.00000	0.09388	-0.01499	0.00000	0.14816	0.97753
7	0.99499	0.00000	0.10039	-0.01798	0.00000	0.16019	0.97305
8	0.99399	0.00000	0.11012	-0.02096	0.00000	0.17004	0.96857
9	0.99299	0.00000	0.12429	-0.02394	0.00000	0.18796	0.96410
10	0.99199	0.00000	0.13387	-0.02692	0.00000	0.19911	0.95963
:	:	:	:	:	:	:	:
990	0.01097	0.00000	0.99994	-1.49922	0.00000	0.01041	-1.24794
991	0.00997	0.00000	0.99993	-1.49926	0.00000	0.01191	-1.24799
992	0.00896	0.00000	0.99996	-1.49928	0.00000	0.01341	-1.24803
993	0.00796	0.00000	0.99997	-1.49931	0.00000	0.01492	-1.24807
994	0.00696	0.00000	0.99998	-1.49933	0.00000	0.01642	-1.24810
995	0.00596	0.00000	0.99998	-1.49935	0.00000	0.01792	-1.24813
996	0.00496	0.00000	0.99999	-1.49937	0.00000	0.01942	-1.24815
997	0.00396	0.00000	0.99999	-1.49938	0.00000	0.02092	-1.24817
998	0.00296	0.00000	1.00000	-1.49939	0.00000	0.02243	-1.24819
999	0.00196	0.00000	1.00000	-1.49940	0.00000	0.02393	-1.24820
1000	0.00096	0.00000	1.00000	-1.49940	0.00000	0.02543	-1.24821

Figure I-3. Sample output for SPHEROID.





## User Instructions

This program is written in Fortran IV and is designed to run on an IBM 370-165 computer. Execution requires 30,000 bytes of core storage and approximately 10 seconds to predict the velocity distribution and pressure coefficient for 1600 points. For a given run, the program requires the following input data:

(1) The 80 characters of the alphanumeric array TITLE which are used as a header for identifying output. It is used to terminate execution by setting the first four characters to "ENDØ".

(2) The x-axis (a), the y and z-axes (b), the free stream x-velocity,  $U_0$ , the mode indicator, IX, and the number of points for this run, N. The mode indicator, IX, may take on two values. If IX is zero a meridian solution of N points is generated by the program. By indicating IX as one, the programmer implies that a meridian solution is not desired and that N specifically selected points will follow.

(3) The points x, y, and z (if IX equals one) at which the solution is to be calculated.

Format specifications for these variables may be found in Figure I-1. A sample data set of a three-to-one prolate spheroid is given in Figure I-2 and the output for that data set is given in Figure I-3.

TITLE					
20A4					
A	B	U0	IX	N	/
F10.5	F10.5	F10.5	I10	I10	/
X	Y	Z	/		
F10.5	F10.5	F10.5	/		
X	Y	Z	/		
F10.5	F10.5	F10.5	/		
etc.	etc.	etc.	/		

Figure I-1. Format specification for SPHEROID.

## APPENDIX J - Supplementary Bibliography

Listed below is bibliographic information on some post-1970 documents in the NASA information collection dealing, at least in a general way, with the estimation of aerodynamic characteristics of subsonic aircraft. The methods described are, for the most part, intended for computer solution. A listing of the appropriate program is given in quite a number of these documents along with user instructions. The documents are available (except where noted) from the National Technical Information Service by requesting the first number (document accession number) shown in each citation.

The list was assembled from a computer search of the NASA information collection for documents indexed under both aerodynamic characteristics and computer methods or numerical methods. Results from a second search employing the terms Prediction Analysis Techniques, Flow characteristics, Aerodynamic Drag, Aerodynamic Coefficient, and Performance Prediction are also included. Titles and mini-abstracts were then examined to select those citations given below. The present authors have not seen the complete document in most cases. The list is intended to provide some contemporary references for the worker just entering the field as well as an indication of the direction in which contemporary research is moving for the benefit of the more casual reader. Because the task of assembling this work as a whole necessarily limited the period of preparing the literature review to late 1972 it was not possible to include the documents listed here in the review.

1. 72B10618      Langley-11047  
Vortex-Lattice Fortran Program for Estimating Subsonic Aerodynamic Characteristics of Complex Planforms  
Margason, R. J.; Lamar, J. E.
2. 71B10153      Lewis-11382  
Computer Program for Calculating Aerodynamic Forces on Blade Sections  
MC Nally, W. D.
3. 74A15445      9 pages  
Computerized Design of Transport Airplane  
Takao, K.  
Japan, Defense Academy, Memoirs, Vol. 13, Sept. 1973, pp. 327-335.
4. 73A22433      2 pages  
Calculation of Forces on Stores in the Vicinity of Aircraft  
Serbin, H.  
Journal of Aircraft, Vol. 10, Feb. 1973, pp. 123, 124.

5. 73A17213      4 pages  
Leading-Edge Force Features of the Aerodynamic Finite Element Method  
Lan, C.-T.; Roskam, J.  
Journal of Aircraft, Vol. 9, Dec. 1972, pp. 864-867.
6. 73A14377      37 pages  
Transonic Profile Theory - Critical Comparison of Various Procedures  
Eberle, A.; Sacher, P.  
Deutsche Gesellschaft Fuer Luft - und Raumfahrt, Symposium Ueber  
Tragfluegel-Aerodynamik Bei Schallnahen Stroemungen, Goettingen, West  
Germany, Oct. 26, 27, 1972, Paper In German.
7. 72A43455      SAWE Paper 908      15 pages  
An Aerodynamics Model Applicable to the Synthesis of Conventional  
Fixed-Wing Aircraft  
Peyton, R. S.  
Society of Aeronautical Weight Engineers, Annual Conference, 31st,  
Atlanta, Ga., May 22-25, 1972.
8. 72A16798      AIAA Paper 72-221  
A Simple Model for the Theoretical Study of Slat-Airfoil Combinations  
Liebeck, R. H.; Smyth, D. N.
9. 71A24253      SAE Paper 710389  
Low Speed Airfoil Analysis Using a Small Digital Computer  
Koepsel, R. E.; Miller, J. A.; Wentz, W. H., Jr.  
New York, Society of Automotive Engineers, Inc., Society of Automotive  
Engineers, National Business Aircraft Meeting, Wichita, Kan., Mar.  
24-26, 1971.
10. 73N70722      GDC-TN-70-AVLABS-09      54 pages  
User's Manual for Tilt Wing and Deflected Slipstream Aerodynamics Program  
Pederson, S. K.
11. 74N14741      NASA-TR-R-421  
A Study of the Nonlinear Aerodynamics of Bodies in Nonplanar Motion  
(Numerical Analysis of Aerodynamic Force and Moment Systems During  
Amplitude, Arbitrary Motions)  
Schiff, L. B.  
Ph.D. Thesis - Stanford University, Calif.
12. 74N14739      NASA-TM-X-62321      31 pages  
Plotting Program for Aerodynamic Lifting Surface Theory -- User Manual  
for Fortran Computer Program  
Medan, R. T.; Ray, K. S.
13. 74N11810      NASA-TM-X-62309  
Geometry Program for Aerodynamic Lifting Surface Theory  
Medan, R. T.

14. 73N31226  
Starting Vortex, Separation Bubbles and Stall -- A Numerical Study of Laminar Unsteady Flow Around an Airfoil  
Mehta, U. B.  
Ph.D. Thesis, Illinois Inst. of Tech., Chicago, Univ. Microfilms Order No. 73-12222.
15. 73N27890      NASA-CR-2217  
Analytical Method for Predicting the Pressure Distribution About a Nacelle at Transonic Speeds  
Keith, J. S.; Ferguson, D. R.; Merkle, C. L.; Heck, P. H.; Lahti, D. J.
16. 73N27889      NASA-TN-D-6933  
On the Numerical Simulation of Three-Dimensional Transonic Flow with Application to the C-141 Wing  
Lomax, H.; Bailey, F. R.; Ballhaus, W. F.
17. 73N27212      NAL-TR-309  
In Japanese; English Summary  
A Numerical Calculation of a Two-Dimensional Incompressible Potential Flow Around a Set of Airfoils Applying the Relaxation Method  
Nakamura, M.  
National Aerospace Lab., Tokyo, Japan.
18. 73N25010      ARC-R/M-3487  
The Calculation of the Spanwise Loading of Sweptback Wings with Flaps or All-Moving Tips at Subsonic Speeds  
Brebner, G. G.; Lemaire, D. A.
19. 73N24997  
Kelvin Impulse Theory Applied to Lift on Airfoils  
Delaney, J. A.  
Ph.D. Thesis, Cincinnati Univ., O.    Univ. Microfilms Order No. 72-31627.
20. 73N24325      SC-CR-72-3182  
Numerical Solution of the Three-Dimensional Boundary Layer on a Spinning Sharp Body at Angle of Attack  
Watkins, C. B., Jr.
21. 73N24319      NASA-TT-F-14918      24 pages  
The Kutta-Joukowski Conditions in Three-Dimensional Flow  
Legendre, R.
22. 73N24302      90 pages  
The Three-Dimensional Structure of Transonic Flows Involving Lift  
Hafez, M. M.  
Ph.D. Thesis, Univ. of Southern Calif., Univ. Microfilms Order No. 72-27661.

23. 73N24054      14 pages  
Review of Two Methods of Optimizing Aircraft Design  
Kirkpatrick, D. L. I.  
In AGARD Aircraft Performance Prediction Methods and Optimization.
24. 73N22998      AFAPL-TR-72-100      124 pages  
Lifting Surface Theory for Statically Operating Propellers  
Murray, J. C.; Carta, F. C.
25. 73N21952      FTD-MT-24-1646-72      20 pages  
Approximate Method of Calculating the Aerodynamic Load Distribution on a  
Low-Flying Wing with a Fuselage  
Tsvetkov, L. G.
26. 73N21913      NWL-TR-2796      122 pages  
Body Alone Aerodynamics of Guided and Unguided Projectiles at Subsonic,  
Transonic, and Supersonic Mach Numbers  
Moore, F. G.
27. 73N21292      MDC-J5679-02      81 pages  
Calculation of Potential Flow About Arbitrary Three-Dimensional Lifting  
Bodies, User's Manual  
Mack, D.
28. 73N19999      NASA-TN-D-7251      35 pages  
Steady, Subsonic, Lifting Surface Theory for Wings with Swept, Partial  
Span, Trailing Edge Control Surfaces  
Medan, R. T.
29. 73N18054      FTD-HT-23-834-72      12 pages  
Flow Around Wing Profile with the Presence of the Surface of a System  
of Sources and Sinks  
Baev, B. S.; Zhuravlev, V. N.
30. 73N17035      AFFDL-TR-72-26-VOL-3      207 pages  
V/STOL Aircraft Aerodynamic Prediction Methods Investigation, Volume 3  
Manual for Computer Programs  
Wooler, P. T.; Kao, H. C.; Schwendemann, M. F.; Wasson, H. R.; Ziegler, H.
31. 73N17033      AFFDL-TR-72-26-VOL-1      238 pages  
V/STOL Aircraft Aerodynamic Prediction Methods Investigation, Volume 1  
Theoretical Development of Prediction Methods  
Wooler, P. T.; Kao, H. C.; Schwendemann, M. F.; Wasson, H. R.; Ziegler, H.
32. 73N16985      120 pages  
A Computer Program for the Prediction of Aerodynamic Characteristics of  
Wing-Body-Tail Combinations at Subsonic and Supersonic Speeds, Part 2  
Anders, S.; Bustavsson, L.  
Aeronautical Research Inst. of Sweden, Stockholm.



33. 73N15035        32 pages  
The Avsyn Air Vehicle Synthesis Program for Conceptual Design  
Sanders, K. L.; Staley, P. A.
34. 73N15004        9 pages  
Design of Airfoils with High Lift at Low and Medium Subsonic Mach numbers  
Wortmann, F. X.  
In AGARD Fluid Dyn. of Aircraft Stalling.
35. 73N14989        NASA-CR-2186        58 pages  
Steady Inviscid Transonic Flows Over Planar Airfoils - A Search for a  
Simplified Procedure  
Magnus, R.; Yoshihara, H.
36. 73N13007        RIAS-TR-72-166        50 pages  
On Lifting Wings with Parabolic Tips  
Jordan, P. F.
37. 73N13006        AFOSR-72-1737TR        50 pages  
Exact Solution for Lifting Surfaces  
Jordan, P. F.
38. 73N12315        NPS-59NN72082A        48 pages  
Flow Studies of Axisymmetric Bodies at Extreme Angles of Attack  
Smith, L. H.; Nunn, R. H.
39. 73N12224        NLR-TR-70088-U        38 pages  
Computer Application of Subsonic Lifting Surface Theory  
Labrujere, T. E.; Wooters, J. G.  
National Aerospace Lab., Amsterdam, Netherlands.
40. 73N11999        NASA-CR-2157        115 pages  
Calculative Techniques for Transonic Flows About Certain Classes of  
Wing-Body Combinations, Phase 2  
Stahara, S. S.; Spreiter, J. R.
41. 73N10242        MDC-J5264-VOL-2        310 pages  
Investigation of Aerodynamic Analysis Problems in Transonic Maneuvering,  
Volume 2 Airfoil Analysis Computer Program  
Gentry, A. E.
42. 73N10042        AFFDL-TR-71-155-PT-1        50 pages  
Takeoff and Landing Analysis (Tola) Computer Program  
Lynch, U. H. D.
43. 72N32302        NASA-TT-F-14547        20 pages  
Subsonic and Supersonic Flow Around Nonaxisymmetric Fuselages  
Rothman, H.

44. 72N31991      18 pages  
Lift-Curve Slope and Aerodynamic Centre Position of Wings in Inviscid Subsonic Flow  
Engineering Sciences Data Unit, London, England, Avail on Subscription from Engineering Sciences Data Unit, 251-259 Regent Street, London, W1R 7AD.
45. 72N31909      SRL-TR-70-0009      24 pages  
A Method for Aerodynamic and Propulsion Design Optimization of the Short Range Dogfight Missile  
Forbrich, C. A.; Gallington, R. W.; Hatlelid, J. E.; Hyde, J. P.; Murrow, R. C.
46. 72N30264      NASA-TT-F-14538      6 pages  
Numerical Study of the Influence of the Wing Tip Shape on the Vortex Sheet Rolling Up  
Rehback, C.
47. 72N29002      RIAS-TR-72-040      70 pages  
Complete Solution for Lifting Wings with Parabolic Tips  
Jordan, P. F.
48. 72N26023      NASA-CR-112065-3      114 pages  
Theoretical Prediction of Interference Loading on Aircraft Stores, Part 3  
Programmer's Manual  
Danfernandes, F.
49. 72N26003      ONERA-TP-1088      16 pages  
In French; English Summary  
Aerofoil Stall Prediction in Incompressible Flow  
Vincentdepaul, M.
50. 72N26001      26 pages  
Calculation of Pressure Distributions for an Airfoil in Subcritical Flow Including the Effect of the Boundary Layer  
Anders, S.; Gustavsson, L.; Hillgren, R. S.; Toll, G. I.  
Aeronautical Research Inst. of Sweden, Stockholm.
51. 72N24005      AFOSR-72-0034TR      19 pages  
The Discrete Vortex Approximation of a Finite Vortex Sheet  
Moore, D. W.
52. 72N24003      MDC-J5108      AFOSR-72-0370      92 pages  
A General Class of Airfoils Conformally Mapped from a Circle  
James, R. M.
53. 72N22002      ARC-R/M-3630  
The Linearized Subsonic Flow Over the Centre-Section of a Lifting Swept Wing  
Rossiter, P. J.

54. 72N15010      48 pages  
In German; English Summary  
Downwash Investigations on a Missile Tail  
Gregoriou, G.  
Messerschmitt-Boelkow-Blohm G. M. B. H., Ottobrunn, West Germany.
  
55. 72N11289      NASA-TN-D-6530      16 pages  
Contribution to Methods for Calculating the Flow About Thin Lifting  
Wings at Transonic Speeds. Analytic Expressions for the Far Field  
Klunker, E. B.
  
56. 71N30488      NASA-TT-F-702  
The Calculation of the Pressure Distribution on a Cascade of Thick  
Airfoils by Means of Fredholm Integral Equations of the Second Kind  
Martensen, E.  
(Translation of Ref. 24).
  
57. 71N19385      9 pages  
A Method for Predicting Interference Forces and Moments on Aircraft  
Stores at Subsonic Speeds  
Fernandes, F. D.  
In AGARD Aerodyn. Interference, Jan. 1971.
  
58. 74N18680      NASA-CR-2334      187 pages  
Correlation of Full-Scale Drag Predictions with Flight Measurements on  
the C-141A Aircraft: Phase 2 Wind Tunnel Tests, Analysis, and Prediction  
Techniques. Volume 2 Wind Tunnel Test and Basic Data, Final Report  
MacWilkinson, D. G.; Blackerby, W. T.; Paterson, J. H.
  
59. 74N18679      NASA-CR-2333      166 pages  
Correlation of Full-Scale Drag Predictions with Flight Measurements on  
the C-141A Aircraft Phase 2 Wind Tunnel Test, Analysis, and Prediction  
Techniques, Volume 1 Drag Predictions, Wind Tunnel Data Analysis and  
Correlation, Final Report  
MacWilkinson, D. G.; Blackerby, W. T.; Paterson, J. H.
  
60. 74N14716      50 pages  
Aircraft Drag Prediction for Project Appraisal and Performance Estimation  
Butler, S. F. J.  
In AGARD Aerodyn. Drag.
  
61. 74N14712      11 pages  
Aerodynamic Drag and Lift of General Body Shapes at Subsonic, Transonic,  
and Supersonic Mach Numbers  
Moore, F. G.  
In AGARD Aerodynamic Drag.

62. 74N14711 38 pages  
A Survey of Drag Prediction Techniques Applicable to Subsonic and Transonic Aircraft Design  
Paterson, J. H.; MacWilkinson, D. G.; Blackerby, W. T.  
In AGARD Aerodyn. Drag.
63. 73N15010 16 pages  
The Effect of Leading Edge Geometry on High Speed Stalling  
Moss, G. F.; Haines, A. B.; Jordon, R.  
In AGARD Fluid Dyn. of Aircraft Stalling.
64. 72N22995 NASA-TM-X-67791 94 pages  
Nonplanar Method for Predicting Incompressible Aerodynamic Coefficients of Rectangular Wings with Circular-Arc Camber  
Lamar, J. E.  
Ph.D. Thesis, Virginia Polytechnic Institute, Avail. NTIS HC \$6.75.
65. 72N11869 NASA-TM-X-67413 9 pages  
A Comparison of Some Aerodynamic Drag Factors as Determined in Full-Scale Flight with Wind-Tunnel and Theoretical Results  
Saltzman, E. J.; Bellman, D. R.  
In AGARD Facilities and Tech. for Aerodyn. Testing at Transonic Speeds and High Reynolds Number.
66. 74N1423 9 pages  
New Investigations for Reducing the Base Drag of Wings with a Blunt Trailing Edge -- Effects of Splitter Plates and Splitter Wedges on Aerodynamic Drag Coefficients  
Tanner, M.  
In AGARD Aerodyn. Drag.
67. 74N14719 20 pages  
Drag of Supercritical Airfoils in Transonic Flow -- Comparison with Conventional Airfoil Drag Coefficients  
Kacprzyński, J. J.  
In AGARD Aerodyn. Drag.
68. 74N14709 AGARD-CP-124 469 pages  
Partly in English and Partly in French  
Aerodynamic Drag  
Advisory Group for Aerospace Research and Development, Paris, France,  
Avail. NTIS HC \$25.50, Proceedings of Specialist Meeting, Izmir, Turkey, 10-13 April 1973.
69. 73N31228 ESOL-71020 ESDU-67010 23 pages  
Aerofoils having a Specified Form of Upper Surface Pressure Distribution  
Details and Comments on Design  
Engineering Sciences Data Unit, London, England, Avail Issuing Activity,  
Sponsored by Min. of Defence and Roy. Aeron. Soc.

70. 73N23362 ESDU-BODIES-02.04.02 3 pages  
 Drag of Streamline Solids of Revolution (Transition at 0.11 Behind Nose  
 (Numerical Analysis of Drag of Streamlined Bodies of Revolution for  
 Various Length to Diameter Ratios)  
 Engineering Science Data Unit, London, England, Avail. Issuing Activity.
71. 74N14729 11 pages  
 The Drag of Externally Carried Stores Its Prediction and Alleviation --  
 Drag Reduction by Redesign or Development of New Aircraft Installations  
 Pugh, P. G.; Hutton, P. G.  
 In AGARD Aerodyn. Drag.
72. 74N14728 22 pages  
 \* The Drag Resulting from Three-Dimensional Separations Caused by Boundary-  
 Layer Diverters and Nacelles in Subsonic and Supersonic Flow  
 Peake, D. J.; Rainbird, W. J.  
 In AGARD Aerodyn. Drag.
73. 74N14724 15 pages  
 A Study of Flow Separation in the Base Region and Its Effects During  
 Powered Flight -- Interaction Between Propulsive Jet and Free Stream  
 Flow  
 Addy, A. L.; Korst, H. H.; White, R. A.; Walker, B. J.  
 In AGARD Aerodyn. Drag.
74. 74N14718 12 pages  
 Remarks on Methods for Predicting Viscous Drag -- Aerodynamic Drag  
 Prediction for High Angles of Attack and Multielement Airfoils  
 Smith, A. M. O.; Cebeci, T.  
 In AGARD Aerodynamic Drag.
75. 74N14717 9 pages  
 Appendix A Data Item Service for Aircraft Drag Estimation -- Collection,  
 Dissemination, and Development of Aerodynamic Drag Prediction Data  
 Engineering Sciences Data Unit, London, England, Avail. NTIS, In AGARD  
 Aerodyn. Drag.
76. 74N12704 ESDU-73028 23 pages  
 Drag of Two-Dimensional Steps and Ridges Immersed in a Turbulent  
 Boundary Layer at Subsonic and Supersonic Speeds  
 Engineering Sciences Data Unit, London, England, Avail Issuing Activity,  
 Sponsored by Roy. Aeron. Soc.
77. 74N10311 ESDU-BODIES-02.04.01-AMEND-A 3 pages  
 Drag of Streamline Solids of Revolution (Transition at Nose)  
 Engineering Sciences Data Unit, London, England, Avail. Issuing Activity.

78. Not in File 23 pages  
 Measurements in the Thick Axisymmetric Turbulent Boundary Layer Near  
 the Tail of a Body of Revolution  
 Patel, V. C.; Nakayama, A.; Damian, R.  
Journal of Fluid Mechanics, Vol. 63, pp. 345-368, April 1974.
79. 74A19581 13 pages  
 Numerical Solution of the Three-Dimensional Boundary Layer on a Spinning  
 Sharp Body at Angle of Attack  
 Watkins, C. B. Jr.  
Computers and Fluids, Vol. 1, Dec. 1973, pp. 317-329.
80. 74A11957 21 pages  
 The Numerical Solution of the Navier-Stokes Equations for Laminar  
 Incompressible Flow Past a Paraboloid of Revolution  
 Veldman, A. E. P.  
Computers and Fluids, Vol. 1, Sept. 1973, pp. 251-271.
81. 72A41264 2 pages  
 Lift on Airfoils with Separated Boundary Layers  
 Ness, N.  
Journal of Aircraft, Vol. 9, Aug. 1972, pp. 607, 608.
82. 74N13984 AFOSR-73-1265TR-PT-7 45 pages  
 Three-Dimensional Laminar Boundary Layer Over Body of Revolution at  
 Incidence, Part 7 The Extremely High Incidence Case  
 Wang, K. C.
83. 73N25006 ARC-R/M-3221 20 pages  
 Numerical Methods for Calculating the Zero-Lift Wave Drag and the Lift-  
 Dependent Wave Drag of Slender Wings  
 (Evaluation of Double Integral Equation for Calculation of Wave Drag  
 Due to Volume and Aerodynamic Lift of Slender Wings)  
 Weber, J.  
 In Arc Aerodyn. Res., Including Heating, Airfoils, and Boundary Layer  
 Studies, Vol. 1, pp. 155-173.
84. 72N32330 200 pages  
 The Optimum Shaping of Axisymmetric Bodies for Minimum Drag in  
 Incompressible Flow  
 (Optimum Hydrodynamic Configurations for Submerged Minimum Drag  
 Axisymmetric Vehicles in Incompressible Fluids)  
 Parsons, J. S.; Goodson, R. E.

85. 72M50104 1 page FORTRAN V Program  
TRW Vortex-Lattice (N-Surface) Subsonic Aerodynamics  
(Aerodynamic Calculations for Single or Multiple Lifting Surface  
Configurations by Improved Vortex-Lattice Method)  
Romere  
National Aeronautics and Space Administration, Lyndon B. Johnson  
Space Center, Houston, Texas.
86. 71M51203 1 page FORTRAN IV Program  
Subsonic Unsteady Aerodynamic  
(Steady and Unsteady Aerodynamic Coefficients for Subsonic Lifting  
Surfaces)  
Harrison  
National Aeronautics and Space Administration, Marshall Space Flight  
Center, Huntsville, Ala., Jan. 1972.
87. 74M10002 1 page CDC FORTRAN Program 1,293 cards  
Modified Multhopp Mean Camber Program -- Mean Camber Surface Required to  
Support Set of Loadings on Composite Wing in Subsonic Compressible Flow  
National Aeronautics and Space Administration, Langley Research Center,  
Langley Station, Va., Price: Program \$275.00/ Documentation \$15.50.
88. 73M10132 2 pages FORTRAN IV Program 6,594 cards  
An Improved Method for the Aerodynamic Analysis of Wing-Body-Tail  
Configurations in Subsonic and Supersonic Flow  
(Aerodynamic Analysis of Wing-Body-Tail Configurations in Subsonic and  
Supersonic Flow)  
Aerophysics Research Corp., Bellevue, Wash., Price: Program \$600.00/  
Documentation \$27.50.
89. 73M10131 1 page FORTRAN IV Program 960 cards  
General Lifting-Line Jet Flap FORTRAN Program for Estimating Subsonic  
Aerodynamic Characteristics  
(Estimation of Subsonic Aerodynamic Characteristics of Jet-Flapped Wings)  
Northrop Corporate Labs., Hawthorne, Calif., Price: Program \$250.00/  
Documentation \$4.00.
90. 74A25062 ONERA, TP No. 1247 14 pages  
In French  
Aerodynamic Problems of the Short Takeoff and Landing Aircraft  
Ceresuela, R.  
(L'Aeronautique et L'Astronautique, No. 41, 1973, pp. 43-56).
91. 74A21893 4 pages In Russian  
An Optimization Method for a Generalized Class of Functionals and Its  
Application to the Problem of Determining the Shape of a Body Exhibiting  
Maximum Aerodynamic Efficiency  
Bunimovich, A. I.; Dubinskii, A. V.  
Moskovskii Universitet, Vestnik, Seriya I - Matematika, Mekhanika, Vol.  
28, Nov.-Dec. 1973, pp. 87-90.

92. 74A21104 11 pages  
The High Subsonic Flow Around a Two-Dimensional Aerofoil with a Trailing Edge Control Surface  
Nixon, D.  
Aeronautical Quarterly, Vol. 24, Nov. 1973, pp. 273-283.
93. 74A20765 AIAA Paper 74-106 28 pages  
Aeroelastic Loads Predictions Using Finite Element Aerodynamics  
Rowan, J. C.; Burns, T. A.  
American Institute of Aeronautics and Astronautics, Aerospace Sciences Meeting, 12th, Washington, D. C., Jan. 30-Feb. 1, 1974.
94. 74A20280 7 pages  
Subsonic Potential Aerodynamics for Complex Configurations - A General Theory  
Morino, L.; Kuo, C.-C.  
AIAA Journal, Vol. 12, Feb. 1974, pp. 919-197.
95. 74A19684 36 pages  
In French  
Flexible Lifting Surfaces -- In Steady Inviscid Compressible Flow  
Vaussy, P.  
(Association Technique Maritime et Aeronautique, Session, 73rd, Paris, France, May 14-18, 1973), Association Technique Maritime et Aeronautique, Bulletin, No. 73, 1973, pp. 361-394, Discussion, p. 395.
96. 74A18878 AIAA Paper 74-107 14 pages  
A Finite Element Method for Potential Aerodynamics Around Complex Configurations  
Chen, L.-T.; Suci, E. O.; Morino, L.  
American Institute of Aeronautics and Astronautics, Aerospace Sciences Meeting, 12th, Washington, D. C., Jan. 30-Feb. 1, 1974.
97. 74A18820 AIAA Paper 74-72 8 pages  
Odin - Optimal Design Integration System for Synthesis of Aerospace Vehicles  
Rau, T. R.; Decker, J. P.  
American Institute of Aeronautics and Astronautics, Aerospace Sciences Meeting, 12th, Washington, D. C., Jan. 30-Feb. 1, 1974.
98. 74A18681 13 pages  
In Russian  
Calculation of the Aerodynamic Characteristics of a Wing System Moving at Subsonic Speed Near Land or Smooth Water Surface  
Ermolenko, S. D.; Khrapovitskii, V. G.  
Samoletostroenie i Tekhnika Vozdushnogo Flota, No. 32, 1973, pp. 3-15.



99. 74A15965 9 pages  
Exact Method of Designing Airfoils with Given Velocity Distribution in Incompressible Flow  
Strand, T.  
Journal of Aircraft, Vol. 10, Nov. 1973, pp. 651-659.
100. 74A15747 22 pages  
Note on the Aerodynamic Theory of Oscillating T-Tails. I - Theory of Wings Oscillating in Yaw and Sideslip  
Ichikawa, T.; Isogai, K.  
Japan Society for Aeronautical and Space Sciences, Transactions, Vol. 16, No. 33, 1973, pp. 173-194.
101. 74A15709 7 pages  
In Russian  
A Problem of Designing the Optimal External Contours of an Aircraft  
Osipov, V. A.; Tereshchenko, A. M.  
Avalatsionnaia Teknika, Vol. 16, No. 3, 1973, pp. 11-17.
102. 73A40427 5 pages  
Simplified Aerodynamic Theory of Oscillating Thin Surfaces in Subsonic Flow  
Jones, W. P.; Moore, J. A.  
AIAA Journal, Vol. 11, Sept. 1973, pp. 1305-1309.
103. 73A37846 7 pages  
In Russian  
Integral Equation in the Theory of Lifting Surfaces  
Poliakhov, N. N.  
Leningradskii Universitet, Vestnik, Matematika, Mekhanika, Astronomiia, Apr. 1973, pp. 115-121.
104. 73A37545 15 pages  
In Romanian  
New Contributions to the Iterative Method for Aerodynamic Calculations of Wings in Subsonic Flows  
Patraulea, N. N.  
Studii Si Cercetari De Mecanica Aplicata, Vol. 31, No. 1, 1973, pp. 15-29  
15-29.
105. 73A36394 5 pages  
A Finite-Element Method for Calculating Aerodynamic Coefficients of a Subsonic Airplane  
Hua, H. M.  
Journal of Aircraft, Vol. 10, July 1973, pp. 422-426.

106. 73A31746 4 pages  
 Remarks on Vortex-Lattice Methods  
 (Optimal Grid Arrangement in Vortex Lattice Method of Lifting Surface  
 Aerodynamic Analysis, Comparing Numerical with Kernel Function Results  
 for Simple Wing Planforms)  
 Hough, G. R.  
Journal of Aircraft, Vol. 10, May 1973, pp. 314-317.
107. 73A27732 5 pages  
 In German  
 FS-28 - A Contribution to a Possible Development Trend in Light-  
 Aircraft Design  
 (Light Motorized Glider-Type Aircraft Design, Development and Flight  
 Testing, Discussing Aerodynamic Configuration, Structural Design and  
 Performance Characteristics)  
Deutscher Aerokurier, Vol. 17, Mar. 1973, pp. 152-156.
108. 73A26256 440 pages  
 In Russian  
 Design and Stability of Airplanes and Helicopters  
 (Russian Book on Airplane and Helicopter Design and Stability Covering  
 Selection of Wing/Rotor/Configuration and Power Plant, Subsystem Design,  
 Strength, Reliability, Lifetime, Etc.)  
 Voskoboinik, M. S.; Lagosiuk, G. S.; Milen'Kii, Iu. D.; Mirtov, K. C.;  
 Osokin, D. P.; Skripka, M. L.; Ushakov, V. S., Chernenko, Zh. S.  
 Moscow, Izdatel'Stvo Transport, 1972.
109. 73A24915 4 pages  
 Symmetrical Airfoils Optimized for Small Flap Deflection  
 Wortmann, F. X.  
Aero-Revue, Mar. 1973, pp. 147-150.
110. 73A23468 4 pages  
 Estimation of Aerodynamics for Slender Bodies Alone and with Lifting  
 Surfaces at Alpha's from 0 Deg to 90 Deg  
 (Aerodynamic Forces and Moments Estimation for Slender Bodies of  
 Circular and Noncircular Cross Section without and with Lifting  
 Surfaces at 0-90 Degree Angles of Attack)  
 Jorgensen, L. H.  
AIAA Journal, Vol. 11, Mar. 1973, pp. 409-412.
111. 73A21611 10 pages  
 In Russian  
 Discrete Vortex Scheme of a Wing of Finite Span  
 Vorob'ev, N. F.  
 Akademiia Nauk, SSSR, Sibirskoe Ctdelente, Izvestiia, Seriia  
 Tekhnicheskikh Nauk, Oct. 1972, pp. 59-68.

112. 73A18510 10 pages  
Pressure Airships - A Review  
(Airships Design, Constructional and Operational Characteristics,  
Discussing Aerodynamics, Flight Control, Performance and Trim)  
Hecks, K.  
Aeronautical Journal, Vol. 76, Nov. 1972, pp. 647-656.
113. 73A11657 39 pages  
In German  
Further Development and Employment of the Subsonic Panel Method  
(Three-Dimensional Potential Flow Past Arbitrarily Shaped Aerodynamic  
Configurations, Using Hess-Smith Numerical Method)  
Kraus, W.  
Deutsche Gesellschaft Fuer Luft-Und Raumfahrt, Jahrestagung, 5th,  
Berlin, West Germany, Oct. 4-6, 1972.
114. 73A10048 1 page  
Simplification of the Wing-Body Interference Problem  
Graham, R. E.; McDowell, J. L.  
Journal of Aircraft, Vol. 9, Oct. 1972, p. 752.
115. 72A44298 18 pages  
In German  
Computation of the Potential-Theoretical Flow Around Wing-Fuselage  
Combinations and a Comparison with Measurements  
Koerner, H.  
Zeitschrift Fuer Flugwissenschaften, Vol. 20, Sept. 1972, pp. 351-368.
116. 72A41150 9 pages  
Experimental Investigations of Separated Flows on Wing-Body Combinations  
with Very Slender Wings at Free-Stream Mach Numbers from 0.5 to 2.2  
Stahl, W.; Hartmann, K.; Schneider, W.  
International Council of the Aeronautical Sciences, Congress, 8th,  
Amsterdam, Netherlands, Aug. 28-Sept. 2, 1972.
117. 72A41138 9 pages  
Potential Flow Calculations to Support Two-Dimensional Wind Tunnel Tests  
on High-Lift Devices  
Labrujere, Th. E.; Schipholt, G. J.; De Vries, O.  
International Council of the Aeronautical Sciences, Congress, 8th,  
Amsterdam, Netherlands, Aug. 28-Sept. 2, 1972.
118. 72A34060 AIAA Paper 72-682  
Analytic Prediction of Dynamic Stall Characteristics  
(Aerodynamic Stall Characteristic Prediction from Static Experimental  
Data for Airfoils, Noting Boundary Layer Effects)  
Ericsson, L. E.; Reding, J. P.  
American Institute of Aeronautics and Astronautics, Fluid and Plasma  
Dynamics Conference, 5th, Boston, Mass., June 26-28, 1972.

119. 72A32250 138 pages  
 Handbook of Airfoil Sections for Light Aircraft  
 (Book on Airfoil Section Designs for Light Aircraft Covering Wind  
 Tunnel Studies of Lift Drag Ratio as Function of Angle of Attacks  
 Rice, M. S.  
 Milwaukee, Wis., Aviation Publications, \$3.95, 1971.
120. 72A31401 22 pages  
 Vortex-Lattice Method for Calculating Aerodynamic Coefficients of a  
 Subsonic Airplane  
 (Vortex-Lattice Method for Subsonic Aircraft Aerodynamic Coefficients  
 Calculation, Verifying Results with Airbus Lifting Surface Wing Tunnel  
 Test Data)  
 Hua, H. M.  
 Astronautical Society of the Republic of China, Transactions, Nov. 1,  
 1971, pp. 1-22.
121. 72A29132 7 pages  
 In Russian  
 Invariant Methods of Determining the Lift Coefficient of Various  
 Aerodynamic Profiles from the Flow Spectrum  
 (Aerodynamic Profiles Lift Coefficient Determination by Empirical  
 Formula Based on Potential Flow Lines Obtained by Conformal Mapping)  
 Suprun, V. M.  
 Samoletostroenie I Tekhnika Vozdushnogo Flota, No. 25, 1971, pp. 8-14.
122. 72A25595 SAE Paper 720337 12 pages  
 Consideration of Application of Currently Available Transport-Category  
 Aerodynamic Technology in the Optimization of General Aviation  
 Propeller-Driven Twin Design.  
 (Transport Aircraft Aerodynamic Design Technology Application to General  
 Aviation Propeller Driven Twin Engine Aircraft, Discussing Wing Loading  
 and Aspect Ratio Optimization)  
 Raisbeck, J. D.  
 Society of Automotive Engineers, National Business Aircraft Meeting,  
 Wichita, Kan., Mar. 15-17, 1972.
123. 72A18958 AIAA Paper 72-188 16 pages  
 Review and Evaluation of a Three-Dimensional Lifting Potential Flow  
 Computational Method for Arbitrary Configurations  
 (Subsonic Three Dimensional Potential Flow Computational Method Lifting  
 Aerodynamic Configurations Analysis and Design)  
 Rubbert, P. E.; Saaris, G. R.  
 American Institute of Aeronautics and Astronautics, Aerospace Sciences  
 Meeting, 10th, San Diego, Calif., Jan. 17-19, 1972.

124. 72A17194 11 pages  
 In French  
 Research and Tests on Laminar Airfoils  
 (Laminar Flow Airfoils for Gliders, Optimizing Profiles for Favorable Velocity and Pressure Distribution)  
 De Lagarde, B.; De Loof, J. P.  
 L'Aeronautique et L'Astronautique, No. 32, 1971, pp. 29-39.
125. 72A16109 5 pages  
 Refinement of the Nonplanar Aspects of the Subsonic Doublet-Lattice Lifting Surface Method  
 (Subsonic Doublet-Lattice Lifting Surface Method. Nonplanar Aspects Refinement, Using Wing-Tail Configurations)  
 Rodden, W. P.; Giesing, J. P.; Kalman, T. P.  
Journal of Aircraft, Vol. 9, Jan. 1972, pp. 69-73.
126. 72A12723 66 pages  
 Experimental Studies of Aerodynamic Coefficients of a Wing-Fuselage Combination and Comparison with the Results of Linear and Nonlinear Theories at Subsonic Speeds  
 (Wing-Fuselage Combination Aerodynamic Coefficients, Comparing Experimental Data with Subsonic Linear and Nonlinear Theoretical Results)  
 Herpfer, E.; Heynatz, J. T.  
 Deutsche Gesellschaft Fuer Luft-Und Raumfahrt, Jahrestagung, 4th, Baden-Baden, West Germany, Oct. 11-13, 1971.
127. 71A43312 14 pages  
 Lifting Line Theory of a Wing in Uniform Shear Flow  
 (Minimum Drag and Lifting Line Characteristics of Large Aspect Ratio Wing in Univorm Shear Flow with Velocity Variations Along Span)  
 Morita, K.  
JSME, Bulletin, Vol. 14, pp. 550-563.
128. 71A39543 3 pages  
 Equations of an Aircraft's Form  
 (Computer Aided Aircraft Design, Analysis and Production, Discussing Numerical Master Geometry Program Developed by British Aircraft Corporation)  
New Scientist and Science Journal, Vol. 51, pp. 410-412.
129. 71A24012 332 pages  
 In Russian  
 Preliminary Design of an Aircraft  
 (Soviet Book on Aircraft Preliminary Design Specifications as Function of Performance, Aerodynamic and Structural Parameters. Discussing Tradeoffs in Operational Requirements for Specific Configurations)  
 Diachenko, A. A.; Fadeev, N. N.; Goroshchenko, B. T.  
 Moscow, Izdatel'stvo Mashinstroenie.

130. 71A18511 AIAA Paper 71-50 19 pages  
Aerodynamics of Finned Missiles at High Angle of Attack  
(Finned Missiles Aerodynamics at High Angle of Attack, Examining  
Body Vortex Wake Region Interaction with Fins)  
Nicolaidis, J. D.; Oberkampf, W. L.  
American Inst. of Aeronautics and Astronautics, Aerospace Sciences  
Meeting, 9th, New York, N. Y., Jan. 25-27, 1971.
131. 71A13737 4 pages  
The Lift of a Slender Combination of a Fuselage of Rectangular Cross-  
Section with a High Wing  
(Lift of Slender Aircraft with Rectangular Cross Section Fuselage and  
High Wing)  
Andrews, R. D.  
AERONAUTICAL JOURNAL, Vol. 74, pp. 903-906.
132. 74N16700 NASA-TM-X-62325 91 pages  
Equation Solving Program for Aerodynamic Lifting Surface Theory  
Medan, R. T.; Lemmer, O. J.
133. 74N16699 NASA-TM-X-62323 67 pages  
Boundary Condition Program for Aerodynamic Lifting Surface Theory --  
Using FORTRAN IV  
Medan, R. T.; Ray, K. S.
134. Not in File 13 pages  
Sting Free Drag Measurements on Ellipsoidal Cylinders at Transition  
Reynolds Numbers  
Judd, M.; Vlajinac, M.; Covert, E. E.  
Journal of Fluid Mechanics, Vol. 48, pp. 353-365, July 1970.
135. 74N14710 11 pages  
Technical Evaluation Report -- Application of Aerodynamic Drag Research  
to Design of Aircraft  
Butler, S. F. J.  
In AGARD Aerodyn. Drag.
136. 72A12723 66 pages  
In German  
Experimental Studies of Aerodynamic Coefficients of a Wing-Fuselage  
Combination and Comparison with the Results of Linear and Nonlinear  
Theories at Subsonic Speeds  
(Wing-Fuselage Combination Aerodynamic Coefficients, Comparing Experi-  
mental Data with Subsonic Linear and Nonlinear Theoretical Results)  
Herpfer, E.; Heynatz, J. T.  
Deutsche Gesellschaft Fuer Luft-Und Raumfahrt, Jahrestagung, 4th,  
Baden-Baden, West Germany, Oct. 11-13, 1971.

137. 73N27209 NASA-TT-F-14962 34 pages  
 Calculation of Potential Flow Around Profiles with Suction and Blowing  
 (Integral Equations for Calculating Incompressible Potential Flows Around  
 Profiles with Suction and Blowing)  
 Jacob, K.  
 Washington NASA Transl. into English from Ing.-Arch., Berlin, Vol. 32,  
 No. 1, 1963, pp. 51-65.
138. 73N27045 AFFDL-TR-72-132 592 pages  
 Optimal Design Integrations of Military Flight Vehicles (ODIN/MFV)  
 (Development of Digital Computing System for Synthesis and Optimization  
 of Military Flight Vehicle Preliminary Designs) Final Report, May 1971 -  
 Sept. 1972  
 Hague, D. S.; Glatt, C. R.  
 Aerophysics Research Corp., Bellevue, Wash.
139. 73N25043 ARC-R/M-3279 ARC-22503 46 pages  
 On the Design of Wing-Body Combinations of Low Zero-Lift Drag Rise at  
 Transonic Speeds  
 (Optimum Design of Wing-Body Combinations for Zero-Lift Drag Rise at  
 Transonic Speeds)  
 Lord, W. T.  
 Ministry of Aviation, London, England  
 In ARC Aerodyn. Res. Progr., Including Turbine, Nozzle, Flutter, and  
 Instrumentation Studies, Vol. 2, pp. 1381-1426.
140. 73N24049 57 pages  
 Parametric and Optimization Techniques for Airplane Design Synthesis  
 (Parametric and Optimization Techniques for Aircraft Design Synthesis  
 to Show Principal Lines of Data Flow for Component Development)  
 Wallace, R. E.  
 In AGARD Aircraft Performance Prediction Methods and Optimization.
141. 73N24042 AGARD-LS-56 345 pages  
 In English and Partly in French  
 Aircraft Performance Prediction Methods and Optimization  
 (Development) and Application of Aircraft Performance Prediction Methods  
 for Subsonic and Supersonic Transport and Fighter Aircraft)  
 Williams, J. A/ED.  
 Advisory Group for Aerospace Research and Development, Paris, France,  
 Avail. NTIS HC \$19.25.
142. 73N21916 157 pages  
 The Design of a Vertical Takeoff and Landing Aircraft for the General  
 Aviation Market  
 (Design and Development of Vertical Takeoff Aircraft Configuration for  
 Use with Air Transportation Services Between Major Population Centers)  
 Harding, J. C.  
 Ph.D. Thesis, Dartmouth Coll., Hanover, N. H., Avail Univ. Microfilms  
 Order No. 72-23515.

143. 73N21899 NASA-CR-112231 32 pages  
 A Parametric Study of Planform and Aeroelastic Effects on Method for Computing the Aerodynamic Influence Coefficient Matrix of Nonplanar Wing-Body-Tail Configurations  
 (Aerodynamic Influence Coefficient Matrix for Nonplanar Wing-Body-Tail Configurations)  
 Roskam, J.
144. 73N15997 222 pages  
 An Optimal Configuration Design of Lifting Surface Type Structures Under Dynamic Constraints  
 (Optimized Design of Supersonic Aircraft Wing Based on Linear Combination of Weight of Wing and Aerodynamic Drag Minimization)  
 Miura, H.  
 Ph.D. Thesis, Case Western Reserve Univ., Cleveland, Ohio, Avail. Univ. Microfilms Order No. 72-18717.
145. 73N14004 41 pages  
 In Italian  
 Theory of Subsonic Lifting Surface (Fixed Mode), Some Considerations and Propositions for Improving the Method of Numerical Solution  
 (Improving Method of Numerical Calculation of Aerodynamic Coefficients for Subsonic Lifting Surface)  
 Polito, L.  
 Pisa Univ., Italy, Faculty of Engineering.
146. 72N32007 12 pages  
 Calculation of the Aerodynamic Characteristics of Lifting Systems Composed of Rectangular Wings  
 (Calculating Aerodynamic Characteristics of Lifting Systems Composed of Rectangular Wings Arranged One Behind Another)  
 Joint Publications Research Service, Arlington, Va.  
 In Its Rept. from the Higher Educational Inst., Aviation Tech., pp. 15-26.
147. 72N29016 404 pages  
 Preliminary Design of an Aircraft  
 (Development of Handbook of Basic Principles of Aircraft Design Based on Technical Specifications and Calculation of Aerodynamic Characteristics)  
 Goroschchenko, B. T.; Dyachenko, A. A.; Fadeev, N. N.  
 Transl. into English from "Eskiznoe Proektirovanie Samoleta", 1970, pp. 1-332, Translation of No. 129.
148. 72N29000 326 pages Unclassified Document  
 Aerodynamics  
 (Application of Aerodynamic Data to Design of Passenger Aircraft with Emphasis on Laws of Gas Motion Flow and Boundary Layer Theory)  
 Mkhitaryan, A. M.  
 Transl. into English from the Publ., "Aerodinamika", 1970, pp. 175-428.



149. 72N23042 AFOSR-72-0369TR 67 pages  
Theoretical Studies on the Aerodynamics of Slat Airfoil Combinations (Aerodynamic Characteristics of Leading Edge Slats Plus Main Airfoil Combinations), Final Report  
Liebeck, R. H.
150. 72N18037 AEDC-TR-71-186 68 pages  
Calculation of Forces on Aircraft Stores Located in Disturbed Flow Fields for Application in Store Separation Prediction (Aerodynamic Characteristics of Bomb in Steady, Incompressible, Potential Flow Based on Model), Final Report, 1 Apr. 1970, - 30 June 1971  
MacDermott, W. N.; Johnson, P. W.
151. 72N11017 AFOSR-71-1079TR 53 pages  
On the Aerodynamic Forces of Oscillating Two-Dimensional Lifting Surfaces (Aerodynamic Lift Characteristics of Oscillating Two-Dimensional Airfoil Subjected to Sinusoidal Gust), Final Report  
Yates, J. E.; Houbolt, J. C.
152. 71N37597 46 pages  
Calculation of Potential Flow About Arbitrary Three-Dimensional Lifting Bodies  
(Computer Program Development for Potential Flow Calculation About Lifting Bodies), Final Report, Dec. 1969 - Oct. 1970  
Hess, J. L.
153. 71N33016 AFFDL-TR-71-26-VOL-1 208 pages  
Stol High Lift Design Study, Volume 1 - State of the Art Review of (Test Data Reduction and Prediction Techniques for High Lift Aerodynamic and Propulsion System Configurations for Short Takeoff Aircraft Design - Bibliographies)  
May, F.; Widdison, C. A.
154. 71N29335 22 pages  
Calculation Methods for Unsteady Airforces of Tandem Surfaces and T-Tails in Subsonic Flow  
(Numerical Analysis of Aerodynamic Loads and Coefficients for Tandem and T-Tail Surfaces Harmonically Oscillating in Subsonic Flow)  
Davis, D. E.  
In AGARD Symp. on Unsteady Aerodynamics for Aeroelastic Analyses of Interfering Surfaces, Part 1, 1971.
155. 71N21973 NASA-TN-D-6243 11 pages  
Charts for Predicting the Subsonic Vortex-Lift Characteristics of Arrow, Delta, and Diamond Wings  
(Predicting Aerodynamic Characteristics of Arrow, Delta, and Diamond Wing Platforms Using Prandtl-Glauert Transformation)  
Polhamus, E. C.

156. 71N20115 80 pages  
 Calculation of the Three-Dimensional Potential Flow Around Lifting Non-Planar Wings and a Wing-Bodies Using a Surface Distribution of Quadrilateral Vortex-Rings  
 (Numerical Calculation of Steady Three Dimensional Potential Flow Around Lifting Nonplanar Aerodynamic Configurations Based on Surface Distribution of Quadrilateral Vortex-Rings)  
 Maskew, B.
157. 71N13402 ONERA-NT-163 34 pages  
 In French  
 Precise Calculation of Unsteady Aerodynamic Pressures in Subsonic Flow (Transient Pressures and Aerodynamic Coefficients of Rectangular Wings in Subsonic Flow Using Linear Equations)  
 Salaun, P.  
 Office National D-etudes et de Recherches Aerospatiales, Paris, France.
158. 74A18897 3 pages  
 In German  
 Investigations Concerning Wing-Fuselage Interference in the Case of Subsonic Velocity  
 Koerner, H.; Ahmed, S.R.; Mueller, R.  
 Dfvlr-Nachrichten, Dec. 1973.
159. 74A17270 18 pages  
 In German  
 Nonlinear Airfoil Theory with Allowance for Ground Effects --- for Aerodynamic Interference Problems Solution  
 Hummel, D.  
Zeitschrift Fuer Flugwissenschaften, Vol. 21, Dec. 1973, p. 425-442.
160. 74A17180 DGLR Paper 33 pages  
 In German  
 The Effect of Wing Planform Modifications on the Aerodynamic Performances of Fighter Aircraft  
 Staudacher, W.  
 Oesterreichische Gesellschaft Fuer Weltraumforschung Und Flugkoerpertechnik and Deutsche Gesellschaft Fuer Luft-Und Raumfahrt, Gemeinsame Jahrestagung, 6th, Innsbruck, Austria, Sept. 24-28, 1973.
161. 74A11606 SAE Paper 730876 9 pages  
 New Airfoil Sections for General Aviation Aircraft --- Cruising and Flap Development Tests  
 Wentz, W. H., Jr.  
 Society of Automotive Engineers, National Aerospace Engineering and Manufacturing Meeting, Los Angeles, Calif., Oct. 16-18, 1973.

162. 73A43028 11 pages  
 In German  
 The Panel Method for the Calculation of the Pressure Distribution on Missiles in the Subsonic Range  
 Kraus, W.; Sacher, P.  
Zeitschrift Fuer Flugwissenschaften, Vol. 21, Sept. 1973, p.301-311.
163. 73A41192 13 pages  
 The Aerodynamic Development of the Wing of the A 300B  
 Mcrae, D.M.  
Aeronautical Journal, Vol. 77, July 1973, p. 367-379.
164. 73A38007 4 pages  
 Prediction of the Lift and Moment on a Slender Cylinder-Segment Wing-Body Combination  
 Crowell, K.R.; Crowe, C.T.  
Aeronautical Journal, Vol. 77, June 1973, p. 295-298.
165. 73A34676 SAE Paper 730318 25 pages  
 Applications of Advanced Aerodynamic Technology to Light Aircraft  
 Crane, H.L.; McGhee, R.J.; Kohlman, D.L.  
 Society of Automotive Engineers, Business Aircraft Meeting Wichita, Kan., Apr. 3-6, 1973.
166. 73A32819 49 pages  
 In French  
 Calculation of the Characteristics of Tail Fins In the Vortical Field of a Wing  
 Yermia, M.  
 Association Aeronautique et Astronautique de France, Colloque D'Aerodynamique Appliquee, 9th, Saint-Cyr-L'Ecole, Yvelines and Paris, France, Nov. 8-10, 1972.
167. 73A25490 AIAA Paper 73-353 10 pages  
 Application of Computer-Aided Aircraft Design in a Multidisciplinary Environment  
 Fulton, R.E.; Sobieszczanski, J.; Storaasli, O.; Landrum, E.J.; Loendorf, D.  
 AIAA, ASME, and SAE, Structures, Structural Dynamics, and Materials Conference, 14th, Williamsburg, Va., Mar. 20-22, 1973.
168. 73A23856 32 pages  
 Transonic Airfoils - Recent Developments in Theory, Experiment, and Design  
 Nieuwland, G.Y.; Spee, B.M.  
 In Annual Review of Fluid Mechanics. Volume 5. (A73-23851 10-12)  
 Palo Alto, Calif., Annual Reviews, Inc., 1973, p. 119-150.

169. 73A1419 2 pages  
Lift of Wing-Body Combination  
Yang, H. T.  
AIAA Journal, Vol. 10, Nov. 1972, p. 1535, 1536.
170. 74N21645 AD-775538 MDC-J5831 277 pages  
Analytical Studies of Two-Element Airfoil Systems  
James, R.M.  
Interim Report, Feb. 1971 - Dec. 1973.
171. 74N21635 NASA-TN-D-7579 15 pages  
On the Use of Thick-Airfoil Theory to Design Airfoil Families in Which  
Thickness and Lift are Varied Independently  
Barger, R.L.
172. 74N20694 AD-774430 91 pages  
Addition of an Arbitrary Body Analysis Capability to the Boeing TEA  
236 Finite Element Computer Program  
Westphal, J. L.  
M.S. Thesis  
Air Force Inst. of Tech., Wright-Patterson AFB, Ohio. (School of  
Engineering)
173. 74N18654 AGARD-R-614 20 pages  
Interfering Lifting Surfaces In Unsteady Subsonic Flow Comparison  
Between Theory and Experiment  
Becker, J.  
Presented at 37th AGARD Structures and Mater. Panel Meeting, The Hague,  
7-12 Apr. 1973.
174. 74N17707 41 pages  
In German; English Summary  
Reciprocal Influence of a Body of Finite Length and a Wing at Mid-Wing  
Position at Subsonic Speed  
Gregoriou, G.  
Avail. Ntis HC \$5.25; Bundeswehramt, Bonn 30 DM
175. 74N13674 24 pages  
Reynolds Number Effects at Low Speeds on the Maximum Lift of  
Two-Dimensional Aerofoil Sections Equipped with Mechanical High Lift  
Devices  
Thain, J.A.  
In Natl. Res. Council of Can. Quart. Bull. of the Div. of Mech. Eng.  
and the Natl. Aeron. Estab. p. 1-24 (see N74-13673 04-34)

176. 74N11821 NASA-TN-D-7428 71 pages  
 Low Speed Aerodynamic Characteristics of a 17 Percent Thick Airfoil Section Designed for General Aviation Applications  
 McGhee, R.J.; Beasley, W.D.
177. 74N11815 NASA-TT-F-15183 25 pages  
 Calculation of Flows Around Zero Thickness Wings with Evolutive Vortex Sheets  
 Rehbach, C.  
 Transl. into English from Rech. Aerosp. (France), No. 2, Mar. - Apr. 1972, p. 53-61.
178. 74N10019 NASA-CR-2344 97 pages  
 The Effects of Leading-Edge Serrations on Reducing Flow Unsteadiness About Airfoils, an Experimental and Analytical Investigation Final Report  
 Schwind, R.G.; Allen, H.J.
179. 73N26000 NASA-TT-F-14959 42 pages  
 Airfoil Profiles in a Critical Reynolds Number Region (Force Measurements and Pressure Distributions on Three Gottinger Airfoil Profiles During Transition From Laminar To Turbulent Boundary Layer Flow)  
 Kraemer, K.  
 Transl. into English from Soderdruck Aus der Z. Forsch. Auf Dem Gebiete des Ingenieurwesens' ' (West Germany), V. 27, No. 2, 1961, p. 33-46.
180. 73N25002 ARC-R/M-3180 19 pages  
 Observations of the Flow Over a Two Dimensional 4 Percent Thick Aerofoil At Transonic Speeds  
 (Wind Tunnel Tests to Determine Pressure Distributions for Four Percent Thick, Circular ARC, Biconvex Airfoil at Transonic Speeds)  
 Henshall, R.D.; Cash, R. F.  
 In ARC Aerodyn. Res., Including Heating, Airfoils, and Boundary Layer Studies, Vol. 1, p. 63-81 (see N73-24999 16-01).
181. 73N24040 AD-757813 81 pages  
 An Exact Method of Designing Airfoils with Given Velocity Distribution in Incompressible Flow An Extension of the Lighthill and Arlinger Methods (Application of Conformal Mapping Procedures for Designing Airfoil Shapes with High Design Lift Coefficients) Final Report  
 Strand, T.  
 15 Jun. - 15 Dec. 1972.

182. 73N24000 ARC-R/M-3238 40 pages  
 The Pressure Distribution on Two-Dimensional Wings Near the Ground  
 (Numerical Analysis of Pressure Distribution in Incompressible Flow  
 on Two-Dimensional Airfoils Near Ground)  
 Bagley, J.A.  
 In ARC Res. Progr. on Aerodyn. Heating, Airfoils, Wings, and Aircraft  
 During 1960, Vol. 1, p. 79-118 (see N73-23995 15-01).
183. 73N22977 NASA-CR-112297 233 pages  
 An Analytical Study for the Design of Advanced Rotor Airfoils  
 (Design and Evaluation of Two Airfoils for Helicopter Rotors for  
 Reduction of Rotor Power Requirements)  
 Kemp, L.D.
184. 73N21914 AD-755480 MDC-J5679-01 166 pages  
 Calculation of Potential Flow About Arbitrary Three-Dimensional  
 Lifting Bodies  
 (Development of Method for Calculating Potential Flow about Arbitrary  
 Lifting Three-Dimensional Bodies with Emphasis on Bound Vorticity and  
 Application of Kutta Condition) Final Technical Report  
 Hess, J.L.
185. 73N21907 NASA-TN-D-7183 41 pages  
 Low-Speed Wind Tunnel Investigation of A Semispan Stol Jet Transport  
 Wing Body with an Upper Surface Blown Jet Flap  
 (Wind Tunnel Tests to Determine Static Longitudinal Aerodynamic  
 Characteristics of Jet Transport Wing-Body with Upper Surface Blown Jet  
 Flap for Lift Augmentation)  
 Phelps, A.E., III; Letko, W.; Henderson, R.L.
186. 73N21054 7 pages  
 Wake Characteristics of a Two-Dimensional Symmetric Aerofoil  
 (Generation of Aerodynamic Noise by Turbulent Wake Behind Rotary  
 Wing Airfoil and Relationship to Drag and Lift Coefficients)  
 Kavrak, I.  
 In AGARD Aerodyn. Rotary Wings (see N73-21031 12-02)
187. 73N20995 198 pages  
 An Analysis of the Design of Airfoil Sections for Low Reynolds Numbers  
 (Design of Airfoil Sections for Low Reynolds Numbers Based on Requirement  
 to Achieve Transition Upstream of Major Adverse Pressure Gradient)  
 Miley, S.J.  
 Ph.D. Thesis  
 Mississippi State Univ., State College. Avail Univ. Microfilms  
 Order No. 72-20272.

188. 73N16283 AD-751075 MDC-J5713 63 pages  
 A New Family of Airfoils Based on the Jet-Flap Principle  
 (Air Foils Based On Utilization of Jet-Flap Principle)  
 Bauer, A.B.  
 Technical Report, Apr. 1971-Apr. 1972.
189. 73N15992 AD-751045 116 pages  
 Circulation Control By Steady and Pulsed Blowing for a Cambered  
 Elliptical Airfoil  
 (Short Takeoff Aircraft Lift Augmentation and Prevention of Airflow  
 Separation on Cambered Elliptical Airfoil Section Using Circulation  
 Control)  
 Walters, R.E.; Myer, D.P.; Holt, D.J.
190. 73N15050 DLR-FB-72-63 42 pages  
 In German; English Summary  
 Theoretical Parameter Studies of Wing-Fuselage Combinations  
 (Prediction Analysis Method to Determine Influence of Geometry  
 Parameters on Aerodynamic Characteristics of Body-Wing Configuration)  
 Koerner, H.  
 Deutsche Forschungs- und Versuchsanstalt fuer Luft- und Raumfahrt,  
 Brunswick (West Germany). (Abteilung fuer Theoretische Aerodynamik.)  
 Avail. Ntis HC \$4.25; Dfvlr. Porz, West Ger. 11 DM.
191. 73N15010 16 pages  
 The Effect of Leading Edge Geometry on High Speed Stalling  
 (Aerodynamic Configurations of Swept Wings to Improve Lift Performance  
 at Stall in Higher Range of Subsonic Speeds)  
 Moss, G.F.; Haines, A.B.; Jordon, R.  
 In AGARD Fluid Dyn. of Aircraft Stalling (see N73-14998 06-02).
192. 73N15009 12 pages  
 A Simplified Mathematical Model for the Analysis of Multielement Airfoils  
 Near Stall  
 (Development of Procedure for Determining Characteristics of High Lift  
 Systems Where Viscous Effects Dominate)  
 Bhateley, I.C.; Bradley, R.G.  
 In AGARD Fluid Dyn. of Aircraft Stalling (see N73-14998 06-02).
193. 73N15008 12 pages  
 The Low Speed Stalling of Wings With High Lift Devices  
 (Analysis of Aerodynamic Stall Characteristics of Wing Sections With  
 High Lift Devices in Two-Dimensional Flow)  
 Foster, D.N.  
 In AGARD Fluid Dyn. of Aircraft Stalling (see N73-14998 06-02).

194. 73N15007 27 pages  
Aerodynamics in High Lift Airfoil Systems  
(Analysis of Aerodynamic Processes Occurring in Flow Past Unpowered  
Multi-Element Airfoils in High Lift Attitude)  
Smith, A.M.O.  
In AGARD Fluid Dyn. of Aircraft Stalling (see N73-14998 06-02).
195. 73N14998 AGARD-CP-102 342 pages  
Partly in English and Partly in French  
Fluid Dynamics of Aircraft Stalling  
(Proceedings of Conference on Fluid Dynamics of Aircraft Stalling to  
Include Stall and Post-Stall Aerodynamic Characteristics of Various  
Military Aircraft)  
Advisory Group for Aerospace Research and Development, Paris (France)  
Avail. Ntis HC \$19.25  
Presented at Fluid Dyn. Panel Specialists Meeting, Lisbon, 25-28 Apr. 1972.
196. 73N14051 AD-749726 FTD-HT-23-181-72 36 pages  
Application of the Wing Impulse Theory to the Determination of Propeller  
Slip Stream Influence on Wing Aerodynamic Characteristics  
(Wing Impulse Theory Applied to Determination of Propeller Slipstream  
Influence on Wing Aerodynamic Characteristics, Using Airfoil of Finite  
Span)  
Kopylov, G.N.  
Transl. into English from Tr. Vyssee Aviatsonnoe Uchilishche  
Grazhdanskii Avlatsii (USSR), No. 24, 1965, p. 24-43.
197. 73N14043 AD-749485 AFFDL-TR-72-96-PT-2 86 pages  
Development of Theoretical Method for Two-Dimensional Multi-Element  
Airfoil Analysis and Design. Part 2 Leading-Edge Slat Design Method  
(Computer Program for Designing Leading Edge Slats for Producing  
Specified Pressure Distribution on Main Airfoil)  
McGregor, O.W.; McWhirter, J.W.  
Final Report, 24 May 1971 - 12 Jun. 1972.
198. 73N10242 AD-740124 MCD-J5264-VOL-2 310 pages  
Investigation of Aerodynamic Analysis Problems in Transonic Maneuvering.  
Volume 2 Airfoil Analysis Computer Program  
(Development of Computer Program for Analyzing Mono-Element and Multi-  
Element Airfoils at Subsonic Speed with Attached Air Flow - Vol. 2)  
Gentry, A.E.  
Final Report, Jun. 1970 - Aug. 1971.











POSTMASTER: If Undeliverable (Section 156  
Postal Manual) Do Not Return

*"The aeronautical and space activities of the United States shall be conducted so as to contribute . . . to the expansion of human knowledge of phenomena in the atmosphere and space. The Administration shall provide for the widest practicable and appropriate dissemination of information concerning its activities and the results thereof."*

—NATIONAL AERONAUTICS AND SPACE ACT OF 1958

## NASA SCIENTIFIC AND TECHNICAL PUBLICATIONS

**TECHNICAL REPORTS:** Scientific and technical information considered important, complete, and a lasting contribution to existing knowledge.

**TECHNICAL NOTES:** Information less broad in scope but nevertheless of importance as a contribution to existing knowledge.

**TECHNICAL MEMORANDUMS:** Information receiving limited distribution because of preliminary data, security classification, or other reasons. Also includes conference proceedings with either limited or unlimited distribution.

**CONTRACTOR REPORTS:** Scientific and technical information generated under a NASA contract or grant and considered an important contribution to existing knowledge.

**TECHNICAL TRANSLATIONS:** Information published in a foreign language considered to merit NASA distribution in English.

**SPECIAL PUBLICATIONS:** Information derived from or of value to NASA activities. Publications include final reports of major projects, monographs, data compilations, handbooks, sourcebooks, and special bibliographies.

**TECHNOLOGY UTILIZATION PUBLICATIONS:** Information on technology used by NASA that may be of particular interest in commercial and other non-aerospace applications. Publications include Tech Briefs, Technology Utilization Reports and Technology Surveys.

*Details on the availability of these publications may be obtained from:*

**SCIENTIFIC AND TECHNICAL INFORMATION OFFICE  
NATIONAL AERONAUTICS AND SPACE ADMINISTRATION  
Washington, D.C. 20546**